2-P

NASA SP-281

SEVENTH ANNUAL CONFERENCE ON MANUAL CONTROL

University of Southern California
Los Angeles, California
June 2–4, 1971

NATIONAL AERONAUTICS AND SPACE ADMINISTRATION

NASA SP–281

SEVENTH ANNUAL CONFERENCE ON MANUAL CONTROL

Proceedings of a meeting held at
University of Southern California
Los Angeles, California
June 2–4, 1971

Scientific and Technical Information Office 1972
NATIONAL AERONAUTICS AND SPACE ADMINISTRATION
Washington, D.C.

Foreword

This volume contains the proceedings of the Seventh Annual NASA/Air Force/ University Conference on Manual Control, held at the University of Southern California, Los Angeles from June 2 to 4, 1971. The format of the program is followed in this report, which contains all the formal papers from the conference, as well as a number of papers which were presented informally and later expanded into complete manuscripts.

As indicated in the title, this was the 7th conference on manual control. The title, location, date, and report number for the first through sixth conference proceedings are listed below for cross reference:

First Annual NASA-University Conference on Manual Control, University of Michigan, December 1964. (Proceedings not printed.)

Second Annual NASA-University Conference on Manual Control, MIT, Feb. 28 to March 2, 1966, NASA SP–128.

Third Annual NASA-University Conference on Manud Control, University of Southern California, March 1–3, 1967, NASA SP–144.

Fourth Annual NASA-University Conference on Manual Control, University of Michigan, March 21–23, 1968, NASA SP–192.

Fifth Annual NASA-University Conference on Manual Control, MIT, March 27–29, 1969, NASA SP–215.

Sixth Annual Conference on Manual Control, Wright-Patterson Air Force Base, April 7–9, 1970, AFIT-AFFDL.

Summary

GEORGE A. BEKEY

University of Southern California

AND

CARL JANOW

NASA Headquarters

The Seventh Annual NASA/AF/University Conference on Manual Control was held at the University of Southern California from June **2–4, 1971.** Some eighty specialists, including colleagues from Canada, Netherlands and West Germany, attended the Conference, which was organized by the authors of this Summary.

Generally at this conference there was less emphasis on theory and more on applications than at some previous meetings. In addition to the well-established areas of human operator modeling and display systems, this conference devoted considerable time to the extensions of manual control theory to such diverse areas as automobile driving, air traffic control and industrial management. This interest in meaningful applications of the existing theoretical knowledge in man-machine systems is encouraging and timely.

Highlights of the major sessions are presented in the following paragraphs.

I. HUMAN OPERATOR MODELS

This session included papers on modeling the tracking as well as the decision aspects of human controllers. Henry Jex presented the opening paper which surveyed the state of the art of human operator models with special emphasis on problems arising from control-vehicle interfaces as occurring via the sensory and motor modalities. Gunnar Johannsen put forth a generalized non-linear multi-parameter model for the human operator which utilized a random search algorithm for parameter identification. The author points out that such an approach would be highly desirable for a systematic comparison of various existing models. William Levison presented an interesting application of the classical level crossing problem in random processes to modeling human decision making in a specific task related to aircraft landing. The model utilizes basic concepts in decision and estimation theory. Continuing in this spirit, John Ware outlined the development of an input-adaptive pursuit tracking model of the human operator. The model presented was that of an optimal mean square predictor constrained to using only position and velocity information.

There were three informal presentations. An on-line, hybrid computer technique for identification of human operator model parameters was presented by

G. A. Jackson and G. Brabant. The technique obtains up-dated parameter values at 15 second intervals. The second paper was concerned with the validity of modeling remnant noise by a sum of sine waves (P. F. Torrey and R. A. Hannen), and the third paper (by R. Mekel and P. Peruo) with the use of a class of Liapunov functions for digital modeling of human operator dynamics.

11. EXTENSIONS OF MANUAL CONTROL THEORY

This session was comprised of four stimulating papers on relevant new applications of manual control theory. The first two papers by R. E. Anderson et al. and D. Graham and W. Clement considered two typical problems in air traffic control operations. In view of the heavy air congestion at certain times at most of our major airports there is a tremendous need for improvements in the pilot/air traffic controller interface. Anderson et al. addressed themselves to this problem by considering the design of an onboard air-traffic situation display. Graham and Clement looked at the safety problem involved in flying aircraft under existing or reduced separation standards. They provide estimates for the effective reaction time delays involved in executing a collision avoidance maneuver. The paper by T. B. Sheridan and W. B. Rouse analyzed the nature of supervisory control and decision processes and the reasons for suboptimal (with respect to some cost) performance on the part of a human supervisor. E. R. F. W. Crossman gave an illuminating presentation on manual control models for industrial management.

III. BIOLOGICAL ASPECTS OF MANUAL CONTROL

This session had six presentations indicating continuing activity in studies of the physiology which underlies manual control. A paper by J. C. Hill dealt with the kinematic aspects of the human skeleton. Digital simulation was used to study the dynamics of an idealized "stick man" moving in the pitch plane. G. Agarwal et al. presented experimental data to support a nonlinear model relating neural input to force and muscle contraction for the ankle joint. J. W. Aldrich et al. discussed the development of a hierarchical, self-regulating, semi-autonomous system which is capable of learning and forgetting complex tasks. They foresee how such systems could be interconnected to obtain adaptive reflex and voluntary control, and thus to synthesize prostheses or remote manipulators. The presentations by R. E. Magdaleno and B. S. Repa et al. were concerned with measurements of neuromuscular system function. In both papers, the results of tracking and manipulation tests were used as indicators of neuromuscular system function. Laurence Young presented the final paper of the session which was concerned with modeling the effects of various forces in a rotating spacecraft on the human vestibular system.

IV. ANALYSIS OF DISPLAY SYSTEMS

Displays continue to be an important area in man-machine system analysis, as demonstrated by a variety of papers in this area. D. Dey showed how predictive displays affect the parameters of a quasi-linear human pilot describing function. Continuous parameter tracking was used to adjust the model parameters. D. L. Kleinman and S. Baron discussed the application of their work on optimal control to prediction of display requirements in a landing situation. The analysis was

based on previously published work where pilot equalization was modeled by a least-squares predictor, a Kalman filter, and a set of optimal gains. A simulated pictorial landing display was also studied by E. Palmer and T. Wempe. The authors showed that pilot performance improved with added guidance symbology in the display.

H. Jex et al. reported the results of a study of display format on pilot describing functions. Their major result was that less desirable displays produce lower closed-loop system bandwidth. A paper by R. Klein documented a series of specially prepared digital magnetic data tapes prepared by Systems Technology, Inc., under contract to NASA-Ames Research Center. The tapes contain synchronized measurements of pilot scanning behavior, control response and vehicle response during ILS approaches made in a DC–8 simulator. The data base provided by these tapes should be useful in many studies of man-machine system performance.

In a very interesting presentation, J. M. Naish described a study on how pilots estimate the movements of their vehicle during an unaided visual approach. The various sources of information available to the pilot are ranked in importance and analyzed.

The final paper in the session was an informal presentation by W. Wilckens, concerned with the effectof automatic landing systems on the pilot's information requirements.

V. VISUAL INFORMATION PROCESSING

The processing of information received by the eyes has been an important area of investigation for many years. A number of questions concerned with this general field were discussed in this session, ranging from models of the perception process to studies of eye movement.

R. E. Curry discussed a model which, according to the author, might unify much of the available experimental data in visual space perception. Its central hypothesis is that the visual system operates centrally as if it were a Bayesian processor.

The generation of visual images which would produce retinal images closely duplicating the outside world was discussed by K. P. Gärtner. The author presented a proposal for using "textured" visual flight information to accomplish this objective.

R. W. Pew and his associates presented two papers in this session. The first was concerned with visualization of an observer's strategy when he adjusts the parameters of a dynamic system to achieve specific objectives. The second paper also dealt with an attempt to understand what aspects of a visual task are important or essential to a human observer. In this case, observers adjusted the angle and exit velocity of a projectile to cause it to fall through a target trap. Apparently, the shape of the trajectory is more important than its evolution in time.

The effect of preview on manual control performance was reported by G. C. Johnson. He showed that up to about 8 millisec of preview was effective in reducing rms error and improving time-on-target scores.

The final paper of the session was presented by J. D. Smith and A. V. Phatak who presented a mathematical model of human eye movements during gaze at a stationary target. Their model exhibits feedback control, a hierarchical structure, a variable retinal gain and movement of the target image within specific areas on the fovea.

VI. AUTOMOBILE DRIVING

While applications of manual control theory to the driver/automobile system have been discussed at previous "Annual Manual" Conferences, this was the first meeting to devote an entire session to this subject. D. H. Weir and C. K. Wojcik discussed the measurement of human driver describing functions in steering tasks using the UCLA driving simulator facility. The describing functions were measured in a simulated crosswind gust and confirmed the feasibility of such measurements in nominal control tasks with real-world visual displays.

P. Delp et al. presented driver describing function estimated for lateral position control obtained using the Berkeley "double steering wheel." Random appearing, gaussian and transient time forcing functions were used in the instrumental car. The time histories showed evidence of pulse-like nonlinear behavior during extended response to step transients.

In a somewhat different view, M. L. Ritchie et al. reported the results of a number of studies which related drivers, vehicles, roadway signs and other roadway variables. Somewhat puzzling results were obtained, indicating the need for careful study of these interactions.

In an informal paper, G. Burnham and G. A. Bekey presented preliminary results of their new studies of simulated multi-vehicle following situations.

VII. PERFORMANCE: PREDICTION & EVALUATION

This was one of the key sessions of the conference, since it was devoted to the payoff of the theory, namely evaluation of performance. In the first paper, R. W. Allen and H. R. Jex presented the results of a series of control tasks performed by the crew of a space station simulator during long term confinement. Good correlation was noted between "clinical" tests (related to the subject's dynamic time delay) and conventional steady-state tracking tasks. Subjects apparently continued to improve their tracking performance during the 90 days of confinement.

S. Baron and D. L. Kleinman presented another application of their work on optimal control by using their model to predict pilot performance in a series of longitudinal hovering tasks. The results showed that their model was able to predict performance with excellent accuracy in most cases. Another application of optimal control technology was given by G. Stein and A. H. Henke, whose paper presents a design procedure for lateral-directional flight control systems. The method is based on minimum quadratic cost optimal control technology and has been applied to the design of a control system for the F4C aircraft.

T. A. Dukes and P. B. Sun introduced a "phase margin performance measure" for manual control systems. When used with multivariable closed-loop experiments, the performance of each loop can be determined independently.

A method for measuring remnant power was discussed by R. Magdaleno. Termed "serial segments," the technique is based on measuring the power spectral density in a frequency band centered on each sine wave in a sum-of-sine-waves forcing function.

R. O. Anderson extended the application of his "paper pilot" (from the 1970 "Annual Manual") to the study of aircraft pitch attitude control.

C. Y. Ng and R. E. Curry described an interesting compensator which tracks the parameters of a quasilinear model and adapts in such a way as to absorb undesirable changes in input signal or in the dynamics of the controlled element.

The final paper of the session, by C. R. Replogle et al., was concerned with the effect of stress on human operator performance. Such stresses as hypoxia were shown to affect error measures in unstable tracking tasks.

VIII. INTERACTION OF SENSORY MODALITIES

The interaction of one sensory channel with another has long been a subject of considerable interest in manual control. D. L. Baty reported on the effect of concurrent audio tasks on human operator performance in compensatory tracking. The study did not provide any evidence for a ceiling on human information processing rates. In a similar problem, R. C. Cliff reported on a study where subjects were asked to verbally shadow an auditory input while performing continuous compensatory control. His evidence supports a single channel model for continuous dual-task control.

The effect of motion cues on tracking behavior were discussed by R. F. Ringland and R. L. Stapleford. The interaction of visual, auditory, vestibular and other proprioceptive signals is analyzed in great detail in the paper.

Aural compensatory tracking and combinations of auditory and visual displays were discussed by E. W. Vinje and E. T. Pitkin. The describing function and remnant data obtained showed that human operators can control as well with aural as with visual signals. However, combined signals did not lead to the expected improvement.

The final paper of the conference was presented by J. W. Hill and J. C. Bliss who discussed manual control of remote manipulators. A tactile feedback system aids the ordinary visual feedback to the operator in controlling the remote arm position.

Contents

Session III. BIOLOGICAL ASPECTS OF MANUAL CONTROL

Chairman: Julia Apter

Session IV. ANALYSIS OF DISPLAY SYSTEMS

Chairman: Richard Pew

Session V. VISUAL INFORMATION PROCESSING

Chairman: John Senders

Session VI. AUTOMOBILE DRIVING

Chairman: George A. Bekey

Session VII. PERFORMANCE: PREDICTION AND EVALUATION

Chairman: M. E. Sadoff

Session VIII. INTERACTION OF SENSORY MODALITIES

Chairman: Arnold Small

SESSION I

HUMAN OPERATOR MODELS

Chairman: DUANE McRUER

1. Problems in Modeling Man-Machine Control Behavior in Biodynamic Environments

HENRY R. JEX

Systems Technology, b c .

The purpose of this presentation is to review some current problems in modeling man-machine control behavior in a biodynamic environment. It is given in two parts: (1) a review of the models which are appropriate for manual control behavior and the added elements necessary to deal with biodynamic interfaces, and (2) a review of some biodynamic interface pilot/vehicle problems which have occurred, been solved, or need to be solved.

MODELS

Basic Manual Control Models

The types of models evolved in the field of man-machine systems are behavioral (i.e., input-to-output) models rather than mechanistic analog models, although the lumped parameter analog models are often used for particular subsystems within the human operator. The development of these models and empirical data is the result of over two decades of research which received its initial impetus during World War II. Manual control technology has been used in numerous practical applications, such as: prediction of military and commercial aircraft handling qualities (and to quantification of the relevant procurement specifications), problems of manned vehicular control systems, and the design of better displays and controls for manned systems (e.g., see refs. 1 through 3, and the bibliography in refs. 1 and 11).

Starting with some basic principles, we will look at an increasingly complex array of models required to interface the man with the machine in a biodynamic environment. Our models are limited to the wide class of tasks which require an operator to act as a very precise sensorimotor link in a closed-loop system. Examples of such tasks are: driving a car, piloting an aircraft, aiming a weapon or telescope, and threading a needle. In such tasks the human operates as an adaptive, learning controller. Subsequent encounters with the same task result in improved behavior, which eventually evolves towards that which is most appropriate for the task. This strategy is remarkably consistent from person to person.

Figure 1 shows the "standard" block diagram for man-machine control situations. Starting from the left, the mission or task context is defined as a set of "forcing functions" comprising command inputs to be followed, and disturbances to be regulated against. Displays couple the command and feedback information to the human operator, who produces the necessary control actions to operate the controlled element in the desired manner. The output motions of the system are then displayed directly or indirectly to the human operator. This completes a feedback loop in which the goal of the operator is to reduce the observed errors between the actual or implied commands and the outputs. Because human behavior in such tasks evolves towards repeatable forms of response, it is thereby meaningful to measure it, to model it, and to seek its underlying laws.

The measured human control behavior in closed-loop tasks has been found to depend on many variables:

- Task variables.—forcing function displays, control stick, and controlled element
- Environmental variables.—vibration, temperature, g-level, and breathing atmosphere

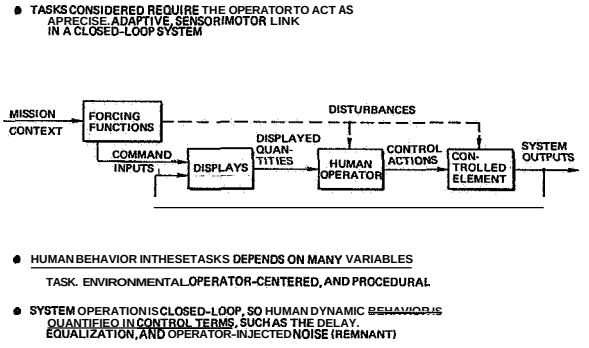

FIGURE 1.—Basic principles for man-machine control situations.

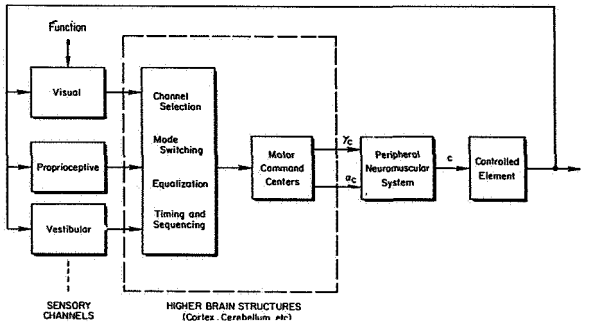

FIGURE 2.—Generalized man-machine system.

• Operator-centered variables.—anxiety, motivation, workload, and fatigue

• Procedural variables.—practice, transfer of training, order of presentation, and even the measurement technique.

We generally try to suppress the procedural variables by suitable experimental design and thorough training, so it is the first three which are of main interest. The effects on both models and parameters of the task variables are fairly well understood (refs. 1 and 8), but measuring the effects of environmental and operator-centered variables are still in an embryonic status.

Because man-machine control systems generally operate in a closed-loop manner, human control behavior is most suitably quantified in terms of control theory. Such concepts as feedback loops, dynamic stability, dynamic loop delays, equalization, and operator-injected noise ("remnant") are central concepts to all man-machine-control models.

Now let's expand the human operator block of figure 1. Here in figure 2 we have a more generalized block system diagram. At the left are shown the three main forms of sensory input, i.e., the visual, proprioceptive, and vestibular neural signals. They interact with the higher brain structures in, as yet, only vaguely understood ways. Within the cortex and the cerebellum a number of processes occur. Among these are channel selection (when more than one channel must be operated concurrently), mode switching between various types of internal loop structure, equalization (in the form of rate anticipating or smoothing), and the timing and sequencing of various discrete events in cases where that is appropriate. All of these operations take a finite amount of time, but as learning proceeds and the same forcing function is encountered again, less time is taken to handle and command the appropriate motor actions. These emanate from the higher brain structure in the form of alpha and gamma motor neuron signals which operate the neuromuscular servo system. A completely accurate and comprehensive neuromuscular model has yet to be evolved; nevertheless, a lot is known. I will expand on this neuromuscular system model later.

The structure of the models for man-machine control systems is not fixed, but can actually change as learning proceeds. This hierarchy of open- and closed-loop feedback structures has been termed the Successive Organization of Perception (SOP) theory of learning (refs. 4 and 5). In figure 3 we see that in the most basic phase the operator merely seeks to correct the errors between the command and response. This "compensatory" loop structure is the only structure allowed when the input or forcing functions are completely unpredictable.

In the second phase the operator takes advantage of any ((coherency," or patterns, in his input (or which he perceives proprioceptively from his control forces) to form other signal paths which can cause the output to follow the input more accurately. Any residual errors are then corrected in a compensatory manner. This so-called "pursuit" loop structure is the most general form of operator control, yet the elements within the blocks at this point can only be inferred, because there is but one input and one output from which the properties of several

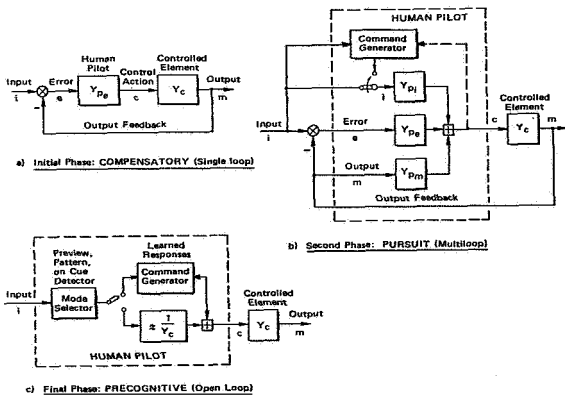

FIGURE 3.—Phases in the successive organization of perception.

blocks must be determined. Consequently, definitive models for the pursuit structures are not well established. Fortunately, it is the error correction portion of this loop which determines the dynamic stability of the man-machine system, so the feedback properties derived for compensatory loop structures continue to dominate the pursuit level of internal organization.

In the final phase, given commands to which prelearned responses are appropriate, the operator can evolve towards a preprogrammed open-loop controller. For example, he could use preview, pattern prediction, or cue detection to select and trigger off a previously learned response. In doing this he incurs increased decision time and a chance of major error. Nevertheless, most of our normal discrete stimulus/response type of actions are correctly modeled in this form. In this case such complexities as closed-loop stability and circulating noise transmission in the control loops cease to be a problem, and the theories of probabilistic learning and optimal control theory play a dominant modeling role.

The ability of the human to form such complex loop structures and to take advantage of the predictability of a command signal leads to great difficulty in the measurement of his dynamic response properties. Unlike the "passive" dynamic models of the body, which mast biodynamicists are used to dealing with, it is not possible to obtain meaningful control response properties of a human controller by forcing him with a pure sinusoid swept through the low-frequency band. Faced with such a predictable input, the operator will rapidly progress through the SOP learning stages. The result is an output which can be closely in synchronism with the input sinusoid up to the limiting neuromuscular bandwidth (on the order of 4 Hz).

Consequently, *to obtain useful dynamic response measures the human operator must be forced with a random-appearing forcing function of fairly low bandwidth* with most of its power below **1 Hz.** Experience has shown that the most efficient way to do this is to provide a sum of randomly phased sinusoids. To prevent the appearance of repetitive wave-forms these are spaced roughly logarithmically in frequency while avoiding simple harmonic frequency ratios. The Successive Organization of Perception considerations make the selection of forcing functions for man-machine measurements a subtle art, requiring great finesse. Just remember that many of the simple frequency-sweep techniques familiar to systems engineers will not work with man-machine systems, and that more sophisticated nonlinear describing function techniques are necessary (e.g., see refs. 6 and 7).

Biodynamic Interfaces

Now consider the additional elements required to interface man and machine in a biodynamic environment. At the top of figure 4 is the now-familiar control loop, including display, human operator, controlled element, and feedback. At the bottom are those additional elements required in a biodynamic environment. There are three

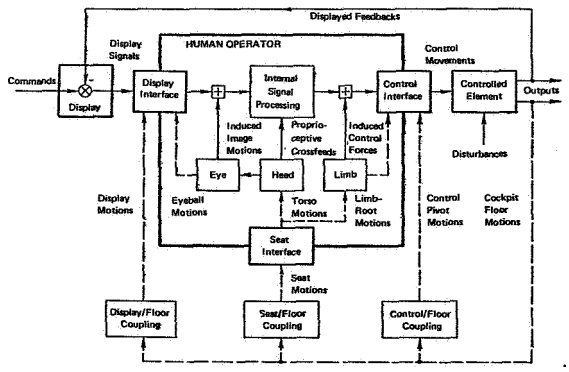

FIGURE 4.—Biodynamic interfaces for man-machine control.

primary biodynamic interfaces of the human operator: at the display, the seat, and the controls. Each of these is, in turn, coupled to the structure **(floor)** of the controlled element via passive or possibly active means. An example of active couplings are the vibration isolation seats currently undergoing tests at U.S. Air Force and NASA facilities.

In a dynamic vibration environment the display, seat, and control can each be vibrating at different large amplitudes and with different phases, so that merely perceiving the display and gripping the stick may become difficult *per se.* The human torso, and through it the motions of the head, eye, and limbs, also may be induced to move out of phase with their respective interfaces. Consequently, a number of spurious (and occasionally favorable) control signals can be developed by the man-machine system in a biodynamic environment. For example, eyeball motions can cause image motions which in turn lead to spurious control signals. Head motions and varying acceleration vectors can cause spurious vestibular signals to be developed, leading to eye motions (nystagmus) or to a number of illusions (i.e., the oculogravic illusion) (ref. **20).** Forces may be applied to the control by the vibration-induced motions between the limb and control pivot. In many cases the mass of the limb (or more correctly, its dynamic impedance properties) acting at the top of the stick act as a "bobweight." This makes the control system unusually sensitive to axial, normal, or transverse accelerations of the coupled pilot-vehicle system. The "bobweight effect" is observed in some automobiles, where resting the hands loosely at the top of the wheel (versus at the bottom) gives rise to markedly different transient responses to side-gusts.

While the modeling **of** the *mechanical* elements between the man and machine interfaces is a straightforward but tedious process, the modeling of the biodynamic feedbacks and interactions is not. Comprehensive biodynamic models such as the ones described in reference **30** are necessary to assess the simultaneous motions **of** the head, eye, and limbs. Even more complex and subtle models are required to handle induced image motions (ref. 42), vestibular crossfeeds (refs. **20** and **21),** and induced control forces (refs. **15** and **16).** As a result, such models are in a more primitive state of development than the basic human operator models.

Example—Model for Limb/Control Interface

To illustrate the additional complexities which can occur, let us look in more detail at what is inside the block previously labeled "control interface" in figure **4.** Figure **5** shows a somewhat simplified, lumped-parameter model for the limb-to-control interface. Its input (from the left) is the command from the central nervous system, and its output (at the right) is the control position. Relative motions may exist between the limb-root (on the torso) and the control pivot.

The middle of figure **5** shows the muscle servo system as a lumped-parameter analog of the agonist/antagonist pair of muscles that actuate the limb. The parameters with arrows through them are some of the many "variable constants" which plague the biodynamic modeling field. These constants are dependent primarily on the tension in the muscle system as set by the gamma

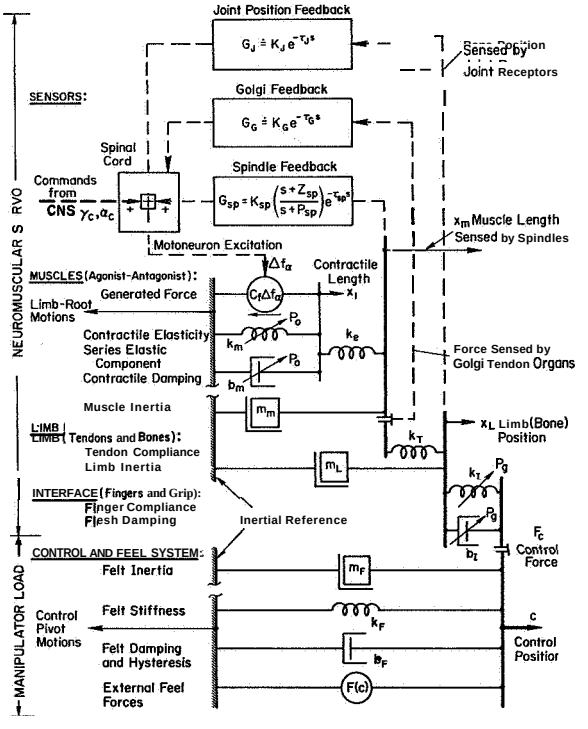

FIGURE 5.—Model for limb-manipulator interfaces.

motor neuron excitation (see refs. 8 and 9). The resulting muscle actuation forces are coupled elastically through the muscle inertia, then through the tendon compliance into the limb inertia to move the bone. Various sensory paths are shown at the top to complete this servo loop. We believe the spindle feedbacks play a dominant role in fine control motions, but Golgi-organ feedbacks and joint-position-receptors are also known to be involved under certain circumstances. The control stick itself is moved through the interface compliance. The picture is not complete without consideration of the "feel system" dynamic properties, including its effective mass, spring rate, damping, nonlinearities, etc.

Any physiologist will attest that this is a somewhat oversimplified neuromuscular model. Nevertheless, we have found it is sufficiently comprehensive to reveal the various dynamic modes observed in neuromuscular describing functions; handle such phenomena as high frequency limb tremor (which occurs at frequencies near 10 **Hz** (ref. 10)); accommodate manipulator feel systems ranging from rigid to free sticks and all forms in between; and correctly account for relative movement between limb root and control pivot. This model can also handle the situation where the limb is acting as bobweight at the end of the feel system, and complicated by its own internal compliances and feedbacks as well. It is well suited to modeling vibration effects such as mechanical feedthrough, resonant modes, and neuromuscular tonus effects on the vibration response.

To illustrate how this limb-manipulator model relates to the vibration problem, consider the case where the manipulator is a light, stiffly sprung control stick operated by finger or wrist action. Systems analysis like that in reference 9 yields the loci of the closed-spindle-loop roots for the neuromuscular dynamics, as shown in figure **6.** Notice that at least two lightly damped modes (ω_N and ω_T) exist within the range from 0 to 10 Hz, and the feel system mode, ω_F, can easily come down into this range for high-mass stick grips. The existence **of** these modes is verified by examination of earlier measurements by Sutton and Sykes (ref. **11)** on hand ('unsteadiness" power spectra when pushing' at various average force levels (as indicated on a galvanometer) against a

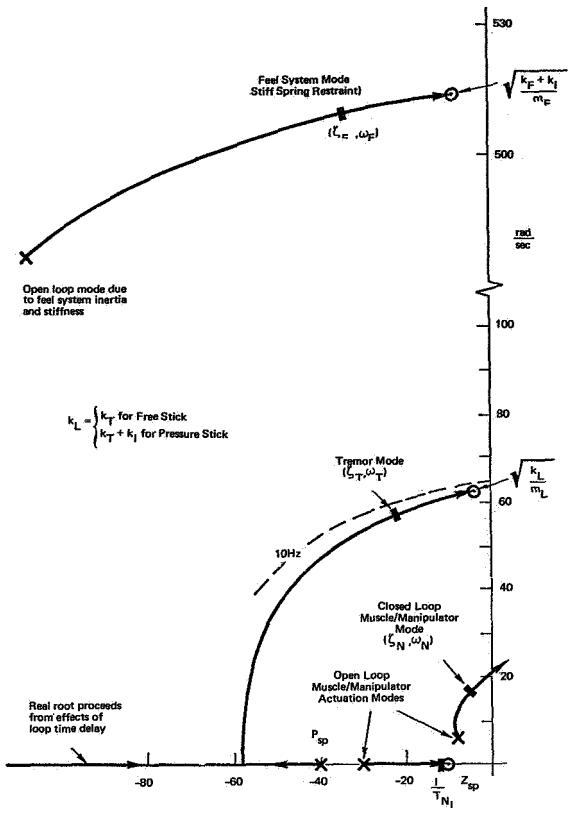

FIGURE 6.—Root locus diagram showing limb-manipulator interface dynamics with a stiffly sprung finger **control** stick.

pressure control (i.e., the case modeled in figure **6).** These data are shown in figure 7 in the form **of** displacement power spectral density plots. The various limb-manipulator modes corresponding to figure **6** are also identified here. The model implications are borne out, and the data clearly show the increase in certain mode resonances (due to lower damping ratio) with neuromuscular tension (here proportional to the average applied force). External vibration motions imposed on the torso or hand or between them both may be expected to result in similar resonances during vehicular control tasks. The particular model details depend on the control and limb configuration used, and several simplifying rearrangement of parameters can often be achieved in a particular case.

It is easy to draw increasingly complex models to represent increasingly precise details. The art comes in knowing how to extract the essential features from a complex model such as this one

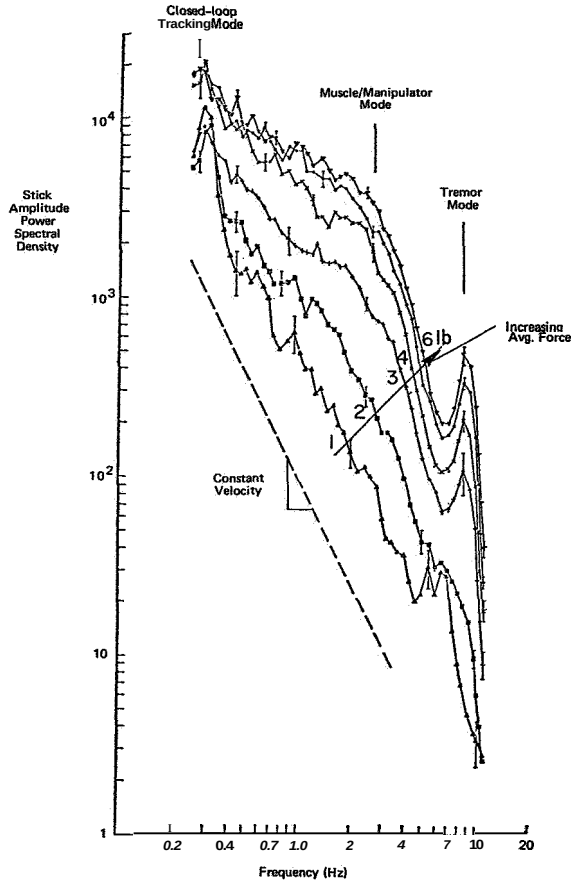

FIGURE 7.—Typical control (error) unsteadiness power spectra for various steady forces on a pressure stick (adapted from ref. 11).

in order to use it to solve practical problems. For ordinary manual control purposes we do not need the complete limb/manipulator model shown here. We simply represent its effects by a simple time delay, or at most a third-order system representing its primary lags and resonance (e.g., ref. **12).** However, under some of the new biodynamic conditions of interest, a model such as figure 5 will be essential. It behooves us all to make sure that efficient, yet well validated, biodynamic interface models are available when they are needed.

SOME BIODYNAMIC PROBLEMS AND THEIR STATUS

I'd like to end this presentation with a review of some specific problems in which biodynamic man-machine interfaces are involved. On the left side of table 1 are some of the important current problem areas, ranging from best to least researched areas. On the right side is an assessment of their status. The first column tells whether sufficiently detailed models are available to represent the phenomena observed. The second column shows by the checks or question marks whether these models have been empirically validated, so that one could have confidence in their use. The last column mentions some of the specific aerospace vehicles on which problems of the type mentioned have occurred, and in some cases solved, by application of biodynamic man-machine models. Let us look at some of these, in succession.

Pilot-Induced Oscillations

Pilot-induced oscillations (PIO) are caused by any of a number of coupling phenomena between the pilot and his vehicle system. By definition, they cease when the pilot releases the controls, or locks them rigidly. Reference **15** gives an overall background of this commonly encountered class of problems. Of the many forms of pilot-induced oscillations, the two of primary interest here are those caused by "limb-bobweight" effects or by "limb-impedance" effects.

Limb-bobweight effects are caused when the accelerations imposed by the control-induced motion of the vehicle are coupled, via the limb's unbalance, back into the control system, thereby forming a closed loop acceleration feedback system. If the mass overbalance of the pilot's arm on the controls has the correct sign and phase lag, this effect can drive the pilot vehicle system to violently unstable oscillations. (For example, in an early T–38, the oscillations reached ± 9 G_z at **1.0** Hs! (ref. **16.))** This can occur even with the pilot acting as a fairly passive element with his hand resting "loosely" on the stick. Analysis of this type of effect using conventional feedback models of the vehicle system, and relatively crude models for the limb's effective inertia have been performed in connection with a number of specific problems that have occurred during flight tests. Among the earliest work is that of Absug on the Douglas A 4 D (ref. 17), of the Northrop people and ourselves on the early T–38 (refs. **16** and 18),

TABLE 1.—*Some Biodynamic Man-Machine Control Problems and Their Status*

Problem	Status		
	Models available	Models validated	Examples
Pilot-Induced oscillations			
Limb-bobweight effects	**Good**	✓	**A-4D, T-38, AH-56**
Limb-impedance effects	**Some**	?	**"Feel" system simulators**
Effects of motion cues on:			
Tracking performance	**Good**	✓	**NASA-ARC, LRC**
Bending-modes excited by:		✓	
Pilot-remnant	**Good**	**(Some)**	**Saturn-V, B-70, C-5**
Vibration effects on:			
Tracking performance	**Some**	**(Pending)**	**UH1-B, A-5**
Isolation seat design	**Partial**	**Some**	**Barry seat, H-21**
Steady-G effects on:			
Tracking performance	**Partial**	...	Ames **F-104B and centrifuge**
Head-mounted sights	...	...	...
Steering motions induced by:			
Terrain or road	...	...	**Jeep**
Rough waves	...	...	**SRN-4**

and more recently by Lockheed on the rigid-rotor AH-56 helicopter, (ref. **19).** One lesson learned from all these analyses is that fairly crude models of biodynamic systems can often be used for these problems, but fairly complete models for the vehicle's control system and the limb/manipulator coupling must be included in order to accurately represent the system dynamics in the frequency range near **1** to **3 Hz.**

In a few instances, simply grabbing the control of an automatic flight control system has caused the system to shake, "quiver," "nibble," or vibrate in some other manner. This is felt to be due to coupling with the limb's complex impedance characteristics, which are included in the model given in figure 5. Anecdotes describing such cases abound in the feel-system simulation field; nevertheless this is an area in which little systematic research has been done and still less has been published.

Effects of Perceived Motion Cues

As illustrated earlier, vehicle motions enter a vehicle control loop through a number of paths, including the vestibular and proprioceptive (seat of the pants) feedbacks which are summed with the visual cues in normal man-machine control. Reasonably good models for the vestibular system crossfeeds now exist. Reference **20** contains a comprehensive review of the vestibular phenomena of interest in man-machine control, and references **21** through **23** summarize some of the recent research on motion cues. Other work is being done on the 5- and 6-degree-of-freedom moving-base simulators at the NASA-Ames Research Center (refs. **23** and **24).** This is an important problem area which is presently undergoing a very fruitful phase of research.

Bending-Mode Excitation

The large aerospace vehicles controlled by pilots are becoming more and more flexible as their length increases and their diameter decreases; for example, the **DC8-63** transport, **B-70** bomber, and Saturn V booster. The first body-bending modes of these vehicles often lie in the range from **1** to 5 **Hz,** and the pilot is usually situated ahead of the main nodal point. Movement of the elevator or rudder strongly excites this bending mode, thereby inducing vibrations at the cockpit. This induced vibration acts on the pilot in a number **of** ways, some mentioned previously. For example, the vibrations can, through limb bobweigth effects, couple into a neutral or divergent oscillation. Particularly in the range near 5 **Hz,** such motions can also

involve unpleasant head and torso vibrations. Because the flight path control commands do not demand responses in this frequency range, the pilot does not intentionally excite these bending modes. However, the wideband pilot-induced remnant noise described earlier in this presentation covers a wider frequency range, and it is the primary source of bending excitation.

Recently, good models to detect the existence of a bending mode excitation problem and to guide the solution (in terms of appropriate stick filtering) are available, and there have been some attempts to validate these models. One of the better documented cases is the analysis of the manual backup control system for the Saturn V booster reported in reference 25. The simulation studies for the vehicle show the dramatic importance of the remnant terms in exciting a 2 **Hz** body bending mode. Subsequent computer simulations at NASA Ames Research Center showed that the analytical man-machine models, including the remnant inputs, could successfully predict the problem and its solution, even though the magnitudes of remnant-induced bending mode excitation were not accurately predicted (ref. 26).

Vibration Effects

Vibration effects on subjective "ride quality" and tolerance of a vibration environment have been well researched and extensively reported (e.g., as summarized in refs. 27 through 30). Vibration effects on man-machine tracking performance are much more scarce, and they have involved relatively crude measurements compared with the kind of behavioral parameters we have been talking about here (refs. 31 through 33). The net tracking error includes both coherent (input correlated) and remnant (noise) contributions, each of which can be influenced in different directions by the direct **or** indirect effects of vibration. For example, tensing up muscles in the presence of mild vibration reduces the neuromuscular timing delays, thereby tending to increase the system bandwidth, but it may also result in higher gain and reduced stability margins, thereby tending to increase the resonances. Effects of the various vibration parameters on remnant are still unknown. Two of the more recent efforts to use modern manual control measurement and techniques are related to low altitude high speed flight (ref. 33), and to weapon aiming from a vibrating helicopter (ref. 34). The latter is still a current problem.

There is current interest in the design of "vibration isolation seats" designed to uncouple the pilot from his vibrating cockpit environment. As noted in figure **4,** this is but one of the *three* interfaces which must be considered in interfacing man-machine performance with the biodynamic environment, so much remains to be done in modeling and validating this interesting problem area. Research using an active vibration isolation seat designed by Barry Controls (ref. 35) is underway both at the 6570th AMRL and at NASA. *Complete* man-machine system models of the type described here are well suited to this problem area. Ideally, this work should be carried along in parallel with the experimental research, both to help in the experimental design, selection of measurements and data analysis, and to reveal concurrent technical advances which should accompany such seats (e.g., vibration-compensated displays and controls).

Steady-G Effects

One of the most studied biodynamic inputs is that of steady accelerations on various bodily functions. Various specialized studies have been done in the last two decades on the effective man-machine performance under steady g's (e.g., refs. 36 through 39). This line of research seemed to reach a plateau a few years ago and is only recently picking up speed again. The much more comprehensive models which are now available for describing the man-machine performance can guide the selection of tasks measurements, and data reduction analysis procedures (e.g., ref. 37 is a pioneering example). There is evidence that those involved in centrifuge research, many of whom are medical people, psychologists, or mechanical engineers, have recently begun to include modern man-machine control techniques in their research. This area urgently needs biodynamic modeling.

A most fascinating problem I wish to mention is that of using head-mounted sights under high-g maneuvering conditions. If any of you have tried to track a moving satellite with a pair of binocu-

lars held against your head, you will understand what a frustrating problem this can be. (It's the remnant that blurs the image!) Now imagine doing this if your head and optics weighed 5 times as much, and you will have an idea of the problem of a pilot trying to track an enemy aircraft with a helmet-mounted magnifying sight during a 5 G_z turn. Some excellent design research has been done on the applications and design features for head-mounted sights (e.g., ref. **40).** Yet, to our knowledge, comprehensive models of the type described here for the ***combined*** system of target, sight, head and eye neuromuscular system, vehicle, and maneuver kinematics have not yet been applied. Here is a problem ideally suited to biodynamic man/machine analysis, and the payoff will be high in terms of problem areas uncovered and avoided, design parameters delineated, and experimental research guidelines exposed.

The last area noted in table **1** has been around the longest, yet has received the least research to date. This is the problem of spurious steering control motions of vehicles traversing rough terrain, or its counterpart **of** high-speed ships crossing rough waves. Although some Jeeps had problems from this cause, the advent of high-sensitivity, low-friction power steering makes modern vehicles particularly vulnerable. **A** suitable model for this phenomenon must include the vehicle pitch, roll, heave, and lateral dynamics (including the suspension effects),seat dynamics, torso effects and a limb-steering wheel model similar **to** that discussed previously herein. Small perturbation linearized analysis is appropriate for modeling surface-induced control motion, but the representation of the torso-limb-control ensemble remains a formidable task for future research. Fortunately, adequate facilities to validate the models presently exist in the form of pitch-roll heave motion simulators and transverse motion simulators at places such as NASA and the U.S. Army Tank and Automotive Command.

Concluding Remarks

In summary, I feel that the field of modeling man-machine control behavior in a biodynamic environment is an extremely fertile one, which is about to enter a new and fruitful era. It will have to draw heavily on the classical lumped-parameter biodynamic response models, especially in the representation of body, limb, head and eye coupling effects (e.g., refs. **30** and **41).** In turn, some of the more sophisticated feedback neuromuscular models and measurement techniques should be of value in biodynamic research, particularly where muscle tension (applied intentionally **or** unconsciously) has a large influence on the results.

A joint Systems Technology, Inc./USAF research program is currently in progress on the effects of vibration on manual control behavior and performance, under the technical direction of Captain D. Wilburn of the Bionics and Biodynamics Branch, 6570th Aerospace Medical Research Laboratories, Wright-Patterson Air Force Base.

ACKNOWLEDGMENTS

I would like to acknowledge the contributions of my colleagues: Duane T. McRuer who started much of the research mentioned here, and Raymond E. Magdaleno who is primarily responsible for our neuromuscular models.

REFERENCES

1. McRuer, D.; and Weir, D. H.: **Theory of Manual Vehicular Control. Ergonomics,** vol. **12,** no. **4, July 1969,** pp. **599–634.**
2. Young, L. R.: On **Adaptive Manual Control. Ergonomics,** vol. **12,** no. **4, July 1969,** pp. 635–674.
3. Clement, W. F.; Jex, H. R.; and Graham, D.: **A Manual Control Display Theory Applied to Instrument Landings of a Jet Transport. IEEE Trans., vol. MMS–9,** no. **4,** Dec. **1968.**
4. Krendel, Ezra S.; and McRuer, Duane T.: **A Servomechanisms Approach to Skill Development. J. Franklin, Institute, vol. 269,** no. **1, Jan. 1960.**
5. Krendel, Ezra S.; and McRuer, Duane T.: **Psychological and Physiological Skill Development— A Control Engineering Model. Fourth Annual NASA-University Conference** on **Manual Control, NASA SP-192, 1969,** pp. 285–288.
6. Graham, Dunstan; and McRuer, Duane: **Analysis of Nonlinear Control Systems.** John **Wiley and** sons, **Inc., 1961.**
7. McRuer, Duane; Graham, Dunstan; Krendel, Ezra; and Reisener, William, Jr.: **Human Pilot Dynamics in Compensatory Systems—Theory, Models, and Experiments with Controlled Element and Forcing Function Variations. AFEDL–TR–65–15, July 1965.**

8. McRUER, D. T.; HOFMANN, L. G.; JEX, H. R.; ET AL.: New Approaches to Human-Pilot/Vehicle Dynamic Analysis. AFFDLTR–67–150, Feb. 1968.
9. MAGDALENO, RAYMOND E.; McRUER, DUANE T.; AND MOORE, GEORGE P.: Small Perturbation Dynamics of the Neuromuscular System in Tracking Tasks. NASA CR–1212, Dec. 1968.
10. MAGDALENO, R. E.; JEX, H. R.; AND ALLEN, R. W.: Fine Motor Unsteadiness: Models, Data Survey, and Sample Measurements. Working Paper 2010-4, Systems Technology, Inc., Aug. 1970.
11. McRUER, D. T.; AND JEX, J. R.: A Review of Quasi-Linear Pilot Models. IEEE Trans., vol. HFE–8, no. 3, Sept. 1967, pp. 231–249.
12. KING-SMITH, ERIC A.: Predictive Compensation in Time-Delay Manual Control Systems. Fourth Annual NASA-University Conference on Manual Control, NASA SP–192, 1969, pp. 253–274.
13. LEVISON, W. H.; BARON, S.; AND KLEINMAN, D. L.: A Model for Human Controller Remnant. IEEE Trans., vol. MMS–10, no. 4, Dec. 1969, pp. 101–107.
14. JEX, H. R.; AND MAGDALENO, R. E.: Corroborative Data on Normalization of Human Operator Remnant. IEEE Trans., vol. MMS–10, no. 4, Dec. 1969, pp. 137–139.
15. ASHKENAS, IRVING L.; JEX, HENRY R.; AND McRUER, DUANE T.: Pilot Induced Oscillations: Their Cause and Analysis. Tech. Rept. No. 239-2 Systems Technology, Inc. (Northrop-Norair Rept. No. NOR 64–143) (AD 481 994), June 20, 1964.
16. JEX, H. R.: Summary of T–38A PIO Analysis. Tech. Rept. No. 239–1, Systems Technology, Inc., Jan. 25, 1963.
17. ABZUG, MALCOLM J.: High-speed Stability and Control Problems as They Affect Flight Testing. AGARD Rept. 120, 1957.
18. LEVI, O. A.; AND NELSON, W. E.: An Analytical and Flight Test Approach to the Reduction of Pilot-Induced Oscillation Susceptibility. J. Aircraft, vol. 1, no. 4, July–Aug. 1964, pp. 178–184.
19. ANON.: Lockheed Flight Testing AH–56 with Modified Controls, Blades. Av. Week, vol. 92, no. 13, Mar. 30, 1970, pp. 66-67.
20. PETERS, RICHARD A.: Dynamics of the Vestibular System and Their Relation to Motion Perception, Spatial Disorientation, and Illusions. NASA CR–1309, Apr. 1969.
21. STAPLEFORD, ROBERT L.; PETERS, RICHARD A.; AND ALEX, FRED R.: Experiments and a Model for Pilot Dynamics with Visual and Motion Inputs, NASA CR–1325, May 1969.
22. RINGLAND, R. F.; STAPLEFORD, R. L.; AND MAGDALENO, R. E.: Motion Effects on an IFR Hovering Task—Analytical Predictions and Experimental Results. Tech. Rept. No. 188–1, Systems Technology, Inc., Oct. 1970.
23. YOUNG, L. R.: The Current Status of Vestibular System Models. Automatica, vol. 5, pp. 369–383, 1969.
24. DOLKAS, CONSTANTINE B.; AND STEWART, JOHN D.: Effect of Combined Linear and Oscillatory Acceleration on Pilot Attitude-Control Capabilities. NASA TN D–2710, Mar. 1965.
25. JEX, H. R.; TEPER, G. L.; McRUER, D. T.; AND JOHNSON, W. A.: A Study of Fully-Manual and Augmented-Manual Control Systems for the Saturn V Booster Using Analytical Pilot Models. NASA CR–1079, July 1968.
26. DENERY, DALLAS G.; AND CREER, BRENT Y.: Evaluation of a Pilot Describing Function Method Applied to the Manual Control Analysis of a Large Flexible Booster. NASA TN D–5149, Apr. 1969.
27. ROTH, EMANUEL M., ED.: Compendium of Human Responses to the Aerospace Environment, Vol. II, Secs. 7–9. NASA CR–1205 (11), Nov. 1968.
28. BEAUPEURT, J. E.; SNYDER, F. W.; BRUMAGHIM, S. H.; ET AL.: Ten Years of Human Vibration Research. Rept. No. D2–7888, Wichita Div., Boeing Co., Aug. 1969.
29. BRYCE, W. D.: A Review and Assessment of Criteria for Human Comfort Derived from Subjective Responses to Vibration. Rept. No. R. 286, National Gas Turbine Establishment, Dec. 1966.
30. VON GIERKE, H. E.: Response of the Body to Mechanical Forces—An Overview. Paper presented at the Conference on Prevention of and Protection Against Accidental Explosion of Munitions, Fuels and Other Hazardous Mixtures, New York Academy of Sciences (New York), Oct. 10–13, 1966.
31. BUCKHOUT, ROBERT: A Working Bibliography on the Effects of Motion on Human Performance. MRL–TDR–62–77, July 1962.
32. CHILES, W. DEAN; AND CUSTER, CAROLYN L.: Summaries of Research on the Human Performance Effects of Vibration. AMRL TR–67–172, Nov. 1963.
33. SOLIDAY, S. M.; AND SCHOHAN, B.: A Simulator Investigation of Pilot Performance during Extended Periods of Low-Altitude, High-speed Flight. NASA CR–63, June 1964.
34. ROSENBERG, BRUCE; AND SEGAL, ROBERT: The Effects of Vibration on Manual Fire Control in Helicopters. Tech. Rept. 1–168, Franklin Institute Research Labs. Mar. 1966.
35. SCHUBERT, DALE W.; PEPI, JEROME S.; AND ROMAN, FRANK E.: Investigation of the Vibration Isolation of Commercial Jet Transport Pilots during Turbulent Air Penetration. NASA CR–1560, July 1970.
36. GILLIES, J. A., ED.: A Textbook of Aviation Physiology. Pergamon Press, 1965.
37. SADOFF, MELVIN; AND DOLKAS, C. B.: Acceleration Stress Effects on Pilot Performance and Dynamic Response. Second Annual NASA-University Conference on Manual Control. NASA SP–128, 1966, pp. 241–257.
38. LITTLE, V. Z.; LEVERETT, S. D.; AND HARTMAN, B. O.: Psychomotor and Physiologic Changes During Accelerations of 5, 7, and 9 $+G_x$. Aerospace Medicine, vol. 39, no. 11, Nov. 1968, pp. 1190–1197.
39. CREER, BRENT Y.; SMEDAL, HARALD A.; AND

WINGROVE, RODNEY C.: Centrifuge Study of Pilot Tolerance to Acceleration and the Effects of Acceleration on Pilot Performance. NASA TN D–337, Nov. 1960.

40. HUGHES, ROBERT J.; HENKE, ALLEN H.; SCHULTZ, ROBERT L.; ET AL.: Helmet-Mounted Sight/Display Applications. Vol. I Summary and Conclusions. AFFDL–TR–69–118, Apr. 1970.
41. YOUNG, RONALD D.: A Three Dimensional Mathematical Model of an Automobile Passenger. Research Rept. 140–2, Texas Transportation Institute, Aug. 1970.
42. LEE, R. A.; AND KING, A.: A Quantification of Oculomotion Due to Whole-Body Vibration. Proc. of 23rd Annual Conf. on Engineering in Med. and Biol. (Washington, D. C.), vol. 12, 1970, pp. 66.

2. Development and Optimization of a Nonlinear Multiparameter Model for the Human Operator*

GUNNAR JOHANNSEN

Forschugsinstitut fur Anthropotechnik

A systematic method is proposed for the development, optimization, and comparison of controller-models for the human operator. This is suitable for any designed model, even multiparameter systems. A random search technique is chosen for the parameter optimization. As valuation criteria for the quality of the model development the criterion function—the comparison between the input and output functions of the human operator and those of the model—and the most important characteristic values and functions of the statistical signal theory (mean values, auto- and crosscorrelation functions, histograms, and power density functions) are used.

A nonlinear multiparameter model for the human operator is being designed which considers the complex input information rate per time in a single display. The nonlinear features of the model are effected by a modified threshold element and a decision algorithm. Different display-configurations as well as various transfer functions of the controlled element are explained by different optimized parameter-combinations. The comparison with the well-known quasi-linear describing function for the human operator shows an essential superiority of the nonlinear model.

INTRODUCTION

For about 25 years models for the human operator as a vehicle controller have been developed. By this research method it was tried to reach the following two objectives:

(1) The capabilities and limitations of the human operator in manual vehicle control problems are to be measured and described as detailed as possible. Thus, valuation and design criteria are provided for the optimal—in the human engineering sense—layout of displays, controls, and automatic auxiliary controllers in integrated man-vehicle-systems.

(2) The human operator possesses features which today's technical systems are lacking extensively: adaptation especially to unforeseen situations, flexibility, capability to learn, and high reliability. By way of the analysis and simulation of these capabilities we find new automatic controllers which have the described features.

The specified objectives, especially the second, are set so high, that one only gets on smoothly with a systematic and economical procedure. This procedure should permit the development, optimization, and comparison of any controller-model for the human operator without time penalty. Simultaneously a reproducible method of test for the investigation of man/model-vehicle-systems is rendered possible with such a procedure. A recommendation of this kind has not been published up to now.

Both a method for the development, optimization, and comparison of controller-models and a nonlinear multiparameter model, which has been designed with the use of the previously mentioned method, are subsequently explained in more detail.

*This study was accomplished at the Institut für Flugführung und Luftverkehr, Technische Universitat Berlin, Germany and is a condensed part of reference 15.

METHOD FOR THE DEVELOPMENT, OPTIMIZATION, AND COMPARISON OF CONTROLLER-MODELS

Figure **1** shows the block diagram for the model parameter optimization in principle. The control of one output quantity is presented. Environmental disturbances shall in this case be excluded from the man-machine-system. From the indicated deviation, the difference between the desired value y_s and the actual value y_i, the human operator deducts a continuous stick signal which is transmitted through a control stick to the input of the controlled element, the simulated vehicle. Through information preprocessing by means of an additional prediction display, which indicates the future state of the vehicle y_v, the control effectiveness for the man-machine system is improved (refs. **1** and **2).** Because of the required transparency, the computation of the prediction value has been omitted in figure **1.**

For the model-machine control loop the same forcing function y_s is used as for the man-machine control loop. The difference between the stick signals of the human operator and the model is minimized. The chosen criterion function is proportional to the mean square error:

$$F(\underline{P}) = \int_0^T (z_V(t) - z_M(t;\underline{P}))^2 \, dt. \qquad (1)$$

The optimization interval T corresponds to the duration of test and equals one minute.

For the parameter optimization a random search technique with local and global search algorithm is used (refs. **3** and **4).** Rastrigin (ref. **5)** has shown that these techniques are especially suitable for the optimization of multi-parameter systems because of their high speed of convergence. Furthermore these techniques allow the criterion-hypersurfaces to be of very complicated shape. In nonlinear optimization problems in which discontinuities can be found in the criterion function, no difficulty results using random search techniques (ref. **6).** These are essential advantages as against the gradient techniques.

The optimal procedure for the development and optimization of controller models is best illustrated by a block diagram (fig. **2).** During "human operator in the loop" tests all input and output functions of the human operator are stored on magnetic tape. If various models are to be designed, the same stored time functions of these tests are used for their parameter optimization.

First the model is optimized as a transfer element in the open control loop (fig. **3).** Thereby the model is supplied with the same input functions which the human operator perceived

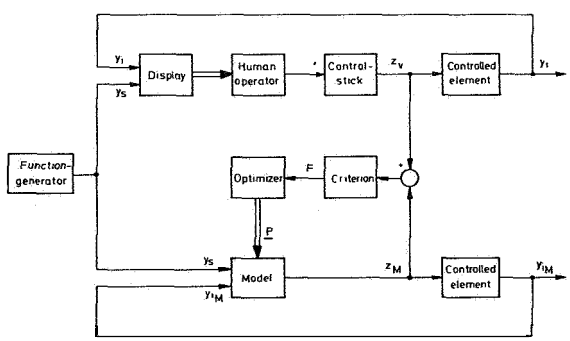

FIGURE 1.—Block diagram for the model parameter optimization in principle.

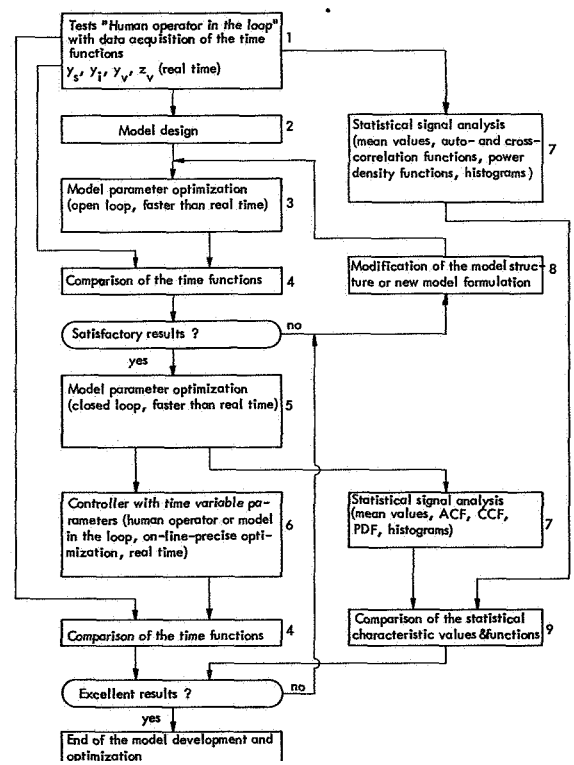

FIGURE 2.—Block diagram for an optimal procedure for the development and optimization of controller models.

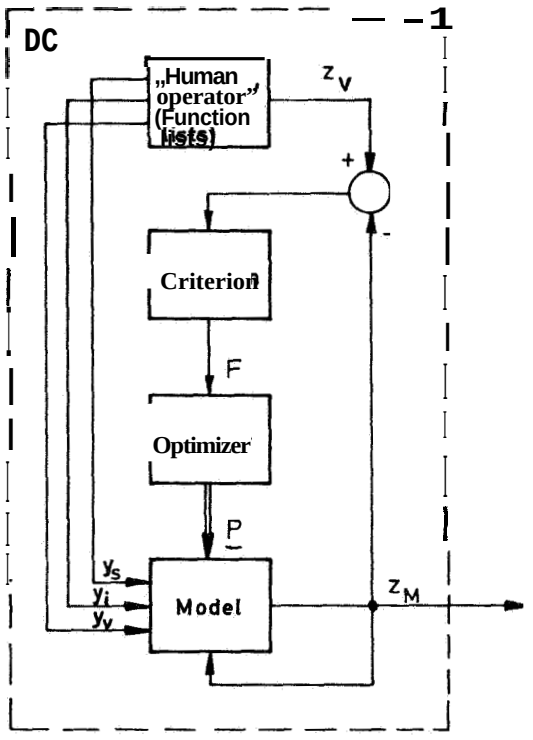

FIGURE 3.—Block diagram for the parameter optimization of the model in the open control loop.

through his sense organs. As manual control tasks are dynamic processes of low frequency they should be run in real time only, if the control is carried out completely or partly by subjects. Therefore, as there are no subjects in the control loop during model parameter optimization the programs shall be run faster than real time.

The time functions of the optimized open loop, plotted with a multichannel recorder, are compared with the corresponding time functions of the "human operator in the loop" tests. Mainly the stick signals (but also the deviations) are used for this coarse valuation criteria. If the comparison does not prove satisfactory, a modification of the model structure has to be considered or a new formulation of the model has to be adopted.

Whenever the model does not produce exactly the same output signal as the human operator after a satisfactory comparison of the time functions—and that will generally be the case—it must be examined whether the control loop, into which this model has been inserted as a controller,

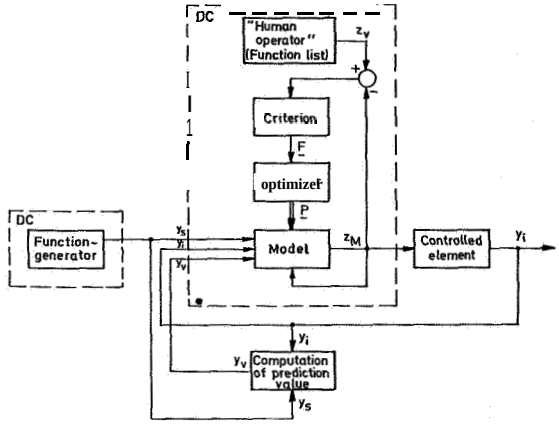

FIGURE 4.—Block diagram for the parameter optimization of the model in the closed control loop.

is stable. That is to say the remnant, the difference between the stick signals of the human operator and the model, is filtered by the controlled element and then included in the input information of the human operator (see fig. 1). With that, it is equally included in those of the model during the optimization of the open loop. In the closed loop this remnant is missing. Therefore it is necessary to continue the model parameter optimization in the closed loop (fig. 4). That is even then convenient, if the control loop is stable, because the criterion function does not necessarily reach its minimum at once, due to the missing remnant, although the optimization of the open loop previously led to a minimum.

The time functions of the closed control loop at the end of the over-all model parameter optimization are once more compared with those of the "human operator in the loop" tests. Additionally, a comparison of the corresponding statistical characteristic values and functions is now made. These are mean values, auto- and crosscorrelation functions, power density functions, and histograms. They have proved suitable for the valuation of man-vehicle control loops (refs. 7 and 8). If the results are excellent in comparison with well-known controller-models, the model-development and optimization is finished.

For the described simulation problems a hybrid computer system is best suitable. The used hybrid computer system consists of an analog computer Telefunken RA 770, a digital computer CAE C 90–40 (this corresponds with the SDS C 90–40),

and an interface Telefunken **HKW** 900. It is programmed in Real-Time Fortran (ref. **9).** The method of test **as** well **as** the model-parameter-optimization are managed by standardized software. It allows in like manner the examination of controller-models which operate on analog, digital, hybrid, and other principles like threshold logic networks. Thereby only the exchange of subroutines is required. The separate systems of the man-vehicle control loop and the optimizer, which work according to the random search technique, are optimally distributed to the analog and digital component of the hybrid computer system. The controlled element, the computation of the prediction value, and the display-generator are realized on the analog computer. The digital computer produces a stochastic time function, which is used as the forcing function, and it calculates parameter change vectors for the random search technique from the sample values of an analog noise generator. The optimizer and the dominant part of the nonlinear controller-model are programmed on the digital computer too. If the well-known quasi-linear describing function for the human operator

$$G_{HO}(s) = \frac{K \cdot e^{-\tau T s}}{1+T_N s} \cdot \frac{1+T_L s}{1+T_I s} \qquad (2)$$

is used, the controller is best simulated on the analog computer, except the dead time term.

The efficiency of the specified method is demonstrated by the development and optimization of a new nonlinear multiparameter model as well as by the comparison of this model with the quasi-linear describing function.

NONLINEAR MULTIPARAMETER MODEL FOR THE HUMAN OPERATOR

The complete nonlinear model for the human operator is shown in figure 5. A clear structure of the model is obtained by dividing it into five subsystems:

(1) The information perception system IP including multiplexer and analog-digital-converter **(ADC)**

(2) The modified threshold element

(3) The decision algorithm

(4) The summing element for the generation of stick signal increments

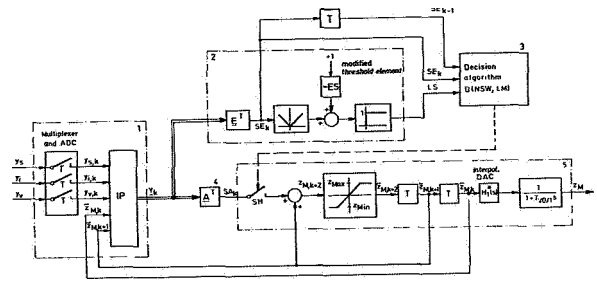

FIGURE 5.—Block diagram of the nonlinear model for the human **operator.**

(5) The system for the synthesis and output of the stick signal.

In the nonlinear model, contrary to most of the known mathematical models, the physiological aspects **of** the human controller characteristics are considered. If the sensory and neuro-physiological foundations of manual control are reflected upon, it is realized **as** one of the most important features of the central nervous system, that parallel information processing takes place already during the perception (ref. **10).** A great number of information is received by the sense organs, especially by the visual apparatus, and it is optimally combined for decisions, which lead to controller output commands for the hand. The complex information, which is included in a single display, is weighted by the nonlinear controller-model. Different display-configurations yield a different input information rate per time not only for the human operator but also for the model. Not only visual but also proprioceptive information is used in the model.

The visual information of the input vector

$$Y_k = \begin{pmatrix} y_{s,k} \\ y_{sp,k-1} \\ e_{i,k} \\ e_{ip,k-1} \\ e_{v,k} \\ e_{vp,k-1} \\ \tilde{z}_{M,k+1} \\ \tilde{z}_{Mp,k} \end{pmatrix} \qquad (3)$$

is the desired value $y_{s,k}$, the actual deviation

$$e_{i,k} = y_{s,k} - y_{i,k}, \qquad (4)$$

the predictive deviation

$$e_{v,k} = y_{s,k} - y_{v,k}, \qquad (5)$$

and the first derivations of these three time functions. These derivations attend to the human prediction capabilities (refs. **11** and **12).** Through the extension of the information rate per time up to a maximum of eight input functions the model differs essentially from all existing models. The multiplication of $\underline{Y}_k$ with the transposed weighting vectors $\underline{E}^T$ and $\underline{A}^T$ gives the scalar products

$$SE_k = \underline{E}^T \cdot \underline{Y}_k \tag{6}$$

and

$$SA_k = \underline{A}^T \cdot \underline{Y}_k. \tag{7}$$

These represent the result of an information reduction.

A modified threshold element and a decision algorithm (fig. 6), which has two parameters NSW and LM, define the nonlinear features of the controller-model by operating the switch SH. Sudden stick signal changes as well as constant stick deflections over longer time intervals are possible. Moreover the model temporarily possesses a linear transfer attitude, if a suitable decision is made depending on the overall input information rate.

Threshold elements are simplified models for the neurons of the human brain (ref. **13).** They are used as classifiers in automatic pattern recognition (ref. **14).** During manual control, dynamic patterns are recognized and analysed. Consequently it is logical to insert threshold elements into controller-models for the human operator.

The nonlinear model possesses a maximum of **19** parameters: twice eight weighting parameters,

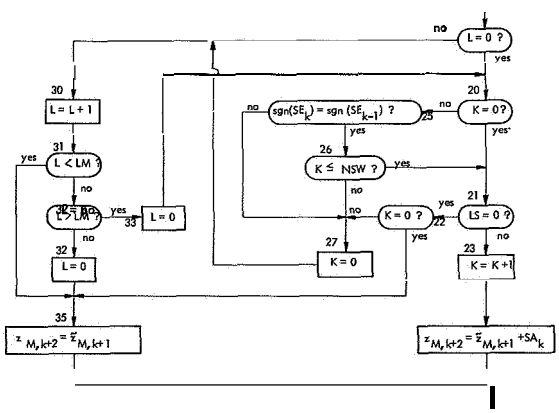

FIGURE 6.—Flow chart for the decision algorithm.

the threshold values ES, and the two parameters of the decision algorithm, NSW and LM. Thus, the parameter vector is

$$P = \begin{pmatrix} \underline{E} \\ \underline{A} \\ ES \\ NSW \\ LM \end{pmatrix}. \tag{8}$$

The generated stick signal $z_{M,k+2}$ is limited according to the mechanical stops of the control stick in use. It is then delayed for two sample intervals, and smoothed by an interpolating digital-analog-converter with a series-connected first order lag term.

RESULTS

Four different display-configurations are studied to show the different weighting of the single input functions. The difference between the compensatory and the pursuit tracking as well as the meaning of the prediction display can be read from the weighting factors of the controller-model. The additional information, which is given through the indication of the desired value during pursuit tracking, is scarcely used by the subjects, whereas an additional indication of the prediction value is weighted considerably. This result corresponds to the improvement of control effectiveness, which can be achieved by the application of the prediction display in tests with a human operator. Moreover the chosen structure of the model explains the human control action for various transfer functions of the controlled element. The parameters of the model were optimized for the control of two acceleration systems, one rate and one position system.

Subsequently only the results for an acceleration system with the transfer function

$$G_S(s) = \frac{1.6}{s^2(1+0.4s)} \tag{9}$$

are considered. The subject S controls the system **1** of equation **(9)** using the display-configuration I (pursuit tracking, additional prediction display). Therefore this test is marked with S1I.

From the comparison of the nonlinear model with the quasi-linear describing function for the human operator it is determined that the stick

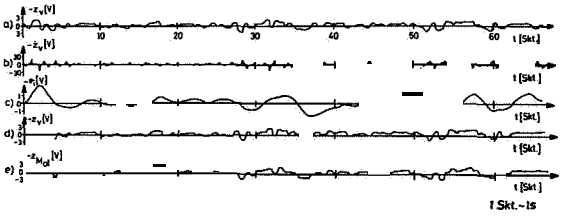

FIGURE 7.—The time functions of the S1I test. (a) and (d) Stick signal of the subject in the closed loop; (b) first derivation of the subject's stick signal; (c) actual deviation for (a); and (e) stick signal of the nonlinear model in the open loop.

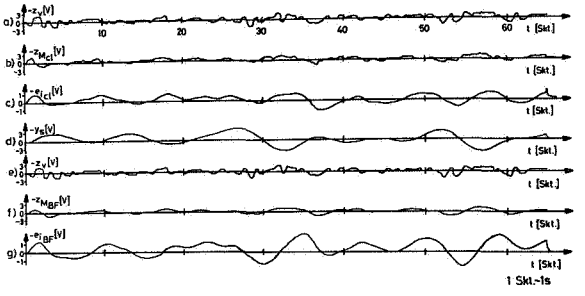

FIGURE 8.—Additional time functions of the S1I test. (a) and (e) Stick signal of the subject in the closed loop; (b) stick signal of the nonlinear model in the closed loop; (c) actual deviation for (b); (d) forcing function; (f) stick signal of the quasi-linear describing function in the closed loop; and (g) actual deviation for (f).

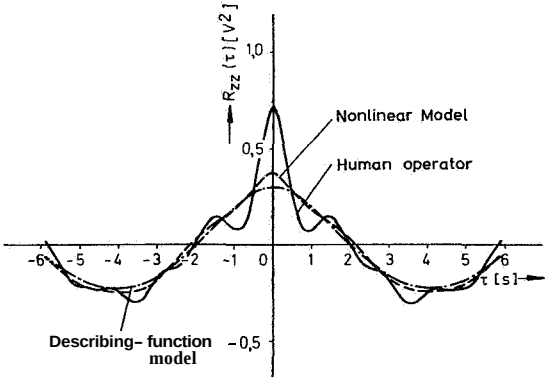

FIGURE 9.—The autocorrelation function of the stick signal for the S1I test.

signals of the nonlinear model in their fine structure look more like those of the human operator than the stick signals at the output of the linear transfer element (figs. 7 and 8). The autocorrelation and power density functions (figs. 9 through 12) as well as the histograms of the deviation and

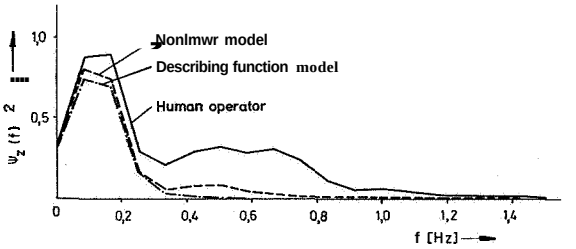

FIGURE 10.—The power density function of the stick signal for the S1I test.

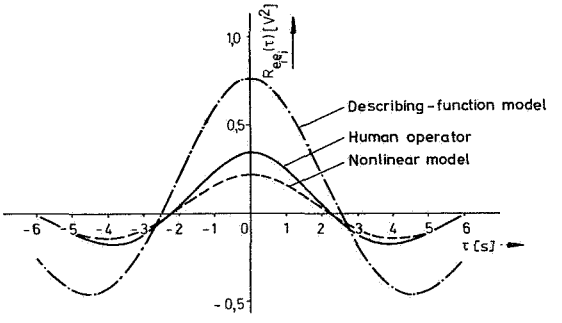

FIGURE 11.—The autocorrelation function of the actual deviation for the S1I test.

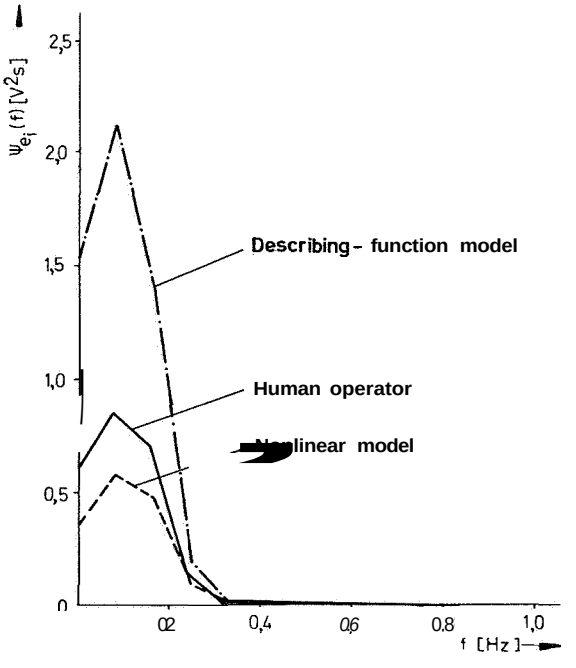

FIGURE 12.—The power density function of the actual deviation for the S1I test.

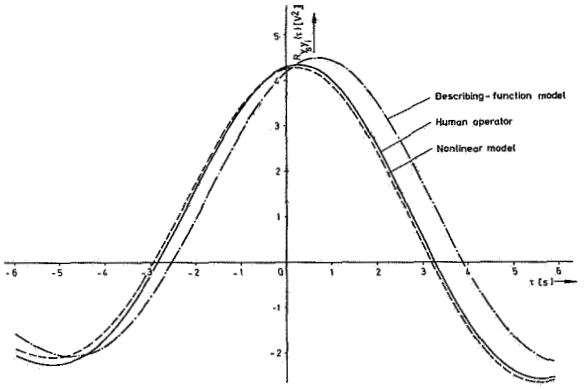

FIGURE 13.—The crosscorrelation between the input and output function of the control loop for the S1I test.

the stick signal show an essential superiority of the nonlinear model over the describing function. This is well marked by the control with an additional prediction display, because the nonlinear model possesses separate inputs for the prediction value and its first derivation. The crosscorrelation functions between the desired and actual value show too, that the control effectiveness is improved by the nonlinear model (fig. **13).**

CONCLUSIONS

An efficient method for the development, optimization, and comparison of controller-models for the human operator was accomplished. An instrument is available to facilitate and accelerate the investigation of manual multiloop control and of the learning and adaptive features of the operator.

By using a heuristic approach the illustrated nonlinear multiparameter model has been designed which considers the complex input information rate per time and the information reduction in manual control as well **as** decision capabilities of the human operator.

REFERENCES

1. BERNOTAT, R.; DEY, D.; AND WIDLOK, H.: Die Voranzeige als anthropotechnisches Hilfsmittel bei der Führung von Fahrzeugen. Forschungsberichte des Landes Nordrhein-Westfalen Nr. **1893,** Westdeutscher Verlag, Koln und Opladen, **1968.**
2. DEY, D.; AND JOHANNSEN, G.: Stabilisierung und Lenkung von Fahrzeugen mit Hilfe der Voranzeige. Bericht Nr. 50 des Instituts fur Flugfuhrung und Luftverkehr der Technischen Universitat Berlin, **1969.**
3. BEKEY, G. A.; GRAN, M. H.; SABROFF, A. **E.;** AND WONG, A.: Parameter Optimization by Random Search Using Hybrid Computer Techniques. AFIPS Proc. Fall Joint Computer Conference, vol. **29, 1966,** pp. **191–200.**
4. BEKEY, *G.* **A.;** AND KARPLUS, W. J.: Hybrid Computation. John Wiley and Sons, Inc., **1968.**
5. RASTRIGIN, L. **A.:** The Convergence of the Random Search Method in the Extremal Control of a Many-Parameter System. Automation and Remote Control **24,1963,** pp. **1337–1342.**
6. KARNOPP, D. C.: Random Search Techniques for Optimization Problems. Automatica **1, 1963,** pp. **111–121.**
7. KREIL, W.; AND SCHWEIZER, G.: Auswertung stochastischer Meßwerte. In: Nachrichtentechnische Fachberichte, Band **33** (Statistische Signaltheorie in der Nachrichten- und Regelungstechnik), **1967,** pp. **111–119.**
8. JOHANNSEN, G.: Der Einfluß einer Voranzeige auf Verteilungsdichte- und Leistungsdichtefunktionen bei der manuellen Folgeregelung eines Beschleunigungs-systems. Regelungstechnik und Prozeß-Datenverarbeitung **18, 1970,** pp. **65–69.**
9. ANON.: Die Programmierung des hybriden Rechnersystems HRS **900** in Real-Time Fortran 11. Institut fur Informationsverarbeitung, Technische Universität Berlin, **1969.**
10. REICHEL, H.; AND BLEICHERT, A.: Leitfaden der Physiologie des Menschen. **2.** Auflage, Ferdinand Enke Verlag, Stuttgart, **1966.**
11. VOSSIUS, G.: Der kybernetische Aspekt der Willkürbewegung. In: Wiener, N., und Schadé, J. P. (Hrsg.): Progress in Biocybernetics, vol. **7,** Elsevier Publishing Company. (Amsterdam-London-New York), **1965,** pp. **111–140.**
12. VOSSIUS, **G.;** AND WERNER, **J.:** The Functional Control of the Eye-Tracking-System and its Digital Simulation. Fourth Congress of IFAC, Techn. Session **70** (Bionics) (Warsaw), **1969.**
13. SHENG, C. L.: Threshold Logic. The Ryerson Press (Toronto), and Academic Press (London and New York), **1969.**
14. MÜYER-BRÖTZ, G.; AND SCHÜRMANN, J.: Methoden der automatischen Zeichenerkennung. Oldenbourg, Miinchen-Wien, **1970.**
15. JOHANNSEN, G.: Entwicklung und Optimierung eines vielparametrigen nichtlinearen Modells fur den Menschen als Regler in der Fahrzeugfiihrung. Dissertation, Technische Universitat Berlin, **1971.**
16. JOHANNSEN, G.: A Method for the Development and Optimization of Controller-Models for Man-Machine-Systems. Proc. Advanced Study Institute on Displays and Controls, Berchtesgaden, **1971.**
17. JOHANNSEN, G.: The Design of a Nonlinear Multi-Parameter Model for the Human Operator. Proc. Advanced Study Institute on Displays and Controls, Berchtesgaden, **1971.**

3. A Control-Theory Model for Human Decision-Making*

WILLIAM H. LEVISON
Bolt *Beranek and Newman Inc.*

The optimal-control model for pilot-vehicle systems has been extended to handle certain types of human decision tasks. The model for decision-making incorporates the observation noise, optimal estimation, and prediction concepts that form the basis of the model for control behavior. Experiments are described for the following task situations: **(1)** single decision tasks, **(2)** two decision tasks, and **(3)** simultaneous manual control and decision tasks. Using fixed values for model parameters, we can predict single-task and two-task decision performance scores to within an accuracy **of** 10 percent. The experiment on simultaneous control and decision indicates the presence of task interference in this situation, but the results are not adequate to allow a conclusive test of the predictive capability of the model.

INTRODUCTION

Considerable effort has been devoted to understanding how a pilot controls his aircraft, and reasonably accurate models for the pilot as a feedback controller have been developed. Continuous control, however, is but one of the functions required of the pilot; he must also make various decisions during the course of a flight. As flight-control systems become more sophisticated, monitoring and decision-making tasks will play an increasingly important role in the pilot's management of the aircraft.

This paper summarizes a theoretical and experimental study recently conducted for NASA-Ames Research Center, to develop a model for human decision-making. In order to provide a common model structure for both decision-making and continuous control, the model for decision-making is based on the existing optimal-control model for pilot/vehicle systems developed by Bolt Beranek and Newman Inc. The optimal-control model contains the concepts of observation noise, optimal prediction, and optimal estimation that can be applied to certain types of decision problems. In addition, the existing pilot/vehicle model is able to account for interference among tasks performed in parallel. The model developed in this study is intended to apply to situations in which the human bases his decision on his estimate of the state of a linear plant.

Considerations of space limit us to a presentation of only the highlights of this study. Additional details are given in reference **1.** The reader is directed to references **2** and **3** for a description of the pilot/vehicle model and to references **4** and **5** for the development and validation of the model for task interference.

DESCRIPTION OF THE DECISION TASK

The following three constraints were imposed on the selection of an experimental decision task: **(1)** the task should be compatible with the existing theoretical structure for optimal control and estimation, **(2)** the correctness or incorrectness of the subject's response should be unambiguous, and **(3)** the experimental task should bear some resemblance to a decision task encountered in flight situations. In addition, we desired to relate this work to a concurrent study **of** aircraft approach and landing conducted both at **NASA**-Ames Research Center (ref. **6)** and Bolt Beranek and Newman Inc. (ref. **7).** Accordingly, we designed and used the following decision task, which was intended **as** an idealization of the

* **This work** was performed for NASA-Ames Research Center under contract **NAS2–5884.**

pilot's task of deciding whether or not he is within the "landing window."

The subject was presented with an oscilloscopic representation of a noisy glide-slope indicator along with two reference indicators showing the "target," or region of acceptable glide-slope error. The subject's task was to keep his response button depressed whenever he thought the true error was within the target area. In order to test the model for task interference, we provided two such decision tasks simultaneously in some of the experimental trials. In the two-task situation, two noisy indicators were presented on the same display and the subject manipulated two response buttons. The two "error" signals were linearly independent and were in no way affected by the subject's response. The display format for the two-task situation is shown in figure **1.**

The quantity displayed to the pilot was constructed as the summation of a "signal') plus a "noise" waveform. Thus,

$$y_d(t) = s(t) + n(t) \qquad (1)$$

where $y_d(t)$ was displayed to the subject, $s(t)$ was a low-frequency random waveform that we defined as the "signal" (say, glide-slope error), and $n(t)$ was a random waveform of higher frequency that we defined as "instrument noise."

Both $s(t)$ and $n(t)$ were generated by simulated Gaussian white noise processes. Signal shaping was accomplished primarily by second-order Butterworth filters. The "bandwidth" of $s(t)$ was fixed at 0.5 rad/sec,* arid the input amplitude was adjusted so that $s(t)$ would be within the target area half the time during the course of an experimental trial. The bandwidth of $n(t)$ was sufficiently greater than that of $s(t)$ to enable the subject to distinguish between the noise and signal components of the displayed variable $y_d(t)$. Noise power and bandwidth were experimental variables. The white noise forcing functions driving the signal and noise filters were linearly uncorrelated.

*For semantic convenience, we refer to the critical frequency of the Butterworth filter as the "bandwidth" of the filter output.

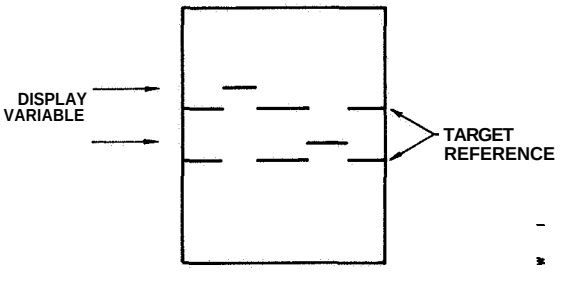

FIGURE 1.—Display format.

A MODEL FOR THE DECISION SITUATION

A block diagram of this decision situation is shown in figure 2. The portion of the model relating to the human's response is denoted by the dotted line. This model is identical to the optimal-control model for continuous tracking except that optimal control activity is replaced by optimal decision behavior.

The equations of motion of the system (i.e., '(system dynamics") are assumed linear and are expressed in state-vector notation, with the state vector denoted as $\underline{x}(t)$. The quantities displayed to the subject are denoted by the vector $\underline{y}(t)$ which is generated by a linear operation on the state vector. The human's inherent limitations are represented by an equivalent perceptual time delay τ and an observation noise process $\underline{v}_y(t)$.

The observation noise process $\underline{v}_y(t)$ is intended to account for the various sources of human randomness (or "internal noise"). The vector $\underline{v}_y(t)$ contains white Gaussian noise terms which account for the noise processes associated with the perception of indicator displacement and indicator velocity. These noise processes are assumed to be linearly independent of each other and of input driving noises. Furthermore, we assume that the power density level of each noise term is proportional to the variance of the corresponding perceptual variable. The constant of proportionality is termed the "noise/signal ratio". This treatment of human randomness is parallel to our treatment of human controller remnant (refs. **8** through 10).

The human's estimation strategy is represented in the model by the operations of optimal prediction and optimal (Kalman) filtering, the joint output of which is $\underline{\hat{x}}(t)$, the best estimate of the state of the system. The optimal predictor and estimator may be used to predict the variances

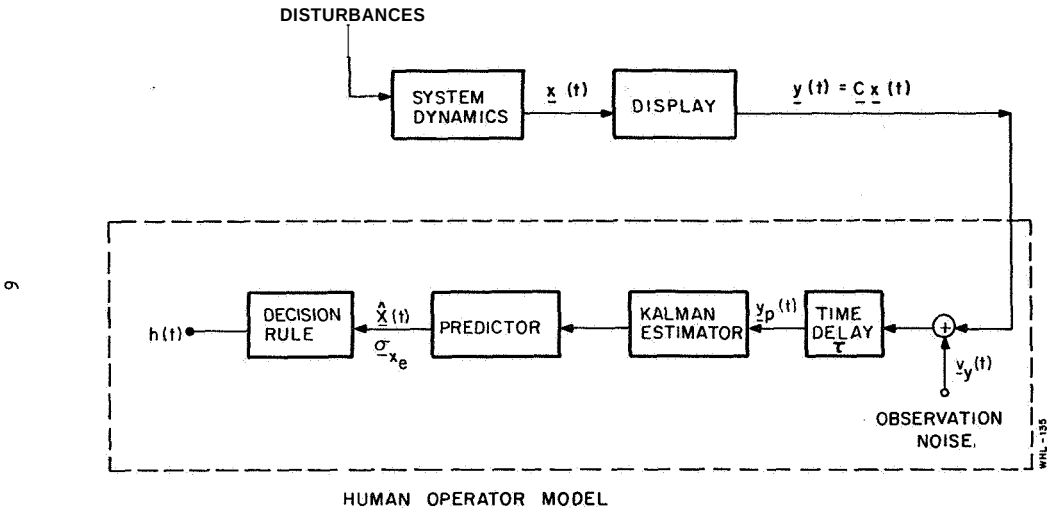

FIGURE 2.—Model for the decision situation.

(or rms levels) of the best estimate of the state vector and of the estimation error. These quantities are needed in order to predict the human's average decision performance.

Since $y_d(t)$ is the summation of linearly filtered white noise processes, this signal, by definition, is a sample function of a Gauss-Markov process (ref. **11).** This type of random process has the following properties which justify our assumptions of optimal estimation and prediction:

(1) The current "state" of the process contains all the useful information about the process. Thus, for most practical purposes, the entire past history of $y(t)$ is "summarized" by the current value of the state vector, $\underline{x}(t)$.

(2) The best estimate of the state vector is given by a Kalman filter cascaded with an optimal predictor which operates on the noisy input variable $\underline{y}_p(t)$ (ref. **11).** This filter is linear and time-invariant, and the difference between the instantaneous value of the state vector and the best estimate of it is a time-stationary random process. (This difference, or "estimation error", has a variance which is denoted by $\underline{\sigma}_e^2$.) The estimate of the state vector, $\underline{\hat{x}}(t)$, is "best" in the sense that it is the minimum-variance as well as the maximum-likelihood estimate (ref. **12).**

(3) The pair $(\underline{\hat{x}}(t),\underline{\sigma}_e)$ constitutes a sufficient statistic to test hypotheses about $\underline{x}(t)$ based on the noisy data $\underline{y}_p(t)$. This is so because all the relevant information that can be extracted from $\underline{y}_p(t)$ is contained jointly in $\underline{x}(t)$ and $\underline{\sigma}_e$ (ref. **12).**

The model that we have described thus far is a model for the human's monitoring behavior. That is, this model will allow us to predict the way in which the human will process the noisy information that is available to him. In order to predict decision behavior, the model for monitoring must be coupled with a rule for generating the appropriate decision response.

The optimal decision element of our model is based on Bayesian decision theory (refs. **13** and **14).** In general, the human's decision strategy will depend on the probabilities of the various correct and incorrect decision situations that can occur and on the "utility" (or "cost") associated with each possible situation. Since space does not permit a generalized analysis, we shall consider only the specific decision situation explored in this study.

Our subjects were instructed to minimize the "decision error," which was defined **as** the fraction of time during an experimental trial during which the subject's response was incorrect. Two types of decision error were possible: the "false alarm" (indicating that the signal $s(t)$ was within the target area when, in fact, it was outside), and the "miss" (the reverse type of decision error). Equal weighting was given to the two types of decision error; that is, the total decision

error score consisted of the sum of the two component error scores. For this situation the subject's decision rule was quite straightforward; namely, he was to respond "in" whenever his best estimate of $s(t)$ was within the target boundaries. (The optimal strategy is somewhat less trivial when the two types of decision error are not equally costly. See reference **1** for a more general analysis of the decision problem.)

PREDICTED DECISION PERFORMANCE

The model described above was used to predict the human's average decision error score for the experimental situations that were explored. The analysis procedure consisted of three steps: **(1)** problem specification, **(2)** computation of the variances of the best estimate $(\sigma_{\hat{s}}^2)$ and the estimation error $(\sigma_{s_e}^2)$ for the signal $s(t)$*, and **(3)** prediction of the decision error. The problem was specified in terms of the state vector $\underline{x}$, the display vector y, the time delay and noise/signal ratio which represented the human's limitations, and the performance requirements (i.e., minimization of decision error as defined above). The model for optimal estimation was implemented on a digital computer, and predictions were obtained for $\sigma_{\hat{s}}^2$ and $\sigma_{s_e}^2$.

The sum of the probabilities of the two types of decision error was used as a prediction of the decision error score. Thus,

$$\text{Predicted decision error} = P(H_1,h_0)+P(H_0,h_1) \quad (2)$$

where $P(H_1,h_0)$ is the joint probability of the subject deciding "in" and the signal being "out." Each of these probabilities was formulated as a joint gaussian distribution of the best estimate $\hat{s}(t)$ and the estimation error $s_e(t)$. Numerical techniques were used to compute average decision error scores, using numerical values for $\sigma_{\hat{s}}$ and σ_{s_e} yielded by the previous step in the analysis procedure. Details of the computational procedure are given in reference **1.**

Two experimental variables were considered: the bandwidth of the simulated instrument noise, and the ratio σ_s^2/σ_n^2. The time-delay parameter of the model was fixed at **0.2** see—a value that is typical of the effective delays inferred from studies of manual control behavior. The noise/signal parameter of the pilot model served as a variable of the analysis procedure.

Predicted decision error is shown as a function of noise/signal ratio in figure **3.** Curves are shown for each of the single-task conditions that were investigated experimentally. The filter bandwidth for the noise process $n(t)$ and the ratio of signal power to noise power is given for each of the conditions in the legend accompanying the figure. For the most part, the theoretical curves behave as one would expect. Predicted decision error increases as the simulated instrument noise power increases and as the human's internal noise level increases. Noise bandwidth, on the other hand, is shown to have little effect on decision performance.

Using the model for task interference that has been developed and validated for multivariable control situations (refs. **4** and 5), we can predict the increase in decision performance that will occur when a multiplicity of decision tasks are to be performed. Task interference is assumed to manifest itself as an increase in the human's internal noise/signal ratio according to the following relationship :

$$P_i^{(M)} = P_{o_i}/f_i \quad (3)$$

where $P_i^{(M)}$ is the noise/signal ratio associated with the i^{th} component task when a total of M tasks are performed, P_{o_i} is the ratio corresponding

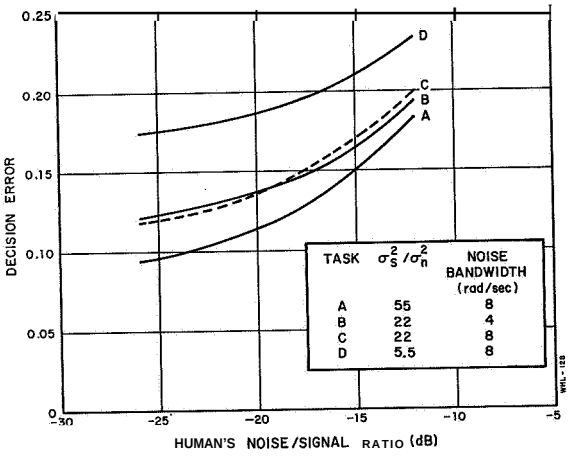

FIGURE 3.—Effect of noise/signal ratio on predicted decision error (signal bandwidth =0.5 rad/sec.)

*The problem was formulated such that $s(t)$ was treated as one element of the state vector $\underline{x}(t)$.

to single-task performance of the i^{th} subtask, and f_i denotes the fraction of attention to that task in the multitask situation. In other words, we assume that the noise/signal ratio varies inversely with attention.

We further assume that the subject has a fixed amount of information-processing capability (or attention) that is allocated optimally among the various subtasks. The notion of fixed capacity is represented by the following mathematical constraint:

$$\sum_{i=1}^{M} f_i = \sum_{i=1}^{M} \frac{P_{o_i}}{P_i^{(M)}} = 1 \qquad (4)$$

The following steps are required to predict the human's decision performance in a multiple-task decision situation. First, we define a total performance measure that is to be minimized (say, a weighted sum of the decision errors associated with the component decision tasks). We then obtain theoretical curves relating decision error to the noise/signal parameter of the model. Finally, using a suitable iteration technique, we find the noise/signal ratios associated with each task which minimize the total performance measure, subject to the constraint of equation **(4).** We thus obtain predictions of total-task performance, performance on the component tasks, and the allocation **of** attention among the tasks as defined by equation **(3).** This analytical procedure may also be used to predict performance when decision and control tasks are performed concurrently, provided a measure of total-task performance can be defined.

THE EXPERIMENTAL PROGRAM

An experimental program was undertaken to test the validity of the model for decision-making presented above and to provide further tests of our model for task interference. The following task situations were explored: **(1)** single decision tasks, **(2)** multiple decision tasks, and **(3)** simultaneous manual control and decision-making. In this section of the paper we briefly describe these experiments and present the principal experimental results. Discussion of results appears in the subsequent section.

Single Decision Tasks

This experiment was conducted to determine the effects of changes in task parameters on decision error and on inferred noise/signal ratios. The four decision tasks identified in figure **3** were explored. Our primary objective was to determine the extent to which decision performance on all tasks could be accounted for with fixed values for time delay and noise/signal ratio.

Four undergraduate engineering students served **as** the subjects for this experiment. The subjects were provided with *six* training trials on each of the four decision tasks.* Following training, three "data" trials of 4 min duration each were conducted per task per subject. The order of presentation **of** tasks was counterbalanced among subjects.

The average decision error was taken as the primary performance measure for each of the four tasks. The standard deviation of the average score was estimated and was defined as

$$\text{Standard deviation} = \left[\frac{\sum_{i=1}^{N} (DE_i - \overline{DE})^2}{N(N-1)} \right]^{1/2} \qquad (5)$$

where DE_i is the average score of the i^{th} subject for a particular task, $\overline{DE}$ is the average score for all subjects on that task, and N is the number of subjects (in this case, four). **A** mean noise/signal ratio was inferred for each task by reference to the appropriate theoretical curve. Standard deviations were estimated for the noise/signal ratio as follows. Ratios were found which corresponded to the mean decision error plus (and minus) one standard deviation; the absolute value of the difference between these noise ratios, divided by two, was taken as the approximate standard deviation.

Figure 4 shows the effects of task parameters on predicted and measured average decision performance. Predictions were obtained with nominal values of **0.2** sec and **−20** dB assigned to the

* For **the most part, the subjects appeared** to **reach a stable level of performance** on **a given decision task after** *six* **training** runs. **Considerably more training was provided in the following two experiments to assure stable levels of performance** in **the two-task decision and simultaneous decision and tracking situations.**

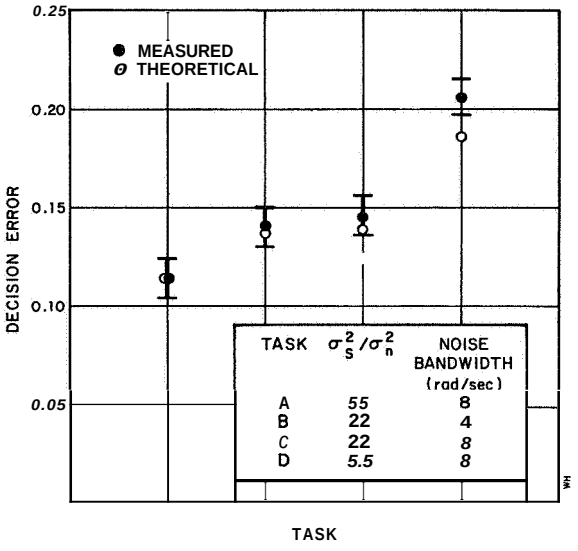

FIGURE 4.—Effect of task parameters on predicted and measured decision error (four subjects, three trials/ subject).

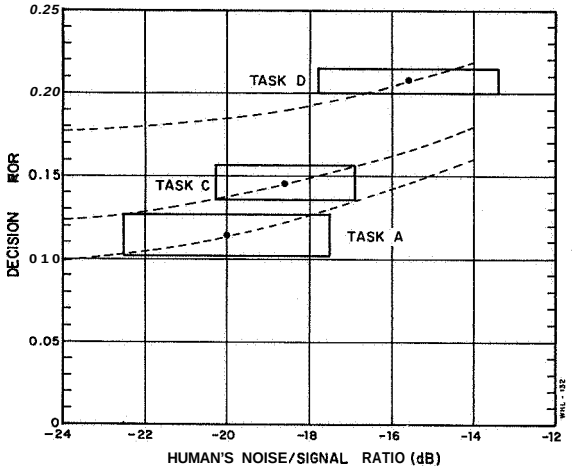

FIGURE 5.—Decision error scores and inferred noise/ signal ratios for three tasks (four subjects, three trials/ subject; dashed lines indicate theoretical relationships).

time delay and noise/signal ratio parameters of the model.

For the most part, predicted and measured scores were in very good agreement. For tasks *A*, *B*, and *C*, the measured decision error score varied by less than one standard deviation from the theoretical prediction. The decrease in "instrument noise" bandwidth from 8 to 4 rad/sec did not appreciably affect decision performance. (We had predicted that this would be the case if the human's noise/signal ratio were −20 dB.) The only notable discrepancy between theory and experiment occurred for the most difficult task (task *D*); in this case, the measured score was about 11 percent greater than the predicted decision error. A t-test performed on the subject means revealed that this difference, while small in absolute terms, was significant at the 0.05 criterion level.

Decision error versus inferred noise/signal ratio is shown graphically for tasks *A*, *C*, and D in figure 5. Rectangular boxes about each datum point indicate ± 1 standard deviation of both the error score and the noise/signal ratio. (The results of task *B* are not shown in this figure since they almost coincide with the results of task *C*.) This figure shows that the noise/signal ratio increases almost linearly with decision performance, ranging from −20.0 dB for task *A* to −15.6 dB for task *D*. Since the ratios inferred for tasks *A*, *B*, and *C* lie within one standard deviation of one another, we cannot ascribe any statistical significance to these differences. The noise/signal ratios associated with tasks *A* and D, however, differ by about two standard deviations; this difference is too large to dismiss simply as experimental variability. Factors which might account for the apparent variation of noise/signal ratio with task parameters are discussed later in this paper.

Multiple Decision Tasks

This experiment was performed to validate our model for task interference in a decision-making context. Decision error scores were obtained for tasks performed singly and two at a time, and the difference between the two-task and one-task scores was tested against the difference predicted by the model.

The subjects were provided with two decision tasks of the type identified as task *A* in figure 3. The statistics of the left- and right-hand tasks were nominally identical, but the two display variables were linearly uncorrelated. When two tasks were performed concurrently, the subjects were instructed to minimize the sum of the decision errors associated with each component task. Each subject performed four data sessions con-

sisting of the following three-task situations: (1) a single task for the left-hand, (2) a single task for the right-hand, and (3) left- and right-hand tasks together.

Average decision error score was 0.110 for the one-task situation and 0.130 for the two-task situation. The difference between these scores was found by a t-test to be significant at the 0.001 level.

If our model for interference is valid in this decision context, then the average increment in decision score should correspond to a doubling of the subject's noise/signal ratio. (That is, the subject devotes an average of half his attention to each task.) In order to obtain a theoretical prediction for the two-task decision error, we refer to the theoretical curve relating decision error to noise/signal ratio. From this curve we associate a noise/signal ratio of −20.8 dB with the average one-task score of 0.110. Taking this point as a reference, we derive the curve shown in figure 6 which relates the predicted increment in decision error to increments in noise/signal ratio (alternatively, to decrements in "attention").

The increments in decision error and inferred noise/signal ratio that we obtained experimentally are shown in figure 6 for comparison with the theoretical curve. The range of decision error and noise/signal ratio corresponding to ± 1 estimated standard deviation are also indicated. The increase of **0.020** in decision errors score that we measured corresponds to an increment of 3.3 dB in the inferred noise/signal ratio. This increase is within one standard deviation of the 3 dB increment predicted by our model for task interference. Similarly, the assumption of a 3 dB increment in noise/signal ratio leads to a predicted increase in error score of 0.018. A t-test of the average two-task, one-task difference scores shows that this prediction is not significantly different from the measured increase of 0.020. On the basis of this very good agreement between theory and experiment, we conclude tentatively that our model for task interference is applicable to the type of decision task explored in this study.

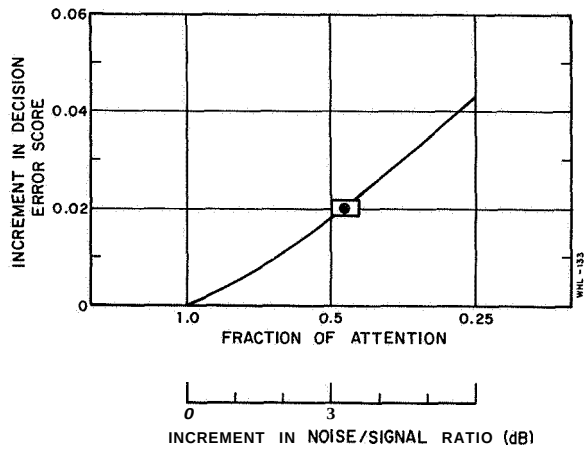

FIGURE 6.—Effect of attention on decision error score, task A (four subjects, three trials/subject).

Simultaneous Control and Decision-Making

The third and final experiment was conducted to determine the extent to which the model would account for interference between a decision task and a continuous control task performed concurrently. The decision task employed in this experiment was of type *A* as described above; the tracking task was a conventional K/s (i.e., velocity control) compensatory tracking task of the type used in previous studies (refs. 5 and 8 through 10). The display format shown in figure 1 was used, with the decision variable displayed on the left and the tracking error displayed on the right. The experimental procedure was similar to that employed in the previous experiment.

The subjects' instructions were to minimize decision error (DE) when performing the decision task alone, to minimize mean-squared tracking error (σ_e^2) when performing the tracking task alone, and to minimize a weighted sum of decision and tracking errors when performing the two tasks concurrently. The total performance measure for the two-task situation was $J = \sigma_e^2 + 3 \cdot \mathrm{DE}$. This combination of decision and tracking errors was selected on the basis of pre-experimental analysis in an attempt to have decision and tracking performance scores contribute roughly equally to the total score.

Each subject yielded higher (worse) performance scores in the two-task situation than in the one-task situation. This was true not only for the total performance measure but also for the component scores as well. The *magnitude* of these differences, however, varied widely from subject-to-subject. The fractional increase in total score

ranged from about 5 percent for one subject to about 45 percent for another subject. For reasons which are detailed in reference 1, the data from these two subjects were considered unreliable and were not subjected to further analysis. The remaining two subjects exhibited an increase of about 15 percent in total score; these results were used to test the model for interference.

The procedure for testing the model for interference was similar to that used in the preceding experiment. Theoretical curves of decision error versus noise/signal ratio and mean-squared tracking error versus noise/signal ratio were used to determine the noise/signal ratios that corresponded to single-task performance. Additional parameters of the model for manual control (time-delay, motor noise ratio, and lag time constant) were chosen partly on the basis of previous experience and partly to provide a good match to the mean-squared error-rate and control scores. Using the rules set forth in equations (3) and (4), we then obtained theoretical curves for total- and component-task performance as a function of attention.

Figure 7 shows the predicted two-task performance scores for combined decision and tracking for two subjects. Total performance, tracking error, and weighted decision error scores are shown as a function of the fraction of attention paid to the tracking task. We see from this figure that optimal performance (i.e., minimum total score) for each subject corresponds to a nearly equal division of attention to the decision and tracking tasks. We note, however, that total score is relatively insensitive to attention in the vicinity of this theoretical optimum.

Superimposed on the theoretical curves in figure 7 are the theoretical two-task performance scores which correspond to no interference and to full interference. Also shown are the two-task scores that were obtained experimentally. The "no interference" theoretical scores are simply the scores obtained in the one-task experiments. (The no-interference total score is the weighted sum of the one-task tracking and decision error scores.) The "full interference" scores are the ones predicted by our model for task interference. These scores are obtained from the theoretical curves of figure 7 for a 50 percent allocation of attention to the tracking task, (which is the allocation of attention that yields the lowest predicted total score).

Both subjects achieved two-task total scores that fell between the theoretical scores associated with no interference and with full interference. Thus, the mutual interference between the tracking and decision tasks was not as severe as that predicted by the model.

Since we have reliable results from only two subjects, we cannot claim with a high degree of assurance that our model for interference either does or does not apply to the combined decision and control situation. There is little question that interference does occur: all four subjects yielded higher total and component scores in the two-task situation. The *degree* of interference remains in question. Accordingly, we must conclude at this stage that the model which we have proposed for combined decision-making and control shows promise, and that a conclusive set of experiments remains to be conducted.

DISCUSSION OF RESULTS

Experimental results agreed very closely with predicted performance scores in situations involving decision-making only. Using fixed values for human time delay and noise/signal ratio, we were able to predict both one-task and two-task decision error scores to within an accuracy of about 10 percent. Agreement was less good for the simultaneous decision and control situation, with prediction errors on the order of 15 percent.

Although the differences between theory and experiment are relatively small, they cannot be attributed entirely to "experimental variability." We consider briefly certain methodological problems associated with the decision task that may account for some of these differences, and we suggest refinements which might improve the predictive accuracy of the model.

Methodological Considerations

Perhaps the most serious drawback of the decision task which we explored—at least with respect to testing our model—was the relative insensitivity of decision error to the human's noise/signal ratio. This insensitivity may be largely responsible for the wide range of noise/signal

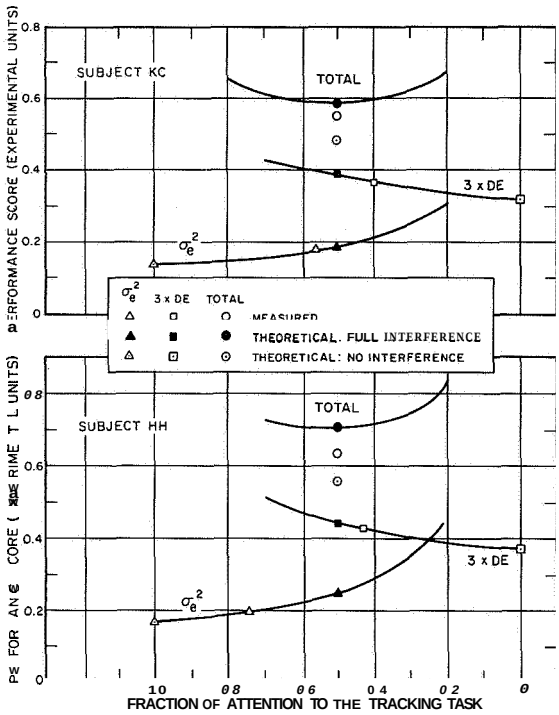

FIGURE 7.—Effect of division of attention on decision, tracking, and total performance scores.

ratios needed to match all single-task decision scores perfectly (fig. *5).*

We have found in previous studies of manual control that, subjects will operate at an unusually low noise/signal level if, by so doing, they can substantially reduce their mean-squared tracking error scores (ref. *5).* By the same token, we would expect subjects to operate at higher than usual levels of noise/signal ratio if task performance is particularly insensitive to noise/signal. From figure **3** we observe that a doubling of the noise/signal ratio from **—20** dB to **—17** dB theoretically produces only about a *5* percent increase in the decision error for task D. The same increase in noise/signal ratio accounts for a **17** percent increase in score for decision task **A** and a **44** percent increase in mean-squared error for the tracking task considered in this study. Thus, it is entirely possible that the subjects were insufficiently motivated to maintain a **—20** dB noise/signal ratio when performing task D.

We suspect that the inability to obtain reliable, conclusive data in the experiment on simultaneous decision and control was also due, in part, to a relative insensitivity of performance score to noise/signal ratio. Note that we can predict the total-task performance score to within **15** percent with either the full-interference or no-interference concept incorporated into the model. In order to obtain a more conclusive set of results, a decision task should be explored which is more sensitive to pilot parameters.

The subjects may have encountered difficulty in learning the strategies appropriate to the various decision tasks because of inadequate knowledge of results during the training period. The only knowledge of performance given to the subject was the decision error score that was given him at the end of each trial. Thus, if a subject were to try various estimation strategies during the course of a single trial, he would not know which strategy was best. Various methods of presenting relatively instantaneous knowledge of performance were considered, but these ideas were rejected because of the high probability that the subject would learn to respond to the performance indicator and not to the signal on the primary display. To some extent, then, the relatively large noise/signal ratio inferred for decision task ***D*** may reflect an inappropriate estimation strategy on the part of the subject.

Refinements to the Model

The first problem discussed above suggests one obvious refinement to the model; namely, that the sensitivity of performance to noise/signal ratio be taken into account. The rules for selecting observation noise levels might be modified to show the noise/signal ratio as an explicit function of this sensitivity. There is enough experimental evidence to indicate that this is a reasonable idea, although further study would be needed in order to determine with any degree of precision what this function should be. A model refinement of this sort would improve the predictive accuracy of models for manual control as well as for decision-making.

Another possible model refinement is to consider the power density level of the observation noise as a time-varying quantity which scales with the instantaneous magnitude of the observed signal. Such a treatment would be consistent with our assumption that human randomness

stems from underlying multiplicative noise sources (ref. 1).

The treatment of observation noise as a time-stationary process is a mathematical convenience that has apparently worked very well for modelling manual control behavior, but one which might introduce non-negligible modelling error in the decision situation. Note that the relation between the magnitude of the estimation error and the instantaneous value of the "signal" $s(t)$ determines the effect that a given amount of estimation error has on decision performance. For example, if the signal is two target widths beyond the target boundary, the subject will make the correct decision even if the error in his estimate of the signal position is relatively large. On the other hand, relatively small estimation errors may cause an incorrect decision if the signal is very close to one of the target boundaries. A more accurate modelling procedure would take account of the relation between the instantaneous signal value and the variance of the accompanying estimation error.

REFERENCES

1. LEVISON, W. H.; AND TANNER, R. B.: A Control-Theory Model for Human Decision-Making. Rept. No. 2119, Bolt Beranek and Newman Inc., Apr. 1971.
2. KLEINMAN, D. L.; BARON, S.; AND LEVISON, W. H.: An Optimal Control Model of Human Response—Parts I and 11. Automatica, vol. 6, pp. 357–369, Pergamon Press, May 1970.
3. KLEINMAN, D. L., AND BARON, S.: Manned-Vehicle Systems Analysis by Means of Modern Control Theory. Rept. No. 1967, Bolt Beranek and Newman Inc., June 1970.
4. LEVISON, W. H.: A Model for Task Interference. Proceedings of the Sixth Annual Conference on Manual Control, Air Force Institute of Technology, Air Force Flight Dynamics Laboratory, Wright-Patterson Air Force Base, Apr. 1970.
5. LEVISON, W. H.; ELKIND, J. I.; AND WARD J. L.: Studies of Multivariable Manual Control Systems: A Model for Task Interference. Rept. No. 1892, Bolt Beranek and Newman Inc., Dec. 1969.
6. PALMER, E.; AND WEMPE, T.: Pilot Performance with a Simulated ILS-Independent Pictorial Landing Display. Proceedings of the Seventh Annual NASA-University Conference on Manual Control, University of Southern California (Los Angeles, Calif.), June 1971.
7. KLEINMAN, D. L.; AND BARON, S.: Analytic Evaluation of Display Requirements for Approach and Landing. Rept. No. 2075, Bolt Beranek and Newman Inc., Mar. 1971.
8. LEVISON, W. H.; KLEINMAN, D. L.; BARON, S.: A Model for Human Controller Remnant. Rept. No. 1731, Bolt Beranek and Newman, Inc., Oct. 1968.
9. LEVISON, W. H.; ET AL.: A Model for Human Controller Remnant. IEEE, Trans. on Man-Machine Systems, vol. MMS–10, no. 4, Dec. 1969.
10. LEVISON, W. H.: The Effects of Display Gain and Signal Bandwidth on Human Controller Remnant. AMRLTR–70–93, Wright-Patterson Air Force Base (to be published).
11. KALMAN, R. E.: A New Approach to Linear Filtering and Prediction Problems. Trans. ASME, vol. 82D, p. 35, 1960.
12. BRYSON, A. E., JR.; AND Ho, Y C.: Applied Optimal Control. Blaisdell Pub. Co. (Waltham, Mass.), 1969.
13. EDWARDS, W.; Lindman, H.; AND PHILLIPS, L. D.: Emerging Technologies for Making Decisions. Published in New Directions in Psychology II, Holt, Rinehart and Winston 1965.
14. GREEN, D. M.; AND SWETS, J. A.: Signal Detection Theory and Psychophysics. John Wiley and Sons, Inc., 1966.

N73-10108

4. An Input Adaptive, Pursuit Tracking Model of the Human Operator*

JOHN R. WARE

Naval Ship Research and Development Center

The purpose of this research was to develop and evaluate a simple model of the input adaptive behavior of the human operator (HO) in a pursuit tracking task in which the plant controlled consists of a pure gain. In such a task the HO must attempt to predict the future position of the input signal to overcome his inherent delay. Figure 1 is a block diagram of the pursuit tracking task.

If it is assumed that the HO is approximately an optimal predictor (in the mean square sense) using only position and velocity information, as suggested by J. I. Elkind, then there is a simple method of computing the values of the model parameters in terms of the autocorrelation function of the input signal. Experimental evidence indicates that the ability of the HO to use velocity information decreases with increasing signal velocity indicating that a biased estimator of the velocity weighting should be used. A suitable approximation is derived which has rapid convergence and low variance. The model thus derived is compared to actual subject transfer functions and is found to be in close agreement.

In addition to tracking random processes the model can adapt to and track deterministic signals, such as sine waves, up to approximately the frequency at which human operators begin to track precognitively.

The optimal position weighting is shown to be a good measure of effective bandwidth and it also possesses the attractive property of being easily calculable using the technique presented.

Possible application, in addition to modelling, are the use of the estimation procedure as an adaptive signal preprocessor to reduce operator workload and the use of the position weighting as an adaptive indicator of sampling rate in multiaxis tasks.

INTRODUCTION

Previously developed input adaptive models, such as those proposed by Angel and Bekey (ref. 1) and Fogel and Moore (ref. 2), are implemented using a finite-state machine approach. However models of this form have several drawbacks, not the least of which is that they are usually cumbersome to simulate.

Elkind (ref. 3) suggested a model for pursuit tracking as shown in figure 2. He then proposed that if the error signal is small, the error feedback loop could be neglected. If, in addition, it is assumed that the plant controlled is a pure gain the problem is reduced to a simple signal tracking task. This is the problem considered in this report, pursuit tracking in which the plant controlled consists of a pure gain.

MODEL FORM

The transfer function of the HO must contain a pure lag which is caused by neuromuscular delay and central processing in the brain. In order to minimize the error due to this delay the HO must make a prediction of the input signal based on previous knowledge of the signal and his present observations of the signal state. Elkind reasoned that the predictor would be such as to minimize the mean square error within the natural limitations of the HO. Minimizing mean square error is used as the criterion mainly because it is the only mathematically tractable function of error, and it is used as the major

* Research supported by NASA under contracts NASr-54 (06) and NSR-23-005-364.

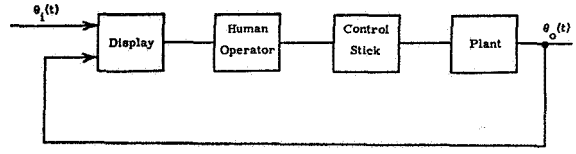

FIGURE 1.—Block diagram of pursuit tracking task.

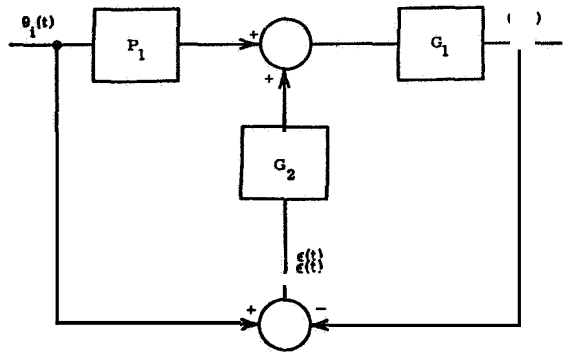

FIGURE 2.—Elkind's (ref. 3) proposed pursuit tracking model.

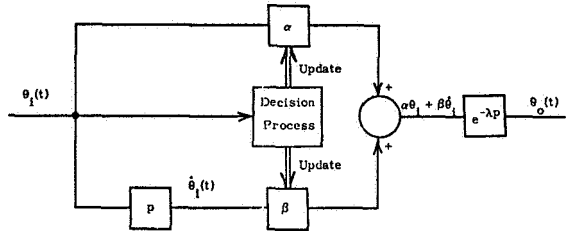

FIGURE 3.—Schematic of proposed pursuit tracking model.

criterion of performance in many studies. If it happens that the signal is a sample function of a Gaussian random process, then the predictor that minimizes mean square error will also minimize any error criterion that is symmetrical and a nondecreasing function for nonnegative argument. Since it is known that the HO can determine position quite accurately, is also able to perceive and use velocity information, but is much less able to use higher derivative information, the predictor model takes the form:

$$\theta_0(t) = (\alpha + \beta p) e^{-\lambda p} \theta_i(t)$$

in which λ is the prediction interval, equal to subject delay.

It is proposed, then, that if it is possible to construct a model in the form shown in figure 3 in which, by observation of the input signal α and β converge to the optimal predictor values, then such a model will be a satisfactory representation of human signal tracking behavior for a wide range of input signals.

It is easy to show (see appendix) that the optimal values of α and β are given by

$$\alpha = \frac{R(\lambda)}{R(0)}$$

$$\beta = \frac{R'(\lambda)}{R''(0)}$$

in which $' = d/d\tau$, if the following conditions are met:

(1) $E\{\theta_i(t)\} = 0$

(2) $R(\tau) = E\{\theta_i(t+\tau)\theta_i(t)\}$

(3) $\dot{\theta}_i(t)$ exists.

If $\hat{R}(0,t)$ is the output of the first order filter shown in figure 4, then it can be shown that $\hat{R}(0,t)$ is an unbiased estimator of $R(0)$. Similar circuits can be used to compute unbiased estimates of $R(\lambda)$, $R'(\lambda)$, $R''(0)$ (see appendix for details) and these may be used to form estimates of the optimal position and velocity weightings:

$$\hat{\alpha}(t) = \frac{\hat{R}(\lambda,t)}{\hat{R}(0,t)}$$

$$\hat{\beta}(t) = \frac{\hat{R}'(\lambda,t)}{\hat{R}''(0,t)}.$$

Experimental evidence indicates that the ability of the HO to use velocity information decreases with increasing signal velocity suggesting that a biased estimator of the velocity weighting should be used. Consider the expression for β

$$\beta = \frac{R'(\lambda)}{R''(0)}$$

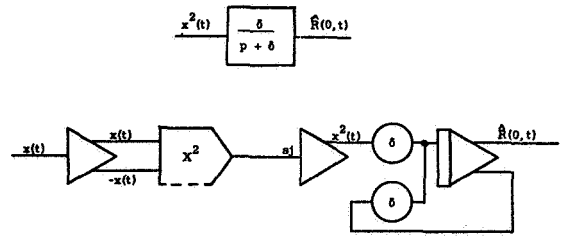

FIGURE 4.—Circuit for generating $\hat{R}(0,t)$ (see appendix for circuit notation).

but since $R'(0)=0$ (which follows from the fact that $R(\tau)$ is symmetrical and that $\dot{\theta}_i(t)$ exists), then

$$\beta/\lambda=\frac{[R'(\lambda)-R'(0)]/\lambda}{R''(0)}$$

and

$$\beta/\lambda\cong\frac{R''(\lambda)}{R''(0)}=\beta^*/\lambda.$$

This approximation is essentially the same as replacing

$$\frac{\theta_i(t+\lambda)-\theta_i(t)}{\lambda}$$

by $\dot{\theta}_i(\lambda)$.

This approximation to the optimal velocity weighting is exactly the same operator as used to generate the optimal position weighting but applied to the derivative of the input rather than the input itself.

PROPERTIES OF THE ESTIMATORS

In order to check the model and compare it with HO behavior tests were run with four different input signals. These consisted of essentially white noise passed through the filter,

$$G(j\omega)=\frac{{\omega_0}^N}{(\omega_0+j\omega)^N},$$

with $\omega_0=1.57, 3.14$ and $N=3,4$. In order to get a reasonable convergence time of the model without excessive variance in the parameters, comparisons were made of the model performance as a function of the time constant of the filter used to compute the autocorrelation functions. A time constant of 10 sec was selected as being a suitable compromise. Table 1 gives the properties of the estimators for the four test signals. Reference 4 contains a study of the linear correlation of the model indicating that the variation in the parameters is sufficiently small that, compared to the HO, the model can be considered as linear and time invariant.

PURSUIT TRACKING TESTS

In order to validate the steady state behavior of the model and compare it with actual HO performance a pursuit tracking experiment was conducted. Three right-handed male subjects practiced tracking each of the four signals with the data presented taken on the fourth day. This amounted to 15 minutes of tracking each signal per subject prior to the final data run. This was deemed sufficient in light of the simplicity of the task. A force stick was used throughout the experiment.

The output of the force stick was passed through a 40 rad/sec first order filter to reduce high frequency noise in the circuit. A plant with such a small time constant (25 milliseconds) is not noticeable during tracking, the major effect being a small phase lag at high frequencies (8.5° at 6 rad/sec). All data are plotted including this filter and with the model outputs also through the same filter for uniformity.

The average subject data is compared with the model transfer function in figures 5, 6, and 7 and also with the optimal predictor in figure 8.

A time delay of 0.200 sec ($\lambda=0.200$ sec.) is used throughout for the model delay. For a complete circuit diagram see appendix.

TABLE 1.—*Estimator Properties for the Four Test Signals*

$\delta=.1$	Position weighting			Velocity weighting		
Signal	α	Mean of $\hat{\alpha}(t)$	Variance of $\hat{\alpha}(t)$	β/λ	Mean of $\hat{\beta}^*(t)/\lambda$	Variance of $\hat{\beta}^*(t)/\lambda$
1.57 4th	0.989	0.988	0.012	0.97	0.95	0.014
1.57 3rd	.983	.981	.013	.95	.89	.024
3.14 4th	.961	.958	.015	.94	.83	.027
3.14 3rd	.947	.934	.018	.88	.66	.033

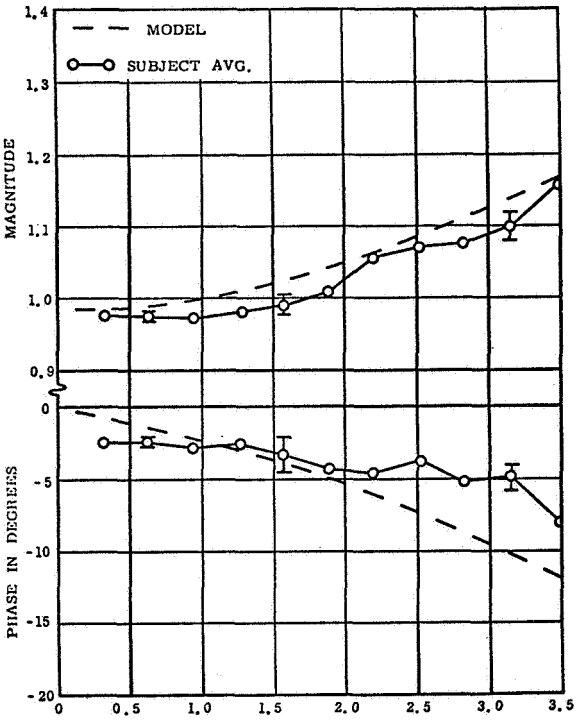

FIGURE 5.—Comparison of model and subject average transfer function: 1.57, 4th.

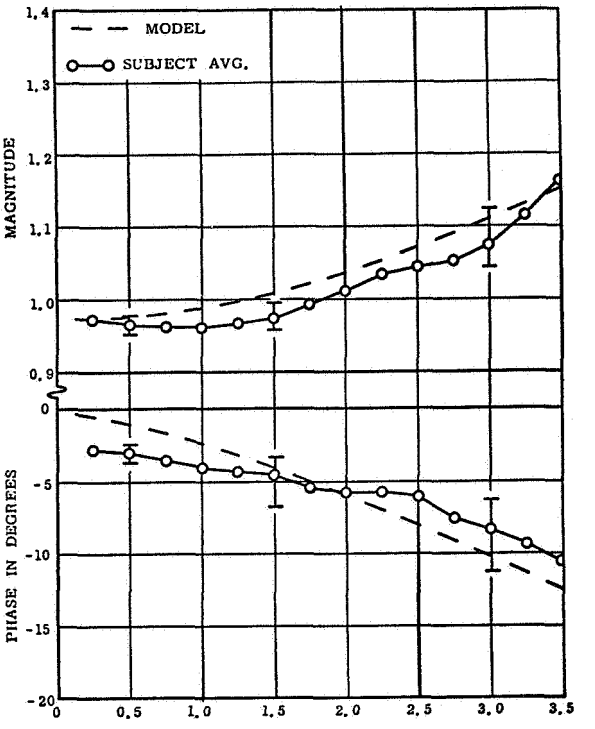

FIGURE 6.—Comparison of model and subject average transfer function: 1.57, 3rd.

As can be seen the model provides a very good fit for the subject data. The major discrepancy appears in the magnitude plots in the low frequency region and the discrepancy is greater for high frequency signals. It can also be seen that in no case does the subject phase lag approach 0°. These effects are no doubt related.

As a check on the quality of the model fit to the subject data, the average absolute difference in magnitude ratio and phase as well as the linear correlation between the two was computed. The results are presented in table 2.

PROBABLE CAUSES OF SUBOPTIMAL BEHAVIOR

Possible explanations for the suboptimal behavior and the low frequency phase droop are:

(1) The subjects are tracking in a partially compensatory manner. Kreifledt (ref. 5) was able to duplicate the suboptimal magnitude ratio at low frequencies obtained by Elkind (ref. 3) by including a compensatory loop in his model.

(2) Subjects are reluctant to correct a small error in a low frequency portion of the signal fearing that a sudden reversal will cause a high error.

(3) For higher frequency signals it becomes increasingly difficult for the subjects to estimate velocity and they therefore appear to decrease their dependence on velocity for prediction. The corresponding increase in the uncertainty of the position weighting is not as pronounced.

POWER MATCH (PM)

A commonly used index of a model performance is called the "power match" (ref. 6). If the difference between model output and subject output is denoted as $e(t)$ then the power match is defined to be

$$\mathrm{PM} = 1 - \frac{\overline{e^2(t)}}{\overline{\theta_i^2(t)}}.$$

If $\mathrm{PM} = 1$ then the model is a perfect match of subject behavior. Table 3 presents the power match and the mean square error averaged over the three subjects for the last day of trials.

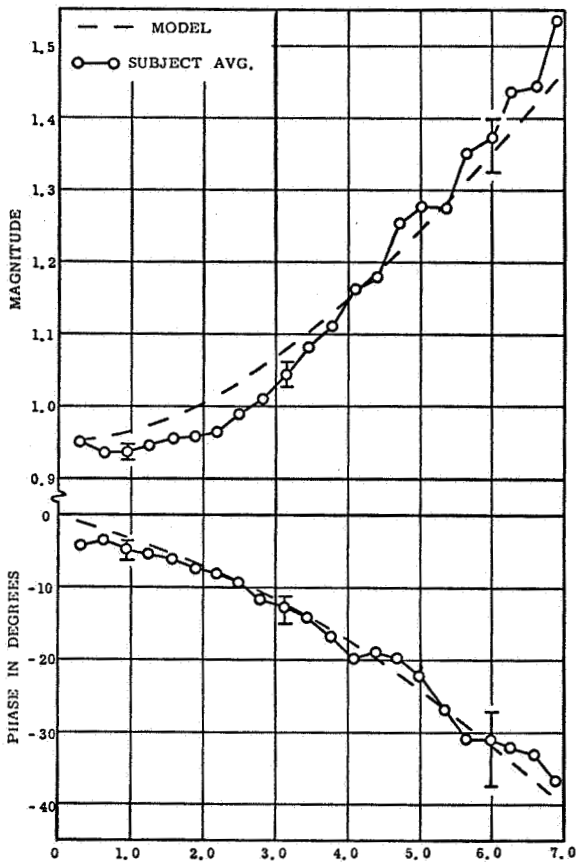

FIGURE 7.—Comparison of model and subject average transfer function: 3.14, 4th.

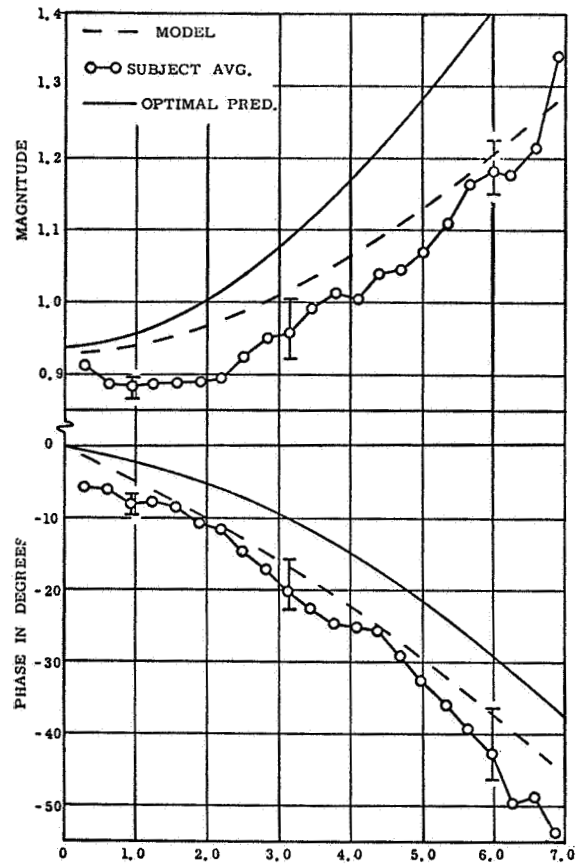

FIGURE 8.—Comparison of model and subject average transfer function: 3.14, 3rd.

TABLE 2.—*Results of Computation of Magnitude Ratio, Phase, and Linear Correlation*

Signal	$\lvert\epsilon\rvert$ Magnitude ratio	$\lvert\epsilon\rvert$ Phase lag, degree	Linear correlation magnitude	Linear correlation phase
1.57 4th	0.023	2.2	0.982	0.926
1.57 3rd	.024	1.4	.978	.985
3.14 4th	.033	1.7	.995	.993
3.14 3rd	.043	3.9	.982	.992

TABLE 3.—Power Match and Mean Square *Error* Averages

Signal	PM	ϵ^{-2}
1.57 4th	0.998	0.00654
1.57 3rd	.996	.0151
3.14 4th	.995	.0275
3.14 3rd	.989	.0720

Because of the low error scores, it is no surprise that the power match is very nearly unity for all signals. A visual comparison of model and subject error, although resulting in no quantitative measure, nevertheless reveals significant qualitative similarities. Figures 9 and 10 are typical time histories.

SINE WAVE TRACKING

Although the model was constructed to follow signals ccnsisting of low-pass filtered white noise it is also useful as a model for tracking low frequency predictable signals such as sine waves. It is not unreasonable to assume that in sine wave tracking subjects change their mode of behavior at a frequency of 2.5 to 3.5 rad/sec (0.4 to 0.5 Hz) (ref. 7). Below this frequency subjects follow the signal apparently using short term prediction but above this frequency subjects use the regularity of the signal to establish a rhythmic pattern which they attempt to match with the input signal. One would expect then that the model, if valid for short term prediction as presented, should be useful for tracking such signals up to about 3.5 rad/sec.

Figure 11 shows the magnitude ratio of the model versus input sinusoid frequency. The magnitude ratio is very nearly unity to 2.0 rad/sec, drops to 0.95 at 3.0 rad/sec, and falls off rapidly at frequencies above that. This is due primarily to the fact that $\hat{\beta}^*$ is a biased estimator. In fact, for sine wave tracking $\beta^*/\lambda = \alpha$.

Figure 12 compares model performance with data obtained by Magdaleno et al. (ref. 7) for pursuit tracking of sine waves.

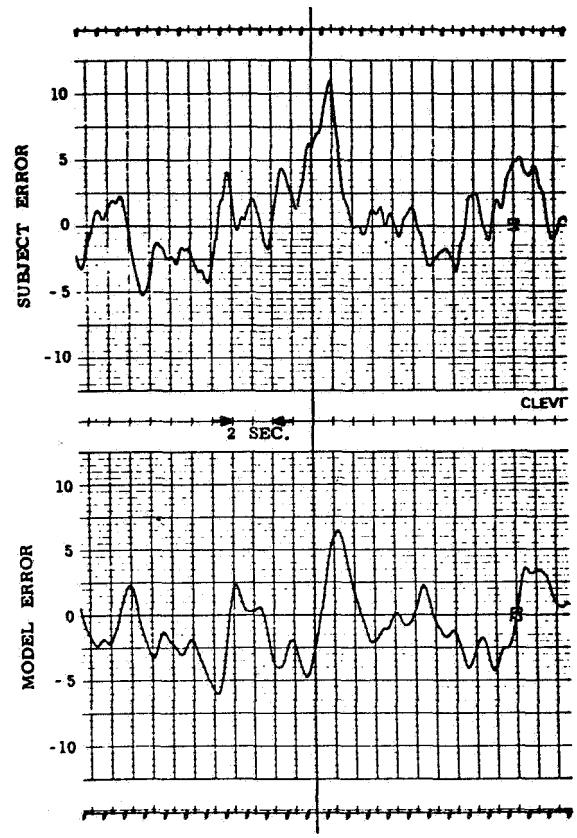

FIGURE 9.—Typical subject and model error time histories. Input signal is 3.14, 4th.

MODEL TRANSIENT BEHAVIOR

Convergence times of $\hat{\alpha}(t)$ and $\hat{\beta}^*(t)$ are functions of the convergence rate, initial conditions and the input signal. It is almost meaningless to try to express convergence times in any other context than of the time required to adapt from one signal to another.

Figure 13 shows what occurs during the transition 1.57, 4th to 3.14, 3rd and figure 14 shows the return. The change in signal characteristics is accomplished within a few milliseconds and in such a way that there is no discontinuity in signal position or velocity.

For the transition 1.57, 4th to 3.14, 3rd the "time constant" (most easily seen from the record of $\hat{\beta}^*(t)$) is about 8 sec. However, for the reverse transition the time constant is about 25 sec. This is because relatively more information about the signal is contained in a segment of a

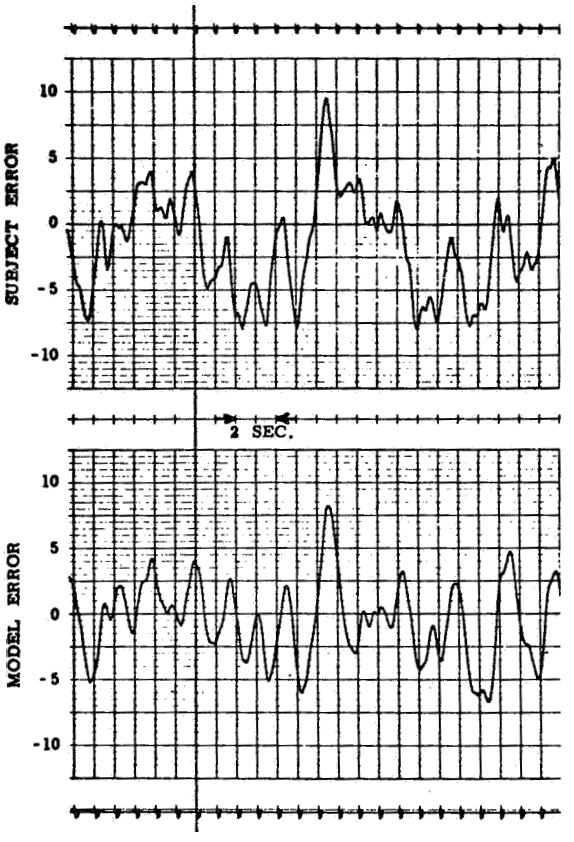

FIGURE 10.—Typical subject and model error time histories. Input signal is 3.14, 3rd.

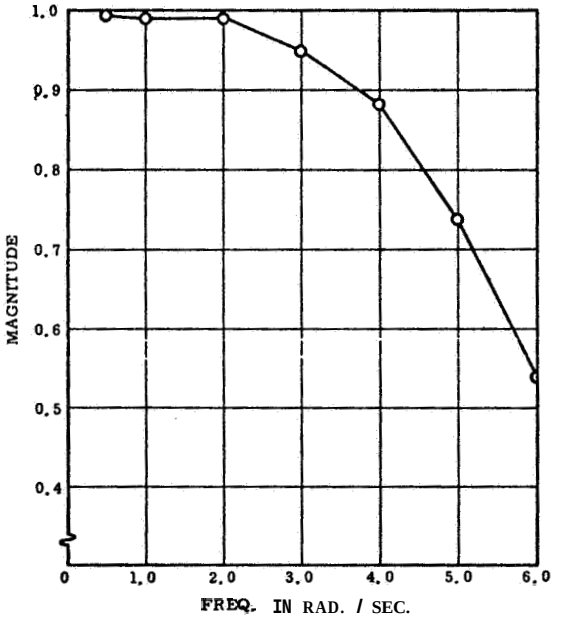

FIGURE 11.—Model response to sine wave inputs.

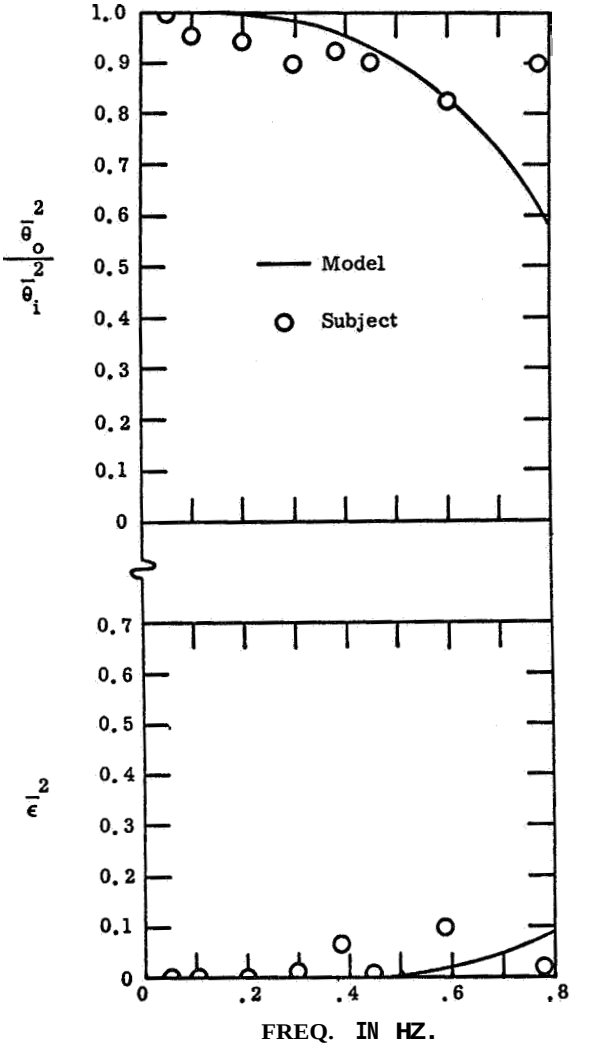

FIGURE 12.—Comparison of subject and model normalized output power and mean square error for sine wave input.

"fast" signal than in the same time segment of a relatively "slow" signal.

The model adapts very quickly to sine waves, as shown in figure **15,** but much more slowly when a transition is reversed as in figure **16.**

Although it is not known how long trained subjects take to adapt to changes in input signal, it is probably less time than the model requires, at least in the case of a change from a relatively fast signal to a relatively slow one. For this reason, the model may not be a valid representation of human behavior during the transition period.

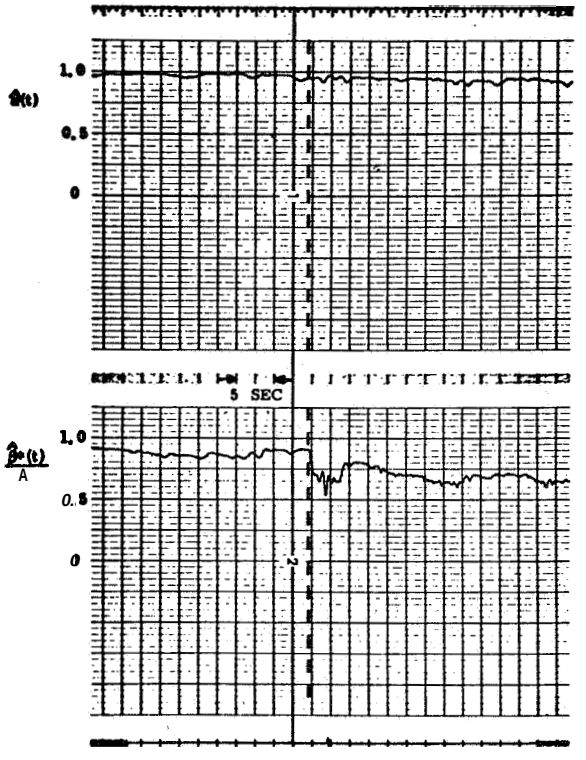

FIGURE 13.—Model parameter response to step change in input signal: 1.57, 4th to 3.14, 3rd.

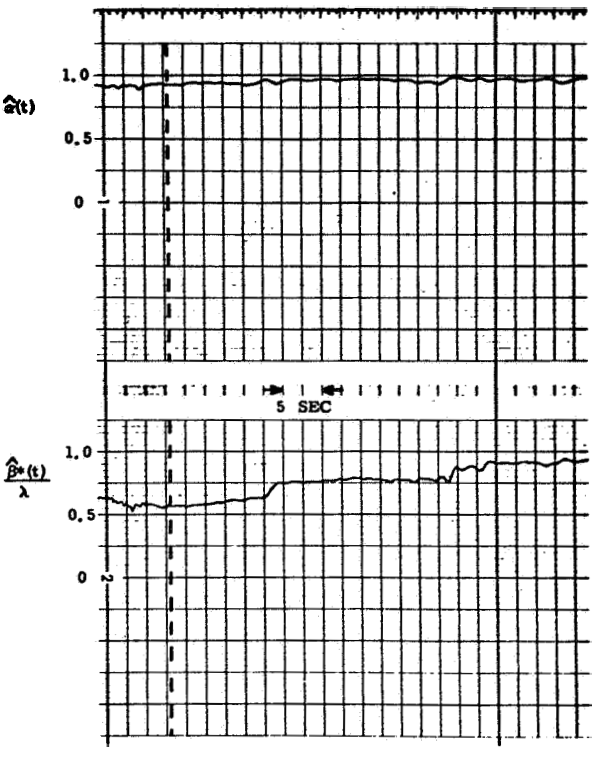

FIGURE 14.—Model parameter response to step change in input signal: 3.14, 3rd to 1.57, 4th.

EFFECTIVE BANDWIDTHS

Since many different forms of input signals are used in the study of human tracking behavior it is desirable to have some measure by which signals may be compared. The most common measure is the "equivalent" or "effective" bandwidth, which compares the nominal cutoff frequency of the input signal to that of a rectangular spectrum.

Magdaleno and Wolkovitch (ref. 8) suggested that the number of axis crossings would be a useful measure. Elkind (ref. **9)** proposed that effective bandwidths be computed by

$$\omega_e = \frac{\left[\int_0^\infty S(\omega)\, d\omega\right]}{\int_0^\infty S^2(\omega)\, d\omega}$$

in which

ω_e =effective bandwidth,
$S(\omega)$ =signal spectrum.

However, this cannot be used if the input signal is composed of the sum of sinusoids. The positive spectrum of this signal is made N delta functions located at $\omega_1, \omega_2, \ldots, \omega_N$. That is, the positive spectrum

$$S(\omega) = \delta(\omega-\omega_1)+\delta(\omega-\omega_2)+ \cdots \delta(\omega-\omega_N)$$

in which, for simplicity, all magnitudes are assumed to be unity. Thus when the magnitudes are all unity the effective bandwidth is

$$\omega_e = \frac{N^2}{N}$$

$$\omega_e = N.$$

This result can hardly be considered valid since the effective bandwidth is totally independent of the frequencies of the sine waves summed.

This difficulty cannot be avoided by assuming that the summed sine waves approximate a continuous function because the spacing and the number of sine waves used are of importance. In order to show this consider another measure of

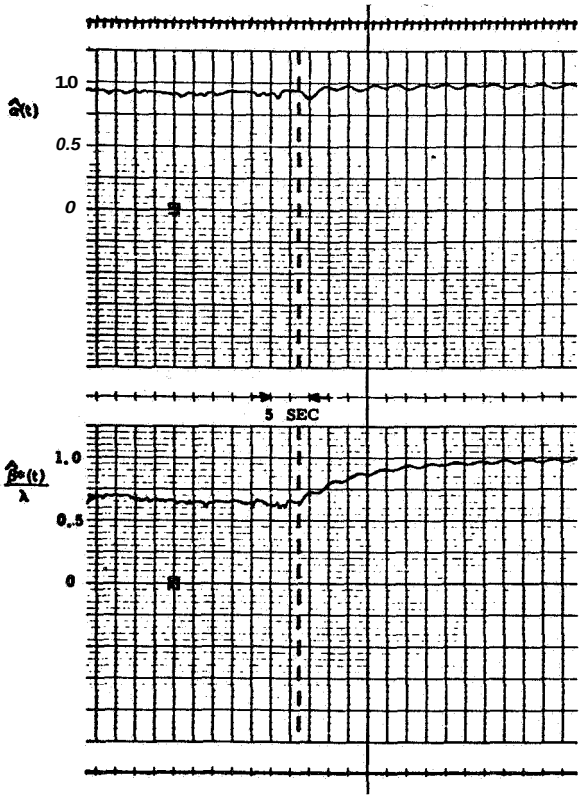

FIGURE 15.—Model parameter response to step change in input signal: 3.14, 3rd to 1.0 rad/sec sine wave,

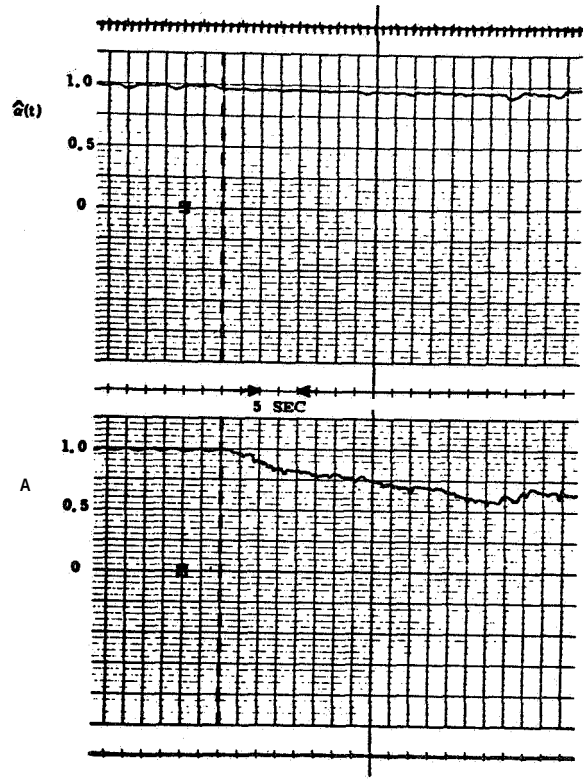

FIGURE 16.—Model parameter response to step change in input signal: 1.0 rad/sec sine wave to 3.14, 3rd.

effective bandwidth. Since the human operator must predict the input signal one time delay ahead the relation between the signal at time t and at time $t+h$ should serve as a useful measure of bandwidth. This number is, of course, the optimal position weighting defined earlier:

$$\alpha = \frac{R(\lambda)}{R(0)}$$

Table 4 shows the effective bandwidths for signals composed of white noise filtered by

$$G(j\omega) = \frac{{\omega_0}^N}{(\omega_0 + j\omega)^N}, \quad N = 1,2,3,4.$$

As can be seen the correlation technique agrees quite well with the other proposed measures. The correlation technique does not give a linear relationship between nominal cutoff frequency and equivalent bandwidth as the others do. See ref. 4 for details.) Figure 17 shows the result of attempting to approximate a rectangular spectrum by summing sinusoids of equal magnitude and random phase. The effective bandwidth, as computed using the correlation technique, is plotted versus the number of sinusoids summed for both equal and logarithmic frequency spacing. The significant observation is that while the effective bandwidth approaches the desired level for equal spacing, it decreases continually for logarithmic spacing. This is due to the concentration of power at low frequencies and sharply points out the possible pitfalls of logarithmic spacing.

TABLE 4.—*Effective Bandwidths as a Function of Nominal CutoffFrequency*

Filter order	Axis crossings	Elkind	Correlation λ = .200
1	1.73 ω_0	3.14 ω_0	2.4 ω_0
2	1.73 ω_0	1.25 ω_0	1.34 ω_0
3	.78 ω_0	0.99 ω_0	0.94 ω_0
4			

The major advantage to using the correlation

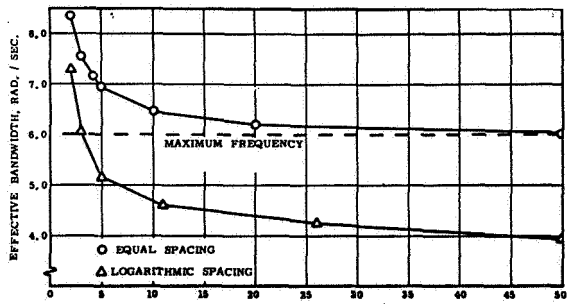

FIGURE 17.—Effective bandwidth vs number of equal amplitude sinusoids summed for different spacing techniques.

technique is that the calculations are easily made given only a time history of the input signal and it is possible to use the recursive estimation procedures outlined earlier to make on-line, quantitative measurements of signal characteristics and changes in signal characteristics.

SUMMARY

For pursuit mode, signal tracking tasks in which the input is low pass filtered white noise it is postulated that the human operator behaves approximately as an optimal predictor attempting to overcome his inherent time delay. Because humans appear to use only position and velocity information the predictor is of the form

$$G(j\omega) = (\alpha + \beta j\omega)e^{-\lambda j\omega}.$$

Test results indicate that the ability to use velocity information decreases with increasing signal velocity indicating a biased estimator of the optimal velocity weighting should be used. A suitable approximation is derived which is equivalent to approximating velocity on the basis of the difference of two successive samples.

A recursive procedure is derived for estimating the position and velocity weighting based on observations of the input signals and applied to an analog simulation. The model thus derived is shown to be a good approximation to human operator steady state behavior and adapts quickly to input signal changes. Since human operators may be very fast in their adaptation the model may not be valid during the transition period.

The model can also be used to track deterministic signals up to approximately the frequency at which human operators would ordinarily begin to track precognitively. The ability of the model to adapt to both random and deterministic signals appears to be a step toward a more general model of tracking behavior.

The optimal position weighting was shown Bo be a simple and convenient measure of effective signal bandwidth.

Since the optimal position weighting is a measure of effective bandwidth, it can be thought of as a measure of signal "coherence". It may be possible to use this measure, perhaps with longer delay times, as an indicator of the sampling rate in a multiaxis task. For example, if an operator is presented with two displays, one consisting of a rapidly moving target and the other consisting of a relatively slow moving target, and asked to track both he must of necessity spend more time observing the faster moving target. Thus an inverse relationship exists between signal coherence and sampling time, and there is a strong likelihood that this relationship could be used for adaptive modelling of this type of system.

The predictive portion of the model could also be used as a signal preprocessor relieving the operator of the burden of prediction and thus reducing his workload, especially in control of systems with delay significantly greater than the operator's.

REFERENCES

1. ANGEL, E. S.; AND BEKEY, G. A.: Adaptive Finite-State Models of Manual Control Systems. IEEE Trans. on Man-Machine Systems, vol. 9, no. 1, Mar. 1968.
2. FOGEL, L. J.; AND MOORE, R. A.: Modelling the Human Operator with Finite State Machines. Fourth Annual NASA-University Conference on Manual Control, Univ. of Mich., Mar. 1968.
3. ELKIND, J. I.: Characteristics of Simple Manual Control Systems. Tech. Rept. No. 111, M.I.T. Lincoln Lab., Apr. 6, 1956.
4. WARE, J. R.: An Input Adaptive, Pursuit Tracking Model of the Human Operator. Ph.D. Thesis, Univ. of Michigan, Ann Arbor, Mich., 1971.
5. KREIFELDT, J. G.: A Sampled-Data Pursuit Tracking Model. IEEE Trans. on Human Factors in Electronics, vol. HFE–6, no. 1, Sept. 1965.
6. TODOSIEV, E. P.; ROSE, R. E.; BEKEY, G. A.; AND WILLIAMS, H. L.: Human Tracking Performance in Uncoupled and Coupled Two-Axis Systems. Rept. 4380–6003–R000, TRW Systems, Dec. 8, 1965.

7. MAGDALENO, R. E.; JEX, H. R.; AND JOHNSON, W. A.: Tracking Quasi-Predictable Displays. Fifth Annual NASA-University Conference on Manual Control, M.I.T., Mar. 1969.
8. MAGDALENO, R.; AND WOLKOVITCH, J.: Performance Criteria for Linear Constant-Coefficient Systems with Random Inputs. ASD-TDR-62470, Jan. 1963.
9. ELKIND, J. I.: A Survey of the Development of Models for the Human Controller. Guidance and Control-11, R. C. Langford and C. J. Mundo eds. Progress in Astronautics and Aeronautics, vol. 13, June 1964.
10. PAPOULIS, A.: Probability, Random Variables, and Stochastic Processes. McGraw-Hill Book Co., 1965.

APPENDIX

OPTIMAL PREDICTION

Suppose $x(t)$ is a real, stationary random process with zero mean whose first derivative exists. That is

(1) $E\{x(t)+\tau)x(t)\} = R_{xx}(t+\tau,t) = R_{xx}(\tau)$
(2) $E\{x(t)\} = 0$
(3) $\frac{d}{dt}(x(t))$ exists.

(Note: since no confusion is possible the subscript xx will be dropped which will greatly simplify notation; i.e., $R(\cdot) = R_{xx}(\cdot)$). Select a and β so that

$$\hat{x}(t+\lambda) = \alpha x(t) + \beta \dot{x}(t)$$

$$= \frac{d}{dt}$$

minimizes

$$\bar{\epsilon}^2 = E((x(t+\lambda) - \hat{x}(t+\lambda))^2\}$$

$$\bar{\epsilon}^2 = E\{(x(t+\lambda) - \alpha x(t) - \beta \dot{x}(t))^2\}.$$

Since the process has zero mean it is possible to apply the orthogonality principle which states, roughly speaking, that in order to minimize mean square error the error vector must be orthogonal to the estimation vectors. Thus the following relationships hold true:

$$E\{(x(t+\lambda) - \alpha x(t) - \beta \dot{x}(t)) x(t)\} = 0 \quad \text{(A.1)}$$

$$E((x(t+\lambda) - \alpha x(t) - \beta \dot{x}(t)) \dot{x}(t)\} = 0 \quad \text{(A.2)}$$

since (see ref. 10)

$$E\{x(t+\tau)\dot{x}(t)\} = -R'(\tau)$$

$$E\{\dot{x}(t+\tau)\dot{x}(t)\} = -R''(\tau)$$

$$' = \frac{d}{d\tau}$$

Equations (A.l) and (A.2) can be simply expressed as

$$R(\lambda) - \alpha R(0) + \beta R'(0) = 0$$

$$-R'(\lambda) - \alpha R'(0) + \beta R''(0) = 0.$$

Since $R(\tau)$ is symmetric and since the derivative $\dot{x}(t)$ exists then

$$R'(0) = 0$$

and the result is the simple relations

$$\alpha = \frac{R(\lambda)}{R(0)}$$

$$\beta = \frac{R'(\lambda)}{R''(0)}.$$

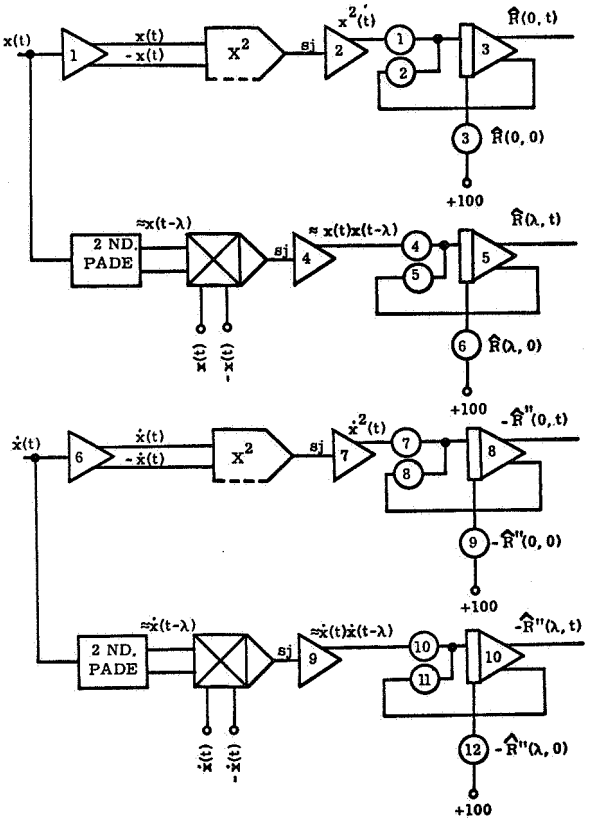

FIGURE A-1.—Circuit for computing estimators of autocorrelation function.

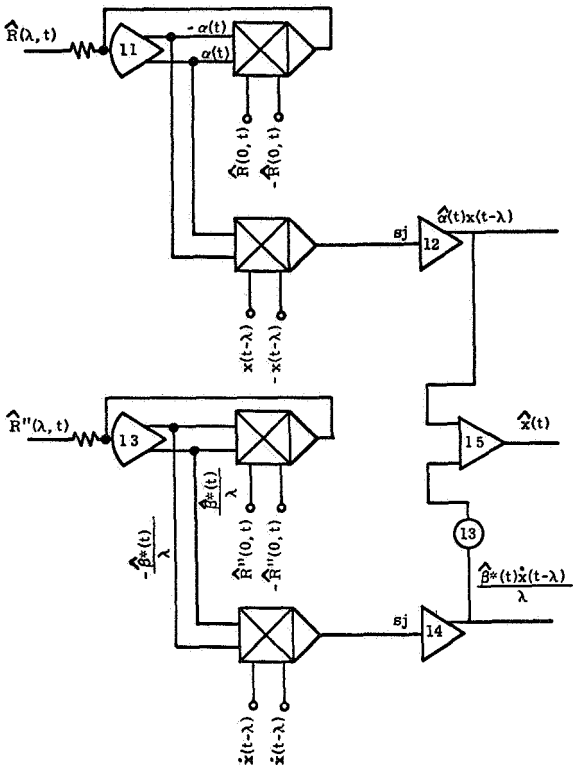

FIGURE A-2.—Circuit for computing position and velocity weighting.

CONTINUOUS ESTIMATION OF AUTOCORRELATION

A very simple method for estimating the autocorrelation function and its derivatives for an analog simulation is given below.

Suppose $x(t)$ is a sample function of a stationary random process. It is easy to show that the output of the simple analog circuit of figure **4** is given by

$$\hat{R}(0,t) = \hat{R}(0,0)e^{-\delta t} + \delta e^{-\delta t}\int_0^t x^2(u)e^{\delta u}\,du.$$

Taking expected values

$$E\{\hat{R}(0,t)\} = \hat{R}(0,0)e^{-\delta t} + \delta e^{-\delta t}E\left\{\int_0^t x^2(u)e^{\delta u}\,du\right\}.$$

On interchanging expectation and integration this becomes

TABLE A-1.—*Suggested Coefficient Settings*

Coefficient device	Setting
1	.3000
2	.1000
3	1.0000
4	.3000
5	.1000
6	1.0000
7	,3000
8	.1000
9	1.0000
10	.3000
11	.1000
12	1.0000
13	.2000

$$E\{\hat{R}(0,t)\} = \hat{R}(0,0)e^{-\delta t} + \delta e^{-\delta t}\int_0^t E\{x^2(u)\}e^{\delta u}\,du$$

$$E\{\hat{R}(0,t)\} = \hat{R}(0,0)e^{-\delta t} + R(0)[1-e^{-\delta t}]$$

$$\lim_{t\to\infty} E\{\hat{R}(0,t)\} = R(0).$$

In a similar manner it is possible to find simple analog circuits (fig. A.1) for estimating the other necessary values of the autocorrelation function and its derivatives. (N.B. All amplifiers are bi-polar.) These will yield the equations given below:

$$\hat{R}(\lambda,t) = \hat{R}(\lambda,0)e^{-\delta t} + \delta e^{-\delta t}\int_0^t x(u)x(u-\lambda)e^{\delta u}\,du$$

$$\hat{R}''(\lambda,t) = \hat{R}''(\lambda,0)e^{-\delta t} - \delta e^{-\delta t}\int_0^t \dot{x}(u)\dot{x}(u-\lambda)e^{\delta u}\,du$$

$$\hat{R}''(0,t) = \hat{R}''(0,0)e^{-\delta t} - \delta e^{-\delta t}\int_0^t x^2(u)e^{\delta u}\,du.$$

These are used to form estimators of α and β by forming:

$$\hat{\alpha}(t) = \frac{\hat{R}(\lambda,t)}{\hat{R}(0,t)} \qquad \frac{\hat{\beta}^*(t)}{\lambda} - \frac{\hat{R}''(\lambda,t)}{\hat{R}''(0,t)}$$

Figure **A.2** is a circuit diagram for computing position and velocity weighting.

Table **A-1** gives suggested coefficient settings.

5. A Hybrid Computer Program for the Visual Display of Compensatory System Model Parameters*

GLENN A. JACKSON AND GERALD BRABANT

Oakland University

A hybrid computer identification program has been developed which determines and displays those parameter values of a model of the compensatory control system that existed over the last fifteen seconds of operation. These values are up-dated every 0.05 sec so that a visual display of the parameters appears to be continuous. Presently, a closed loop crossover model is being used as the compensatory system model with the parameters K and τ displayed, however, any suitable model could be used in its place.

INTRODUCTION

The hydrid computer program discussed in this paper is the outgrowth of research that is dedicated to the development of a system that will meet two main specifications:

(1) Develop a parameter identification method that will quickly and accurately identify the parameters of a compensatory control system model using only short lengths of input-output data from the compensatory system under test.

(2) Convert this method into an on-line system that will continuously display to the operator the average values of his associated compensatory system model. These average values should again be calculated over as short a time span as possible so that the display will indicate to the operator essentially his present parameter state. The hybrid computer method developed, referred to as "hybrid parameter tracking" (ref. 1), satisfies both of these specifications.

Parameter identification via hybrid parameter tracking is accomplished by using short lengths of sampled input-output data from the compensatory system. These data, ≤ 15 sec in length, are used repetetively as the driving signals for a fast-time analog continuous parameter tracking system utilizing the crossover model (refs. 1 and 2). Since only 5 to 10 iterations of these data are required for parameter convergence, and since each iteration requires only 0.05 sec, parameter identification is achieved less than half a second after the data are taken. In addition, once started, the program continues sampling the compensatory system input-output signals, while simultaneously iterating these data through the continuous parameter tracking system.

The final result is that every 0.05 sec new values of the crossover model parameters, K and τ, are calculated and displayed with each calculation using only the last 15 sec of compensatory system data. The visual display is thus a running record of the K and τ values that existed over the last 15 sec of operation.

A BRIEF DESCRIPTION OF THE PROGRAM

A simplified block diagram of the overall hybrid system is given in figure 1. In this figure only main signal lines are shown. All sense lines and control lines have been omitted for simplicity of presentation.

The basic operation of the system is as follows:

(1) The compensatory system input and output signals, $r(t)$ and $c(t)$, are sampled via ADC's

* This research was supported by NASA contract NGR 23-054-003.

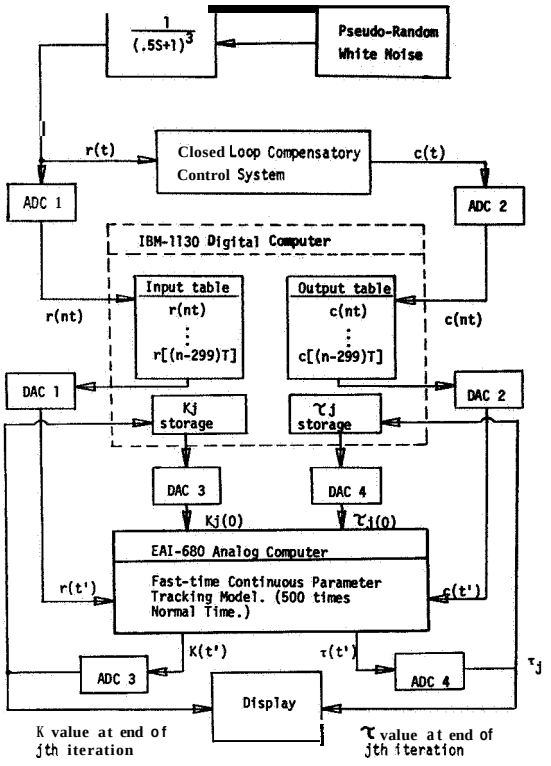

FIGURE 1.—Simplified block diagram of the identification system.

1 and 2 at a rate of 20 samples/sec with the samples stored alternately in a 600 word table in digital core.

(2) After 600 samples have been taken (300 samples of both $r(t)$ and $c(t)$), and before the 301st samples of $r(t)$ and $c(t)$ arrive, the sampled input and output values are fed via DAC's 1 and 2 into a fast-time analog continuous parameter tracking identification system. The analog time scale is 500 times normal time. At the end of this fast-time run three things occur:

(a) The parameter values present at the end of the run are recorded using ADC's 3 and 4. These values are stored so they can be analyzed later; sent to the visual display; and also used as initial conditions for the next fast-time analog iteration.

(b) The 600 values in the input-output table are moved down two words in core. This eliminates the first samples of $r(t)$ and $c(t)$ that were taken, and provides room for the next samples to be taken. In addition, the gradient gains on the K and τ integrators of the continuous parameter tracking system are adjusted. These gains are reduced systematically for five iterations and then recycled back to their initial values. This is done to ensure that a short length of high remnant data will not cause the continuous parameter tracking system to go unstable.

(c) The system waits for the next samples of $r(t)$ and $c(t)$ to arrive.

(3) At $t = 15.05$ sec the 301st samples of $r(t)$ and $c(t)$ are taken and placed in the 600 word table. The program returns immediately to (2) above, and the next fast-time identification run begins.

The timing sequence used during a single period of operation is given in figure 2, with the timing intervals labeled to correspond to the word descriptions given above. In this figure it is assumed that the system has been in operation for at least 15 sec. Figure 3 presents the general functional level flow diagram of the system.

TESTS IDENTIFYING A KNOWN CROSSOVER MODEL WITH STEP CHANGES IN K AND τ

To check the accuracy and transient response of the identification method, three tests were run using a known model in place of the normal compensatory system. A crossover model with nominal values of $K_0 = 3.8$ and $\tau_0 = 0.235$ was used. The input signal $r(t)$ was pseudo random gaussian white noise passed through a third order low pass filter of the form $1/(\frac{1}{2}s+1)^3$. After the identification system was on-line, step changes

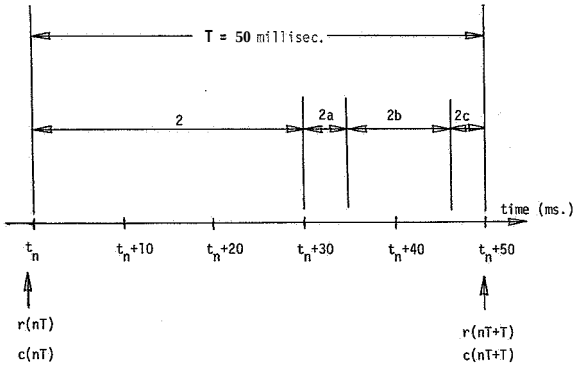

FIGURE 2.—Timing sequence for a single iteration.

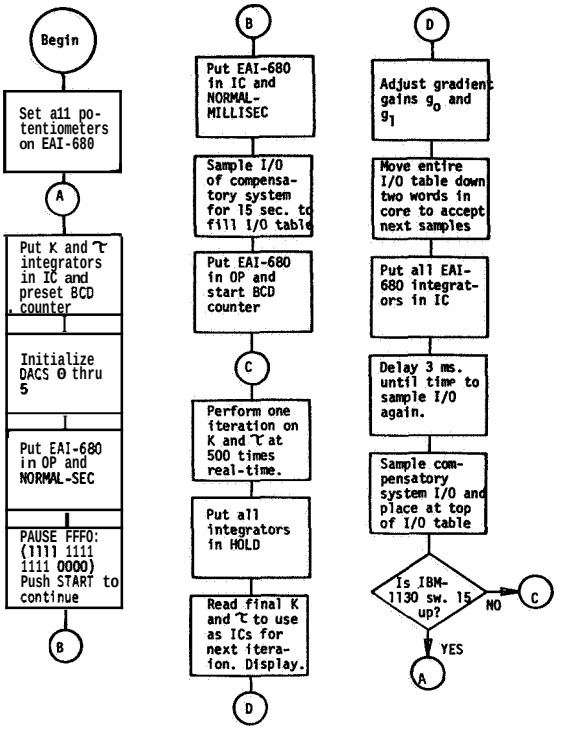

FIGURE 3.—Functional level flow chart for the hybrid parameter tracking program.

in K_0 and τ_0 were made in the known model, and the resulting identified values were recorded.

Figure 4 shows the response to a step change in K_0 from 3.8 to 4.8 with τ_0 held fixed at 0.235. The total transient response time is seen to be 15 sec, which is the time it takes for the 600 word data table to be converted from "$K=3.8$ data" to "$K=4.8$ data." Figure 5 shows the response to a step change in τ_0 from 0.235 to 0.285 with K_0 held fixed at 3.8. Again, the response time is 15 sec, as expected. Figure 6 shows the system response to simultaneous step changes in both K_0 and τ_0. The responses are similar to those found following individual step changes in K_0 or τ_0. It can be seen that in these particular cases, the determination of one parameter was relatively independent of the other. This is undoubtedly not always the case.

TESTS ON HUMAN OPERATORS

Following the tests on a known model, the hybrid parameter tracker was evaluated on a standard compensatory control system. The com-

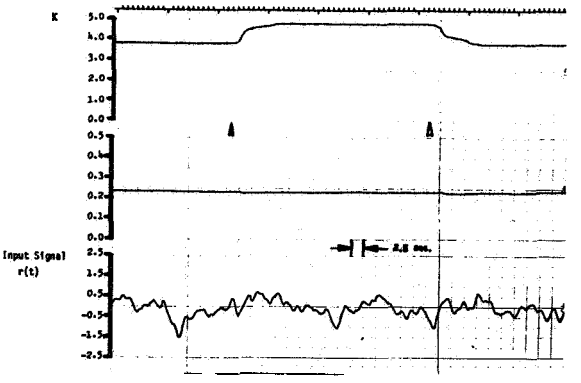

FIGURE 4.—τ_0 held at 0.235 while K_0 is step changed between 3.8 and 4.8.

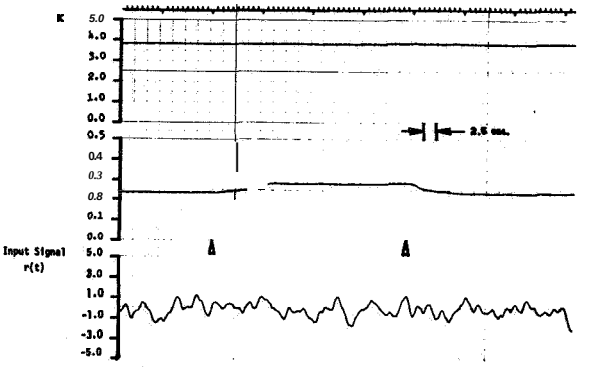

FIGURE 5 - K_0 Held At 3.8 While τ_0 is STEP Changed Between .235 and .285

FIGURE 5.—K_0 held at 3.8 while τ_0 is step changed between 0.235 and 0.285.

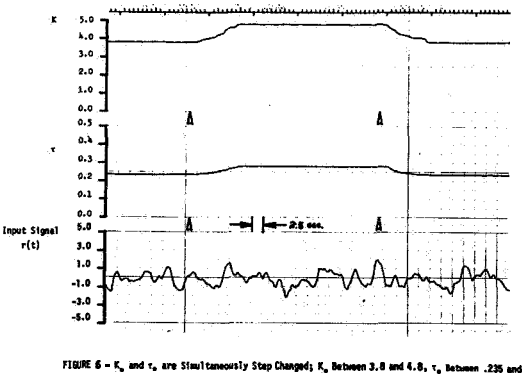

FIGURE 6 - K_0 and τ_0 are Simultaneously Step Changed; K_0 Between 3.8 and 4.8, τ_0 Between .235 and .285

FIGURE 6.—K_0 and τ_0 are simultaneously step changed; K_0 between 3.8 and 4.8, τ_0 between 0.235 and 0.285.

pensatory system used an arm movement control stick, a k/s plant, and the same $1/(\frac{1}{2}s+1)^3$ filter that was used on the known model. The main point of concern prior to the running of these tests was the distinct possibility that remnant would cause high variability in the K and τ values being identified and displayed. Fortunately, these fears appear to have been unwarranbed, at least when data lengths of 15 sec are used.

Figure 7 is a typical section of data found while identifying an untrained subject. Figure 8, on the other hand, is a similar section of data obtained from a subject who had some previous tracking experience. In both cases the variability of K and τ was not large enough to degrade the visual display by any significant amount. As expected, parameter variability was greater in the untrained case (ref. 3).

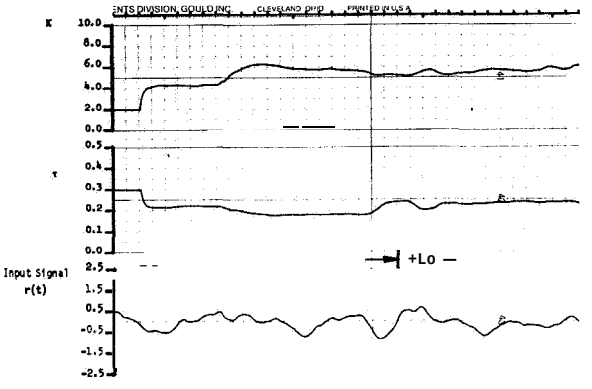

FIGURE 7.—Hybrid parameter identification of an untrained human operator.

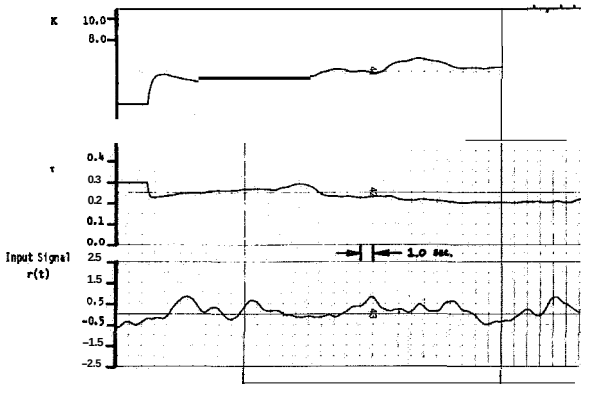

FIGURE 8.—Hybrid parameter identification of a trained human operator.

CONCLUSIONS

The hybrid parameter tracking identification method has been shown to accurately identify crossover model parameters using input-output data only 15 sec in length. Theoretical analysis indicates that with an input filter of the form $1/(\frac{1}{2}s+1)^3$ the method should be successful using data only 7 sec long (ref. 1). This has not been tried to date. However, since the identification time, even in the present state, is relatively short when compared to the times required by other identification methods, several specific uses for the method are proposed.

(1) The method can be used as a test device to display to the human operator his present parameter state. In this manner several interesting experiments could be run: Can the operator alter his parameters on command? Can he learn his tracking task more quickly by monitoring his progress? Can he reduce parameter variability? Can he reduce remnant by reducing parameter variability? Can he adjust K and τ in some specified optimum sense?

(2) The method can be used as a data analysis device to determine the correlation between short-term parameter variability and other pertinent system variables: How does the variance of the short-term average parameter values change with practice? How does it vary between subjects? Is parameter variability a function of parameter magnitude? Is it directly related to remnant? Is it related to the plant being controlled? Some of these questions will be investigated during the coming year.

To date only a limited amount of human operator testing has been completed using the hybrid parameter tracking technique. Thus, no firm statements concerning its utility can be made at this time. However, it has the potential of becoming a valuable tool in the measurement of human performance.

NOTE ON COMPUTATION

The hybrid facility used in evaluating the hybrid parameter tracking method consists of an

IBM 1130 digital computer, an EAI **680** analog computer and an EAI **693** interface package. The digital program was written in Assembler language.

REFERENCES

1. JACKSON, G. A.: An Investigation of Two Hybrid Computer Identification Techniques for Use in Manual Control Research. Final Report on NASA/ERC contract No. NGR 23–054-003, vol. II, June 30, 1970.
2. JACKSON, G. A.: A Method for the Direct Measurement of Crossover Model Parameters. IEEE Transactions on Man-Machine Systems, vol. MMS–IO, no. 1, Mar. 1969, pp. 27–33.
3. BURGETT, A. L.: A Study of the Variability of Human Operator Performance Based on the Crossover Model. Fifth Annual Manual Control Conference, Mar. 27–29, 1969.

6. Input Noise Approximations in Tracker Modeling*

PAUL F. TORREY AND RUSSELL A. HANNEN

Wright-Patterson Air Force Base

INTRODUCTION AND RESULTS

This study was conducted to investigate the validity of approximating random Gaussian-distributed inputs used in human response modeling by sums of discrete sinewaves. An ideal rectangular power density spectrum was simulated using both filtered Gaussian white noise (Butterworth Filter) and sums-of-discrete sinewaves spaced as in reference 1. These two input spectrums were used with three different input cutoff frequencies ($\omega_i = 1.5$, 2.5, and **4.0** rad/sec) in the same compensatory tracking task ($Y_c = K/j\omega$) and the resultant normalized tracking error (NTE) and qualitative operator observations to investigate the apparent discrepancies in human operator characteristics. A block diagram of the experimental setup is shown in figure 1. A comparison of normalized tracking error and input cutoff frequency is given in figure 2 for the discrete and continuous spectra. An analysis of variance was performed at each input cutoff frequency ($\omega_i = 1.5$, 2.5, and **4.0** rad/sec) to determine if the differences were statistically significant. The results of the analysis of variance based on a confidence level of 0.95 show that the discrete and continuous spectra are statistically similar at the two lower breakpoints but there is a statistically significant difference at $\omega_i = 4.0$ rad/sec.

There are at least two explanations that can be offered for the differences in response at **4.0** rad/sec. The first is that the Butterworth filter is not a perfect approximation of the ideal rectangular spectra and thus there is power in the crossover region. The second explanation is based

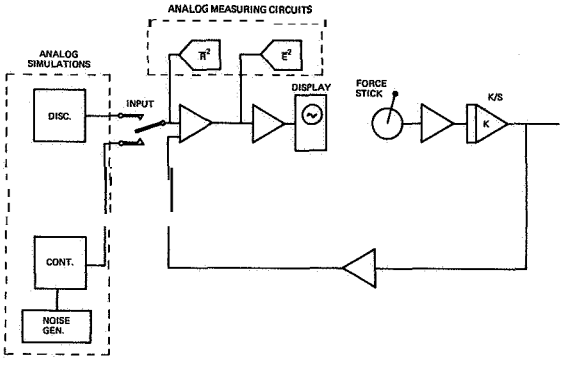

FIGURE 1.—Analog computer simulation: compensatory tracking task.

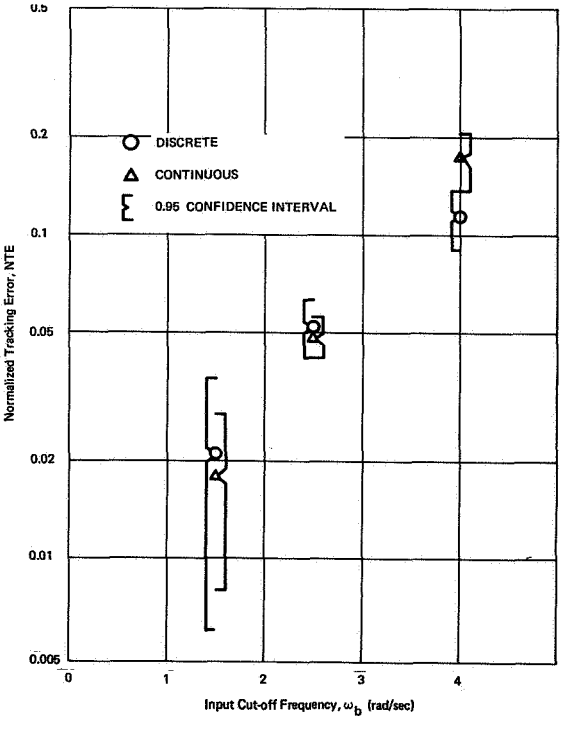

FIGURE 2.—Comparison of NTE: discrete vs continuous rectangular input spectra.

* The work described herein is the M.S. thesis work of Paul F. Torrey (ref. 4).

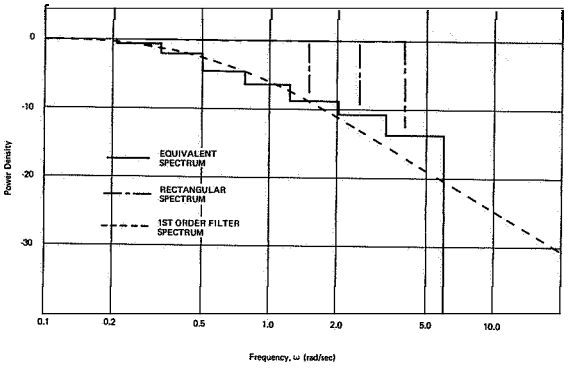

FIGURE 3.—Equivalent power density spectrum for discrete rectangular input.

on the logarithmic frequency distribution of the discrete sinewaves. As shown in figure **3** the equivalent spectrum of the discrete spectrum and the first order filter spectrum are approximately the same. Thus, there may be a better filter than the eighth order Butterworth filter for the continuous input.

To support these explanations and to validate these results with other research efforts, we compared the normalized tracking error and normalized crossover frequency for the three input cutoff frequencies (w_c = 1.5, 2.5, and 4.0 rad/sec). Figure **4** is a plot of NTE vs $\tau_e\omega_c$ where the solid lines are calculated for a continuous rectangular input spectrum. Data from references 1 and **2** as well as parameter track data obtained in this study are also displayed in figure **4.** Figure 5 is a plot of NTE vs $\tau_e\omega_c$ where the solid lines are calculated for a continuous first order filter spectrum. Again data from references 1 and 2 as well as parameter track data obtained in the present study is presented in figure 5. Note the good correspondence between the reference 2 and **3** data and the data taken in this study with the dashed line on figure 5. The dashed line is the loci of minimum points for NTE vs $\tau_e\omega_c$ and is the loci of operating points predicted in references **1** and **3.**

CONCLUSIONS

There is a statistical difference in the tracking behavior at the 4.0 rad/sec cutoff frequency between the filtered Gaussian white noise inputs and sums-of-discrete sinewaves inputs. Based on

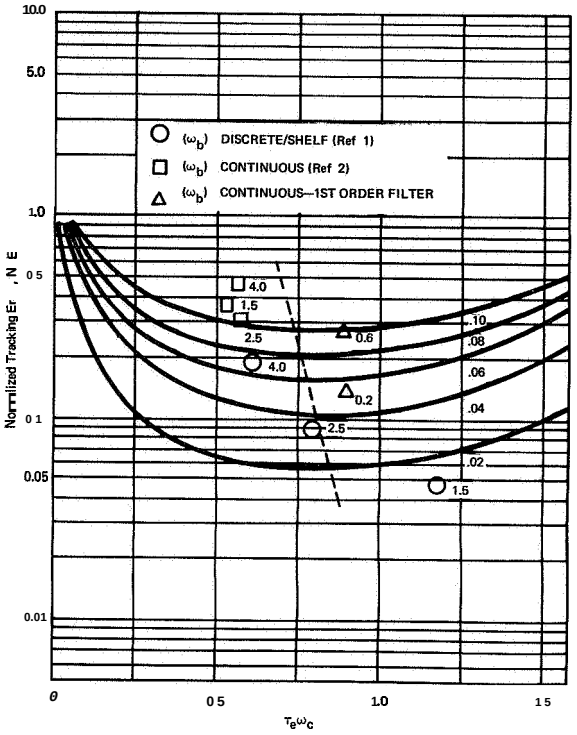

FIGURE 4.—NTE vs $\tau_e\omega_c$: rectangular input spectrum (from ref. **1).**

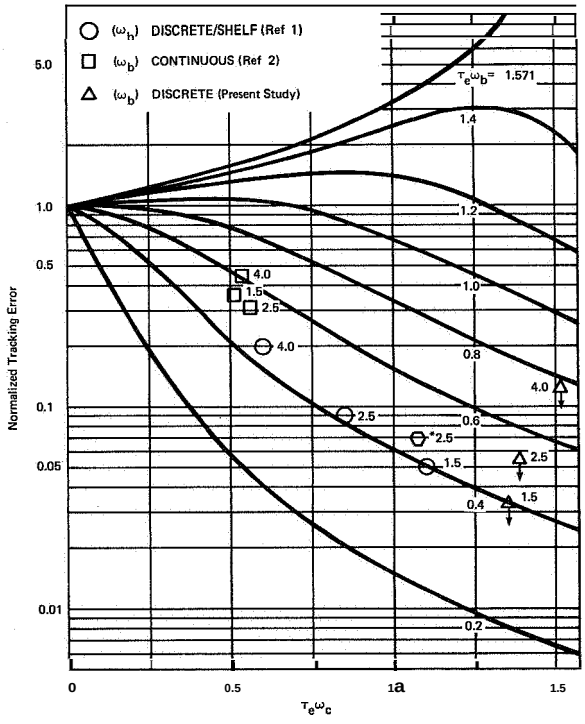

FIGURE 5.—NTE vs $\tau_e\omega_c$: first **order** filter input spectrum.

tracking behavior data from other investigations and data gathered in this study it was found that the discrete and continuous input tracking data compared favorably when the power in the crossover region was taken into account. Any power in the crossover region has a pronounced effect on pilot parameters. The best correspondence between discrete and continuous input tracker behavior was found using a continuous input with a first order filter.

REFERENCES

1. McRuer, Duane T.; et al.: Human Pilot Dynamics in Compensatory Systems. AFFDLTR–65–15. Research and Technology Div., Air Force Systems Command, Wright-Patterson Air Force Base, July 1965.
2. Gordon-Smith, Michael: An Investigation into Certain Aspects of the Describing Function of a Human Operator Controlling a System of One Degree of Freedom. UTIAS Rept. no. 149, Univ. of Toronto Institute of Aerospace Studies, Toronto, Feb 1970.
3. Heifferon, John *C.:* The Effects of Input Power Spectra on Human Operator Compensatory Tracking. Master's Thesis, Department of Electrical Engineering, Air Force Institute of Technology, Wright-Patterson Air Force Base, Mar. 1970.
4. Torrey, Paul F.: Investigation of Input Noise Approximations on Human Response Modeling. Masters Thesis, Department of Electrical Engineering, Air Force Institute of Technology, Wright-Patterson Air Force Base, June 1971.

7. Digital Modeling of Human Operator Dynamics Via a Class of Liapunov Functions*

RALPH MEKEL AND PATRICK PERUO, JR.

The City College of The City University of New York

This paper describes a technique which is utilized for modeling human operator dynamics. The technique is based upon a model-reference system configuration and a class of Liapunov functions formulated for this purpose. Since human operator characteristics change with changes in environment as well as with variable processes within the operator himself, it is therefore desirable that the class of Liapunov functions with their time derivatives also possess variable characteristics. It is shown in this paper how such a class of Liapunov functions and their time derivatives is formulated. The crux of the formulation lies in three variable positive definite matrices used for the construction of the class of Liapunov functions. The form and order of these matrices depend upon the form and order of the error differential equation of the human operator model-reference system. These matrices can be modified to include nonlinear functions of the human operator model.

The purpose of this study is to synthesize a controller dedicated to identify parameter variations and provide corrective dynamics to the mathematical model of the human operator. In order to describe briefly the modeling technique, consider the human operator model-reference system depicted in figure **1.** The mathematical model system is described by the vector differential equation

$$\dot{\underline{x}} = B\underline{x} + C\underline{r} \tag{1}$$

where $\underline{x}$ is the model's output state vector, $\dot{\underline{x}} = d\underline{x}/dt$ and r is the input vector. The square matrices B and C consist of zeros, ones and the postulated parameters of the model system including parameter variations. It is assumed that the reference system is a human operator whose response due to an input $\underline{r}$ can be obtained experimentally. The output vector of the human operator is denoted by $\underline{z}$. The difference between the mathematical model output and the human operator output is the model-reference system error and is denoted by vector $\underline{e}$. The error differential equation is given by

$$\dot{\underline{e}} = A\underline{e} + \underline{b}\underline{u}^T(\underline{e}+\underline{z}) + \underline{d}\underline{w}^T\underline{r} \tag{2}$$

where $\dot{\underline{e}} = d\underline{e}/dt$ and A is a square matrix consisting of zeros, ones and the postulated nominal values of the model parameters. It is the B matrix without the parameter variations. The controller outputs are denoted by vectors $\underline{u}$ and $\underline{w}$. These vectors when modified by the vectors $\underline{b}$ and $\underline{d}$ provide the corrective dynamics for the postulated parameters in the mathematical model. Note that the superscript T denotes the transpose.

The Liapunov function and its time derivative, denoted by V and $\dot{V}$ respectively, have the forms

$$V = \underline{e}^T M\underline{e} + \underline{u}^T N\underline{u} + \underline{w}^T Q\underline{w} \tag{3}$$

and

$$\dot{V} = -\underline{e}^T D\underline{e} + 2[\underline{\dot{u}}^T N + (\underline{e}+\underline{z})^T(\underline{b}^T M\underline{e})]\underline{u} + 2[\underline{\dot{w}}^T Q + \underline{r}^T(\underline{d}^T M\underline{e})]\underline{w} \tag{4}$$

where

$$D = (A^T M + MA + \dot{M}). \tag{5}$$

One way to comply with Liapunov's criterion for stability is to constrain the elements of the D matrix, denoted by d_{ii} and d_{ij}, to satisfy the conditions

$$d_{ii} \geq 0 \tag{6}$$

* This research is supported by NASA-Langley Research Center grant NGR-33-013-053.

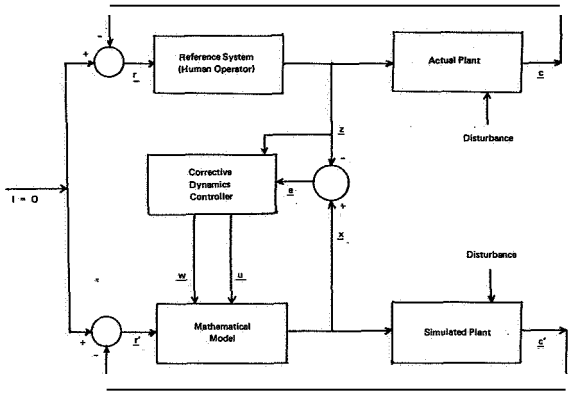

FIGURE 1.—Block diagram of the model-reference system.

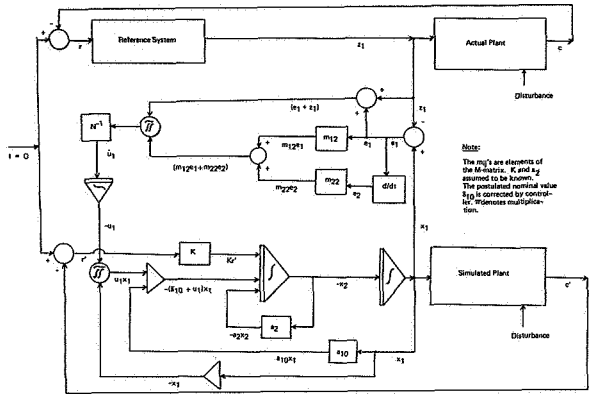

FIGURE 2.—Controller structure which provides corrective dynamics for a second-order mathematical model.

and

$$d_{ij}+d_{ji}=\mathbf{0} \tag{7}$$

where i and j denote row and column respectively and let

$$\dot{\underline{u}}=-N^{-1}(\underline{e}+\underline{z})(\underline{b}^{T}M\underline{e}) \tag{8}$$

and

$$\dot{\underline{w}}=-Q^{-1}\underline{r}(\underline{d}^{T}M\underline{e}). \tag{9}$$

The conditions given by equations (6) and (7) permit the evaluation of the elements in the D and M matrices in terms of the mathematical model's nominal parameters. At this point a test is performed to insure the positive definiteness of these matrices. Matrices N and Q must satisfy the condition $N>0$, $Q>\mathbf{0}$ and are design parameter matrices at the discretion of the investigator. Equations **(8)** and (9), when integrated and modified by vectors $\underline{b}$ and $\underline{d}$ respectively, provide the corrective dynamics for the postulated mathematical model of the human operator.

A very useful feature of this study is the development of a digital computer program which is easily implemented and modified concurrent with experimentation. In this way the modeling process interacts with the experimentation process in a mutually beneficial way. It is the systematic and logical use of the digital computer that permits one to effectively apply the class of Liapunov functions to the modeling of the human operator.

An illustrative example shown in figure 2 describes a controller structure which provides corrective dynamics to a second order mathematical model.

ACKNOWLEDGMENT

The first author wishes to thank James J. Adams, NASA-Langley Research Center, for experimental data and useful discussions.

SESSION II

EXTENSIONS OF MANUAL CONTROL THEORY

Chairman: JOHN **LYMAN**

8. Considerations for the Design of an Onboard Air Traffic Situation Display*

R. E. ANDERSON, R. E. CURRY, H. G. WEISS, R. W. SIMPSON
M. E. CONNELLY, AND T. IMRICH

Massachusetts Institute of Technology

INTRODUCTION AND SYSTEM DESCRIPTION

Major changes in the air traffic control (ATC) environment will occur during the coming decade as the result of increased automation, improvements to the beacon and radar surveillance systems and upgrading of the runways and taxiways at the major airports. The introduction of computers and improved displays into the 20 enroute air traffic control centers and the implementation of the automated radar terminal system (ARTS) at the major airports, coupled with a steady increase in data link communications will contribute to the more effective utilization of airspace. This automation will substantially aid the controllers by improving the processing of the surveillance and flight data, by providing electronic identity and altitude labels on the display scopes and by assisting in the sequencing and flow control process. In addition, area navigation and the curved path microwave landing system will make it possible to feed more traffic into those airports which are upgraded with parallel runways and high-speed turnoffs.

To most effectively capitalize on this advanced capability and fully utilize the limited facilities at an airport, it will be increasingly important to more tightly couple the controller and the pilot. The flow of information to pilots should include a means of understanding the intentions of the controller in addition to the specific real-time commands. Various types of data links have been proposed for this function, ranging in capability from a simple readout display for replacing the voice channel, to an advanced system which would automatically transfer instructions from the ground computer directly into the aircraft flight director. With this latter mode of operation, the controller and the pilot would monitor all operations and intervene when appropriate.

The underlying concept in these systems is to provide an effective command-response relationship between the controller and his supporting computer and the pilot and his avionics. This concept is a logical extension of the current practice of vectoring aircraft and is deeply embedded in the historical development of air traffic control. The extensive use of vectoring is viewed as an essential yet undesirable change from the clearance-response relationship which still exists throughout the majority of a flight, during which pilots are cleared to execute a flight plan and do so with little communication with the ground system.

Advances in technology have now made it reasonable to question if the command-response relationship between controllers and pilots in congested terminal areas is either necessary or in fact beneficial. Computers are now capable of generating flight routes from runway to runway which are conflict-free of other controlled aircraft. It is also feasible to present to pilots a display of all pertinent air traffic, controlled and uncontrolled. The combination of these new capabilities with an appropriate data link now permits a safe return to the clearance-response relationship

* This describes a portion of the work on traffic situation displays being performed jointly by the Lincoln Laboratory, Electronic Systems Laboratory, Flight Transportation Laboratory, and Man-Vehicle Laboratory at MIT.

throughout a flight, while retaining or enhancing the increased capability provided by the other new equipment being developed.

About 18 months ago, it became apparent to the ATC group at Lincoln Laboratory that as a result of recent advances in airborne computers, digital data links, and computer-driven CRT display technology, it was technically feasible to provide a system in the aircraft that would enable the pilot to have access to the NAS/ARTS data base. The ARTS data base will, at a future date, include flight routes in **4–D** in addition to the traffic data. Furthermore, since the pilot would be only interested in the segment of NAS/ARTS data on his flight route, it seemed that it could probably be assimilated by a busy aircrew.

The basic concept of remoting information to the cockpit is not new. It was explored in TELERAN (1966), RATCA (1963), and televised radar **(1966).** However, the important difference between these early systems and the system now proposed is that currently available technology permits only data of interest to each particular aircraft to be automatically selected and presented. In addition, the traffic data will be more adequately processed by the ground computer and target altitude information will be available.

Our studies indicate that a high-quality replica of a selected segment of a controller's scope could be relayed over a narrow-band digital data link and that this data could be integrated with aircraft heading and navigation information to provide the pilot with a display which would be useful in congested air space. The ability to employ small airborne computers enormously increases the display flexibility and this factor coupled with the improved quality of the NAS/ARTS computer-processed data should enhance the operational utility of the system. The display might include alphanumeric symbols, air route maps, and controller instructions.

Since the terminal area problem is most severe from the traffic management standpoint, we have investigated the task of remoting ARTS data into the cockpit. There are many variations of the basic concept which are technically feasible, but the scheme which appears most practical is the class of system (fig. **1)** which broadcasts all of the pertinent information on a common channel.

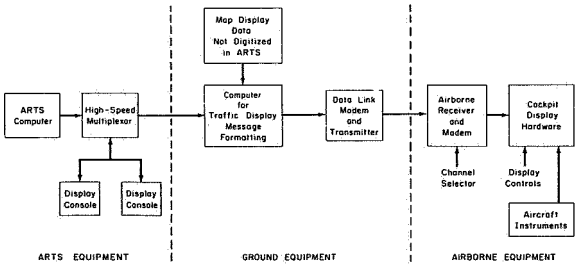

FIGURE 1.—Traffic display system block diagram.

Using available technology, traffic information in a **64** by **64** mile sector of air space would be digitized and transmitted once every few seconds over a narrow-band VHF channel. The digital data stream would contain the identity, geographical coordinates, altitude, ground speed, and heading of each aircraft. The airborne computer would select the identity code of its own aircraft from the common stream and would thereby obtain its position coordinates and altitude as observed by the ARTS ground facility. The pilot could select the range and altitude band which he wished to have displayed and only those targets in the selected categories and navigation reference fixed would appear on the display.

This type of data link has a number of attractive features. It provides to the pilot information on all aircraft which are under ground surveillance either by beacon or radar and it presents the information to him in the same frame of reference as is being observed by the ground controller. The pilot can quickly confirm if his air-derived flight information agrees with the ARTS data. The controller can quickly and precisely send instructions to one or a limited number of aircraft in a form which is both quantitatively and readily interpretable. This could be accomplished through the use of a light pen or keyboard to issue commands or to show graphically vectors indicating the flight route to be followed. This information would be available simultaneously to all aircraft in the system. The controller monitoring the information could rapidly sense if the aircraft was obeying commands. Similarly the aircraft could observe his performance with respect to the ground navigation fixes and his nearby neighbors.

THE IMPACT OF THE TSD ON THE ATC SYSTEM

Traffic Situation Display (TSD) and the present ATC system.—The provision of better information in the cockpit can be used in many ways. It is not necessary to associate either centralized or distributed management concepts with the existence of the traffic situation display on board the aircraft. The congruency of the information available to the pilot and his ATC controller allows the pilot to understand the traffic situation and the commands that a controller is issuing to him and to other aircraft. The pilot can assist the controller by anticipating his commands, and reacting more quickly, or at a proper rate to achieve the ATC controller's intentions. He can also make small or minor corrections to maintain a desired traffic situation such as following another aircraft in trail at a given distance. Thus without any change in present ATC procedures, it is likely that the traffic would flow easier and that the ATC controller's workload would be reduced.

Reduction of A*TC* separation standards.—The most important benefits that a TSD can bring lie in achieving a reduction in the present IFR separation standards. By tightening the control over aircraft separations through including the pilot as a monitor and active control agent, it would seem to be possible to demonstrate reduced standards at higher levels of safety than the present system offers.

The basic aircraft separation of three miles is partially based on time delays between controller observance of a situation and the initiation of target response. With the pilot in the loop observing the separation, this time delay is much reduced through avoiding communications delays on a busy radio channel. When the separation is small, but the gap is widening the pilot can be assured of safety, and will be confident of allowing a much smaller separation to occur.

Examples of traffic situations where improved information offered by the TSD are

(1) Airborne separations in the departure area between successive takeoff aircraft, or between a missed approach and a preceding departure. Here both the relative position and present altitude of the preceding target can be seen by the following aircraft which can ensure that the separation is positive and increasing.

(2) Air to ground separations between an aircraft on approach and aircraft landing or taking off on the runway. If beacon information is available for surface targets, the pilot will be able to monitor runway occupancy and progress towards clearing the runway, and to call his own missed approach if necessary. The present 2 mile requirement for a takeoff in front of an approach could be greatly reduced, and would depend upon the departure standards established in **(1)** above.

(3) Separation standards for approaches on parallel runways could be reduced because of pilot monitoring of the joining procedures at different altitudes and the ability of the pilots to coordinate their longitudinal position relative to approach aircraft on the other runway. In the event of a blunder, a pilot would see aircraft from the parallel approach wandering into his approach zone and could initiate corrective action much earlier.

Change of ATC procedures.—There are a number of procedures which one can envisage for an ATC system which has targets with TSD capabilities. Aircraft could be commanded to follow another aircraft in trail at a given distance simplifying control commands for a string of aircraft, although this raises the question of string stability. An IFR spacing pattern similar to the VFR square landing pattern can be established where pilots are responsible for their final spacing on landing for a sequence established by the ground controller. Successive aircraft on standard, instrument departures could be commanded to maintain "1000 ft below" separation during climbout until lateral radar separation is established by the controller. Similar instruction could be issued for arrival aircraft where the following aircraft on descent track "1000 ft above" the preceding aircraft.

At crossing points, aircraft with a TSD could be issued altitude clearances conditioned upon passage of other traffic, e.g., "clearance below *X* thousand feet after observing passage of target *Y* at crossing point. Report starting descent." Thus a controller could set up in advance a control action to be initiated by the pilot after the traffic situation has resolved itself.

Introduction of guidance commands.—ATC in-

structions for guidance of targets which are generated on the ground by a controller or computer can be displayed to the pilot on the TSD. There are various concepts and situations where one can envisage such usage in the terminal area.

The desired position for a target to achieve a landing slot can be displayed as a "bucket" along arrival routings and onto final approach. Speed commands and speed changes could be issued such as to achieve metering into the terminal area and rough final spacings.

Alternatively, the "time to turn" command could be counted down on the TSD to avoid a radio transmission by the ground. The inbound vector and desired speed would also be displayed. Elimination of this transmission delay would improve the accuracy of the "time to turn" process.

The scheduling of "buckets" for the runway system would allow setting up staggered spacings for parallel runway operations, and would open up the possibility of operating coordinated landings on crossing runway systems. This would allow substantial increases in IFR operating capacities at certain airports, and certain wind conditions.

From the above, it is clear that a potential exists for a number of new and beneficial applications which would be possible if a substantial portion of the air traffic were to be equipped with a TSD. There is a need for simulation of these concepts, and a detailed analysis of possible new procedures to establish the value in proceeding further with this line of ATC development.

THE IMPACT OF THE TSD IN THE COCKPIT

Normal operations.—At present, pilots construct a mental image of the traffic environment from information received through radio communications, visual scanning for other traffic, knowledge of standard procedures and previous experience. A pictorial situation display provides this traffic information to the pilot at a glance. The uncertainty and ambiguity associated with mentally synthesizing a time varying traffic situation is largely eliminated. A TSD provides a continuous display of information with predictable quality. Unlike the information received from present sources, data from a TSD are available whenever a pilot needs it. Both pilot and controller responses can be based on information received through a common data base.

The information transfer process between controller and pilot is more efficient. Controller instructions can be simplified and abbreviated without sacrificing message content. Messages of advisory nature may often be eliminated (such as transmitting spacing advisories to traffic following in trail or giving reasons for speed changes, etc.). With a TSD pilots will be able to see more clearly the reason for clearances which are being issued to their own aircraft and other aircraft, and a means will be provided to independently cross-check the validity of a clearance. Because of advanced cues provided by a TSD, a crew can plan ahead and make better decisions. Flap schedules, pressurization regulation, and other items related to aircraft management can be more appropriately timed. Response to controller requests can be reduced because pilots are continuously aware of the ATC situation. In general, reactions are quicker and more precise. The proper rates of control can be applied to achieve the controller's intention.

Emergency situations.—When unusual circumstances arise the pilots will receive cues from a traffic display much sooner than can now be expected. Because of this advanced notice, the pilots can be awaiting an amended clearance, and preparations to execute that clearance can be initiated much sooner. In emergency situations which involve an aircraft in the near vicinity deviating from its expected course, the TSD becomes a critical source of information for evaluating the threat, considering alternative courses of action and executing an evasive maneuver. If, and when, an amended ATC clearance is given, the pilots will be able to immediately see the reason for its issuance. The TSD will give the pilot confidence that the command is appropriate, and it will convey a measure of the urgency of the situation.

A TSD will provide assurance when the ATC system is functioning properly. Positive and continuous indication will be given when adequate separations exist. When certain types of ATC failures occur, a TSD can offer an added margin of safety or even an avenue of escape. (Failures such

as loss of a ground communication channel during radar vectors.) The time delays associated with detecting, evaluating, and reacting to a threat can be greatly reduced when a common source of information is available to both the controller and pilot. In the coming years, this will be even more important because efforts to increase the capacity of the ATC system are resulting in new procedures which greatly reduce the longitudinal and lateral separations between aircraft (such as conducting simultaneous approaches to closely spaced parallel runways).

Collision avoidance.—TSD will be a valuable aid in helping to avoid mid-air collisions or near mid-air collisions within the terminal area. As it is currently structured, the display would operate as a proximity warning indicator or pilot warning indicator (PWI). (We make the distinction here between PWI systems and collision avoidance systems (CAS). A CAS provides a command to the pilot (e.g., fly up, fly down) to avoid collision, while a PWI system only informs the pilot of nearby traffic.) In the PWI system, it is the function of the pilot or other crew members to detect that a hazardous situation exists, assess the degree of threat posed by the other aircraft, and then take appropriate action to avoid collision.

The primary trade-off in using this traffic situation display as a PWI device comes from the desire to have, on the one hand, a very large field of view so that aircraft with high closing velocities can be seen in time to make small corrections to avoid a near miss, and on the other, a small field of view is desirable for the stationkeeping and following tasks in the terminal area. In fact, it has been suggested by some people that perhaps two displays will be required to accommodate these two functions.

Display format and symbology should be designed with the PWI function in mind so that the probability of detecting a threat is high and so that a rapid assessment of the situation can be made which leads to the correct evasive maneuvers if required.

Crew workload allocation.—A preliminary assessment of the TSD is that the workload of the pilot in traffic following tasks will remain comparable to that which currently exists. However, when one considers the additional functions which the display might perform including merging with other traffic, area navigation, and collision avoidance, it is clear that even greater demands will be made on the pilot if he is to perform all of these tasks and fly the aircraft as well.

Can we reduce this additional load imposed upon the pilot by having other crew members perform some of these functions? For example, it might be possible for the flight engineer to watch the display and use it as a PWI device. The first officer might use it to report to the pilot on the progress of making good courses and times to various waypoints in an area navigation scheme, and he might also be responsible for inserting and modifying waypoints.

It is well within the realm of possibility that the TSD will eventually be placed in the center of the instrument panel where the HSI is currently located. In this case, the pilot will then be using the display as one of his primary guidance and navigation displays, and it no longer will be relegated to the role of a secondary information display.

DISPLAY FORMAT, SYMBOLOGY, AND PRESENTATION

This section is a review of what may be called presentation variables or display parameters for the design of a TSD using data uplinked from an ARTS-I11 system. We shall describe the important elements of the display and the considerations peculiar to this application for a horizontal situation display.

Background reference and display *orientation.*—The background reference element can take form in various levels of complexity. Between the extremes of no background reference and a facsimile of a Jeppesen chart lie a nondescript grid and a simple map with only standard air routes and navigation fixes. Several considerations which will influence the selection of the reference to be provided are the desirability of some area navigation capability and the fact that Jeppesen charts will be available in the cockpit to provide any detailed information which is desired. A reasonable compromise would be some form of map containing key navigation facilities but less information than is available on standard charts and approach plates.

Whatever the form or content of the map, certain other decisions regarding its orientation and motion must be made. For translation, the first level of decision is whether the map will move so own aircraft is always in the same position of the display, or the map will be fixed and the symbol of own aircraft will move across it. Very simple estimates of the greatest number of miles per inch that it is reasonable to put on the display and the number of miles travelled in terminal area operation quickly indicate the difficulty with a fixed map for our applications. In the case of own aircraft symbol remaining fixed near the center of the display, there still remains a number of variations for the presentation.

The map can be oriented so that UP on the display corresponds to north, the aircraft's heading, or the direction defined by the ground track. Numerous reports have shown that confusion arises when travelling south on a north-up display. Visual acquisition of landmarks and other aircraft should be easiest using heading-up display information and most difficult with the north-up display.

The position of own aircraft, which is needed for centering the map on the display, will come from uplinked ground radar data in the system described here. Since the radar update occurs every 4 sec, the map translation would most easily be accomplished every 4 sec. Prediction computations done onboard would be required to project a continuously translating map. This problem is independent of the display orientation, but similar options are available for the track-up display. (The heading-up display might be continuously oriented from an external heading reference.)

Other *traffic.*—Probably the most important feature of the overall concept is the presentation of selected traffic information. Simple operations on the new data which is available every 4 sec can provide the relative position of other traffic. The past few positions of those aircraft can be displayed as history tracers to aid the pilot. Tracking and prediction of relative motion is another option, but this appears to be a costly option from the implementation point of view. However, it would allow the traffic to move continuously on the display and could be used to generate predicted paths of flight.

If the map translation is discontinuous, there will probably not be any question about how the traffic moves since they will jump together. However, if the map has continuous translation, a choice exists for displaying continuous traffic or unpredicted traffic (having discontinuous motion) between updates. Their coordinates may be frozen so they stay fixed relative to the translating map, or they can stay at a fixed range from own aircraft's symbol on the display. Either case can result in extremes of misrepresentation.

Data rates higher than once every 4 sec may be available in the future. These rates would reduce the significance of any differences which are found to exist between the acceptability of traffic symbols moving continuously through prediction and those jumping at the basic update rate.

Alpha-Numeric data tags.—The proposed data link provides identification, altitude, and tracking estimates of ground speed for selected transponder-equipped aircraft. The type of alpha-numeric information useful to the pilot depends on the task he is performing. One possibility is to have the data tag move with the symbol of the other aircraft. The effects on display legibility and interpretation of the characters moving across the display face, possibly in jumps, will depend upon the beam width and persistence properties of the particular scope. An alternative method is to present the alpha-numerics in tabular form. This may improve legibility and reduce clutter, but will introduce difficulty in associating an aircraft with its data tag.

Display scales.—There are three variables which have a direct relationship upon one another: the display scale (in miles/inch), the field of view of the display (in miles), and the scope size (in inches). Specifying any two determines the third. Since each phase of an approach has a characteristic range of viewing interest (field of view) and a set of tolerances for performing maneuvers, a variety of scales (miles per inch) will be required. Each viewing scale must display enough range to provide basic collision avoidance capability as well as presenting all of the picture needed to plan and execute the current maneuver. The precision possible in an aircraft-following task will depend on the display gain, the number

of inches on the display corresponding to the desired separation. The value of the scale setting must be easily and unambiguously identifiable.

Scope size.—If, as stated in the previous paragraph, the phase of the flight specifies a desired field of view, then the scale of the display can be adjusted so that this desired view fills whatever size of a display is available. This means that there will be more miles per inch on a smaller display, and the alpha-numerics which will have to remain a legible size, will occupy a larger percentage of the display area. The results of this imposed change in scale and added clutter on task performance will have to be examined to determine the limitations of a small scope which may be required in certain aircraft.

Command information.—For more advanced systems, the ground might provide commanded position information for each aircraft, or onboard systems might generate commands for the aircraft based on arrival times and/or spacing with other aircraft. The symbology and scales for such command information will require studies to ensure compatability with the other data presented and to avoid excessive clutter of the display.

THE SIMULATION FACILITY

Graphics computer.—The cockpit simulation facility assembled at M.I.T. to evaluate the potential applications of airborne displays has as its central elements an Adage AGT–30 computer (fig. 2) and a prototype SST cockpit shell donated by Boeing (fig. 3). The AGT–30 computer (fig. 2) is only moderately fast having a 16 K core memory with a 2 microsecond memory cycle time, but it does feature a unique peripheral hybrid array that can rototate, translate, and scale 3D vectors at rates ranging from 5 to 40 microseconds per vector depending on the vector length. This fast hardware operator permits the display of very complex 3D line images at flicker-free rates. Moreover, as each line is being drawn, the central processor may continue on with other calculations while awaiting an interrupt signifying the completion of the draw. As a consequence, the computer in real-time solves the equations of motion of the simulated aircraft, maintains three independent displays (two in the cockpit and one at the operator's console), monitors and responds to discrete and continuous inputs by the pilot, provides selected analog outputs to an x-y plotter and six strip chart recorder channels, and processes experimental data online so that selected statistical summaries are available at the end of each run.

Cockpit.—With respect to the cockpit, the objective was to provide a full-workload environment for a transport pilot approaching a major terminal so that a realistic evaluation of various display options could be obtained. Analog pick-offs were installed for the pilot inputs for aileron, elevator, rudder, throttle, speed brake, flaps, heading set, and course set. Up to 60 discrete

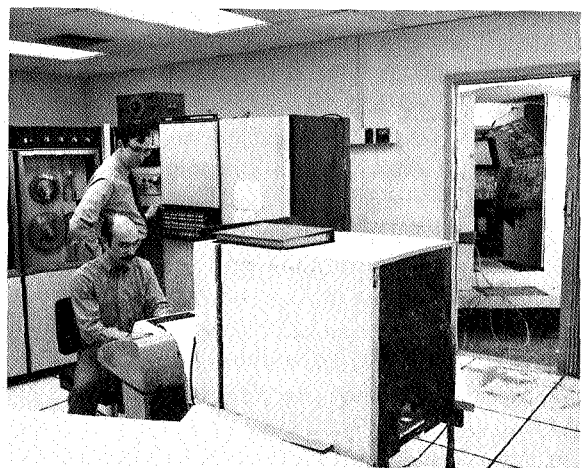

FIGURE 2.—Adage AGT–30 graphics computer.

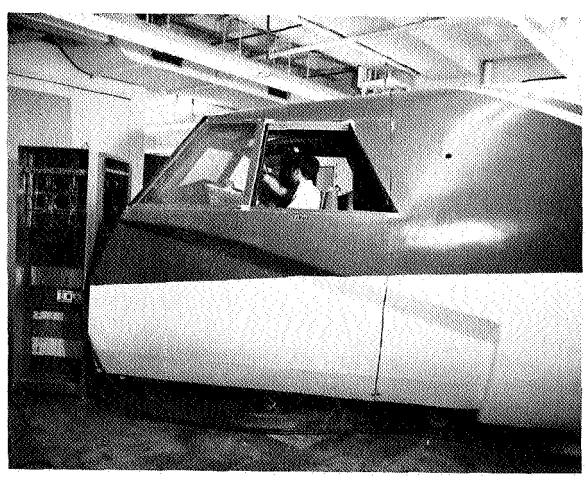

FIGURE 3.—Boeing prototype SST cockpit shell.

pickoffs indicated landing gear setting, stabilizer trim action, VHF COMM/NAV frequency settings, VOR/ADF selection, and display control inputs. Computer-generated discrete outputs were provided for marker beacon lights and intensity control.

Figure 4 shows the interior of the cockpit simulator during operation. Two cockpit displays were 16-inch Digital Equipment Corporation Type 30A CRT units modified so that they could be driven by the continuous voltages from the Adage hybrid array and vector generator. One display presents a set of basic flight instruments (altimeter, vertical speed, airspeed, radio magnetic indicator, attitude indicator, and horizontal situation indicator) whose dynamic response corresponds to the simulated flight conditions. The second unit positioned between the two pilot stations is used to present the various ATC display options being investigated such as an aircraft-centered navigation map, other aircraft in the vicinity, alpha-numeric information, etc. The third display at the computer console is a standard Adage unit which is used to monitor experiments or is used by the ATC ground controller when one is required. A set of built-in function switches, a light pen, and two foot pedals supply additional control inputs by which the experiments may be directed. In addition to the dynamic instruments and numerous dummy switches and knobs representing checklist items, photographic reproductions of the remaining cockpit panel instruments were mounted at the captain, first officer, and flight engineer stations. The present configuration corresponds to a Boeing 707–123B transport.

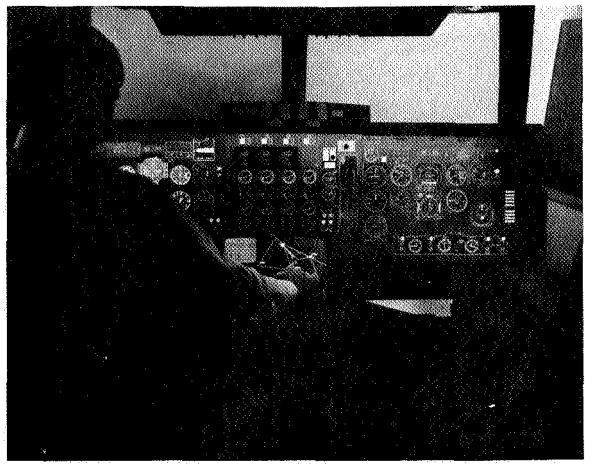

FIGURE 4.—Interior view of simulator.

Interface equipment.—The logic interface between the cockpit and the computer was largely constructed from commercial DEC building blocks. Nexus encapsulated operational amplifiers were used as buffers between the cockpit pickoffs and the multiplexer channels feeding the analog-to-digital encoder in the AGT–30. Some dynamics, such as the time lag between actuating the throttles and the buildup of thrust (EPR reading), were simulated by active RC circuits at the interface.

DESCRIPTION OF THE EXPERIMENTAL PLAN

The previous sections outlined some of the features which require consideration when designing a TSD. A set of symbols and reasonable fields of view were selected to reduce the number of variables confronting us when planning the experiments which are being performed to evaluate the various display options. Another set of experiments (ref. 1) is being done to investigate the TSD in the ATC system.

The display option experiments are being divided into two phases.

Phase 1 Experiments

The first phase of testing addresses the following factors: (1) display format for alpha-numerics, (2) scope utility for different sizes and shapes, and (3) effects of continuous and jumping traffic on the extraction of information from the display.

To elaborate briefly on these factors:

(1) With various alpha-numeric data (identification, altitude, and ground speed) selectively available, consideration must be taken to present this data in a way which makes it easy to associate the data with its respective aircraft. Two forms of data presentation have been considered. One is a traditional moving tag which stays along side of the actual aircraft symbol. This tag remains horizontal in the heading-up orientation. The other form is a stationary tabu-

lar presentation with a single character affixed to the aircraft symbol to establish the tie between an aircraft and its data.

(2) These formats were tried out on a rectangular scope (13.3 cmX18.4 cm) and on a scope **18.4** cm square.

(3) Here we are concerned with the effect of jumping or continuously moving symbols on the ability to extract information from the display.

Figures 5 and **6** show two examples of the display used during this phase of testing.

Phase **1** *test plan.—*

Situation: With the subject sitting in a normal pilot position, a variety of display options will be presented. There will be no primary or even secondary flying task, but rather the subject is instructed to give his full attention to the traffic display.

Task: With no traffic on the display, the subject is verbally given the flight identification for one **of** the test aircraft (e.g., TWA 426). This aircraft as well as one to four others then pop up on the display and the subject hits a response button as soon as he has identified the relative position, the altitude, and the ground speed of the selected aircraft.

Measures: The computer records the response time, and the accuracy of the subject's observations is recorded externally.

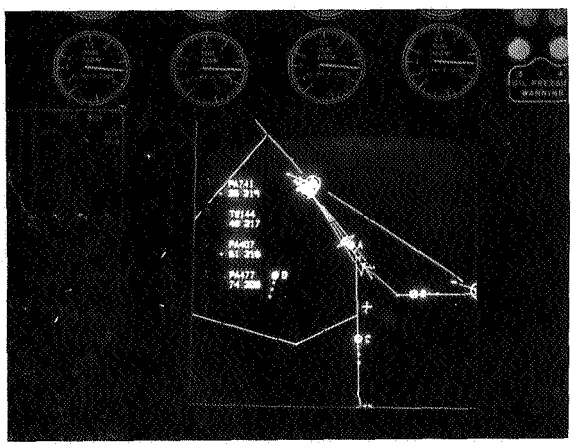

FIGURE 5.—Alpha-numeric **data in vertical table. Own aircraft at cross; other** aircraft **with tracers. Display size is 7-1/4 in. by 7-1/4** in.

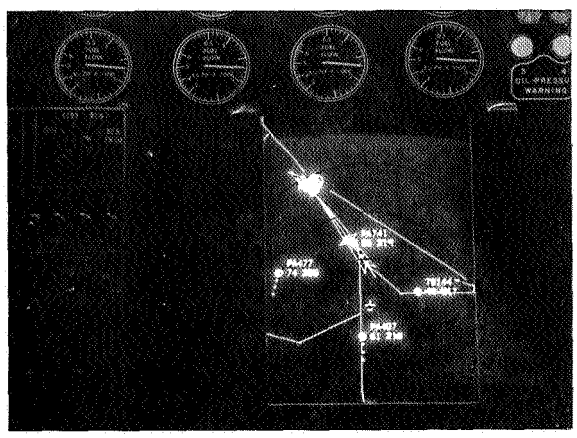

FIGURE 6.—Alpha-numeric **data in moving tag. Display size is 5-1/4 in. by 7-1/4 in. Note symbols for outer-marker and airport.**

Phase **2** Experiments

The second phase of testing requires piloting a simulated jet transport class aircraft through a variety of maneuvers within a simulated traffic situation. The flight is composed of a series of maneuvers which might be expected when following another aircraft into a terminal area; included among these are (1) acquisition of an assigned spacing directly behind the other aircraft, **(2)** following through a turn, and **(3)** maintaining spacing through a deceleration.

With these flight conditions and requirements, the following display options are to be investigated:

(1) Ground reference frame (GRF) and traffic translation
  (a) Continuous GRF translation with continuous traffic translation
  (b) Continuous GRF translation with traffic frozen in the GRF between 4-sec updates.
  (c) Both GRF and traffic frozen in translation between 4-sec updates
(2) Display orientation
  (a) North-up
  (b) Heading up with continuous update
(3) Background reference
  (a) With a background map showing nominal traffic routes
  (b) With no background reference
(4) Scope size
  (a) Large—providing 12.0 cm of forward viewing distance on the scope

(b) Small—providing 9.9 cm of forward viewing distance.

Figures 7 and 8 show two examples of display options used during the second phase of testing.

This list of feature options gives 24 different conditions. The experimental design employs four test subjects. Each subject is tested in two sessions. Half of them have a heading up display for the first session and north up for the second session. The others encounter the displays in the opposite order. One subject in each of the two orientation groupings has no background reference for his first session and does have this reference in his secbnd session. The reverse is true for the other two subjects. Within each session, half view the three translational options

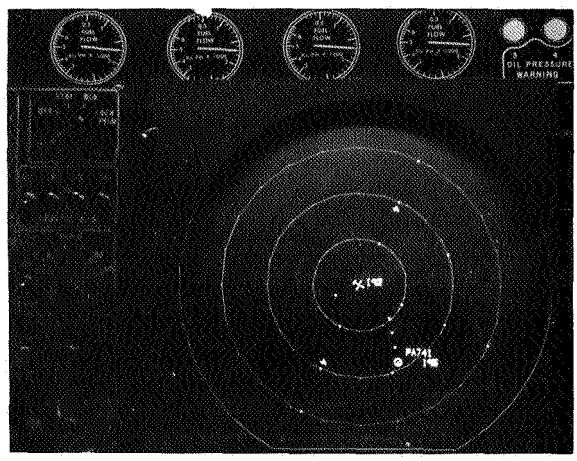

FIGURE 7.—North-up display without map. PA 741 shown with tracers and ground speed tag. Scale is 2 miles per range ring.

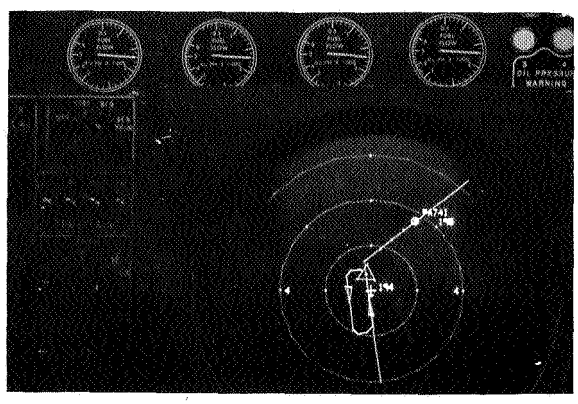

FIGURE 8.—Heading up display with map; 2 miles per range ring.

first on a large scope, then on a small scope. The order of presenting translation cases is also randomized among the subjects.

The subjects were experienced pilots : a current instrument instructor; Navy reservist; 707 flight engineer; and a first officer on Electras. Each subject had at least three hours of familiarization training on the simulation, about half of the time was devoted to practice with the actual test situation which the subject would first encounter in the testing. At the beginning of each test session the subjects were given two more practice runs before starting data runs. When the scope size was changed midway through the session a 15-minute break was taken, and an abbreviated practice run was made before recommencing data cases. The translational options could be changed at any time without stopping the flight, and they were all interspersed throughout the practice cases.

EXPERIMENTAL RESULTS

This section contains a brief review of the experimental results. See reference 2 for a more complete description.

Observations of the data from phase 1 tests show the search time does not increase greatly as one goes from a case having two aircraft on the screen to a case with three, but the time rises more abruptly as one goes to four or five aircraft being present. The increase is not as sharp when going from three to four aircraft in the tabular presentation as for the moving tag case. The tabular data experiments require a tearch for the specific aircraft identification and shen a search for the associated aircraft. This double search tends to increase the response times by 30 to 50 percent over the times required for collecting data from moving tags. Of the two styles of tabular data, the side presentation appears more favorable.

In the flight tests of phase 2, data on range, lateral error, course deviation, side task performance, and the head monitor were recorded. Plots of the ground track were also generated on a map. The pilots were found to be able to perform the flight task with virtually the same high level of precision on all the display options. With no map present, the turn at ACTON tended to be a little late or a little early, but in

all cases the error was immediately recognized and the turn was appropriately extended or cut short to bring the aircraft in line with the traffic. The measures used to compare the displays were ones indicating workload rather than absolute performance, since the performance was so steady. Viewing time for the traffic display, as extracted from head monitor data, and side task scores were used.

Preliminary results from this data show a reduced workload for the heading up display, but all other features show less clear preferences.

Three measures of workload were selected for intense analysis to find differences between the display options. Viewing time for the traffic display was entered in two forms: **(1)** Dwell time—average time the subject's head orientation remained in the selected position, hopefully corresponding to viewing the TSD, and *(2)* Total time spend in the prescribed orientation as a percentage of the time over which the record is taken. The third measure was the time average value of the magnitude of the side task deviation.

Analysis of variance and subsequent student's t-tests were applied to each of these measures for each of the four intervals over which data were collected.

A five dimensional array of data—(3 measures over 4 intervals) × (4 subjects) × (2 display orientations) × (2 display sizes) × (3 translation styles)—was set upon an IBM 360–67 by use of the time-share program APL. APL possesses capabilities for easy restructuring of and operating on multidimensional arrays, providing immediate results, and thus allowing various forms of analysis to be applied conveniently. Considering a single workload measure on a particular data interval, the experimental design reduces to a 3-way classification, with four replications (subjects) per cell.

The same four subjects performed all the tests, so the within cell (among subjects) variance estimate is the appropriate factor for testing the significance of all other variances by an F-test. Before the analysis was cerried out, the scores for each subject for each measure on each section of the flight were reduced to zero mean. This was done because we are interested in preferences and variations in preferences as indicated by the data, rather than variations in the level of the scores for the different subjects. The variations between the operating levels of the four subjects were generally greater than the variations of any single subject, so an effect to first minimize these differences in operating levels was in order.

The results of such an analysis are presented in table 1. For each major feature which showed significant variance between its indices, individual t-tests were examined for each subject on the particular measure and data interval. For the student's t-test, the data were treated by calculating the differences between the scores of those cases differing only by the feature being examined.

Interval 3 of the data begins with the third section of the flight and interval 4 of the data takes over after 2 min of flight section three, by which time the deceleration transients have supposedly died out.

Statistically significant findings at the 10 percent level were

(1) Of the 12 data sets (three measures on four data intervals) eight showed a significant variance between orientations. All but one of these eight data sets lead to t-tests which showed significantly better scores for heading-up cases. The one other data set exhibited a north-up preference at a significant level.

(2) The display size did not show a eignificant effect.

(3) The translation options require close examination. Section 3 of the flight (data intervals 3 and 4) is a case in which the necessary control actions are fairly well established, so the display provides a check that the pilot's action had the expected effect. For these intervals of the data, the differences showing significance favor both other options over the case of continuous map translation with traffic jumping every 4 sec. For this unfavored case it can be noted that the pilot must watch until he sees the traffic jump to be sure of the correct measure of the spacing. Conclusions for sections 1 and 2 are tenuous, though the pilot questionnaires fill in the guidelines which the data are weak in providing. The data for side task performance show the case of both continuous traffic and map to be significantly better than the case of both jumping.

TABLE 1.—*Analysis of Variance Table* for *Phase 2 Experiments*

	Or.	Sz.	Tran.	Or.-sz.	Or.-tran.	Sz.-tran.	Or.-sz.-tran.	Data interval
Dwell time	"9.766	1.191	[c]11.531	[b]4.153	08.713	0.028	0.277	1
	"3.012	0.328	[c]4.358	1.625	[a]2.736	0.503	0.706	3
	0.027	0.011	0.710	1.385	0.848	0.753	0.984	3
	c10.943	0.004	82.558	0.976	1.146	0.371	0.488	4
Attention, %	0.177	0.410	2.304	0.827	0.904	1.156	1.207	1
	0.821	0.124	82.786	0.270	0.985	1.763	1.932	2
	"3.478	0.709	1.176	3.289	2.186	0.462	1.037	3
	[c]7.423	[a]3.519	[b]5.514	[a]7.045	0.856	0.427	0.724	4
Side task	2.832	0.843	0.389	2.226	0.181	0.008	0.066	1
	3.954	0.998	0.630	2.362	0.021	0.844	1.076	2
	[b]6.598	[b]4.243	[a]2.718	"8.900	0.241	0.908	1.971	3
	[b]5.208	0.158	0.525	0.641	1.911	1.676	2.152	4

Notes:
(1) Data structure: Orientation (Or.) by size (Sz.) by translation (Tran.) with entries from each of four subjects composing each cell. Each subject's scores have been reduced to zero mean within each cell.
(2) F-test figures for principle features and interactions are shown, with significance indicated by [a] = 0.10 level, [b] = 0.05 level, [c] = 0.01 level.

However, the other two measures show the reverse preference at a lower level of significance. Other investigations (ref. 1) have found the after image of jumping traffic to be useful in judging relative motion for more complex tasks.

(4) The interactions which are indicated are not too ambiguous because generally two of the primary features have already shown significant variation. Perusal of the original data reveals that the cases which fail to provide two variables of significant variation require the qualification that the heading-up orientation is favored most when appearing in a large display. Note that this interaction is only significant in three of the 12 data sets, and a heading-up smallinteraction is favored once.

Summary of Experimental Findings

Phase I.—Unless a terribly cluttered map is to be presented on the display (which would lead to unresolvable conflicts of data tags with map elements) it appears very desirable to implement moving tag alphanumerics. If tabular data are used, however, a slight preference exists for the table appearing in a single column at the side of the display, rather than in rows at the bottom.

Phase 2.—For the flight tasks employed in these tests, which were a combination of navigation through a familiar flight pattern and following predictable traffic in this pattern, a heading oriented display generally leads to lower workload scores and better pilot acceptance than a north oriented display. Neither performance nor workload measures appear to be influenced significantly by the display sizes tested. Pilot opinion was not critical of the smaller scope, while the larger one was naturally favored. For the translation options, either the case of continuous map and traffic or that of jumping map and traffic appear acceptable, with the pilot preference going to the fully continuous case. The continuous map with jumping traffic is undesirable from the standpoints of both workload and pilot opinion.

REFERENCES

1. IMRICH, T.: System Concept Development and Evaluation of Airborne Traffic Displays. S.M. Thesis, Dept. of Aeronautics and Astronautics, Mass. Inst. of Technology, Cambridge, Mass.
2. ANDERSON, R. E.: Format Evaluation for an Airborne Traffic Situation Display. M.S. Thesis, Department of Aeronautics and Astronautics, Mass. Inst. of Tech., Cambridge, Mass.

N73-10113

9. Manual Control Theory Applied to Air Traffic Controller-Pilot Cooperation

DUNSTAN GRAHAM, WARREN F. CLEMENT, AND LEE GREGOR HOFMANN

Systems Technology, Inc.

Reduced runway separation standards are among the means which have been proposed for increasing airport capacity. The probability of a blunder will dominate the calculation of safe separation standards. Then the determinant of safe system performance will be the system reaction time comprised of the air traffic controller's detection, decision and communication delays, and the response times of the pilot and aircraft in executing a collision avoidance manuever. Estimates of these times, based on existing data, show that the delays ascribable to the human portions of the man-machine system are comparatively unimportant. New developments in radar, computers, and data links will be required to provide any substantial improvement of the existing system, and the goal of 2500 ft of separation may not be achievable.

INTRODUCTION

By the summer of **1969,** in the United States, the growth of air carrier traffic and of operations by elements of the general aviation fleet had led to readily apparent distress and to certain dislocations with respect to the capacity of major airports and the functioning of the air traffic control system. Very lengthly departure delays were frequently encountered. In the eyes of some travellers, the matter seemed to approach the quality of a civil disaster when some members of the organized air traffic controllers staged a "sick out" in the middle of the summer. The peak travel period in the summer of **1970,** however, did not seem quite as bad. At the present time, the air carriers have cut back their schedules, the Boeing **747** aircraft (capable of carrying many more passengers per departure or arrival) have come into service in substantial numbers, and in some cases, such as at JFK International Airport, the imposition of high landing fees has discouraged air taxi operators and commuter airlines from using the airport. This has led, at least by comparison, to a breathing spell during which new solutions to the problems may be sought.

The problems, of course, are by no means entirely technological. The proposed solutions are increasingly subject to economic and particularly to political constraints. In the vicinity of New York City, for example, *every* proposed location for the "fourth" jetport has been opposed by some groups, and two of the locations considered promising by the Port of New York Authority have been defeated in voter referendums.

While clearly recognizing the often conflicting interests of airport developers and the airport's neighbors, the report of the Department of Transportation Air Traffic Control Advisory Committee (the Alexander Committee) (ref. **1)** says flatly:

> Air traffic is in crisis . . . major improvements in current airport capacity must be achieved. (Emphasis added)

In another place, the same report says:

> The conclusions reached on air traffic control for the **1980's** and **1990's** *assume* that runway capacity in the dense traffic areas will be provided. This is our present severe bottleneck, and the improvements to the ATC system discussed in this report will not *be* significant unless the airport (runway) problems are also resolved. (Emphasis added)

Further on, the report says, in part:

> . . . additional capacity can be provided by utilizing airport acreage more efficiently by decreasing the 5,000-foot separation between independent IFR runways. The Committee believes it will be possible to safely reduce

this separation between runways to 2,500 feet and the final spacing on approach to two mites. This will require an improved landing aid, such as the scanning beam microwave ILS, as *well as provisions for precise monitoring and data linked commands* in case of blunders.

At the present time, and for the forseeable future, the enforcement of safe separation standards will require the joint efforts of human air traffic controllers and pilots and will involve a geographically vast and technologically complex array of "machines" including radars, beacons, digital computers, displays, and communications, as well as aircraft with their primary and secondary flight control and propulsion subsystems. In short, the augmentation of runway capacity by means of reduced separation standards will demand the utmost performance of a truly named man-machine system. Faithful adherents of the '(Annual Manual," over a comparatively short period of time, have witnessed explosive development of a theory of manual control for at least certain problems in man-machine systems. We take it that manual control theory is understood to involve an abstraction of the performance of human operators in such a way as to allow an analysis of the relationship between the controller(s) and the "object of control." In particular, in our view, the abstraction and the analysis are mathematical. Can manual control theory contribute to the determination of safe separation standards for terminal area air traffic control? We propose in this paper to demonstrate that it can. It will, however, eventuate that the performance of the system with respect to separation standards is not critically sensitive to the performance of the air traffic controller and the pilot.

Determination of safe separation standards for operations on independent IFR runways may be influenced by consideration of an inordinately large number of *combinations* of system parameters and subsystem performances. Among these are

- Runway configurations
- Aircraft types (e.g., CTOL and STOL aircraft)
- Airborne equipment complement (e.g., flight director or automatic coupled approach)
- Gust, wind, and wind shear environment
- Data acquisition system capabilities (e.g., airport surveillance radar)
- The type of operation (e.g., front course or back course approach with or without simultaneous departures, etc.)
- The frequency of occurrence of blunders
- Controller intervention rules
- Controller response
- Pilot response

as well as, possibly, still other factors. We are unprepared to deal with all these factors in anything like an exhaustive fashion. Instead, we shall assume a prototype problem which will serve the primary purpose of providing a setting or background for considering the influence of controller and pilot responses on the performance of the system.

THE PROTOTYPE PROBLEM

Consider two conventional aircraft approaching an airport along parallel paths. These paths are separated laterally by a distance which is currently set at 5000 ft for 'independent" IFR operations. (Independent here means that no account is taken of any possible separation of the aircraft in a direction parallel to their tracks.) Because of gusts and wind shears, radio beam anomalies, spurious control actions, etc., the motion of each airplane is a random function of time which can be presumed to take place with respect to some mean or average motion which carried each aircraft toward its landing runway.

In the absence of better information, we can assume that the distributions of the three cartesian displacements and the corresponding velocities of each aircraft with respect to their mean paths are Gaussianly distributed and independent. This appears to be reasonable for small displacements and velocities, but it is generally conceded that the assumption will seriously underestimate the frequency of large deviations. This is because of the possibility of "blunders."

A blunder is a random process in the sense that its occurrence is probabilistic, but, for our purposes at least, where it occurs it is a single deterministic function of time. An example of a dangerous blunder would be a maneuver which would place one of the approaching aircraft on a collision course with another.

A typical case of parallel approaches has the aircraft on extended runway centerlines **762** m (2500 ft) apart. Without air traffic controller intervention, in order for the variances of the time functions representing the random motions of each aircraft with respect to its mean motion to contribute as much as **1** percent to the overall probability of a collision, we have calculated that it would be necessary that any blunder occur less frequently than once in 7.787×10^{17} approaches. (This has been done by a method similar to the one given in references **2** and **3.** The exposition of the method is worth a paper in itself.) Another representation of this fact is that at the mean level of instrument approaches in the United States in the years **1964–1966** inclusive (6.16×10^5 instrument approaches per year), if blunders occurred more often than approximately once in a million years, the statistics with respect to blunders would completely dominate the determination of safe separation standards. We may easily believe and act on the belief that this is the case.

Given that blunders can and do occur, we wish to inquire as to the effect of air traffic controller intervention in maintaining the safety of operations.

In our prototype problem, we, therefore, assume that the progress of both of the airplanes on parallel approach paths is being monitored by a final controller using a display of secondary surveillance radar data. (This is currently the case at major airports). Where, on the basis of the information available to him, the final controller detects a violation of one aircraft's collision threat space by the other, he will issue a warning to one or both pilots. (We shall neglect, for simplicity, the probability that the controller does not detect the threat.) One or both pilots will then execute a collision avoidance maneuver. This will allow the system to be "safe" provided only that the parallel approach paths are sufficiently separated so that there is ***time*** for the controller to detect the threat, to communicate a warning, and for the pilot(s) to complete an avoidance maneuver. This time may be very considerable. The total time is called the system reaction time T_R. It has the following components:

- Data acquisition delays
- Data processing delays and uncertainty
- Controller decision delays
- Controller/Pilot communication delays
- Pilot effective reaction time delays
- Aircraft response delays as determined by its
  - Speed
  - Maximum rate of climb
  - Maximum bank angle.

In order to be able to place the controller's and the pilot's performances in perspective, we choose a particular example blunder scenario. This is illustrated in figure **1.** The numbers associated with the graph are choosen for convenience, but they are approximately representative. The aircraft are on "independent" parallel approach paths at the same altitude and separated by **1250** m **(4100** ft) laterally. (This latter is a little less than the current minimum separation, but it is rather more than what it is hoped can be achieved.) Each aircraft is proceeding at **61** m/sec **(200** ft/sec). At time $t=0$, aircraft ***A*** preceeds aircraft *B* by **488** m **(1600** ft). At that point in time, aircraft ***A*** initiates a postulated blunder, banking to an average bank angle of 35° for approximately **7** sec and then

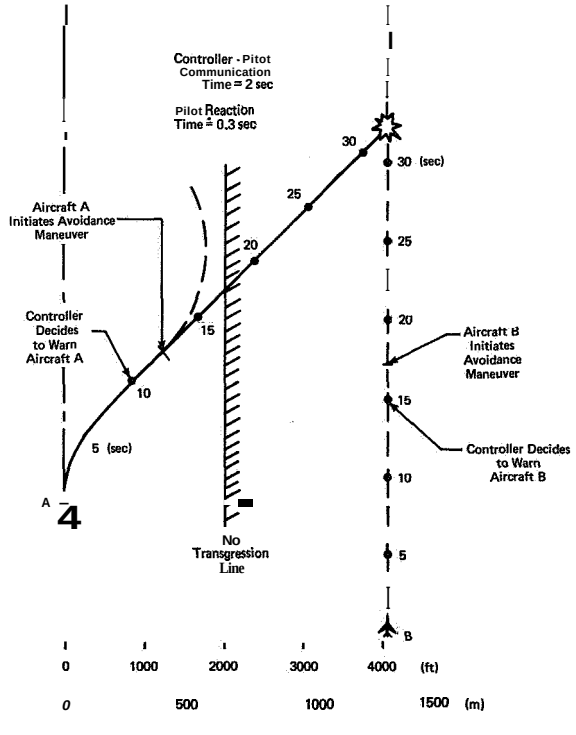

FIGURE 1.—A blunder scenario.

recovering to straight flight. The surveillance radar beam sweeps over the positions of both aircraft once every **5** sec. (The airport surveillance radar at JFK International Airport rotates **13** times per min.) Assuming that the beam has just passed both aircraft at $t=0$, the positions of both aircraft at 5 sec intervals, as they might appear to the air traffic controller, are indicated by the heavy dots in figure **1.** In the absence of controller intervention there will be a collision between the two aircraft at $t=32$ sec. Is there time in which to detect the threat, issue a warning, and have the innocent pilot and aircraft respond?

ESTIMATE OF THE SYSTEM REACTION TIME

In principle, without rate weighting, the average effective time delay in radar data, sampled once every **5** sec, is half the sampling period. We may, however, take a more pessimistic view with respect to the geometry of figure **1.** At t=**5** sec the blunderer, aircraft ***A***, is only a little more than **76.2** m **(250** ft) off course. The data are somewhat noisy in any case and on the scale of the display this error would be nearly imperceptible to the controller. When the radar next determines the position of aircraft ***A***, it might be clear to the traffic controller that he should intervene. Conventionally (ref. 4), this is done so as to command aircraft ***A*** to turn away from the "no transgression line" perhaps established half-way between the approach paths. We shall shortly justify in more detail a figure of **2.3** sec for the time required for the controller to communicate a warning to the pilot and for the pilot to respond. Beginning at $t=12.3$ sec we have shown (dotted) in figure **1,** a compensating left turn by aircraft ***A*** which is similar but opposite to the turn which initiated the blunder. This, it may be observed, carries aircraft ***A*** well clear of the no transgression line.

But suppose that the pilot of aircraft ***A*** does not receive the warning, or for some reason fails to heed it. Because **of** the small displacement between the uncorrected and corrected tracks, this may or may not be evident to the air traffic controller at $t=15$ sec. We will presume, however, that he at least suspects the danger, and that he practically instantaneously decides to command a collision avoidance manuever for aircraft **3.**

What is a reasonable estimate for the controller decision and communication time as well as for the reaction time of the pilot of aircraft ***B?***

Data on which to base such an estimate are not abundantly available.

A lower bound for the estimate, however, might be discovered by reconsidering the two-operator tracking tests conducted by Russell (ref. 5). In these experiments a "director" observed a compensatory display of tracking error and gave verbal instructions to a "tracker" who then operated a handwheel control so as to null the error perceived by the director. The controlled element was a pure gain. The course or forcing function was a sum of four sine waves. Figure **2** is a replot of a sample of Russell's two operator data and the corresponding single operator data for the same tracker. The effective time delay, τ_e, for the single tracker is estimated, from a fit to the phase lag data, to be **0.2** sec. The two operators together seem to be characterized by a lag-lead describing function which includes a larger delay. If the phase angle contribution of the lag-lead characteristic is subtracted from the total phase Iag of the two-operator describing function, the residual phase lag corresponds to a time delay of 0.8 sec. This leads us to conclude that (exclusive of the tracker's delay) the *average* time delay ascribable to the director's decision and communication delays is:

$$\Delta\tau_{e_c} = \mathbf{0.6}\ \text{sec.}$$

This estimate is rather neatly supported by the observation that, on the average, instructions from the director to the tracker were communicated 48 times per minute, or equivalently with an intersample interval of **1.25** sec. The effective *average* time delay is almost exactly half the sample interval. The nature of the instructions from the director in this case, however, was extremely simple, comprising a series of commands such as "left, left, right, right, right, left . . ." to each of which the tracker responded with standardized increments of control deflection. Furthermore, it may be that this continuous tracking experiment is not representative of what might be expected in the case of discrete events. Nevertheless, considering the necessity

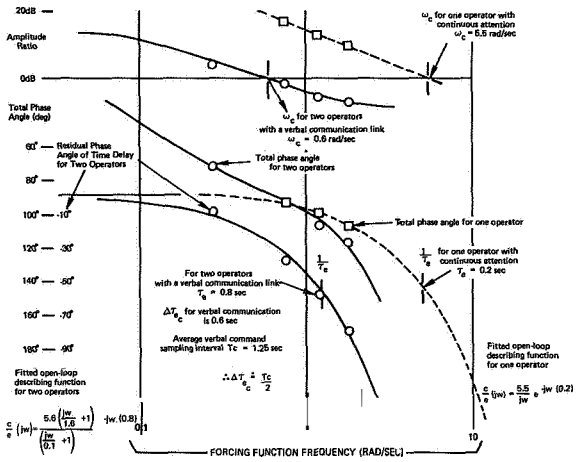

FIGURE 2.—Comparison of Russell's (ref. 5) measured open-loop describing functions for one- and two-operator tracking.

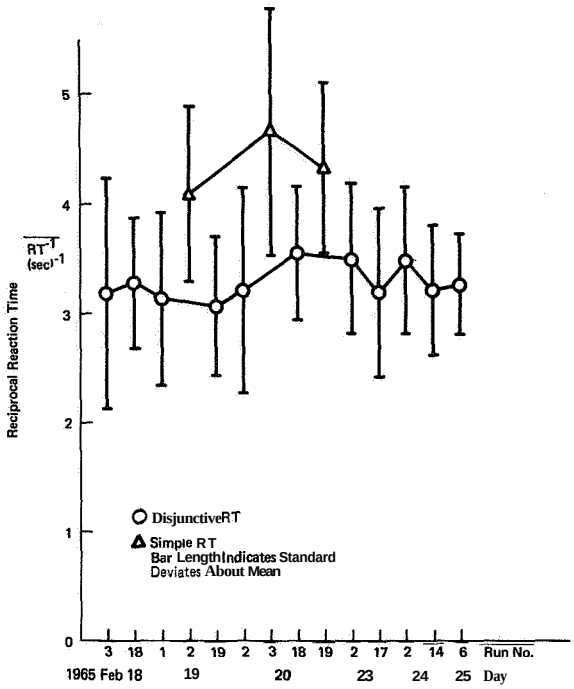

FIGURE 3.—Run-to-Run variability of the 20-trial step reaction time samples.

for more complicated messages and the fact that the message is not necessarily expected by, in the second case, the pilot, we might guess that in the case of air traffic control, the controller's decision and communications delay might be as little as two to three times the average decision and communications delay from the two-operator tracking tests.

One source of data on actual two-way transmissions between air traffic controllers and pilots is reference *6* which discusses several examples of two-way transmissions of nonurgent messages in which the time difference between the initiation of the message and the reply or acknowledgment is as little as **4** to *5* sec.

From this we conclude that the controller's decision and communication time, as it enters into our problem, is unlikely to be much less than **2** sec, nor more than **4.** We shall take **2** sec as representative. It would be interesting to measure controller's decision and communication times in simulator experiments if this has not already been done.

Assuming that the pilot of aircraft B is alert and that he knows that at approach altitudes, for an intrusion from the side, a pull-up and climb is the preferred avoidance maneuver; we ask: What are the response times of the pilot and the aircraft?

Figure **3** (taken from reference **7)** shows step reaction times for visual stimuli. It shows that if the direction of the response is not known beforehand (disjunctive reaction time) the mean reciprocal reaction time is approximately 3^{-1} sec. In the absence of better information on step responses to aural stimuli we take as representative of the step response of the pilot of aircraft B to the warning of the controller a time delay of **0.33** sec.

The response of the aircraft to pilot control may be represented by a flight path response to pitch attitude commands. In transfer functions form this is

$$\frac{\gamma(s)}{\theta_c(s)} = \frac{\exp(-\tau_\theta' s)}{T_{\theta_2}' s + 1} \tag{1}$$

where

τ_θ' = is the closed-loop system delay (a fraction of a second)

$T_{\theta_2}' \doteq \dfrac{2(W/S)}{g\rho U_0 C_{L_\alpha}}$

$\dfrac{W}{S}$ = wing loading

g = acceleration of gravity

ρ = air density

U_0 = trimmed airspeed

C_{L_α} = aircraft's lift curve slope.

The quantity T_{θ_2}' is often termed the flight path response time constant. Note how it depends on the aircraft's performance, notably on the wing loading and approach speed. Small time constants are, of course, desirable. For the DC-8, T_{θ_2}' is approximately ***1.56*** sec in approach. It is only about ***0.5*** sec for the Navion.

The minimum pull-up maneuvering time, following receipt of the climb command by the pilot, can be computed as the sum of the effective closed loop time delay, τ_θ' plus the time to establish the flight path acceleration $3T_{\theta_2}'$ plus the time to terminate the flight path acceleration $\tau_\theta'+3T_{\theta_2}'$ plus an interval of steady acceleration $(\dot{h}_c-\dot{h}_0)gn_{z_{\max}}$. Here $n_{z_{\max}}$ is the maximum normal acceleration in g units. It is limited in the case of interest here by the approach to a stall. In the form of a sum, the minimum pull-up maneuvering time T_m then becomes

$$T_m=2\tau_\theta'+6T_{\theta_2}'+\frac{\dot{h}_c-\dot{h}_0}{gn_{z_{\max}}} \qquad (2)$$

where

$\dot{h}_c$ = the rate of climb command

$\dot{h}_0$ = the initial rate of climb or descent.

The displacement d which can be achieved at time t after command of the pull-up maneuver and steady climb can be calculated with good approximation by assuming constant velocity U_0 and using the equation

$$d(t)=\dot{h}_c[u(t-T_m)]t+U_0\int_0^{T_m}\gamma(t)\,dt \qquad (3)$$

where $\gamma(t)$, the aircraft's flight path angle, is the inverse Laplace transform of the product of equation *(1)* multiplied by the transform of the pitch attitude command θ_c, viz.,

$$\theta_c(s)=\dot{\gamma}_{z_{\max}}\frac{1-e^{-T_s}}{s} \qquad (4)$$

Here

$\dot{\gamma}_{c_{\max}}=gn_{z_{\max}}/U_0$

$T=\tau_\theta'+3T_{\theta_2}'+\dfrac{\dot{h}_c-\dot{h}_0}{gn_{z_{\max}}}$

$u(\cdot)$ = unit step function applied at time (°)

$\tau_\theta'=\tau_\theta+\dfrac{2\zeta_{sp}'}{\omega_{sp}'}$

τ_θ = pilot's reaction time delay for a deterministic input $\doteq 0.33$ sec

ζ_{sp}' = modified aircraft short period damping ratio (modified by the pitch attitude feedback)

ω_{sp}' = modified aircraft short period natural frequency (rad^{-1}) (modified by the pitch attitude feedback).

For the case of a D G 8 going from an initial glide path sink of rate -3.05 m/sec (-10 ft/sec) to a steady rate of climb at $+3.05$ m/sec (***600*** ft/min) (low, but convenient), substitution in equation (2) yields $T_m=10.35$ sec.

A more elaborate calculation, which is capable of showing the effect of the steady climb after the T_m sec have elapsed, yields the results shown in figure **4.** Plotted there is the time required to reach a given displacement above an initially descending path. Note that the effect of the incremental load factor in the pull-up is comparatively small. The biggest effects are, of course, to be found in the steady rate of climb which may be achieved. This depends primarily on the thrust to weight ratio. The actual formula is

$$(R/C)=\frac{(T-D)U_0}{W} \qquad (5)$$

where

(R/C) = rate of climb

T = thrust

D = drag

U_0 = aircraft velocity

W = aircraft weight.

In a missed approach pull-up, the drag is small compared to the thrust, and the climbout velocity is likely to be nearly the same for a variety of aircraft. The big differences between aircraft will

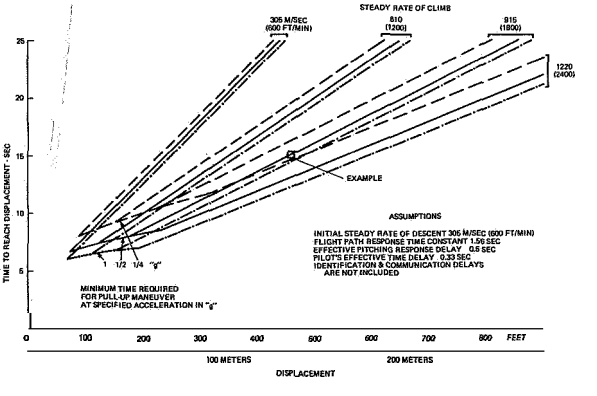

FIGURE 4.—Theoretical minimum time to reach a given displacement above the glideslope by a pull-up avoidance maneuver and steady climb.

then reside in their different thrust to weight ratios. This, of course, is one of the most important determinants of performance in many different respects, but we are not likely to see any spectacular improvements here because high thrust to weight ratios tend to make airplanes uneconomic.

Figure **4** may be used to estimate a lower bound on the elapsed time interval required to achieve, say, **140** m **(460** ft) of displacement above the glideslope, for example; if the maximum incremental acceleration is limited to one-half g and the final steady rate of climb is **1800** ft/min. By entering on the abscissa of figure **4** at **140** m **(460** ft), the time ordinate corresponds to the solid line for **9.15** m/sec **(1800** ft/min) (denoted by the square symbol). It may be read as **15** sec elapsed time. To this time interval following receipt of the climb command by the pilot must be added the ATC surveillance, identification, intervention, and communication delay. Thus, a typical overall latent period between the initiation of a lateral threat to an aircraft of the approach and achievement of **140** m **(460** ft) separation ***above*** the intruder is on the order of one-half minute or about one-quarter of the time required to fly from the outer marker to the middle marker.

The results are similar if we consider intrusions from above in which the most correct response is a lateral avoidance maneuver. Such a maneuver is the familiar side-step whereby lateral displacement is achieved by a double sinusoidal aileron command which recovers the original direction of flight. After achieving a safe lateral standoff, the pilot of the evading aircraft can then execute a missed approach.

Figure **5** (fig. 28 of ref. 8) shows the time required to achieve a given lateral separation by a double banking maneuver (X-turn). (Ref. **9** has shown that the approximate theory is confirmed by experiments with **14** aircraft flown by airline and professional test pilots.)

In Figure **5,** the maximum bank angle, φ_{max}, and the maximum roll rate, p_{max}, might possibly be somewhat altered and the results recomputed. The values assumed are typical, however.

We may use figure **5** to estimate a lower bound on the elapsed time interval required to achieve, say, **152** m (500 ft) of lateral separation if the

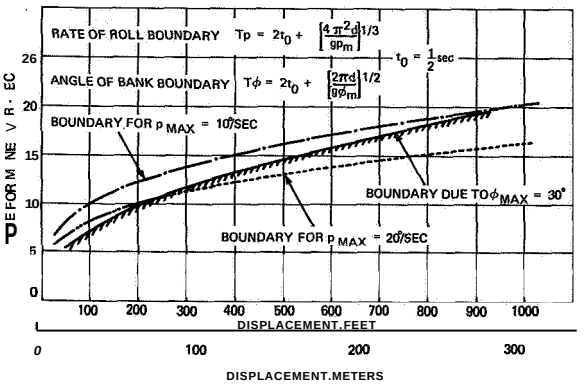

FIGURE 5.—Theoretical minimum times for sinusoidal maneuvers limited **by** rate **of** roll **(fig.** 28 of ref. 8).

maximum roll rate (p_{max}) is limited to 10 deg/sec. By entering the abscissa of figure **5** at **152** m **(500** ft), the time ordinate corresponding to the boundary for $p_{max} = 10$ deg/sec (denoted by the circular symbol) can be interpolated between **16** and **17** sec elapsed time for the maneuver. This value is seen to be similar to the one for the pull-up maneuver.

If the evasive maneuver were considered to be a turn away from the course and then flight in a straight line, the same separation distances would be achieved in somewhat shorter times. The improvement would not, however, be astounding. It appears that the pilot aircraft combination will typically require about **15** sec to achieve **152** m (500 ft) of lateral separation with aircraft as we have known them to be configured. Can anything else be done? Very large thrust to weight ratios, the availability of large amounts of direct lift control, and anything that would induce the pilots to use larger bank angles would help. No dramatic improvement in these factors, however, is likely to be brought about.

We have now seen that, at least for the choice of a miss distance of **140** to **152** m **(460** to **500** ft), either the side-step or the pull-up takes approximately **15** sec for typical values of the parameters for transport aircraft. Since we have also seen further above, that in connection with the prototype problem the effective controller's delay (including data acquisition (three scans = **15** sec) and communication delays **(2** sec)) is currently, perhaps, of the order of **17** sec, the total system

response time T_R is likely to be approximately 32 sec. Thus, in our prototype problem, the system is ((safe" at a runway separation of 1250 m (4100 ft), if a miss distance of 140 m (460 ft) is considered acceptable.

CONCLUSION

For a typical case of independent approaches to parallel runways, there is an appreciable probability of a blunder. The safe spacing of runways depends on making the system reaction time T_R sufficiently small so that adequate miss distances can be achieved between aircraft on collision courses when the air traffic controller must intervene.

The dominant effects are comprised within the times required to predict the impending collision and for the aircraft to respond to a collision avoidance maneuver command. Of the 32 sec system response time calculated in connection with the prototype problem, only 2 sec are ascribable to the controller's decision and communication delays, and only 0.33 sec to the pilot's response time. No effective improvement is to be expected from attempts to improve the performance of the human operators. The response time of the aircraft is likewise not readily amenable to improvement. The installation of track-while-scan (phased array) radars, and computer prediction of conflicts possibly based on down-link transmission of airborne sensor data could reduce the system reaction time by perhaps 5 sec. This would allow the runways to be safely spaced at 1036 m (3400 ft) in the prototype problem. The data linking of collision avoidance maneuver commands could possibly obviate the necessity for the 2 sec communication time we have allowed. This would then allow the runways to be separated by only 945 m (3100 ft). Further reduction in the spacing to the 762 m (2500 ft) called for in reference 1 would then be at the expense of miss distance in the event of a critical blunder.

REFERENCES

1. ANON.: Report of Department of Transportation Air Traffic Control Advisory Committee. Vol. 1, Department of Transportation, Dec. 1969.
2. STEINBERG, H. A.: A Safety Model for Evaluating Risk Involved in Airport Landing Operations. Rept. of Department of Transportation Air Traffic Control Advisory Committee, Vol. 2, Dec. 1969, pp. 9–20.
3. STEINBERG, H. A.: Collision and Missed Approach Risks in High-Capacity Airport Operations. Proc. IEEE, Mar. 1970, pp. 314–321.
4. BLAKE, N. A.; AND SMITH, E. E.: Data Acquisition System Design Considerations. Rept. of Department of Transportation Air Traffic Control Advisory Committee. Vol. 2, Dec. 1969, pp. 271–285.
5. RUSSELL, L.: Characteristics of the Human as a Linear Servo-Element. MS Thesis, MIT, 1951.
6. ANON.: Collision-Course Illusion Cited in Accident. Aviation Week, vol. 86, no. 1, 2 Jan. 1967, pp. 84–98.
7. MCDONNELL, J. D.; AND JEX, H. R.: A "Critical" Tracking Task for Man-Machine Research Related to the Operator's Effective Delay Time Pt. 11. NASA CR–674, Jan. 1967.
8. ASHKENAS, I. L.: A Study of Conventional Airplane Handling Qualities Requirements. Part I, Roll Handling Qualities. AFFDL-TR-65-138, part I, Nov. 1965.
9. PERRY, D. H.; PORT, W. G. A.; AND MORRALL, J. C.: A Flight Study of the Sidestep Manouvre During Landing. R and M 3347, Aeronautical Research Council, July 1961.

N73-10114

10. Supervisory Sampling and Control: Sources of Suboptimality in a Prediction Task

THOMAS B. SHERIDAN AND WILLIAM B. ROUSE

Massachusetts Institute of Technology

A process supervisor is defined as a person who decides when to sample the process input and what values of a control variable to specify in order to maximize (minimize) a given value function of input sampling period, control setting, and process state. This paper presents experimental data in such a process where the value function is a time-averaged sampling cost plus mean squared difference between input and control variable. The task was unpaced prediction of the output of a second order filter driven by white noise. Experimental results, when compared to the optimal strategy, reveal several consistently suboptimal behaviors. One is a tendency not to choose a long prediction interval even though the optimal strategy dictates that one should. Some results are also interpreted in terms of those input parameters according to which each subjects' behavior would have been nearest optimal. Differences of those parameters from actual input parameters served to quantify how subjects' prediction behavior differed from optimal.

INTRODUCTION

The literature of man-machine systems has long implied that a human operator might best function as a supervisory controller, aloof from instant-by-instant in-the-loop error nulling. The supervisor, instead, programs or adjusts the control variables (or parameters of a lower level open or closed loop process) in order to optimize with respect to some performance function. He does this on a time scale which he tends to make cognitively comfortable and usually different from that of the controlled process itself. Though his actions may be intermittent the controlled process may nevertheless go on continuously.

Several modes of supervisory control may be distinguished. A first (most sophisticated) mode is where the supervisor specifies a subgoal and lets a computer algorithm select the parameters of how and when the process implements its state trajectory to the subgoal. This mode occurred, for example, in controlling the Apollo spacecraft, (ref. 1) and is also characteristic of supervisory control of teleoperators (refs. 2 and 3). This mode elevates the human to the highest level of authority with the least effort on his part in performing the actual control function.

A second mode is where the supervisor manually searches the parameter space of an automatic process to optimize performance, without direct regard for the process state trajectory. Nolan (ref. 4) and Pew and Jagacinski (ref. 5) measured how the human operator adjusted parameters of one system to make its output match that of another system.

A third (least sophisticated) mode is where the supervisor preprograms a process state trajectory as far as he thinks will optimize the performance function (which may include the cost of his own sampling or attention). This is the mode explored in these experiments. This mode has many analogies from everyday human supervisory situations. It requires of the human operator more detailed control functions than either of the above levels.

These experiments build on the previous human operator sampling models of Senders (ref. 6), Smallwood (ref. 7), and Carbonell (ref.

8). The Baron and Kleinman model of the human operator as an optima1 controller also includes an optimal sampling assumption (ref. 9).

THEORY

In a previous paper (ref. 10) it is shown that given

(1) A process input x characterized by a random time series of probability density (%) and by conditional probability density $\{x'|x_0t\}$, where x' is a value of x at time t after a known value of x, x_0 at time $t=0$,

(2) A value function $V(x,y)$, indicating the reward (in a positive sense) or penalty (in a negative sense) acquired per unit time when input is x and control variable is y,

(3) The cost C of sampling the input, the optimal control y at each t after sampling x is

$$y_{\text{opt}}=y[V(x,y),x_0,t]=\max_{y}\int_{x'}\langle V|x'y\rangle\{x'|x_0t\}. \quad (1)$$

Brackets ( ) indicate an (ensemble) expected value and $\int_{x'}$ indicates integration over all z'.

The optimal sampling interval T was similarly shown to be

$$T_{\text{opt}}=T_{\text{opt}}[V(x,y),\ \{x'|x_0t\},\ \{x\}]$$
$$=\max_{T}\left\{\frac{1}{T}\int_{t=0}^{t}\left[\int_{x_0}y_{\text{opt}}[V(x,y),x_0t]\{x_0\}\right]-\frac{C}{T}\right\} \quad (2)$$

While in certain cases analytical expressions for $\{x'|x_0t\}$ are analytically tractable, this function can also be generated montecarlo fashion by computer. Use of the latter is a convenient procedure when computer solution of values of y_{opt} and T_{opt} is desirable.

The above theory applies for any input time series $x(t)$, with its corresponding $\{x\}$ and $\{x'|x_0t\}$, and any value functions of control and sampling, $V(x,y)$ and C. However, it is obvious that arbitrary inputs and value functions will result in tasks which may be unnatural (not be like any familiar real-world experiences) and virtually impossible to learn.

EXPERIMENTS

The task considered in these experiences consisted of asking subjects to make predictions (in a least-squared error sense) $y_j(\Delta t)$, $y_j(2\ \text{At})$, . . . , $y_j(i\ \Delta t)$, . . . , $y_j(T_j\ \Delta t)$ of the future values of a time series $x_j(\Delta t)$, $x_j(2\ \text{At})$, . . . , $x_j(i\ \Delta t)$, . . . , $x_j(T_j\ \Delta t)$. These values were outputs of **a** second-order digital filter driven by white noise. T_j* is the prediction interval for the j^{th} trial of an experimental run and was chosen by the subjects. **As** initial conditions, subjects were given $x_{j-1}[(T_{j-1}-1)\ \text{At}]$ and $x_{j-1}[(T_{j-1})\ \text{At}]$ which are also equal to $x_j(-\text{At})$ and $x_j(0)$. The end of the $\text{j}-1^{\text{th}}$ interval serves as initial conditions for the j^{th} interval.

After inputing $y_j(\Delta t)$, $y_j(2\ \text{At})$, . . . , $y_j(i\ \text{At})$, . . . , $y_j(T_j\ \Delta t)$, subjects were shown the actual output $x_j(\Delta t)$, $x_j(2\ \text{At})$, . . . , $x_j(i\ \text{At})$, . . . , $x_j(T_j\ \text{At})$ and their score for the j^{th} trial given by

$$V_j=\frac{\sum_{i=1}^{Ti}[x_j(i\ \text{At})-y_j(i\ \text{At})\ ]^2+C_j}{T_j}, \quad (3)$$

where, C_j = the cost to the subject of updating his information about the actual x's. The subjects' monetary reward for performance on the j^{th} trial monotonically increased with decreasing V_j. Thus, a trade-off developed between the cost of making prediction errors and the cost of information (referred to as sampling cost).

For the $j+1^{\text{th}}$ trial, subjects specified T_{j+1} and used $x_j[(T_j-1)\text{At}]$ and $x(T_j\ \Delta t)$ as initial conditions. They then input T_{j+1} y's and the experiment continued as above.

The task was self paced, not forced pace; subjects had plenty of time to think through decisions before making them.

As previously indicated, the x's were generated by passing zero mean white noise through a second order filter. The transfer function of the filter $G(s)$ is given by

$$G(s)=\frac{w^2}{(s+w)^2} \quad (4)$$

where w = filter bandwidth in radians per At (unity damping ratio). The noise was realized

* The prediction interval can also be called a sampling period because the subjects' information concerning the actual x's is updated after T_j. Thus, prediction interval and sampling period are **used** synonymously in this paper.

digitally using a gaussian random number generator which was proven satisfactory by calculating its autocorrelation function.

The filtered output x was generated by using equations for the statistics of the distribution of the state of knowledge of x (after sampling at $t=0$) given by

$$m_{j+1}(t) = x_j(T, At)(1+wt)e^{-wt} + \hat{x}_j(T_j\,\Delta t)te^{-wt}, \quad (5a)$$

$$v_{j+1}(t) = v_0[1-(1+2wt+2w^2t^2)e^{-2wt}], \quad (5b)$$

where

$m_{j+1}(t)$ = mean of probability density function representing our state of knowledge of x during the $j+1^{\text{th}}$ trial

$v_{j+1}(t)$ = variance of x during the $j+1^{\text{th}}$ trial

v_0 = steady-state variance of signal

t = zero at beginning of $j+1^{\text{th}}$ trial.

Computationally, it was not necessary to use equation **(4)** as the filter output was directly obtained by using equations (5a) and (5b) which were discretely realized by letting $v_0 = 225$ and using

$$x(T_j\,At) = \frac{x(T_j\,At) - x[(T_j-1)\,At]}{At}. \quad (6)$$

To determine the optimal solution for the j^{th} trial, the optimal prediction interval T_0 (the subscript j is omitted because T_0 was generally constant over the entire j trials of a run) was found by minimizing the expected value of equation *(3)* V_j with respect to T_0. This expected value is given by

$$\langle V_j \rangle = \frac{\sum_{i=1}^{T_0} v_j(i\,At) + C_j}{T_0} \quad (7)$$

Once T_0 is determined, the optimal prediction strategy is to follow the nonstationary mean $m_j(t)$ until the next sample. For this procedure $\{x'|x_0t\}$ is characterized by $m_j(t)$ and $v_j(t)$. These were estimated on-line by simulating the filter output one hundred times from the given initial conditions and averaging across the results. This estimation technique was employed to eliminate problems that arose from using approximation of equation **(6).**

The experiments were performed entirely on a PDP-8 digital computer using a teletype as input and display apparatus. Each subject made his specification of inputs by typing numbers at his own comfortable pace.

The experimental input and display arrangement was identical for both experiments. A sample trial is illustrated in figure *1.* The subject input the bandwidth, sampling cost, and run number at the beginning of each run. These were specified by the experimenter. He was given an initial X and x. He chose T_j and input the appropriate number of y's (integers between 0 and *100).* As feedback he received the x's that occurred during the interval and his sampling cost per unit time C/T, squared error per unit time F/T, and V_j which is $(C+E)/T$. At the end of each run, he was told how much he made during that run. During all nine sessions of these experiments, sample signal plots for each of the bandwidths were posted within the subjects' view and subjects were encouraged to use them as necessary. After each session, the subjects' comments were gathered and recorded.

The experiments were performed using four male subjects including one graduate student and three undergraduates. All of the subjects had some familiarity with system dynamics. Each subject was told that the input he was predicting was the output of a second-order filter and that this output had a mean equal to fifty and a variance of v_0.

The optimal strategy was completely explained to the one graduate student hence referred to as

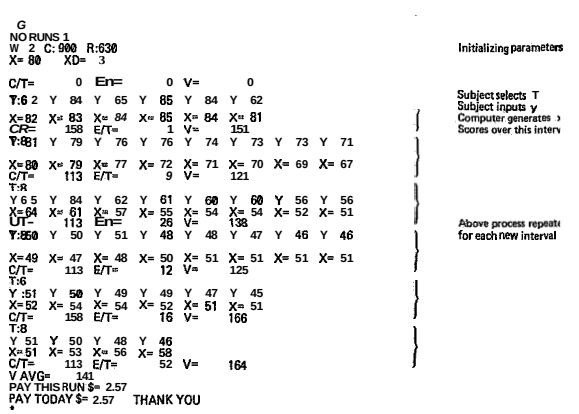

FIGURE 1.—Input and display arrangement on teletypewriter.

the "trained subject" S_1 before the experiments began to assess the affect **of** such knowledge on performance.

The subjects were rewarded per session according to the following pay structures, where minimizing expected value of criterion function, V_j, (eq. *(3))* is equivalent to maximizing expected pay.

$$P_1 = \$1.00 + \$\frac{1}{N}\sum_{k=1}^{N}(C_k - V_k), \tag{8a}$$

$$P_2 = \$1.00 + \frac{1.5}{N}\sum_{k=1}^{N}\left(\frac{C_k - V_k}{P_k C_k}\right) \tag{8b}$$

$$P_3 = \frac{\$2.5}{N}\sum_{k=1}^{N}\left(\frac{C_k - V_k}{P_k C_k}\right) \tag{8c}$$

where

N = number of runs during session,
P_k = a normalizing percentage for k^{th} run,
V_k = cumulative score for the trials of the k^{th} run $= \sum_{i=1}^{j} V_i$
C_k = sampling cost for k^{th} run.

P_1 was used during the first three sessions for S_1 and S_2, P_2 during the remaining six sessions for S_1 and S_2, and P_3 with S_3 and S_4 for all nine sessions. These modifications in pay structure were made in an effort to improve the sensitivity of reward to performance and to insure a reasonable incentive to do well. However, discussions with S_1 and S_2 showed that they were not particularly conscious of the changes in pay structure.

Experiment I consisted of two parts. Each part included three **1-1/2** hour sessions. Before the experiment began each subject performed three practice trials. The individual runs lasted 40 to **60** time units. Runs were terminated at this fixed time regardless of whether or not a subject was in the middle of a prediction interval. This termination was necessary because subject and optimal predictor must run over the same length of time for a valid comparison.

During the first part of this experiment eight combinations of input bandwidth w and optimal sampling period T_0 were employed as indicated below

w \ T_0	3	5	8
0.2	1	2	3
.3	4	5	6
.4	7	8	...

Subjects were assigned a random sequence of the above eight runs configurations. Each run was forty units of time in length. Three replications of this matrix of assignment of runs constituted the first three sessions of the first part of experiment **I.**

The second part of experiment I used the following experimental matrix:

w \ T_0	3	5	8	12
0.2	1	2	3	4
.3	5	6	7	8
.4	9	10	11	12

A new random sequence of the above **12** runs was used to assign runs to each subject. Each run was 40 time units in length. Three replications of this sequence constituted the three sessions of the second part of experiment **I.**

Experiment II consisted solely of measuring the subjects' prediction ability as they were told what prediction period to use. The experimental matrix was

w \ T_0	5	8	12	17
0.2	1	2	3	4
.4	5	6	7	8

A new random assignment of the above eight runs was used for each subject. Each run was **60** time units in length. Three replications of this sequence constituted the three **1** hour sessions of this experiment.

Summarizing this section, two experiments were performed to study the human operator's ability to pick optimal prediction intervals and to predict between samples.

RESULTS

Experiment **I** included two variables of interest: prediction or sampling period chosen by the subject and the average criterion function V resulting from tracking. Figures **2, 3,** and **4** illustrate the sampling periods chosen by the subjects plotted versus the optimal sampling periods. These data from the sixth session represent the steady state choices of sampling periods and shows the subjects to have consistently underestimated these periods except on the low *T's.*

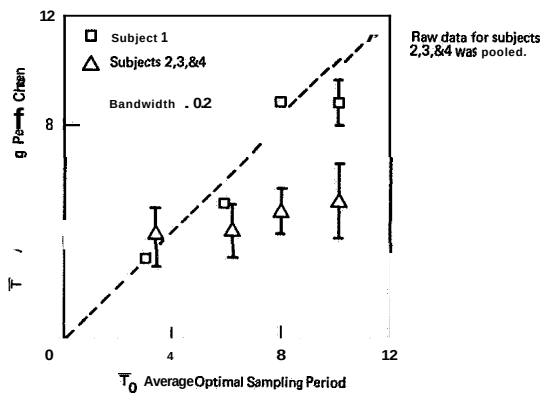

FIGURE 2.—Average sampling periods (at 0.2 bandwidth) chosen **for** the sixth session.

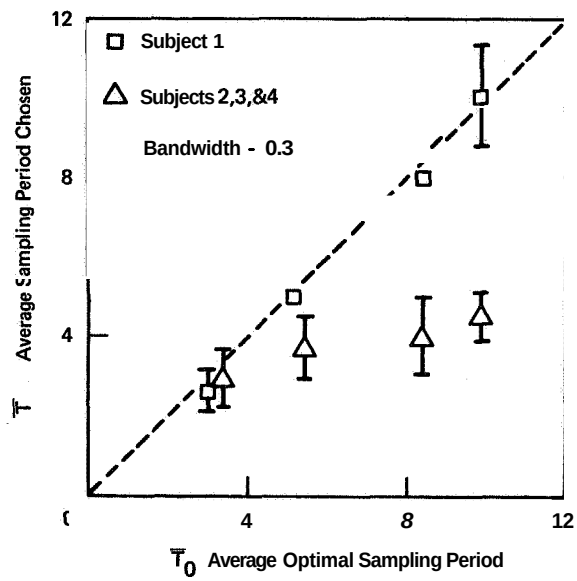

FIGURE 3.—Average sampling periods (at **0.3** bandwidth) chosen for the sixth session.

The trained subject did much better since he was aware of the range of *T's* before the experiment began.

Since the subjects chose *T's* much smaller than they should have, their scores were much different than optimal, due mainly to higher sampling cost per unit time. The subjects' and optimal *V's* are compared in figures 5, **6,** and 7. On the basis of the ratio V optimal/*V* subject, the subjects were found to be closest to optimal for $T = 5$ with a percentage of **0.864.** This experiment does not provide a fair comparison between *V's* because optimal and subject used different *T's.* However, the data do indicate that a different optimal sampling strategy may exist if a subject's tracking strategy is not optimal. Thus his picking a large *T* (given that he doesn't really predict optimally over that long of an interval) may actually give him a worse score than picking a smaller T. This phenomenon did not occur often enough to permit any more than conjecture on this point.

Experiment II only investigated the subject's ability to predict in the interval between samples, as they were told what T to use. The subjects' and optimal *V's* are compared in figures 8 and 9.

The long *T* trials show the effect of a suboptimal prediction strategy more than the short

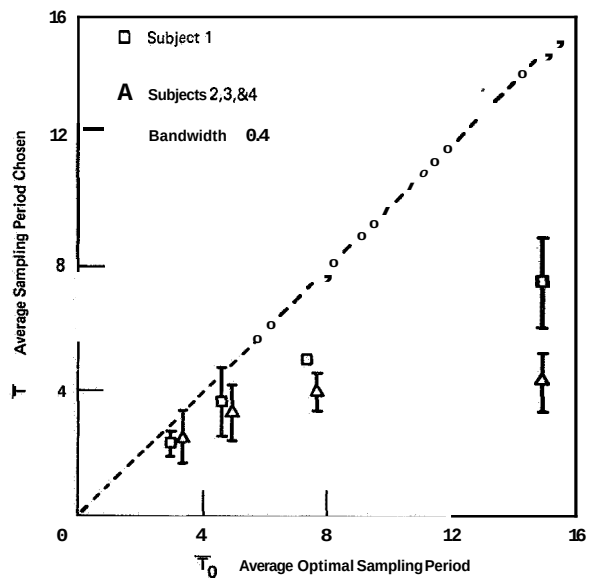

FIGURE 4.—Average sampling periods (at **0.4** bandwidth) chosen **for** the sixth session.

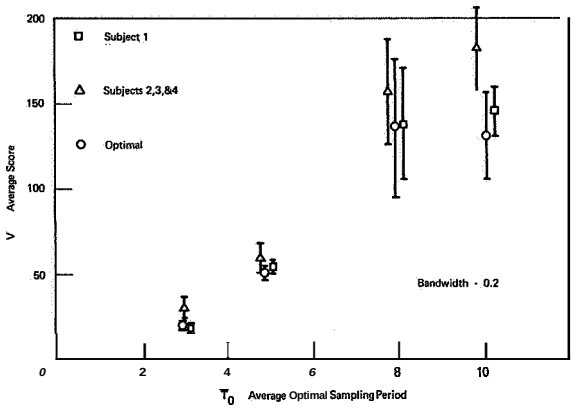

FIGURE 5.—Average scores (at 0.2 bandwidth) for experiment I.

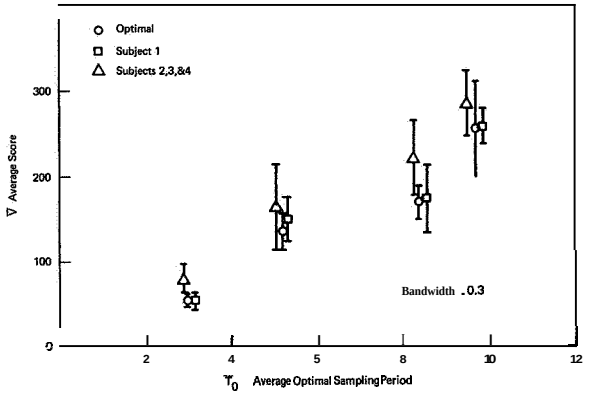

FIGURE 6.—Average scores (at 0.3 bandwidth) for experiment I.

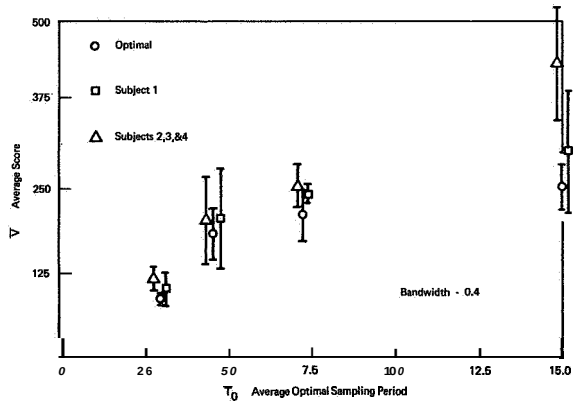

FIGURE 7.—Average scores (at 0.4 bandwidth) for experiment I.

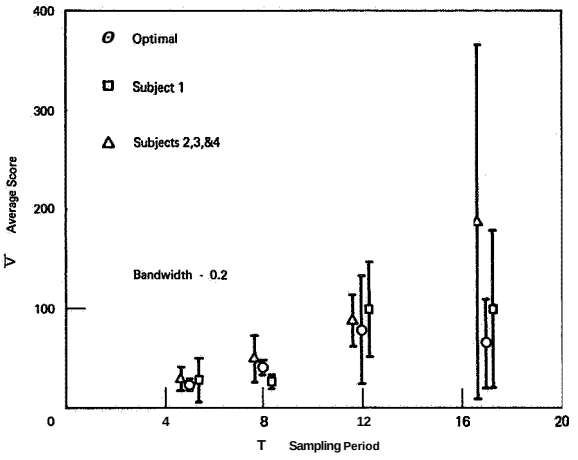

FIGURE 8.—Average scores (at 0.2 bandwidth) for experiment 11.

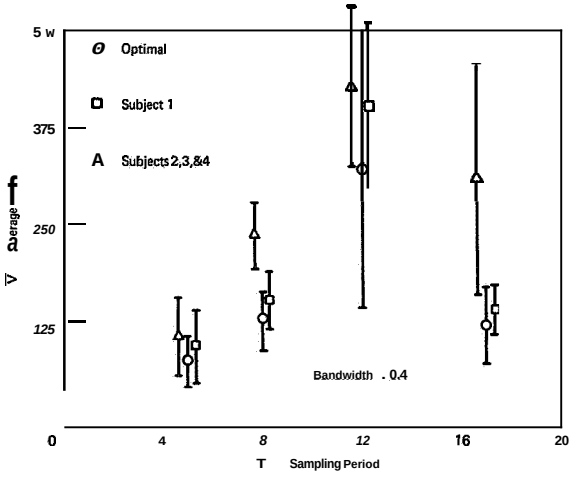

FIGURE 9.—Average scores (at 0.4 bandwidth) for experiment 11.

T trials. This is reasonable because approximations to the optimal strategy of predicting the mean diverge more for longer T's.

Plots of subjects' trajectories versus optimal trajectories, figures **10** through **13,** show that certain subjects consistently tend to extrapolate linearly and all subjects return to the mean much more slowly than the optimal. Thus, for T's of **5,**

Notes:

(1) Bars on data of figures 2 through 9 represent ±1 standard deviation.

(2) Raw data for subjects 2, 3, and 4 were pooled (figs. 2 through 9).

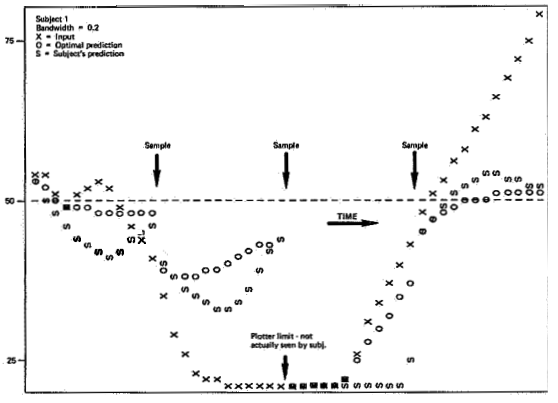

FIGURE 10.—Example of experimental time histories (subject 1).

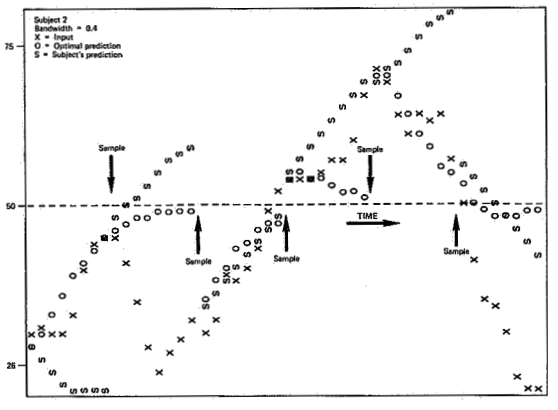

FIGURE 11.—Example of experimental time histories (subject 2).

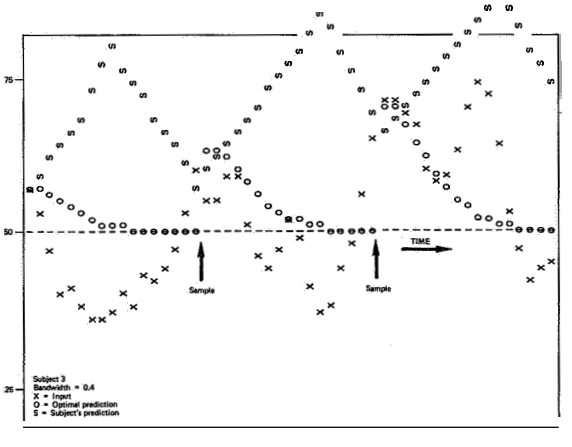

FIGURE 12.—Example of experimental time histories (subject 3).

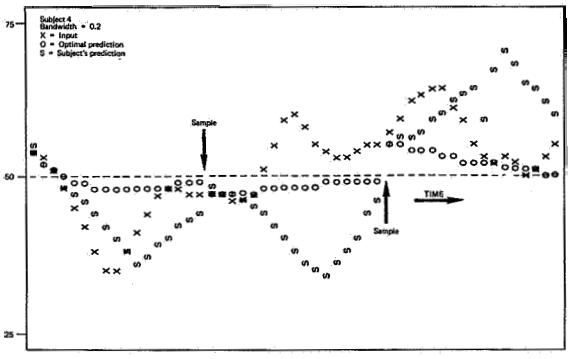

FIGURE 13.—Example of experimental time histories (subject 4).

subject and optimal are not very different while longer $T's$ emphasize the difference between a linear and an exponential prediction. The one well-trained subject did fairly well, but of course on the average could not score better than the optimal.

Reasons for suboptimality include the subjects having an erroneous internal model of the process. The model could be erroneous by being of the wrong order or may be of the correct order but with the wrong parameters. Many other reasons are possible but will not be considered at this point.

If we assume that the subjects each used some second-order internal model and performed optimally with respect to that model we then find a least-squared error fit of the following model to the data:

$$y\{[T_j-(T_j-1)]\,At) = K_1 \times (T_{j-1}\,At) + K_2 \frac{x(T_{j-1}\,At) - [(T_{j-1}-1)\,At]}{At}. \quad (9)$$

From this we can see how the subjects weight position and derivative in their prediction strategy. The above second order model was fit only to the subjects' first choice after sampling. (Fitting the subjects whole trajectory would require assuming a model for the whole trajectory.) Figures **10** through **13** show that it is hard to justify the same model (different parameters as optimal for points further away from the sample than one or two). However, modeling only the first point yields an idea of the sources of subjects' suboptimality. Fitting equation **(9)** to the

data from session nine of experiment II results in the following parameters:

w	Control	K_1	K_2	K_1/K_2
0.2	Optimal	0.98	0.91	1.09
	S_1	.99	.95	1.04
	S_2	.99	.68	1.33
	S_3	.98	.14	6.83
	S_4	1.05	.89	1.11
0.4	Optimal	0.94	0.67	1.40
	S_1	.98	.83	1.18
	S_2	.97	.39	2.51
	S_3	1.01	.14	7.07
	Sa	1.05	.62	1.70

Using these constants, we can quantify the performance of the subjects as displayed in figures 10 through 13. In general, the subjects overestimated K_1 which kept them from returning to the mean as quickly as they should. Some subjects overweighted the derivative while others underweighted it. In either case, this caused a degradation of performance.

DISCUSSION AND CONCLUSIONS

None of the subjects were able to score as low as the optimal (although training helped). This was due to their inability or unwillingness to pick appropriate sampling or prediction periods and to predict optimally.

Inappropriate choice of T is attributable to two sources. First, inability on the part of the subjects to predict over longer periods of time without sampling may have caused them to choose shorter sampling periods over which they felt their skills more closely resembled optimal. Second, the subjects were unwilling to take the chance of a large error that might arise from a longer sampling period even though this also gave them a very small time-averaged sampling cost and thus a chance at a very high reward. This tendency is termed risk aversion and is evidenced by the subjects' comments that were collected.

Inability to predict optimally resulted from various sources. The subjects' internal model of the input process may have been erroneous as previously discussed. Also, subjects may not have fully realized what prediction strategy would minimize the specific value function. In particular, some of the subjects obviously did not know that predicting the estimated mean of the signal distribution was the optimal strategy and consequently they attempted to make their y's look like the x's. This strategy is disastrous if the subject guesses the wrong direction after sampling. Subjects' comments also indicated that they may need more than the last two points to predict the next point. In effect this amounts to their assuming a higher order filter than actually existed.

Summarizing, these experiments have enabled us to study sources of suboptimality in a specific task. These sources are perhaps applicable to many other tasks (i.e., systems, value functions, etc.).

REFERENCES

1. NEVINS, J. L.; JOHNSON, I. S.; AND SHERIDAN, T. B.: Man Machine Allocation in the Apollo Navigation, Guidance and Control System. Draper Lab Memo, M.I.T., 1968.
2. SHERIDAN, T. B.: Use of Artificial Computation Loops within Human Control Loops for Remote Manipulation. Unpublished memo, Department of Mechanical Engineering, M.I.T., Oct. 28, 1964.
3. FERRELL, W. R.; AND SHERIDAN, T. B.: Supervisory Control of Remote Manipulation. IEEE Spectrum, vol. 4, no. 10, Oct., 1967.
4. NOLAN, G.: Human Response in Matching the Parameters of an Operating Dynamic System. SM Thesis, Department of Mechanical Engineering, M.I.T., 1959.
5. PEW, R. W.; AND JAGACINSKI, R. T.: Mapping an Operator's Perception of a Parameter Space. Proceedings of the Seventh Annual Conference on Manual Control (Los Angeles), June 1971.
6. SENDERS, J. W.: The Human Operator as a Monitor and Controller of Multidegree of Freedom Systems. IEEE Trans. Human Factors in Electronics, vol HFE–5, no. 1, Sept., 1964.
7. SMALLWOOD, R. D.: Internal Models and the Human Instrument Monitor. IEEE Trans. Human Factors in Electronics, vol. HFE–8, pp. 181–187, Sept., 1967.
8. CARBONELL, J. R.: A Queuing Model of Many-Instrument Visual Sampling. IEEE Trans. Human Factors in Electronics, vol. HFE–7, pp. 157–164, Dec., 1966.
9. BARON, S.; AND KLEINMAN, D. L.: The Human as an Optimal Controller and Information Processor. IEEE Trans. Man Machine Systems, vol. MMS–IO, no. 1, Mar., 1969.
10. SHERIDAN, T. B.: On How Often the Supervisor Should Sample. IEEE Trans. System Science and Cybernetics, vol. SSC–6, pp. 140–145, Apr., 1970.

N73-10115

11. "Manual" Control Models of Industrial Management*

E. R. F. W. CROSSMAN

University of California

The industrial engineer is often required to design and implement control systems and organization for manufacturing and service facilities, to optimize quality, delivery, yield, and minimize cost. Despite progress in computer science most such systems still employ human operators and managers as real-time control elements. Manual control theory should therefore be applicable to at least some aspects of industrial system design and operations.

Formulation of adequate model structures is an essential prerequisite to progress in this area; since real-world production systems invariably include multilevel and multiloop control, and are implemented by timeshared human effort, this is a nontrivial problem. Since structures proposed by Haberstroh (ref. 1), Beer (ref. 2) and others appear inadequate, a modular structure incorporating certain new types of functional element, has been developed. This forms the basis for analysis of an industrial process operation.

In this case it appears that managerial controllers operate in a discrete predictive mode based on fast time modelling, with sampling interval related to plant dynamics. Successive aggregation causes reduced response bandwidth and hence increased sampling interval as a function of level.

Data of Jaques (ref. 3) on the so-called "time-span of discretion" are cited in support of specific hypotheses concerning the influence of level of control on manual control requirements of managers.

INTRODUCTION

Dated from Arnold Tustin's pioneer study of tank gunnery (ref. **4),** the engineering approach to manual control is now *25* years old and well advanced both in theoretical and design capability. The time therefore seems ripe for a serious attempt to extend its range beyond the original fields of weaponry and vehicular control and find potential applications in other major system design areas. Interpreting the term manual control in a relatively broad sense, there would appear to be many possibilities, since nearly all systems and institutions from the largest† to the smallest use manual control in one form or another. Reviewing various fields, engineers are likely to be attracted to those where **(1)** existing control structures are relatively stable, environments well-defined, and performance specifications can be agreed; *(2)* there is an existing quantitative approach with supporting data; and **(3)** some possibility exists of persuading clients to implement new or modified designs. An additional criterion would be: **(4)** an evident need due to shortcomings in, or total lack of, existing design techniques.

One field meeting the first three of the above criteria is plant level industrial process control, used extensively in the oil, chemical, paper, food, and other industries. My earlier explorations (ref. **6)** suggested that manual control models could be of significant value in process plant design; however, automatic control techniques, implemented first with analog instruments and now increasingly with online computers, have been so successful here as to leave only a small field for manual control technology, however expert.

* This research was supported in part by the Office of Naval Research under contract N00014-69-A-0200-1043 with the Univ. of Calif.

† Tustin himself gave an early automatic control (frequency domain) analysis of macroeconomics (ref. 5), and suggested some "Equalization" policies. However, he did not consider manual control as found at Treasury level!

The picture is entirely different and in my view more promising at the next higher level of industrial control. We consider the production sector only here, though marketing and sales present similar problems. Analog instrumentation cannot be used, and as yet there are extremely few (if any) fully effective online computer control systems operating above the plant level, even in process industries which at first sight would appear to lend themselves to total automatic control (see for example, refs. 7 and 8). Thus almost all industrial control (as distinct from data acquisition, storage, and retrieval) is still implemented manually, sometimes based on explicit decision rules but much more frequently on human judgment. At a conservative estimate, a typical industrial plant employing 100 people implements some 500 to 1000 manual control loops, effective in frequency bands ranging from seconds to years; this estimate of course includes only sampled data or continuous control, and excludes other manual activities such as manipulation, data acquisition, and communication.

Techniques used by industrial engineers and management consultants to design and assist in implementing these highly important control processes, which are needed to meet product specifications and maintain quality, minimize cost, increase yield, and insure prompt delivery, do not currently include automatic control in any form, still less human operator theory. Among quantitative tools used are statistical quality control which is based on time domain statistics, and such operations research techniques as static optimization by linear programming, and network flow models. However, fully engineered dynamic design methods are conspicuously lacking, and in most practical cases good or improved dynamic response is secured only by online intuitive trial and error. In other words, viable control systems are not designed, but grow (if they do) organically.

This situation appears to present a direct challenge to the automatic and manual control fraternity, a challenge which has as yet elicited little response except from a few pioneers such as Sheridan (ref. 9). The present paper seeks to structure some of the problems involved in responding and to draw attention to some existing data which may be useful for this purpose. It also presents, on an admittedly speculative basis, the beginnings of a model structure which I feel may form the necessary basis for a rational design procedure. Unfortunately time and space constraints have permitted no more than a sketch map, which I hope will be expanded into a substantive contribution at a later date.

SYSTEM MODELS FOR INDUSTRIAL CONTROL

To arrive at a workable system model incorporating human control elements, we need (1) a valid flow diagram showing the control relationships between systems elements, both human and otherwise, and (2) compact quantitative characterizations of the various elements, expressed in input/output form.

Role Structures

In the industrial management case we cannot readily specify or trace a precise wiring diagram, since the intercommunication pattern found in even a small industrial plant is very involved (ref. 10). Nor are the individual response patterns of managers amenable to simple description. Brief field observation will readily confirm these statements. To simplify reality we must work with idealized role relationships and prescribed role behaviors, as indicated for example in job descriptions, rather than with actual behavior. Roles can be conceived as idealized "programs" which each role incumbent is supposed to execute; programmed behaviors include seeking and accepting specific types of data, processing it in a certain manner, outputting specific types of data or commands to other role players, and in some cases manipulating machine controls. The operating role structure and programs of a particular organization may, of course, depart widely from that given in written job descriptions; in case of doubt we must ascertain or reconstruct the true role structure from interview data. The control system is then abstracted from the role structure thus determined. Conversely, a control system designed for an industrial control application is implemented by written instructions to role players, supplemented by training on the job.

Previous Model Structures

The classical control model, after which most industrial organizations are patterned, is the bureaucratic hierarchy first described by the sociologist Max Weber late in the 19th century (ref. 11) and now familiar as the "organization chart" (see fig. 1). Taken literally, this describes an open-loop command structure, the only parameters being number of levels and span of control. A United Kingdom study by Joan Woodward (ref. 12) recently showed (fig. 2) that both of these vary widely with type of product and production technology. Span of control frequently, but by no means universally, decreases with managerial level. This parameter clearly describes a human timesharing phenomenon, and some attempts have been made to derive optimum values from a queueing model, but without marked success.

Considered as a control flow model the organization chart is obviously incomplete, making no provision for feedback and failing to identify system inputs and outputs. Despite much discussion, for instance by Beer (ref. 2) and Buckley (ref. 13), very few attempts have been made to construct more realistic and satisfactory structures adapted to theoretical analysis. Haberstroh (ref. 1) has provided perhaps the best case study to date, concerning the safety subsystem of an integrated steelworks. Figure 3 presents his model structure, together with a time history giving some indication of dynamic response. While interesting, this study was obviously far from complete, and failed to cover the actual production process for producing steel. A recent paper from the glass industry by Mouly (ref. 7) comes nearer to presenting a true system and begins to exploit the frequency domain approach to system response.

Proposed Model Structures

Model *elements.*—In this section we develop a control flow * model structure which seems in principle capable of representing fully functional control systems found in industrial production plant, without undue forcing or resort to ill-specified functions. The structure is based primarily on the familiar type of single or dual input/single output elements, here identified according to function as effectors, control elements, and receptors (see table 1). These are

*One must, of course, carefully distinguish flow of control from flows of materials, power, labor, etc.

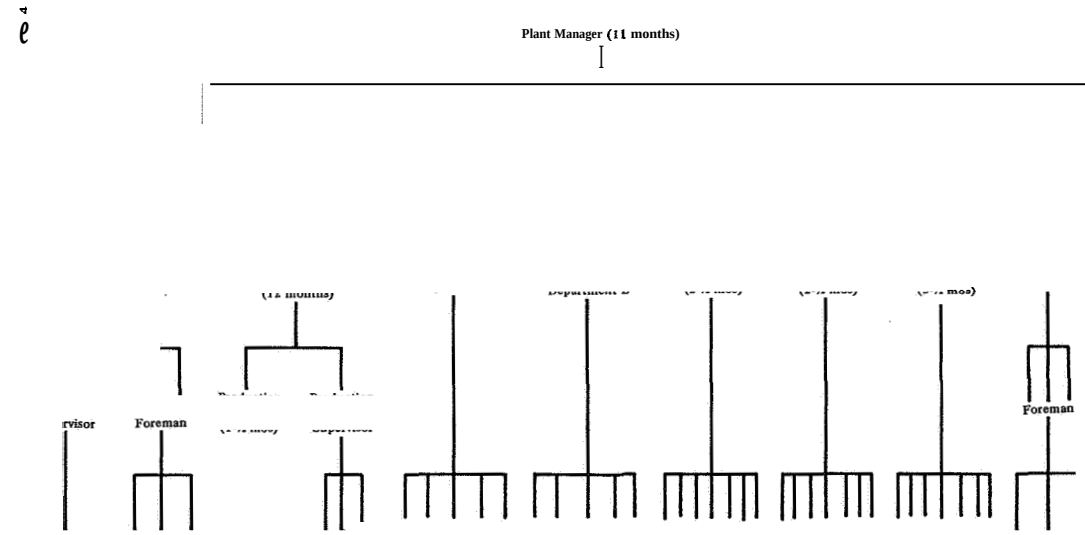

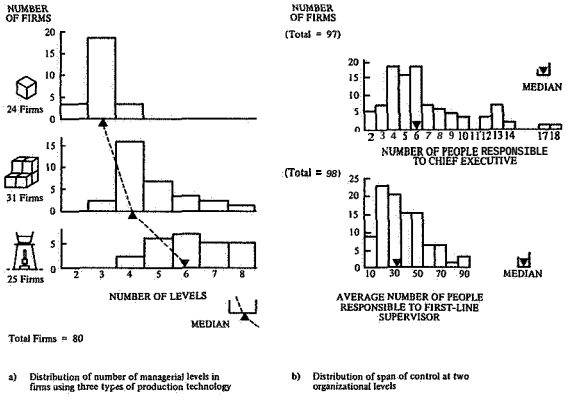

a) Distribution of number of managerial levels in firms using three types of production technology

b) Distribution of span of control at two organizational levels

FIGURE 2.—Field data on organizational levels and span **of** control (from ref. **12).**

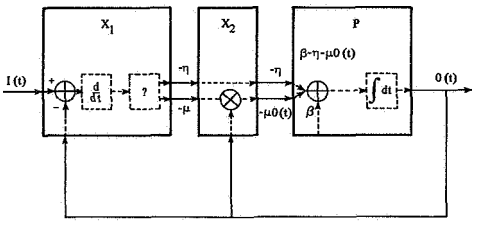

a) Model Structure

Year	Average All Plants	Disabling Injuries					Total Injuries			
		Error	Δ Error	Plant Performance	Error	Target	Plant Performance	Error	Target	Innovation
1	529	98	98	6 17			357			moderate
2	495	13	.85	5.08			422			none
3	541	1.77	1.64	7.18			407			heavy
4	466	124	53	5.90			302			none
5	366	61	51	433			244			
6	355	65	- 02	420	46	374	210	0	238	light
7	3 W	83	18	383	50	333	196	0	210	moderate
8	238	.81	02	319	12	247	183	11	172	light
9	2.07	63	18	210	.54	2.16	133	0	168	none
10	193	.91	28	284	80	2.04	128	0	133	heavy

connected in cascade, with loops closed around those elements (the effectors) which are most susceptible to disturbance and loading. Where implemented by human role players, these elements are assumed to function only intermittently, multiplexing switches being included to indicate the presence of timesharing.

Despite several attempts I found it impossible to construct a complete model using only these three elements and I have therefore introduced two new ones, termed respectively "multifiers" and "unifiers." These are intended to represent control aspects of the branching structure seen on the organization chart (fig. 1), a structure which arises in practice out of three specific functional requirements, **(1)** more than one operation (or transformation) is usually needed to turn raw material into product, **(2)** most processes and operations are multidimensional, **(3)** production volume usually requires simultaneous performance of the same operation on different batches of raw material or semifinished product.

The unifier element represents the combination **or** melding of several initially distinct product dimensions or process outcomes into a single complex but measurable result or product dimension. For example, in blending gasoline, measured amounts of various paraffins and additives combine or are ('unified)'to yield a certain octane rating. The unifier is a multi-input single-output element characterized by single-valued function of several variables, which may or may not include time.

The multifier element performs an inverse function to the unifier, and represents the process of generating two or more simpler subobjectives, goals or reference signals from a single complex objective. Thus the objective of producing a certain quantity of gasoline of a given octane rating must be "multified" or split up, into a series of production targets (or purchase orders) for the various components later to be blended. The multifier is a single-input multioutput element, and is characterized as a set of functions of a single input variable and time.

For simplicity, only four types of control variables or signals are identified here; these are **(1)** command or control variables c, **(2)** output or result variables r, **(3)** feedback variables f, and (4) disturbance or noise variables d. These will generally be available as time functions, but can be transformed into spectral functions for analysis.

Nested structure.—Using the five elements described above and listed in table 1, we can readily construct a multiloop hierarchical control structure capable of controlling or ('managing'' any number of effectors in the pursuit of a single complex time varying objective. The simplest possible inner-loop structure would be that of figure 4(a), with a single output dimension of a given process following up a single-dimensioned

TABLE *1.—Inventory of Model Elements*

	Function	Input	Transfer	output
Effector	Transforms incoming raw material or data into a desired state using power and other expendable resources	**1** Reference signals or commands. *2* Disturbances **3** Feedforward data (above level **1)**	Usually transport lag +lowpass filter. Often high-order	Dimensions of process or product.
Receptor	Samples, measures and encodes process or product quality **or** quantity dimensions	**1** Process or product dimensions, etc. *2* State of environment	Sampling with small lag; sometimes high-pass filter	**1** Feedback signals to controller. *2* Feedforward signal to controller.
Controller	Computes and issues reference or command to a single effector.	**1** Reference signal from multifier **2** Feedback signals from receptor. **3** Feedforward data from receptor.	Generally the approximate inverse of corresponding effector.	Reference signal(s) or command to effector
Unifier	Combines two or more diverse product **or** process dimensions into a single "result", itself measurable.	Two or more process or product outputs.	**A** single-valued function of two or more variables.	Single dimensional result
Multifier	Derives two or more subobjectives or reference signals from a single complex objective.	**A** single reference signal from a higher level controller	**A** set of functions of a single variable.	Two or more reference signals to lower-level controllers.

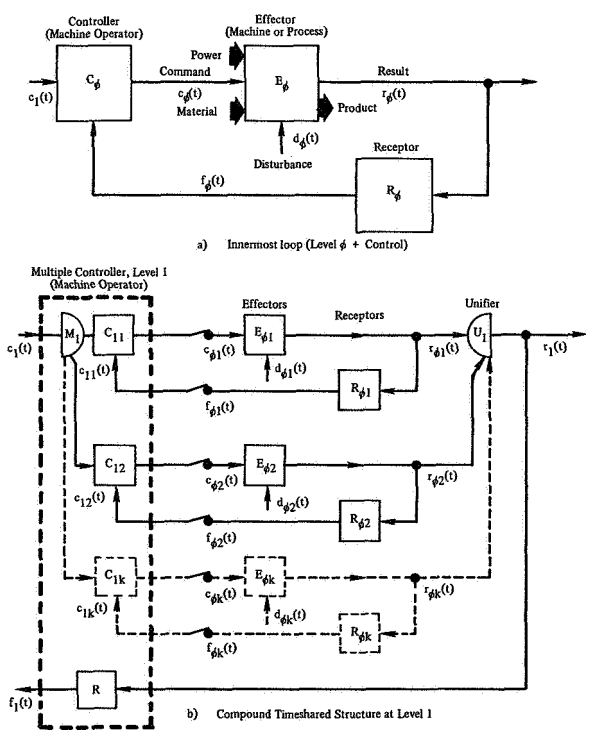

FIGURE 4.—Production control structure.

reference input under command of a controller supplied with feedback through a receptor. Typically this is implemented either as one subtask performed by a machine operator, or by a single analog process controller.

The typical skilled machine operator, however, both timeshares several such loop closures and determines for himself what the reference inputs to each loop shall be.* The outputs of the various effectors appear jointly in the product, whose overall quality and quantity should be that specified in the overall command input. Figure 4(b) shows the corresponding structure.

Since this parallel multiloop structure is self-contained, having only a single input and output, it can be regarded as a compound effector, and incorporated as a module in a larger structure

* We note in passing that timesharing need not occur at the micro level; the same structure applies to sequential performance of complete operations.

2

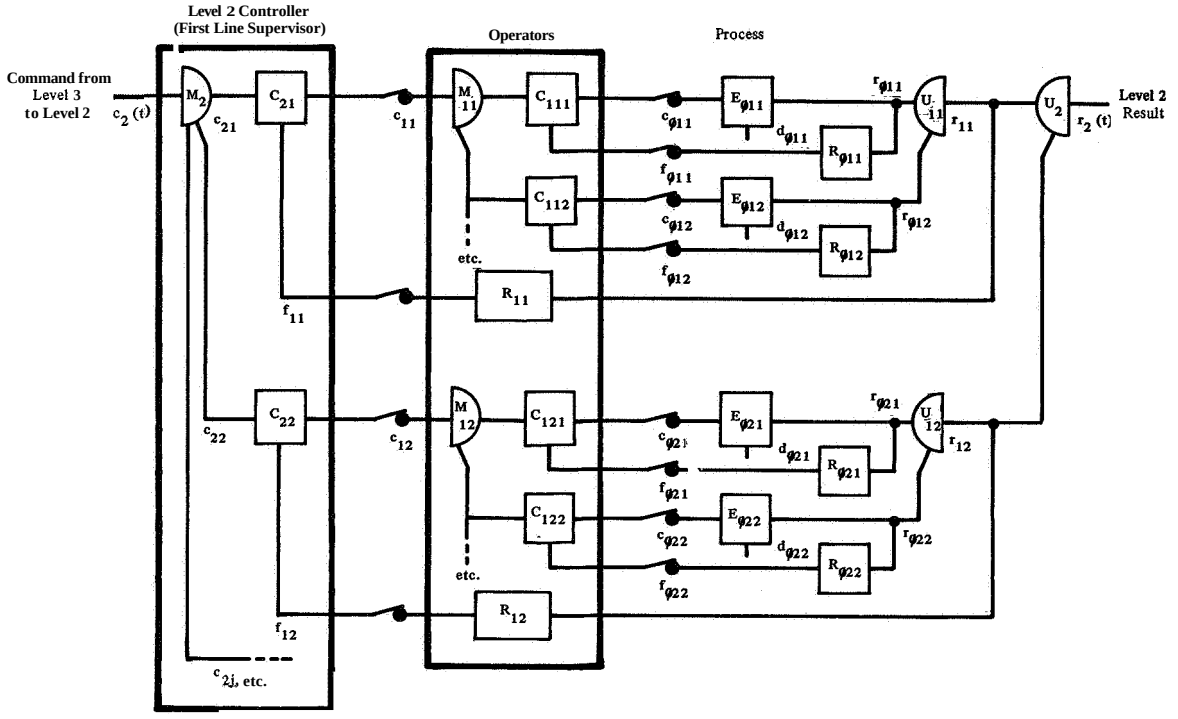

a) Full Level 2 Structure

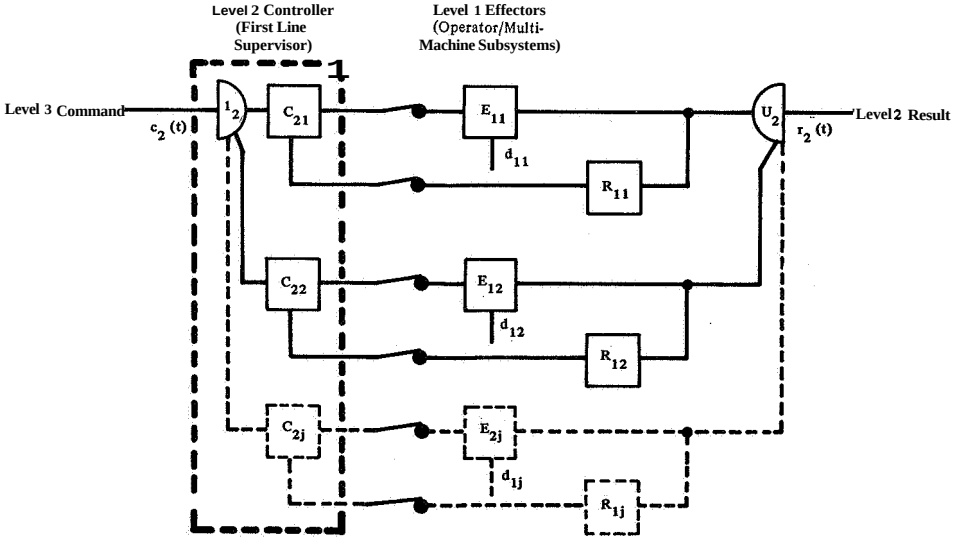

b) Level 2 Structure Simplified by Treating Each Operator/Multi-Machine Combination as a Single Effector

FIGURE 5.—Production control structure.

comprised of elements with exactly the same interconnections as those already described. Thus we arrive (fig. 5(a)) at a representation of the industrial foreman or supervisors' function in delegating objectives to, and monitoring the results of, a number of operators, shown in simplified form in figure 5(b).

The modular structure thus developed can be nested to any desired depth (fig. **S),** provided that **(1)** all component results are at some stage molded in a single overall result, **(2)** all subobjectives devolve ultimately from a single global objective, and **(3)** all activities can be related in the same time frame. We note that forcing functions are represented as being injected into specific control loops by two distinct routes, one deriving ultimately from the global objective, and the other through individual innermost loop effectors. While the latter does not directly model human error, little is lost by failing to distinguish this from machine and environmental disturbance.

Cross-coupling between effectors is a leading feature of most production systems, but is not represented in the above structures. Its control effects can be shown by transfers between effectors as shown in figure 7.

A case study.—With Office of Naval Research support, we have recently been able to obtain field data to permit modelling of the control aspects of two actual production systems using the structure described above, with coordinated time-span measurements as outlined below. The full details are, of course, quite voluminous and no attempt will be made to present them here. *As* an illustration of the structures obtained, figure 8 shows a single operator/machine model, including six loop closures and using a further subordinate man/machine system. This system produces a continuous product by processing given incoming materials to quality specifications laid down in standing instructions to the operator, in quantities specified in production schedules supplied by the foreman. Overall quality is subjected to inspection, but, as shown in the diagram, the operator performs online quality checks in each of the several quality dimensions involved. The operator in this case is experienced but not highly skilled in the conventional industrial sense. Disturbances arise as drifts and fluctuations in the process itself, in its environment (such as the power supply) and from fluctuations in raw material composition. In practice these are largely eliminated by the control mechanisms shown in the diagram, at least as far as the operators control "authority" reaches.

We hope to give a complete account of this case on a later occasion.

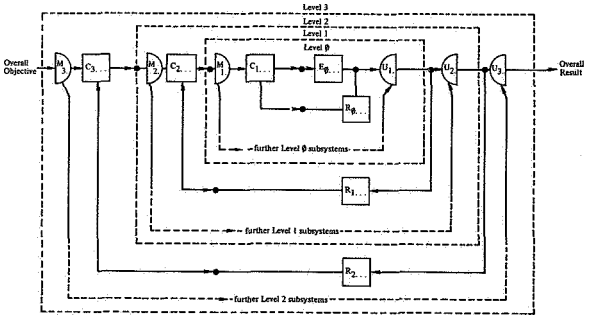

FIGURE 6.—Generalized multilevel **timeshared production control system configuration.**

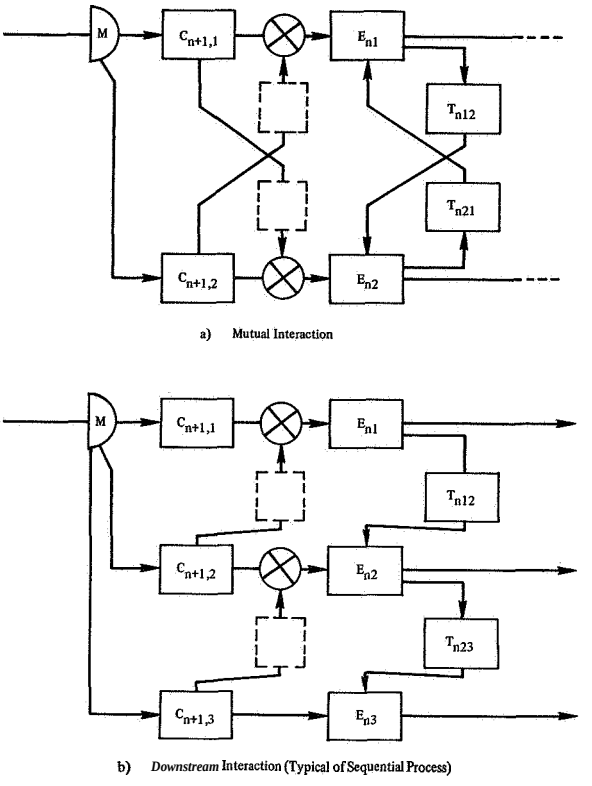

FIGURE 7.—Representation of interaction patterns among effectors in an industrial process.

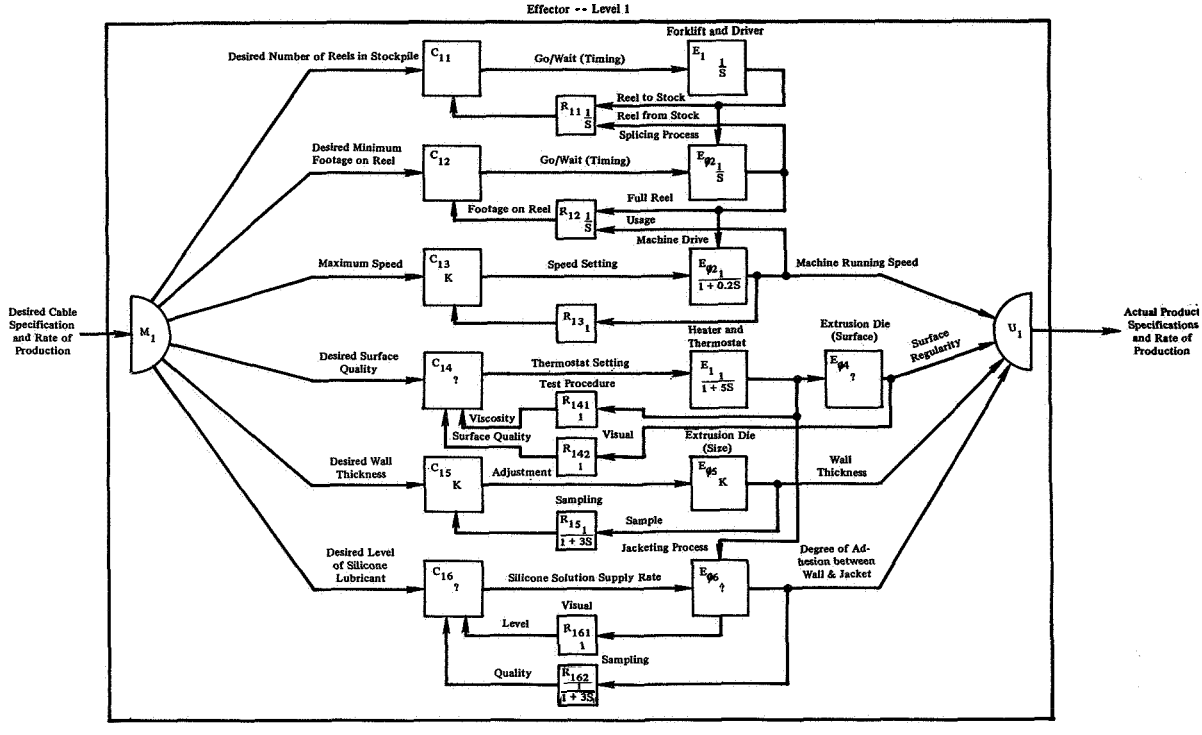

FIGURE 8.—Control structure for level 1 of a manufacturing process involving a continuously running special-purpose machine. Transfers expressed in cycles per minute. Control and receptor functions are timeshared by a single operator. One effector function is performed by a separate man-machine system (forklift truck and driver).

Application Goals

Assuming that models such as that described could be completed, and spectral descriptions of the various inputs and linearized transfers developed without large remnant terms, it would become possible to analyze system response to objective functions in the frequency band of interest to top management and disturbances expected to continue in the future. Components primarily responsible for steady state error, avoidable lag, and instability (if any) could then be identified and equalization forms developed. These would be implemented either by way of instrumental aids to the operator or manager (including computer-processed data) or through changes in role structure and required response of operators or managers. The latter would be installed by instruction and training; continued until the desired transfer was obtained. Such application possibilities seem, however, somewhat remote at present.

MANAGEMENT CONTROL CHARACTERISTICS

Since the control structure developed above is modular, it can in principle be nested to any desired depth; or, put the other way round, expanded to any level. We now consider the generalized role behavior required of the n^{th} level manager.

Desired Transfer

Figure 9 shows the generic control model of the level n manager, implementing one multifier function and two or more online controllers, the latter serving to regulate corresponding effectors, which (except at level 1) themselves contain complex control systems. Each such effector will be subject to disturbances not entirely eliminated by its own control system, hence creating a certain workload for its corresponding level n controller. Some of these disturbances will be predictable based on environmental data, and others

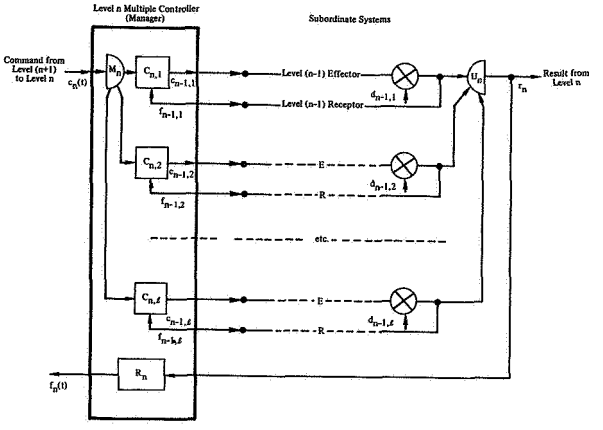

FIGURE 9.—Generalized manager model.

will arise from known cross-couplings between effectors, while still others will be random, hence unpredictable. Generally speaking, only disturbances within the pass band of the level $(n-1)$ effectors can be entirely eliminated, while the bandwidth of response to inputs from level $(n+1)$ is limited by the lowest level $(n-1)$ cutoff frequency. Hence, we would broadly expect managers at successively higher levels to operate in successively lower pass bands, and adequate control would require successively lower sampling rate.

The minimum transfer tolerable in the time-shared level n controllers would presumably be lagged (due to timesharing) proportional error feedback following up the current objective. However, low frequency disturbance would be poorly corrected by this policy, and a degree of integral feedback control would seem highly desirable. With effectors having second and higher order dynamics, some damping, by derivative control would also be needed for stability. Classical human-operator research has demonstrated human capacity to provide all these types of error feedback at high frequencies (on the order of radians per second). To cover the managerial case, however, radical relocation of the operating frequency band down to frequencies on the order of radians per day, week, month, and year is required and direct data in these ranges appear to be entirely lacking.*

* Though indications may perhaps be gleaned from Forrester's studies of Industrial Dynamics (ref. 14).

In addition to responding to error in a three term manner, we may also, following various studies of pursuit, preview and precognitive tracking (ref. 15) expect the level n controller to improve system response **by (1)** use of feedforward data to assist in regulating against predictable disturbances, both internal and external, and **(2)** use of fast time effector response modelling (Ziebolz control) to optimize approach to desired states and generate relatively high order control policies. These modes are less well understood, and it is not at present clear how much weight should be attached to them even in the fast tracking case, still less in low frequency managerial control.

Possible Relevance of "Time-Span of Discretion"

Some empirical evidence for frequency domain rnodels of managerial control at successive levels can be gleaned from the work of Elliott Jaques and his successors on the nature and level of managerial work. Starting in the early fifties in a United Kingdom metal working company* (refs. **3, 16,** and **17)** Jaques has developed a quantitative technique for measurement of the so-called "level" of work in managerial roles, which in the present context may be recognized to require mainly control system implementation. His earliest method (described fully in ref. **3)** consisted in determining, by interview of the immediate (level $n+1$) superior, the longest extended period over which the level n manager's exercise of discretion is allowed to remain unreviewed; or, to be more precise, the earliest time at which possible substandard exercise of discretion in the given role would be positively identified by the superior. **As** applied by Jaques, this quantity, termed "task extension," varies from assignment to assignment and the longest extension is taken to measure the "time-span of discretion," itself identified with level of work. While Jaques' method has proved difficult to apply in practice, and has certain theoretical difficulties (ref. 18), our own field trials have resulted in development of what we regard as an improved method, without changing the essentially time based criterion for measuring level of work (ref. 19).

* Glacier Metal Co., London.

Jaques obtained striking support for the validity of time-span as an index of level of work by studying its relation to salary level, either directly or through what he termed "felt-fair pay." In widespread industrial sampling, salary levels were found to increase monotonically with measured time-span over a very wide range (1 hr to 10 yr); the regression takes a roughly bilinear form, with a breakpoint around **3** months (see fig. 10).

Jaques has (so far unsuccessfully) proposed adoption of wage and salary policies based solely on level of work as determined by time-span. While this scheme has obvious difficulties, it is nevertheless clear that the industrial value of a manager is closely related to his time-span capacity; that is, the role of highest time-span that he is capable of successfully occupying. Salary progression curves show that this capacity develops predictably through a given individual career, and can be used to provide advance warning of organization problems (refs. **17,** 19, and 20).

Workers in the time-span field have also found a definite relationship between organizational level and time-span of role, to the point where some analysts are prepared to recommend organization structures with successive time-spans in a ratio not less than two. Our field studies show that, overlapping and discrepant time-spans are frequently associated with organization dysfunction. The organization depicted in figure 1 is a case in point; the general association between time-span and level will be evident to the reader, but a discrepancy is seen at plant manager level. This was associated with organizational trauma which cannot for reasons of confidence be described here.

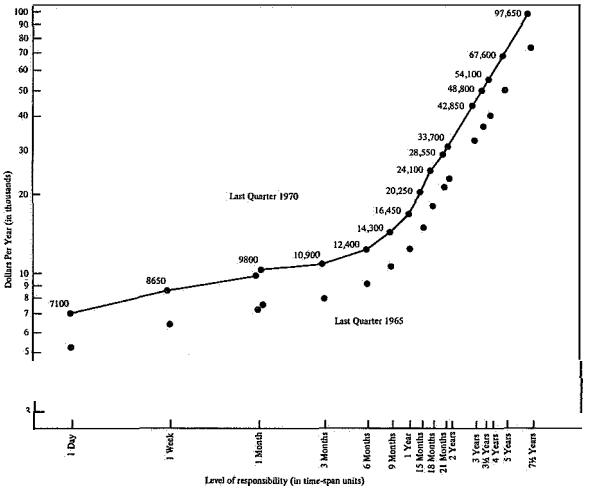

FIGURE 10.—Average managerial salary **as a** function of "time span of discretion." (Prepared by Laner and Caplan (ref. **20)** after Jaques (ref. 17).)

A Hypothetical Half Bandwidth Rule

These time-span results could be plausibly translated into the frequency domain by viewing the review interval used at level $(n+1)$ as a sampling interval adjusted to optimize information transfer from level (n). Since the feedback data being transferred represent disturbances transmitted through the level n effector, they will in general be confined to its response bandwidth. By the sampling theorem, therefore, the review interval should be not greater than twice the reciprocal of the effector cutoff frequency at level (n).* Hence the reciprocal of the estimated time-span of discretion at level n (as determined by interview at level $(n+1)$) could be viewed as an estimate of effector cutoff frequency at that level, and we would conclude that effector bandwidths decline on average by a factor of two between successive levels. This interpretation, however, yields unduly low cutoff frequency estimates and also fails to explain the higher value set on higher level controllers as shown by salary data.

An Alternative Double Planning Horizon Rule

In my view a more plausible interpretation of the time-span data can be given by considering low rather than high frequency phenomena, and assuming that many disturbances take the form of random walks rather than zero mean Gaussian processes. For forcing function frequencies in the range studied by, for example, Elkind (ref. 21), human operators appear to behave essentially as first-order low pass filters down to a breakpoint dependent on the amount of low frequency power present in the forcing function. While we have no data for forcing functions measured in radians per minute and below, it would be plausible to suppose (1) that the low pass break frequency declines with forcing function cutoff, and **(2)** that

* Assuming that this can be defined.

response falls off again beyond a still lower break frequency. In other words, the human controller may be imagined to behave generally as a first order bandpass filter adjusted to match the forcing function spectrum currently experienced.

The ability to provide a proportional band at relatively low frequencies with sampled data input depends, of course, on the possession of what one may loosely term leak-free memory; or in other words, the ability to retain and utilize instructions over long periods without refreshment, together with the ability to predict effector response to command inputs and known disturbances; and to output relatively precise correction signals. These requirements appear to place more demands on human control capability than does the fast action implied by extended high frequency response.

With these considerations in mind we may interpret the time-span data as reflecting the minimum input data rate required from level $(n+1)$ to support specified controller performance at level n, rather than the reverse. In this connection it is perhaps of interest that our field informants respond better to inquiries about their subordinates' projected future deployment of resources, than to those about the periods used for (retrospective) review of past performance. Managerial control appears to be based more on feedforward than feedback, and the time extent of the planning horizon used in resource deployment seems more important than the feedback sampling period (ref. 18).

Within this frame, we may perhaps interpret time-span as reflecting the low frequency cutoff applying to feedforward control at a given managerial level. The recommended time-span ratio of two between successive levels, would then imply successive halving of the managerial controllers' low frequency cutoff. In other words, higher level managers must respond coherently to lower frequency inputs, a principle extending down to cycles per decade at the very top. This principle would not of course prevent the same manager from also responding to high frequency inputs; but if extended low frequency cutoff were a rare individual quality, market forces would dictate delegation of high frequency control to less rare (and hence less expensive) talent.

The above two frequency domain interpretations of the time-span data are, of course, speculative; further data will be needed to decide between them, and further alternatives which may be proposed. What does seem clear is that data of this type are relevant to frequency domain modelling of industrial management. And, as I have said, management is a very widespread form of "manual" control.

REFERENCES

1. HABERSTROH, C. J.: Control as an Organizational Process. Management Science, vol. 6, no. 2, 1960, pp. 165–171.
2. BEER, STAFFORD: Cybernetics and Management. John Wiley and Sons, 1964.
3. JAQUES, E.: Time-Span Handbook. Heinemann, (London), 1964.
4. TUSTIN, A.: The Nature of the Operator's Response in Manual Control and its Implication for Controller Design. J. Inst. Elect. Eng., vol. 94, 1947, pp. 190–202.
5. TUSTIN, A.: The Mechanism of Economic Systems. Heinemann, (London), 1953.
6. CROSSMAN, E. R. F. W.: Fitting Man into Automatic Process Control. Proceedings of 17th Annual Industrial Engineering Institute (Berkeley, Calif.), 1965.
7. MOULY, R. J.: Systems Engineering in the Glass Industry. IEEE Trans. Sys. Science and Cybernetics, vol. SSC–5, no. 4, 1969, pp. 300–312.
8. CROSSMAN, E. R. F. W.; ET AL.: Impact of Technological Change on Manpower and Skill Demand. Human Factors in Technology Research Group Final Report to U.S. Department of Labor, Univ. of Calif. (Berkeley), 1969.
9. SHERIDAN, T. B.: On How Often the Supervisor Should Sample. Human Factors in Technology Research Group Working Paper HFT 69-12, Department of Industrial Engineering and Operations Research, Univ. of Calif. (Berkeley), 1969.
10. BURNS, TOM: The Directions of Activity and Communication in a Departmental Executive Group: A Quantitative Study in a British Engineering Factory with a Self-Recording Technique. Hum. Rel., vol. 7, 1954, pp. 73–97.
11. WEBER, MAX: The Theory of Social and Economic Organizations. (Translated by A. M. Henderson and Talcott Parsons.) Oxford Univ. Press (New York), 1947.
12. WOODWARD, JOAN: Industrial Organization, Theory and Practice. Oxford University Press (New York), 1965.
13. BUCKLEY, W.: Sociology and Modern Systems Theory. Prentice-Hall, 1967.
14. FORRESTER, J. W.: Industrial Dynamics. John Wiley and Sons, 1961.

15. KELLEY, C. R.: Manual and Automatic Control. John Wiley and Sons, 1968.
16. JAQUES, E.: Equitable Payment. John Wiley and Sons, 1961.
17. JAQUES, E.: Progression Handbook. Heinemann (London), 1968.
18. CROSSMAN, E. R. F. W.: Task Extension and Responsibility for Resource Deployment. Human Factors in Technology Group, Working Paper HFT 69–3, Department of Industrial Engineering and Operations Research, Univ. of Calif. (Berkeley), 1969.
19. LANER, STEPHEN: Measuring Work that Cannot Be Measured. 5th Annual MTM Western Conference (Anaheim, Calif.), 1971.
20. LANER, S.; AND CAPLAN, S.: Earnings Progression Data Sheets Expressed in U.S. Dollars. Human Factors in Technology Group Working Paper HFT 69–2, Department of Industrial Engineering and Operations Research, Univ. of Calif. (Berkeley), 1969.
21. ELKIND, J. I.: Characteristics of Simple Manual Control Systems. Technical Report III, Lincoln Laboratory, M.I.T., 1956.

SESSION III

BIOLOGICAL ASPECTS OF MANUAL CONTROL

Chairman: **JULIA APTER**

12: A Dynamic Model of the Human Postural Control System*

J. C. HILL

Oakland University

A digital simulation of the pitch axis dynamics of the stick man of figures 1 and 2 is described. Difficulties encountered in linearizing the equations of motion are discussed; the conclusion reached is that a completely linear simulation is of such restricted validity that only a nonlinear simulation is of any practical use.

Typical simulation results obtained from the full nonlinear model are presented in this paper.

INTRODUCTION

In reference 1 the equations of motion of the seven-element linked figure of figures 1 and 2 were derived. The links represent the trunk, thigh, shank, foot, upper arm, forearm, and head as seen in a side view of the human body. Each link is considered to have mass and rotational inertia. Thus for the trunk, we have a link of total length ℓ_{TR}, moment of inertia J_{TR}, and mass M_{TR}, located at the trunk center of mass, which is a distance ℓ_{TRM}, above the hip. Similar nomenclature is used to define the properties of the other links. The trunk orientation is described in terms of the x and y coordinates of the trunk c.g. and the rotation θ of the trunk center line clockwise from the vertical. All other limb orientations are described by angles as shown in figure 1.

In figure 2, a preliminary model of the forces and torques acting on the seven-element stick man of figure 1 is shown. The muscle systems are assumed to produce torques T_α about the ankle, T_β about the knee, etc. It is assumed that both the heel and toe can be in contact with the ground, where the x and y components of the ground reaction forces acting on the model are F_{H_x} and F_{H_y} at the heel, and F_{T_x} and F_{T_y} at the toe.

Gravitational forces acting at the centers of mass of each link are not shown.

The preceding constitutes the definition of a possible set of generalized coordinates in the sense of Lagrange.

LAGRANGE'S EQUATIONS

To develop the equations of motion of the postural control system model shown in figures 1 and 2, use was made of Lagrange's equations in the form of equation (1),

$$\frac{d}{dt}\left(\frac{\partial T}{\partial \dot{q}_i}\right)-\frac{\partial T}{\partial q_i}+\frac{\partial V}{\partial q_i}=Q_i \qquad i=1, 2, \ldots, n \quad (1)$$

where q_i denotes the i^{th} generalized coordinate (taken here in the order $(x,y,\theta,\gamma,\beta,\alpha,\delta,\epsilon,\zeta)$, $\dot{q}_i$ is the time derivative of the i^{th} generalized coordinate, V is the total potential energy of the system, T is the total kinetic energy of the system, and Q_i is the i^{th} generalized force arising from the muscle torques and the ground reaction forces. Gravitational forces are included through the potential energy V. Hence expressions for T and V in terms of the generalized coordinates and their derivatives must be derived, the indicated differentiations with respect to q_i, $\dot{q}_i$, and t must be carried out for $i = 1, \ldots, n$, the generalized forces must be evaluated, and the results collected according to equation (1).

The resulting equations are far too lengthy for

*This research was supported by NASA under contract NGR 23-054-033.

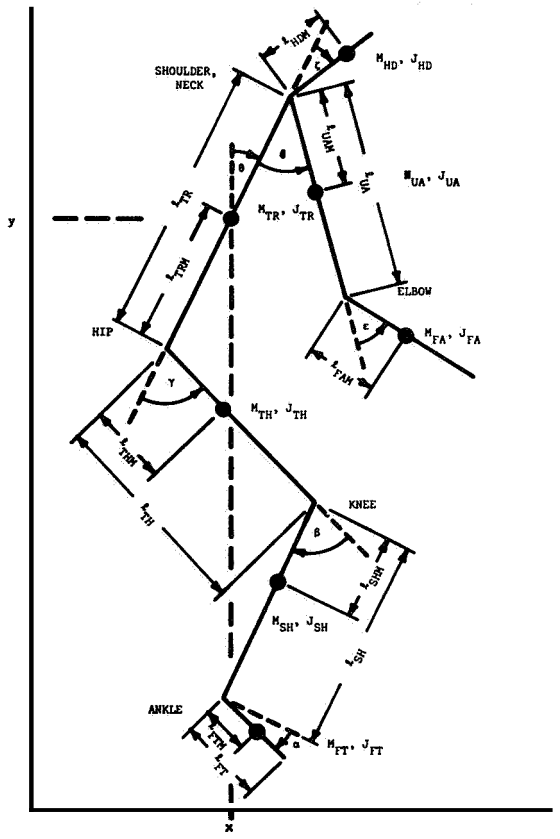

FIGURE 1.—Seven-element linked model of the human postural control system.

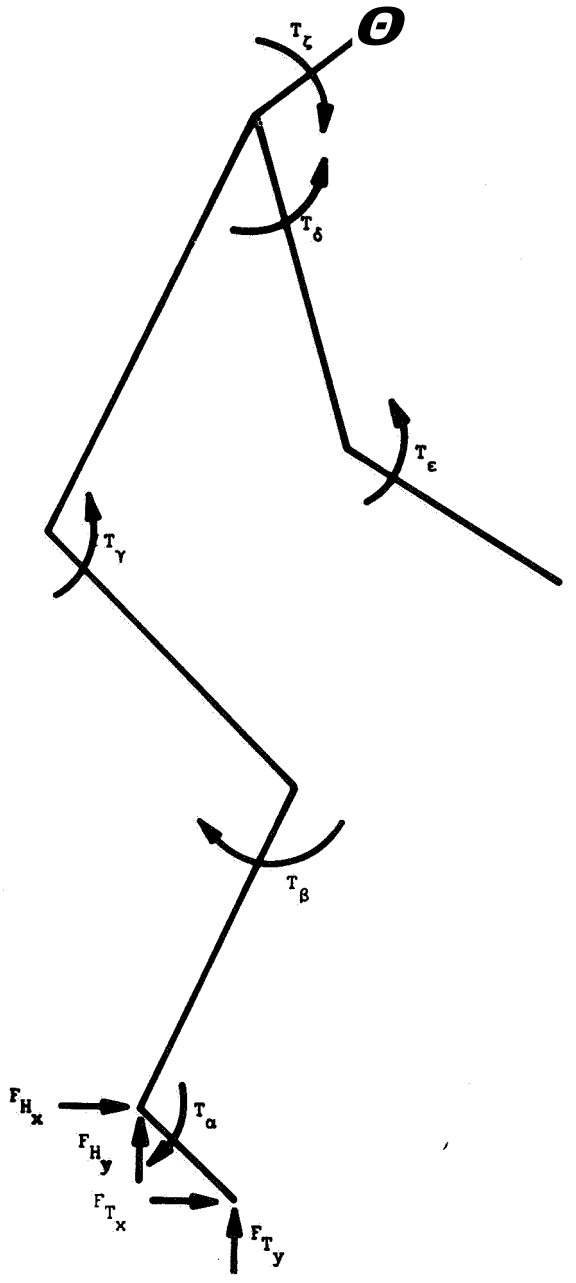

FIGURE 2.—Forces and torques acting on the postural control system.

inclusion here. They are contained in their entirety in reference **1.**

LINEARIZATION

For a variety of reasons, it would appear desirable to have a linear model valid for small deflections. First, standard techniques from linear control theory are available to assist in designing control laws for the system. Second, a linear model would be much easier to simulate on an analog computer, and the speed possible from an all-analog simulation is much to be desired in future work. Third, if a linear model is acceptable, considerable algebraic simplification in the preceeding equations may be achieved by keeping only terms of degree one or less.

The results thus obtained may best be represented in the form of the vector-matrix differential equation

$$A\ddot{x} = Cx + y \tag{2}$$

where A is a square matrix of order 9×9, C is a square matrix of order 9×9, and x and $\ddot{x}$ are 9-vectors whose components are defined in equation (3),

$$\underset{\sim}{x} = \begin{Bmatrix} x \\ y \\ \theta \\ \gamma \\ \beta \\ \alpha \\ \delta \\ \epsilon \\ \zeta \end{Bmatrix}, \qquad \ddot{\underset{\sim}{x}} = \begin{Bmatrix} \ddot{x} \\ \ddot{y} \\ \ddot{\theta} \\ \ddot{\gamma} \\ \ddot{\beta} \\ \ddot{\alpha} \\ \ddot{\delta} \\ \ddot{\epsilon} \\ \ddot{\zeta} \end{Bmatrix} \tag{3}$$

and $\underset{\sim}{y}$ is a 9-vector of constants.

For the parameter values given in table 1, which are rough estimates of the lengths, masses, and inertias appropriate to a 160 lb man, A, C, and v may be estimated as shown below.

From equation (4), since A is not diagonal, equation (2) is badly cross coupled in the accelerations; an analog computer programmer would say that equation (2) has an algebraic loop problem. Although algebraic loops on an analog computer usually are troublesome only if they lead to instability in the solutions, numerical integration of equation (2) requires that the coupling be removed (actually, it is only necessary that the matrix multiplying $\ddot{\underset{\sim}{x}}$ be lower left-

TABLE 1.—Numerical Parameter Estimates for a 160 lb Man

$M_{TR}=2.1$ slugs	$\ell_{TR}=2.0$ ft
$M_{TH}=1.3$ slugs	$\ell_{TH}=1.3$ ft
$M_{SH}=0.6$ slug	$\ell_{SH}=1.5$ ft
$M_{FT}=0.1$ slug	$\ell_{FT}=0.6$ ft
$M_{UA}=0.4$ slug	$\ell_{UA}=1.0$ ft
$M_{FA}=0.2$ slug	$\ell_{TRM}=1.2$ ft
$M_{HD}=0.3$ slug	$\ell_{THM}=0.5$ ft
$J_{TR}=0.5$ slug-ft^2	$\ell_{SHM}=0.6$ ft
$J_{TH}=0.25$ slug-ft^2	$\ell_{FTM}=0.2$ ft
$J_{SH}=0.1$ slug-ft^2	$\ell_{UAM}=0.4$ ft
$J_{FT}=0.01$ slug-ft^2	$\ell_{FAM}=0.4$ ft
$J_{UA}=0.05$ slug-ft^2	$\ell_{HDM}=0.8$ ft
$J_{FA}=0.02$ slug-ft^2	
$J_{HD}=0.03$ slug-ft^2	$g=32.18$ ft/sec^2

$$A = \begin{bmatrix} 5.000 & 0.000 & -3.949 & 2.069 & -0.509 & 0.000 & 0.439 & 0.079 & 0.239 \\ 0.000 & 5.000 & -0.019 & 0.019 & -0.019 & -0.019 & 0.000 & 0.000 & 0.000 \\ -3.949 & -0.019 & 12.990 & -6.122 & 1.829 & 0.014 & -0.173 & -0.067 & 0.413 \\ 2.069 & 0.019 & -6.122 & 3.638 & -1.217 & -0.014 & 0.000 & 0.000 & 0.000 \\ -0.509 & -0.019 & 1.829 & -1.217 & 0.554 & 0.014 & 0.000 & 0.000 & 0.000 \\ 0.000 & -0.019 & 0.014 & -0.014 & 0.014 & 0.014 & 0.000 & 0.000 & 0.000 \\ 0.439 & 0.000 & -0.173 & 0.000 & 0.000 & 0.000 & 0.525 & 0.131 & 0.000 \\ 0.079 & 0.000 & -0.067 & 0.000 & 0.000 & 0.000 & 0.131 & 0.052 & 0.000 \\ 0.239 & 0.000 & 0.413 & 0.000 & 0.000 & 0.000 & 0.000 & 0.000 & 1.221. \end{bmatrix} \tag{4}$$

$$C = \begin{bmatrix} 0.000 & 0.000 & 0.000 & 0.000 & 0.000 & 0.000 \\ 0.000 & 0.000 & 0.000 & 0.000 & 0.000 & 0.000 \\ 0.000 & 0.000 & -127.110 & 14.159 & 2.574 & 7.723 \\ 0.000 & 0.000 & 66.612 & 0.000 & 0.000 & 0.000 \\ 0.000 & 0.000 & -16.411 & 0.000 & 0.000 & 0.000 \\ 0.000 & 0.000 & 0.000 & 0.000 & 0.000 & 0.000 \\ 0.000 & 0.000 & 14.159 & -14.159 & -2.574 & 0.000 \\ 0.000 & 0.000 & 2.574 & -2.574 & -2.574 & 0.000 \\ 0.000 & 0.000 & 7.723 & 0.000 & 0.000 & 7.723 \end{bmatrix} \tag{5}$$

$$v = \begin{Bmatrix} 0.000 \\ -160.899 \\ 0.643 \\ -0.643 \\ 0.643 \\ 0.643 \\ 0.000 \\ 0.000 \\ 0.000 \end{Bmatrix} \tag{6}$$

half triangular, for then each acceleration may be solved for in sequential fashion). Complete decoupling may be achieved by premultiplication of equation (2) by A^{-1}, yielding equation (7):

$$\begin{aligned} A^{-1}(A\ddot{\underline{x}}) &= A^{-1}(C\underline{x}) + A^{-1}\underline{y} \\ I\ddot{\underline{x}} &= (A^{-1}C)\underline{x} + A^{-1}\underline{y} \\ \ddot{\underline{x}} &+ (A^{-1}C)\underline{x} + A^{-1}\underline{y} \end{aligned} \tag{7}$$

The matrices A^{-1}, $A^{-1}C$, and the vector $A^{-1}\underline{y}$ are shown below.

It is of interest to note that although A, C, and A^{-1} are symmetric, $A^{-1}C$ is not. Symmetricity (or lack of it) has proved useful in ferreting out errors in A and C.

MODEL VALIDATION: THE FREE FALL TESTS

In view of the large amount of hand derivation and computer programming involved in the development of equations (7 through 10), it is clearly desirable to test the model to see if it is at all reasonable. As no provision has been made for the addition of external forces and/or torques via the generalized forces of equation (1) at this stage in the analysis, one is limited to free fall conditions, several of which may be defined:

(1) Free fall with zero initial conditions on all angles

(2) Free fall with a small initial condition, say 0.1 radian, on only one angle at a time

$$A^{-1} = \begin{bmatrix} 0.366 & 0.000 & 0.130 & -0.076 & -0.263 & 0.056 & -0.454 & 0.759 & -0.640' \\ 0.000 & 0.201 & 0.000 & 0.000 & 0.000 & 0.287 & -0.000 & 0.000 & -0.000 \\ 0.130 & -0.000 & 0.713 & 1.431 & 0.912 & -0.195 & -0.157 & 1.130 & -1.472 \\ -0.076 & -0.000 & 1.431 & 4.262 & 4.610 & -1.779 & 0.105 & 1.721 & -2.586 \\ -0.263 & 0.000 & 0.912 & 4.610 & 8.796 & -5.098 & 0.334 & 0.751 & -1.417 \\ 0.056 & 0.287 & -0.195 & -1.779 & -5.098 & 75.354 & -0.071 & -0.160 & 0.303 \\ -0.454 & -0.000 & -0.157 & 0.105 & 0.334 & -0.071 & 5.800 & -14.230 & 0.783 \\ 0.759 & -0.000 & 1.130 & 1.721 & 0.751 & -0.160 & -14.230 & 55.663 & -2.930 \\ -0.640 & -0.000 & -1.472 & -2.586 & -1.417 & 0.303 & 0.783 & -2.930 & 7.942, \end{bmatrix} \tag{8}$$

$$A^{-1}C = \begin{bmatrix} 0.000 & 0.000 & -26.815 & 9.484 & 0.926 & 0.000 & 6.325 & -0.449 & -3.934 \\ 0.000 & 0.000 & 0.000 & -0.000 & -0.000 & 0.000 & 0.000 & -0.000 & -0.000 \\ 0.000 & 0.000 & -21.043 & -32.815 & -3.205 & 0.000 & 9.418 & -0.669 & -5.858 \\ 0.000 & 0.000 & 12.325 & -112.958 & -29.198 & 0.000 & 14.338 & -1.019 & -8.920 \\ 0.000 & 0.000 & 42.453 & -101.959 & -83.683 & 0.000 & 6.260 & -0.445 & -3.894 \\ 0.000 & 0.000 & -9.083 & 21.816 & 57.690 & 0.000 & -1.339 & 0.095 & 0.833 \\ 0.000 & 0.000 & 73.056 & -12.007 & -1.173 & 0.000 & -47.714 & 21.297 & 4.840 \\ 0.000 & 0.000 & -122.207 & -27.022 & -2.639 & 0.000 & 74.198 & -103.755 & -13.895 \\ 0.000 & 0.000 & 103.021 & 50.942 & 4.976 & 0.000 & -24.401 & 1.734 & 49.969. \end{bmatrix} \tag{9}$$

$$A^{-1}\underline{y} = \begin{Bmatrix} -0.000 \\ -32.179 \\ -0.000 \\ 0.000 \\ 0.000 \\ 0.000 \\ 0.000 \\ -0.000 \\ 0.000 \end{Bmatrix} \tag{10}$$

(3) Free fall with a small initial condition, say 0.1 radian, on all angles.

Tests (1), (2), and **(3)** provide a sequence of increasingly severe tests that the simulation must pass.

In test (1), the model is initially "lined out," and would be expected to remain that way since there are no forces or torques other than gravitational forces acting on the system. Test **(1)** essentially verifies that the origin of the state space is indeed an equilibrium point.

Test **(2)** allows the system to be perturbed from its equilibrium point in one coordinate at a time. Test **(2)** is, in essence, a test of the stability of the equilibrium point under restricted conditions. Intuitively, one would expect the perturbed angle to remain at its initial value of **0.1** radian while all other angles remain at their initial value of zero.

Finally, test **(3)** allows a general perturbation of the system from its equilibrium point. Intuitively, one again expects no action—all angles should remain at their initial values as the model drops straight down in free fall.

Several comments about these tests are in order. First, it might be argued that the system is linear. Therefore either test **(2)** or test **(3)** is redundant—they both give the same information. Although this is true of the way the simulation *ought* to behave, it is not necessarily true of how the simulation *does* behave, the difference presumably being due to a mistake somewhere. Both tests **(2)** and **(3)** are therefore useful in debugging the simulation.

Secondly, with the initial conditions of, say, test **(3)** one would not necessarily expect the angles to remain *precisely* at their initial values. An exact simulation of the physical system would be expected to do so, but the model presently under discussion is inexact in at least three ways:

(1) The equations have been linearized, and are therefore valid for small deflections only.

(2) A numerical integration technique (Runge-Kutta or Euler) is used, which inherently produces only approximations to the exact solution.

(3) Even if **(1)** and **(2)** were not a factor, the finite word length of a digital computer introduces errors into the results.

Strange or unwelcome behavior of a properly coded simulation can usually be identified as arising from one or another of these three causes by making use of the following properties of each type of error:

(1) Errors due to linearization only become smaller as the system variables remain closer to their equilibrium point. Hence these errors can be made as small as desired by the simple expedient of assuming smaller initial conditions. Behavior of the linear system should approach behavior of the nonlinear system as the initial conditions are made smaller and smaller.

(2) Functional truncation errors introduced by the integration technique used tend to zero as the integration step size approaches zero. Subject only to consideration of the amount of machine time required, these errors usually may be made as small as desired.

(3) Errors introduced by the finite word length of the computer used can usually be eliminated or at least estimated by running the simulation in extended or double precision. If the arithmetic precision can, practically speaking, be extended without limit, these truncation errors can, practically speaking, be reduced without limit. Again, the only real consideration often is the increased running time implied thereby.

In summary.—Provided that the initial conditions on the angles are small enough, provided that the integration step size is small enough, and provided that the word length used is long enough, it would be expected that the linear simulation angles would, at worst, drift *slowly* away from their initial values if indeed the exact solutions were constant. Fast changes in θ, γ, a, . . . would be interpreted as behavior common to the approximate linear model and the exact nonlinear system.

Application of the Free Fall Tests to the Linear Model

In figure **3,** time histories of the joint angles are presented for the initial conditions of test **(3).** It is seen that by the time only 100 msec have passed, the angles have departed from their initial value of **0.1** radian by amounts up to 80 percent. During this time, the system has fallen **0.14** ft or only about **1.6** in.

In comparison, figure **4** presents the time his-

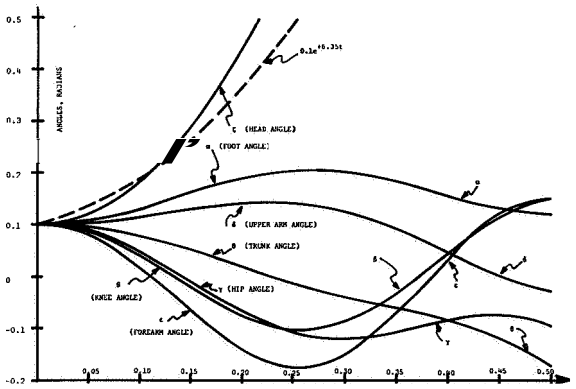

FIGURE 3.—Linear model, test (3): 0.1 radian initial conditions on each angle.

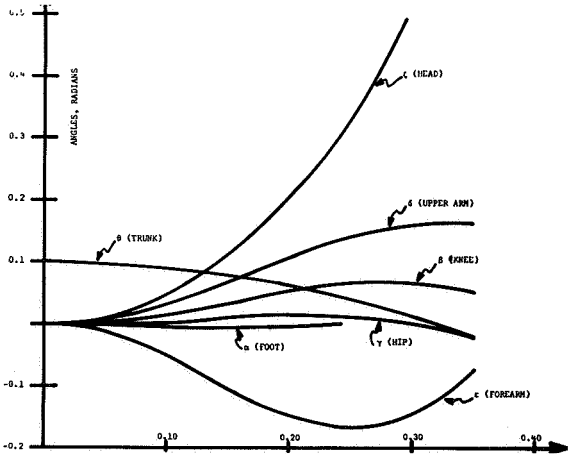

FIGURE 4.—Linear model, test (2): 0.2 radian initial condition on θ only.

tories of the angles for a typical test **(2):** an initial condition of **0.1** radian is placed on θ, and all other angles are set to zero initial conditions. The simulation is allowed to free fall, θ drifts away from **0.1** radian, and the other angles move relatively rapidly away from zero.

The system is a (constantly) forced linear system, and it is not immediately apparent whether the divergences seen in figures **3** and **4** are a result of instability of the model or are in response to the forcing function (gravity) or perhaps both. Accordingly, the pole locations of the linear system were calculated, and are given in table **2.** The Linear Approximating System (LAS) has *six* poles at the origin, five pure imaginary pole pairs with natural frequencies ranging

TABLE 2.—*Linear Approximaiing System Pole Locations in the Couplex Plane*

Real	Imaginary
0	0 (multiplicity = 6)
0	$\pm j$ 12.32
0	$\pm j$ 11.03
0	$\pm j$ 6.71
0	$\pm j$ 5.42
0	$\pm j$ 3.35
+6.35	0
−6.35	0

from $\sqrt{3.35}$ to $\sqrt{12.32}$, and two real poles—one stable at **−6.35,** one unstable at **$6.35.** It is clear that for large t the initial condition response will be dominated by the $e^{6.35t}$ term associated with the unstable pole. For comparison purposes, $0.1e^{+6.35t}$ is plotted on figure **3,** and appears to be closely connected to the response of the head.

The fact that the behavior presented in figures **3** and **4** is substantially independent of the magnitude of the initial conditions, substantially independent of integration step size, and substantially independent of word length, together with the fact that during the **100** msec or so it takes the angles to depart significantly from their theoretical values the simulation has time to fall only **0.14** ft or **1.6** in. precludes interpretation of these changes as the slow drifts from the exact solution discussed in the preceeding section. If the possible causes of error are only those previously discussed and if the observed behavior cannot be accounted for in terms of these causes, then it would appear that we are suffering from a different kind of not-so-sophisticated error—the mistake.

Accordingly, the results of figures **3** and **4** triggered an extensive and arduous period of differentiation-checking, algebra-checking, coefficient-checking, and program-checking including two completely different derivations and programs developed independently—all in an attempt to find the mistake and all to no avail. The results lead inexorably to the conclusion that the analysis leading to equations **(3)** and (4), and the pole locations given in table **2** are completely correct (useless, maybe—but correct). Either our intuition is wrong and the physical system really

behaves as shown in figures **3** and **4,** or there is some other as yet unappreciated explanation of the discrepancy. The system clearly knows what it is doing.

Investigation of some simpler systems led to the conclusion that a completely linear simulation would be of such restricted validity as to be essentially useless. Consequently, the full nonlinear equations of motion were derived (ref. **1);** the next section presents preliminary results obtained with this model.

SIMULATION RESULTS WITH THE FULL NONLINEAR MODEL

In this section simulation results of the following three physical situations will be presented. These simulations utilize the full nonlinear equations of motion.

(1) Free *fall wiih* ***no*** muscle torques.—The model is in free fall until it touches the ground, after which it collapses under the action of the ground reaction forces and gravity (fig. 5). Figures ***6*** and **7** are strip charts of free fall data.

(2) *Stand erect.*—Muscle torques proportional to a linear combination of joint angle and joint angular rate are applied so as to attempt drive all joint angles to zero, resulting in a stable upright position (fig. 8).

(3) The leap.—The control laws specifying muscle torques are modified to cause the hip and thigh to extend and the foot to deflect in such a way as to propel the model back into the air after impact in an imitation of a "graceful leap" (fig. 9).

Simulation Results: Free Fall With No Muscle Torques

Figure 5 is the result of releasing the model slightly above the ground in a slightly deflected attitude. The system configuration is drawn at **30** msec intervals. The sequence of events can easily be identified: the toe hits, the vertical ground reaction at the toe causes the foot to flex around the ankle, eventually the heel hits, initiating significant flexure of the hip and knee, etc. It should be remembered that the muscle system is not attempting to oppose the tendency of the model to collapse on the ground since all muscle torques (T_α, T_β, . . .) have been set to zero.

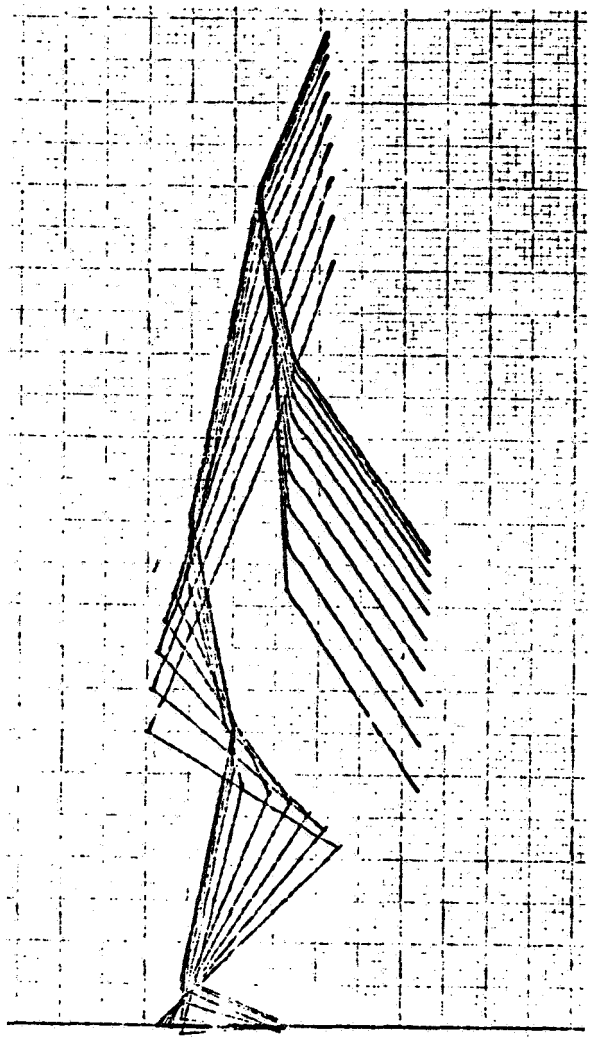

FIGURE 5.—Simulation results: free ball with **no** muscle torques.

Therefore the behavior indicated in figure 5 would continue until either the knee or the hip touched the ground—at which point the simulation would become invalid, since the possibility of ground reaction forces at these points has not been included in the model.

The principal value of figure 5 is verification of the ground reaction force simulation. Numerical data pertinent to figure 5 are given in table **3.**

Strip chart recordings (figs. ***6*** and **7)** of key variables depict the sequence of events with greater clarity. The initial free fall is clearly visible in the parabolic nature of y_T. When $y_T = 0$

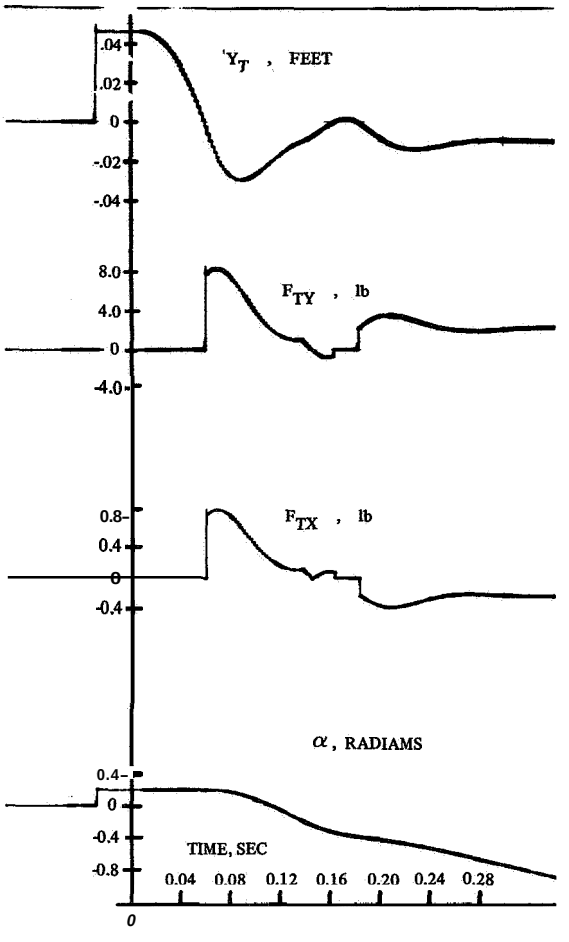

FIGURE 6.—Strip chart recordings of free-fall data: toe forces and angles.

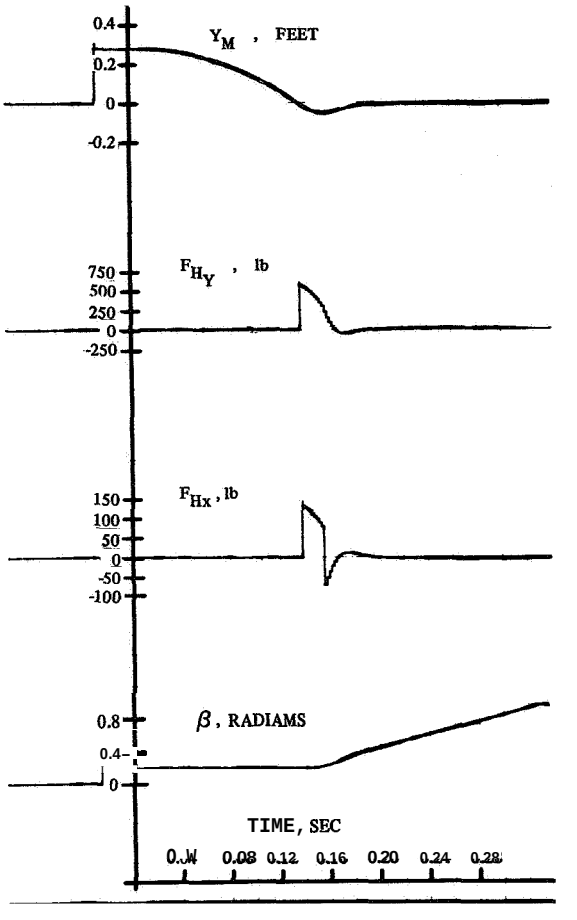

FIGURE 7.—Strip chart recordings of free-fall data: heel forces and knee angle.

(first contact with the ground), F_{Ty} is seen to jump discontinuously to 8 lb and then decrease as sufficient angular velocity is imparted to the foot to cause the toe to rest gently slightly below the ground. Similar behavior is observed for the heel-ground interaction in figure 7.

Simulation Results: Free Fall with Subsequent Stand Erect

In this case, it is desired to use the muscle torques to cause the model to come to rest in an upright position after being dropped from an initial position slightly above ground. The model is initially in a flexed attitude with all muscle torques set equal to zero as long as $y_T > 0$ (the toe is above ground). When the toe touches ground, the following form of *control law* is *assumed,* expressing muscle torques in terms of joint angles and angular rates,

$$T_\gamma = K_\gamma \gamma + K_{\dot\gamma}\dot\gamma \tag{11}$$

$$T_\beta = K_\beta \beta + K_{\dot\beta}\dot\beta \tag{12}$$

$$T_\alpha = K_\alpha \alpha + K_{\dot\alpha}\dot\alpha \tag{13}$$

$$T_\delta = K_\delta \delta + K_{\dot\delta}\dot\delta \tag{14}$$

$$T_\epsilon = K_\epsilon \epsilon + K_{\dot\epsilon}\dot\epsilon \tag{15}$$

$$T_\zeta = K_\zeta \zeta + K_{\dot\zeta}\dot\zeta \tag{16}$$

in the (possibly forlorn) hope that by attempting to drive all angles to zero the model will assume

FIGURE 8.—Simulation results: free fall with subsequent stand erect.

its reference position. Note, however, that the torques as given by equations (11) through (16) exhibit no dependence on the inertial trunk angle θ; it is therefore quite possible for the model to line out in an inclined position relative to horizontal. The rate feedback terms are included to provide damping to stabilize the system.

Figure 8 presents pictorial results obtained using the control law of equations *(11)* through (16), with numerical values for the coefficients as specified in table 4. The time increment between drawings is 90 msec, and the results have been de-superimposed for clarity. The initial conditions are the same as for figure 7. The tendency to assume an erect position is clearly evident—which is somewhat surprising considering the complexity of the system and the ad hoc nature of the control law.

Simulation Results: The Graceful Leap

As a final result, figure 9 shows the model behavior when given an initial translational velocity in X, and with the control law of equation

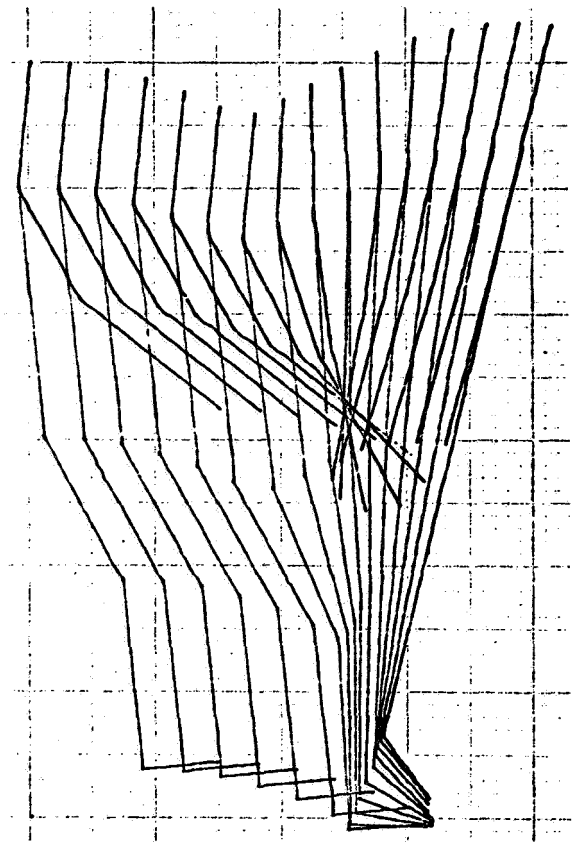

FIGURE 9.—Simulation results: the graceful leap.

TABLE 3.—*Numerical* Data *for* ***Figure 5: Free Fall***

Initial conditions	Parameter values
$x(0) = 0.0$ ft	
$y(0) = 4.2$ ft	$k_T = -100.0$ (lb-ft)/rad
$\theta(0) = 0.2$ rad	$\dot{k}_T = -2.0$ (lb-ft)/(rad/sec)
$\gamma(0) = 0.4$ rad	$\mu_T = 0.21$
$\beta(0) = 0.4$ rad	$k_H = -5000.0$ (lb-ft)/rad
$\alpha(0) = 0.2$ rad	$\dot{k}_H = -125.0$ (lb-ft)/(rad/sec)
$\delta(0) = 0.4$ rad	$\mu_H = 0.23$
$\epsilon(0) = 0.4$ rad	
$\zeta(0) = 0.2$ rad	

(13) modified to

$$T_\alpha = K_\alpha(\alpha - 0.7) + K_{\dot{\alpha}}\dot{\alpha} \qquad (17)$$

which has the effect of causing the foot to flex strongly toward an angle of *0.7* rad (about 40°) with respect to the perpendicular to the shank. The form of the other torque equations is left

TABLE 4.—*Numerical Data for Figure 8: Xtand Up*

Initial conditions	Parameter values	
$x(0) = 0$ ft	$k_T = -5000$	$k_H = -5000$
$y(0) = 4.2$ ft	$\dot{k}_T = -100$	$\dot{k}_H = -150$
$\theta(0) = 0.2$ rad	$\mu_T = 0.5$	$\mu_H = 0.5$
$\gamma(0) = 0.4$ rad	.....	
$\beta(0) = 0.4$ rad	$K_\gamma = -1000$ (ft-lb)/rad	$K_{\dot{\gamma}} = -10$ (ft-lb)/(rad/sec)
$\alpha(0) = 0.2$ rad	$K_\beta = -200$ (ft-lb)/rad	$K_{\dot{\beta}} = -15$ (ft-lb)/(rad/sec)
$\delta(0) = 0.4$ rad	$K_\alpha = -500$ (ft-lb)/rad	$K_{\dot{\alpha}} = -5$ (ft-lb)/(rad/sec)
$\epsilon(0) = 0.4$ rad	$K_\delta = -150$ (ft-lb)/rad	$K_{\dot{\delta}} = -7$ (ft-lb)/(rad/sec)
$\zeta(0) = 0.2$ rad	$K_\epsilon = -60$ (ft-lb)/rad	$K_{\dot{\epsilon}} = -3$ (ft-lb)/(rad/sec)
$(0) =$	$K_\zeta = -90$ (ft-lb)/rad	$K_{\dot{\zeta}} = -3$ (ft-lb)/(rad/sec)

TABLE 5.—*Numerical Data for Figure 9: The Graceful Leap*

Initial conditions	Parameter values	
$X(0) = 0$ ft	$K_T = -5000$	$K_H = -500$
$\dot{x}(0) = 10$ ft/sec	$K_{\dot{T}} = -100$	$K_{\dot{H}} = -150$
$y(0) = 4.2$ ft	$\mu_T = 0.5$	$\mu_H = 0.5$
$\theta(0) = -0.1$ rad	.....	.....
$\gamma(0) = 0.4$ rad	$K_\gamma = -200$ (ft-lb)/rad	$K_{\dot{\gamma}} = -25$ (ft-lb)/(rad/sec)
$\beta(0) = 0.4$ rad	$K_\beta = -900$ (ft-lb)/rad	$K_{\dot{\beta}} = -75$ (ft-lb)/(rad/sec)
$\alpha(0) = 0$ rad	$K_\alpha = -350$ (ft-lb)/rad	$K_{\dot{\alpha}} = -4$ (ft-lb)/(rad/sec)
$\delta(0) = 0.4$ rad	$K_\delta = -150$ (ft-lb)/rad	$K_{\dot{\delta}} = -7$ (ft-lb)/(rad/sec)
$\epsilon(0) = 0.4$ rad	$K_\epsilon = -60$ (ft-lb)/rad	$K_{\dot{\epsilon}} = -3$ (ft-lb)/(rad/sec)
$\zeta(0) = 0.2$ rad	$K_\zeta = -90$ (ft-lb)/rad	$K_{\dot{\zeta}} = -3$ (ft-lb)/(rad/sec)

unchanged. Clearly the form of equation (17) has been chosen to mimic to some degree the action of the foot in propelling the body into the air.

Numerical data pertinent to figure 9 is as in table 5.

SUMMARY AND CONCLUSIONS

The conclusion reached from the results obtained so far is that a linear simulation is of such restricted validity as to be almost useless. While a linear *analysis* might occasionally be of use, a nonlinear *simulation* now seems essential if further progress is to be made.

Although it was recognized that a nonlinear representation of the ground reaction forces would be necessary, it was hoped that the basic system dynamics could be linearized with attendant simplicity and ease of analog computer mechanization. This does not appear to be the case. However, figures 5, 8, and 9 make it clear that reasonable simulation results can be obtained for this complex system.

It now appears that although the coordinate system chosen in figure 1 is in terms of those angles most likely to be physiologically instrumented, it is not the one that leads to the simplest set of equations of motion. The frequent occurrence in the derivation of inertial angles such as $(\gamma - \theta)$, $(\beta - \gamma - \theta)$, etc., suggests that a great deal of simplification would occur if inertial angles were used as generalized coordinates. An early task for future work is the development of a full nonlinear simulation in terms of inertial angles.

The present nonlinear simulation is slow. Extensive comparison of simulation results with experimental data taken on human subjects would be time-consuming and expensive. Unfortunately, there is no obvious way of speeding up the present simulation. It is hoped that the nonlinear simulation in terms of inertial angles will

be less complex and therefore faster. Improvement in the speed of the simulation is clearly a continuing goal for future work.

The ideal torquemotor assumption of equations **(11)** through **(16)** is greatly at variance with physiological fact. Clearly, before extensive work is done on more realistic control laws, it would be desirable to have a more realistic representation of the geometry and dynamics of the human muscle structure. Developing this representation is a priority item for future work, and some initial effort has already been made in this direction, Tn addition, a few minor improvements in the ground reaction forces need to be made.

It is important to realize that the hypothetical control law described by equations **(11)** through **(16)** is entirely for the purpose of debugging the parts of the simulation describing basic system dynamics, and no assertion is made **or** implied that this form of control law has any basis in fact. Indeed, information on the form **of** the control law is the desired long term output **of** the present research.

REFERENCE

1. **HILL, J. C.: A Dynamic Model of the Human Postural Control System. Vol. I, Final Report on Biosystems Engineering Research. NASA/ERC contract NGR–23–054–003, Oakland Univ., School of Engineering TR 70–5, Nov. 1970.**

13. Further Observations on the Relationship of EMG and Muscle Force*

GYAN C. AGARWAL, LAWRENCE R. CECCHINI, AND GERALD L. GOTTLIEB

Rush Presbyterian-St. Luke's Medical Center
AND
University of Illinois at Chicago Circle

Human skeletal muscle may be regarded as an electro-mechanical transducer. Its physiological input is a neural signal originating at the alpha motoneurons in the spinal cord and its output is force and muscle contraction, these both being dependent on the external load.

In this paper some experimental data taken during voluntary efforts around the ankle joint and by direct electrical stimulation of the nerve are described, Some of these experiments are simulated by an analog model, the input of which is recorded physiological soleus muscle EMG. The output is simulated foot torque. Limitations of a linear model and effect of some nonlinearities are discussed.

INTRODUCTION

Modeling of biological systems requires us to face three most challenging problems. First, we sometimes do not know and often cannot measure the inputs to the real system we are modeling. Second, it is usually extremely difficult, if not impossible, to measure all state variables, and third, such systems almost inevitably contain significant nonlinearities which cannot be avoided by common analytical devices of piecewise linearization or small signal analysis. In the following paper we wish to discuss some models of muscle contraction in normal humans, and show how we have attempted to resolve or avoid these difficulties.

Human skeletal muscle may be regarded as an electro-mechanical transducer, converting the electrical signals from the alpha motor-neurons into a mechanical force at its origin and insertion. For all practical purposes we cannot measure this neural input. Associated with muscle activation is the electrical activity of the contracting muscle itself, which we may record as the electromyogram (EMG). There is a one-to-one relationship between an action potential in a single motor nerve and the EMG of its muscle fibers. Using surface electrodes on the belly of the muscle, however, we get only a single scalar measure from the many motor units which fire in varying spacial and temporal patterns.

Nevertheless, there is some theoretical justification for expecting the average rectified EMG (refs. 1 and 2) to be proportional to the level of innervation and we have used this signal (ref. 3) as our model's input.

The only other variables we can measure are muscle force and length. For simplicity we have fixed muscle length and measured only the isometric force (actually torque) generated by the gastrocnemius-soleus muscles (GSM) at the ankle joint. This avoids those nonlinearities in both the EMG measurement and in the mechanical parameters which are associated with changing muscle length.

One of the intrinsic state variables of the muscle which we cannot measure is termed the "active state" (ref. 4). This rather loosely used term describes two conceptually distinguishable changes, one the generation of an active force of contraction and the other an increase in the passive

*This work was partially supported by NSF grant GK–17581.

mechanical impedance of the muscle. Measurements of both these phenomena have been made in animals (ref. *5)* but only the impedance changes have been measured in man (refs. **6** and **7).**

LINEAR MODEL

At the Sixth Annual NASA-University conference we presented a linear model for the EMG-force relationship ((ref. 8), see also (ref. **9)).** The topology of this model is shown in figure **1.** For the linear model, B, K_1, and K_2 are constant, passive elements and activation of the muscle implies generation of an active force F_m.

The model transfer function is given by

$$\frac{F}{\mathrm{EMG}} = K \cdot G_1(S) \cdot G_2(S),$$

where

$$G_i(S) = \frac{1}{T_i S + 1}, \; i = 1, 2.$$

Separation of the transfer function like this allows us to tentatively designate $G_1(S)$ as the active state component while $G_2(S)$ may be considered the linearized mechanical component of the muscle model shown in figure **1.** The input is recorded physiological EMG data. For our simulation the model parameters were chosen as $T_1 = 0.105$ sec, $T_2 = 0.105$ sec, and $K = 0.25$ to *0.35.* Figure 2 shows muscle and model response to a rapid contraction. Figure *3* shows the impulse response of this linear model. The "impulse response" of the muscle was obtained by delivering a single maximal shock to its motor nerve.

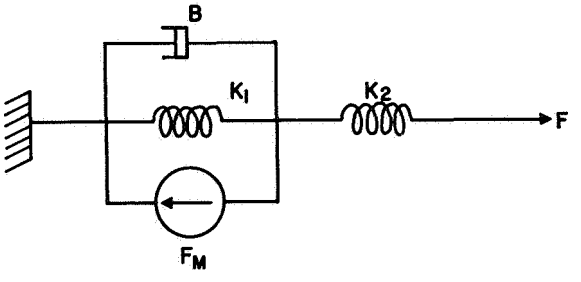

FIGURE 1.—A mechanical model of skeletal muscle. The series and parallel elastic elements (K_2 and K_1) and the viscosity B are defined only by the mechanical behavior of the muscle and should not imply a mechanism. The force generator F_m represents the contractile "active state" of the muscle.

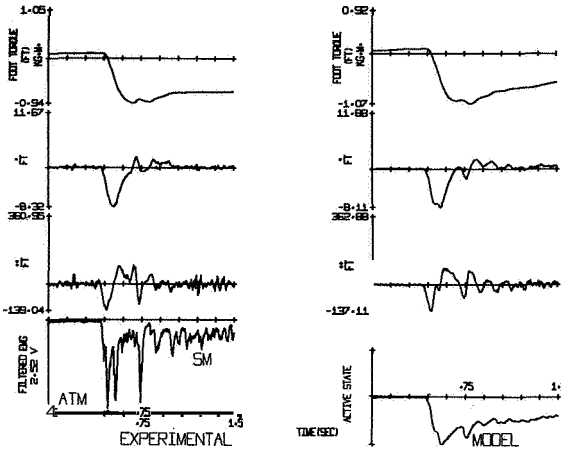

FIGURE 2.—Left: subject's step torque response and EMG. Right: model response to subject's EMG. Instead of replotting EMG on the right, the output of the active state stage G_1 is the fourth curve plotted.

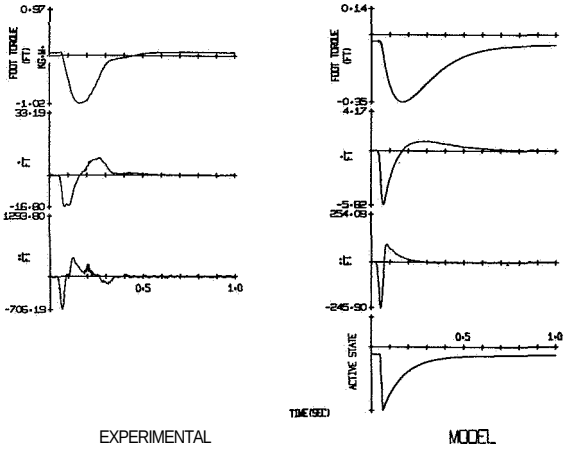

FIGURE 3.—Left: foot twitch in response to a single supramaximal shock to the tibial nerve. Right: model impulse response and the output of the active state stage G_1.

Figure 2 shows that the model is reasonably successful in mimicking rapid muscle contraction. The output of the first stage of the model is plotted as the active state in the lower part of the figure. However, it was shown in an earlier paper (ref. 8) that these time constants are too long to reproduce a sudden relaxation. Reducing one time constant ($T_2 = 0.01$) improves the rate of fall of the force (see fig. 8 of ref. 8). It is clear that a constant coefficient linear model is not adequate to reproduce both contraction and relaxation.

The impulse response in figure 3 shows three interesting deficiencies. The negative peak in the experimental acceleration curve at 300 msec is not due to intrinsic muscle activity but is produced by the stretch reflex loop causing reactivation of the muscle as it relaxes and returns to its resting length.

The second error is the apparent saturation of the velocity curve and the third is the double hump of the acceleration curve between 100 to 250 msec. The active state variable does behave much like measurements in animal preparations indicate it should. It rises abruptly and falls slowly but does not remain on a plateau at its peak value.

NONLINEAR MODEL

The nonlinear model incorporates two limiter type nonlinearities in order to improve the impulse response of the model and its performance with soleus EMG as the input signal. A block diagram of the analog model is shown in figure 4. The first limiter N_1 is situated after the first stage to limit amplitude of the active state thus producing a plateau at its peak value. The second limiter N_2 is situated in the second stage to limit the maximum rate of change of foot torque. Figure 5 shows the effect of the active state limiter and figure 6 shows the effect of the velocity limiter.

DISCUSSION

The nonlinearities used in this model only show that the simple first order dynamics of the two stages are easily improved upon. However, these nonlinearities (which were used because they were easy to implement) are not suitable because we are still dealing with linear phenomena. What is actually needed are higher order linear stages

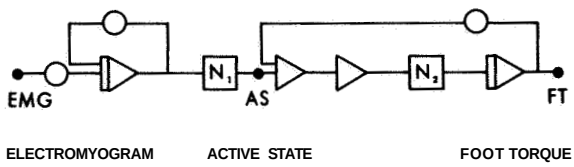

FIGURE 4.—Analog diagram of the model showing the position of the nonlinear elements.

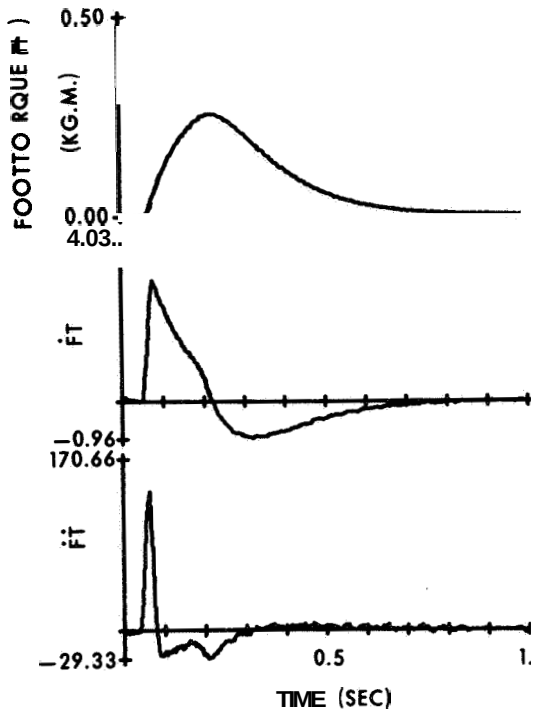

FIGURE 5.—Effect of the active state limiter.

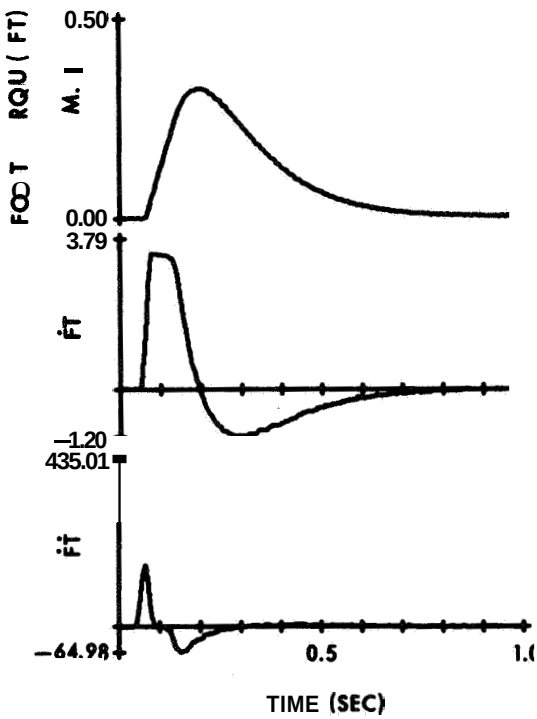

FIGURE 6.—Effect of the velocity limiter.

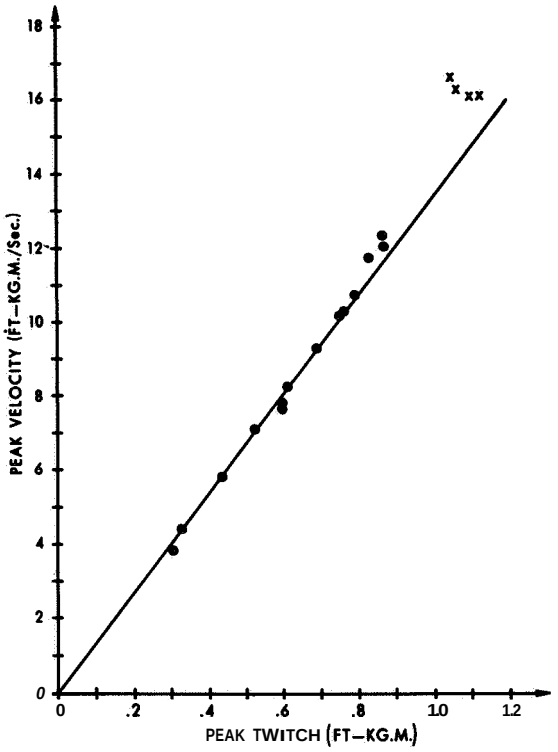

FIGURE 7.—A plot of the peak velocity of the isometric twitch contraction vs the peak twitch in the soleus at different levels of stimulus voltage.

which have a plateau in their response. That, at least, will improve the impulse response but its impact on the response with EMG inputs is not clear.

The impulse response of the physiological system is much more complex than what is shown in figure 3. In a slightly different experiment the tibial nerve at the back of the knee in popliteal fossa is stimulated with different levels of voltage stimulus. The EMG at the soleus at the lower levels of stimulus shows the familiar H-wave. As the stimulus level is increased, the alpha motor fibers are directly stimulated producing the M-wave (ref. 9). A plot of the peak velocity (with plateau) versus the peak twitch in such electrically evoked twitches is shown in figure 7. The circles are for H-wave response and the crosses are for M-wave response. Note that this relationship is nearly linear. The peak velocity is a function of the response, i.e. the input level itself. Thus the major change that is required in this model is that the mechanical parameters must be made functions of the input.

It seems clear, though, that a relatively simple model can be used to predict isometric muscle activity from the EMG.

REFERENCES

1. MOORE, A. D.: Synthesized EMG Waves and Their Implication. Amer. J. Phys. Med., vol. 46, 1967, pp. 1302–1316.
2. LIBKIND, M. S.: II Modelling of Interference Bioelectrical Activity. Biophysics, vol. 13, 1968, pp. 811–821. (English transl.)
3. GOTTLIEB, G. L.; AND AGARWAL, G. C.: Filtering of Electromyographic Signals. Amer. J. Phys. Med., vol. 49, 1970, pp. 142–146.
4. HILL, A. V.: The Abrupt Transition From Rest to Activity in Muscle. Proc. Roy. Soc., London, Ser. B, vol. 136, 1949, pp. 399–420.
5. BAHLER, A. S.; FALES, J. T.; AND ZIELER, K. L.: The Active State of Mammalian Skeletal Muscle. J. Gen. Physiol., vol. 50, 1967, pp. 2239–2253.
6. WILKIE, D. R.: The Relation Between Force and Velocity in Human Muscle. J. Physiol., vol. 110, 1950, pp. 249–280.
7. AGARWAL, G. C.; BERMAN, B. M.; AND STARK, L.: Studies in Postural Control System. I. Torque Disturbance Input. IEEE Trans. Systems Science and Cybernetics, vol. SSC–6, 1970, pp. 116–121.
8. GOTTLIEB, G. L.; AND AGARWAL, G. C.: A Model of Muscle Activity. Proceedings of the Sixth Annual Conference on Manual Control. Wright Patterson Air Force Base 1971, pp. 177–193.
9. GOTTLIEB, G. L.; AND AGARWAL, G. C.: Dynamic Relationship Between Isometric Muscle Tension and the Electromyogram in Man. J. App. Physiol., vol. 30, 1971, pp. 345–351.

N33-10118

14. The Use of a Battery of Tracking Tests in the Quantitative Evaluation of Neurological Function*

B. S. REPA, J. W. ALBERS, A. R. POTVIN, AND W. W. TOURTELLOTTE
The University of Michigan

The potential of tracking tasks for use in clinical applications has been recognized for many years. While investigators have demonstrated the usefulness of these tasks in drug research and in measuring the performance of pathological subjects, (e.g., Stark and Iida (ref. **1)** and Angel et al. (ref. **2)** few have made effective use of tracking measures in clinical trials. At the University of Michigan's Neurology Research Laboratory, a tracking test battery has been applied in a drug trial designed to compare the efficacy of L-DOPA and amantadine to that of L-DOPA and placebo in the treatment of **28** patients with Parkinson's disease. The drug trial provided an ideal opportunity for objectively evaluating the usefulness of tracking tests in assessing changes in neurologic function.

Evaluating changes in patient performance resulting from disease progression and controlled clinical trials is of great importance in establishing effective treatment programs. Clinicians are usually able to classify a given neurologic function of the patient into broad categories such as supernormal, normal, and abnormal (mild, moderate, or severe); but they often have difficulty in detecting small but significant changes in the patient's function over time. One attempt at a more objective and quantitative neurologic examination was initiated at The University of Michigan Medical Center several years ago by Dr. Wallace W. Tourtellotte. Investigators have long known that the total performance capabilities of an individual cannot be specified on the basis of a single performance test. For this reason, Dr. Tourtellotte devised a battery of sensory and motor performance tests which are now collectively referred to as the Clinical Quantitative Neurological Examination (CQNE) (table **1).**

TABLE **1.**—*The Clinical Quantitative Neurological Examination (CQNE) Test Items*

- Vision: Visual acuity
- Upper Extremities—
  - Strength of movements:
    - Grip
    - Wrist dorsiflexion
    - Shoulder abduction
  - Control of movements:
    - Steadiness
      - Hole steadiness, supported and unsupported
      - Force steadiness, supported and unsupported
      - Finger tremor, resting and sustension
    - Simple reaction time
    - Speed of hand
    - Speed-coordination of hand
    - Rotary pursuit
    - Finger dexterity
      - Purdue Pegboard
      - Pencil rotation
  - Fatigue of movements:
    - Grip strength
    - Speed of hand
    - Speed-coordination of hand
  - Sensation:
    - Touch, hand
    - Vibration sense, index finger
    - Position sense
    - Two-point discrimination

Considerable experience has been gained with the CQNE as it has been used in a number of studies using asymptomatic subjects to obtain

* This research effort has been supported in part by NIH training grant 5 to 1 GM01289-07, 1970–71, NASA contract NSr 23–005–364, and an equipment grant from the University of Michigan Institute of Science and Technology.

normative data and in several therapeutic trials involving multiple sclerosis and Parkinson's disease patients (Tourtellotte et al. (ref. **3)** and Kuzma et al. (ref. **4)).**

As part of a continuing effort to improve the clinical testing program, a tracking test battery was studied as a possible source of future tests for inclusion in the CQNE. To be effective in a clinical environment, the battery had to provide measurements that required minimum run lengths and the fewest trials possible to establish stable parameter estimates. Extensive training time was a luxury that simply could not be afforded. Furthermore, all tests and measures had to allow the use of on-line data reduction schemes. The battery that was selected is very similar to the one described by Jex and Allen at last year's meeting (ref. *5);* it includes step tracking, random tracking, and critical tracking (table **2).** The tests were kept as simple, yet as comprehensive and challenging, as possible. Modifications in the display screen and control stick were necessary to accommodate patients with various sensori-motor disabilities.

Whenever new quantitative tests for measuring neurologic disorders are developed it is of interest to examine the performance of normal subjects as well as patients on the tests. Reliabilities and learning effects are more effectively measured with normal subjects due to the possibility of large variations in patients' performance which can be justifiablyattributed to their pathological condition. Ten age-matched normals were used in a test-retest study to determine reliability measures for the tracking battery (table **3).** All reliability coefficients were found to be significant at or above the **5** percent level with the exception of movement time for a right to left transition, and the coefficient for this test

TABLE 3.—*Reliability of Tracking Test Battery Involving 10 Matched Normals With a 3 Week Interval Between the First and Second Examinations*

Test	r [1]	$\frac{2r}{1+\lvert r\rvert}$ [2]
Step tracking		
Reaction time, right to left	[3] **0.75**	**0.86**
Reaction time, left to right	[4] **.82**	.90
Movement time, right to left	**.60**	**.75**
Movement time, left to right	[3] **.67**	.80
Random tracking		
Integral of absolute error	[5] **.91**	**.95**
Critical tracking		
Reciprocal of critical root	[5] **.96**	.98

[1] Pearson product moment correlation coefficient.
[2] Spearman-Brown split-half correlation formula.
[3] $p \leqq .05$. [4] $p \leqq .01$. [5] $p \leqq .001$.

TABLE 2.—*General Tracking Task Descriptions*

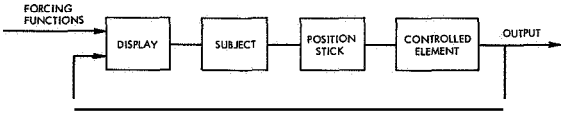

Type of tracking	Forcing function	Display	Controlled element	Performance measures
Step	**Rectangular pulse with alternating ± 14 centimeter amplitude and pulse width from 2.7 to 5.7 sec.**	**Pursuit**	**K**	**Reaction time, movement time**
Random	**Random noise with cutoff frequency of 1.0 rad/sec.**	**Compensatory**	**K**	**Integral of absolute error**
Critical	**None**	**Compensatory**	$\frac{K}{S-\lambda}$; $\lambda_0 = 1.0$ rad/sec $\lambda = 0.05$ rad/sec	**Reciprocal of critical root**

TABLE 4.—*Learning in Tracking Test Battery Involving 10 Matched Normals With a 3 Week Interval Between the First and Second Examinations*

Test	Exam I Mean	Exam I SD	Exam II Mean	Exam II SD	Difference	% Change [1]	*t*-Difference	*t*-% Change
Step tracking [2]								
Reaction time, right to left	308	44	305	43	−3	−.3	.27	.10
Reaction time, left to right	297	37	297	51	0	−.2	.00	.07
Movement time, right to left	510	80	493	106	−17	−2.7	.62	.53
Movement time, left to right	596	109	530	116	−66	−10.5	2.29	2.41 [4]
Random Tracking [3]								
Integral of absolute error	1.93	.54	1.89	.52	−.04	−1.4	.68	.35
Critical tracking [2]								
Reciprocal of critical root	371	56	361	61	−10	−2.6	1.77	1.79

[1] $\%\ \text{Change} = \frac{1}{10}\sum_{i=1}^{10}\frac{\text{Score 2i} - \text{Score 1}_i}{\text{Score 1}_i} \times 100.$

[2] Units are in milliseconds.

[3] Units are in $\frac{\text{centimeter-seconds}}{\text{second}}$

[4] $= p \leqq .05$.

measure just barely missed the cutoff point. The same group of 10 normals was used to measure learning effects(table **4).** Although all test scores showed an improvement on the aecond exam, none of the improvements were statistically significant.

Another important reason for using normal subjects on new tests is to establish normative performance levels. Since it is the goal of the physician to bring the performance of patients to the predisease level, it is meaningful to express patient data as a percentage of that obtained from matched normal controls. This was done for the drug study, which used a randomized, double-blinded, crossover design. The 28 Parkinson's disease patients were randomly assigned to two groups, the first group receiving L-DOPA +amantadine first and L-DOPA+placebo second, with the second group receiving just the opposite schedule (table *5).* Treatment groups were combined for analysis, and scores were expressed as a percentage of matched normal levels (table **6).** Relative to the normal subjects, patients performed better on step tracking and critical tracking than on random tracking. Improvements were modest when amantadine was taken in addition to L-DOPA.

TABLE 5.—*Experimental Paradigm*

Group	No. of patients	Medication taken during week 1–3	4–6
1	14	*L−D+A* *	*L − D+P*
2	14	*L−D+P*	*L − D+A*

* *L − D=L-DOPA.* *A* =Amantadine. *P* =Placebo.

Based on other tests administered in the drug trial, the effect of adding amantadine to L-DOPA was found to be beneficial but weak. Thus, while the trends in the CQNE scores favored L-DOPA+ amantadine, only grip strength, hand coordination, pencil rotation, 2-point discrimination, and resting tremor showed statistically Significant changes. The tracking test measures all showed improvements favoring the L-DOPA+amantadine treatment group (table **7).** The critical task measure and left to right movement time showed improvements significant at the *5* percent level. While changes in random tracking scores and right to left reaction time scores were 10 percent or more, large variations in scores among patients prevented these changes from being statistically significant. The tracking

TABLE 6.—*Performance of Patients in the Tracking Test Battery Expressed as a Percentage of Matched Adult Normal Function*

Test	Matched adult normal function Mean ± 2SD	Patients on placebo %	Patients on placebo SD	Patients on drugs %	Patients on drugs SD
Step tracking [1]					
Reaction time, right to left	303 ± 78	83	19	90	22
Reaction time, left to right	294 ± 67	83	17	86	18
Movement time, right to left	489 ± 220	78	22	80	20
Movement time, left to right	568 ± 234	76	22	84	23
Random tracking [1]					
Integral of absolute error	1.8951.16	61	23	65	17
Critical tracking [2]					
Reciprocal of critical root	362 ± 128	78	17	81	18

[1] Units are in millisec.

[2] Units are in $\frac{\text{centimeter-sec}}{\text{sec}}$

TABLE 7.—*Results of Tracking Test Battery Involving 28 Parkinson Patients: Comparison Between L-DOPA+Placebo and L-DOPA+Amantadine Treatment Groups*

Test	L-DOPA + amantadine Mean	L-DOPA + amantadine SD	L-DOPA + placebo Mean	L-DOPA + placebo SD	Difference	% Change [1]	*t*-Difference	*t*-% Change
Step tracking [2]								
Reaction time, right to left	359	91	385	102	27	10	1.61	2.32 [4]
Reaction time, left to right	358	84	368	81	10	4	.75	1.32
Movement time, right to left	642	145	679	215	4	7	1.18	1.46
Movement time, left to right	717	191	820	289	10	16	2.32 [4]	2.89 [5]
Random tracking [3]								
Integral of absolute error	3.04	.74	3.36	1.35	.32	11	1.42	1.66
Critical tracking [2]								
Reciprocal of critical root	463	96	486	110	22	5	2.23 [4]	2.58 [4]

[1] $\%\ \text{Change} = \frac{1}{28}\sum_{i=1}^{28}\frac{\text{Score } 2_i - \text{Score } 1_i}{\text{Score } 1_i}$.

[2] Units are in millisec.

[3] Units are in $\frac{\text{centimeter-sec}}{\text{sec}}$

[4] $p \leqq .05$. [5] $p \leqq .01$.

measures still appeared to be at least as sensitive as most measures in the CQNE in detecting changes in performance.

The final selection of a test for inclusion in the CQNE depends upon the test's satisfactory fulfillment of a number of criteria relating to the neurological function being tested, instrumentation, test data, subject requirements, and examiner-requirements (table 8). The direct application of tracking tasks to a clinical trial has shown that they are indeed capable of satisfying these criteria. In closing, it should be mentioned that tracking tasks and other quantitative testing procedures are not meant as a substitute for

TABLE 8.—*Criteria for Test Selection*

Criteria related to the neurological function tested:
The function must relate meaningfully to the status of the subject's nervous system.
Criteria related to the instrument:
The instrument must be small and capable of being used in a small area.
Initial, operating, and maintenance costs of the instrument must; not be prohibitive.
Criteria related to the test data:
The data must be truly quantitative, i.e., at least of interval strength.
The data must be objective, i.e., reliable.
The data must be sensitive enough to detect changes in the neurological function being evaluated.
Criteria related to the subject:
The "supernormal" healthy young adult should be challenged by the test, and yet at the same time the test should not be beyond the ability of the patient.
The subject should be reasonably interested and motivated by the test.
Learning effects should be at a minimum.
The subject must not be *so* fatigued by the test as to prohibit the completion of succeeding tests in the battery.
The idea of the test must be simple enough to be easily communicated to the subject.
Criteria related to the examiner:
A trained physical therapist must be capable of administering the test.

sound clinical judgement, but they do provide the medical investigator with information that is often impossible to obtain from observation alone, particularly in detecting and documenting changes in a patient's condition.

REFERENCES

1. STARK, L.; AND IIDA, M.: Dynamical Response of the Movement Coordination System of Patients with Parkinson Syndrome. Quarterly Progress Rept. No. 63, Research Laboratory of Electronics, MIT, Oct. 15, 1961, pp. 204–213.
2. ANGEL, R. W.; ALSTON, W.; AND HIGGINS, J. R.: Control of Movement in Parkinson's Disease. Brain, vol. XCIII, pp. 1–14.
3. TOURTELLOTTE, W. W.; HAERER, A. F.; SIMPSON, J. F.; KUZMA, J. W.; AND SIKORSKI, J.: Quantitative Clinical Neurological Testing. I. A Study of a Battery of Tests Designed to Evaluate in Part the Neurological Function of Patients With Multiple Sclerosis and Its Use in a Therapeutic Trial. N.Y. Acad. Sci., vol. 122, 1965, p. 480.
4. KUZMA, J. W.: TOURTELLOTTE, W. W.; AND REMINGTON, R. D.: Quantitative Clinical Neurological Testing. 11. Some Statistical Considerations of a Battery of Tests. J. Chron. Dis., vol. 18, 1965, pp. 303–311.
5. JEX, H. R.; AND ALLEN, R. W.: Research on a New Human Dynamic Response Test Battery. Presented at Sixth Annual Conference on Manual Control, Air Force Institute of Technology, Wright-Patterson Air Force Base, Apr. 7–9, 1970.

15. Human Disorientation in a Rotating Spacecraft*

LAURENCE R. YOUNG

Massachusetts Institute of Technology

The problem of disorientation in a rotating spacecraft is treated as an example of the general case of habituation to an unusual motion environment using all sensors and active movements. The dynamic response of the sensors is stressed. Several avenues for work on combatting disorientation are mentioned.

INTRODUCTION

Before the first manned space flight launches, there were numerous predictions, many of them quite dire, about the deleterious vestibular reactions to be expected in weightlessness. Fortunately, at least in the early days of space flight, vestibular problems were minimal. We should not be led into a state of overconfidenceregarding the possible seriousness of disorientation or motion sickness in future space programs. Although the concern about motion sickness prior to the first manned space flight proved to be unfounded, the Soviet cosmonauts did report several instances of stomach awareness. The problem was raised again during the Apollo program, when the astronauts had a high incidence of vestibular related problems. Berry (ref. 1) reports five of the six crewmen on Apollo 8 and 9 reported symptoms of motion sickness, and one on Apollo 10. In all cases, adaptation took place. Berry (in ref. 1) summarized his views of this problem in 1969:

> It appears that the opportunity to move about more freely in the Apollo cabin than in previous spacecraft is a factor producing the motion sickness problem. Sensory inputs from the semicircular canals to the central nervous system during head movements in space are thought to be enhanced due to altered activity of the otolith organs in the weightless state. This is a significant problem which must receive continued attention in the space program, for it can markedly affect astronaut performance.

Later Apollo flights (through 14) were apparently not subject to the motion sickness symptoms. Astronaut Ed Mitchell (ref. 2) has commented on the recognition of a requirement for some pre-flight "vestibular training." The Apollo 14 crew did considerable active flying in jets prior to their mission, and experienced no symptoms of motion sickness. The situation in regard to possible disorientation and motion sickness symptoms for non-astronauts in a space vehicle rotating to achieve artificial gravity is even less clear.

The pending development of a space station to be used not only by pilot astronauts, but also by scientists for experiments and observation further points out the need to try to understand the expected orientation responses, both in weightlessness, and in a rotating spacecraft with its attendant problems of bizarre stimulation. The only direct experimental evidence which relates to this problem is from the Pensacola rotating room work which, although quite valuable in itself, is of course limited by the ever present 1 g from the earth's gravitational field. One approach to research on possible disorientation in a rotating spacecraft is through the extension of modelling of the vestibular system to make predictions as to the expected system response for different types of head and body motions in a rotating spacecraft. The physical forces, centrifugal and Coriolis, can be well predicted and, we feel, can be used to make accurate predictions of vestibular outputs not only from

* Supported by NASA grants NGR–22–009–025 and NGR–22–009–156.

semicircular canals and otoliths individually, but also on the basis of combined canal and otolith stimulation.

The physical force field resulting from translation or rotation inside a rotating spacecraft has been described in reference **3.** In vector form, the linear and angular acceleration stimulating the vestibular system are

$$\ddot{\bar{r}}_{h\text{-}I} = \ddot{\bar{r}}_{h\text{-}B} + 2(\bar{\omega}_v \times \dot{\bar{r}}_{h\text{-}B}) + \bar{\omega}_v \times (\bar{\omega}_v \times \bar{r}_{h\text{-}B})$$

$$\dot{\bar{\omega}}_{h\text{-}I} = \dot{\bar{\omega}}_{h\text{-}B} + \bar{\omega}_v \times \bar{\omega}_{h\text{-}B}$$

where the subscripts

h-I indicate head, with respect to inertial space,

h-B indicate head, with respect to the rotating base, measured from the hub,

$\bar{\omega}_v$ is the angular velocity of the space station with respect to inertial space,

$\bar{r}$ is the vector from the hub of the spacecraft to the subject's head.

In each of these equations, the acceleration sensed visually, with respect to the rotating spacecraft, is only the first term on the right-hand side.

The term $2(\bar{\omega}_v \times \dot{\bar{r}}_{h-B})$ represents the Coriolis acceleration associated with linear velocity not parallel to the axis. It results in variations in radial force, which is higher when walking in the direction of spacecraft rotation, and lower when walking away. It also produces tangential acceleration when moving radially, toward or away from the center.

The term $\bar{\omega}_v \times \bar{\omega}_{h-B}$ represents the cross-coupled angular accelerations which stimulate the semicircular canals about an axis normal to the head rotation and the spacecraft axis of rotation.

To apply the vestibular models which have been developed for predicting human dynamic spatial orientation, the total acceleration must be used as stimulus, as seen in figure **1.** (See also ref. **4.)**

MODELLING DISORIENTATION IN UNUSUAL ENVIRONMENTS

Jones (ref. *5)* has pointed out the need to consider the dynamic characteristics of the vse-

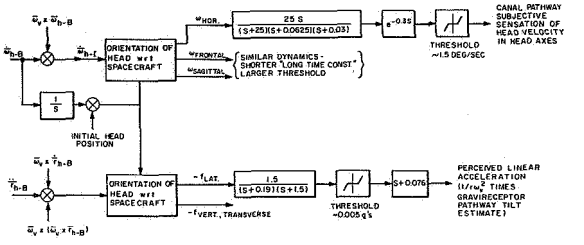

FIGURE 1.—Vestibular model applied to sensation in a rotating spacecraft.

tibular sensors as well as the "bizarre stimulation" in predicting spatial orientation in a rotating environment, and refers to analog simulation using models such as shown in figure **1** as perhaps the best approach to the problem. At the present time, however, these models are still in their infancy and serve a true predictive role only in the most elementary case of dynamic space orientation : when the stimulus is pure rotation about an "earth vertical" axis or vertical linear acceleration. The dynamic interaction between vestibular pathways and among different orientation sensors is being investigated for active and passive motion in normal and unusual motion environments (ref. **6).**

A useful starting point is a taxonomy of dynamic orientation situations, as follows:

Case 1.—Passive motion, no visual cues, pure rotation or translation. Examples : post rotation sensation; oculogravic illusion.

Case 2.—Passive motion, no visual cues, consistent combined vestibular stimulus. Example: head motion in pitch or roll.

Case 3.—Passive motion, all sensors, normal environment. Example : automobile passenger.

Case 4.—Passive motion, all sensors, conflict between sensors. Examples : simulator sickness, airplane turning illusions.

Case 5.—Active motion, all sensors, not habituated to unusual environment. Example : first hours aboard ship.

Case 6.—Active motion, all sensors, habituation to specific motion pattern. Example: skater's habituation to spins.

Case 7.—Active motion, all sensors, habituation to general motion in unusual environment. Example: "sea legs."

Clearly, the situation of free motion in a

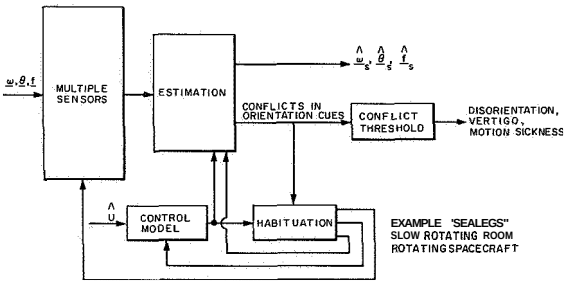

FIGURE 2.—Case 7: active motion, all sensors, habituation to general motion in unusual environment.

rotating spacecraft belongs to case 7, which is shown schematically in figure 2.

SOME APPROACHES TO REDUCING DISORIENTATION

Consideration of practical solutions to the problem of reducing to a minimum the discomfort and performance decrement in a rotating spacecraft leads to several avenues to be explored (refs. 7 through 9). Many of these have been mentioned by others and some of them appear highly impractical at this point. Nevertheless, the suggestions for investigation are

(1) Devise active movement training schedules for habituation. Regulate schedule by measuring disorientation so as to minimize habituation time and symptoms of disorientation.

(2) Design the visual surround to have no outside view which cannot be shut out, no strong visual verticals or horizontals, distinctive colors for all walls having the same orientation with respect to the spacecraft motion.

(3) Orient cabins and work stations so that most walking is parallel to the axis of rotation; and head movements are nodding motions about that axis (ref. 8).

(4) Construct radial stairs or ladders to curve (against the direction of spacecraft rotation for ascending and in the direction of rotation for descending) so that the direction of the apparent vertical does not change relative to the subject ascending or descending at a constant rate. (Of course, this condition does not apply to the limbs because of their reciprocating motion.) The transcendental equation for angle θ away from the radial is

$$\cot \theta = (r\omega_v - 2v \sin \theta)/v \cos \theta$$

where r is the radius and v is the man's relative velocity.

As an example, for $\omega_v = 0.5$ rad/sec (4.8 rpm) at a radius of 6.1 m (20 ft) and relative velocity of 0.58 m/sec (1.9 ft/sec), the passageway should be tilted by ten degrees. Of course, a simpler solution is to provide two-sided radial ladders in which one ascends by facing into the direction of spacecraft rotation and descends facing away from this direction, so that Coriolis forces always push the subject toward the ladder.

(5) Finally, variable individually controlled visual surrounds could be further investigated. We have had initial success in reducing disorientation in single axis rotations by displaying a pattern of moving stripes which is driven in agreement with the semicircular canal model prediction of this sensation of rotation. We are currently experimenting with a three axis system using a diffuse large field Moiré pattern.

One could imagine a device utilizing a head mounted CRT and head position monitor to display a "combatible scene" during head movements. This visual pattern could be arranged to approach the actual spacecraft visual surround as the subject habituated to the effects of active head movements in a rotating environment.

REFERENCES

1. BERRY, C. A.: Summary of Medical Experience in the Apollo 7–11 Manned Spaceflights. Recent Advances in Aerospace Medicine, Douglas E. Busby, ed., Dordrecht, Holland. D. Reidel Publishing Co., 1970, pp. 3–41.
2. MITCHELL, E.: Personal communication. Cambridge, Mass., Apr. 1971.
3. STONE, R. W., JR.; AND LETKO, W.: Some Observations on the Stimulation of the Vestibular System of Man in a Rotating Environment. The Role of the Vestibular Organs in the Exploration of Space. NASA SP–77, 1965.
4. YOUNG, L. R.: The Current Status of Vestibular System Models. Automatica, vol. 5, 1969, pp. 369–383.
5. MELVILL JONES, G.: Dynamic Cross-Coupling in the Semicircular Canals. Recent Advances in Aerospace Medicine, Douglas E. Busby, ed., Dordrecht, Holland. D. Reidel Publishing Co., 1970, pp. 235–248.
6. GUEDRY, F. E., JR.: Conflicting Sensory Orientation

Cues as a Factor in Motion Sickness. Fourth Symposium on the Role of the Vestibular Organs in Space Exploration. NASA SP–187.

7. GRAYBIEL, ASHTON; THOMPSON, ALLEN B.; DEANE, ROBERT; FREGLY, ALFRED R.; COLEHOUR, JAMES K.; AND RICKS, EDWARD L., JR.: Transfer of Habituation of Motion Sickness on Change in Body Position Between Vertical and Horizontal in a Rotating Environment. Aerospace Medicine, vol. 39, no. 9, Sept. 1968, pp. 950–962.
8. LORET, B. J.: Optimization of Space Vehicle Design with Respect to Artificial Gravity. Aerospace Medicine, vol. 34, no. 5, May 1963, pp. 430–441.
9. HELD, RICHARD; AND FREEMAN, SANFORD J.: Plasticity in Human Sensorimotor Control. Science, vol. 142, no. 3591, Oct. 25, 1963, pp. 455–462.

SESSION IV

ANALYSIS OF DISPLAY SYSTEMS

Chairman: RICHARD PEW

16. The Influence of a Prediction Display on the Quasi-Linear Describing Function and Remnant Measured With an Adaptive Analog-Pilot in a Closed Loop

D. DEY

Institut fur Flugführung und Luftverkehr

THE PREDICTION DISPLAY

The prediction display shows the desired value x_s, the actual value x_i and additionally the anticipated system output $x_v(t) = x_i(t+\tau)$. The predicted value x_v is computed through a Taylor series in which the number of derivatives used designates the order of prediction *(m)*. The prediction time is called τ. Refer to figure 1.

Investigating the manual attitude stabilization of one axis of a hovering VTOL aircraft, it was shown in several experiments, that a prediction display facilitates and improves the manual stabilization (refs. 1 and 2). The transfer function of the controlled system is $K_F/s^2(1+T_V s)$ with $T_V = 0.4$ sec and $K_F = 20$ cm/sec²/full deflection. Refer to figure **1.**

The disturbance is taken from a pseudo-random noise generator, which consists of a 10 stage shift register with a **0.64** sec clock period, a digital to analog converter and a first order analog filter of the form $1/(1+j\omega)$.

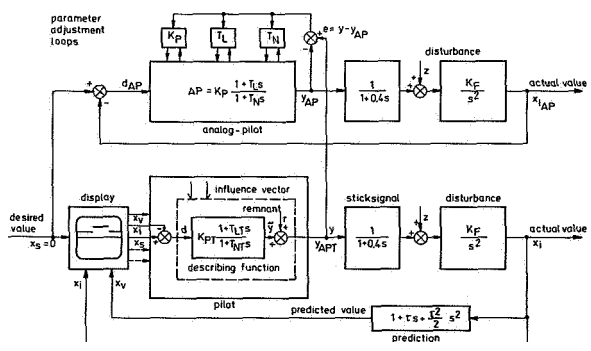

FIGURE 1.—Measuring **of** the human control characteristics in a closed loop by means of an adaptive analog pilot.

With a prediction display the damping of the man-machine control loop is increased and untrained test persons are able to stabilize the control loop from the first moment onward. The facilitation of a continuous control task by a prediction display can be shown by additional tasks. The improvement of the manual control is defined as a minimization of the rms value of the control deviation (control error e) with a simultaneous reduction of the rms value of the stick signal (stick deflection κ). The best prediction for the investigated system is a second order prediction

$$x_v = x_i + \tau\dot{x}_i + \frac{\tau^2}{2}\ddot{x}_i$$

with a prediction time of $\tau = 0.7$ sec. Refer to figure **2.**

The reason for the improvement of manual control by the additional pilot information about the anticipated system output must be seen in a change of the human transfer characteristics. This will now be explained by means of the parameter changes in a linear model.

THE **HUMAN** OPERATOR MODEL

The known application-orientated model of a linear describing function, a remnant, and an additional "influence vector" has been chosen to describe the human transfer characteristics, because much experience has been acquired for this model (ref. **3).** The describing function relating the stick signal y to the control deviation $d = 0 - x_i$ used is $AP(s) = K_P(1+T_L s)/(1+T_N s)$. The pre-

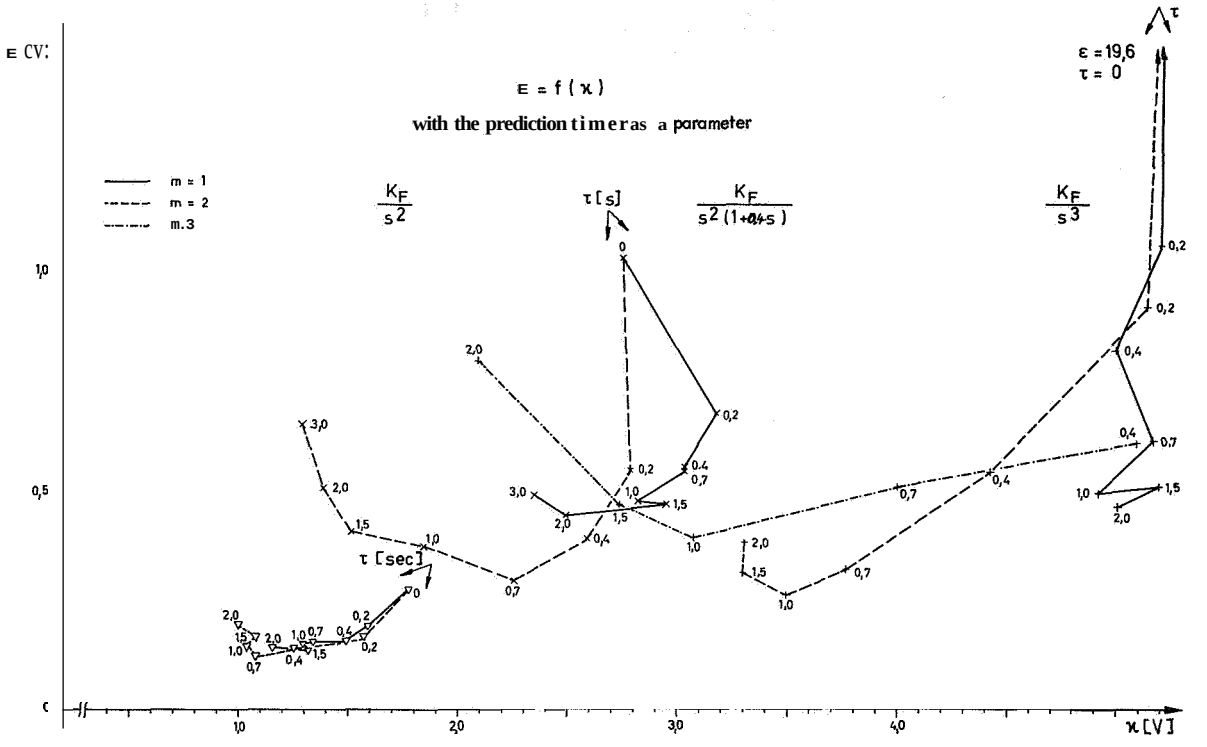

FIGURE 2.—Rms control deviation ϵ as a function of rms stick signal with τ as a parameter for the systems K_F/s^2, $K_F/s^2(1+0.4 \text{ sec})$ and K_F/s^3.

dicted system output is always considered as additional information (like other a priori information) of the simulated task.

The remnant includes all nonlinear parts of the transfer characteristics as, for instance, observation and movement noise, the influence of an indifference threshold, stick positioning limits, and effects of discrete signal procession. The influence vector stands for all the parameters of the simulation and task which influence the transfer characteristics, which we attempted to hold constant during this investigation. The quasi-linear model is shown in figure **1.**

To get an insight into the effect of different coefficient values on the mean square control deviation it is calculated without a remnant from the known disturbance.

Figure 3 is a 3-dimensional picture showing the mean square control deviation as a function of K_P, T_L, and T_N. The lowest control deviation can be obtained with high gain values. To obtain a stable loop in these cases T_L values must be high and T_N values low.

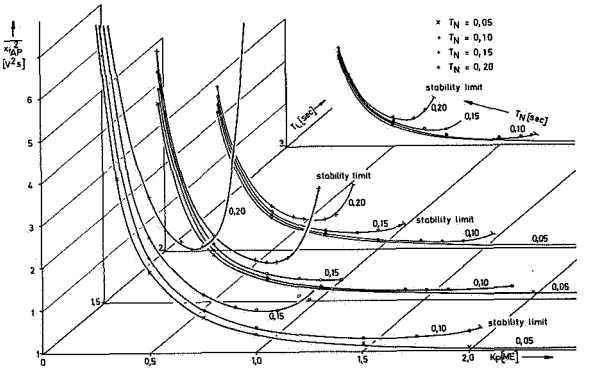

FIGURE 3.—The mean square value of the control deviation as a function of the analog pilot's coefficients.

THE CONTINUOUS ADAPTION OF THE MODEL

A model matching technique is used as a method of measurement because the simultaneous observation of the human and the model with its variable parameters yields a good view of the control process. When controlling a third order

acceleration system, a great remnant portion is to be expected in the human output. The model matching technique is therefore used in a closed loop, that is, the adaptive analog-pilot works parallel to the manual control in its own loop. By this method of measurement the coefficients are not affected by the human remnant (ref. **4).** Refer to figure **1.** Under the assumptions that the structure of the model is chosen well and the adaption is finished the power density spectrum (PDS) of the remnant can be calculated directly from the PDS of the adaption difference ***e.***

By means of the gradient method the coefficients K_P, T_L and T_N are adapted on-line, continuously and simultaneously, so that the difference of the output of the test person y and the analog pilot y_{AP} is minimized (ref. ***5).*** The principle of adaption, for instance for the gain constant K_P is shown in figure **4.** For adaption an even error function is defined:

$$f=\frac{1}{2}e^2=\frac{1}{2}(y-y_{AP})^2$$

and a modified gradient method is chosen for the continuous adaption of coefficients

$$\dot{c}_i=-k_i\frac{\partial f}{\partial c_i}=k_i\cdot e\cdot u_i$$

$\dot{c}_i$ describes the derivative of the desired coefficient, k_i represents the gain constant of the adaptive loops and

$$u_i=\frac{\partial y_{AP}}{\partial c_i}$$

describes the sensitivity functions. For each coefficient it is continuously computed. Since this is only valid for constant coefficients the adaption is performed iteratively. To begin with, initial values are chosen, then an adaption is performed and after that the measured coefficients are considered in the differential equations for the sensitivity functions before starting a new measurement.

The object of the experiments is a high speed of adjustment. The speed of adjustment is dependent on the number of parameters, the remnant, the power density spectrum of the disturbances, and the amplification factors of the adaptive loops. It is, after all, a stability problem. Since the stability of these measuring systems

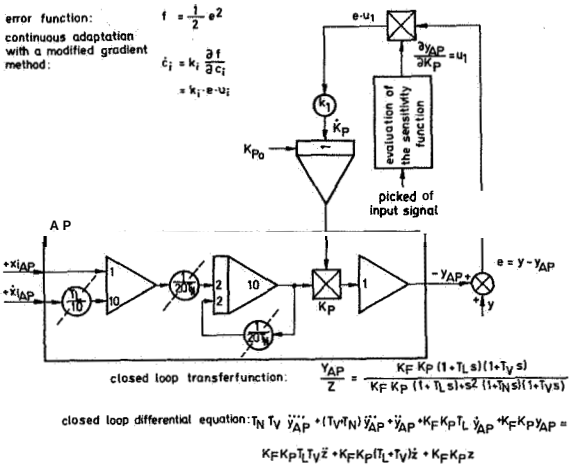

FIGURE 4.—The structure of the analog pilot and the K_P adaption loop.

cannot be calculated so far, and since the entire method leaves a number of questions to be answered, it is tested by a test analog pilot with simulated remnant.

THE TESTING OF THE MEASURING METHOD

The testing of the measuring method can be seen in figure **1.** Instead of a human, a test analog pilot with a simulated remnant is operating in the control loop. Now, the known coefficients of the test analog pilot are measured by the analog pilot.

The investigation proved that the measuring method operates well. The remnant causes considerable reduction of the adjustment speed. After complete adaption the adaptive difference will not be zero, owing to the remnant. The difference is always minimized even if the known coefficients cannot be found exactly. The power density spectrum of the simulated remnant can be calculated from the adaptive difference. Therefore the power density spectrum of the remnant, occurring during experiments with the human can also be calculated.

THE MEASURING OF THE HUMAN CONTROL CHARACTERISTICS

For the investigation of human control characteristics a special experimentation technique

was developed which provides a stationary attitude of the test persons. They were screened optically and acoustically. They were able to manage the control tasks owing to former experiments and were trained additionally for **1** week.

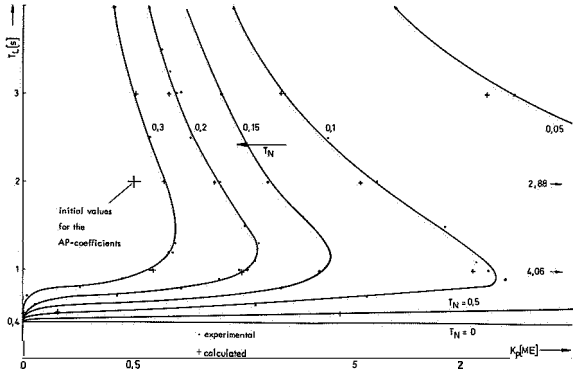

FIGURE 5.—The stability limit of the closed loop for 'different coefficients of the analog-pilot **(AP).**

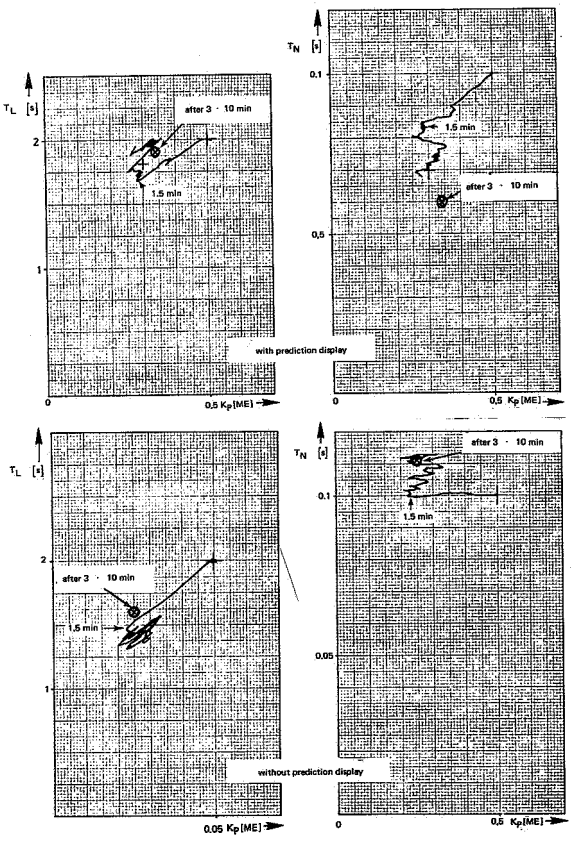

FIGURE 6.—An example for the adaption of coefficients during first day 10 min measurement.

The test lasted *10* minutes and was conducted twice during *3* days. The measuring time is a compromise between the frequency resolution and the statistic certainty of the results on the one hand and the exhaustion of the test persons on the other.

The initial values to begin with were derived from an investigation of the possible parameter space in respect to the stability of the control loop. Figure **5** shows the stability limits **as** a function of the parameters K_P, T_L, and T_N.

Figure **6** shows an example of the parameter adaption on the first day beginning with the initial values. The fast adaption within the first **1.5** min is obvious. The mean coefficient values, which were read after **3** days of tests were also recorded. They are shown in table *1.* **It** can be seen, that the test persons by means of the prediction display increase their effective gain constant and their effective lead constant and diminish their lag constant. This variation of coefficients already effects a reduction of the mean square value of the control deviation (see table *2* and figure *3).* The remnant decreases also by the prediction display.

TABLE *1.—Mean Values of Coefficients Measured by the Analog Pilot*

VP	Task	$\bar{K}_P[ME]$	$\bar{T}_L[s]$	$\bar{T}_N[s]$
K	With prediction	0.78	2.87	0.036
G	display	0.34	1.90	**0.060**
K	Without prediction	0.60	1.75	0.154
G	display	0.25	1.60	0.111

TABLE *2.—The Mean Square Values of the Control Deviation for the Test Persons and for the Adapted Analog Pilot*

VP	Task	$\bar{x}_i^2[V]^2$	$\bar{x}_{i\,AP}^2[V^2]$
K	With prediction	0.12	0.205
G	display	2.48	1.82
K	Without prediction	1.14	0.75
G	display	7.92	4.62

TABLE 3.—*The Adaption Factor* $\tilde{\rho}$

Trial	VP	Task	$\bar{y}_{T_1}{}^2\bar{y}^2[V^2]$	$\bar{e}^2[V^2]$	$\tilde{\rho}^2$	$\tilde{\rho}$
E4	APT	Test	1.46	0.50	0.66	0.81
V9	K	With PD *	2.08	0.94	0.54	0.74
V10	K	Without PD	3.45	1.77	0.49	0.70
V11	G	With PD	1.08	0.36	0.67	0.82
v12	G	Without PD	1.06	0.49	0.54	0.73

* PD—prediction display.

For that part of the stick signal which can be explained by the analog pilot an adaption factor $\tilde{\rho}$ is defined

$$\tilde{\rho}^2 = 1 - \frac{\bar{e}^2}{\bar{y}^2}.$$

The adaption factor is a measure for that part of the human stick signal which is explained by the linear model and thus is a quality factor for the model. The results are depicted in table 3. By means of the chosen simple model 70 to 80 percent of the human output can be explained.

Figure 7 shows an example of the power density spectra for the human stick signals, the analog pilot's stick signals, as well as the adaptive difference during control with and without prediction display. It is seen (1) that the prediction display increases the damping within the loop, and (2) the low frequency components of the human output are well explained by the analog pilot. The high frequency components remain in the adaptive difference.

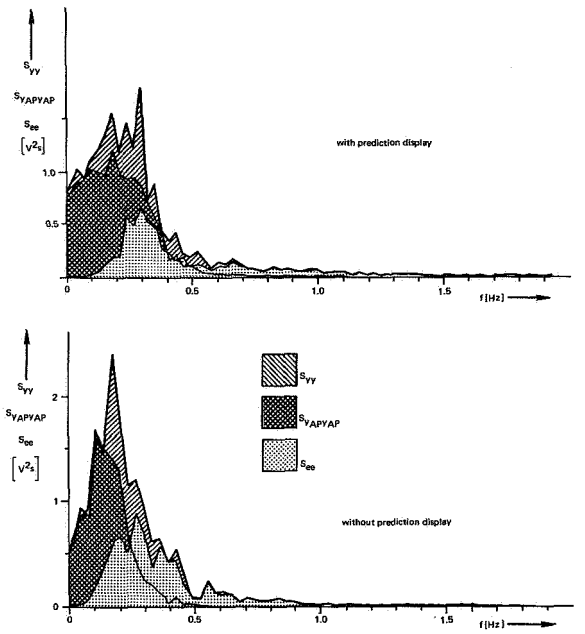

FIGURE 7.—An example for the power density spectra of the human stick signal S_{yy}, the analog pilot stick signal $S_{yap\,yap}$, and the adaption difference S_{ee}.

CONCLUSION

Summing up, one can say, that the effect of a prediction display on the human transfer characteristics can be explained with the aid of a quasi-linear model. The prediction display causes an increase of the gain factor K_P and the lead factor T_L, a diminishing of the lag factor T_N and a decrease of the remnant. Altogether, these factors yield a smaller mean square value of the control deviation and a simultaneous decrease of the mean square value of the stick signal.

REFERENCES

1. BERNOTAT, R.; DEY, D.; AND WIDLOK, H.: Die Voranzeige als anthropotechnisches Hilfsmittel bei der Fiihrung von Fahrzeugen. Forschungsberichte des Landes Nordrhein-Westfalen, Nr. 1893, Jan. 1967.
2. DEY, D.; AND JOHANNSEN, G.: Stabilisierung und Lenkung von Fahrzeugen mit Hilfe der Voranzeige. Bericht Nr. 50 des Instituts fur Flugfuhrung und Luftverkehr der TU Berlin, 1969.
3. MCRUER, D.; GRAHAM, D.; KRENDEL, E.; AND REISENER, W.: Human Pilot Dynamics in Compensatory Systems. Air Force Flight Dynamics Laboratory, Tech. Rept. Nr. AFFDL-TR-65-15, Wright-Patterson Air Force Base, Ohio, July 1965.
4. JONES, J. G.: A Note on the Model Matching Technique for the Measurement of Human Operator Describing Functions. Tech. Rept No. 65290, Royal Aircraft Establishment, Dec. 1965.
5. BEKEY, G. A.; MEISSINGER, H. F.; AND ROSE, R. E.: A Study of Model Matching Techniques for the Determination of Parameters in Human Pilot Models. Für die NASA hergestellter Bericht von TRW Space Technology Laboratories, Redondo Beach, 1965.

17. Analytic Evaluation of Display Requirements for Approach to Landing*

DAVID L. KLEINMAN AND SHELDON BARON

Bolt, Beranek and Newman Inc.

In recent years we have developed an integrated approach to the analysis of manned vehicles systems (refs. 1 through **4).** We have blended human response constraints within an optimal control theoretic framework to represent the pilot's limitations as a decision and control element. The resulting pilot-vehicle-display model can be used to study information and display requirements and the effects on system performance and reliability of pilot-induced randomness, wind gusts, configurational changes, etc. In this paper, we give a brief description of our control theoretic systems model and demonstrate its use and validity by applying it to a piloted approach to landing situation.

The analysis procedure assumes that the vehicle dynamics (which may also include actuator and sensor dynamics) are represented by the linearized equations of motion

$$(\dot{\underline{x}}t) = \underline{A}\,\underline{x}(t) + \underline{B}\,\underline{u}(t) + (\underline{w}t). \qquad (1)$$

$\underline{x}(t)$ is a vector that describes the vehicle state; $\underline{u}(t)$ is the pilot-generated control input; $\underline{w}(t)$ represents external disturbances (turbulence, wind-gusts, up-drafts, etc.).

Several system outputs

$$\underline{y}(t) = \underline{C}(t)\underline{x}(t) \qquad (2)$$

may be of concern, and it is assumed that they are presented continuously to the pilot via some visual display or instrument panel. The observations of $\underline{y}(t)$ represent the information set upon which the pilot bases his control actions.

The methods for representing the human's limitations and the resulting optimally compensating elements are the unique and crucial features of our approach. Several pilot limitations that we represent explicitly in the model are

(1) The various internal time-delays associated with visual, central processing, and neuromotor pathways are represented by a lumped "equivalent" perceptual time-delay τ.

(2) Observation noise represents the combined effects of sensory and central-processing sources of pilot randomness, as well as display-related noise sources. This noise process is modeled by associating with each displayed output $y_i(t)$ a white observation noise $v_i(t)$ with power-density level V_i. Values for V_i depend on the nature (quality, type, and form) of the display panel, where the pilot is looking, etc.

(3) Visual and/or indifference thresholds that represent human nonlinear characteristics for small signals.

(4) A motor noise $\underline{v}_u$ is added to $\underline{u}(t)$ and represents the fact that a pilot cannot generate commanded control inputs perfectly. The sum of $\underline{v}_u(t)$ and $\underline{v}_y(t)$ represents inherent pilot "remnant," or randomness.

The pilot is assumed to adopt a control strategy that minimizes a weighted sum of averaged state and control variances (i.e., a quadratic cost functional conditioned on the displayed information and subject to his inherent constraints. With this assumption, the human's control characteristics are determined by the solution of an optimal linear regulator problem with time-delay and observation noise. Pilot equalization is modeled by the cascade combination of three elements: **(1)** a least-mean-squared predictor that compensates optimally for the inherent delay, **(2)** a Kalman filter that yields a best estimate of the system state from (noisy) observations of $\underline{y}(t)$,

* **Entire paper** to **appear in Proceedings of 1972 IFAC Congress.**

and (3) a set of optimal gains that operates on the best estimate of the state to produce the desired control response. The general expressions for these model elements, in the time-invariant case, are given in reference 4. The extensions of the model to a time-varying approach to landing situation are covered in this paper.

The analysis procedure that we developed is used to investigate pictorial display requirements for the landing approach of a light aircraft. Input disturbances include vertical drafts and random gusts. Pilot variability is accounted for, leading to statistical performance predictions even in the absence of external random disturbances. The effects on system performance of several display modifications and different wind disturbances are predicted by the model and are compared with data obtained in an independent experimental study. The comparison affirms the validity of our system model and demonstrates its utility in manned-vehicle analysis and synthesis.

REFERENCES

1. KLEINMAN, D. L.; AND BARON, S.: Manned Vehicle System Analysis by Means of Modern Control Theory. Rept. No. 1967, Bolt, Bernak and Newman, Inc., June 1970.
2. BARON, S.; AND KLEINMAN, D. L.: The Human as an Optimal Controller and Information Processor. IEEE, Trans. on Man-Machine Systems, vol. MMS-10, no. 1, Mar. 1969.
3. LEVISON, W. H.; BARON, S.; AND KLEINMAN, D. L.: A Model for Human Controller Remnant. IEEE, Trans. on Man-Machine Systems, vol. MMS-10, no. 4, Dec. 1969.
4. KLEINMAN, D. L.; BARON, S.; AND LEVISON, W. H.: An Optimal Control Model of Human Response. Automatica, vol. 6, pts. I and II, no. 3, May 1970.

N73-10122

18. Pilot Performance With a Simulated ILS–Independent Pictorial Display

EVERETT PALMER AND THOMAS WEMPE

Ames Research Center
National Aeronautics and Space Administration

As part of a general investigation of the effectiveness of pictorial displays for manual control and monitoring of aircraft approaches and landings, a simulator study was conducted in which pilot performance with three pictorial display? was evaluated. These displays differed in the type of guidance symbology added to the basic perspective runway display. The effect of decreased resolution and update rate of the runway image on pilot performance was also determined.

The results indicate that for pictorial displays with added guidance symbology, there was a marked improvement in pilot performance compared to results of a previous study in which the display consisted of only a runway image and aircraft attitude. However, approach precision was inadequate to meet category II tolerances. Landing performance was also improved by providing additional guidance information on the display. The moderate degradation in runway image resolution and update rate had a negligible effect on performance; nevertheless, it was disliked by the pilots.

INTRODUCTION

New transport aircraft are being equipped to perform completely automatic approaches and touchdowns in low visibility weather. If the redundancy and reliability provided by the presence of the pilot on board these aircraft is to be effectively utilized, the pilot must remain actively in commandand not become merely a system status monitor. Studies have shown that current displays are inadequate for this task (refs. **1, 2,** and **3).** Displays should allow the pilot to commit the airplane to a landing if the approach is successful, reject all marginal approaches, and assume manual control to complete the approach or execute a missed approach.

In addition, there is a strong feeling, especially among pilots (ref. **4),** that the guidance for such a display must be independent of the guidance for the autoland system. The display should provide a redundant source of information and thereby increase pilot confidence in the use of the automatic system. Such a display is generally referred to as an independent landing monitor (ILM).

One type of ILM generates a perspective image of the terrain and runway ahead of and below the aircraft. This display would be generated by an airborne system such as perspective radar, low light level TV, or a microwave radiometer that could penetrate low visibility atmospheric conditions (ref. *5).* This type of imaging pictorial display has several advantages. It provides an integrated and easily interpreted picture of the outside world. The pilot should be able to use many of the same visual cues that he haslearned to use during extensive visual flight. The perspective format should improve the pilot's ability to visualize his position with respect to the real runway and thus facilitate the transition from instrument to visual flight. Finally, symbolic guidance information can be naturally integrated into the display to provide quantitative information and to improve the precision with which the pilot can use the information provided by the perspective image of the runway. However, such

display systems usually produce runway images with insufficient content, degraded resolution, and a delay in time.

Two simulator studies have been conducted to investigate the attributes and deficiencies of imaging pictorial displays for manual control and monitoring of aircraft approaches and landings. The first study (ref. 6) isolated and studied the basic display element: the perspective runway image. Results of that study indicate that although the display had good pilot acceptance and could be degraded in resolution and update rate with little effect on performance, it was inadequate for making precise approaches and landings. The purpose of the present study was to investigate various methods of adding guidance symbology to augment the information contained in the runway image. Three display configurations and two image resolution and update rates were studied, and the results are compared with those of the first study. Results are also provided on pilot ability to monitor approach performance at a decision altitude of 30 m (100 ft).

TESTS AND PROCEDURES

Display Configurations

Approach and touchdown configurations of the three displays evaluated are shown in figure 1. Each display comprised basically the same runway image, horizon bar, and airplane reference symbol used in the previous experiment (fig. 2); and additional symbology (fig. 3) to aid the pilot in using the natural visual cues provided by the runway image and to provide other guidance information in symbolic form. The central display element was a perspective view of the runway reflectors (fig. 4). This particular reflector or beacon configuration was designed to improve lateral offset and distance-down-the-runway information when the aircraft was close to the ground. Other configurations with more beacons positioned to simulate actual runway lights were tested, but they added too much clutter for the low-resolution display condition.

Each display configuration contained the following basic information:

(1) Digital readouts of airspeed, altitude, and vertical velocity.

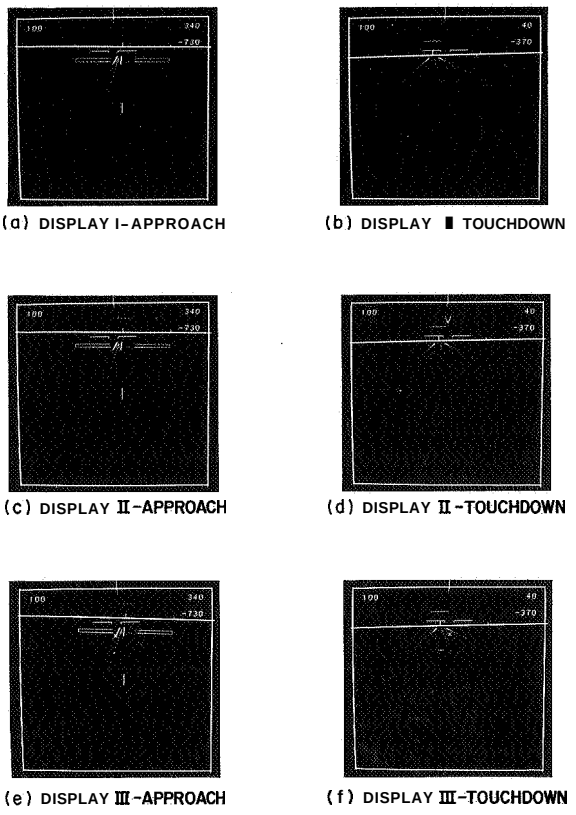

FIGURE 1.—Approach and touchdown configurations of the three experimental displays.

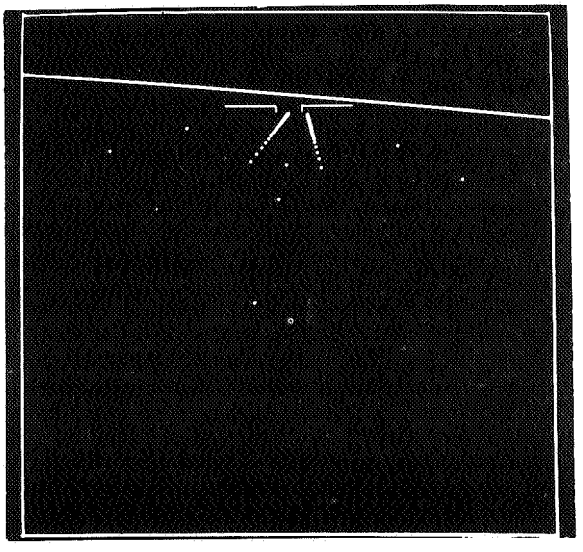

FIGURE 2.—Pictorial display A used in prior experiment (ref. 6).

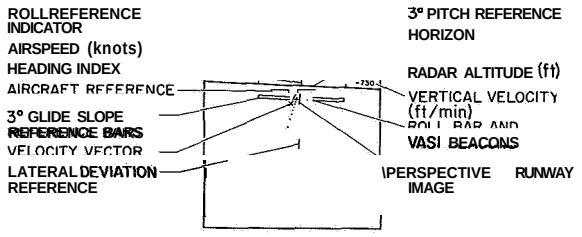

FIGURE 3.—Identification of display elements of display III during the approach.

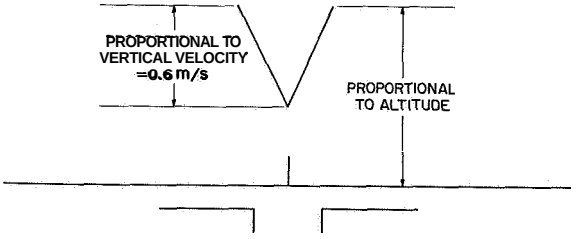

FIGURE 5.—Integrated altitude and vertical velocity symbol during touchdown with display 11.

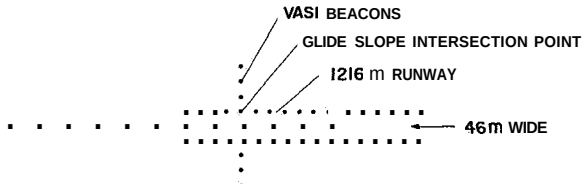

FIGURE 4.—Runway configuration (not to scale).

(2) Pitch, heading, and roll reference marks.

(3) Glide slope reference (GSR) bars, which were depressed 3° below the horizon. If the glide slope intersection point on the runway was held 3° below the horizon, the aircraft would remain on a 3" glide slope. The gap between the glide slope reference bars indicated a $\pm 0.3°$ glide slope tolerance.

(4) A lateral deviation reference (LDR) bar, which was a short line perpendicular to the horizon on the same heading as the runway. If the airplane was over the extended runway centerline, the runway lead-in beacons were perpendicular to the horizon. The LDR bar helped the pilot maintain this relationship.

(5) At an altitude of 36 m (120 ft) above the runway, a minimum decision height (MDH) marker flashed on the display to indicate to the pilot that he was approaching the MDH. At an altitude of 30 m (100 ft) the MDH marker was removed, and an integrated display of radar altitude above the runway appeared. At an altitude of 15 m (50 ft) the GSR bars and LDR bar were removed to reduce clutter and to cue the pilot that he was 15 m above the runway.

The experimental displays contained the following additional symbology:

Display I.—The approach symbology was the same as described above. At an altitude of 30 m, the short bar shown above the horizon in figure 1(b) appeared. Its distance above the horizon was proportional to wheel height above the runway. The scaling was 6 m per degree.

Display II.—During the approach, the roll bar lights at the glide slope intersection point formed a visual approach slope indicator (VASI). If the aircraft was at a glide slope angle of between 2.85" and 3.15°, two roll bar lights were visible. Below 2.85" only one light was visible, and above 3.15" three lights were visible. At an altitude of 30 m the chevron shown in figure 1(d) appeared. It provided an integrated measure of both wheel height above the runway and vertical velocity (fig. 5). The display gains were set so that the chevron could be used as a flare command. If the pilot began his flare when the point of the chevron touched the horizon and then continued to pitch up just enough to hold the point of the chevron on the horizon, he would execute an exponential flare and touchdown with a vertical velocity of 0.6 m/sec (2 ft/sec). The display gains on altitude and vertical velocity were 6 m/deg and 1 m/sec/deg, respectively.

Display III.—In addition to the VASI lights, this display included a velocity vector symbol (the X in fig. 1(e)), which indicated the point on the ground toward which the aircraft was aiming at any instant. Vertically, it provided flight-path angle; laterally, it provided track information. At 30 m, the radar altitude bar shown in figure 1(f) appeared. It was scaled the same as the bar in display 11. If the velocity vector was held on the runway aim point until the radar altitude bar passed through the velocity vector and then the flare was initiated, holding the velocity vector just below the altitude bar, an exponential flare would be executed.

Display Quality

Two runway image qualities were tested for each of the three display conditions. These were "good display quality" (horizontal resolution, **0.05";** vertical resolution, **0.05";** and update interval, 0.1 sec), and "poor display quality" (horizontal resolution, 0.4°; vertical resolution, 0.4°; and update interval, 0.3 aec). The resolution of the displayed runway image was degraded by reducing the effective digital resolution of the computer display. The update interval, the time between new frames of information, was simulated by adjusting the updating in the digital program. The horizon and other display symbols were updated every **0.05** sec and always had a resolution of **0.05"** relative to the "real world." All display elements were refreshed at the rate of 60 frames/sec to prevent flicker.

The field of view of the perspective display was 40" by 40° in the "real world." The display was generated on a cathode ray tube and transmitted by a 946-line closed-circuit TV system to a monitor in the pilot's cab. The pilots viewed the TV monitor from a distance of about 45 cm. The display was thus compressed to a scaling of approximately **1**:2 as compared to a "real world" view of the runway.

Test Setup

The piloting tasks were performed by pilot-subjects seated inside a small portable cab. The pilot had three controls: a side-arm controller with a flexible plastic fiber control stick, a combination recycle and start switch, and a decision switch. Figure **6** shows the interconnection between the cab and the simulation equipment.

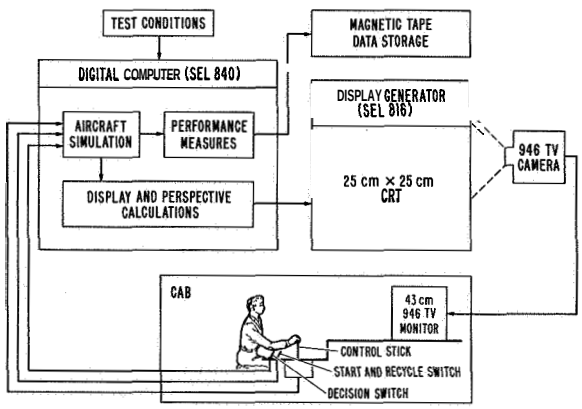

FIGURE 6.—Cab and simulation equipment.

An aircraft with good handling qualities was selected so that the effects of the flight display variables considered in this study on pilot performance could be more easily determined. The dynamics of a Navion low-wing, four-passenger, light plane were simulated on a digital computer using the linear equations described in appendix A. To reduce the effects of differences in piloting techniques, pilot options such as power adjustments and flap settings were not included in the simulation. The power and trim were set to maintain an airspeed of **53** m/sec (104 knots) on a **3"** glide slope. The yaw rate was computed so that the aircraft always made coordinated turns; hence, rudder control was not required or provided. At the beginning of each flight the simulated aircraft was positioned 3040 m **(10** 000 ft) from the threshold on a 3" glide slope to a point 304 m **(1000** ft) down the 1216-m (4000 ft) long runway.

Test Subjects and Procedure

Six airline pilots with extensive backgrounds in instrument flying were selected to participate in these experiments. They had very little prior experience with pictorial displays or laboratory simulation experiments. Their flight experience is summarized in table **1.**

The experiment was divided into two phases. Phase **1** provided the pilots with initial practice on the displays and included a test to identify pilots with a tendency to make control reversals on an inside-out display in a fixed-base simulator. Phase 2 was designed to measure the overall performance levels of the different displays, the relative differences between the displays, and the effect of poor display image quality on pilot performance.

Phase 1.—Each pilot was informed of the background and objectives of the experiment. He then was given a detailed description of the particular display he would fly, the aircraft dynamics, the environmental disturbance, and the task to be performed.

The pilot was seated in the cab and allowed to fly the simulated aircraft. The display provided only numeric readouts of airspeed, altitude and

TABLE 1.—*Pilot Experience*

Pilot	Position	Aircraft	Flight time		
			Total	Night	Instrument
1	2nd officer	707	3,000	700	1,000
2	Captain	720	14,500	.....	.....
3	1st officer	707	2,700	1,200	500
4	2nd officer	DC–8	4,000	1,500	500
5	1st officer	707	5,000	1,800	700
6	2nd officer	DC–8	5,000	500	500

vertical velocity, and aircraft attitude information. The runway image, glide slope reference bars, and lateral reference bar were removed. After about 10 min of flying, a series of 36 random disturbances in bank, pitch, and yaw angle were introduced and the pilot was instructed to correct for them. The pilot was subjectively scored by the experimenter on the number of control reversals he made.

If a pilot made any control reversals during the the last 18 disturbances he was not asked to participate in phase 2. Six pilots were eliminated in this way. There was no apparent difference in experience or position between these pilots and those selected to participate in phase 2 of the experiment. All pilots then made 32 approaches and landings for practice with one of the three displays with the runway image quality degraded.

Phase 2.—Six pilot-subjects who passed the control reversal test spent 2 hr on three different days on phase 2. Each pilot was briefed on the display he would fly that day and then made 32 flights. The first 16 flights were made with one runway image quality and the second 16 flights with the other; the first 8 flights of each group of 16 were for practice. The flights were made in sets of four. In each set of four flights, initial crosswinds were drawn randomly without replacement from the set (-2.7, -1.35, $+1.35$, and $+2.7$ m/sec). Vertical drafts were drawn in the same manner from the set (-0.9, -0.45, $+0.45$, and $+0.9$ m/sec). At a range of 1520 m (5000 ft) from the threshold, the constant vertical drafts were reduced to zero. The crosswinds for the remainder of the flight were drawn randomly without replacement from the set (0, 0, 0.6, and 1.2 m/sec). The sign of these winds was the same as the initial crosswind. A moderate level (0.9 m/sec rms) of vertical and horizontal turbulence was also included on every other flight. This turbulence faded out below an altitude of 30 m (100 ft). On all flights the pilots were instructed to land. At an altitude of 30 m (100 ft), when the MDH light went off, they were instructed to judge whether or not they were within 0.3" of a 3" glide slope and within the extended runway confines, and to indicate their decision by pushing the decision switch in the appropriate direction.

The pilot-subjects were arbitrarily divided into two groups and the order of display conditions was balanced in a Latin square for each group. The order in which the display qualities were presented was also balanced between the two groups of three subjects.

Performance Measures and Pilot Opinion

Altitude, lateral displacement from an extension of the runway centerline, and sink rate were recorded at distances of 1520 and 304 m from the threshold for each simulated flight. These same measures and the distance down the runway from the threshold were also recorded at touchdown. When the pilot pushed the decision height switch, his decision as well as the aircraft range, altitude, and offset at that instant were recorded. At the end of the 16 flights for a given display condition, each pilot rated the usefulness of the display for both the approach and landing according to the Cooper-Harper rating scale (ref. 7). At the end of the experiment, each pilot was interviewed.

RESULTS AND DISCUSSION

Means and variances of the data taken at ranges of 1520 and 304 m from threshold and at touchdown were computed for the 288 data

Aights. In addition, the data for each Aight at *304* m *(1000* ft) and at touchdown was converted to a qualitative performance description. The altitude and lateral position at *304* m were converted into one of three qualitative performance descriptions according to the definitions provided in table *2*. The touchdown data were categorized in a similar way (table *3)*. The resulting performance data for the *288* flights were subjected to chi-square tests; results for *304* m and touchdown are summarized in tables *4* and **5,** respectively.

TABLE 2.—*Qualitative Dejtnition* of *304-m Approach Window Performance* *

Approach window performance	Lateral displacement from centerline L, m	Altitude error from glide slope Ae, m
Excellent	$\|L\| < 11.2$	$\|Ae\| < 1.8$
Successful	$11.2 < \|L\| < 22.8$	$1.8 < \|Ae\| < 3.6$
Unsuccessful	$22.8 < \|L\|$	$3.6 < \|Ae\|$

* The rating for each flight was the worst of the two variables, L or Ae.

Display Symbology Effects

Approach performance: 1520-m range.—The mean and standard deviation of altitude error and the rms lateral offset at the 1520-m window are shown in table 6; rms lateral offset was used to include the effect of crosswind biases to obtain the worst case dispersion. **A** Cochran's test for homogeneity of altitude variances of the three displays indicated that the displays were significantly different at the 0.05 level. Table **6** indicates a progressive reduction in altitude variability from display I to display III. This was as expected since the VASI beacons in display II should improve the pilot's ability to see glide slope errors, and the velocity vector symbol in display III allowed the pilot to immediately estimate and correct for the constant vertical drafts, thereby reducing his overall altitude variability. There was a similar trend in the lateral offset data, but the differences were not statistically significant. The addition of turbulence did not cause any significant difference in performance.

TABLE 3.—*Qualitative Dejtnition* of *Touchdown Performance* *

Touchdown performance	Lateral displacement from centerline L, m	Distance down the runway D, m	Sink rate S, m/sec
Excellent	$\|L\| < 3.0$	$365 < D < 547$	$S < 0.9$
Successful	$3.0 < \|L\| < 12.1$	$182 < D < 365$ or $547 < D < 730$	$0.9 < S < 1.5$
Marginal	$12.1 < \|L\| < 21.9$	$0 < D < 182$ or $730 < D < 1034$	$1.5 < S < 2.4$
Unsuccessful	$21.9 < \|L\|$	$D < 0$ or $3400 < D$	$2.4 < S$

* The rating for each flight was the worst of any of three variable, L, D, or S.

TABLE 4.—*Chi-Square Analysis* of *304-m Approach Window Data*

Controlled variable	Degrees of freedom	Chi square	Level of significance
Display I vs II vs III	4	7.79	$p < 0.10$ (not sig.)
Calm vs turbulent air	2	21.28	$p < 0.01$ (very sig.)
Good vs poor picture quality	2	4.20	$p < 0.20$ (not sig.)

TABLE 5.—*Chi-Square Analysis of Touchdown Data*

Controlled variable	Degrees of freedom	Chi square	Level of significance
Display I vs. II vs. III	4	31.05	$p < 0.01$ (very sig.)
Calm vs. turbulent	2	3.57	Not sig.
Good vs. poor picture quality	2	12.46	$p < 0.01$ (very sig.)

TABLE 6.—*Altitude Error and Lateral Offset Statistics at 1520 and 304 m From the Threshold for All Flights in Calm and Turbulent Air; 48 Flights Per Statistic*

		1520-m range			304-m range		
		Altitude error		Offset	Altitude error		Offset
Display	Disturbance	Mean, m	Sigma, m	rms, m	Mean, m	Sigma, m	rms, m
I	Calm	−1.1	7.7	17.5	−0.6	2.3	**4.5**
	Turbulent	2.9	7.8	15.7	−2.1	3.4	4.8
II	Calm	***−0.5***	6.3	15.6	**−0.5**	2.1	***5.8***
	Turbulent	−0.8	7.1	14.3	−0.4	3.7	6.0
III	Calm	−1.9	***5.5***	11.6	−0.6	1.8	3.6
	Turbulent	−2.1	4.8	10.1	−1.1	3.2	**4.5**

Approach performance: 304-m range.—The chi-square test for display effects summarized in table 4 indicates that there were no significant differences among the approach window performance data for the three displays. The results suggest that the use of display I in turbulent air might result in poorer performance (fig. 7); however, as indicated above, this was not statistically significant. A Cochran's test of the altitude and lateral offset data in table 6 also showed that there were no significant differences among the displays. It appears that although the addition of the VASI beacons and the velocity vector symbol improved altitude performance at the 1520-m window, there was no similar improvement at the 304-m window. The pilot ratings (fig. 8) agreed with the 304-m window data in that the pilots felt there were no real differences among the displays of the current study in their utility for making the approach.

Figure 9, which compares data of the current study with the data of the prior study (fig. 2, display A), shows that there was a dramatic improvement in altitude performance due to the addition of the glide slope reference indicator. Though display I differed from display A in other ways, such as including a heading reference and

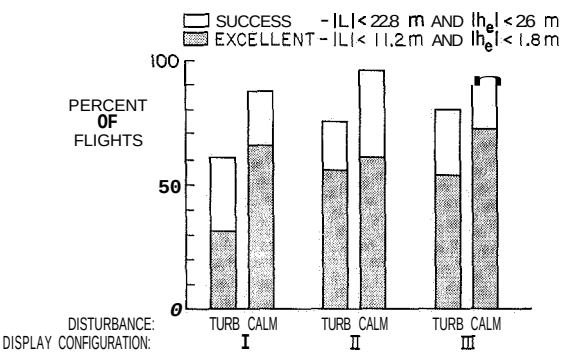

FIGURE 7.—Approach window performance—48 flights per condition.

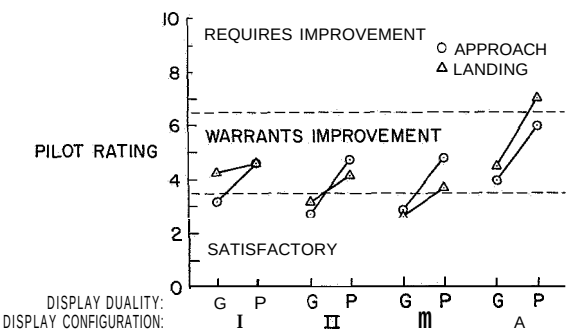

FIGURE 8.—Average Cooper-Harper ratings for each display and picture quality.

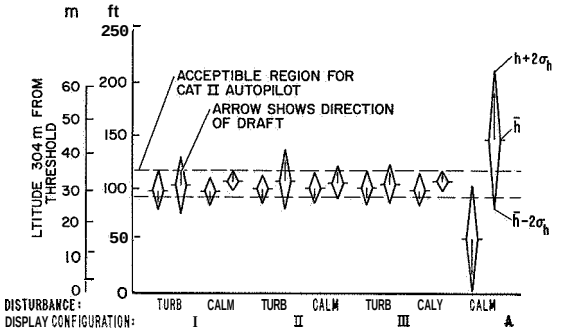

FIGURE 9.—Average altitude performance at the 304m approach window for both the current and prior study. Only flights with a ±0.9 m/sec vertical draft are shown. Flights in the prior study were made in calm air only.

digital instrument data, the addition of the glide slope reference is considered to be the principal factor that would account for the large improvement in reducing glide slope error.

With respect to the requirement to penetrate a category II approach window (less than **f3.7** m **(12** ft) height error and ±22.9 m **(75** ft) lateral offset error (ref. 8)) **95** percent of the time, with the various wind conditions of this experiment, the displays provided inadequate glide slope information but adequate lateral offset information. The data in table **6** indicate that in calm air the displays allowed barely acceptable altitude control since the 2σ value of altitude dispersion is about **3.7** m **(12** ft). With turbulence the variability was nearly twice this value. One reason for this inadequate longitudinal performance is believed to be the low display gain on glide slope deviation inherent in an imaging pictorial display. The display gain is fixed by perspective geometry and the image magnification. On these displays the magnification ratio of 0.5 caused a 0.3° error in glide slope to produce only a 0.15° deviation as measured at the pilot's eye. A standard ILS indicator has a display gain roughly four times this great. A second related reason for poor glide slope performance is that at an altitude of **30** m **(100** ft) the pilot was naturally attending to the runway and was not very concerned about what appeared to be small deviations from the specified glide slope. The only way to provide a higher glide slope gain on a pictorial display is to provide artificial symbols such as highways in the sky (ref. **9).** This type of symbology was not considered in the study because it depends on an external guidance source like the ILS.

The largest rms lateral deviation of **6.0** m **(19.6** ft) was more than adequate to meet the category II criterion of a **22.9** m **(75** ft) absolute limit from the centerline. None of the flights was as far as **22.9** m from the runway centerline at the 304-m **(1000** ft) window.

As indicated in table **4,** the effect of turbulence on performance was very significant. In figure **7,** note the degradation in window performance for each display when the simulated **(0.9** m/sec rms) turbulence was present. Table **6** presents the standard deviations for all flights (including all conditions of up- and downdrafts and crosswinds) in calm and turbulent air; the principal effect of turbulence was to almost double the variability in altitude, while little turbulence effect on the variability in lateral position is noted.

Touchdown performance.—The progression of improved touchdown performance from display **I** through display III is evident in figure **10.** Both display II and III provided better control over distance to touchdown (table **7** and fig. **11).** The maximum 2σ dispersion of **231.0** m **(760** ft) was about one-half the FAA-specified 2σ limit of **456** m **(1500** ft) for an autoland system (ref. **9).** This demonstrates that the inclusion of a flare command scheme offers improvement in touchdown distance over the presentation of altitude alone.

Improved lateral performance was obtained with display III, which had the advantage of

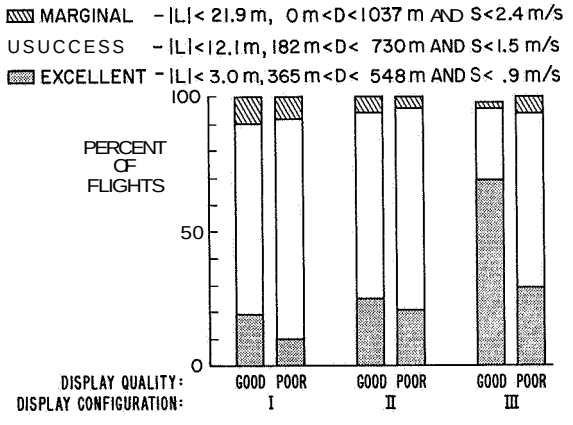

FIGURE 10.—Touchdown performance, all flights (48 landings per condition): L—lateral displacement from centerline of runway; D—distance down runway; S—sink rate.

TABLE 7.—*Touchdown Statistics* for *All Displays and* ***For Good*** *and* ***Poor*** *Display Quality; 48 Landings* ***Per*** *Statistic*

Display	Display quality	Distance, *D*		Sink rate, *S*		Offset, *L*
		Mean, m	Sigma, m	Mean, m/sec	Sigma, m/sec	rms, m
I	Good	461.7	134.4	0.85	0.42	4.1
	Poor	428.8	143.8	.91	.33	4.9
II	Good	437.6	90.2	.79	.33	5.1
	Poor	415.4	106.6	.82	.33	5.5
III	Good[1]	416.0	76.5	.70	.36	2.0
	Poor	429.7	115.8	.79	.42	4.02
A	Average of all conditions	417.3	157.8	1.21	.41	3.2

[1] Data for this condition exclude the one unsuccessful touchdown (D = 382.8, S = 3.62, and L = −0.9).
[2] Large value due to one touchdown at 18.5 m left of center.

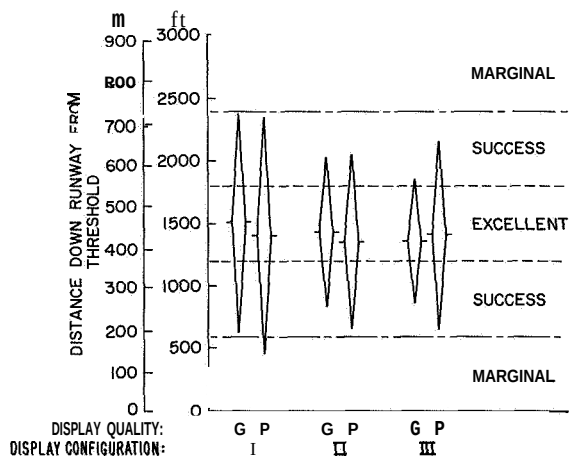

FIGURE 11.—Average distance down the runway at touohdown.

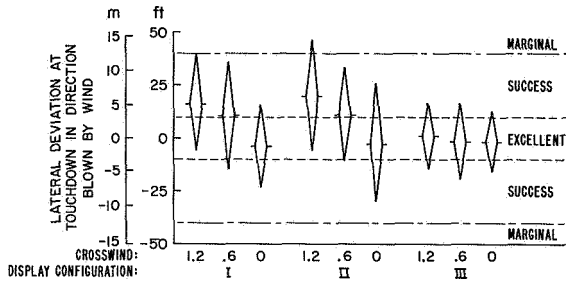

FIGURE 12.—Average lateral dispersions at touchdown for different crosswinds and displays: N = 24 for non-zero crosswinds; N = 48 for zero crosswind.

indicating the true direction that the aircraft was tracking near the runway (table 7 and fig. 12); in fact, performance with display III was relatively impervious to crosswinds during the landing (fig. 12).

Table 7 indicates that there were no essential differencesamong the performance measures with the displays relative to sink rate at touchdown. Thus, contrary to expectations, neither display II nor display III, both of which included information on sink rate, showed any improvement over display I, which only showed altitude above the runway. In the prior study (ref. 6), one conclusion was that the unaided pictorial of the runway provided inadequate information to control sink rate near touchdown. The mean touchdown sink rate for that study was 1.2 m/sec (4.0 ft/sec) with a standard deviation of 0.43 m/sec (1.4 ft/sec); thus, the displays of the current study indicated a sizable overall improvement of about 0.39 m/sec (1.3 ft/sec) less sink rate at touchdown.

The finding that there was no apparent effect due to turbulence was unexpected; even when the turbulence was reduced to zero between 30 and 21 m, the turbulence caused a significant increase in altitude dispersion at the 304-m window, which could have affected touchdown performance. However, there was very little correlation between altitude at the window and touchdown performance (product-moment correlations were less than 0.25).

Display Quality Effects

Approach ***performance.—The*** results of varying the runway image quality were similar to prior results (ref. 6) in that there was no sig-

nificant difference in performance due to image quality at either 1520 or 304 m, even though the pilots preferred the better display. The better quality display was rated two units lower on the Cooper-Harper rating scale (fig. 8). The responses to questions 2 and 3(c) during the debriefing (appendix B) further substantiated the pilot's preference for the better runway image quality. Most of the pilots complained that with the poor display quality they had trouble seeing the runway image as that of a real runway, and two pilots responded that poor display quality was the most disturbing aspect of the display configuration they preferred over the other two.

Touchdown performance.—The effect of display quality on overall touchdown performance is shown in figure 10. Although performance with displays I and II was slightly better with the better picture quality, performance with display III was more significantly affected by display quality. When performance data for displays I and II were subjected to the chi-square test, there was no significant effect from display quality ($\chi^2 = 1.74$, $df = 2$); display III data tested alone still revealed highly significant effect of picture quality ($\chi^2 = 15.05$, $df = 1$). In the case of display 111, there were so few failures and marginals that they were added to the successes, yielding a fourfold table for the chi-square test and one degree of freedom.

Table 7 indicates that the effects of poor display quality with display III were apparent in greater dispersion in lateral and distance down the runway but not in sink rate (fig. 11).

The height bar, the velocity vector symbol, and the horizon were not affected by picture quality; thus, there is no apparent reason for the influence of poor display quality on the distance-down-the-runway measure when the pilots were using display 111. It was presumed that these three symbols were used to establish the flare and sink rate just prior to touchdown.

The poorer performance in lateral dispersion due to picture quality with display III can be associated with the fact that to make a touchdown near the centerline, the pilot was required to first be over the centerline and then to set and hold the velocity vector symbol on the center of the far end of the runway. With poor resolution and a time delay in updating the runway pictorial, it is possible that the pilots had difficulty in holding the velocity vector centered on the end of the runway and thus were distracted from the flare maneuver, resulting in more variability in lateral and distance performance.

The pilot ratings for display quality (fig. 8) showed little preference for the better picture quality with display I and a one-unit preference for the better display quality with displays II and 111.

Performance Monitoring

Of the total of 286 flights in which the pilots made judgments as to whether they were inside or outside of the specified category II approach window at an altitude of 30 m (±3.7 m in altitude or ±0.3° in glide slope and ±22.9 m laterally), 42 (15 percent) of the judgments were incorrect. These judgment errors were biased such that the pilots estimated their performance to be better than was actually the case. Of the 38 flights that failed to make the specified performance window (all failures were in altitude), 19 (50 percent) were judged by the pilots to be inside the window; of the 248 flights that were inside the window, 23 (9 percent) were judged to be outside. The lack of precision in making these judgments is indicated in figure 13; as extreme examples, a flight as deviant as 1.4° from the glide slope nominal was judged to be within 0.3° and one flight within 0.1° of the glide slope nominal was judged to be outside. It ap-

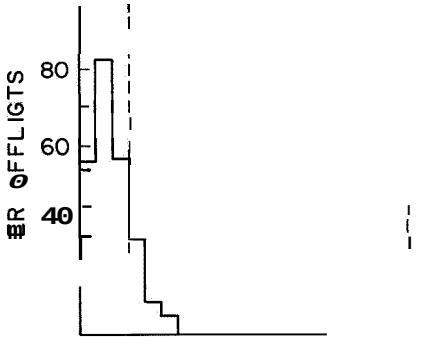

FIGURE 13.—Pilot judgment data averaged over all display conditions, display qualities, and disturbances; N = 286.

pears that the requirement for a pilot to make accurate judgments of glide slope error, at least while also manually flying the aircraft, is beyond his capability with the displays of this study. In another study conducted at Ames (ref. 1), it was shown that pilot judgments of lateral offsets with a pictorial display designed for pilot monitoring were considerably more accurate than those made with a conventional flight director and associated instrumentation.

The judgment data were examined to determine if the different displays, the turbulence, or the display quality had any effect. The results were negative. Pilot judgments were equally good (or bad), regardless of the display, turbulence condition, or display quality.

Pilot Interviews

A summary of the pilots' responses on each question of the interview is given in appendix B. In general, for the good runway image quality, none of the six pilots had any trouble seeing the picture of the runway as a real runway. However, four pilots said that they had some difficulty with the poor runway image quality, which was the most disturbing feature of the display. During the approach the pilots preferred the displays with the VASI lights. Three pilots also felt that the velocity vector was helpful during the approach. During the flare and touchdown, the pilots preferred displays II and III with integrated vertical velocity information. With regard to the category II judgment task, the pilots generally felt that their responses were accurate.

CONCLUDING REMARKS

A study has been conducted in which airline pilots flew manual approaches and landings using simulated ILS-independent, imaging pictorial landing displays. Approach and touchdown performance was evaluated as a function of display configuration, turbulence, and display quality. In addition, pilots' judgments of their success in penetrating a category II approach window during manual approaches were obtained. In general, the results indicated that the displays with added guidance symbology allowed control considerably more precise than that obtained with an unaugmented pictorial display studied in a prior study, and the pilots' acceptance of these displays was good. Moderate degradation in image resolution and update rate did not affect performance but was disliked by the pilots. Simulated turbulence doubled the variability in altitude at **304** m from the threshold but had little effecton lateral or altitude performance at **1520** m from the threshold.

During the approach, lateral control with these displays was good, and the pilots made no lateral judgment errors at the 30-m (100 ft) decision height. Although altitude control performance with the addition of the glide slope reference bars, VASI, and velocity vector symbols was improved dramatically relative to results with an unaugmented display from a prior study, consistent **(95** percent probability) penetration of a category II approach window in turbulence was not accomplished. Furthermore, **15** percent of the pilot's judgments as to whether they were within a category II approach tolerance were in error, indicating that the displays did not provide adequate information for the pilot to judge glide slope deviations during manual approaches.

Touchdown performance also showed an improvement over results of a prior study in which no guidance symbology was added to aid the pilot in making the flare. Touchdown distance dispersion and mean sink rate were both reduced, but the lateral offset dispersion was only marginal.

SYMBOLS AND ABBREVIATIONS

Ae	altitude error from 3° glide slope, m
D	distance down runway from threshold, m
g	acceleration due to gravity, m/sec²
GSR	glide slope reference
HR	horizontal resolution, deg
ILM	independent landing monitor
ILS	instrument landing system
L	lateral displacement from runway centerline, m
LDR	lateral deviation reference
MDH	minimum decision height
p	roll rate, rad/sec
q	pitch rate, rad/sec
r	yaw rate, rad/sec
s	Laplace operator, rad/sec

S sink rate, m/sec
u perturbed forward velocity, m/sec
U_0 steady-state forward velocity, m/sec
UI update interval, sec
VASI visual approach slope indicator
VR vertical resolution, deg
w perturbed downward velocity, m/sec
w_g vertical wind gust, m/sec
X forward ground velocity, m/sec
Y side ground velocity, m/sec
$\dot{Z}$ vertical velocity, m/sec
p_0 lateral wind gust, rad/sec
δ_a aileron control surface deflection, rad
δ_e elevator control surface deflection, rad
θ pitch angle, rad
ϕ roll angle, rad
ψ yaw angle, rad

REFERENCES

1. GARTNER, W.; AND BALDWIN, J.: Improved Display Support for Flight Management During Low Visibility Approach and Landing. NASA CR 73495, Nov. 1970.
2. GARTNER, W. B.: A Simulator Study of Flight Management Task Performance During Low Visibility Approach and Landing Using Baseline Category II Flight Instrumentation. NASA CR 73478, Dec. 1969.
3. MONROE, R. D.; VREULS, D.; AND SEMPLE, C. A.: Summary of All Weather Landing Simulation Studies. SRDS Rept. RD 68–13, FAA, 1968.
4. DECELLES, J. L.: The Fail-safe Landing. A Report of the ALPA All-Weather Flying Committee. Paper presented at ALPA's 17th Air Safety Forum, July 1970.
5. YOUNG, D.; AND SUZANSKY, J.: Research Study of an Aircraft-Contained Radar Zero-zero Landing System. Vol. 1. NASA CR 73184, 1967.
6. WEMPE, T.; AND PALMER, E.: Pilot Performance With a Simulated Pictorial Landing Display Including Different Conditions of Resolution and Update Rate. Proc. 6th Annual Conference on Manual Control, Wright Patterson Air Force Base, 1970.
7. COOPER, G.; AND HARPER, R., JR.: The Use of Pilot Rating in the Evaluation of Aircraft Handling Qualities. NASA TN D–5153, 1969.
8. ANON.: Criteria for Approval of Category II Landing Weather Minima. FAA Advisory Circular 120–20, effective June 6, 1966.
9. WILCKENS, V.; AND SCHATENMANN, W.: Test Results With New Analogy Displays for All Weather Landing. AGARD Conf. Paper 55 (Amsterdam), 1968.

APPENDIX A

Aircraft Simulation

The following linear differential equations were programmed on a digital computer to simulate the dynamics of a Navion single-engine, four-place light aircraft.

AIRFRAME DYNAMICS

$$\begin{bmatrix} \dot{u} \\ \dot{w} \\ \dot{q} \end{bmatrix} = \begin{bmatrix} Z_u & X_w & -U_0 s \\ O & M_w & M_q \end{bmatrix} \cdot \begin{bmatrix} u \\ w \\ q \end{bmatrix} + \begin{bmatrix} O \\ Z_{\delta_e} \\ M_{\delta_e} \end{bmatrix} \delta_e - \begin{bmatrix} O \\ Z_w \\ M_w \end{bmatrix} w_g$$

$$\dot{p} = L_p \cdot p + L_{\delta_\alpha} \cdot \delta_\alpha - L_\beta \cdot \beta_g$$

The following values of the stability derivatives were obtained from reference **11.**

$Z_{\delta_e} = -8.45\ \text{msec}^{-2}$	$M_w = -0.166\ \text{msec}^{-1}$
$M_{\delta_e} = -11.1892\ \text{sec}^{-2}$	$M_q = -2.0767\ \text{sec}^{-1}$
$X_w = 0.03607\ \text{sec}^{-1}$	$U_0 = 53.0\ \text{sec}^{-1}$
$X_u = -0.0451\ \text{sec}^{-1}$	$L_p = -8.402\ \text{sec}^{-1}$
$Z_w = -2.0244\ \text{sec}^{-1}$	$L_{\delta_\alpha} = 23.984\ \text{sec}^{-2}$
$Z_u = -0.3697\ \text{sec}^{-1}$	$L_\beta = 16.0\ \text{sec}^{-1}$

The following approximation for yaw rate r resulted in coordinated turns for small bank angles.

$$r = p \cdot g / (U_0 \cdot s)$$

Control forces.—An MSI Model **438** 2-axis side-arm force controller with a flexible fiber control stick was used. The fiber stick had a **28** N/cm restoring force. The stick gains were:

Longitudinal:	**113.0** N/rad of δ_e
Lateral:	**69.2** N/rad of ϕ

Turbulence.—w_g and β_g were both first-order filtered white noise with a break frequency of ***0.5*** rad; rms turbulence levels for w_g and β_g were **0.9** m/sec and **0.017** rad/sec. The turbulence was faded out below an altitude of **30** m.

COORDINATE TRANSFORRIATIONS

Approximate Euler transformations.—

$$\dot{\theta} = q \cdot \cos(\phi) - r \cdot \sin(\phi)$$

$$\dot{\psi} = q \cdot \sin(\phi) + r \cdot \cos(\phi)$$

$$\dot{\phi} = p$$

Ground coordinate approximations.—

$$\dot{X} = U_0 \cdot \cos(\theta) \cdot \cos(\$)$$

$$\dot{Y} = U_0 \cdot \sin(\$) + \text{crosswind velocity}$$

$$\dot{Z} = U_0 \cdot \sin(\theta) + (w + 0.05236 \cdot U_0) \cdot \cos(\$) + \text{draft velocity}$$

APPENDIX B

Pilot Concluding Interviews

At the end of the last session, each pilot was asked a number of questions and the responses were recorded. The following paragraphs summarize these interviews.

Question 1. How did the workload of the approach and landing task with the displays compare with that with an instrumented ILS system?

Two pilots said a flight director command display was easier down to 30 m altitude; one said the pictorial display required more attention; and the other three said the display was as easy or easier than an ILS.

Question 2. Did you have difficulty in seeing the picture of the runway as being a real runway?

Four of the pilots said they had some trouble with the poor image quality, but none had any difficulty with the good image quality picture. One pilot said it looked surprisingly good—like Pittsburgh in bad weather.

Question 3(a). Which display did you like best? Did you develop any special strategy for this display?

One pilot preferred display I, one preferred display II, and four preferred display III. None of the pilots said that he developed any special strategy.

Question 3(b). How would you like this display improved?

One pilot wanted the digital instruments moved in closer to the center. One wanted a dial instrument for sink rate. One wanted the lead-in beacons placed farther out from the runway, and the pilot who preferred display I wanted the VASI lights added to it.

Question 3(c). What was the most disturbing aspect of this display?

Two pilots complained about the poor runway image quality. One felt that the airplane symbol got in the way when he was high and had to pitch down. One of the pilots who preferred display III was confused by the velocity vector on the approach and only used it during the flare.

Question 4(a). Which display did you like next best? Any special strategy?

One pilot preferred display I, three preferred display II, and two preferred display III. The pilots did not mention any special strategy other than what they were instructed to do.

Question 4(b). How improved?

One pilot had trouble flaring with display II and felt it needed better sink rate information near the ground. A pilot who preferred display II wanted to add the velocity vector of display III, and a pilot who preferred display III wanted to add the touchdown symbol of display II.

Question 4(c). Most disturbing aspect?

The poor image quality was mentioned by one pilot. Another complained that the velocity vector symbol did not stand out enough from the runway beacons.

Question 5. Discuss the CAT II window judgment task.

The pilots generally felt that their judgments were quite accurate. Two pilots stated that they sometimes said that they were in the window if they felt they could make a good landing or if they were almost in and were correcting in the right direction.

Question 6. Would you use one of these displays if installed in your aircraft? How?

All pilots said that they would use the display. Four pilots said that they would use it to monitor an autocoupled approach and to crosscheck other instruments. One pilot felt that if it was developed enough he could use it right down to touchdown.

Question **7.** Were your instructions clear?

All pilots answered ('yes."

Question 8. Did you have enough practice to do a reasonably good job?

All pilots answered "yes," although one pilot did not think he had a feel for the display after only one day.

Question 9. Do you think that your performance would improve much with more practice?

Five pilots answered in the affirmative, the other felt that his performance would not improve much.

Question 10. Have you had any recent light plane experience?

Only one pilot had flown a light plane recently.

Question 11. What did you think of the two-control Navion?

The pilots felt that the simulation was adequate, though two complained about the control being too sensitive.

Question 12. What are your usual errors in making an ILS approach as a percent of full scale?

Five pilots stated they kept the glide slope indication within **25** percent of full scale. One pilot kept it less than **50** percent of full scale. All of the pilots stated that they were able to maintain the localizer needle within **25** percent of full scale.

N73-10123

19. Effects of Display Format on Pilot Describing Function and Remnant*

HENRY R. JEX, R. WADE ALLEN, AND R. E. MAGDALENO

Systems Technology, Inc.

As part of a program to develop a comprehensive theory of manual control displays, six display formats were used by three instrument-rated pilots to regulate against random disturbances with a controlled element of $Y_c = K/s(s \$2)$ (which requires mild lead equalization), under both foveal and 10° parafoveal viewing conditions. The six display formats were: CRT line, CRT thermometer bar, 14-bar quantized on a CRT, a rotary dial and pointer (meter movement), and two variations of a moving scale tape-drive (C-141 VSI). All were scaled to equivalent movement and apparent brightness. Measures included overall performance, describing functions, error remnant power spectra, "critical instability" scores, and subjective display ratings. Other controlled elements and parafoveal angles were partially investigated.

The results show that the main effect of display format is on the loop closure properties. Less desirable displays induce lower bandwidth closures with consequent effects on the closed-loop remnant and performance. The normalized injected error remnant remains roughtly similar for all cases except quantized formats. The quantized display induces larger pilot lags and observation remnant. The moving tape display (off-reference case) could not be tracked parafoveally. Parafoveal viewing affected each display differently. The second-order critical instability task seems to provide a sensitive and convenient test for overall display format problems. Simple analytical models are presented which show good agreement with the preliminary-test data, and a tentative set of rules for estimating format effects of the display/pilot/vehicle system are given.

INTRODUCTION †

The complete program covered the three areas shown under '(Scope" of table **1** which have been reported in full in STI Technical Report **191–1** (dated June **1971)** which will soon be released as an AMRL report (see ref. **1).** Only the experiments are covered in this presentation.

Experimental Design for Display Format Experiment

The main features of this experiment are (see figs. **1** and 2)

- Standard single-axis setup in the STI fighter cockpit fixed-base simulator.
- Controlled elements were: $K/s(s+2)$ for the instrument format experiment, and K/s and K/s^2 for some preliminary experiments.
- Input: sum of five sinusoids.
- Measurements included: error performance σ_e^2, remnant error component $\sigma_{e_n}^2$; open- and closed-loop describing functions of pilot-controlled element-display; input-correlated and remnant error spectra at input frequencies (via serial segment technique, described in another Annual-Manual paper); subjective display rankings on a **1** to **5** scale from "best" to "worst;" and three sets of critical instability scores, including one set having the same lead equalization requirement as the tracking task.
- Viewing angles of 0" (foveal), **10°, 20°** (parafoveal).
- Two to three instrument-rated pilots were

* This research was sponsored by the Aerospace Medical Research Labs., Aerospace Medical Div., AF Systems Command, Wright-Patterson AFB, under contract F33615-69-C-1808 with Systems Technology, Inc. (STI).

† This is a summary of the points made on each slide of the informal presentation. These slides are now the tables and figures **of** this paper.

TABLE 1.—Display *Format Effects*

OBJECTIVE:
Effects of instrument display format on pilot's closed-loop behavior and performance
SPONSOR:
USAF AMRL/MRHD
SCOPE:
Reanalysis of extant remnant data for "ideal displays" in terms of recent "processing noise" concepts
Experiments with several display formats
Revised models and adaptation rules
REPORT:
STI–TR–191–1 (forthcoming USAF AMRL Rept. (ref. 1))

subjects; well trained on the task before measurement.

- At least two replications per cell were made.

The six instrument formats tested are shown on figure 2. The CRT line display served as a reference condition for the others. The coarsely "quantized" format had about **2** to **3** bars per 1a of error. The moving scale tape format was the fine-altitude scale of a standard C–141 VSI altimeter. The "on-reference" case was at the well marked white null, while the "off-reference" case required visual interpolation of the 270 ft position. All displays were scaled to the same linear sensitivity (for the dial at the pointer end) of 0.75 cm for 1a of input.

Typical Data for Error Spectra

The top half of figure **3** shows the closed-loop circulating error spectrum, Φ_{ee}, computed at input frequencies. The key points are

- The input-correlated component, Φ_{ee_i} is well above the remnant at all input frequencies, assuring accurate pilot describing functions.
- The remnant component, Φ_{ee_n} is usually well above the basic system noise level of −40 dB, except at the highest frequency.
- The mean square error is dominated by the closed-loop error peak near *2* to **3** rad/sec, and is thus sensitive to loop closure changes induced by the various formats.
- The data for successive replications is quite consistent for a given operator, but differs somewhat among subjects.

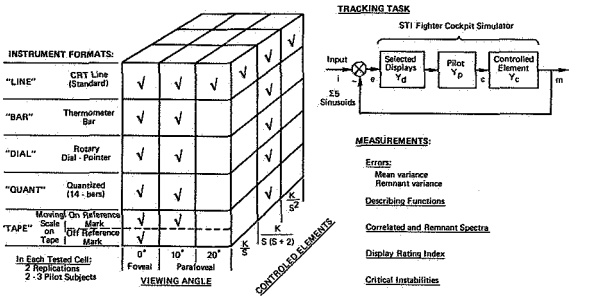

FIGURE 1.—Experimental design for display format exeriments.

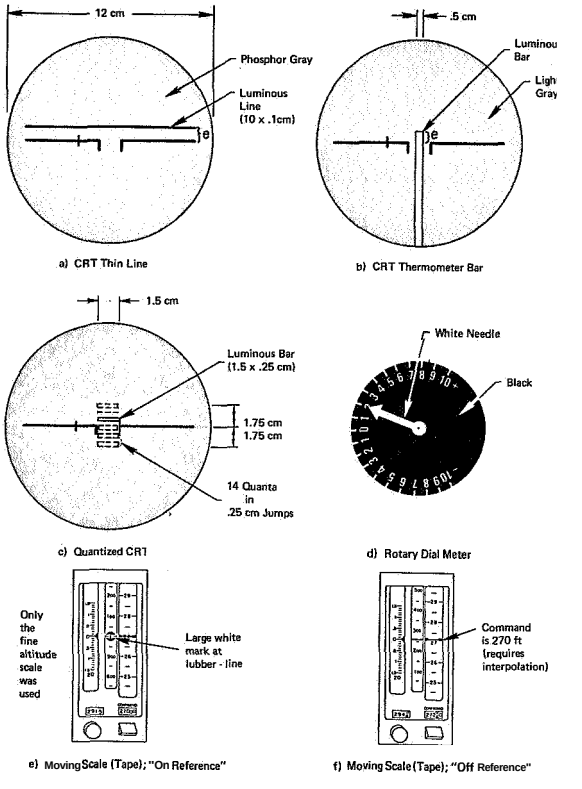

FIGURE 2.—Display formats investigated.

The normalized injected noise or processing remnant gradient $(\Phi'_{n_e} = \Phi_{nn_e}/\sigma_e^2)$ is shown in the bottom half of figure **3.** The main points are

- The shape of Φ'_{nn_e} is typically not that of noise through a first-order filter.
- The level is typical of much prior and concurrent research at other laboratories.

(Display format effects on Φ'_{nu_e} will be shown later.)

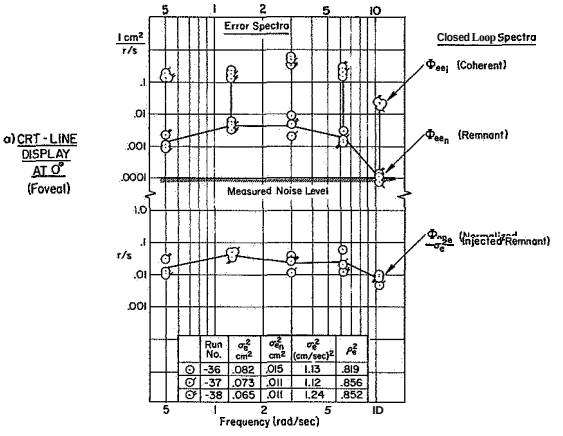

FIGURE 3.—Typical data for error spectra.

Error Performance Summary

The top of figure 4 shows total mean-square-error; the bottom shows the remnant component to an expanded scale. The bars show average. (Further data are in the Final Report (ref. 1).) The main points are

- Foveally, the line, bar, and dials (and tape: on-reference) were about equal in performance.
- Parafoveally, all formats suffered, but the line and dial held up best (dial's angular cue helped). Worst were quantized and tape: off-reference (latter could not be tracked at all).
- Remnant contributions due to format (foveal viewing) were small except for quantized display, where increase is on order of 1 quanta squared.
- Most of total error increases were due to the looser or lower stability closures induced by non-ideal formats (e.g., see quantized case).

Describing Function Parameter Summary

Detailed describing functions of figure 5 (shown also in Final Report (ref. 1)) showed that all subjects generated sufficient lead to roughly cancel the controlled element lag at $(s+2)$, and the open-loop data were reasonably well fit by the extended crossover model:

$$Y_{OL} = Y_D Y_p Y_c \doteq \frac{\omega_c}{(j\omega)} e^{-j\left(\tau_e \omega + \frac{\alpha}{\omega}\right)}.$$

An interpolation routine, part of the post-run data reduction, gave estimates of the parameters for the two frequencies nearest crossover, denoted by subscript c. The left side of figure 5 shows that format induced consistent effects in both subjects, in their delays and lead decrements (decrease in a, below the 0.3 to 0.4 value for the line case is associated with a similar decrease in the lead break frequency, which is well below the crossover region). Nonideal formats induce higher loop delays, and reduced displacement gains (hence lower lead break $(1/T_L \doteq K_D/K_R)$, evidenced here by lower a, and lower ω_c). Similar effects noted parafoveally, again Line and Dial held up best. One pilot used much more aggressive (and less typical) loop closure strategy parafoveally, evidenced by his higher gain and lower phase margin.

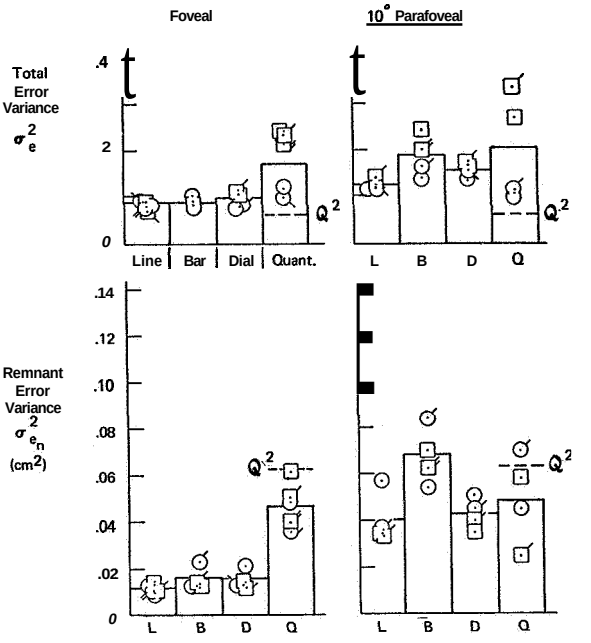

FIGURE 4.—Error performance summary.

Φ'_{nn_e} Comparisons Across Displays and View Angles

In figure 6 the lines are averages of Φ'_{nn_e} (see fig. 3) across subjects for each condition. The left side shows the the observation or noise, when normalized by the perceived signal variance, is remarkably insensitive to quite different formats.

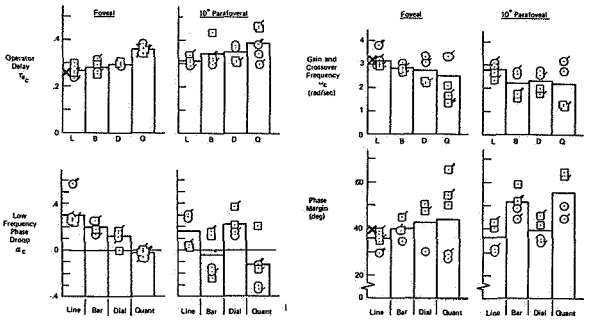

FIGURE 5.—Describing function parameter summary.

The right side shows that all data cover only a range of about 2:1 across the spectrum. This implies that a "processing noise" remnant source is dominant here.

Few of the shapes are clearly first-order, but a first-order noise model would represent typical effects adequately. The simple "Pew model" (so-named because Professor Pew pointed it out in the 1968 Annual Manual) ($\Phi'_{nn_e} = A\omega^B$, with $A \doteq 0.06$ rad/sec and $B \doteq -0.7$ or -7 dB/decade) is about as good a fit as any, albeit not very tractable analytically.

Other Measures

Scores for the "one-and-a-half-order" critical instability task (shown at bottom of table 2), which require the same lead as the tracking case, showed sensitive and significant decrements from the ideal CRT line format. These decreases in λ_c imply an increase in the apparent delay time, and correlate well with the increased crossover model delays, τ_{e_c}.

The critical instability task, with stable roots placed to induce the desired lead equalization, proved to be an easily learned, sensitive way to objectively rank an array of display formats. The subjective rankings (of overall suitability of each format for precision control purposes) corresponds to the critical task scores. Although the quantized format showed up poorly in performance and preference for tracking purposes, pilot comments revealed that its blinking action during a rate-of-change of error signal was readily perceivable parafoveally, even though its displacement was not.

TABLE 2.—*Other Measures*

Foveal case		
Display	Critical instability [1]	Display rating [2]
CRT line	3.9	1.0
Dial	**3.4**	2.5
Bar or tape (on ref.)	3.2	2.8
Quantized	2.5	3.7

[1] $Y_c = \frac{\lambda}{-(s+2)(s-\lambda)}$ (req'd $T_L \approx 0.5$ sec)

[2] Average ranking.

TABLE 3.—*Conclusions*

- Display-induced remnant is best modeled as a "processing-noise"

$$\Phi_{nn_e}(\omega) = \underset{\text{(residual)}}{\Phi_{nn_0}(\omega)} + \underset{\text{(gradient)}}{e^2\Phi'_{nn_e}(\omega)}$$

- $\Phi'_{nn_e}(\omega)$ is similar to first-order white noise
  Data also fit Pew Model:

$$\Phi'_{nn_e} \doteq A\omega^B;\ A \approx .06;\ B \approx -.7$$

- Main effects of reasonable display formats are due to second-order decrements in loop closure tightness, and some increase in Φ'_{nn_e} for worst displays.
- Decrements due to format in critical task scores and subjective rankings correspond to describing function changes.

Conclusions

The following conclusions were reached (see table 3 for additional conclusions):

(1) The reanalysis of extant remnant data (not discussed here), as well as these experiments, verify that most display-induced remnant is best modeled as an injected '(processingnoise" :

$$\Phi_{nn_e}(\omega) = \underset{\text{(residual)}}{\Phi_{nn_0}(\omega)} + e^2 \cdot \underset{\text{(gradient)}}{\Phi'_{nn_e}(\omega)}.$$

The gradient component is dominant for most cases of interest.

(2) The spectral shape and closed-loop effects of the processing remnant gradient can be modeled by white noise through a first-order filter, but out data are not closely first-order in shape. The simple Pew model with a slope of -7 dB/decade is about as good a data fit.

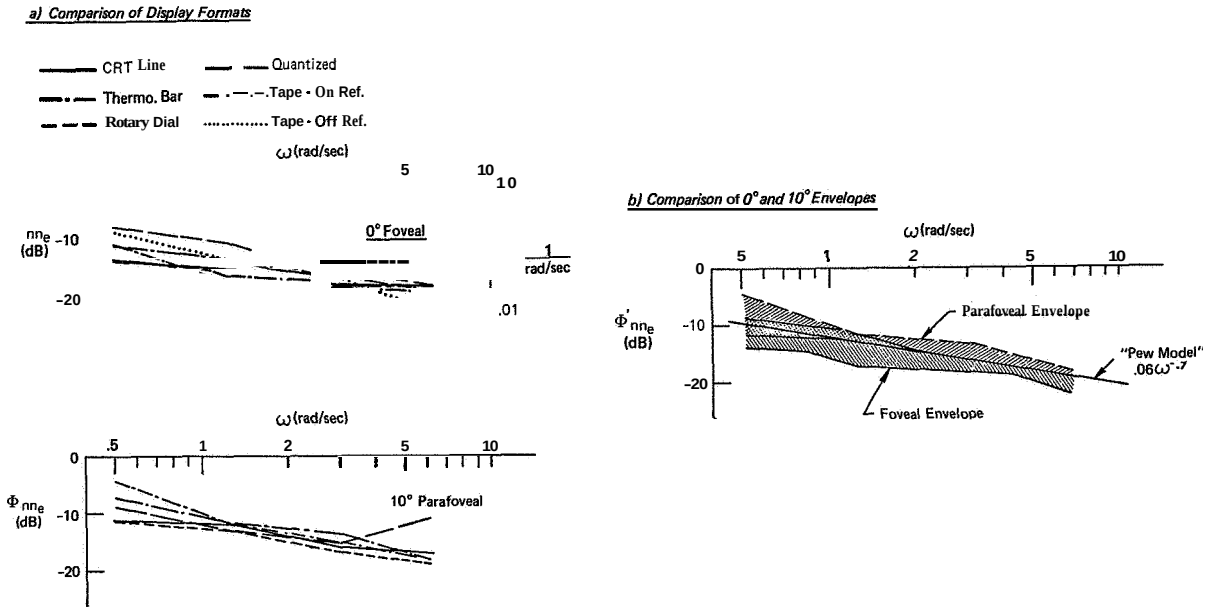

FIGURE 6.—Φ'_{nne} comparisons across displays and view angles.

(3) The main effects of nonideal tracking instrument format under nonscanned single-axis conditions are increased operator (and/or display motion) delays, which causes looser or less damped loop closures and, hence, poorer performance. The remnant gradient is also somewhat worse for nonideal formats or view angles, but represents second-order effects on the errors.

(4) There was a rough rank-order correlation among the subjective rankings, Critical Instability scores, and tracking parameters.

(5) When equally scaled, the CRT line and dial formats are roughly comparable, allowing for the extra lag in the dial instrument drive. The bar and moving tape displays suffered most under parafoveal viewing. Coarsely quantized displays (having only **2** to **3** quanta per desired 1σ of the error) should be avoided where lead generation is required.

(6) Further research on quantized displays is recommended using the efficient techniques developed during this program.

(7) Changes to the extant human operator models and adaptation rules to account for display format effects are discussed in the Final Report (ref. **1).**

REFERENCE

1. JEX, HENRY R.; ALLEN, R. WADE; AND MAGDALENO, RAYMOND E.: Display Format Effects on Precision Tracking Performance, Describing Functions, and Remnant. AMRL TR–71–63 (to be published). Obtainable by request from: Philip Kulwicki, 6570th AMRL/HED, Wright-Patterson AFB, Dayton, Ohio 45433.

20. A Dynamic Response and Eye Scanning Data Base Useful in the Development of Theories and Methods for the Description of Control/Display Relationships*

RICHARD KLEIN

Systems Technology, Inc.

This paper documents a set of specially prepared digital tapes (STI master tape I) which contain synchronized measurements of pilot scanning behavior, control response, and vehicle response obtained during instrument landing system (ILS) approaches made in a fixed-base DC–8 transport simulator at the NASA-Ames Research Center. The objective of the master tape is to provide a common data base which can be used by the research community to test theories, models, and methods for describing and analyzing control/display relations and interactions.

The experimental conditions and tasks used to obtain the data and the detailed format of the tapes are described. Conventional instrument panel and controls were used, with simulated vertical gust and glide slope beam bend forcing functions. Continuous pilot eye fixations and scan traffic on the panel were measured. Both flight director (zero reader) and standard localizer/glide slope (manual) types of approaches were made, with both fixed and variable instrument range sensitivities.

INTRODUCTION

The experimental data described in this paper represent the results of one phase of a multiple-year research program to develop and validate a theory of manual control displays. The early phases included

- Evolution of a model for the display/pilot/vehicle system from extant data (refs. 1 and 2)
- Specific experiments aimed at developing and refining multiple instrument scanning models (ref. 3).

Development and validation of this work required simultaneous eye movement and pilot response data in flight control tasks under realistic approach conditions. This experimental phase has been accomplished, and selected data are now in hand for 31 simulated instrument approaches in a subsonic jet transport performed by three airline pilots. Detailed scanning statistics have been computed for these runs (ref. 4), and a concurrent phase is now under way to reduce the pilot response data for 12 of the 31 data runs.

As a by-product of this program it was decided to make the response and scanning data available to other researchers in this area. This would provide a common data base that could be used to test theories, models, and methods for describing and analyzing manual control/display relations and interactions. To this end, this paper will

(1) Summarize the experimental situations, pilot tasks, panel arrangement, forcing functions, etc., relevant to the data.

(2) Review the eye point-of-regard (EPR) manual data interpretation and reduction process.

(3) Describe the recorded variables and physical arrangement of the three specially prepared digital tapes (master tape I).

*This work was performed in part under contract NAS2–5690 for NASA-Ames Research Center.

SUMMARY OF THE EXPERIMENT

The experiment involved pilot control in a conventional category 11-like instrument approach in a six-degree-of-freedom fixed-base simulation of a DC–8 aircraft. The panel layout shown in figure 1 was typical of a subsonic jet transport, with some configurations employing a flight director (FD). The subjects were airline pilots and copilots. The task was to fly an ILS approach from the outer marker (30 000 ft from threshold) to the middle marker in the presence of pitch attitude disturbances, θ_c, and glide slope beam bends, ϵ_{GS_c}. Aircraft motions, displayed signals, pilot response, and pilot eye point-of-regard were FM-analog tape recorded during the experimental runs.

Experimental Configurations

The experimental configurations are described in table 1. Configuration *A* was a pitch attitude tracking task designed to provide single-loop response data on the present subjects for correlation with past data and models. Configurations *B*, *C*, and *D* involve a "raw presentation" of localizer and glide slope deviation, pitch and roll attitude, and peripheral instruments, but no flight director display. These tasks varied in their detail in order to explore effects of scanning and statistical stationarity. Configurations *E* and *F* employed all the displays of *C* and *D*, respectively, plus a lateral and longitudinal flight director display superimposed on the artificial horizon.

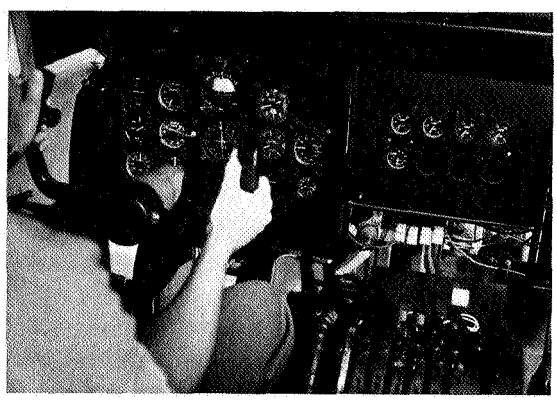

FIGURE 1.—Cockpit instrument layout.

TABLE 1.—*Experimental Configurations*

Configuration	Description
A (Pitch attitude regulation only)	Single-axis tracking task with pitch attitude display and θ_c forcing function. Other instruments masked. Other axes controlled by autopilot.
B (Split-axis manual ILS, fixed-range)	Three-degree-of-freedom longitudinal task. θ_c and ϵ_{GS_c} forcing functions on. Lateral axes under autopilot control, but meters visible.
C (Manual ILS, fixed-range)	All-axis approach task with both forcing functions on. The glide slope deviation computer range was fixed at 30000 ft from threshold.
D (Manual ILS, varying range)	All-axis approach task with forcing functions on. The range varied throughout the run. Glide slope deviation per unit altitude error increases with decreasing range.
E (Flight director, fixed-range)	All-axis approach task with forcing functions on. Flight director on and driven by forcing function. Same as configuration *C* plus flight director.
F (Flight director, varying-range)	All-axis approach task with forcing functions on. Flight director on. Glide slope component of *FD* forcing function attenuated with range by flight director computer. Same as configuration *E*, except range-varying.

The flight director provided pitch and roll commands. The longitudinal director mixed pitch attitude and "altitude" errors. The latter was computed from the angular glide slope deviation by multiplying by the range to the glide slope transmitter. This caused the forcing function amplitude (component due to the glide slope command) to decrease during configuration *F* runs. The lateral director mixed roll angle, heading angle, and (angular) localizer deviation errors. The flight director guidance equations are given in reference 4.

Properties of the other controlled elements are detailed in reference 4. The dynamics of the simulated vehicle were defined by a linearized set of perturbation equations in six degrees of freedom. The simulator was stabilized with full flaps and gear down at 135 kt on the approach path at the outer marker at the start of the run. No changes

in flaps, trim, or power setting were required during the run. The dynamic properties of the flight instruments and elevator, aileron, and rudder controls were also measured and are given in reference **4.** The rudder pedals moved in a normal manner, but were disconnected from the lateral equations of motion to insure single-axis control.

Run Sequence

Each pilot was given several initial familiarization runs of both manual ILS and flight director tasks without input forcing functions. This enabled the pilots to evaluate the aircraft's flying characteristics, become familiar with new instrumentation, and experience the cockpit procedures.

Practice runs followed the familiarization and enabled the pilots to experience the input forcing functions as applied to the three basic configurations *(B, C,* and *E).* Fixed-range tasks were used in practice because they could be of any run length, allowed stationary pilot behavior, and were to comprise the bulk of the final data runs. During the practice runs the EPR system was explained and the equipment fitted to the subject.

All formal record runs (after the familiarization and practice sessions) included two or three "warm-up" runs. The final data runs were made with the EPR system. A data session usually involved five or six 100 sec runs in succession, divided at random between manual ILS and flight director configurations. Fixed-range and varying-range configurations were not mixed in the same session, but were run on separate days.

Rest periods of 15 to 20 min for every five runs (about **30** min of data taking) were required. Normal data taking sessions were **2** to **2-1/2** hr duration, including EPR setup, with only one session per day per pilot.

Signals Recorded

The displayed signals, pilot response, vehicle motions, and eye movements recorded on **14-**channel FM tape included

Vertical coordinate of eye point-of-regard, EPR_V
Horizontal coordinate of eye point-of-regard, EPR_H
Pitch attitude command, θ_c
Glide slope command, ϵ_{GS_c}
Pitch attitude error, θ_e
Glide slope deviation error, ϵ_{GS_e}
Elevator deflection, δ_e
Displayed roll angle, φ_d
Displayed localizer deviation, ϵ_{LOC_d}
Aileron deflection, δ_a
Displayed rate of climb, $\dot{h}_d$
Heading angle, ψ
Voice commentary and identification
40 Hz digitizing tone.

During flight director runs (configurations *E* and *F* the pitch and roll director commands were recorded in lieu of rate of climb and heading angle.

The 40 Hz digitizing tone, signifying the start of the **100** sec run was turned on about 10 sec after the start of the run. After approximately **2** min of running, the experimenter would call "run completed," at which time the digitizing tone was turned off and the simulator reset. The digitizing signal enabled a common time base to be maintained regardless of recorder speed variations.

EPR DATA INTERPRETATION

This section describes the data interpretation procedure that was used to obtain a unique set of eye point-of-regard data from the raw vertical and horizontal coordinates of the EPR records. This involved the allocation of *all* elapsed time into discrete intervals, each corresponding to a dwell on a given region of the panel. The six instruments and other regions of the panel were numbered as shown in figure 2. There were no looks to regions 9 and **10,** and looks at region **8** were usually blinks.

Using a high-speed strip chart playback of the horizontal and vertical EPR signals, it was possible to very accurately distinguish between dwells. **A** typical bona fide dwell was usually greater than **0.3** sec. The transition time was defined as the time between looks at two different instruments, and was assumed to be no greater than **0.13** sec. Normally there is a clear-cut switch (of about 0.02 sec duration) in the trace, as shown in figure **3.** For this case the transition is divided evenly between adjacent dwells. If the duration was greater than **0.13** sec

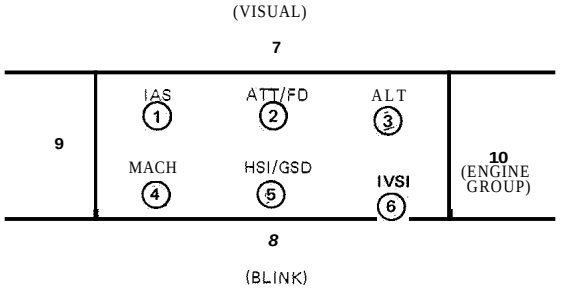

FIGURE 2.—EPR regions on instrument panel.

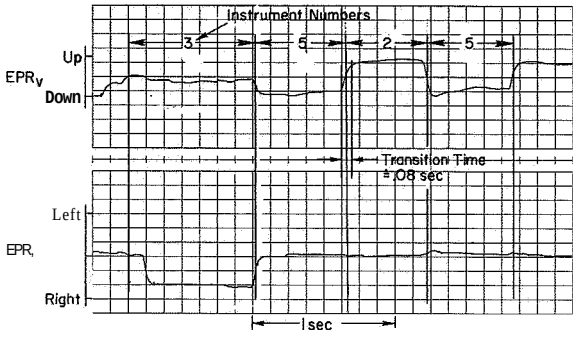

FIGURE 3.—Raw EPR data showing normal transitions.

it was included in the tabulation as a separate entry, rather than allocated to adjacent dwells.

Once the dwells were discretized and assigned to regions, the region number and dwell duration were transferred to punch cards. The region numbers were then digitized and merged with the other recorded variables using a BOMM* program.

To maintain time correlation with the other variables, EPR data reading began at the first complete dwell following the digitizing tone, and proceeded through exactly 100 sec. This resulted in truncation of the last dwell. In reference 4, however, the nearest complete dwell to 100 sec was used. Hence EPR statistics obtained from master tape I will differ slightly from those presented in reference 4.

DESCRIPTION OF MASTER TAPE I

The master tape contains a total of 34 data runs, each exactly 100 sec long. These runs were selected from over 100 total runs because of the quality of the EPR data, motivation of the pilot subjects, and compatibility of the response data with that of actual approaches (based on pilot comments and tracking errors). Thirty-one of the data runs contain EPR data. Three additional runs (with no EPR data) include two single-axis (configuration *A)* for tie-in to other single-axis compensatory tracking data, and one analog pilot run for checkout of data reduction techniques.

* BOMM—A system of programs for the analysis of time series. Written by E. C. Bullard, F. E. Oglebay, W. H. Munk, and G. R. Miller of the Institute of Geophysics and Planetary Physics at the University of California at La Jolla, Apr. 1964.

The 34 data runs are recorded on three 7-track digital tapes which together comprise master tape I. The allocation of runs, in order of their appearance on the tapes, is presented in table 2. The column labeled "recorder key" specifies the set of variables recorded for that run. Table 3 defines this recorder key and gives the units and sign convention of each variable.

Each tape has the following digital characteristics:

Tape tracks = 7
Tape density = 556 bits/in.
BCD format = (1X, 11E, 10.3)
Sampling rate = 20 samples/sec
2000 records per file
11 variables (words) per record
10 characters per word.

One file of data may be read using the following FORTRAN IV statements:

```
      DIMENSION (22000)X
      READ (TAPE UNIT, 1)X
    1 FORMAT (1X, 11E 10.3)
```

Copies of STI master tape I may be obtained from NASA-Ames* or through STI.

REFERENCES

1. McRuer, Duane; Jex, Henry R.; Clement, Warren F.; and Graham, Dunstan: Development of a Systems Analysis Theory of Manual Control Displays. Tech. Rept. 163–1, Systems Technology, Inc., Oct. 1967.

* Man-Machine Integration Branch.

TABLE 2.—*Master Tape Index*

Tape	File no.	Config-pilot	Run no.	Recorder key
I	1	A1	17–14	1
	2	D1	17–16	1
	3	B1	17–18	1
	4	B1	19–5	1
	5	B2	19–17	1
	6	A2	19–20	1
	7	D1	26–05	1
	8	D1	26–09	1
	9	D1	27–03	3
	10	D1	27–06	3
	11	D3	28–05	3
	12	D3	28–08	3
2	1	Analog pilot	17–08	1
	2	C1	17–15	1
	3	C1	19–04	1
	4	C1	19–10	1
	5	C1	19–11	1
	6	C1	19–13	1
	7	c2	19–16	1
	8	c2	19–19	1
	9	c 2	19–21	1
	10	c2	19–23	1
	11	c2	19–25	1
3	1	E l	17–19	2
	2	E l	19–08	2
	3	E l	19–12	2
	4	E2	19–18	2
	5	E2	19–22	2
	6	E2	19–24	2
	7	E l	13–20	2
	8	F1	26–07	2
	9	F1	26–08	2
	10	F1	27–05	3
	11	F3	28–07	3

TABLE 3.—*Recorded Variables*

Position within record	Recorder key*			Name	Sign convention and symbol	Positive value	Units
	1	2	3				
1	TE	TE	TE	Pitch attitudeerror	$+\theta_e$	Meter indicates nose down	rad
2	GE	GE	GE	Glide slope error	$+\epsilon_{GS_e}$	Meter indicates below beam	rad
3	TI	TI	TI	Pitch attitude command	$+\theta_c$	Meter indicates nose down	rad
4	GI	GI	GI	Glide slope command	$+\epsilon_{GS_c}$	Meter indicates below beam	rad
5	DE	DE	DE	Elevator angle	$+\delta_e$	Trailing edge down	rad
6	DA	DA	DA	Aileronangle	$+\delta_a$	Right aileron up	rad
7	PH	PH	PH	Display bankangle	$+\phi_d$	Right wing down	rad
8	LO	LO	LO	Display localizer angle	$-\epsilon_{\mathrm{loc}_d}$	Left of localizer	rad
	HD			Display altitude rate	$+\dot{h}_d$	Climbing	ft/sec
9		FP		Pitch flight director error	$+FD_{pe}$	Bar up	units
			R	Range	$+X$	Before glide slope trans.	ft
	PS		PS	Heading angle	$+\psi$	Right turn	rad
10		FR		Roll flight director	$+FD_r$	Bar counterclockwise	units
11	EPR	EPR	EPR	Eye-point-of-regard		All positive	integers 1to 8

* Abbreviated symbol names for use in digital analysis.

2. McRUER, D. T.; AND JEX, H. R.: A Systems Analysis Theory of Manual Control Displays. Third Annual NASA-University Conference on Manual Control, NASA SP-144, 1967, pp. 9–28.
3. ALLEN, R. W.; CLEMENT, W. F.; AND JEX, H. R.: Research on Display Scanning, Sampling, and Reconstruction Using Separate Main and Secondary Tracking Tasks. NASA CR–1569, July 1970.
4. WEIR, DAVID H.; AND KLEIN, RICHARD H.: The Measurement and Analysis of Pilot Scanning and Control Behavior During Simulated Instrument Approaches. NASA CR–1535, June 1970.

21. Control Information in Visual Flight*

J. M. NAISH

Douglas Aircraft Company

The purpose of the inquiry is to determine how precisely a pilot can estimate the movements of his vehicle, and thus exercise control, during an unaided visual approach. The method is to relate changes in the forward view, due to movements along and across the approach path, to human visual thresholds and errors. The scope is restricted to effects of inclination, expansion, size, and rotation in runway features during approaches at small angles of elevation.

Quantitative relations are given which provide a basis for ranking the several information mechanisms. Alignment by inclination of a ground line is found to be an accurate lateral mechanism, probably superior to the expansion mechanism. Vertical control mechanisms are complex, of questionable accuracy, and difficult to rank. The results throw some doubt on the usefulness of a runway symbol as a source of displayed information.

INTRODUCTION

When an approach is made without the help of flight instruments or ground aids, the pilot depends heavily on observations of the external visual world. If he is able in these circumstances to make good a selected flight path, his control actions must be in some way related to visual information derived from external sources. On the other hand, an erratic approach would indicate the absence of an adequate relation between what is seen and what is done.

Previous investigations of this subject have perhaps given the impression that much information is available for control purposes in visual flight. For example, Gibson (ref. **1)** has stated that the pilot is able to see accurately a continuous visual world in which he moves with precision, and this view has frequently found embodiment in displays which imitate the forward view in flight. But it must first be asked *how* precisely the pilot moves in his visual flight path, if a complete description of the control process is to be given. Unfortunately, the quantitative aspect of visual flight has attracted very little attention.

Another feature of previous work is the variety of visual characteristics considered able, through dependence on the position or speed of an observer, to contribute to the control of visual flight. But not all visual characteristics are equally admissible, because of variability under differing meteorological conditions. Thus, color, contrast, and sharpness of detail can vary markedly with changes in weather, while the form, size, and apparent movement of visible ground objects are hardly affected. The latter characteristics are therefore more likely to provide a quantitative basis for a process which, obviously, may take place under a range of weather conditions.

It is not difficult to establish relationships between the form, size, and apparent movement of ground objects and the observer's position, or change of position. For example, Belik (ref. **2)** has recently shown the relationship of position and speed to the size and apparent velocity of ground objects, for different sighting angles. What is needed for control purposes, however, is to relate the visual changes, due to movements along or across the approach path, to known visual capabilities of the human observer. If this can be done, it will be possible to determine the

* This paper summarizes work performed at the Douglas Aircraft Company under the sponsorship of the Independent Research and Development Program (IRAD) of the McDonnell Douglas Corporation.

smallest changes of the observer's position and speed causing detectable effects in the external scene and, thus, to estimate the precision with which a vehicle may be controlled in purely visual flight.

Another limitation desirable in selecting material from the external visual scene is in choosing only those ground objects suitable for building up quantitative relations for all visual approaches. Clearly, an invariable feature of the pilot's forward view is the outline shape of the runway, to which approaches are made over varying, or even featureless terrain. This geometrical pattern, or one of its component sides, will therefore be taken as providing the basic visual characteristics of the external scene, which are to be related to the observer's state variables, of position and speed. (The attitude of the observer's vehicle will not be considered as a state variable because it is without effect on the shape, size, and apparent velocity of ground objects.) The appearance of a ground line, such as a runway side, provides characteristic effects of inclination, expansion, size, and rotation, which will be considered for a conventional approach at a small elevation of the flight path, and without considering any secondary effects due to the windshield frame.

FIGURE 1.—Appearance of runway during approach.

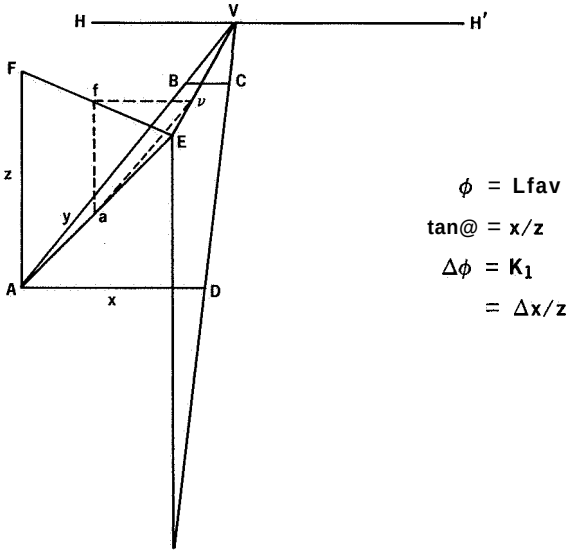

FIGURE 2.—Inclination of ground line.

INCLINATION EFFECTS

Lateral Alignment

A prominent runway feature during the approach is the appearance of a side or centerline. It is evident from figure 1 that each appears as a more-or-less straight line which is inclined to the vertical at an angle depending on the position of the observer. Ground lines to the left of the observer extend from lower left to upper middle, and those to his right are inclined in the opposite sense. It is not difficult to show that the apparent inclination of the ground line increases with the lateral offset of the observer, but decreases with an increase in height of the observer's eye. This relation is important in the lateral alignment of an approaching vehicle.

Let A, figure 2, be the origin of a rectangular coordinate system, of which the x-axis AD and the y-axis AB lie in a horizontal plane containing the rectangle $ABCD$. Let the observer be at the point E (x, y, z) lying in a vertical plane through DC. Then the observer's horizon HH' lies in a horizontal plane through E, which also cuts the z-axis in a point F, and the parallel lines AB and DC appear to meet at a point V on HH'.

Suppose a transparent reference plane is held between the observer and the scene before him, at a convenient distance, and inclined so as to be perpendicular to the y-axis. The points A, F, and V will be seen by the observer at the points a, f, and v, where the lines EA, EF, and EV intersect this plane. Now the ground line AB will

be seen in this plane as the line av, extending from the position of A to the position of the vanishing point V. The apparent inclination of AB will therefore be the inclination of av, or the angle fav, since af is a vertical line formed by two intersecting vertical planes, afv and EAF. Then by similar triangles,

$$\tan fav = \tan \phi = fv/fa = x/z. \quad (1)$$

It follows from this simple relation that, for any height of eye, z, the inclination of the ground line is zero when the observer's lateral offset, x, is zero. In practice, however, it is difficult to observe zero inclination because it is not always possible to estimate the vertical with great precision, as can be seen in figure 1. The process of lateral alignment will therefore be inexact to an extent depending on the ability to estimate the vertical, in field conditions. Laboratory studies, such as those of Werner and Wapner (ref. 3), suggest that this kind of estimation may be made to better than 1°, but a larger error, perhaps as great as 5°, would no doubt occur in the less settled conditions of flight. The quantitative relationship governing lateral alignment of the observer's vehicle is therefore of the form

$$\Delta(\phi) = \Delta(\tan \phi) = \Delta xz = k_1 \quad (2)$$

where $\Delta(\phi)$ is the error in estimating zero value for the inclination of the ground line, and k_1 is a constant expected to be about 1/12. With this value for k_1, the minimum detectable lateral offset will be about 42 feet at a height of 500 feet, or a range of 10000 feet on a 3° approach. Smaller offsets are discernible at smaller ranges, and the order of magnitude of the result suggests an accurate means of lateral control.

Vertical Alignment

Since the runway is essentially a plane surface, it does not readily lend itself to the vertical alignment of an observer, by showing whether he is above or below a chosen approach path. Few features of vertical extent are available which reveal the kind of differential inclination so easily observed in the lateral plane. It may nevertheless be possible to gain some control information in the vertical plane from the absolute value of the inclination of a ground line.

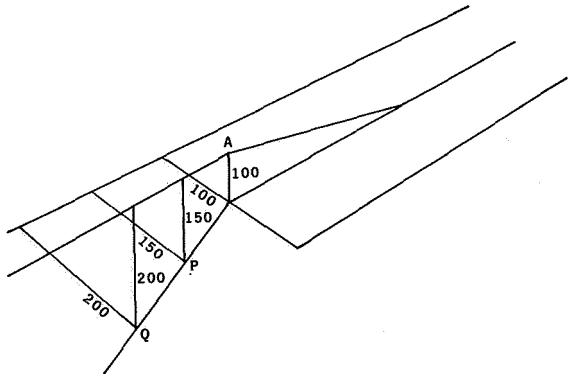

FIGURE 3.—Approach at constant included angle.

In the special case where the observer's height of eye is equal to the lateral offset from a ground line, its apparent inclination is 45° (eq. (1)). Thus, at an eye point 100 feet above the centerline of a runway, A, figure 3, the included angle between the runway sides would be 90" for a runway width of 200 ft. Given an ability to judge an absolute value of 90°, it would thus be possible to make an oblique approach to this point, at a constant glideslope angle, by passing over points equispaced in the ground plane and offset from a runway side by amounts increasing in arithmetical progression, P, Q, etc. But no very precise control could be expected by this method because an error of only 5" in estimating the included angle would result in a height error of about 8 percent; moreover, accuracy of alignment in the lateral plane would be sacrificed by using an oblique approach.

The more commonly practiced method of making an approach along a line of constant offset, such as the runway centerline, leads to the condition that inclination of the ground line varies only with height

$$\tan \phi = k/z. \quad (3)$$

The trained observer may then be able to estimate height from inclination, and this technique, with the further stipulation that distance to touchdown is known, may be sufficient to control the flight path in the vertical plane. But without knowledge of position along the approach path this method cannot yield usable information.

Estimation of range to touchdown is obviously influenced by the existence and visibility of

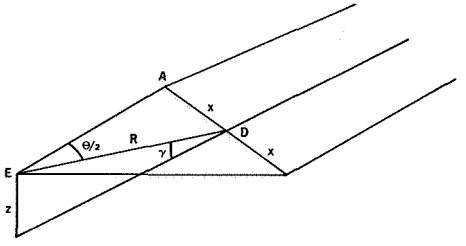

FIGURE 4.—Runway width and range.

recognizable ground features. This visual information is not always available, however, or it may not be usable because of unfamiliarity with the terrain. The pilot may nevertheless estimate range to touchdown from the apparent size of ground objects. For example, in a centerline approach to a runway of width $2x$, figure 4, the nearest edge subtends an angle θ such that

$$\tan \theta/2 = x/R \tag{4}$$

where R is the visual range to the midpoint of the edge. At the same time, either side of the runway appears inclined to the vertical at an angle ϕ such that

$$\tan \phi = x/z$$
$$= x/R \sin \gamma \tag{5}$$

where γ is the elevation of the sight line to the same midpoint. It follows from equations (4) and (5) that

$$\tan \theta/2/\tan \# = \sin \gamma \tag{6}$$

so that the elevation of the sight line may be held constant if this ratio of tangents can be observed always to have the same value. This suggests a possible mechanism for controlling a straight-line approach in elevation along the centerline of a runway.

The judgment required in maintaining a constant relationship between the apparent width of the runway and the apparent inclination of a runway side is more complicated than the simple judgment needed in observing alignment with a ground line. Accuracy in the vertical plane may therefore be more difficult to achieve than in the lateral plane, if the supposed mechanism is responsible for mediating the control information. And it is hard to relate this mechanism to known human capabilities. But if it is assumed that a measurable value may be given to the ability to estimate an angular ratio of this type, the governing relation for vertical control by means of the width/inclination ratio is

$$k_2 = \mathrm{A}\ (\tan \theta/2/\tan \#) = \mathrm{A}\ (\sin \gamma) \tag{7}$$

where k_2 is the error in estimating the angular ratio. If this error is 10 percent, the height error at a range of 10 000 ft, or a height of 500 ft on a 3° glideslope, would be about 50 ft. That is, this angular ratio would need to be held constant to within one part in ten in order to achieve a control accuracy similar to that calculated for the lateral plane by equation (2). This possibility is conjectural.

EXPANSION EFFECTS

It is well known that objects near the path of a vehicle appear to move outward as the vehicle advances. During an approach, for example, the runway appears to expand in all directions about the (inertial) flight path. This phenomenon suggests a mechanism providing information about the probable outcome of the pilot's control actions. Clearly, its usefulness depends on the quality of information provided, and this can be judged for the visual approach situation by calculating the apparent expansion in the region of the touchdown zone.

Lateral Aim

Suppose the observer at E, figure 4, is moving with velocity v, and approaching the point D, which is on the centerline of a runway of width 2s. A diameter through this point subtends the angle θ at the observer's eye, and each of its ends, such as A, appears to move outward from the approach path at an angular rate given (with sufficient accuracy) by

$$\frac{d}{dt}(\theta/2) = -\frac{s}{R^2}\frac{dR}{dt}$$
$$= sv/R^2 \tag{8}$$

(an increase in angle corresponding to a decrease in range).

If the observer fixates on the center point *D* and observes both extremities to move outward, he may conclude that his vehicle is proceeding to a point lying between them. Further, if the outward velocities are observed to be equal and opposite, it may be concluded that the destination is in fact point D, although this kind of judgment may be almost impossible to make at the limit of perception. Assuming that only the simpler type of observation is made, this will first be possible when the lateral angular velocity given by equation (8) exceeds the human threshold for perceiving movement. This threshold is quite large when the observation has to be made without the help of a fixed visual reference, as may be the case during a visual approach, and under these conditions the threshold will probably not be less than 10 min of arc per sec, or 1/344 sec (ref. 4). The impact point, at a range R, will then be estimated simply as lying somewhere within the runway width; that is, there will be an uncertainty of aiming position, $\pm Ax$, where

$$Ax = R^2/344v. \tag{9}$$

Then at a range of 10000 feet and with an approach speed of 200 ft per sec, the aiming uncertainty is ±1450 ft, or an angular uncertainty of ±8°. Because this value is a predicted or future offset, it cannot be compared directly with the lateral offset of 42 ft calculated by equation (2), which is a presently detectable offset. It is nevertheless clear that the expansion mechanism is less sensitive than the alignment mechanism because, at the same range of 10000 ft, the alignment mechanism can show an acceptably small error but the expansion mechanism can only show ambiguity. It cannot even show whether the impact point is within a 200-ft runway until the range is very much reduced (to about 2600 ft), according to the assumed threshold.

Vertical Aim

Basic features of the forward view which are significant to the expansion mechanism, for aiming the flight path in the vertical plane, are shown in frontal elevation in figure 5. The near and far ends of the runway, *N* and *F*, respectively, are the two relevant ground lines. There is also a visible horizon *V* and this is displaced below the true horizon *T* by the angle of dip 6 according to the approximate relation

$$\delta = \sqrt{z} \tag{10}$$

where 6 is expressed in minutes of arc, and the height z is in feet.

Since the true horizon is invisible, the largest observable vertical angle is *NV*. The rate at which this angle increases can be calculated by noting that the angle *NT* is nearly constant for a good approach, when the vehicle moves along an approximately straight line to touchdown, so the angle *NV* increases at about the same rate as the angle *VT* decreases. This is easily obtained from equation (10),

$$\frac{d}{dt}(\delta) = \frac{1}{2\sqrt{z}}\frac{dz}{dt} \tag{11}$$

and for a typical descent rate of 10 ft per sec, the angle *NV* increases at less than 0.5 min of arc per second at heights above 100 ft, and only changes at an observable rate when the height is reduced to about 0.25 ft. In other words, the near end of the runway is not seen to move away from the visible horizon during a normal visual approach.

The rate at which the runway length *NF* appears to expand can be calculated from the geometry of figure 6, which shows the visual

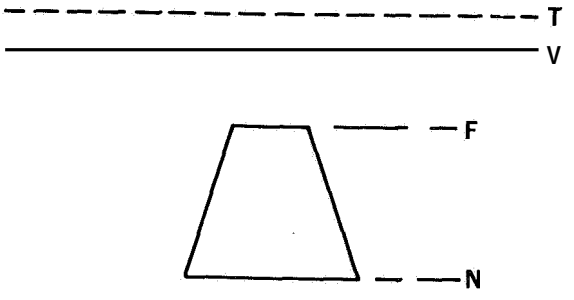

FIGURE 5.—Expanding runway features in frontal elevation.

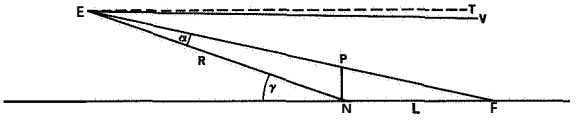

Vertical Expansion	Height/Range Ratio
$a = \angle\gamma/(L+R)$	$\gamma = z/R$
$\dot{a} = -\angle\gamma\, v/(L+R)^2 = \angle\dot{z}/(L+R)^2$	$\Delta\gamma/\gamma = \Delta z/z - \Delta R/R$

FIGURE 6.—Runway features in side elevation.

features of figure 5 in side elevation through the eye point E. If the visual range to the near end is R, and the runway length is L, the vertical angle α subtended by the runway is given to the first order of accuracy by

$$\alpha = PN/EN = \frac{L\gamma}{L+R} \tag{12}$$

where PN is a vertical through N and γ is the elevation of the inertial flight path. The expansion rate is then

$$\frac{d\alpha}{dt} = -\frac{L\gamma v}{(L+R)^2} = \frac{L}{(L+R)^2}\frac{dz}{dt} \tag{13}$$

which, for a typical runway length of 8000 feet and the same descent rate of 10 ft per sec, increases to a maximum of only about 4 min of arc per sec as R reduces to zero, and is thus never usefully observable. This result means that the expansion mechanism does not allow the flight path to be aimed within the length of the runway during an approach at a small glideslope angle (where the approximation of eq. (12) is valid). It does not even show that the flight path lies below the horizon.

SIZE EFFECTS

Lateral Position

In a conventional approach, the ratio of visual range to height is large, of the order of twenty to one, and the runway therefore subtends only a small visual angle until quite a low altitude is reached. Thus, when the elevation of the approach path is 3°, a 200-ft runway subtends less than 6" until height is decreased to 100 ft. Under such small-angle conditions, it is possible to be offset from the centerline by quite large amounts, of the order of half the runway width, without appreciably altering either the visual range or the projected width of the runway. The apparent width of the runway is therefore an insensitive clue to lateral position, except at very short range, and is unable to provide information for control purposes during the greater part of a normal visual approach.

Vertical Position by Height and Range

It has already been suggested that the flight path may be controlled in the vertical plane by maintaining a relationship between the inclination of a ground line, which can be related to height, and the apparent size of the runway, which is related to range. But height may sometimes be estimated directly from the apparent size of a known object beneath the airplane, such as a motor vehicle, and this kind of judgment is not dependent on local topographical knowledge. If such objects are available, position in the vertical plane may be known by combining this type of observation with the estimation of range: that is, by combining two observations of apparent angular size.

The path accuracy achieved in attempting to maintain a constant ratio of height to range is then given directly,

$$\frac{\Delta\gamma}{\gamma} = \frac{\Delta z}{z} - \frac{\Delta R}{R}. \tag{14}$$

If estimates of height and range can be made within 5 percent of the true values, the flight path will be accurate to within 10 percent, according to this mechanism, and the result will be commensurate with the lateral accuracy achieved by the alignment mechanism, equation (2). Such accuracy in judging distances is perhaps possible when the intermediate space is a continuum of observable detail; for example, a golf shot of 200 yd can probably be estimated within 10 yd. But there are no intermediate objects in the airborne situation. Moreover, the two distance judgments are to be made in different directions, and can hardly be simultaneous. For these reasons, the vertical accuracy achieved by a height and range mechanism based only on angular size, is likely to be less than the lateral accuracy achieved by alignment.

Vertical Position by Depression of Touchdown Zone

A more direct method of locating the flight path in the vertical plane may consist in observing the depression of the touchdown zone below the true horizon. Thus, if the angle TEN, figure 6, has the value y, the aircraft is on the line EN, since from any other position the ground point N is depressed by a different amount. If this value is maintained, the vehicle is also proceeding along the straight line EN and the flight path is known if the angular values are correctly judged.

Unfortunately, more is involved than estimation of an absolute angular value. It is also necessary for the angle to be judged with respect to an invisible horizon. Thus, in figure 5, the position of T has to be established before the subtense of NT can be given a value. Clearly, angular estimation can be practised, and the associated error might be reduced to an acceptable level. But it is less straightforward to compute mentally, and estimate visually, the position of the true horizon, especially as the visible horizon may itself be displaced through changes of visibility and local variations of terrian. The total error in estimating the flight path by this mechanism is thus:

$$\Delta\gamma = \Delta(\gamma) + k_3\sqrt{z} \qquad (15)$$

where $\Delta(\gamma)$ is the error in judging the absolute value of a small angle, and the second term is derived from equation *(10)*. If the factor k_3 has a value as great as unity, as may happen if the significance of the angle of dip is not appreciated, the second term contributes nearly three-fourths of a degree during an approach from *1600* ft, and no great accuracy is achieved. On the other hand, if time is available and care is taken to establish the true horizon, it may perhaps be possible to operate with the accuracy typical of the lateral alignment mechanism, assuming accurate angular judgment within 10 percent. The true situation may lie between these two cases.

ROTATION EFFECTS

Since the inclination of a ground line depends on lateral offset and height of eye, according to equation (1), each runway side will appear to rotate during lateral and vertical movements of the observer. The consequent motions are distinguished by the sense in which the sides appear to rotate. For an observer on the centerline, the offsets and therefore the inclinations are opposite in sign, as in figure 7(a). As he moves laterally, one offset increases as the other decreases, and the inclinations change in the same algebraic sense. The lines thus appear to rotate about the vanishing point in the same sense. For an observer moving vertically above the centerline, figure 7(b), the offsets are constant, and as height changes, each inclination of opposite sign changes in opposite algebraic sense. The runway sides thus appear to rotate in opposite sense. In the general case, lateral and vertical motions occur together, and the total rotational effect is a combination of the two kinds of apparent rotation.

Lateral Motion

If the observer is assumed simply to move laterally at constant height, the apparent rotation of a runway side may be estimated by differentiating equation (1), using the small-angle approximation

$$\frac{d\phi}{dt} = \frac{1}{x}\frac{dx}{dt}.$$

This is a rotation in the observer's frontal plane of a line having an apparent (angular) length given by equation (12), with sufficient accuracy, so that either end appears to move about the other at the approximate rate

$$\alpha\frac{d\phi}{dt} = \left(\frac{L\gamma}{L+R}\right)\frac{1}{z}\frac{dx}{dt} = \frac{L}{R(L+R)}\frac{dx}{dt}. \qquad (16)$$

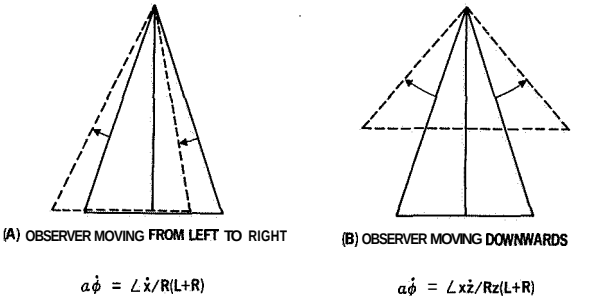

FIGURE 7.—Apparent rotations of runway sides.

But during an approach, the observer's sink rate must also be taken into account, and the apparent rotation of a runway side is

$$\frac{d\phi}{dt} \quad \frac{1}{z}\frac{dx}{dt} \quad \frac{x}{z^2}\frac{dz}{dt}$$

so that either end appears to move about the other at approximately

$$\frac{d\phi}{dt} = \frac{L}{R(L+R)}\frac{dx}{dt} - \frac{L}{R(L+R)}\frac{x}{z}\frac{dz}{dt}. \qquad (17)$$

This is the speed at which the far end of the runway will appear to move if the near end is fixated. It is an angular speed at the eye, and will be discernible if it exceeds about 1/344 sec.

It can be seen that until the approach is far advanced, the second term of equation *(17)* is unimportant, and the combination of lateral and downward motion of the observer yields a rotational effect adequately described by equation *(16)*. Thus, for an observer on the centerline of a runway *200* ft wide and 8000 ft long, the second term first exceeds the value 1/344 sec when height is reduced to about *120* ft, for a sink rate of *10* ft per sec. The minimum discernible lateral speed can therefore be estimated as

$$\frac{dx}{dt} = \frac{R(L+R)}{344L} \qquad (18)$$

which, at a range of 10 000 feet from the same runway, gives a value of about 65 ft per sec. Clearly, this is a large fraction of a typical approach speed of *200* ft per sec and gives a drift angle of about 18°, so that this mechanism of detecting lateral motion is scarcely adequate for control purposes.

Vertical Motion

It has already been shown that vertical motion of the observer during the approach results in a negligible rotation effect, for normal sink rates, until the airplane is quite close to the ground. Departures from an optimum sink rate will not therefore result in observable effects during most of the approach, unless the departures are large. Moreover, a consequent rotation may be concealed by contrary rotation due to lateral motion. The apparent rotation of a runway side thus provides insufficient information for controlling vertical speed.

DISCUSSION

It is evidently possible to derive quantitative relationships 'connecting the information available in the pilot's forward view with the position and motion of his vehicle. Several mechanisms can be advanced which allow calculable changes in the visual scene to be linked with human capabilities of visual judgment. These depend on the apparent inclination, expansion, size, and rotation of prominent runway features, and their magnitudes throw light on the accuracy of the control process in visual flight.

Results of the analysis, for an approach of conventionally small elevation, are collected in table *1*. An important mechanism depends on the inclination of a ground line, at a given position of the observer, which yields a simple and direct method of control in the lateral plane. With a conservatively estimated ability to judge vertically within 5°, alignment within less than 50 ft is possible at a range of 10000 ft, and within smaller offsets at shorter ranges. In other words, it is readily possible to place the vehicle within the width of the runway during most of the approach. A connection may also be traced between the appearance of the runway and the position of the observer, for control in the vertical plane. But for this to be used it is necessary to propose an ability to make a somewhat complicated comparison of apparent size and apparent inclination. The supposed ability has not been linked with human performance data, and the accuracy of the mechanism has not therefore been ranked.

Contrary to expectations, the expansion mechanism is unable to provide an accurate basis for controlling the flight path. Without the help of a stabilized reference mark, angular velocities less than *10* min of arc per sec can scarcely be discerned, and calculation shows that this level of visual performance will only support a crude estimation of the impact point. In the lateral plane, there is an aiming uncertainty of ±8° at a range of *10* 000 feet, for an approach at **200** ft per sec. And it only becomes possible to tell whether the vehicle will arrive within the width of the runway when the range is reduced to about

TABLE 1.—*Information Mechanisms of Visual Flight*

Visible effect	Application	Quantitative relation	Rank order Lateral	Vertical
Inclination	Lateral alignment	$Ax = k_1 z$	1	. .
	Vertical alignment	$k_2 = \Delta(\tan \theta / 2 / \tan \phi)$ $= A (\sin \gamma)$	...	?
Expansion	Lateral aim	$Ax = R^2/344v$	2	...
	Vertical aim	$L_z = (L+R)^2/344$	...	u *
Size	Lateral position	.....	U	...
	Vertical position by			
	Height and range	$\Delta\gamma/\gamma = \Delta z/z - \Delta R/R$	...	1
	Depression of TDZ	$\Delta\gamma = \Delta(\gamma) + k_3 z^{1/2}$	...	2
Rotation	Lateral motion	$\dot{x} = R(L+R)/344L$	3	...
	Vertical motion	$\dot{z} = zR(L+R)/344xL$	...	U

* u Signifies unusable.

one-half mile. The expansion mechanism thus provides less information in the lateral plane than the alignment mechanism, which allows continued monitoring of the offset from runway centerline. In the vertical plane the situation is worse: the flight path cannot be observed to lie below the horizon, or to fall within the length of the runway till after touchdown. The vertical expansion mechanism is therefore unusable, according to the assumption made about velocity perception.

The apparent size of the runway provides little clue to lateral position, except at short range, but yields two possible mechanisms for the vertical plane. In one of these, combined estimations of height and range may perhaps be used to determine the elevation of the flight path. But since these estimations are made in different viewing directions, and largely without the help of intermediate objects, it may be difficult to achieve optimum judgments of distance, which might otherwise yield an overall accuracy of 10 percent. An alternate vertical mechanism is based on the angular size of the depression of the touchdown zone, and this is subject to errors of estimating an angle and of establishing the position of the true horizon. Because of the unpredictable, and potentially large influence of the horizon effect, it seems necessary to rank the touchdown depression mechanism below the height and range mechanism in which, at least, the objects to be judged are visible.

Information mechanisms can also be described which depend on the apparent rotation of runway sides, but their yield is insufficient for control purposes. Rotation due to lateral motion of the observer is only discernible for cross track speeds capable of causing drift angles of 18° in either direction at 10 000-foot range, and this mechanism is ranked below the lateral expansion mechanism. Rotation due to vertical motion is only observable below a height of about 120 ft and is scarcely usable, especially as it may be masked by contrary rotation due to lateral motion.

In brief, it is clear that a more satisfactory situation exists in the lateral plane than in the vertical plane. According to the analysis, the alignment mechanism provides a simple and accurate basis for lateral control and is superior to other mechanisms, including the expansion mechanism. But in the vertical plane, all of the usable mechanisms involve some kind of double judgment, whether of width and inclination, of height and range, or of depression and horizon position, and a simple mechanism of unquestionable accuracy has not been found. Without experimentation, there is some uncertainty about the visual performance data which apply, and some difficulty in determining rank order.

Finally, an important application of the results is to displays which include a runway representation. For although this kind of symbol may inspire a certain amount of confidence, through the familiarity of its shape and the ease with which it can be understood, it may be less than satisfactory as a source of information for control purposes.

SYMBOLS

x displacement perpendicular to runway side (length)
y displacement along runway side
z height
ϕ apparent inclination of ground line to vertical
k_1 error in judging vertical
θ subtense of runway width
γ elevation of flight path (or sight line)
k_2 fractional error in estimating angular ratio
R range to touchdown or ground point
s half width of runway
V vehicle velocity
α' apparent (angular) length of runway
L length of runway
k_3 fractional error in estimating dip angle

REFERENCES

1. GIBSON, J. J.: Perception of the Visual World. Houghton Mifflin (Cambridge, Mass.), 1950, p. 129.
2. BELIK, YA. YA.: Modelling of the Optic Distance Perception in Vertically Taking-Off and Landing Aircraft. Kosmicheskaya Biologiya i Meditsina, vol. 3, no. 3, May–June 1969, pp. 66-70.
3. WERNER, H.; and WAPNER, S.: Experiments on Sensory-Tonic Field Theory of Perception. Vol. IV Effect of Initial Position of a Rod on Apparent Verticality. Jour. Exp. Psychology, 1952, pp. 68-74.
4. GRAHAM; BARTLETT; BROWN; HSIA; MUELLER; AND RIGGS: Vision and Visual Perception. J. P. Wiley and Sons, 1965, p. 575.

N73-10127

22. On the Dependence of Information Display Quality Requirements Upon Human Characteristics and "Pilot/Automatics"-Relations

V. WILCKENS

Deutsch Forschungs-U.

INTRODUCTION

Basically, the title selected has to deal with the characteristics of, and relations between, many and complex components. Due to the short time available some of these contributing factors can only be touched and I am very aware of the risk of over-simplification. So I can only try to give a representative cross section.

Although this paper primarily offers generalized statements, these are based on operational and experimental flight and simulator experience, on literature- and some theoretical studies, and on an evaluation of a new display concept. Information on more specific results is, or will be, presented in other papers (refs. **1** through **4).**

Manual control e.g., of an aircraft landing would be (under the impression of the previous paper of Dr. Naish I should modify to: "seems to be) no problem, if best visual contact with the outside environment would be continuously available. In general, this is true even for poor aircraft dynamics.

Actual operating conditions, however, are more or less below optimum, down to absolute zero visibility. We all know that under these conditions aircraft control becomes critical as soon as solid objects in the environment of the aircraft severely restrict the use of one or more **of** the six degrees of freedom, especially when the speed is extremely low or high. Several remarks in literature try to base the "all" weather landing problems on limited human abilities in manual control. The pilot as a controller should be substituted by automatics, as shown by the quotes from reference *5*

> . . . even with the best available displays the pilot has not been able to control (the blind landing) with the precision required . . .

and reference *6*

> There is no doubt that in complex flying tasks like blind landing . . . automatics become essential . . .

Sometimes, certain limitations of man are reached and exceeded, indeed. For example, when a pilot tries to suppress high frequency oscillations. However, such critical flight characteristics do not prevail in the landing phase.

Of course, man cannot penetrate fog with his eyes; However, in order to remain consequent, it would be unreasonable to blame *him* for this fact. Otherwise, he should be considered to be blameworthy, too, because he needs tools, machines to carry heavy loads, artificial wings to fly, etc.

The characteristics of the aircraft, **of** the controls, and of the gust disturbances in principle do not change and the same human sensors remain active as soon as flight conditions change to IMC. **A** rigorous change happens in the type of information only. Therefore this and it's interference with basic human characteristics must be the main source of the problem. Furthermore, this suggests, that the substitutes for visual contact presently in operation are not yet equivalent, although visual contact itself has been shown to provide poor information in some respect, too (see paper **21** and (ref. **7)).**

Finally, the inevitable predominance of the automatic in landing control is justified only if the present information display concepts are approximately the best that can be achieved at all.

EVOLUTION OF THE DISPLAY PROBLEM

A quick look at the evolution of the display problem may help to emphasize the main "knots in the network" (fig. **1).**

Some aspects of the field of aeronautics are composed here according to different applicable activities of man. However, let us concentrate on man in his role as a systems component, especially as a pilot. In his other activities within the whole, he has more or less direct, or secondary, influence with the central display problem. The other part of the "link systems" the controls are eliminated here, although their man-compatible outlay plays a remarkable role in the limitations of the total systems performance.

Aircraft performance increased rapidly under the powerful drive of basic human desires. On the other hand, the human "ability for unaided information pick-up" and "some desire" or, at least: "acceptance to perform difficult tasks" delayed the development of the artificial information sources. Economy and the desire for independence from day time and meteorological conditions partly provided for some accelerating as well as unfavorable inputs to the display development. The other part of this influence made use of the human "readiness to adapt to almost every demand." This combination of inputs necessarily led, via a "completion" of the information step by step, to the "logic" result, the additive display as we know it from present cockpits. The built-in "lag-mechanism," however, is responsible that even this simplest requirement for complete information relative to the demands of operation was fulfilled in rare cases only. It should not be surprising that there are still gaps to be filled. The following is quoted from reference 8.

> . . . None **of** the parameters . . . flare initiation, decrab, touch down point . . . are available on the instrument panel . . . (inusable form) . . .

The *visual switching* of man operates at a high performance level, when compared with other motion functions of the human body. The fact that basically the additive display—in whatever stage of maturity—does not allow the systems optimum to be reached has been obscured for some time:
Sinaiko (ref. 9) stated

> . . . man can perform several **kinds** of tasks simultaneously or in rapid succession and keep them all integrated.

This is true in normal every-day conditions. However, as soon as a complex riskful task has to be performed under severe time constraint, the opposite unfavorable side of the (minutely examined) organization principle of the human

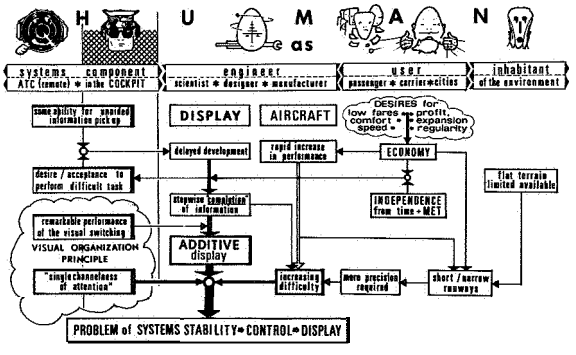

FIGURE 1.—Evolution **of** the display problem.

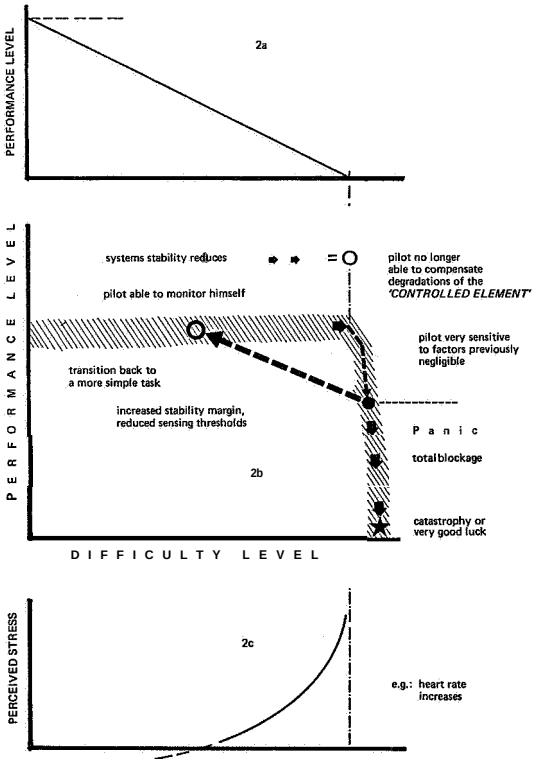

FIGURE 2.—Human performance behavior.

visual becomes apparent. Kelly in reference **10** mentions

The human operator can attend to only **one thing at a time; he is a single channel device in this sense . . .**

The increasing performance of the aircraft, on the one hand, impaired the flight characteristics; but on the other hand, the step from circular grass airfields to narrow concrete runways was necessary and required a much more precise guidance.

The following is a translated remark in a **1935** paper by Schulz (ref. 11):

Landing in poor weather (dense fog included) is a problem, the main part of which is considered to be solved; within a few years the last difficulties will have been overcome.

We know, the progress "by-passed the last difficulties," which grew in the meanwhile and was "baked" to be a very resistant problem now. After all, the "single channelness of attention" of man in a task of increasing difficulty made the manual control with information from an additive display critical. Operation under marginal conditions primarily became a stability problem.

Human Performance Behavior

We saw that the willingness of man to adapt had an unfavorable influence in the evolution process. This would have been avoided, if the "man in the loop" would allow the performance of the system to drop, e.g., linearly, with increasing difficulty (fig. 2(a)). He does not. Instead of this, he amplifies his effort and maintains the overall performance approximately constant (fig. 2(b)), as demonstrated by Henry Jex during this conference. Due to the raised effort man perceives stress as soon as a certain difficulty level is exceeded (fig. 2(c)).

Compensating the difficulty with effort necessarily reduces the reserves of man and thus of the system's stability. As soon as the human capacity is saturated, a steep break down occurs and either a simpler task is adopted or, if this is impossible, a catastrophy may result.

TRIED SOLUTIONS

Figure **3** shows a rudimentary diagram of known efforts to overcome a problem. Some impressions and knowledge of limitations as well as abilities of man and automatics, respectively, split the activity—some of which diverged into opposite directions. Not all of these are indicated here and two, the improved education and simplification of machine are mentioned only. Figure **3** concentrates on the trends towards display improvement for manual control and towards substitution of man by fully competent automatics.

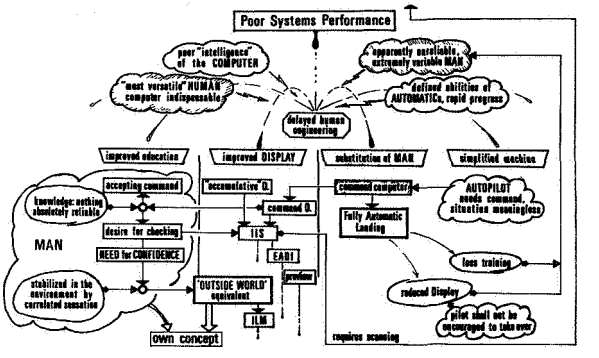

FIGURE 3.—Types of known solutions.

Improvement of Controllability by Displays

Display improvements have been achieved, for example, by compressing the distributed indicators into—I prefer to call it—"accumulative displays."

Steering commands, which combine the different separate variables are obligatory for automatic control. They were made available for the pilot, too, in the form of command displays, e.g., director needles.

While the first step, the accumulation, reduced information scanning, command should have completely eliminated this main destabilizer on the first superficial view.

What can be effected in terms of stabilization with a "fully integrated" display is symbolized in figure **4** by a simple mechanical model. In control tasks with "distributed information" the pilot has to stabilize (dependent upon the difficulty level) a more or less unstable system. Unstable, because too much relaxation in information scanning activity increases deviations from the desired conditions and thus the control diffi-

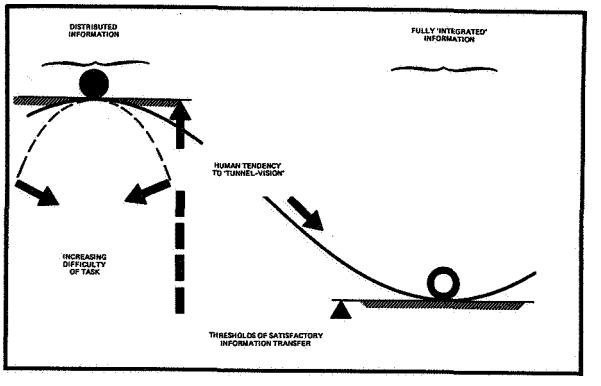

FIGURE 4.—Effect of tunnel-vision=function of display.

culties. This in turn, tends to further reduce the scanning frequency.

As soon as the stabilizing capability of man is exhausted, the information transfer runs "downhill" below the satisfactory threshold. If, on the other hand, the pilot is provided with fully integrated information, which has it's threshold of satisfactory information transfer at "the bottom of a valley" (fig. 4), the destabilizing scanning process is no longer required. It may be used to gather additional secondary or detail data; however, in cases where attention must be concentrated, man automatically returns to the main source of a continuous fully integrated flow of information. In this case, the information transfer would be inherently stable. In other words, since the pilot has a strong tendency to "tunnel-vision," it is reasonable not to fight against this but to give him the "tunnel."

Returning to figure 3 we can say that the pure command display already is some type of fully integrated information. However, pure imperative indications are not satisfactory. Although there are some pilots (and people) who accept or even like command, most of them feel a natural need at least to check its validity. So the accumulated situation indicators were combined with command in the so-called integrated instrument systems (IIS), which are the well known ADI/HSI-instruments, presently in wide use.

Progress in electronics has led to conversion of the ADI-display into the CRT-equivalent: the electronic attitude director indicator (EADI). Although to a lesser extent than before, the problems of single channelness of attention and information scanning and systems stability were adopted again with the IIS and EADI. Furthermore, in operations under marginal visibility it became obvious that the present state of the art does not cover, to a satisfactory extent, the human psychological need for confidence. The following observations of Stout and Naish (ref. 12) emphasize this:

> . . . pilots anxiety level increased at an alarmingly fast rate below 100 ft (altitude in true blind landings, manually controlled with a certain modern Flight Director).

Obviously, the conventional type of situation display, although sometimes provided with the term "pictorial," is not yet realistic enough. The following remark of Armitage (ref. 13) indicates a possible solution:

> There appears to be a great need for a real world-type display derived from . . . data of a source other than ILS.

TV- and infrared techniques and the recent progress in radar have made possible a picture of the runway during the final phase of a landing even through dense fog. In some displays this picture is combined with the EADI-Information. The independent landing monitor (ILM), a radar-image according to the statement of Armitage (ref. 13), is intended to be used not as an aid for manual control but as a separate 'confidence producer' for the pilot who supervises the automatic landing.

Another important type of outer loop-information, the preview-display, should, at least, be mentioned here. There is no instrumentation of this type in general use today.

Both, pure command or IIS, as well as pure contact analog, had been shown to be unsatisfactory, as has been presented in separate displays. In a paper presented at the AGARD Symposium in 1968 (ref. 14) we can find the following surprising remark of Douwes Dekker which shows that superimposition of different elements is undesirable:

> . . . Complete obedience to the HUD-director signals was required. This was best achieved with windshield blanked out, to prevent the pilot from being disturbed by the outside world. This most curious contradiction . . . indicates that FD-signals, having no direct relationship with the visual cues, should not be superimposed on the outside world.

AIMS FOR DISPLAY DESIGN

Obviously, the question is now, how we can achieve the desirable complete integration of quantitative indications, outer **loop** information and real-world display, in order to fulfil the requirements of controllability and confidence, respectively.

Gibson (ref. **15)** and Metager (ref. **16)** and probably other psychologists have shown the high extent which man is emotionally stabilized in his habitual fixed environment. This is primarily achieved by the realistic, and in motions quickly changing, the appearance of near-by objects which are reasonably distributed in the visual world, and, furthermore, by a very intense correlation of the inputs from all the affected human senses.

Since the natural environment of an aircraft is not filled with space-fixed objects, a simple copy of the real world has proven unsatisfactory. More or less abstract superimposed additives are undesirable. However, the useful part of the real world can be extended by suitable imaginary objects apparently fixed in space. Such a complex pictorial presentation can provide for each desired sensitivity.

The symbology of pictorial displays can be designed to provide for all necessary quantitative information content by pure pictorial means. It is a wrong assumption that pictorial displays in principle are less accurate and qualitatively only.

Furthermore, such pictorial displays which meet the aims mentioned before inherently contain some outer loop-information to a much higher degree than generally recognized. Separate indicators for command, preview, and flight path vector will thus be superfluous.

These display qualities are evaluated in detail in reference **17.**

The presentation until now has only touched the controllability and the confidence components of the problem area. However, the requirements for really advanced displays extend beyond these aims. Modern aircraft operation demands for a maximum of flexibility, e.g., for noise abatement — STOL-operation on small airfields which may be surrounded by high obstacles. We know that modern instruments do not allow an approach such as is possible in visual

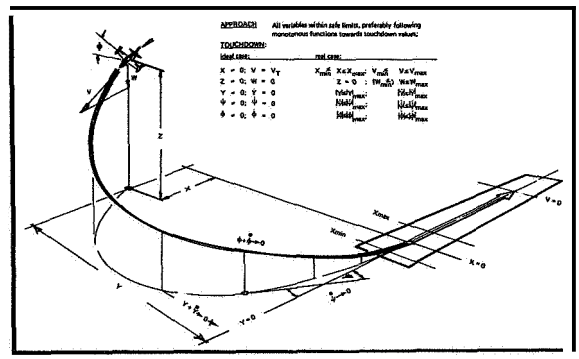

FIGURE 5.—Desirable flexibility in landing approach.

contact turning approaches (fig. *5).* Present instruments require all dynamics of motion, except speed, to be suppressed in a 5 to 8 mile long straight-in approach in order to effect a safe landing. Straight approach suits the desire for comfort, yes. However, up to now not much more in terms of flexibility is possible.

Turning approaches, contradictory as it may seem, are safer and easier to perform (ref. 18) and, therefore, are used by fighter pilots and recommended for space shuttle landing (ref. **19).**

A true precision task in terms of a tight control of all degrees of freedom prevails in relatively short phases of flight only—if at all. In general, the last **10** sec of a landing might be considered as such. But, more accuracy is required in close formation flight and flight refuelling. In spite of that, these tasks are performed with admirable perfection which indicates that landing cannot be too difficult a task for manual control if a suitable display is provided.

The proficiency of a pilot depends upon his training in precision control. Thus, presenting a display which continuously demands a reasonably high precision of guidance would raise the average manual skills to a remarkably higher level.

The ability of man to "differentiate" and "integrate" is much better than sometimes assumed; it can be raised to an artistical level as an overwhelming number of examples, even in every-day life, demonstrate. This should consequently be used for improvement of manual control of an aircraft by better display techniques.

The following summarizes the main aims of display quality requirements:

Controllability of the system:

(1) Not as easy **as** possible, when achieved by artificial task simplification only.

(2) According to demands of high performance activities of man

(3) Economic use of superb human dynamic capabilities.

Flexibility of the system:

(1) Free selection of safe flight trajectories

(2) Response to operational requirements.

Proficiency of the pilot:

(1) Raised beyond the present state

(2) Maximum use of human reflexes+intelligence

(3) Selection of the most suitable individuals.

Confidence of the pilot:

(1) In space orientation

(2) In his own ability as pilot in the loop

(3) In the overall situation

(4) In the functional reliabilities may be less important.

FINAL REMARKS

Let me add a further statement to confidence. My impression is that we cannot hope for any spontaneous confidence when we base it only on partly experienced, finally extrapolated, and believed or not believed high reliability of the equipment. The pilot needs a back-up by a confidence-immanent information display!

With respect to the acceptance of advanced automatics, we cannot derive that the automatic solution is near-optimum if pilots accept the role of a manager without being able to demonstrate true competence in manual control during each phase of flight. They must and probably will accept a dominating autopilot and reduced instead of improved displays, if no convincing alternative is in sight; otherwise, they will probably lose their job. The extreme tendency of man to adapt allows him to develop a fatalistic type of confidence. On the other hand, a pilot will like to delegate the complete landing even to a less reliable automatic if the display enables him to chose and perform alternative decisions in case of not only an overshoot but a take over.

Two examples of our approach to solve the problem are shown in figure ***6, 7,*** and 8.

The main display element is a channel or a tunnel, which has been developed by consequently applying the street-shaped symbol for lateral and vertical guidance in all flight phases. This concept is described in more detail in references **5** and 17.

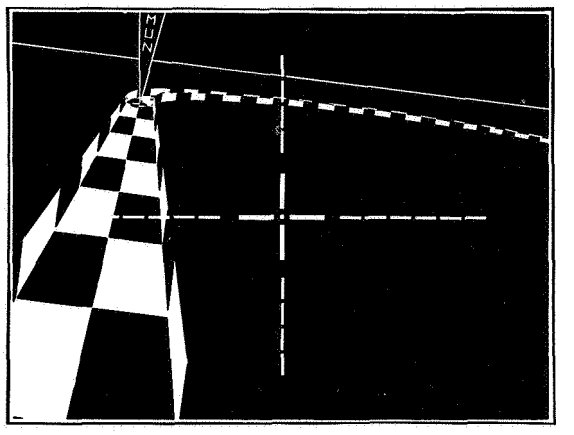

FIGURE 6.—Entering MUN holding pattern.

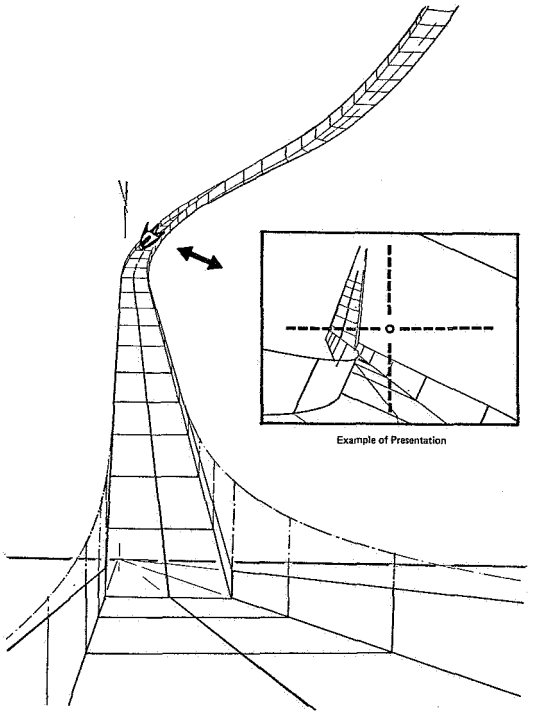

FIGURE 7.—A channel for unpowered landings; glide angle variability, wind, and flare capability have been accounted for.

We feel sure that we can meet the requirements of controllability, flexibility, and proficiency. We believe that we have a good chance to fulfil the confidence-requirement, too. However, we are aware that this is very difficult to demonstrate.

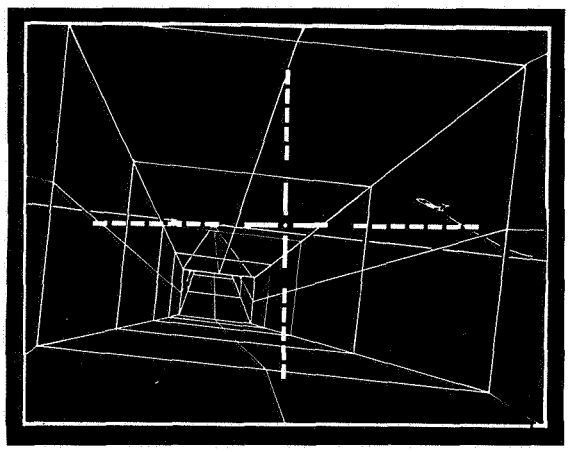

FIGURE 8.—Channel information for collision avoidance.

REFERENCES

1. WILCKENS, V.: Flugeigenschafts- und Leistungsmessungen an einem Propellerflugzeugvom Typ "RW 3". DVL-Bericht Nr. **271,** June **1963,** pp. **48** and **49.**
2. WILCEENS, V.: Uber ein Verfahren zur Fuhrung von Flugzeugen auf vorgegebenen Bahnen, vornehmlich bei manuell gesteuerten, vollstandigen Blindlandungen. Vortrag Nr. **66–100** der DGRR/WGLR-Jahrestagung, Bad Godesberg, **1966.**
3. WILCKENS, V.; AND SCHATTENMANN, W.: Test Results with New Analog Displays for All Weather Landing. Paper No. 10, AGARD Conf. Proc. No. **55** (Amsterdam), Nov. **1968.**
3. WILCKENS, V.: On the Design Philosophy and Operational Capabilities of the CHANNEL-Display. Interner Bericht Nr., der DFVLR, Oberpfaffenhofen, Mar. **1971.**
5. ANON.: Automatic Landing. Aircraft Engineering, Apr. **1969.**
6. O'HARA, **F.:** Stability Augmentation in Aircraft Design. The Aeronautical Journal of the RAeS, Apr. **1971.**
7. WEMPE, E., AND PALMER, E.: Pilot Performance with a Simulated Pictorial Landing Display Including Different Conditions of Resolution and Update Rate. 6th Annual NASA/University Conference on Manual Control, Wright-Patterson AFB, Apr. **1970.**
8. JOHNSON, E. W.; CARMACK, D. L.; AND HADLEY, L. M.: Psychological and Procedural Aspects Related to ILS-Approaches and Landings in Visibilities less than **1200** ft. Paper No. **3,** AGARD-Symposium Aircraft Landing Systems, Conf. Proc. No. **59** (Cambridge, Mass.), May **1969.**
9. SINAIKO, H. W.; AND BUCKLEY, E. P.: Human Factors in the Design of Systems. NRL Report **4996,** Wash. D.C. **1957.** Reprinted in Selected Papers on Human Factors in the Design and Use of Control Systems, Dover Publications Inc. (New York), **1961.**
10. KELLEY, C. R.: Manual and Automatic Control. John Wiley and Sons (New York), **1968.**
11. SCHULZ, R.: Schlechtwetterflug. Luftwissen, Band **2;** Nr. **11,** Nov. **1935.**
12. Stout, **C.** L.; AND NAISH, **J.** M.: The Total Systems Concept for CAT III Operations. SETP Technical Review **of** the XI Symposium Proceedings (Beverly Hills), Sept. **1967.**
13. ARMITAGE, H. B.: A Pilot's Evaluation of the **C–141** CAT III b All Weather Landing System. SETP-Cockpit, Dec. **1968** and Mar. **1969** (in Letters to the Editor).
14. DOUWES DEKKER, F. E.: Head-Up Display Symbology. Paper No. **23,** AGARD Conf. Proc. No. **55** (Amsterdam), **1968.**
15. GIBSON, J. J.: The Perception of the Visual World. The Riverside Press (Cambridge, Mass.), **1950.**
16. METZGER, W.: Gesetze des Sehens. Ed. Senckenberg, Naturforsch. Gesellschaft Frankfurt Main. Waldemar Kramer (Frankfurt), **1953.**
17. WILCKENS, V.: Die Entwicklung der KANAL-Information. To be published as a DLR-FB (research report).
18. LANE, **J.** C.; AND CUMMING, R. **W.:** The Role of Visual Cues in Final Approach to Landing. ARL-Human Engineering Note **1.**
19. DANA, W. H.; AND GENTRY, **J.** R.: Pilot Impressions **of** Lifting Body Vehicles. NASA TM **X–2101,** June **30, 1970.**

SESSION V

VISUAL INFORMATION PROCESSING

Chairman: JOHN SENDERS

23. A Bayesian Model for Visual Space Perception

RENWICK E. CURRY

Massachusetts Institute of Technology

A model for visual space perception is proposed that contains desirable features in the theories of Gibson (ref. 1) and Brunswik (ref. 2). This model is a Bayesian processor of proximal stimuli which contains three important elements: an internal model of the Markov process describing the knowledge of the distal world, the a priori distribution of the state of the Markov process, and an internal model relating state to proximal stimuli. The universality of the model is discussed and it is compared with signal detection theory models. Experimental results of Kinchla are used as a special case.

INTRODUCTION

There have been two broad theories of visual perception expounded in the past several decades; they are usually attributed to Gibson (ref. 1) and Brunswik (ref. 2). Gibson seems to be the first to present a unified picture of all the various cues about the three-dimensional world that are available from the two-dimensional retinal image, especially motion cues and cues of the gradient of texture. Gibson's theory is a deterministic one, and it is his thesis that the visual stimulus contains enough information to provide veridical perception of distal objects. However, Gibson's theory does not account for the fact that perceptual responses are inherently stochastic.

Brunswik (ref. 2), on the other hand, proposes the perceptual theory of probabilistic functionalism. Unlike Gibson, he assumes that the perceptual process is random, and that people are continually learning about the validity of the cues of the proximal stimuli. Brunswik proposed that massive ecological surveys be taken to determine the correlations between the range of stimuli and the perceptual response. He, unlike Gibson, felt that a detailed examination of the proximal stimulus would not be a worthwhile course of action because the real scenes observed everyday do not contain these limited number of stimuli. The major criticism of Brunswik's approach seems to be that there is no hope or interest in finding the stimuli which determine the various responses. (See Hochberg (ref. 3) for a further discussion of Gibson's and Brunswik's theories.)

In this paper we present a model of visual space perception which has been influenced by Gibson and Brunswik. Briefly, it models visual space perception by a Bayesian processor which operates on the proximal stimuli; the percept is a conditional probability density function. The model has the advantage that the many stimuli noted by Gibson are incorporated, yet it describes the randomness and ambiguities observed in experiments.

This paper contains a review of the very basic concepts of Bayesian estimated theory; a description and discussion of visual space perception model; a notation of the similarities and differences to signal detection theory in psychophysics; and an application of the model to some experimental results by Kinchla and Allen (ref. 4).

REVIEW OF BAYESIAN ESTIMATION THEORY

In thissection we give a very brief review of some important results in the field of estimation theory. A discussion of the results for estimating constant but unknown parameters is presented first, and a treatment for dynamic systems Markov processes) follows. Jazwinski (ref. 5) and Nahi (ref. 6) are general references.

Let us denote by X the (column) vector of variables which we are trying to estimate, and let $z(t)$ be a vector of "measurements" or variables observed at time t. Let $Z(t)$ be thecollection of all known information up through time t, i.e., the a priori distribution and the set of all measurements taken between t_0 and t; $p(x)$ represents the a priori probability density function of the vector X at t_0. In concept, the Bayesian processor does nothing more than find the conditional distribution of X from the measurements z and the a priori distribution. This is shown schematically in figure **1.**

Parameter Estimation

The Bayesian processor requires the joint probability density function (PDF) $p(x,z)$. Many times this is not available directly and must be calculated from a measurement equation

$$z = h(x,v) \tag{1}$$

and the PDF $p(x,v)$, where v is a vector of observation disturbances. The PDF of x conditioned on one observation z and the a priori distribution, i.e., $Z = \{p(x),z\}$ is given by Bayes' Rule

$$p(x|Z) = \frac{p(x,z)}{p(z)} = \frac{p(z|x)p(x)}{p(z)} \tag{2}$$

where $p(z)$ is the scale factor found by integrating the numerator with respect to x. This conditional PDF can be used to find a variety of estimates, e.g., conditional mean, conditional median, or conditional mode.

Figure **2** shows an example of an a priori probability density function for a scalar x and examples of conditional probabilities that result from particular realizations of z.

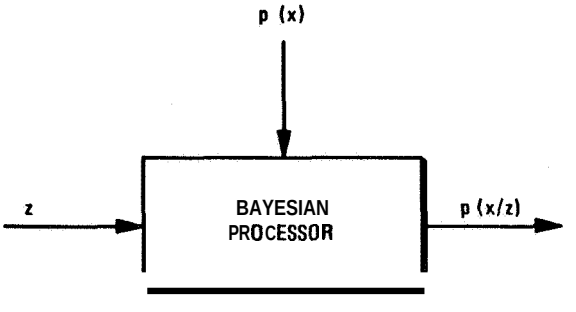

FIGURE 1.—Inputs and output of a Bayesian processor.

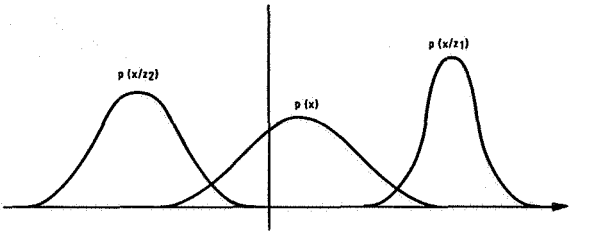

FIGURE 2.—Examples of a priori and conditional probability density functions.

Linear regression is a Bayesian estimation technique which uses the first two moments of $p(x,z)$. For X and z of zero mean, the minimum variance linear estimate $\hat{x}$ is

$$\hat{x} = E(xz^T)E(zz^T)^{-1}z \tag{3}$$

where the superscript T denotes transpose.

Markov Processes

A Bayesian processor for a Markov process can be found when observations related to the state of the process are available. In general the processor computes $p[x(t_1)|Z(t_2)]$ where $x(t_1)$ is the state of the process at time t_1, and

$$Z(t_2) = \{p[x(t_0)],\ z(s),\ t_0 \leq s \leq t_2\}.$$

This corresponds to predicting, filtering, and smoothing when t_1 is greater than, equal to, and less than t_2, respectively.

The Bayesian processor requires the following items to carry out the computations of the conditional PDF. The discussion will be limited to continuous-state, continuous-time situations with the knowledge that the general concepts hold for discrete-state and/or discrete time models.

(1) *The state* equation.—This is an equation which describes the evolution of the state of the Markov process with time. This may be written

$$\frac{dx(t)}{dt} = \dot{x}(t) = f(x(t),\ w(t),\ t) \tag{4}$$

where $x(t)$ is the state at time t, and $w(t)$ a random forcing function (sometimes called the process noise). For equation **(4)** to be a Markov process with state $x(t)$, $w(t_1)$ and $w(t_2)$ must be independent for $t_1 \neq t_2$. It is also referred to as white noise since its power spectral density func-

tion is a constant, that is, it contains equal amounts of power at all frequencies. The prescription of $p(w(t))$ is part of the specification for the state equation.

(2) The *a* priori distribution.—The a priori distribution of $x(t_0)$ is required not only to describe the state before any observations are taken but it is the "initial condition" for the computation of the conditional distribution. The state equation (4) and the a priori distribution can be used to calculate $p[x(t)]$ the a priori distribution of the state for $t > t_0$, i.e., without the benefit of any observations. In general, this requires a solution to a partial differential equation, although the linear-Gaussian ease can be solved with a vector and matrix differential equation for the mean and covariance (Jazwinski (ref. 5)).

(3) The measurement equation.—The measurement equation describes the instantaneous relationship between the observations $z(t)$ and the state. It may be written as in equation (1) but now $z(t)$ is a vector of time functions:

$$z(t) = h(x(t), v(t), t). \tag{5}$$

The observation noise $v(t_1)$ is independent of $v(t_2)$ if $t_1 \neq t_2$; $p[v(t)]$ is needed to complete the description of the measurement equation.

The following example may help to solidify the Bayesian concepts. Suppose we have a linear RC circuit being driven by white noise $w(t)$. We measure the voltage across the capacitor with a voltmeter which gives erroneous readings, and wish to find the probability density function of the capacitor voltage as a function of time. In this case $x(t)$ is the capacitor voltage, $w(t)$ is the input voltage to the circuit, $z(t)$ is the voltmeter reading and $v(t)$ is the source of error in the voltmeter. The result of the calculating $p[x(t)|Z(t)]$ continuously might appear as shown in figure 3 which shows a particular realization for $x(t)$, $z(t)$, and $p[x(t)|Z(t)]$ at several time instants. This conditional PDF can be used to derive an estimate for the voltage at any time.

A MODEL FOR VISUAL SPACE PERCEPTION

In this section we present a probabilistic model for visual space perception that exhibits important characteristics of the human response:

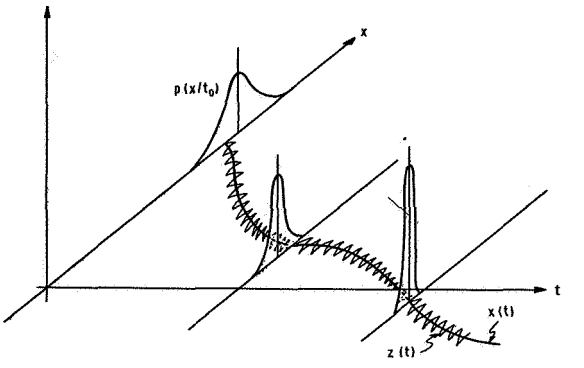

FIGURE 3.—Sketch of conditional probability density function.

(1) On any one trial observers may express uncertainty about objects' relationships (e.g., distance).

(2) Repeated presentation of stimuli results in a distribution of responses. These may fall into multiple categories if the stimulus is ambiguous (for example, the Necker Cube).

The proposed model for visual space perception is shown in figure 4. The central element in this model is a Bayesian processor consisting of a state equation, an a priori distribution, and a measurement equation. The processor operates on $z(t)$, which is the vector of stimuli as modified by the sensory processes, and yields a conditional probability density function for the state. There is some justification for calling this conditional PDF the percept because it recognizes the possibility of uncertainty of interrelationships between objects after observations have been made.

The state equation describes the behavior of the perceiver's knowledge of the distal world. The process noise is used to account for the two types of uncertainties that the perceiver has about the distal world. The first type is the imprecise modeling of distal constraints, e.g., assuming constant velocity motion when an object is actually accelerating. The second type is the degradation of certainty due to imperfect memory process.

The sensory process and/or response processes shown in figure 4 must be of a random nature to yield different responses in different trials to the same proximal stimulus if the parameters of the Bayesian processor remain constant. The determination of these two processes is similar to a problem faced by early users of signal detection

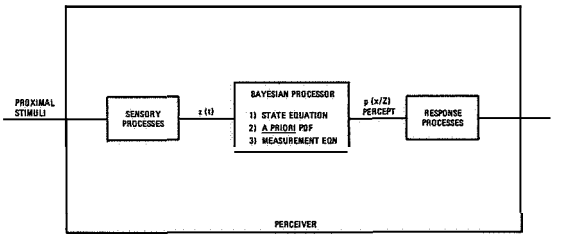

FIGURE 4.—A Bayesian model for visual space perception.

theory in psychophysics, and we postpone discussion on sensory and response processes until the section which compares the Bayesian processor with signal detection theory.

DISCUSSION OF THE MODEL

Rationale for the Model

There are four major reasons for postulating the model described above. The first is that the model is probabilistic: it describes the uncertainty on any one trial through a conditional PDF (the percept), and the ensemble of percepts which may exhibit ambiguous responses. These are two major characteristics of visual space perception.

A second reason for choosing a model of this type is that it provides the capability for modeling perception of state variables of which there is no direct observation. An example of this is the perception of velocity even though only the instantaneous position is contained in the proximal stimulus.

A third advantage of this model is that it provides the capability for modeling space perception in a time-varying dynamic environment. Arbitrary motion of objects relative to the observer or to other objects is allowed, and the static scene used in so many studies (e.g., size-distance, shape-slant) is just a special case. Whether or not the distal stimulus changes, the conditional distribution of the internal state will exhibit transient behavior.

The fourth reason for choosing this model is the possibility for unifying many of the concepts and experimental results in visual space perception. The model is general and perhaps should be considered as a framework for organizing the important variables and their interplay. It is not necessary that all three parts of the model receive equal attention, and in fact, portions of the model might be ignored in certain situations. See the discussion below on how the model might be applied in some specific situations.

Relationship to Other Work

There are two aspects of the proposed model that are related to prior work in human information processing: Bayesian processing, and internal models. Bayesian models have been used to describe decision making (see, for example, Edwards (ref. **7)).** It has been found that humans accumulate information at approximately one half the rate of an optimal Bayesian processor in discrete observations. The same effect can be realized in visual space perception by postulating noise sources to reduce the rate of accumulation of information. The primary difference between the Bayesian model for space perception and the Bayesian decision maker is that the former is more of a reflex action (Brunswick (ref. *2))* whereas the latter involves conscious deliberation and thought.

The concept of an internal model of the distal stimulus has been found useful in other models of information processing (e.g., Carbonell (ref. 8), Smallwood (ref. 9), and Carbonell, Ward, and Senders (ref. 10)). In these papers the internal model is used for extrapolation, that is, to describe the time evolution of the observer's knowledge in the presence of null stimuli; this function is performed by the state equation in the visual space perception model. Another role of the internal model is to relate distal to proximal stimuli, and this is accomplished through the measurement equation in the space perception model.

It is interesting to note that the concept of an internal model may have a physiological basis. In discussing the orienting reflex, Sokolov (ref. **11)** gives some justification for a neuronal model of the stimulus. The orienting reflex is activated when a mismatch occurs between the afferent signals and the extrapolations of the model. On the behavioral level, Berlyne (ref. **12)** uses the concept of the novelty of a stimulus as a determinant of arousal and exploratory behavior. The

very notion of novelty implies a standard for comparing stimuli, i.e., an internal model.

Potential Applications of the Model

The overall purpose of the model is that of predicting visual space perception with some degree of certainty, and that of providing insight into the perceptual process. Very little has been done in the way of experimental verification of this model, so at this point in time no definite statements can be made concerning the constancies of the model nor the range of validity. Corroboration of the model with previously published results is usually difficult because of the lack of proper data presentation to evaluate the model.

However, there are several situations in which the model may prove valuable. One of these is the problem of determining the relative strengths of visual cues and higher order variables in perception, especially in an environment which is more or less uncontrolled (Brunswick (ref. 2)) but which may be measured. This includes the possibility of taking observer motion into account. If the parameters of the model are sensitive indicators, then it might be useful as a descriptor of changes in perceptual response in learning, attention, and other studies.

Application of the Model

The model as presented is limited to visual space perception, i.e., the perception of position, orientation, and motion of objects relative to the observer. The studies of figure, form, etc. cannot be treated in this formulation because they imply spatial processing of the proximal stimulus as opposed to the temporal processing considered here.

The model is general, and one of the major criticisms of it is that there are too many degrees of freedom to provide useful quantitative insight into the perceptual process. Yet the model is simple in concept, and we feel that judicious use of the general framework will be fruitful. Some specific applications have already been carried out by other investigators and one of these (on movement perception) will be discussed in detail.

The basic procedure in determining the form of the model is to first derive an estimate of the conditional PDF of the internal state, and from these experimental data, determine an a priori distribution, a state equation, and a measurement equation which would produce the measured conditional PDF. We note here that the results of this type of analysis will not, in general, yield unique results. First, the number and choice of internal state variables must be determined, that is, the internal state variables might be a subset of the distal state variables, but which subset? Second, there may be intervening parameters incompletely specified for a given input/output function. For example, their sum or product is a known quantity, but no other equations exist.

The freedom in choosing the state equation and measurement equation is immense, yet simplifications in each application can be made to reduce the choice to a manageable level. Care must be exercised, however, since as Brunswik (ref. 2) points out, perception is an irrational process, and assumptions which are reasonable on the basis of physical laws may be inappropriate. However, some general guidelines can be used. In situations involving the (perhaps) complex motion of a simple object, the emphasis should be placed on the state equation since there is no complexity in determining what parameters make up the proximal stimuli. For studies of depth perception, size estimation, and orientation from static scenes, the state equation can be ignored, and the effort concentrated on the measurement equation which contains a myriad of cues (Gibson (ref. 1)) and functional relationships between the proximal stimulus and the elements of the internal state vector. There are many situations, however, where both the state and measurement equations are necessary, as would be the case for depth perception when there is relative motion between the object and the observer.

The a priori distribution represents such effects as experimental set and previous knowledge of the state variables, e.g. "familiar size" in depth perception experiments. (Whether familiar size is beneficial in depth perception or not is another matter.) The conditional PDF may also undergo abrupt changes if discrete (rather than con-

tinuous) measurements are incorporated. This situation arises when a subject is given some feedback on his errors in perception, leading to improved performance, reductions of illusions, etc.

COMPARISON WITH STATISTICAL DECISION THEORY MODELS IN PSYCHOPHYSICS

The main purpose of the application of detection theory in psychophysics is to separate the detectability of a signal from the decision processes of the observer (Green and Swets (ref. **13)).** The Bayesian model of perception is an attempt to model perceptual behavior and to examine the interactions of visual cues and the internal models. In most of the experiments using signal detection theory (SDT), the signal is a single point in signal (state) space, whereas we are dealing with a continuum. Moreover, the stimuli are usually discrete time presentations whereas we are allowing for a continuous presentation of signal and noise.

As a further comparison of the two techniques, we next formulate the signal detection problem as a special case of the Bayesian processor. Although the majority of the work seems to have been done in psychoacoustics (see, for example, Swets (ref. 14)), the original application was in visual detection (Tanner and Swets (ref. **15)).** This exercise will also point up the need for random elements in the sensory and response processes in the Bayesian perception model.

Let x be the signal level which has a probability p of being X and $(1-p)$ of being zero. An observation z of signal x plus noise v is made:

$$z = x + v. \tag{6}$$

Using this information and Bayes' Rule the a posteriori probability density function for x becomes

$$p(x|z) = \frac{p(z|x)p(x)}{p(z)} \tag{7}$$

$$= \frac{p_v(z-x)[(1-p)\delta(x) + p\delta(x-X)]}{(1-p)p_v(z) + p_v(z-X)} \tag{8}$$

where $p_v(\ )$ is the PDF of the observation noise v. Because the a priori distribution of the signal level is limited to two values, the a priori PDF of x is a pair of impulses at $x=0$ and $x=X$, of areas $(1-p)$ and p respectively. The a posteriori PDF remains at two impulses, but of modified areas depending on the distribution of the noise and the observed value of z.

The SDT model assumes that the decision is based on the likelihood ratio * being greater or less than some criterion level. Because the response process is perfect, there must be some source of uncertainty in the model to account for incorrect responses when the proximal stimulus consists of a small signal and no noise. The SDT model, therefore, assumes an internal source of noise between the proximal stimulus, which is the block labeled "sensory processes" in figure 4, in addition to the ideal response process.

As shown in Green and Swets (ref. 13), and as can be easily derived from equation (8), the ratio of a posteriori probabilities and the likelihood ratio are related by

$$\frac{P(x=X|z)}{P(x=0|z)} = \frac{p}{1-p}\ell(z). \tag{9}$$

Since these are monotonically related, the likelihood criterion and the ratio of a posteriori probabilities are equivalent statistics upon which decisions can be based (Green and Swets (ref. **13)).** The most important point, however, is that the wealth of experience in using SDT techniques may be used to great advantage in experimental verification of the model proposed in this paper if the response processes are assumed ideal, and the sensory processes introduce uncertainty. In other words, we can use SDT to help identify and measure the conditional PDFs of the perceptual process.

Perfect response may not always be the most accurate model, however, since the criterion level of the observer may change from trial to trial, and optimal thresholds involve precisely defined probabilities and entries in the payoff matrix which can hardly be expected to be realized internally by the observer (Swets (ref. **14,** ch. **4)).** In addition to these noisy decision processes, faulty memory of the signal will produce behavior not predicted by the model. This can easily be

*The likelihood ratio for this problem is $\ell(z) = p(z|x=X)/p(z|x=0)$.

modelled with the Bayesian processor by defining the signal level to come from the following distribution

$$x = \begin{matrix} 0 & \text{with prob. } 1-p \\ \text{X+m} & \text{with prob. p} \end{matrix}$$

where m is a memory "error" drawn from $p_m(\ )$. The a posteriori distribution of x conditioned on an observation z is then

$$p(x|z) = \frac{p_v(z-x)[(1-p)\,\delta(x) + p \cdot p_m(x-X)]}{p(z)} \quad (10)$$

APPLICATION OF THE MODEL TO VISUAL MOVEMENT PERCEPTION

Experimental Apparatus

In this section we apply a special case of the Bayesian model of visual space perception to the problem of absolute movement perception and use data reported in Kinchla and Allan (ref, **4).** The experiments involve the presentation of clearly visible tungsten sources subtending an angle of 0.036° energized for **0.1** sec. A *stimulus* pattern (Xi) is the successive presentation of two lights with intervening time intervals of **0.5, 1.0, 1.5** or *2.0* sec. The movement *(m,)* of the stimulus pattern is the angular displacement of the second light relative to the first. Stimulus patterns were presented in pairs (with equal probability) to well trained observers familiar with the patterns. This allows the use of SDT to remove the effects of response thresholds from the data.

The Bayesian Model

We now proceed to specify the form of the model for the experiment described above. Four sources of uncertainty will be accounted for:

(1) Unperceived eye movement

(2) Recorded but unexecuted eye movement commands (efferent copy)

(3) Memory uncertainty

(4) Sensory noise.

State equation.—Rather than deal with an explicit form of the state equation, we will be concerned with the conditional distributions which it describes, and these will be considered shortly.

A priori distribution.—The experiment was performed in the dark with almost no information about the position of the first light. Thus we will assume that the a priori position of the light is $N[0, \infty]$.

Measurement equation.—At the time of the first light we assume that the stimulus received by the Bayesian processor is

$$z(0) = x(0) + v(0) \quad (12)$$

where $x(0)$ is the "position" of the light in a stimulus domain and $v(0)$ is sensory noise assumed to be $N[0,\sigma_v^2]$. At the time of the second light we bave

$$z(T) = x(T) + v(T) + w_e(T) \quad (13)$$

where $x(T)$ is the position of the light at time T, $v(T)$ is sensory noise $N[0,\sigma_v^2]$, and $w_e(T)$ is the change in stimulus due to unperceived eye movements, with distribution $N[0,\sigma_e^2(T)]$.

Conditional Distributions

We now present the calculations that would be carried out under the conditions described above. The general form of these calculations may be found in Nahi (ref. **6)** or Jazwinski (ref. *5).*

Because the a priori variance of the initial position is very large (specifically, much larger than σ_v^2), it can be shown that the conditional distribution of $x(0)$ just after the first light $(t=0^+)$ is $N[z(0),\sigma_v^2]$. Just prior to the second light the conditional distribution of $x(0)$ is $N[z(0)+u(T),\sigma_v^2+\sigma_{\text{mem}}^2(T)]$ where $u(T)$ is the effect of unexecuted eye movement commands and $\sigma_{\text{mem}}(T)$ is the increase in uncertainty due to faulty memory.

The stimulus received by the processor at time T can be expressed by

$$z(T) = x(0) + m + v(T) + w_e(T) \quad (14)$$

where m is the movement m_i or m_j. Thus, when $z(T)$ arrives, the Bayesian processor must decide whether it comes from a Gaussian distribution with variance $2\sigma_v^2+\sigma_e^2(T)+\sigma_{\text{mem}}^2(T)$ and mean either $z(0)+u(T)+m_i$ or $z(0)+u(T)+m_j$.

To evaluate the parameters of the model from experimental data, we assume that the ideal decision making portion of the model behaves as follows. Let R_j denote the response "stimulus

S_j," and the probability of this response conditioned on S_j is

$$P(R_j|S_j) = P[z(T) > z(0) + u(T) + m_i + \beta | m = m_j] \quad (15)$$

where β is the threshold criterion relative to the smaller mean of the conditional distributions of $z(T)$. Using equation **(14)** this becomes

$$P(R_j|S_j) = P[x(0) - z(0) + v(T) + w_e(T) - u(T) > \beta - (m_j - m_i)] \quad (16)$$
$$= 1 - F[Z(R_j|S_j)]$$

where $F(\ )$ is the cumulative distribution function for a normalized Gaussian variable, and $Z(R_j|S_j)$ is given by

$$Z(R_j|S_j) = \frac{\beta - (m_j - m_i)}{\sqrt{2\sigma_v^2 + \sigma_u^2(T) + \sigma_{\text{mem}}^2(T) + \sigma_e^2(T)}} \quad (17)$$

Similarly, the probability of response R_j conditioned on stimulus S_i is

$$P(R_j|S_i) = P[z(T) > z(0) + u(T) + m_i + \beta | m = m_i] \quad (18)$$
$$= 1 - F[Z(R_j|S_i)]$$

where

$$Z(R_j|S_i) = \frac{\beta}{\sqrt{2\sigma_v^2 + \sigma_u^2(T) + \sigma_{\text{mem}}^2(T) + \sigma_e^2(T)}} \quad (19)$$

At this point we specify the functional form for the time-dependent variances. In particular it is assumed that

$$\sigma_u^2(T) + \sigma_{\text{mem}}^2(T) + \sigma_e^2(T) = \Phi T \quad (20)$$

where Φ is a constant. This form assumes that the variables are drawn from random walk processes, but as Kinchla and Allan (ref. **4)** point out, there is little if any experimental data on the variances of these variables, although Carbonell et al. (ref. **10)** have found this form to be of some value in other contexts.

Figure **5** shows the equivalent detection problem. The "discriminability index" (Kinchla and Allan, ref. **4)** is the normalized distance between distributions, and is given by

$$D_{j,i} = Z(R_j|S_i) - Z(R_j|S_j) \quad (21)$$

$$= \frac{m_j - m_i}{\sqrt{2\sigma_v^2 + \Phi T}}. \quad (22)$$

The parameters of the model are found by observing the empirical probabilities $\hat{P}(R_j|S_i)$ and $\hat{P}(R_j|S_j)$, looking up the corresponding values of Z in a normal probability table, and then

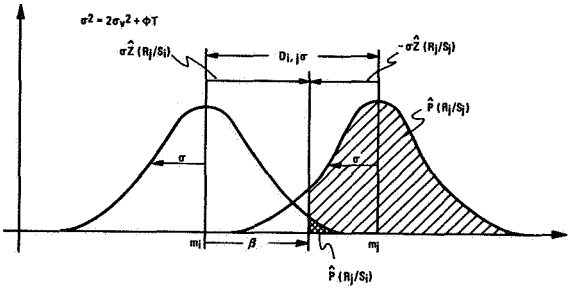

FIGURE 5.—Equivalent detection problem.

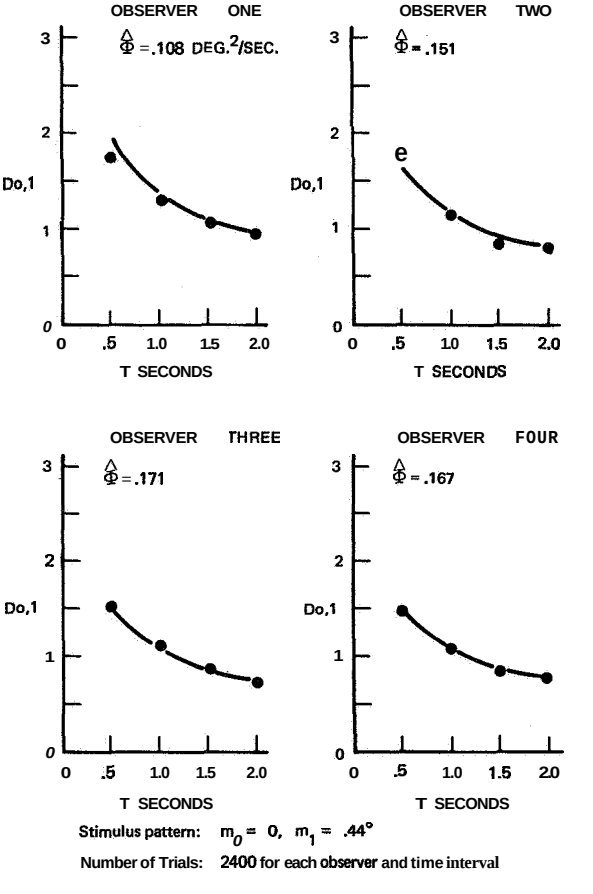

FIGURE 6.—Data from Kinchla and Allan (ref. 4) for stationary judgement task (stimulus pattern: $m_0 = 0$, $m_1 = 0.44°$; number of trials: 2400 for each observer and time interval).

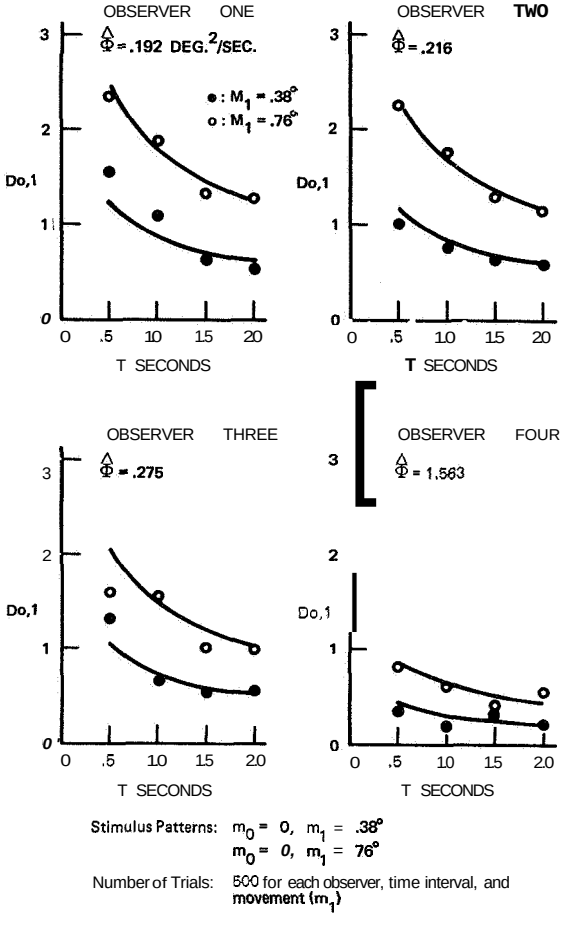

FIGURE 7.—Data from Kinchla and Allan (ref. **4)** for stationary judgement task (stimulus patterns: $m_0 = 0$, $m_1 = 0.38°$, $m_0 = 0$, $m_1 = 76°$; number of trials: 500 for each observer, time interval, and movement m_1).

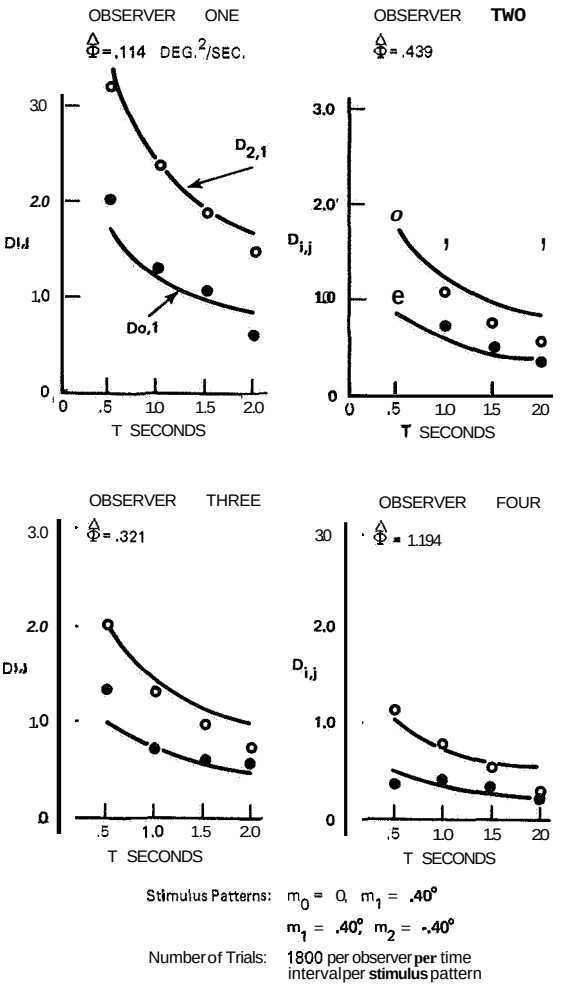

FIGURE 8.—Data from Kinchla and Allan (ref. **4)** for stationary judgment and movement discrimination tasks (stimulus patterns: $m_0 = 0$, $m_1 = 0.40°$, $m_1 = 0.40°$, $m_2 = -0.40°$; number of trials: 1800 per observer, per time interval, per stimulus pattern).

finding $\hat{D}_{j,i}$ from equation **(21).** Those values of $\hat{\sigma}_v^2$ and $\hat{\Phi}$ which give closest agreement in the least squares sense via equation **(22)** are the parameters of the model.

Experimental Results

Figures 6, **7,** and 8 show data from three experiments. The first two are stationary judgment tasks with $m_0 = 0$ and $m_1 = 0.44°$ in experiment **1;** $m_0 = 0$ and $m_1 - 0.38°$ or **0.76"** in experiment **2.** Experiment 3 contained both stationary and directional judgment tasks for which $m_1 = 40°$, $m_2 = -0.40"$ in one pair of stimulus patterns, and $m_1 = 0$, $m_2 = -0.40"$ for the other pattern. These curves are found by minimizing sum of squared discrepancies between the observed statistic and that predicted by the model. In all cases the observation noise σ_v^2 was negligible and the curves are determined by one parameter $\hat{\Phi}$. The model accounts for at least 90 percent of the variance of $\hat{D}$ in all cases, and typically accounts for 95 percent. The behavior of Φ for the four observers is shown in table **1.** Note that there are individual differences for $\hat{\Phi}$ between subjects (which might be the basis for evaluating certain skills), as well as some variation within subjects. It is not known what time interval elapsed between experiments.

TABLE 1.—*Estimates of Φ in Three Experiments (Kinchla and Allan, ref. 4)*

Experiment	Subject 1	2	3	4
1	0.108	0.151	0.171	0.167
2	.192	.216	.275	1.563
3	.114	.439	.321	1.194

CONCLUSIONS

We have proposed a model for visual space perception in which a Bayesian processor provides the percept, a conditional probability distribution of the knowledge of distal objects. This model incorporates desirable qualities of the theories of Gibson and Brunswik and has the potential for unifying many of the concepts and results in visual space perception. Signal detection theory may be considered as a special case of the model, but its primary power lies in its ability to extract percepts independently of response thresholds. The model was applied to the problem of visual movement perception and its parameters evaluated with previously published data.

REFERENCES

1. GIBSON, J. J.: The Perception of the Visual World. Houghton Mifflin Co. (Boston), 1950.
2. BRUNSWIK, E.: Perception and the Design of Psychological Experiments. Univ. of Calif. Press (Berkeley, Calif.), 1956.
3. HOCHBERG, J. E.: A review of Perception and the Representative Design of Psychological Experiments by E. Brunswik. Am. Jour. of Psychol., vol. 70, 1957, pp. 480–485.
4. KINCHLA, R.; AND ALLAN, L.: A Theory of Visual Movement Perception. Psych. Rev., vol. 6, 1969, pp. 538–558.
5. JAZWINSKI, A.: Stochastic Processes and Filtering Theory. Academic Press, 1970.
6. NAHI, N.: Estimation Theory and Applications. John Wiley and Sons, 1969.
7. EDWARDS, W., ED.: Special Issue on Revision of Opinions by Men and Man-Machine Systems. IEEE Trans. on Human Factors in Electronics, vol. HFE–7, Mar. 1966.
8. CARBONELL, J.: A Queuing Model of Many-Instrument Visual Sampling. IEEE Trans. on Human Factors in Electronics, vol. HFE–7, Dec. 1966.
9. SMALLWOOD, R.: Internal Models and the Human Instrument Monitor. IEEE Trans. on Human Factors in Electronics, vol. HFE–8, Sept. 1967.
10. CARBONELL, J.: WARD, J.; AND SENDERS, J.: A Queuing Model of Visual Sampling-Experimental Validation. IEEE Trans. on Man-Machine Systems, vol. MMS–9, Sept. 1968.
11. SOKOLOV, E. N.: Higher Nervous Functions: The Orienting Reflex. Annual Review of Physiology, vol. 25, 1963, pp. 545–580.
12. BERLYNE, D. E.: Conflict, Arousal, and Curiosity. McGraw-Hill, 1960.
13. GREEN, D.; AND SWETS, J.: Signal Detection Theory and Psychophysics. John Wiley and Sons, 1966.
14. SWETS, J., ED.: Signal Detection and Recognition by Human Observers. John Wiley and Sons, 1964.
15. TANNER, W.; AND SWETS, J.: A Decision-Making Theory of Visual Detection. Psychol. Rev., vol. 30, 1954, pp. 922–928.

N73-10129

24. A Proposal for Pre-Processing, Reduction, and Selection of Visual Information in Airborne Flight Simulation

K.-P. GÄRTNER

Forschungsinstitut für Anthropotechnik

Every pilot who has flown on instruments knows the difficulty of learning to translate a number of indicators into a mental image to provide him with the feeling of the attitude, level, and orientation of his aircraft. Even the most intimate familiarity with the cockpit instruments does not lend to the pilot the flight sensation which he knows from the familiar references of the horizon, the earth surface, and the sky.

With the increasing level of aircraft complexity numerous technical sensors have been developed to assist human perception, e.g., radar altimeters, interial platforms, etc. The information picked up by these sensors is presently in most cases still displayed on single independent instruments. In critical situations, however, the pilot is overstrained by observing the wide variity of instruments. The time he has availableto read all instruments relevant to a specific flight situation, frequently is not sufficient for reactions adequate to critical phases of the flight. Furthermore the pilot is known to read preferably only those display parameters which he subjectively selects as important parameters. Thus he becomes a limiting factor for the efficiency and safety of modern man-machine systems.

Integrated displays comprise on a single screen information, which formerly has been obtained by checking a variety of different instruments. The introduction of flexible electronic displays made possible, on the one hand the technical verification of integrated flight displays, and on the other hand the presentation of complex image information.

This development resulted in the need for the selection of the most suitable data to be presented to the pilot in order to facilitate the interpretation of flight situations and to optimize the decision process with regard to the displayed information.

This paper will give a contribution to the solution of this fundamental problem.

For the purpose of onboard visual simulation the image contents of the out-of-the-window scene are to be simulated by technical means. The purpose is to produce artificially as a stimulus field on the eye retina a nearly true image of the heterogeneous textured outside world, in order to obtain a realistic impression of the simulated out-of-the-window scene.

The entire scope of practically relevant complex situations could be covered by the so called "textured" visual flight simulation. This assumes an image generator of very high optical fidelity which, till date is not to be realized technically.

In order to overcome this difficulty, the necessary information contents of the image can be reduced by means of a critical analysis of the information contents of the real world scene. This image analysis and the information reduction derived from this are essentially based on psychological rules and lead to flight scenes of characteristically modified, so-called "stylized" image contents: Coarse structures of the scene remain almost unchanged, while fine structures are simplified or modified. The described procedure, i.e., simulate an artificial out-of-the-window scene by considering the special image contents, is referred to as "stylized visual flight simulation." This method of visual simulation forms an alternative to the textured visual flight simulation mentioned earlier, which processes arbitrary empirical image contents without critical modification.

There are two tasks remaining in regard to application of stylized visual flight simulation:

(1) Clarification as to the image stylization method. In this respect, primarily psychological aspects must be considered.

(2) Examination of technical means for generation of abstracted visual flight scenes.

At first, images are examined as to their subjective information content. Objective and subjective image contents are visual image information carriers. Objective image contents appear as colorimetrically measurable local color valence distributions. The subjective image contents constitute the essential object of the psychological perceptual process. With the perception of the out-of-the-window scene, certain image content elements prove to be of predominant importance for three-dimensional perception, so that these elements have to be reproduced with ahigh degree of fidelity in the stylized visual flight simulation. Other elements are of minor importance and may, therefore, be resorted to for the technically necessary reduction in information capacity by abstraction, without making this process a disturbing factor noticed by the pilot in the aircraft. The image content elements thus compiled and determined to be important constitute the psychological main components for the construction of stylized synthetic visual flight images.

Figure **1** illustrates the difference between the textured and the stylized visual simulation. Both methods aim to create an artificial replica of the outside visual scene. The direct approach via a noncritical empirical detail-by-detail transformation of the environmental information into the simulated image by purely physical methods characterizes the textured visual simulation, whose result would, ideally, be indiscernibly identical with the real scene.

The generation of a stylized image starts from an analysis of the original image contents with

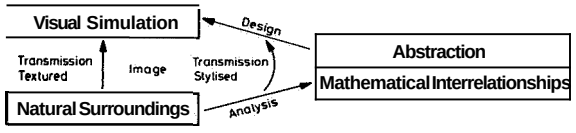

FIGURE 1.—Schematic illustration **of** the stylized visual flight simulation.

respect to mathematical, mainly statistical regularities and to possibilities of simplifying abstractions justified psychologically. The stylized image consequently is built up constructively from the analytical results.

The analysis is compiled by questioning and observation of reactions of test persons. Evaluation of respective statements would require a quantitative perceptual psychology. However, a quantitative psychology is nonexistent, neither is the mechanism of perception understood. However, a rough understanding of the perceptual process briefly described below is assumed to be achieved in perceptual psychology today.

The information acquired by man through his sensors is not processed as an entity by the brain; due to a preprocessing in the sensory areas only a very limited flow of information is fed to the brain. Although this model of the perceptual process is not quantitatively understood as yet, it may be used to justify the stylization of images.

With the knowledge of how preprocessing of visual information takes place such preprocessing, performed already during image generation, appears justified, which means that the eye receives already processed information and that the physiological preprocessing system becomes "unemployed."

Today, the central element of modern aircraft is the electronic computer, and it is the aim to accomplish also airborne visual simulation with computer systems. This requirement poses the question as to whether the information quantities provided by the flight scene can be processed by electronic means. This appears to be possible only with reduced image quality, i.e., image simplification or information quantity reduction, which provides for the desired technical feasibility since it seems quite possible to produce simplified visual flight images with electronic computers. In this case, however, the degree of realism must, at least, be so high that the objective information content is sufficient to supply the pilot with the subjective information required by him.

Therefore only those technical solutions appear usable, which start from a comprehensive description of the original image contents and comprise a subsequent abstraction. The best

applicational future aspects for generators of stylized images result from the selection of suitable flight missions. In these image generators the simplification still acceptable has to be balanced against the psychological and operational fidelity requirements for visual flight scenes.

Now the task remains to examine the technical possibilities for stylized visual simulation. The process of visual flight simulation consists of four subprocesses (ref. **1)** :

image storage→readout→image transformation -+display

The image storage contains the total information to be presented to the pilot during flight (fig. **2).** From this, however, only a small fraction is read out. In image transformation a true perspective of the scene is created.

The result of image transformation is a synthetic true-perspective and true-color visual flight image which is presented to the pilot on board the aircraft.

At present, and presumably for a long time to come, only the cathode ray tube, preferably in the proven form as used in TV, is available for image displays. It is envisaged to generate in a purely electronic manner stylized visual flight images to be displayed by standard TV techniques. After close examination the analog-hybrid computer technique appears to be a very suitable means for the solution of the new task.

As suggestions for solution of the simulation of landing approach, stylized flight images have been verified in a purely electronic manner, employing the analog-hybrid technique (ref. 2).

Figure **3** shows as an example the landing approach scene computed according to the raster method (ref. **3).** Storage of the image content "runway" is achieved through applicable dimensioning of electronic computers, e.g., resistors.

Such an airborne stylized visual simulation

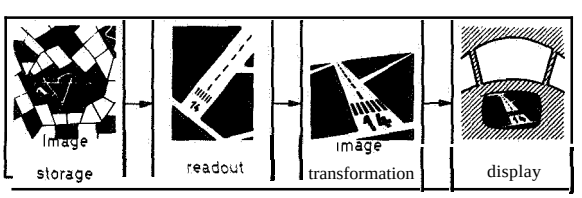

FIGURE 2.—The process of visual flight simulation.

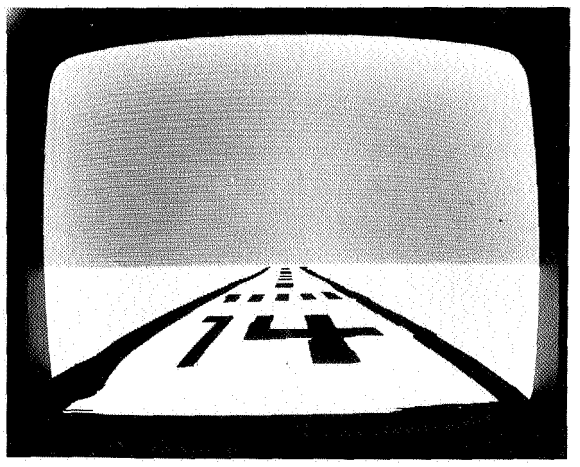

FIGURE 3.—TV screen photograph at a moment **of** a simulated landing approach.

may be used for visibility zero-landing in the future.

The novel methods described permit for the first time by means of an accessory system to the flight instruments of an aircraft the generation of extremely well focused, high-contrast, color-true stylized images on standard TV screens with a very high freedom of maneuver. Future tendencies will presumably aim to utilize the control board computer of the aircraft instead of an independent accessory system, so that the following conclusion should be permissible.

The visual flight simulation onboard an aircraft has up to now been a rather difficult and complex hardware problem. Through abstraction, approaches become evident which suggest that visual simulation of out-of-the-window scenes, e.g., runway will become a software detail in the future and will thus cease to constitute a technical bottleneck within the field of visual flight displays.

REFERENCES

1. GÄRTNER, K.-P.; AND WERNICEE, J.: Verfahren der Sichtsimulation. Zufiihrung und Verarbeitung von Information durch den Menschen, Drei-Nationen-Tagung Mannheim, Sept. 1968—Verlag Krupinski, Mondorf bei Bonn, 1968.
2. GÄRTNER, K.-P. : Stilisierte Flugsichtsimulation. Dissertation, Technische Universitat Berlin, 1970.
3. WERNICKE, J. : Flugsichtsimulation mit Bildspeichern hoher Informationsdichte. Dissertation, Technische Universitat Berlin, 1969.

25. Mapping an Operator's Perception of a Parameter Space*

RICHARD W. PEW AND RICHARD J. JAGACINSKI

University of Michigan

Operators monitored the output of two versions of the crossover model having a common random input. Their task was to make discrete, real-time adjustments of the parameters k and τ of one of the models to make its output time history converge to that of the other, fixed model. A plot was obtained of the direction of parameter change as a function of position in the (τ, k) parameter space relative to the nominal value. The plot has a great deal of structure and serves as one form of representation of the operator's perception of the parameter space.

INTRODUCTION

The major thrust of manualcontrol research, including our own, has been concerned with closed loop, moment-to-moment control of dynamic systems by the human operator, the so-called inner loop control problem. This area is still important and work on it has led to many practical developments. However, as we learn to design more appropriate and sophisticated automatic control systems and to model plants more successfully, more emphasis should be shifted toward understanding man's higher level control processes, such as those involved in adjusting the parameters of an automatic flight control system or in deciding exactly when to override the automatic system to abort a landing.

There are many systems in which men participate directly in process control operations as system optimizers or parameter adjusters. However, there are also many jobs that involve great levels of responsibility for processes, but very little actual controlling. These jobs demand intimate knowledge of the system dynamics. The monitors need to keep abreast of the current status of system variables, but their information and expertise are rarely utilized. They are highly skilled, but it is difficult to specify in a job description exactly what they need to know, for their skills involve subtleties that are hard to express verbally.

One approach to the study of parameter controllers and systems monitors is to analyze their tasks in a decision theoretic structure as Sheridan (ref. 1) or Carbonell (ref. 2) have done: namely, to define the predictability of the information sources probabilistically, to define values and costs for taking samples of information, to derive a performance index, and to postulate what observers *should* do if they are to behave optimally. Although that is a useful and important approach, it has difficulty taking account of the operator's knowledge of system behavior. This probabilistic structure cannot easily capture his level of "understanding" of the system dynamics. The approach taken by Smallwood (ref. 3) and by Kelly (ref. 4) in which a state of internal knowledge is postulated comes closer to the conceptualization presented here.

In the development that follows we are attempting to derive ways of describing the operator's knowledge of the dynamics of a system as it should be used in a parameter control or monitoring situation. We will describe a paradigm, based on that of Nolan (ref. 5), that permits the experimeter to keep track of the operator's parameter adjustments as he converges on a match between a fixed and a variable set of dynamics under his control. By summarizing his

* This research was supported by NASA under contract NSR–23–005–364. The second author was supported by a National Science Foundation Graduate Fellowship. The paper was completed while the first author was on leave as a Visiting Scientist at Bolt, Beranek and Newman.

adjustment behavior at each of several points in a two-dimensional parameter space, we have obtained a crude representation of his uncertainty in choosing which way to move in the space. We believe this representation may be useful for inferring how the operator perceives the space.

METHOD

Figure 1 shows the basic paradigm. Two systems are operated in parallel and are subjected to the same band-limited random input signal. One of the systems has its parameters set to fixed values that remain constant throughout an experimental trial. The other system has parameters that are under the control of the system operator. On a CRT the operator views the inputs to the two systems as two single dots aligned vertically and moving horizontally. The output for each system is represented as a pair of vertically aligned dots 3/4-in. apart and centered about an imaginary horizontal line passing through the corresponding input dot. Since the inputs to the two systems are identical, the operator may compare the relationship between each input and output, or he may pay attention primarily to the two outputs, which will be perfectly aligned in their horizontal motion when the variable system is adjusted to correspond to the fixed one. The subject's task is to adjust the parameters of the variable system from some initial setting until its behavior matches the behavior of the fixed system as closely as possible.

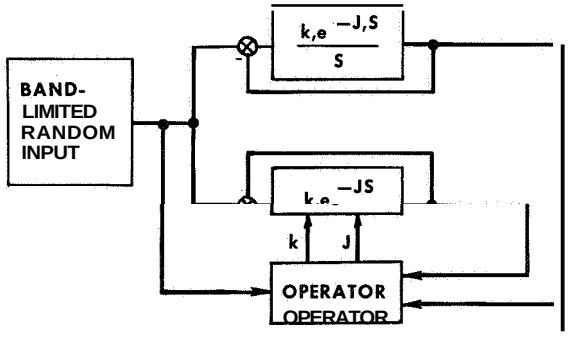

FIGURE 1.—Block diagram showing human operator as a parameter controller that attempts to match the variable parameters k and τ, to the values of the fixed system, k_1 and τ_1.

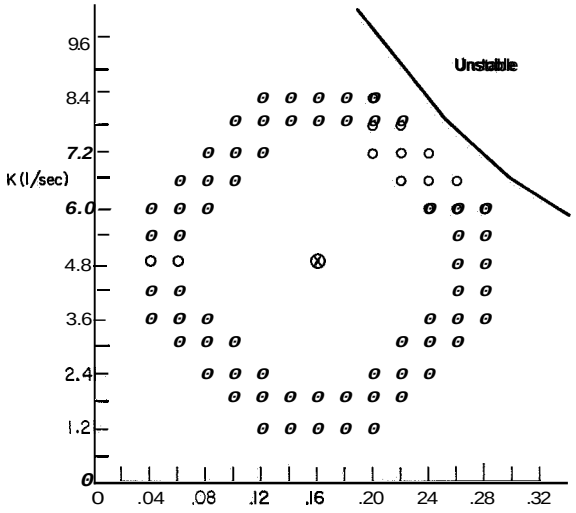

6 sec for the onset of a 700 Hz tone before they could proceed with the next adjustment. They were given 3 min in which to complete all adjustments on a given trial.

In order to give the subjects some initial intuition regarding the effects of the τ and k adjustments, they were told that the displayed inputs represented winding roads, and the displayed outputs represented the centers of two automobiles. The drivers were attempting to keep the centers of their automobiles aligned with the centers of the roads. However, their ability to do this was limited by two factors, τ and k. τ is the driver's reaction time, which is a pure time-delay that elapses before he can *start* to make a steering correction when the road takes a sudden turn. k is the relative "tightness" or "looseness" of the driver, and determines how quickly or slowly he will attempt to complete a steering correction once it has begun. The subjects' task, then, was to match the performance of the driver in the adjustable system to the performance of the driver in the fixed system. Subjects were also told that while these descriptions of τ and k were not meant to be misleading, they were only first order approximations to an accurate verbal description. They were therefore encouraged to characterize the effects of τ and k to themselves through their experience in making the adjustments. They were also encouraged by the original instructions and by trial-to-trial feedback to bring about correspondence with as few parameter changes as possible. The feedback concerned the minimum possible number of adjustments, how many they had made, and how many more, if any, would have been required to make a match.

Three college students who volunteered to serve in paid experiments and had no technical knowledge of control theory participated for 8 days each. They completed 18 trials per day for 4 days in order to complete the set of 72 initial conditions shown in figure 2. One trial for subject A was aborted because of an equipment failure. Each subject was tested in a different random order. On days 5 to 8 they completed a second replication of the 72 conditions in a new random order.

The direction that each subject chose to move at each point in the adjustment trajectory for each initial condition constitutes the major raw data of the experiment. In a few cases, especially for subject A, the adjustments were divergent to the point of exceeding the scaling limits of the parameters. In these cases the subjects were permitted to continue after being told that they had exceeded the limits.

RESULTS

One measure of the subjects' success at parameter control is the number of trials in which they failed to converge on the target values of k and τ within the allotted time. In the first block of days 1 to 4, out of a total of 72 trials subjects A, B, and C failed to converge on 41, 9, and 8 trials, respectively, within the given time limit. During block 2 on days 5 to 8, all subjects eventually converged on all trials.

The data were then analyzed in terms of the grid of possible states in τ-k parameter space in which the operator could find himself in relation to the target position at $k = 4.8, \tau = 0.16$. Depending on the starting point the optimal subject could reach the target position in 5, 6, 7, or 8 moves. Summing over all 72 initial position, the optimal subject would need 492 moves to complete all the trajectories optimally. As an indication of the success of the subjects, on days 5 to 8, the second replication, subjects A, B, and C took 922, 608, and 568 moves, respectively.

For each state in the space at which a trial was initiated or that was reached as a result of the operators' actions, a tally was made of the direction of movement away from that state. An example of such a tally is shown in figure 3. The subjects could decide to increase or decrease τ by one unit or increase or decrease k by one unit. For each state the transition probabilities of movement in each direction were computed. This analysis treats the subjects' behavior at each state as independent of that at every other state, and therefore, as independent of how they got there. This independence assumption permits a rather simple graphical representation of these transition probabilities which is shown in figures 4, 5, and 6. The thin-lined vectors represent the actual transition probabilities on a scale such that the sum of the four possible probabilities equals a unit length of 1 cm. The bold vector

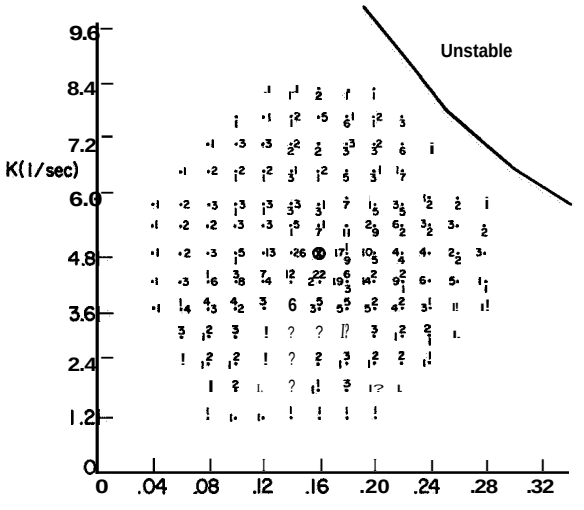

FIGURE 3.—Tally of subject B's movement through the parameter space.

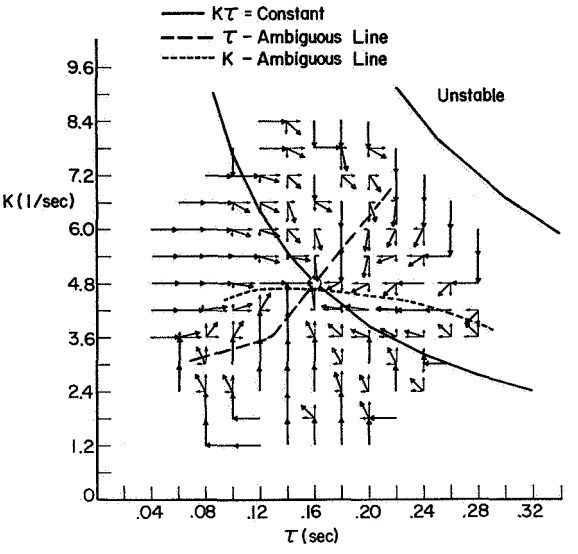

FIGURE 5.—Vector diagram illustrating subject B's average movement through the parameter space to reach the target dynamic condition.

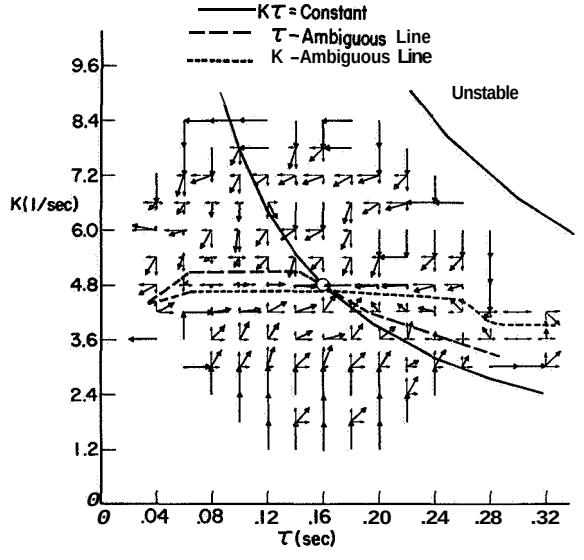

FIGURE 4.—Vector diagram illustrating subject A's average movement through the parameter space to reach the target dynamic condition.

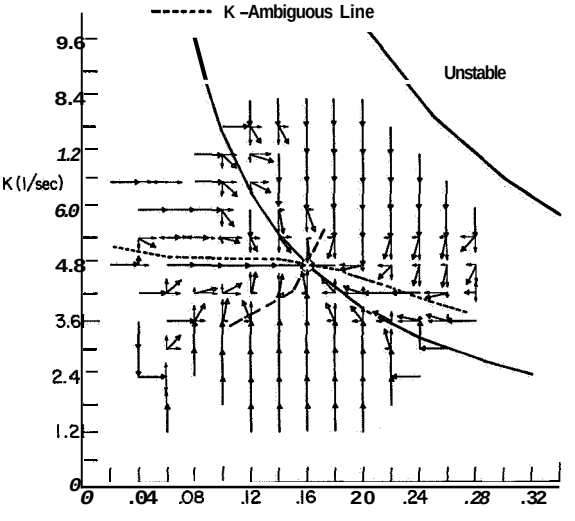

FIGURE 6.—Vector diagram illustrating subject C's average movement through the parameter space to reach the target dynamic condition.

represents the vector sum of the individual components of that state. In the plot for subject A any adjustments made after a parameter boundary was reached have been eliminated from consideration.

Since the states close to the target state are reached more frequently, (refer to fig. 3) the vectors close in are more reliable than those near the 72 starting points. On the other hand, it is also intrinsic to this kind of analysis that the most data are available about state regions where the subjects are least certain what to do since, on

the average, they spend more time making nonoptimal moves in these regions.

DISCUSSION

In general terms, the subjects displayed an impressive ability to decide which direction of change will bring them closer to the criterion condition. Subjects B and C are much more efficient than Subject **A,** but even he is able to converge on all the trials in the second block.

The vector representations of figures **4, 5,** and **6** are remarkably coherent and homogeneous. As one travels down a row or column of states, it is usually possible to observe a gradual change from movement predominant. in one direction to movement in another direction. Even in the case of subject **A,** who does not exhibit as much consistency as the others, it is frequently possible to map trends from state to state within the space. This coherence supports the idea that this record of the direction subjects choose to move from any particular state is indicative of their larger view of the space. They have not learned something that is specific to a particular state, but rather they have acquired a general model of the relation between points in the space and the target parameter values. It would be interesting to test how general this understanding is by measuring subjects' success when the target state is shifted to a new location. How much have they learned about the specific relationship and how much about model input-output behavior at states throughout the space.

Although there is homogeneity of the vector patterns, and, in general, the subjects tend to move efficiently toward the target state, the individual patterns of movement reflect a lack of orthogonality and symmetry in terms of the τ, k coordinates. On the basis of inspection a pair of lines have been drawn on the plots of Figures **4, 5,** and **6** to represent the point of transition from increasing to decreasing k adjustments and increasing to decreasing τ adjustments. In some regions, the path of these partitions of the space are ill-defined; in other areas they are quite well defined. The partitioning curves for subjects B and C are rather similar. For k adjustments, the line of ambiguity corresponds roughly to the $k = 4.8\ \text{sec}^{-1}$ line, implying that the interpretation of k in the subjects' mind corresponded closely with objectively-defined k. The same cannot be said for τ. Subjects B and C agree that the line of ambiguity lies roughly **45°** clockwise from the objectively defined line at $\tau = 0.16$ sec. Subject A's line for ambiguous τ closely resembles the line for ambiguous k, suggesting that perhaps subject **A** did not perceive two independent parameters. In any case, the ambiguous line for τ does not correspond with the $\tau = 0.16$ sec axis. The conclusion from these observations is that the subjects introduce their own distortions and interpretations of τ adjustments, and that it seems likely that a more meaningful transformation of the space might be found.

The stability boundary is shown in figures 4, 5, and **6** and the solid line passing through the target state is a line of constant $k\tau$ product. It represents a level of stability corresponding to a phase margin of approximately **48".** In the case of subjects B and C it appears that the more efficient adjustment might be produced by replacing the τ adjustment control with a new adjustment parameter, z, that would permit simultaneous increases or decreases in k and τ by fixed amounts in the ratio of **0.6** $\text{sec}^{-1}/0.02$ sec. Then, adjusting z would produce movement through the parameter space parallel to the line of ambiguity for τ revealed in this study. Of course, it could turn out that this new choice of adjustment parameters, k and z, is also distorted in a similar manner to k and τ.

OPEN QUESTIONS

This experiment has demonstrated the feasability of obtaining information directly from an observer that is useful for characterizing his general strategies for adjusting the parameters of a dynamic system. This method may also provide some insight concerning the properties of representation or model that these observers develop about the parameter space with which they are working. If such a map could suggest for some realistic systems the choice of parameters that is most directly and easily utilized by human observers, that would be a step forward.

Many questions remain. For example, do control system specialists or pilots deal with the space in the same way naive subjects do? How

sensitive to the location of the target state is the generalized map of the space? Is the assumption of independence of states justified? What are the effects on convergence and map structure of introducing a fixed level of broadband noise in the output of the fixed model? Could subjects learn to match the dynamic properties of the two models if each were subjected to different, linearly uncorrelated, random input signals?

Whether or not this particular approach is ultimately judged productive, the problem of human monitoring and control of the parameters of relatively automatic systems remains an important one in need of further exploration.

REFERENCES

1. SHERIDAN, T. B.: Three Models of Preview Control. IEEE Transactions on Human Factors in Electronics, vol. HFE–7, 1966.
2. CARBONELL, J. R. : A Queuing Model of Many-Instrument Visual Sampling. IEEE Transactions on Human Factors in Electronics, vol. HFE–7, 1966.
3. SMALLWOOD, R. D.: Internal Models and the Human Instrument Monitor. Transactions on Human Factors in Electronics, vol. HFE–8, 1967, pp. 181–186.
4. KELLY, C. R.: Manual and Automatic Control. John Wiley & Sons, 1968.
5. NOLAN, G. R.: Human Response in Matching the Parameters of an Operating Dynamic System. Unpublished SM Thesis, Department of Mechanical Engineering, MIT, June, 1959.

SESSION VI

AUTOMOBILE DRIVING

Chairman GEORGE **A.** BEKEY

26. The Measurement of Driver Describing Functions in Simulated Steering Control Tasks*

DAVID H. WEIR

Systems Technology, Inc.

AND

CHARLES K. WOJCIK

University of California

Measurements of driver describing functions in steering control tasks have been made using the Driving Simulator at UCLA. The simulator facility includes a **1965** Chevrolet sedan mounted on a chassis dynamometer, a moving model roadway and landscape, analog computation for the vehicle's handling dynamics, and a black and white TV camera-projector display system to provide the driver's visual display. The visual image was projected on a **6**×8 ft screen in front of the driver, giving a subtended horizontal angle of about **40".**

The task was to regulate against a random crosswind gust input on a straight roadway, in order **to** stay in the center of the lane. Five male drivers of varying age and driving experience were used in these exploratory studies. Although driving is a multiloop task in general, the forcing function and situation were configured *so* that an inner-loop visual cue feedback of heading angle **or** heading rate would dominate, and the driver's response was interpreted to be primarily single-loop. The driver describing functions were measured using an STI describing function analyzer. Three replications **for** each subject showed good repeatability within a subject. There were some intersubject differences as expected, but the crossover frequencies, effective time delays, and stability margins were generally consistent with the prior data and models for similar manual control tasks.

The results further confirm the feasibility of measuring human operator response properties in nominal control tasks with full (real-world) visual field displays, and they provide some verification and quantification of existing engineering models for the driver and the driver/vehicle system.

INTRODUCTION

Recent experimental studies using the UCLA driving simulator show the validity of simulator results relative to field studies, and provide an estimate of the driver's dynamic response in random input steering tasks. This paper describes the TV-projected model landscape driving simulator and presents experimental measures of driver-vehicle system response. Emphasis is placed on driver steering control of passenger vehicles on two-lane rural roads. Simulated tasks included overtaking and passing maneuvers and regulation against crosswind gusts. By mechanizing the vehicle's equations of motion on an analog computer, a broad range of vehicle handling can be simulated by adjusting the dynamic coefficients.

Simulation is useful in driving research because

- Limiting, critical situations can be studied safely.
- Controlled conditions can be created.

* This paper describes research results which are derived in part from work accomplished in cooperation with the California Business and Transportation Agency and **the U.S.** Department **of** Transportation, Bureau of Public Roads.

- Task variables can be changed systematically.

Typical practice (e.g., refs. **1** through **5)** generates the visual field image with

- Closed-circuit TV on scale models.
- Point light source shadowgram.
- Preprogrammed film.
- Computer generation of roadway abstraction.

The driver's station generally consists of a mockup of seat, controls, instrument panels, and windshield display. It is usually fixed-base, although simple moving-base devices have been used with limited success. Common deficiencies include

- Inadequate visual field size, framing, and reference points to indicate orientation of the driver or vehicle in the external world.
- The lack of realistic vehicle response as reflected in the movement of the displayed cues.
- Improper steering feel and deficient self-centering properties.

These deficiencies can be particularly troublesome in the study of steering control and vehicle handling tasks.

The newly developed simulator at UCLA tries to overcome some of these shortcomings. Its description comprises the next part of the paper. More details of its construction are given in reference **1.** In the remainder of the paper some exploratory describing function results are given for driver response with simulated random-appearing crosswind gust inputs.

SIMULATOR DESCRIPTION

The driver is seated in a **1965** Chevrolet sedan mounted on a chassis dynamometer facing the TV projection screen. A separate room contains the analog computer, **1**:72 scale model landscape, TV camera servo, and associated recording equipment. The setup is shown in figure **1.**

The functional block diagram is shown in figure **2.** The analog computer is an EAI TR–20. It contains the coupled lateral-directional equations of motion for the car which are summarized in appendix A, and provides heading rate and

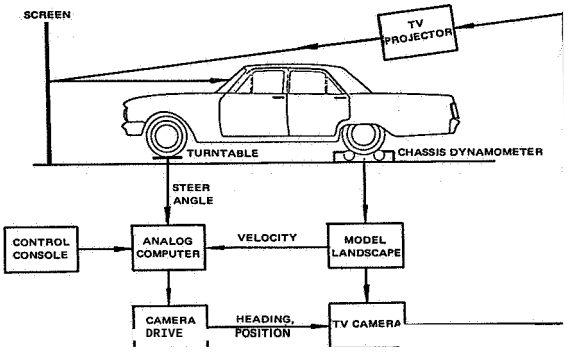

FIGURE 1.—Topological diagram of driving simulator.

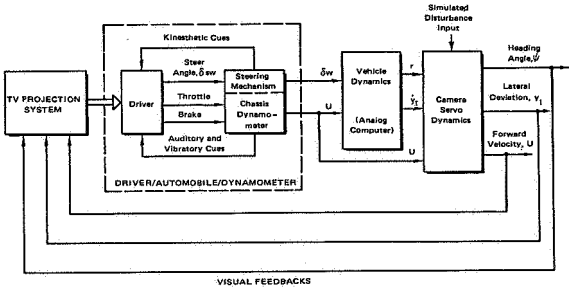

FIGURE 2.—Overall functional block diagram.

inertial lateral velocity signals to the two camera servos. Driver steering actions are fed to the analog computer, and the vehicle handling properties can be modified by changing the dynamic coefficients. Forward speed is controlled by the motion of the model landscape, slaved to the chassis dynamometer. The basic variables are shown in figure 2, using the notation of references **6** and 7. Table **1** summarizes this notation, the units commonly used, and the range of variables expected during simulator operation.

Although the simulator is fixed-base, the vibration of the rear wheels on the dynamometer provides tactile sensation which varies with speed. The car contains conventional power steering, with the front wheels mounted on spring-restrained swiveling turn tables to provide fairly realistic feel and self-centering properties. The self-centering properties are not perfect, however, and there is some hysteresis which the driver must remove to avoid drifts. The speedometer displays twice the actual rear wheel speed (the landscape belt speed is doubled accordingly) in order to keep road noise to a realistic level.

TABLE 1.—*Dejinition of Ximulation Variables*

Variable	Notation	Range
Forward velocity	U or U_0	0–100 ft/sec
Steer angle	δ_w	±0.2 rad
Heading angle	Ψ	±0.2 rad
Heading rate	r	±0.3 rad/sec
Lateral acceleration	a_y	±0.3 g
Lateral velocity	v	±10 ft/sec
Inertial lateral velocity	$\dot{y}_I$	±20 ft/sec
Lateral deviation	y_I	±20 ft

FIGURE 3.—Road scene as viewed by driver.

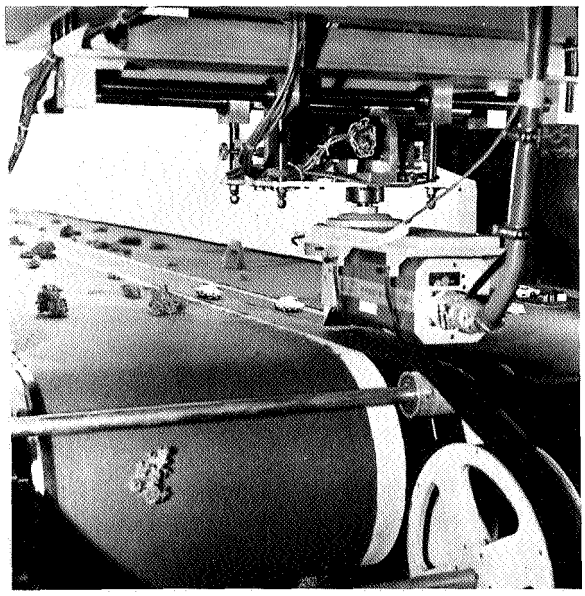

FIGURE 4.—TV camera, other vehicles, and model landscape.

This very approximately doubles the available acceleration rate at any given speed and gives a sensitive throttle response.

The TV camera is a black-and-white GPL Model 1000, with up to 1000 lines horizontal resolution, 15 H_z bandwidth, and a scan rate of 525 lines per frame. The camera lens is an f2.0 Schneider Xenon with 16 mm focal length, operating through two 1.5 in. silvered prisms to lower the optical axis to 0.75 in. (equivalent to a full-scale eye height of 48 in.). The TV projector is a Prizomatic 5XTP, mounted directly above the vehicle. It has a fixed orientation. The included horizontal angle of the visual field is about 40°, and the driver is seated relative to the projected image in correspondence to the camera image. The streamer and geometric cues used for directional control are strong and seem adequate for foveal and parafoveal vision. The resolution of the projected image is such that an object the size of an oncoming vehicle can be distinguished as present (if not identified) at an equivalent full-scale distance of about one quarter mile (the length of the moving belt landscape). The overall impression is one of driving in desert terrain under a heavy, dark overcast. After familiarization, the subjects reported that it seemed very realistic. A typical projected scene as viewed by the driver is shown in figure 3.

Provision is also made to control and measure the position of lead and oncoming cars relative to the subject vehicle. These other vehicles are fixed to tapes (roadway lanes) which move relative to the model landscape. This is shown in figure 4, together with the TV camera mount.

The lack of motion cues always has at least a minor effect on a fixed-base simulation of this type. In driving maneuvers and disturbance regulation the lateral acceleration motion cue provides a useful high frequency (rapid) cue which alerts the driver to an input onset, as well as providing feedback regarding the initial results of his steering response. Without vestibular cues the driver must wait until the change in the visual display exceeds threshold, and this delay is increased by any camera servo deadband. The net effect can be treated as an increase in the driver's effective time delay, and this results in reduced performance potential. In this simulation the effect does not appear to be significant. This is confirmed by the experimental results (ref. 1), which show good comparison between field and simulator results for the same tasks and subjects.

SIMULATED VEHICLE DYNAMIC RESPONSE

Several vehicles with different handling properties have been simulated to date. The one used in the experiments reported here was a nominally loaded full-size station wagon with less than ideal handling properties.

The assumed design parameters and vehicle stability derivatives are given in table *2*, using the notation of the appendix to this paper. Substituting these stability derivatives into the lateral-directional equations of motion and rearranging, gives the following vehicle motion to steer angle input transfer functions.

Lateral velocity:

$$\frac{v}{\delta_w} = \frac{91(s-16.4)}{[s^2+2(.79)(3.3)s+(3.3)^2]} \qquad (1)$$

Heading rate:

$$\frac{r}{\delta_w} = \frac{19.5(s+2.8)}{[s^2+2(.79)(3.3)s+(3.3)^2]} \qquad (2)$$

Lateral deviation (position in lane):

$$\frac{y_I}{\delta_w} = \frac{91[s^2+2(.19)(7.4)s+(7.4)^2]}{s^2[s^2+2(.79)(3.3)s+(3.3)^2]}. \qquad (3)$$

The dynamic response properties are similar to those of the test vehicle used in prior field experiments (ref. 8).

The analog computer diagram is shown in figure **5**. The kinematic variation of speed in the equations (i.e., the $U\psi$ term) was accounted for by using the speed sensed by a belt-driven tach-generator. Some of the stability derivatives Y_v, Y_r, N_v, and N_r are inversely proportional to speed in the nominal driving range (**45** to **60** mph), however, fixed settings corresponding to **60** mph were used for simplicity. Where possible, the experimental tasks were planned for a constant **60** mph. Operation at speeds below the design values results in a less responsive vehicle than would normally be the case if the derivatives were speed varying (see ref. **6).**

TABLE 2.—*Dynamic Parameters for Simulated Car*

Design parameters		Stability derivatives	
m, slugs	151	Y_v, sec^{-1}	−2.8
U_0, ft/sec	88	Y_r, ft/sec-rad	1.33
Y_{α_1}, lb/rad	6860	N_v, rad/ft-sec	.05
Y_{α_2}, lb/rad	11700	N_r, sec^{-1}	−2.45
a, ft	5.77	Y_{δ_w}, ft/sec^2-rad	91
b, ft	4.14	N_{δ_w}, sec^{-2}	19.5
I_z, slug-ft^2	4060	N_v, rad/ft-sec	−,003
ℓ, ft	9.91	Y_v, sec^{-1}	−,035

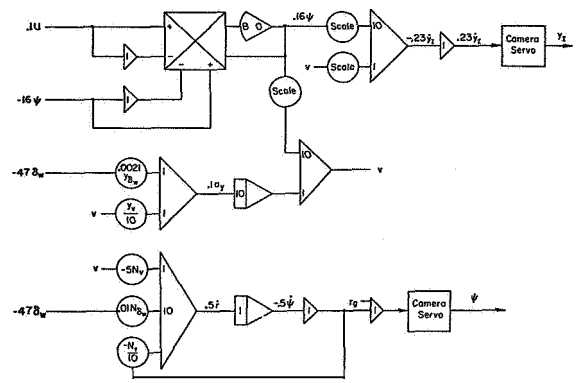

FIGURE 5.—Analog computer mechanization.

Although the analog computer provides a good representation of the vehicle's steering response, the camera servo drive for heading has a small amount of backlash which results in a deadband and hysteresis. The magnitude of the deadband is less than a degree, but it may be important for small heading corrections and accurate disturbance error regulation.

OVERTAKING AND PASSING EXPERIMENTS

A major objective of the overall research study was to replicate full-scale field measurements of driver control for simulator validation. Previously published response and performance measurements for overtaking and passing tasks with and without an oncoming vehicle (ref. 8) provided a useful field data base. These tasks were repeated in the simulator using the same driver subjects so that at least some subjects served as their own control. If transfer effects are negligible, for these subjects any differences would be due to physical effects such as lack of vestibular cues, degree of visual realism, and differences in handling dynamics.

Details of these experiments are given in reference **1.** To summarize, the simulator results

were in good agreement with the previously published field data (ref. **6)** for comparable tasks. The same relative changes occurred in field and simulator as the tasks changed. With comparable controlled element dynamics and the same driver subject, both the absolute levels of driver/vehicle response in a given task and the magnitudes of the change between situationswere quite similar in field and simulator. These results confirmed the validity of the simulator task with respect to evoked response and performance for nominal steering tasks.

RANDOM CROSSWIND GUST EXPERIMENTS

In contrast to overtaking and passing, continuous closed-loop operation by the driver dominates in the presence of a random-appearing disturbance input such as a crosswind gust. With continuous control, on-the-average frequency response properties of the driver can be measured as a describing function.

Models for the driver in continuous control task have been described previously (e.g., refs. **7** and **9).** Several feedbacks such as heading angle or rate, and path angle or rate, were shown to be good "inner-loop" control cues; while a necessary "outer loop" for trim control seems to be lateral deviation in the lane. With a dynamic simulator of the sort used in the experiments it is possible to structure regulation tasks and measure the driver's response under the interpretation that certain feedbacks are dominant; and this is accomplished below. Investigation of the more fundamental question of which feedback structures are operant in a given driving situation requires extension of these experimental techniques, and has yet to be accomplished.

These experiments were set up so that the driver's steering response resulted from his operation on heading angle, ψ, and lateral deviation y_I cues. The multiloop block diagram for this case is the simplified version of figure 2, as shown in figure **6.** The driver's task is to maintain the car in the center of the lane (at **60** mph) in the presence of the equivalent crosswind gust signal.

Because only one gust input is being used, the analyses concentrated on the middle and high frequency driver response data which are dominated by the heading disturbance in this task. Then the lateral deviation outer loop is assumed to result in low frequency corrections to reduce errors which accumulate despite the driver attempting to maintain the car's heading parallel with the roadway. The fidelity of the measurements is reflected in the linear correlation in the data between the disturbance input and the driver's steering response, as measured by $\bar{\rho}_e^2$.

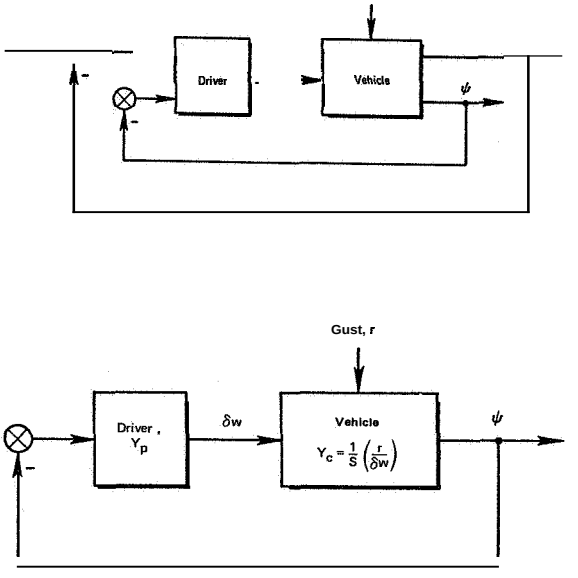

FIGURE 7.—Simplified system for data interpretation.

With this interpretation, the driver/vehicle system takes the single-loop form of figure **7,** which accounts for its dominant characteristics in this task. The vehicle's dynamics Y_c are given by integrating the heading rate to steer angle transfer function in equation (2); and the result is approximately a simple integration or K/s controlled element; i.e.,

$$Y_c = \frac{\psi}{\delta_w} = \frac{1}{s}\left(\frac{r}{\delta_w}\right) \doteq \frac{K_c}{s}. \tag{4}$$

In this case the driver model Y_p takes the form of a pure-gain-plus-time-delay,

$$Y_p = \frac{\delta_w}{\psi_e} = K_p e^{-\tau_e j\omega} \tag{5}$$

as shown in references **7** and **9.** The complex frequency $j\omega$ is used (instead of s) in the driver

describing function because the describing function is computed by taking the ratio of cross spectra which are Fourier transforms.

The heading rate gust disturbance signal r_g was a random-appearing sum of equal amplitude sine waves with component frequencies at 0.5, **1.26, 3.0,** and **6.3** rad/sec, and an rms amplitude **of 1.8** deg/sec. The camera servo acted as an integrator which produced a heading angle disturbance that rolled off at **20** dB/decade, **as** if low pass filtered. The resulting heading angle disturbance appeared to have a bandwidth of about **0.7** to **1.0** rad/sec on the display, with an rms amplitude of approximately **1.7°.** The subjective effect is not unlike that of driving a very gust–sensitive car in an intermittent crosswind.

DRIVER DESCRIBING FUNCTION DATA

The driver model (ref. **7)** provides for his equalization of the vehicle dynamics such that the combined driver/vehicle system properties are approximately invariant. The result is that the driver/vehicle describing function for closed-loop operation on a displayed cue has the general form:

$$\frac{\psi}{\psi_e} = Y_p Y_c \doteq \frac{\omega_c}{j\omega} e^{-(\tau_e j\omega + \alpha/j\omega)} \qquad (6)$$

where Y_p is the driver and Y_c is the controlled element. The parameter ω_c is the Bode crossover frequency (or closed-loop system gain) and provides a good estimate of the driver/vehicle system bandwidth. The effective time delay is τ_e as shown in equation (5). The additional parameter α accounts for the driver's low frequency phase lag (often attributed to his neuromuscular properties) which is sometimes observed.

The output-to-error describing function of equation **(6)** was measured directly, on-line, using a Systems Technology, Inc., Describing Function Analyzer (DFA), Model **1001.** This DFA also supplies the random-appearing heading rate disturbance input described above. The driver describing function Y_p is computed from ψ/ψ_e by dividing by the assumed vehicle dynamics or controlled element, $Y_c = \psi/\delta_w$. Each experimental run lasted **100** sec.

Estimates of driver/vehicle model parameters given in equation **(6)** have been made using the DFA results for several runs on each **of** five driver subjects whose backgrounds are given in

TABLE 3.—*Subject Background*

Subject	Age	Years driving	Personal vehicle	Passes on rural roads in last: Month	Passes on rural roads in last: Year	Remarks on simulator realism
B	**48**	**18**	Mercury Comet **(1962)**	**0**	**10**	.....
C	**23**	**7**	Ford Econoline Van **(1969)**	...	...	Steering oversensitive. Simulation seemed OK for cues.
D	**34**	**18**	Ford Mustang **(1965);** VW squareback **(1969)**	**15**	**50**	Vehicle response realistic. Easy to project oneself into task ***so*** that lack **of** visual field acuity and limited peripheral cues are not noticed. Lateral acceleration cues are missed in first fraction of second following steering inputs.
E	**30**	**14**	Volvo **144 (1968)**	0	**20**	Visual scene like heavy overcast with light rain. Some ill effects due to lack **of** motion cues. Vehicle seemed somewhat oversensitive and gusts were too lively. Considering limitations, however, simulator seemed surprisingly realistic.
F	**30**	**13**	Buick station wagon **(1964);** Karman Ghia **(1968)**	**10**	**30**	Couldn't judge center **of** lane well. Vehicle handled naturally. Visual scene was like light snow condition.

table **3.** The individual data runs are shown in figure 8(a) through (e), with Y_pY_c on the right and the computed Y_p on the left. The averaged parameters for the fitted Y_pY_c curves are summarized in table **4.** Also shown in table **4** are the closed-loop phase margin φ_m, gain margin G_M, and zero phase margin crossover frequency, ω_u, which relate to system stability and the quality of control. The average linear correlation, ρ_e^2, is the fraction of the total heading rate error which is linearly correlated with the gust input—the average coherence. Values in the range of 0.5 to **0.6** indicate that the majority of the driver's steering actions are heading angle or heading rate corrections that are correlated with the gust input, and these values are consistent with comparable instrument panel data. σ_e^2/σ_i^2 is the heading rate error variance over the heading rate input r_g variance, and the larger values in figure 8 may imply that the driver is using a low frequency heading bias to correct residual errors in lateral deviation (see fig. **6).**

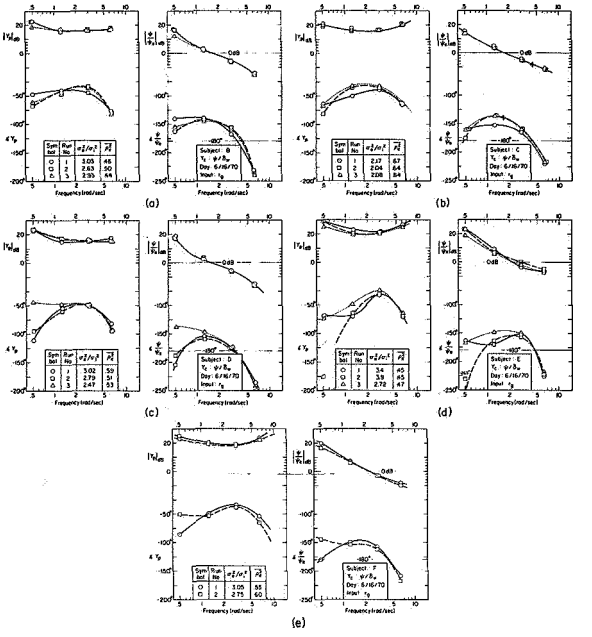

FIGURE 8.—Describing function data.

The dominant features of the data are the consistent similarity in crossover frequency, effective time delay, and stability margins. This is not only true within one subject (as expected), but over all subjects. The crossover frequency is bounded on the low side by the gust bandwidth—the former has to be nearly twice the latter to achieve effective control (e.g., ref. 9). Crossover frequency is limited on the upper side by the effective time delay (due to driver and car) and stability considerations. The repeatability in the data is associated with these task-related constraints.

The measured driver response properties and stability margins are compatible with inner-loop crossover frequency predictions made for similar vehicle/task situations in prior studies (e.g., refs. **7** and **S),** suggesting that heading angle is a reasonable inner-loop cue in the multiloop driver/vehicle system structure. Note that lagged heading rate is a reasonable alternative, but simple proportional operation on (unlagged) heading rate is not a compatible alternative because **(1)** it is inconsistent with the previously noted form of Y_pY_c based on a large body of prior data, and **(2)** the effective gust bandwidth of **6.3** rad/sec would then be prohibitively large. Finally, the observed values of τ_e and φ_m are more consistent with prior data for $Y_c=K/s$ (i.e., heading angle) than for $Y_c=K$ (i.e., heading rate).

The "peaking up" of the high frequency amplitude ratio for subjects C, E, and F, in figure 8(b), (d), and (e), indicate that they are using lead equalization to offset the additional high frequency lag in the simulated car. The result is

TABLE 4.—*Summary of Describing Function Results*

Subject	ω_c, rad/sec	φ_m, deg	G_m, dB	τ_e, sec	ω_u, rad/sec	ρ_E^2
B	**1.7**	**35**	**8.3**	**0.34**	**3.8**	**0.47**
C	**1.8**	**36**	**7.5**	**.35**	**4.1**	**.65**
D	**1.7**	**24**	**6.9**	**.41**	**3.3**	**.54**
E	**2.9**	**27**	**2.9**	**.24**	**4.3**	**.46**
F	**2.3**	**28**	**5.6**	**.32**	**4.3**	**.58**

reflected in table 4 as a lower effective time delay which in turn permits a higher crossover frequency (with the same stability margins) and better gust regulation performance. The stability margins for each driver are large enough to give smooth (comfortable) response, as well as rapid error reduction. The α measures are somewhat unreliable because they represent a least square fit to only the middle two frequency points.

These exploratory data show that repeatable measures of driver response in closed-loop steering control tasks can be made. Not unexpectedly, the results are consistent with predictions from prior (empirically derived) driver/vehicle models, and they provide added insight into the multiloop feedback structure the human operator may adopt when provided with a cue-rich, real-world visual field.

CONCLUSIONS AND IMPLICATIONS

A major objective was to implement and exercise a driving simulator useful in the study of driver control processes, and to establish the validity of simulation results by comparison with published field data for similar subjects and tasks. This has been accomplished. The dynamic response and performance of the simulator are subjectively realistic, and it yields data which are similar to field data. It also shows the same sensitivity to variations in tasks and conditions as the field data. By mechanizing the vehicle's differential equations on an analog computer, a broad range of vehicles can be simulated by simply adjusting dynamic coefficients.

Driver describing functions have been measured in a simulated crosswind gust regulation task. These exploratory results were repeatable and compatible with existing driver/vehicle system models. The numerical parameters confirmed prior estimates of closed-loop properties and provided new insight to the possible driver/vehicle system multiloop structure.

ACKNOWLEDGMENTS

The authors wish to thank Richard Klein and R. Wade Allen of Systems Technology, Inc., for their assistance in simulating the vehicle dynamics and accomplishing the driver describing function measurements; and Richard Maynard of the Institute of Transportation and Traffic Engineering, UCLA, for his part in operating and maintaining the simulation system.

REFERENCES

1. WOJCIK, C. H.; AND WEIR, D. H.: Studies of the Driver as a Control Element, Phase No. 2. Rept. 70–73, UCLA Inst. of Transportation and Traffic Engineering, July 1970.
2. ANON.: Proceedings of a Conference on Mathematical Models and Simulation of Automobile Driving. Mass. Instit. of Tech. Sept. 28–29, 1967.
3. HULBERT, SLADE: Survey and Comparisons of Simulation Techniques for Automobile Driving Research. Paper No. 69–WA/BHF–11, ASME, Nov. 1969.
4. ANON.: Proceedings of General Motors Corporation Automotive Safety Seminar, No. 24. July 11–12, 1968.
5. SUNAGA, KAZUO; IIDA, SHIN; AND FUJIOKA, SHIZUO: A Driving Simulator for Stability of a Motor Vehicle. Stability and Control Committee, Society of Automotive Engineers of Japan, Inc., Oct.–Nov. 1969.
6. WEIR, D. H.; SHORTWELL, C. P.; AND JOHNSON, W. A.: Dynamics of the Automobile Related to Driver Control. Tech. Rept. 157–1, Systems Technology, Inc., July 1966 (also SAE Paper 680194).
7. WEIR, DAVID H.; AND MCRUER, DUANE T.: A Theory for Driver Steering Control of Motor Vehicles. Highway Research Record No. 247, 1968.
8. WEIR, DAVID H.; ALEX, FREDERIC R.; AND RINGLAND, ROBERT F.: Driver Control During Overtaking and Passing Under Adverse Conditions. Tech. Rept. 174–1, Systems Technology, Inc., May 1969.
9. MCRUER, D.; AND WEIR, D. H.: Theory of Manual Vehicular Control. Ergonomics, vol. 12, no. 4, 1969, pp. 599–633.

APPENDIX

Lateral-Directional Vehicle Dynamics

The lateral motions of a car which dominate in steering control and are represented in the simulator system are shown in figure **A–1.** The symbols are defined in table **1.**

The lateral-directional matrix equation for a car with lateral velocity v and heading rate r degrees of freedom are derived in reference **6** and summarized below:

$$\begin{bmatrix} s-Y_v & U_0-Y_r \\ -N_v & s-N_r \end{bmatrix}\begin{bmatrix} v \\ r \end{bmatrix}=\begin{bmatrix} Y_{\delta_w} \\ N_{\delta_w} \end{bmatrix}\delta_w+\begin{bmatrix} Y_{v_g} \\ N_{v_g} \end{bmatrix}v_g \qquad \text{(A–1)}$$

s is the Laplace Transform complex variable. The front wheel steer angle is δ_w and v_g is a lateral velocity gust. The stability derivatives are defined in terms of vehicle and tire design parameters by the following expressions:

$$Y_v=\frac{-2}{mU_0}(Y_{\alpha_1}+Y_{\alpha_2})$$

$$Y_r=\frac{2}{mU_0}(bY_{\alpha_2}-aY_{\alpha_1})$$

$$N_v=\frac{2}{I_{zz}U_0}(b\,Y_{\alpha_2}-aY_{\alpha_1})$$

$$N_r=\frac{-2}{I_{zz}U_0}(a^{2}Y_{\alpha_1}+b^2Y_{\alpha_2})$$

$$Y_{\delta_w}=\frac{2}{m}Y_{\alpha_1}$$

$$N_{\delta_w}=\frac{2a}{I_{zz}}Y_{\alpha_1}$$

$$Y_{v_g}=\frac{qA}{mU_0}C_{y_{\beta_g}}$$

$$N_{v_g}=\frac{qA\ell}{I_{zz}U_0}C_{n_{\beta_g}}.$$

The design parameters on the right of these equations are as follows

- m is the total vehicle mass
- U_0 is the nominal forward velocity
- Y_{α_1} is the side force due to front tire slip angle
- Y_{α_2} is the side force due to rear tire slip angle
- a is the distance of the c.g. aft of the front axle
- b is the distance of the c.g. aft of the rear axle
- I_{zz} is the total vehicle yaw moment of inertia

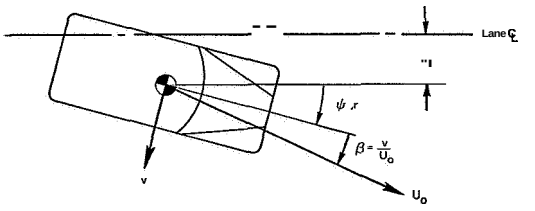

FIGURE A-1.—Motion quantities for directional control.

q is the aerodynamic pressure
A is the projected frontal area
$\ell = a + b$ is the wheel base
$C_{y_{\beta_0}}$ and $C_{n_{\beta_0}}$ are the aerodynamic coefficients.

More detailed descriptions are given in reference 6.

Normally $|Y_r|$ is much less than U_0. Another simplification shown in equation (A–1) is the deletion of the gust terms (Y_{v_g} and N_{v_g}) from the left-hand side because they are small relative to the tire forces and moments (Y_v and N_v) at reasonable speeds. They are included on the right side to provide for force and moment disturbance inputs to the simulation.

These two-degree-of-freedom equations do not include the roll mode. It can have considerable influence on them by modifying the effective Y_{α_1} and Y_{α_2}, mainly due to roll steer and camber thrust effects. Knowledge of the complete three-degree-of-freedomequations and data allows this correction to be made in the two-degree-of-freedom model. Another result of including a roll degree of freedom is the appearance of a usually inconsequential high frequency dipole pair in the lateral-directional transfer functions. Hence, the two-degree-of-freedom equations used in the simulation reflect the major effects of the roll without including it explicitly.

N73-10131

27. Some Interactions Among Driver, Vehicle, and Roadway Variables in Normal Driving

MALCOLM L. RITCHIE, JOHN M. HOWARD, AND W. DAVID MYERS

Wright State University

At the Fourth Annual Manual (ref. 1) I reported on a study of driving behavior in which we had related lateral acceleration in curves to the forward velocity. We plotted the data for 50 subjects, each of which drove a course containing 227 identifible curves. The relationship which was obtained was

$$g = P - 0.068\left(\frac{v}{20} - 1\right) \qquad (1)$$

where g is the lateral acceleration in gravitational units, P is a constant for an individual but variable between individuals (90 percent of the P values were between 0.33 and 0.19 g) and V is the forward velocity in miles per hr between 20 and 60. Since then we have gathered more data, have read some interesting reports by others, and have thought more about the problem. In this report I will discuss all three developments.

In the January 1971 issue of Sports Car Graphic there is an article entitled, "World's Most Advanced Race-Driving School" (ref. 2). At this school aspiring drivers drove an instrumented car which allowed them to study their individual performance. The instrumentation produced a recording of lateral acceleration and forward velocity. The results for the aspiring drivers were compared with those for Mark Donahue in an effort to discover why Donahue could beat them through the course.

The velocity and lateral acceleration data for Mark Donahue were presented in such a way that an equation could be derived to express the relationship between g and V for those curves in which he had a free choice of speed. For Mark Donahue the expression is

$$g = 1.25 \qquad (2)$$

No velocity term is in the expression because the lateral acceleration did not vary with velocity. The car would stay on the road at 1.25 g and apparently Donahue's technique for each curve was to achieve and hold that speed which produced 1.25 g.

We may assume that the vehicle used by Mark Donahue would lose adhesion at a g value slightly higher than 1.25. It is estimated that the Buick station wagon which was used in all our experiments will lose adhesion at about 0.67 g. Where Mark Donahue stayed at something like 98 percent of breakaway g at all speeds, our ninetieth percentile driver achieved 50 percent of breakaway g at 20 mph, and eased off to about 30 percent at 60 mph.

We have become a little more ambitious and would like to be able to account for vehicle and roadway variables in addition to personal variables. We can expand equation (1) as follows:

$$g = (P_1, P_2 \ldots P_n)(v_1, v_2 \cdots v_n)(R_1, R_2, \ldots R_n) - 0.068\left(\frac{V}{20} - 1\right) \qquad (3)$$

where P_1, P_2 etc., are the family of personal variables, v_1, v_2 etc. are the family of vehicle variables, and R_1, R_2, etc. are the family of roadway and environmental variable. We have begun to consider which variables in each family account for most of the variance.

In the first study of this series (ref. 3) we found that men drove faster and pulled more lateral g's than women. Partially completed analyses suggest that most of this difference may be due to the fact that men drive more miles per year than women. In addition to miles per year we have some data on driver's age, number of years driving,

and hand dominance. We have found no significance to age and number of years driving. Our left-handed drivers drove faster than right handed, but the number is too small to be conclusive. In observing our subjects it appeared that there was a relatively large variability due to level of aspiration. Some subjects appeared quite in awe of the experimenter, while others appeared to be making a game of trying to toss the recorder in his lap. We plan an experiment soon in which we hope to measure the influence of the subjects' understanding of what he is trying to do.

In the original experiment all the subjects were run in the same vehicle, a **1962** Buick Invicta station wagon with power steering and brakes. Experimental controls were applied to insure that no vehicle variables entered into the experiment. Since the original study we have run **60** more subjects (making **110** total) in the same car on the same **110** mile course over Ohio state highways. Fifteen of these were run with the tire pressure lowered to **21** lb cold (from the standard **29).** Another **15** subjects were run with the speedometer covered. The same Buick station wagon was used for these runs also. Low tire pressure was used as a simple way to get a change in the vehicle's dynamic characteristics. The covered speedometer eliminated some of the information which the machine normally provides the driver. Fifteen more subjects were run through the course at night, and a final **15** subjects acted as a control group, repeating the conditions of the first experiment.

The results of these four conditions are shown in figures **1** and **2.** The data points for each curve are grouped by the mean velocity for that curve in the first experiment. Figure **1** shows the recorded speed plotted against the reference speed for each curve. It will be seen that the speeds for the night and the control condition are indistinquishable statistically from each other, but both may be distinquished from the low tires and the no speedometer condition, which are in turn indistinquishable from each other. The general statement is that the group with low tires and the group with no speedometer drove faster than the control group, but the night group did not drive faster than the control.

Figure **2** shows lateral acceleration plotted

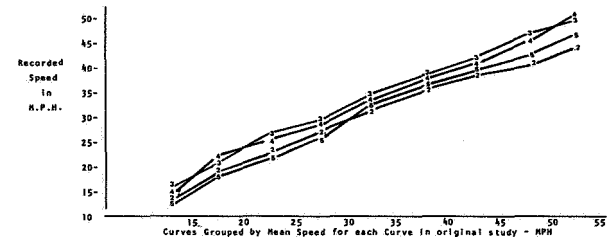

2 Night	Mean	13.106	18.856	22.806	27.131	31.369	36.031	39.056	41.756	14.331
	S.D.	2.344	3.027	2.667	3.612	3.662	4.198	4.461	4.200	4.343
3 Speedometer	Mean	15.753	20.053	26.187	30.060	35.500	39.353	43.407	46.780	49.293
	S.D.	2.488	5.948	5.023	1.170	4.252	3.936	4.269	5.169	5.417
4 Low Tires	Mean	16.269	22.197	24.607	28.240	33.313	37.993	41.600	45.767	49.367
	S.D.	2.883	5.187	3.437	3.859	4.504	4.973	5.142	5.281	5.966
5 Control	Mean	12.629	18.821	22.421	26.864	32.036	36.307	40.171	43.450	46.714
	S.D.	2.632	3.352	3.122	4.043	3.949	1.876	4.422	4.125	1.607

FIGURE 1.—Comparative speed in turns for night (2), no speedometer (3), and low tires (4).

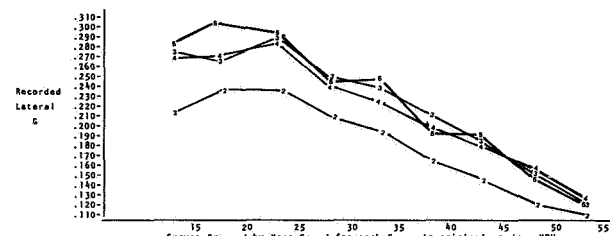

2 Night	Mean	.216	.239	.238	.211	.198	.169	.150	.123	.112
	S.D.	.065	.064	.050	.064	.038	.038	.026	.024	.029
No 3 Speedometer	Mean	.275	.264	.288	.250	.241	.213	.184	.150	.127
	S.D.	.056	.092	.065	.056	.055	.048	.041	.035	.037
4 Low Tires	Mean	.270	.273	.284	.240	.228	.199	.183	.152	.129
	S.D.	.035	.037	.057	.048	.040	.051	.034	.028	.042
5 Control	Mean	.282	.306	.291	.241	.249	.194	.191	.149	.127
	S.D.	.024	.064	.067	.054	.050	.063	.037	.022	.023

FIGURE 2.—Comparative lateral acceleration for night (2), no speedometer (3), and low tires (4).

against the reference speed for each curve. It will be seen that the night group produced lower accelerations than the low tires, no speedometer, and the control groups; these latter three being statistically indistinquishable.

How is it possible that the control group drove no faster than the night group but still produced higher lateral accelerations? When the data from the two-channel Brush recorder were read, the acceleration value read was the peak acceleration produced in a given curve. The velocity was then read at that point. If the control group drivers systematically jerked the wheel to a greater degree than the night group, thus producing greater spikes on the lateral acceleration trace, the result would be as observed in the two figures.

In the report we gave at the 4th Annual Manual (ref. **1)** we showed figure **3,** which is a plot of the recorded speed as a function of the speed values of advisory signs. Our subjects drove faster than

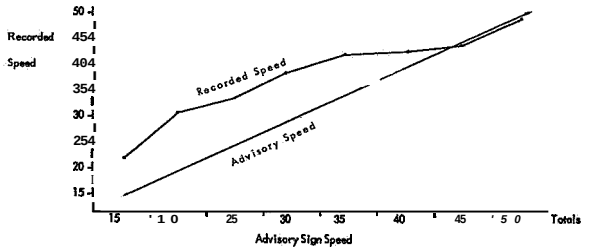

Recorded Speed	Mean	21.950	30.460	32.383	37.900	42.177	42.109	44.425	49.633	39.006
	SD	1.900	5.001	2.060	2.036	2.996	3.361	4.187	3.984	7.919
	N	4	10	6	6	13	11	12	6	68
	F = 38.1515		DF = 7/60							
Lateral Acceleration	Mean	0.253	0.251	0.228	0.226	0.210	0.197	0.162	0.138	0.205
	SD	0.072	0.057	0.061	0.015	0.039	0.053	0.049	0.041	0.059
	F = 5.1144		DF = 7/64							

FIGURE 3.—Actual speed in curves in relation to advisory sign speed.

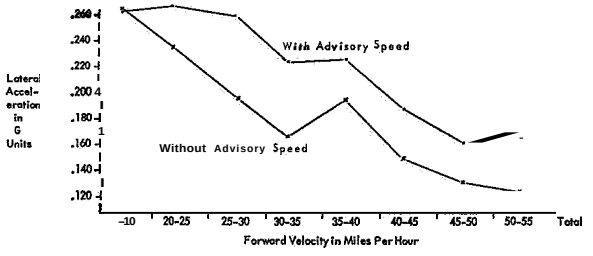

With Advisory Speed	Mean	0.263	0.268	0.257	0.222	0.224	0.185	0.161	0.169	0.205
	SD	0.	0.081	0.061	0.053	0.037	0.053	0.043	0.032	0.059
	N	1	4	6	10	12	19	13	3	68
Without Advisory Speed	Mean	0.264	0.234	0.193	0.165	0.195	0.146	0.130	1.126	0.155
	SD	0.059	0.059	0.043	0.021	0.045	0.035	0.039	0.041	0.059
	N	8	2	5	6	8	9	22	34	94
Between Groups	F	0.0003	0.265	3.989	6.319	2.445	4.064	4.726	3.156	28.305
	DF	1/7	1/4	1/9	1/14	1/18	1/26	1/33	1/35	1/160

FIGURE 4.—Effect of the presence of advisory speed sign upon choice of speed in curves.

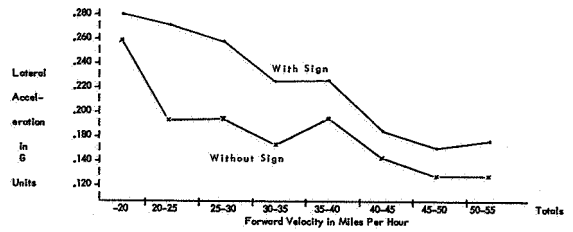

With Sign	Mean	0.280	0.270	0.257	0.222	0.223	0.183	0.159	0.174	0.224
	SD	0.024	0.071	0.061	0.053	0.035	0.051	0.037	0.028	0.0582
	N	2	5	6	10	13	21	18	4	79
Without Sign	Mean	0.259	0.193	0.193	0.165	0.192	0.140	0.124	0.124	0.1503
	SD	0.062	0.	0.043	0.021	0.048	0.139	0.042	0.040	0.0582
	N	7	1	5	6	7	7	17	33	83
Between Groups	F	0.193	0.993	3.989	6.319	2.753	4.180	7.109	6.002	32.492
	DF	1/7	1/4	1/9	1/14	1/18	1/26	1/33	1/35	1/160

FIGURE 5.—Effect of the presence of a curve sign on the choice of speed in curves.

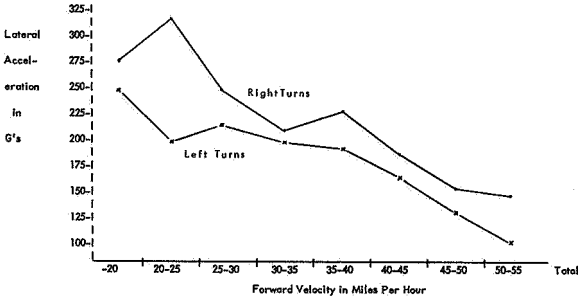

Right Turns	Mean	0.276	0.317	0.247	0.109	0.226	0.188	0.151	0.145	0.188
	SD	0.054	0.037	0.070	0.070	0.038	0.062	0.048	0.038	0.068
	N	5	3	5	5	12	13	19	23	85
Left Turns	Mean	0.249	0.198	0.212	0.197	0.191	0.159	0.131	0.102	0.162
	SD	0.061	0.020	0.054	0.033	0.040	0.037	0.034	0.033	0.056
	N	4	3	6	11	8	15	16	14	77
Between Groups	F	0.477	23.593	0.850	0.192	3.878	2.405	2.020	12.381	7.086
	DF	1/77	1/4	1/9	1/14	1/18	1/26	1/33	1/35	1/160

FIGURE 6.—Effect of the direction of turn on the choice of speed in curves.

the signs reading below 40, but did not drive faster than advisories of **45** and **50.** Figure **4** shows the lateral acceleration for those curves with advisories and for the curves without advisories. We have looked at the individual curves with advisories in relation to their advisory speeds. Mean values for our **110** subjects show considerable variability in speed and acceleration with a given advisory speed. Using these data we are negotiating with the Ohio Department of Highways a contract to revise considerably the methods by which advisories are assigned.

Selecting **162** curves which gave the drivers a free choice of speeds, we had **79** with a curve sign and **83** without. Figure **5** shows the plot of lateral acceleration for these two conditions. (Note that all **68** curves with advisory signs in figure **4** are among the **79** curves in figure **5** which had curve signs. No curve had an advisory without a curve sign, but **11** had curve signs and no advisory.)

These **162** curves consisted of **85** right turns and **77** left turns. The speed versus lateral acceleration data for right versus left are shown in figure **6.** The difference is reliable because the two curves do not overlap. It is a small difference, however, and is about the same order as the limits of the relatively simple instrumentation system. Therefore, these data must be considered as being subject to revision.

REFERENCES

1. RITCHIE, MALCOLM L.: Some Relations Between Visual and Kinesthetic Displays in Normal Driving. Proceedings of the Fourth Annual NASA–University

Conference on **Manual Control, Univ. of Michigan (Ann** Arbor, **Mich.), Mar. 21–23, 1968, pp. 459–463.**

2. **VAN VALKENBURG, PAUL: World's Most Advanced Race-Driving School. Sports Car Graphic, Jan. 1971, pp. 58–61, 67.**

3. **RITCHIE, MALCOLM L.; MCCOY, WILLIAM K.; ADN WELDE, WILLIAM L.: A Study of the Relationship Between Forward Velocity and Lateral Acceleration in Curves During Normal Driving. Human Factors, vol. 10,** no. **3, 1968, pp. 255–258.**

N73-10132

28. Estimation of Automobile-Driver Describing Functions From Highway Tests Using the Double Steering Wheel*

P. DELP, E. R. F. W. CROSSMAN, AND H. SZOSTAK

University of California

The automobile-driver describing function for lateral position control was estimated for three subjects from frequency response analysis of straight road test results. The measurement procedure employed an instrumented full size sedan with known steering response characteristics, and equipped with a lateral lane position measuring device based on video detection of white stripe lane markings. Forcing functions were inserted through a servo driven "double steering wheel'' coupling the driver to the steering system proper. Random appearing, Gaussian, and transient time functions were used.

The quasi-linear models fitted to the random appearing input frequency response characterized the driver as compensating for lateral position error in a proportional, derivative, and integral manner. Similar parameters were fitted to the Gabor transformed frequency response of the driver to transient functions. A fourth term corresponding to response to lateral acceleration was determined by matching the time response histories of the model to the experimental results. This model parameter also accounted for the driver's direct response to steering wheel reaction torques.

The time histories show evidence of pulse-like nonlinear behavior during extended response to step transients which appear as high frequency remnant power.

INTRODUCTION

The present entirely manual controlled approach to road vehicle operation demands high performance of the man-vehicle closed-loop system to ensure safe transportation. In this paper we consider the lateral control or steering subsystem alone. Here the prime requirement is to minimize lateral position error relative to a driver selected path on the pavement or other surface, despite disturbances due to mechanical and aerodynamic forces acting on the vehicle. This requirement implies good closed-loop regulation, conventionally accomplished by a combination of vehicle handling qualities and driver responsiveness. Previous researchers have demonstrated the feasibility of a frequency domain analytical approach to steering subsystem performance using now classical human operator theory (Weir (ref. **1);** McRuer and Weir (ref. 2)), and at a previous Annual Manual we have reported initial measurements of driver describing functions obtained under highway conditions using the newly developed "double steering wheel" forcing function injector (Crossman and Szostak (ref. **3)).** The present paper reports the results of extended application of this technique, and considers various possible driver models that can be fitted to the data. As pointed out in the previous paper, one can also employ highway curvature to force the steering system, and describing function estimation for this case, together with the relevant psychophysics, will form the subject of a later report.

We have previously shown (ref. **3)** that the vehicle yields a zero order path curvature response to steering wheel angle, so that the driver could ideally employ an open-loop control mode

* This research was supported in part by the **U.S.** Public Health Service under contract R01 **AC 00260–02** with the University of California, Berkeley. Reproduction in whole or in part is permitted for any purpose **of** the United States Government.

for typical highway geometry.* However, it is clear that this system configuration offers inadequate precision under typical real highway conditions. When traversing a path of approximately constant (or zero) curvature defined by lane markings or other visible features in the highway environment, an additional forcing function is injected partly in visible form, as lane marking deviations, and partly invisible as lateral force on the car due to crosswind and surface irregularity. Hence the driver experiences a mixed compensatory and pursuit tracking task. Some advance information may be obtained from visible surface undulation, permitting a preview mode, and on a well-known road there may be some precognition. In normal circumstances, quickening, via vehicle heading is also available. Thus the total steering task presents a complex generally time-varying mixture of tracking modes, and a driver model based purely on the single input compensatory case is unlikely to yield adequate precision.

Nevertheless, Weir (ref. 1) has surveyed the various possible compensatory loop closures using a nominal operator describing function, and shown that pure lateral position response would be poor, yaw rate response relatively good, and so forth.

As noted by McRuer and Weir (ref. 2) there are significant differences between a laboratory task where stimuli are explicit and the task of car steering with its proprioceptive and motion stimuli, and which has a visual field rich in cues. The gap may be bridges by simulation. Wierwille et al. (ref. 4) and Weir and Wojcik (ref. 5) have reported describing functions estimated in fixed-base automobile simulators, but to our knowledge no genuine field test data have yet been reported.

In the present study we sought to estimate parameters of the random-appearing, Gaussian, and transient open-loop describing functions representing the regular automobile driver responding to unpredictable steering disturbance inputs under essentially compensatory tracking conditions on an actual highway in a standard sedan car.

A leading feature of the results has been the appearance of a low frequency first order gain increase and phase lag corresponding to pure integration down to frequencies on the order of 0.02 Hz. This may be related to the phenomenon of low frequency "phase droop" as noted by McRuer et al. (ref. 6). The extended crossover model for compensatory control tasks accounts for low frequency phase lag occurring with no measured break point in the amplitude ratio, as being directly related to the operator's neuromuscular system response. However, Taylor (ref. 7) found no supporting evidence for the low frequency phase lag in his time domain models with extended record lengths. Both the classical Goodyear study (Cacioppo (ref. 8)) and certain Japanese researchers (Iguchi (ref. 9) and Kobayashi (ref. 10) have represented the human operator as a parameter-adaptive Proportional-Integral-Derivative (PID) controller, and this is particularly attractive in the highway case since, as pointed out by Weir (ref. 1) both proportional and derivative data are directly available to the driver. Response based on a suitable weighted sum of these together with timed repetitions to correct small lateral position errors, seemed initially plausible to us in the light of earlier highway studies, and would indeed generate a PID model form. The specific experiments were planned with this in mind.

EXPERIMENTAL EQUIPMENT AND DESIGN

Figure 1 shows the experimental configuration in schematic form. Novel features were the use of a special purpose forcing function injector and a lateral position recording device. The "plant" consisted of a standard sedan car whose steering response had been previously determined. The experimental trials were run during a single day on a preselected stretch of test road, all equipment and test subjects being transported to the site in the experimental car.

*The "double steering wheel" forcing function injector.**—This device consisted of a second steering wheel mounted concentrically on the

*Anecdotal evidence suggests that this may offer a realistic model of highly skilled racing and circuit driving.

*Fuller descriptions are given in report HFT 66–10 (ref. 11).

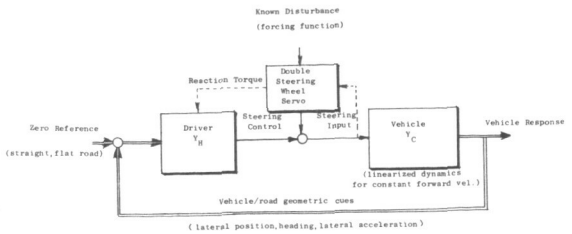

FIGURE 1.—Compensatory driving task: disturbance injected into the vehicle-driver steering control loop via the double steering wheel.

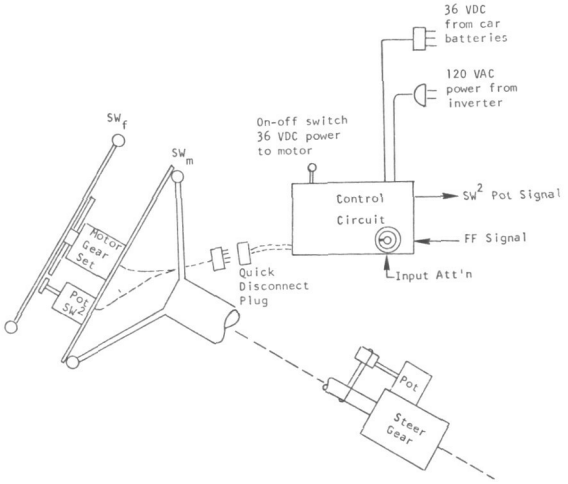

FIGURE 2.—Mechanical layout of the double steering wheel differential drive forcing function system.

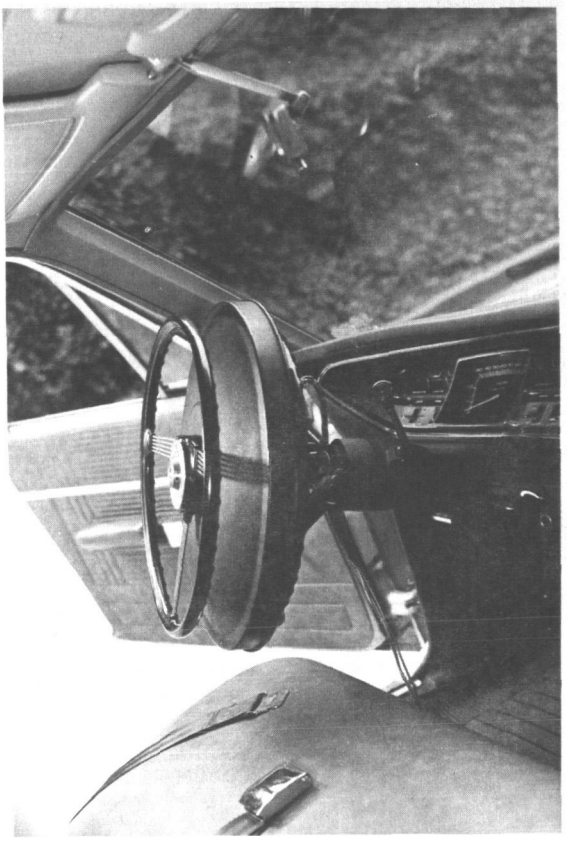

FIGURE 3.—The double steering wheel.

car's regular steering wheel and linked to it through an angular positioning servomechanism comprising an electric motor, gear train and servo amplifier, their relative angular position being commanded by a voltage reference signal (fig. 2). The driver steered the car via the second (top) steering wheel and the required forcing function was thus introduced as a time-varying angular increment to his steering output. The unloaded dynamic response of the servomechanism to voltage inputs was essentially second order with $f_{co}=1.8$ cps and $\zeta=0.5$, but the damping factor was increased under field conditions due to loading by the driver's limbs and the vehicle steering system. Consequently, a true step command voltage input would appear to the driver to yield an overdamped second order approach to a new angular displacement. However, the forcing function θ_F, assumed in the data analysis, was the measured output rather than the input to the angular positioning servomechanism.

The driver's view of the lower steering wheel was obscured by a cover to prevent direct visual feedback (fig. 3).

*The lateral position recording system.**—An optical sensing system based on a closed-circuit television camera provided a continuous record of the lateral position of the vehicle relative to the painted highway centerline stripe. This was accomplished as follows. A convex mirror reflected an image of the pavement surface into the lens of a commercial TV camera mounted at the rear of the car, the horizontal sweep being aligned with the lane markings while the vertical sweep provided a lateral scan. The video voltage output was filtered to remove the horizontal scan component, leaving a radar-type pulse waveform

* Fuller descriptions are given in report HFT 66–9 (ref. 11).

with 60 Hz repetition rate. The peak voltage due to the relatively bright lane marking triggered a rectangular pulse and this in turn caused sampling of a synchronized timebase, providing a voltage level proportional to the lateral displacement of the centerline on the camera screen. This level was maintained between sweeps, and in the absence of the white stripe, by a zero order hold circuit. The resulting signal was recorded by an onboard instrumentation tape recorder.

Since the camera was mounted approximately 12 ft rearward from the C.G. of the vehicle, the lateral position trace was delayed approximately 0.27 seconds at 30 mph. Interruptions in the painted centerline, bridged by the zero order hold circuit, introduced a further delay averaging 0.20 ± 0.05 sec at 30 mph, for a total time delay of 0.47 ± 0.05 sec. This was corrected during off line data analysis.

The test car dynamics and instrumentation.*— The test vehicle was a 1965 Ford sedan whose sinusoidal steering response dynamics had been previously determined. This was done at a series of test frequencies by manual application of sinusoidal steering inputs, the inputs (steering wheel angular displacement, speed), and outputs (yaw rate, roll rate, and lateral acceleration) being recorded at different points relative to the vehicle's C.G. In the frequency range of interest in the present context, the vehicle lateral position response to steering wheel angular displacement can be characterized as lagged double integration, the constant of integration being a function of forward speed:

$$\frac{y}{\theta_s} = \frac{K}{s^2} \cdot \frac{1}{T_c s + 1}$$

where, at 30 mph, $K \approx 2.13$ cm/sec²/deg
$T_c \approx 0.25$ sec.

The *test* road and conditions.—The test road was a straight, almost flat, country road in new condition with 11 ft lanes and 5 ft paved shoulders, 8900 ft in length, permitting test runs of from 150 to 180 sec duration. There was some mist, visibility being estimated at 300 ft, and no wind at the time of the test, which was mid-day. There were solid white lane markings between the road lanes and shoulder and a dashed center line striping.

Subjects and instructions.—All three subjects were Univ. of Calif. students with previous driving experience, but only one (subject C) had had previous experience with the double steering wheel. Their ages ranged from 22 through 40.

The subjects were requested to keep the vehicle within the right half driving lane and to maintain a constant speed: for subject A and B, 30 mph; for subject C, 40 mph. An auxiliary tachometer was mounted on the dash to the side to display the speed since the cover between the two steering wheels blocked the view of the vehicle's standard speedometer. If necessary, the subject could regain normal control of the cay by simply reaching around the cover and grasping the vehicle's steering wheel.

Experimental design.—The three distinct forcing functions used are referred to below as random appearing (RA), gaussian noise (GN) and transient disturbance (TD). Each subject performed one run with RA and TD, and two with GN, in the order given in table 1. As noted above, subject C maintained an average speed some 5 to 10 mph faster than the other subjects.

(1) Random appearing. The sum of sinusoidal components with the following amplitudes and frequencies (table 2)

(2) Gaussian noise. White noise from an electronic generator * passed through a fourth-order band-pass filter † with the following settings:

Low pass cut-off frequency = 0.02 cps
High pass cut-off frequency = 0.25 cps

The peak disturbance amplitude was ±90°.

(3) Transient disturbance. This included positive and negative impulses, steps and truncated ramps in random sequence. The bandwidth of the step and impulse inputs were limited by the response of the angular position servo, as follows.

(a) Step-wide disturbances with ±65° and ±130" amplitude, rise time respectively of 0.2 and 0.5 sec

(b) Impulse excursions of 40" to 60" with approximately 0.3 sec duration and symmetrical waveshape (0.15 sec rise, 0.15 sec fall)

(c) Ramp disturbances at ±60°/sec., terminating at ±65° and ±130".

* Further details are reported in an unpublished report HFT 67–8 (ref. 12).

* Elgenco Model.
† Kronhite Model.

TABLE 1.—*Test Run Sequence*

Run number	Subject	Duration	Type of forcing function	Peak amplitude double steering wheel	Average speed, mph
1	A	182 sec	RA: (Mixed sinusoid)	±120"	29
2	B	171 sec			33
3	C	159 sec			34
4	A	181 sec	GN : (Gaussian noise)	±90"	31
5	A	180 sec			30
6	B	181 sec			32
7	B	167 sec			33
8	C	156 sec			36
9	C	140 sec			39
10	A	191 sec	TD: (A mixture of step,	±65°	30
11	B	180 sec	ramp, and impulse	and 130" peak to peak	32
12	C	144 sec	inputs)	swings	40

TABLE 2.—*Forcing Functions Used in the Experiment* *

	Normalized amplitude	Frequency	
		Rad/sec	Cycles/sec
1	1.0	0.070	0.0111
2	1.0	.157	.0250
3	1.0	.393	.0625
4	1.0	.602	.0957
5	1.0	.969	.1540
6	1.0	1.490	.2370
7	1.0	2.540	.4040
8	0.1	4.030	.6410
9	0.1	7.570	1.2100

*** Peak amplitude = ±120°**
Note: This is identical with the STI forcing function.

DATA ANALYSIS

The data analyzed were sample time histories of the following variables recorded on instrumentation tape:

(1) θ_F The measured angular output of the forcing function injector

(2) 8, The angular displacement of the steering wheel, as sensed by a potentiometer coupled to the steering shaft

(3) e_P The lateral position of the white stripe relative to the vehicle, sensed by the TV camera system

(4) θ_D The driver's output to the second steering wheel, obtained during playback by summing θ_F and θ_s, before further processing.

To remove components above the Nyquist frequency, the above signals were passed through a linear phase second order low pass filter with cutoff frequency *1.8* Ha, and damping constant $\pi/4$. They were then digitized at 2.5 samples/sec with *12* bit precision.

Spectral response estimates with RA forcing functions were obtained from the digital data using two distinct techniques.

(1) A fast Fourier transform routine identified as BMDX92, part of a biomedical data processing package (Massey (ref. **13))** running on the Berkeley CDC *6400* computer.

(2) A routine based on the recently described Gabor transform principle (Crossman and Delp (ref. 14)), and running on the laboratory PDP–8 computer.

Estimates formed by the two methods agreed quite closely where they could be validly compared.

TD forcing function data could only be analyzed by the Gabor transform technique. The GN data did not yield satisfactory results with either technique, due probably to inadequate run length, and are not considered further here.

RESULTS

Mixed Sinusoidal Input Driver Describing Function

Estimates $\hat{H}_F$ and $\hat{Y}_H$ respectively relating system (closed-loop) angular response to forcing function angle and driver response to lateral position error were formed once for each experimental run, and are presented in Bode plot form in figures 4, **5,** and **6.**

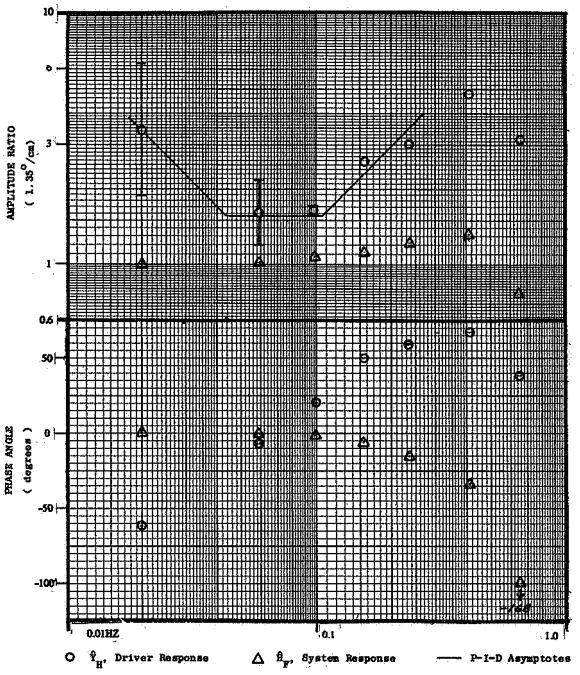

FIGURE 4.—Driver frequency response to lateral position error and system (closed-loop) response to mixed sinusoidal disturbance (run No. 1, subject A).

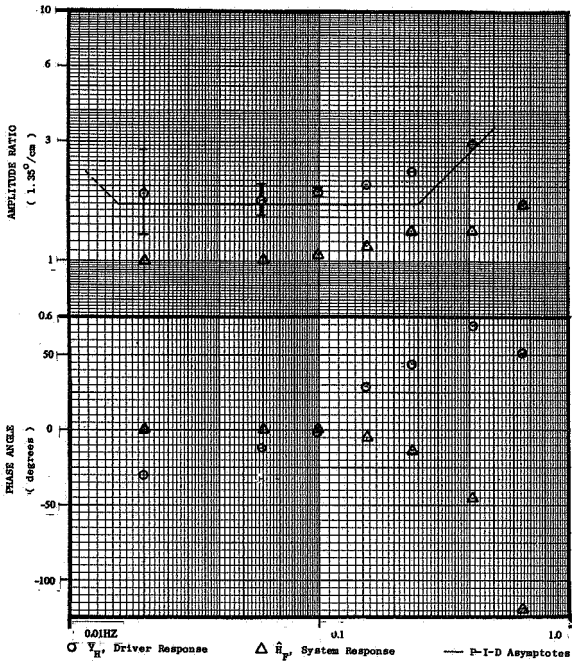

FIGURE 6.—Driver frequency response to lateral position error and system (closed-loop) response to mixed sinusoidal disturbance (run No. 3, subject C).

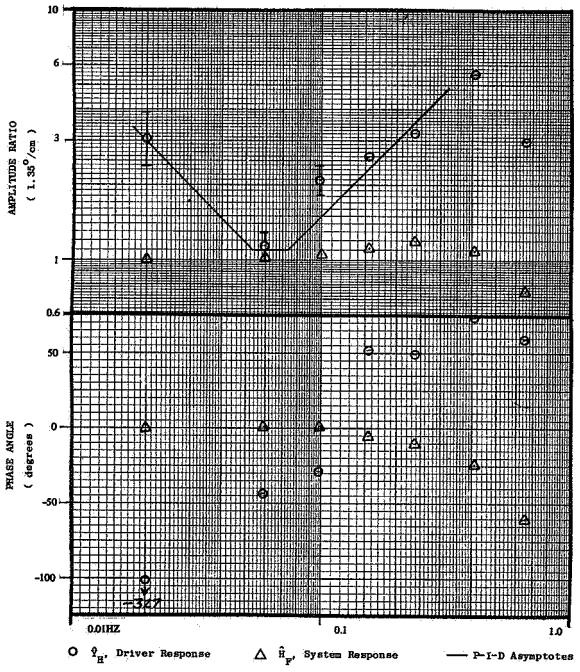

FIGURE 5.—Driver frequency response to lateral position error and system (closed-loop) response to mixed sinusoidal disturbance (run No. 2, subject B).

The closed-loop system shows good regulation with near unity gain and zero phase at low frequency (≤ 0.3 Hz). The slight rise in amplitude ratio at middle frequencies (0.2 to 0.4Hz) may be ascribed to driver response to position error resulting from his lagging response to high frequency disturbances. The expected high frequency rolloff is not clearly delineated due to decreasing coherence at frequencies above 0.5 Hz, but a system cutoff frequency in the range 0.6 to 0.8 Hz can be extrapolated from the data. This general pattern of behavior appears to be consistent with one's subjective experience of steering.

Plots of $\hat{Y}_H$, the driver's angular response to lateral position error are presented because lateral position is the state variable of prime importance in system operation and will usually be treated as the system output, for instance in congested traffic and on narrow roads. The other main state variable directly sensed by the driver is relative heading, γ which under normal highway conditions at constant speed is the first derivative of lateral position:

$$\gamma \approx \frac{1}{V}\frac{de_p}{dt}.$$

The estimated phase of $\hat{Y}_H$ has been corrected for estimated delay in the recording of e_p, the correction being enough to make the frequency response of the vehicle (Θ_s/E_p, not shown) agree with previously determined phase response.

The Bode plots (figs. **4** and **5)** for subjects **A** and B respectively, show tho presence of integral, proportional, and derivative compensation with varying break frequencies. Subject C (fig. **6)** does not show evidence of integrator action, nor is the derivative action strongly evident; however, he does show high average amplitude ratio. The first order slope at high frequencies can be readily interpreted to mean that in this frequency range the subject responds proportionally to relative heading or else to lateral velocity. The low frequency rise in amplitude ratio, described above as integral control action, indicates that the subject nulls out accumulated position error relatively slowly. The phase data are consistent showing a considerable lag ($-40°$ to **$-60°$)** with decreasing frequency for all three subjects. Further evidence for this type of compensation in a quasi-linear describing model is presented below.

Transient Input Describing Functions

The data for runs No. **10, 11,** and **12** were filtered and digitized at **5** Hz and analyzed using the Gabor transform technique; this centers a Gaussian weighted "data window" at the onset or center of the transient disturbance and forms response estimates as the ratio of Fourier transform of the input and output series, utilizing the fact that the Fourier transform of a Gaussian time function is also a Gaussian frequency function. The transient input is thus convolved with the Fourier transform of the normal curve. The theoretically infinite integration period required for a Fourier transform is adequately approximated by the $\pm 3\sigma$ limits of the data window. For transient inputs with finite rise time, departure from the ideal spectrum begins at a frequency greater than $\sim 0.8/T_R$, where T_R is, for example, rise time of a step input. Since the high frequency response of the double steering wheel was limited (discussed earlier), the forcing transients θ_F as actually applied had a rise time in the order of 0.8 sec; the variance of the spectral estimates was significantly increased above **1 Hz.**

The transfer from E_p, the lateral position error to driver output, Θ_D, was obtained from the ratio

$$\hat{Y}_H = \frac{\Theta_D}{E_p}.$$

The time history used as input to this transformation was obtained by averaging several step responses of each subject. The steps were selected such that sufficient time separated the transients so that low frequencies could be resolved, and only suprathreshold events were used, i.e., where enough lateral position error had occurred to provoke a driver response. This time averaging process tends to smooth the data by obliterating the driver's high frequency output leaving only the gross response (see fig. **7).** This point is discussed further below.

The time averaged responses are shown in figures **8** through **10** for step disturbances and figure **11** for truncated ramp disturbances, and the results of the averaged transient input analysis are sketched in the Bode plots of figures **12** through **14** for each subject. Again three-term controller response yields an adequate driver

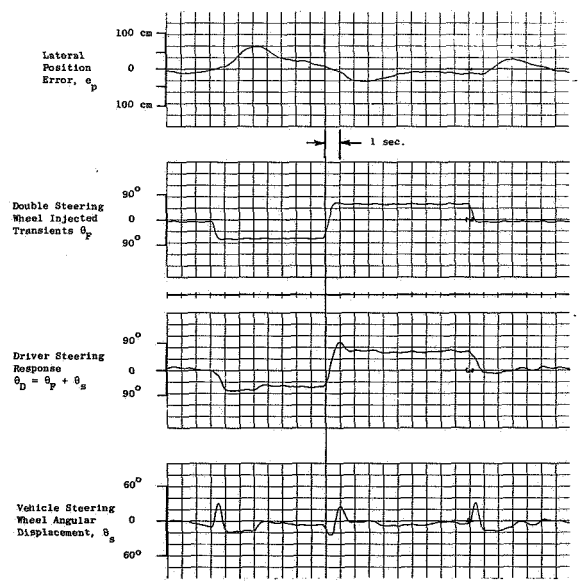

FIGURE 7.—Typical time responses due to transient disturbances (subject B, run No. 11, events 9, 10, 11 used in time average, figs. 12 through 15).

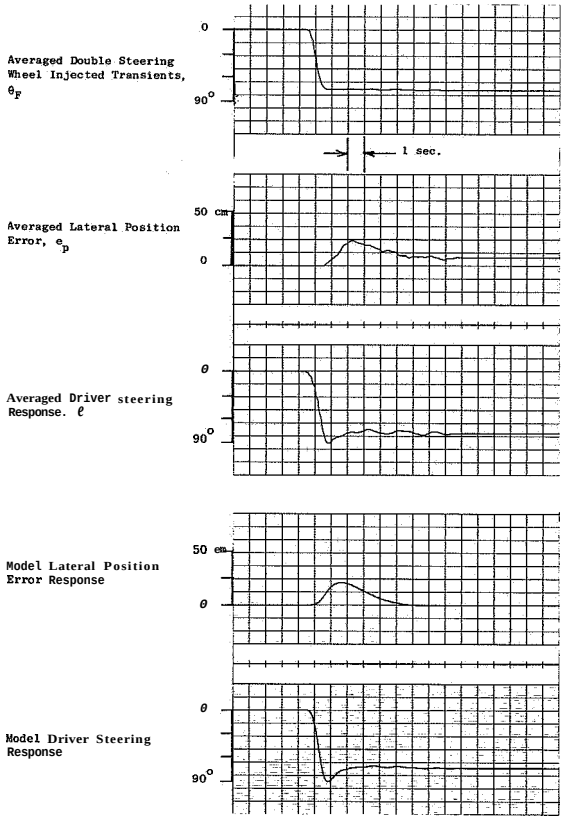

FIGURE 8.—Run No. 10, time average response for subject A and P-I-D model response to time average θ_F (3 steps).

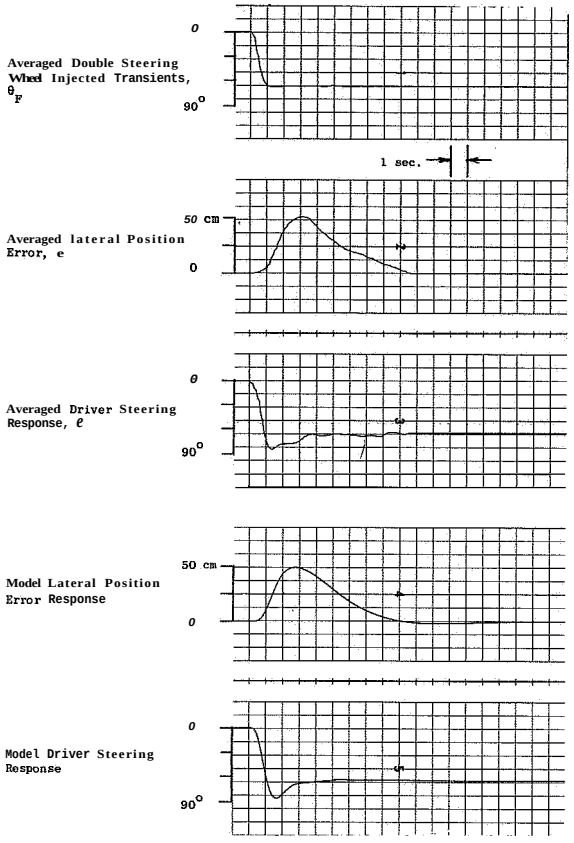

FIGURE 9.—Run No. 11, time average response for subject B and P-I-D model response to time average θ_F (6 steps).

model. Intuitively, the driver, after responding to the torque input of the double steering wheel and correcting his heading to avoid immediately leaving the roadway, must then null out any accumulated lateral position error duplicating the response of an integral controller. The increasing phase lag at low frequency also supports this view.

Agreement between transient and sinusoidal driver response is apparent from table **3** where the parameters of proportional/integral/derivative control determined from the Bode plots are tabulated. These values were obtained for each case by application of Ausman's unfactored polynomial method.

$$Y_H = \frac{\Theta D}{E_p} = \left[K_p + \frac{K_I}{s} + K_D s + K_A s^2 \right] \frac{e^{-\tau s}}{Ts+1} \Bigg|_{s=j\omega<0.5\ \mathrm{Hz}}$$

As a check against the loss of information by time averaging, each step used in the average response for subject C was Gabor transformed and plotted. Figure **15** shows these values with the time average values. The vector average of the transfers of these steps was computed at each frequency and found to coincide with the time average transfer. A fit of PID parameters to each transfer was made and the values are given in table **3.** This indicates a great deal of variability from one step response to another by each subject. Therefore, the Bode plots of figures **12** through **14** can be said to indicate only a central tendency for the driver.

DISCUSSION

The results presented above contain the major substantive outcome of the study. However, subjective reports of the subjects together with time

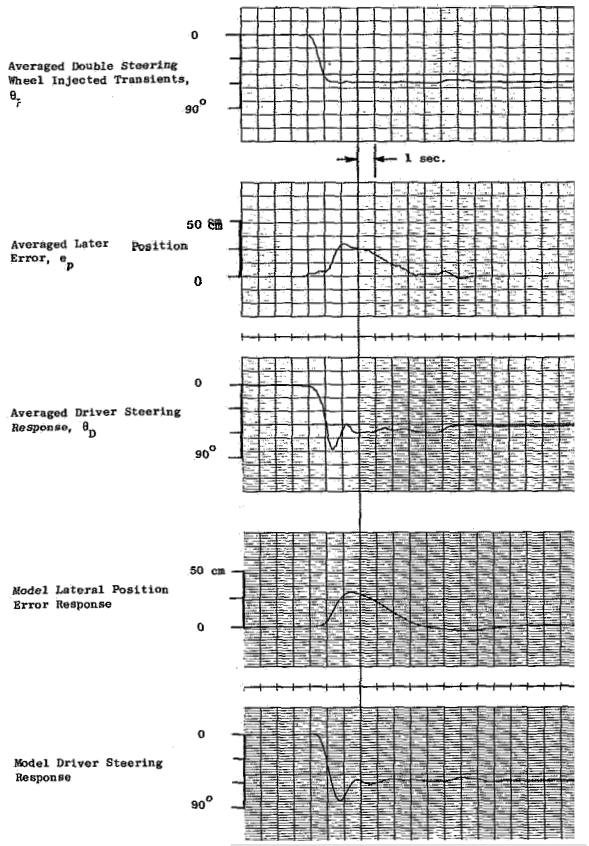

FIGURE 10.—Run No. 12, time average response for subject C and P-I-D model response to time average θ_F (3 steps).

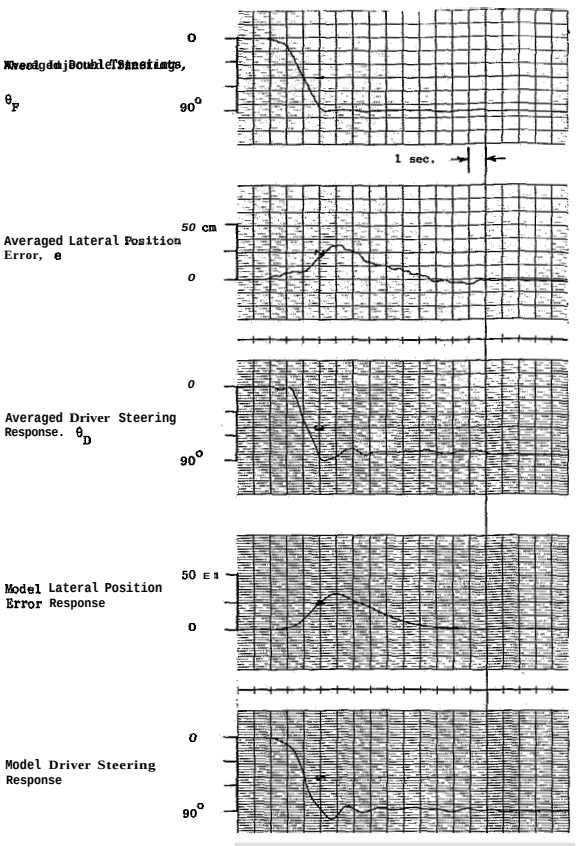

FIGURE 11.—Run No, 10, time average responses for subject A and P-I-D model response to time average θ_F (2 ramps).

domain modelling of the driver's feasible control policy may throw further light on the validity and generality of the results presented.

Subjects Learned Response to the Forcing Function Injector

Since most drivers sense the torque being applied during steering corrections, it would be natural for them to correct their steering responses if unexpected "feel" were introduced by the experimental double steering wheel inputs. From subject comments, it appears that they are sensitive to larger than normal reaction torques and respond to them. The time histories of transient responses show an initial proportional response with small lag (≈ 0.25 sec) and some overshoot. This fast response cannot possibly be ascribed to visual feedback, since the vehicle response is at best that of a lagged single integrator. Therefore, the driver clearly responded directly to the reaction torque at his hands created by the forcing function injector's angular displacement.

From this evidence, it would seem necessary to evaluate the driver's response Y_{H2} to torque variation, as well as his response Y_{H1} to road/vehicle geometric cues.

The reaction torque of the steering wheel, τ_{fb}, is generally proportional to the angular acceleration of the car, which at small angles is itself proportional to lateral acceleration for a given forward speed. The driver estimates a steering wheel torque, τ_{est} necessary to maintain the steering angular position decided on the basis of visual cues, and follows up the estimated torque τ_{est} by closed loop control. However, his estimates are imperfect particularly under dynamic conditions, and there will be a residual "error" torque tending to force the steering

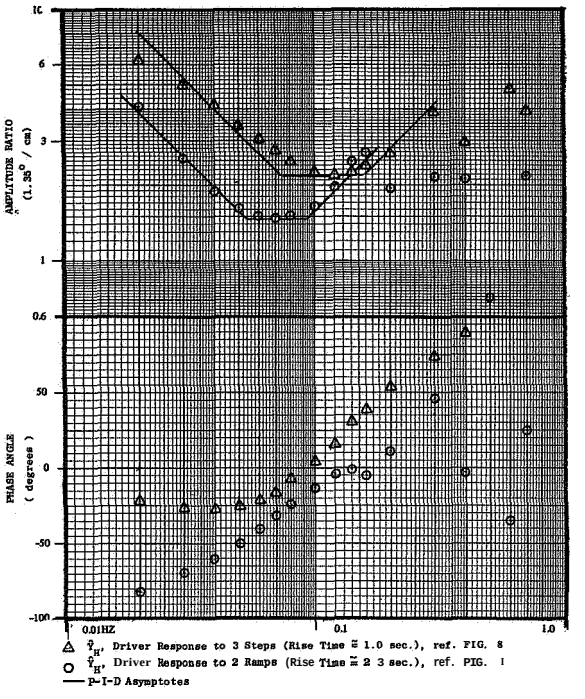

FIGURE 12.—Driver frequency response to lateral position error from Gabor transform analysis of time averaged transient disturbance responses (run No. 10, subject A).

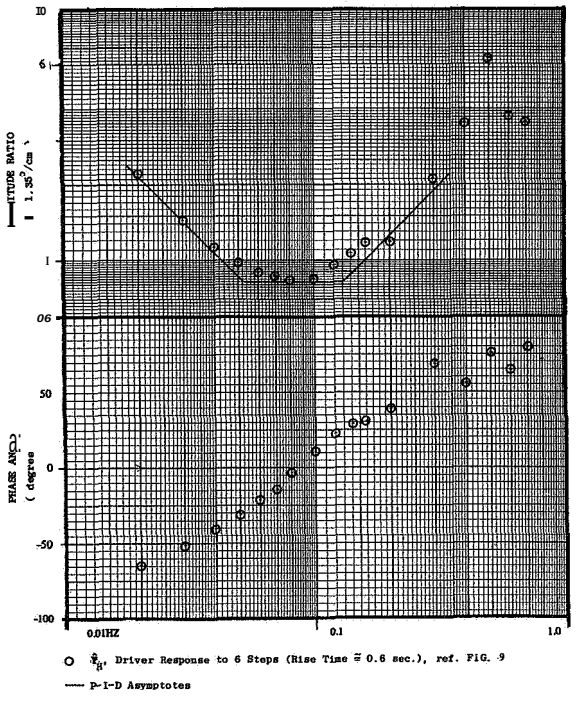

FIGURE 13.—Driver frequency response to lateral position error from Gabor transform analysis of time averaged transient disturbance responses (run No. 11, subject B).

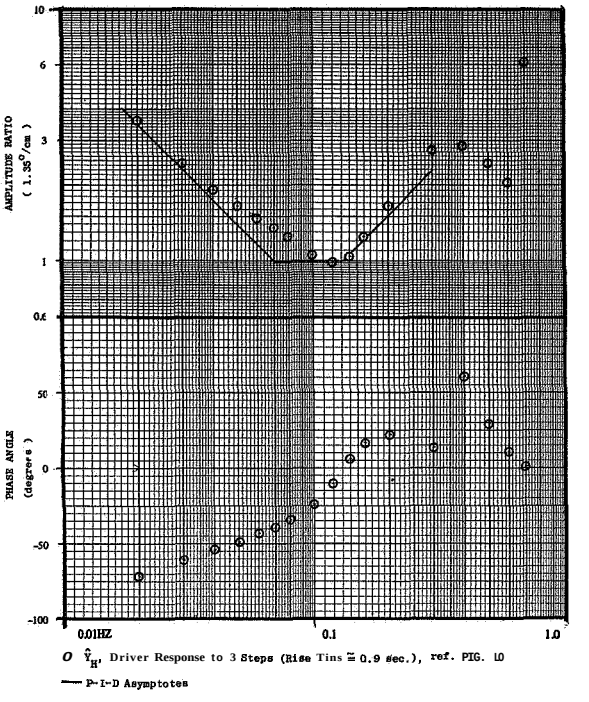

FIGURE 14.—Driver frequency response to lateral position error from Gabor transform analysis of time averaged transient disturbance responses (run No. 12, subject C).

system. The resulting control flow diagram is shown in figure **16.** The results given must therefore be interpreted in the light of the existence of two linked control subsystems.

It was observed that as a subject becomes more familiar with the double steering wheel torques produced by a given forcing function, he can diatort the effect of the forcing function on steering output and road position by passively allowing the top ateering wheel to displace backwards. His arms, torso, and the inertia of the wheel respond like a soft spring. He might also choose to react to changing outer feedback loop error signals by attempting to null out all effects of the forcing function while controlling to the desired steering wheel torque level. He would maintain this torque by backing off with the forcing function utilizing his torque feedback loop so that the net response corrects the outer loop error.

These problems could possibly have been overcome by adopting zero force feedback system for the double steering wheel system using a vehicle equipped with modified power steering.

TABLE 3.—*Proportional, Integral, Derivative Acceleration Model Parameters for Frequency Response of Subjects to Lateral Position Error*

		Run no.	Subject	Frequency response, fig. no.	Time response, fig. no.	Parameters: Proportional K_P, deg/cm	Integral K_I, deg/sec / cm	Derivative (heading) K_D, deg / cm/sec	Lateral acceleration K_A,* deg / cm/deg²
Double steering wheel injected forcing function	Mixed sinusoids	1	A	4	...	2.07	0.57	3.1	.....
		2	B	5	...	1.5	0.51	3.2	.....
		3	C	6	...	2.3	0.23	1.5	.....
	Averaged transients	10	A	12	8	2.96	1.35	2.96	1.9
		10	A	12	11	1.98	0.66	3.5	0
		11	B	13	9	1.1	0.36	1.35	0.7
		12	C	14	10	1.35	0.62	1.66	0.28
	Individual transients	12–9	C	15	...	1.35	0.62	1.9	.....
		12	C	15	...	0.9	0.97	1.08	.....
		12–14	C	15	...	0.9	0.35	1.08	.....

* The parameter K_A accounts for the driver response to a variety of feedback cues including steering wheel reaction torque as well as lateral acceleration.

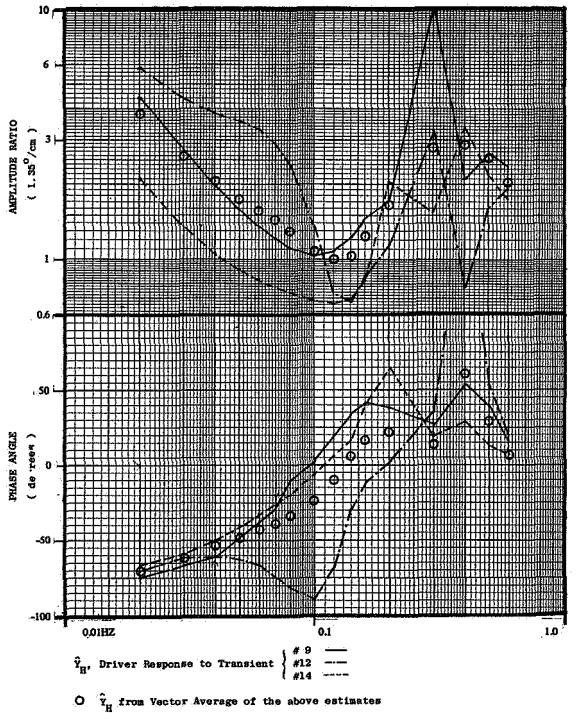

FIGURE 15.—Frequency response and vector average response from Gabor analysis of driver response to lateral position error due to three transient disturbances (run No. 12, subject C).

In the present experiment the effect was reduced as far as possible by using two subjects unfamiliar with the double steering wheel and by the use of random appearing forcing functions which slowed down the learning process.

Subsequent discussion will also indicate that the possible effects on the results occur at the upper limit of the resolvable spectral measurements at the frequency associated with response to lateral acceleration and thus have little effect on the low frequency parameter estimation.

A Comprehensive Frequency Domain Model of the Vehicle/Driver System for Straight Road Driving With Injected Angular Steering Disturbances

A complete model of the vehicle/driver system has been developed on the assumption that the driver will utilize the simplest forms of available feedback signals for his control actions, and thus will not need to develop any lead compensation nor signal differentiation when the derivative signals are available directly. Thus all driver responses have been represented as proportional to directly observable signals, including:

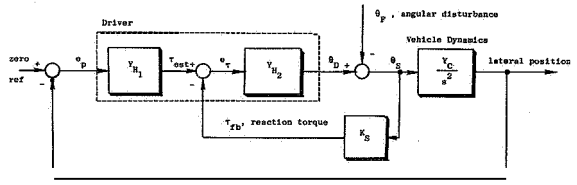

FIGURE 16.—Reaction torque compensation modeled as an inner loop response of the driver.

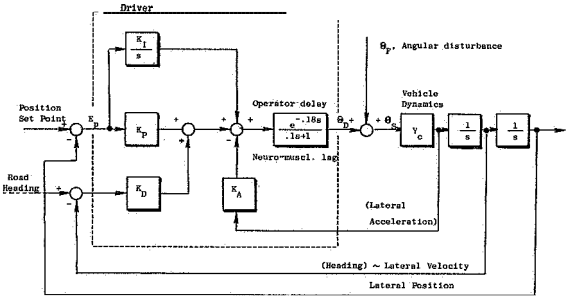

FIGURE 17.—Driver model for straight road steering control (constant speed) with injected angular disturbances.

(1) Lateral position error, the difference from actual car position to lane set point.

(2) Lateral position error when present over long periods (or with low frequency).

(3) Heading error (between car trajectory and road).

(4) A differential level of car response feedback directly estimated by the driver in several forms:

(a) Lateral (and angular) acceleration

(b) Car body roll angle

(c) Steering torque feedback.

The model is shown in figure 17. The parameter for K_P, K_I, and K_D are tabulated in table 3. The K_A term is estimated by matching model and averaged time history responses, θ_D and e. Further clarification and discussion of the various loops shown in figure 17 follows.

Integral control term.—This permits precise positioning over relatively long periods.

Lateral acceleration response.—This control mode is modelled as a response to the car's lateral acceleration. However, as shown above, it may in reality reflect a closed-loop response to torque disturbance sensed at the steering wheel. This response has low resolution since the driver must first estimate the "correct" torque associated with the desired steering angle before attempting to null out deviations from it resulting from forcing function injector action. Since steering wheel torque is highly correlated with angular and lateral acceleration of the vehicle the two response modes (aceeleration and torque) cannot be separately modelled.

We may note the driver's modelled response to forcing angle alone, without considering lateral position or heading errors, whichever cue is used (acceleration or torque). Initial driver response to the lateral acceleration (or torque) is modelled as

$$\frac{\theta_D}{\theta_F} \approx K_A Y_C.$$

The driver can apparently eliminate a large portion of the forcing function amplitude without resorting to outer loop feedback. This may be better described as feedforward regulation, since the driver estimates and cancels the sensed disturbance before it has had an opportunity to disturb the plant.

Reaction time and neuromuscular lag terms.—The reaction time and neuromuscular lag terms were estimated from the time histories, with some uncertainty. However, the values are common values found in the literature. For an equivalent control task and forcing function bandwidth, classical data on test pilots suggest a time delay of 0.18 sec (McRuer and Krendel (ref. 15)). The neuromuscular lag time constant is less sharply defined, ranging from 0.1 to 0.2 sec. But a close examination of test run No. 1 subject A's response to step inputs shows an overall lag from θ_F to θ_D of 0.25 to 0.30 sec, as measured during the initial signal rise period. Thus a physical response lag time constant of $0.275 \text{ to } 0.18 \approx 0.10$ sec appears to be a good approximation on an average basis.

This estimation has an effect on the determination of the lateral acceleration response parameter. For example, when the lag term was increased to $1/(0.2s+1)$, the only real change required in the model was to double the lateral acceleration control gain K_A.

Figures 8 through 10 show the time history response of the model to the time averaged "step" transients for subjects A, B, and C, respectively. A truncated ramp response for subject C is shown in Figure 11. It was observed that the driver

corrected lateral position error only to within a tolerance threshold, while the linear model nulled out the error completely by the K_I/s compensation. Excessive integral action may result in overshoot in the lateral position response. Also, the actual time averaged responses indicate possible pulse-like behavior (0.5 to **0.9** Hz). This may account for part of the spectral variation shown in figures **12** through **15** for that frequency range.

CONCLUSIONS

The double steering wheel forcing function injector is a viable experimental tool for producing a known disturbance in the driver/vehicle steering control loop permitting measurement of low and mid frequency compensation by the driver.

Using this method, the results have indicated an integral control-like action in response to a transient disturbance which is used by the driver to reduce the vehicle lateral position error to within his tolerance limits.

The frequency and response analysis also strongly supports earlier conjectures that feedback cues related to the first time derivative of lateral position viz. relative heading or lateral velocity, and the second derivative, viz. lateral acceleration or steering torque reaction are used by the driver in steering the vehicle. This assumption yielded good models of driver response both to random appearing mixed sinusoidal disturbances and to transient disturbances. Drivers also learned to respond directly to reaction torque from the angular displacement injected into the steering control loop. This state variable is highly correlated with lateral acceleration and was not distinguished from it in the model.

Results were unsatisfactory above about **1** Hz. This may have been due to unwise selection of a relatively low sampling rate in digitization, and further processing of the data may yield improved high frequency estimates. It may also have been due to genuine driver remnant, but this cannot confidently be estimated from the data analyzed to date. The time histories show evidence of pulse-like nonlinear behavior during extended response to step transients which could appear as high frequency remnant power.

Further experimentation will further define the high frequency response of the driver and seek to delineate evidence of pulse-like corrections (minimum effort compensation) which are an equally viable explanation of the integral control effect observed in the tests. This would lead to a nonlinear model of possible driver steering behavior in which an initial quasilinear response to a transient disturbance is followed by timed steering wheel pulses whenever the projected path of the vehicle exceeds some intrinsic threshold for allowable lateral position error.

SYMBOLS

Time functions are in lower case; frequency functions in upper case; and ^ indicates experimental estimate.

θ_F angular displacement of the forcing function injector

θ_s angular displacement of the vehicle steering wheel

$\theta_D = \theta_F + \theta_s$ angular displacement of the second steering wheel, i.e., driver output

e_p lateral position error, i.e., vehicle displacement from white stripe

$Y_{H_1} = \dfrac{\Theta_D}{E_p}$ driver response to lateral position error

$Y_{H_2} = \dfrac{\Theta_D}{E_\tau}$ driver response to the torque imbalance generated by the forcing function injector

$H_F = \dfrac{\Theta_D}{\Theta_F}$ system response to forcing function

$Y_C = \dfrac{s^2 E_p}{\Theta_s}$ vehicle lateral position response to angular displacement of the regular steering wheel

$Y_C \approx \dfrac{K}{s^2(T_c s + 1)}$ where

$K \approx \left.\begin{cases} \dfrac{2.13 \text{ cm/sec}^2}{\text{degree}} \\ \text{at 30 mph} \end{cases}\right\}$ up to 0.5 Hz

$K \approx \left.\begin{cases} \dfrac{2.93 \text{ cm/sec}^2}{\text{degree}} \\ \text{at 40 mph} \end{cases}\right\}$

T_c = vehicle response lag

V vehicle forward velocity

$\gamma = \frac{s}{V} e_p$ relative heading of car—lateral velocity for constant V

$K_s = \frac{\tau_{fb}}{e_\gamma}$ vehicle model self-aligning torque feedback constant

$\frac{451 \text{ cm gm}}{\text{degree}}$ at 30 mph

$\approx \frac{634 \text{ cm gm}}{\text{degree}}$ at 40 mph

τ_{fb} steering feedback torque from steering gear

τ_{est} the driver estimated steering wheel torque

$e_\tau = \tau_{est} - \tau_{fb}$ torque imbalance (error)

K_P driver model response to lateral position error

K_I driver model response to integrated lateral position error

K_D driver model response to heading angle or lateral velocity

K_A driver model response to lateral acceleration or steering torque

T neuro-muscular time constant

T_R rise time of transient input

s laPlace domain operator

REFERENCES

1. WEIR, D.: Closed-Loop Directional Control of Automobiles. IEEE Eighth Annual Symposium on Human Factors in Electronics, 1967.
2. MCRUER, D.; AND WEIR, D. H.: Theory of Manual Vehicular Control. IEEE Trans., vol. MMS–IO, Dec. 1969.
3. CROSSMAN, E. R. F. W.; AND SZOSTAK, H.: Man-Machine Models for Car Steering. Fourth Annual NASA/University Conference on Manual Control, NASA SP–192, 1968.
4. WIERWILLE, W. W.; ET AL.: An Experimental Study of Human Operator Models and Closed-Loop Analysis Methods for High-speed Automobile Driving. IEEE Trans., vol. HFE–8, Sept. 1967.
5. WEIR, D.; AND WOJCIK, C. K.: The Measurement of Driver Describing Function in Simulated Steering Control Tasks. Seventh Annual NASA/University Conference on Manual Control, Univ. of Southern California (Los Angeles), 1971.
6. MCRUER, D.; ET AL.: Human Pilot Dynamics in Compensatory Systems. AFFDL TR 65–15, 1965.
7. TAYLOR, L. W.: A Look at Pilot Modelling Techniques at Low Frequencies. Sixth Annual NASA/University Conference on Manual Control, 1970.
8. CACIOPPO, A. J.: Pilot Information Utilization: A Study in Human Response Dynamics. GER–7686A, Goodyear Aircraft Corp., 1956.
9. IGUCHI, M.: Man-Machine Systems. Kyoritsu Publishing Co. (Tokyo), 1970.
10. KOBAYASHI, M.: Research on Characteristics of Human Control Behavior. Thesis, M.E., Univ. of Tokyo, 1967.
11. CROSSMAN, E. R. F. W.; SZOSTAK, H.; AND BECHARD, J.: A Device for Continuously Recording the Lateral Position of a Vehicle on the Highway by Optically Sensing Its Distance from Painted Lane Markings. HFT Group Working Paper 66–9, Univ. of California, Berkeley, 1966.
12. SZOSTAK, H.: Investigation of the Dynamic Steering Response of a 1965 Ford Sedan Test Vehicle. HFT Group Working Paper 67–8, Univ. of California, Berkeley, 1967.
13. MASSEY, F.; AND JENRICH, R.: BMDX92, Time Series Spectrum Estimation. UCLA, Los Angeles, 1966.
14. CROSSMAN, E. R. F. W.; AND DELP, P.: Application of Gabor's Elementary-Signal Theorem to Estimation of Nonstationary Human Spectral Response. Fifth Annual NASA/University Conference on Manual Control. NASA SP–215, 1969.
15. MCRUER, D.; AND KRENDEL, E. S.: Dynamic Response of Human Operators. WADC–TR–56–524, Wright-Patterson AFB, Oct. 1957.

SESSION VII

PERFORMANCE: PREDICTION AND EVALUATION

Chairman: M. E. SADOFF

29. Visual-Motor Response of Crewmen During a Simulated 90-Day Space Mission as Measured by the Critical Task Battery*

R. WADE ALLEN AND HENRY R. JEX

Systems Technology, Inc.

In order to test various components of a regenerative life support system and to obtain data on the physiological and psychological effects of long-duration exposure to confinement in a space station atmosphere, four carefully screened young men were sealed in the McDonnell-Douglas Astronautics Space Station Simulator for 90 days with no pass-in's allowed. Under contract to the NASA-Ames Research Center, Systems Technology, Inc., administered a tracking test battery during the above experiment. The battery included a "clinical" test (critical instability task) related to the subject's dynamic time delay, and a conventional steady tracking task, during which dynamic response (describing functions) and performance measures were obtained. The subjects were extensively trained prior to confinement and generally reached asymptotic performance levels.

Good correlation was noted between the clinical critical instability *scores* and more detailed tracking parameters such as dynamic time delay and gain-crossover frequency. The levels of each parameter spans the range observed with professional pilots and astronaut candidates tested previously. The chamber environment caused no significant decrement on the average crewman's dynamic response behavior, and the subjects continued to improve slightly in their tracking skills during the 90-day confinement period. Some individual performance variations appeared to coincide with morale assessments made by other investigators. The comprehensive data base on human operator tracking behavior obtained in this study demonstrates that sophisticated visual-motor response properties can be efficiently and reliably measured over extended periods of time.

INTRODUCTION

A 90-day sealed chamber test of a regenerative life-support .system was performed at the McDonnell-Douglas Astronautics Corporation (MDAC) under NASA Contract NAS1-8997 from the Langley Research Center. Among the stated objectives of the official test plan and procedures (ref. 1) were the following:

. . . D. To demonstrate man's capability . . . for in-flight monitoring of necessary human . . . parameters.

E. To obtain . . . data that will assist in determining the precise role of man in performing in-flight experiments . . . and . . . in validating mathematical models of [manned] space missions.

F. To obtain data on physiological and psychological effects of long-duration exposure to confinement in the cabin atmosphere . . .

To accomplish these objectives, four men, carefully screened for compatibility with each other and with a confined environment, were sealed in the MDAC space station simulator (SSS) for 3 months with no pass-in's allowed, and only a limited number of pass-outs allowed for medical sampling purposes. The primary workload of the subjects included monitoring and maintenance of SSS life support equipment and monitoring and recording their metabolic, medical, and mood characteristics. The SSS environment was "closed-cycle" and included a subnormal air

* This research was sponsored by the Man-Machine Integration Branch of the NASA-Ames Research Center under contract NAS2-4405 (modification-5). The tasks and associated hardware used in this study were previously developed under the same contract.

pressure of **3/4** atmosphere with normal oxygen partial pressure. A complete description and preliminary results of this simulated mission are given in reference **2.**

This program also provided a unique opportunity to evaluate certain other psychomotor and cybernetic functions in a realistic space station environment (except for zero-gravity) and under operational type work-rest cycles and ambient stresses. Among the more important of such psychomotor tasks are the broad class of tracking tasks: star tracking for navigation or astronomical purposes; telescope pointing for earth-resource or reconnaisance purposes; fine tuning of apparatus for research or communications purposes; and, last but not least, piloting tasks such as rendezvous in orbit and reentry into the earth's atmosphere. (At least one of the crew members is likely to be a pilot or trained as a pilot for such emergencies.)

In order to measure behavior appropriate to such tracking tasks, Systems Technology, Inc., under sponsorship by the NASA-Ames Research Center's Man-Machine Integration Branch, provided a battery of tracking tasks to be performed during the 90-day mission. The objectives of this experiment were:

(1) To obtain a simple "clinical" measure of the crewmember's visual-motor dynamic performance on a routine basis using the so-called "critical instability task" (ref. **3).**

(2) To obtain comprehensive measures of the intrinsic dynamic response properties on a less frequent basis by means of advanced cross-correlation techniques, and to correlate this standard tracking-task data with the critical instability measure.

(3) To present data obtained in this tracking experiment for correlation with medical physiological and psychological data from other experiments run concurrently.

The tracking task test battery and associated apparatus employed in this experiment were developed under NASA sponsorship and are detailed in references **3** through **6.** Systems Technology's role in the present experiment was to provide test specifications, experimental design and procedures; to participate in indoctrination and training; and to reduce and analyze the data. Douglas personnel were responsible for integrating the equipment and tests into the 90-day Experiment, and for administering the control task test sessions.

CONTROL TASKS AND EXPERIMENTAL SETUP

Control Tasks

The psychomotor tests used in this experiment are continuous, compensatory visual-motor tracking tasks. A general block diagram representation of these tasks and associated data measures and analysis is shown in figure **1.** Further details on these tasks are given in reference **6.** Basically, the subject is required to control the motion of a luminous horizontal CRT line with an isometric (force) control stick whose output controls a dynamically unstable controlled element (first-order: $Y_c=\lambda_1/(s-\lambda_1)$; second-order: $Y_c=\lambda_2/s(s-\lambda_2)$). If the subject provides the appropriate dynamic equalization behavior he will be able to not only stabilize the man-machine system, but also to minimize CRT line motions away from the null point or reference line. Two variations of this unstable tracking task employed in the present experiment are described below:

Critical instability task.—The subject is required to maintain stable control as the controlled element's instability is steadily increased. No external disturbance need be introduced in this task because "(remnant" noise sources internal to the human operator (e.g., unsteadiness, tremor) provide ample excitation for the unstable element. In the face of the increasing instability the subject will lose control of the task at some

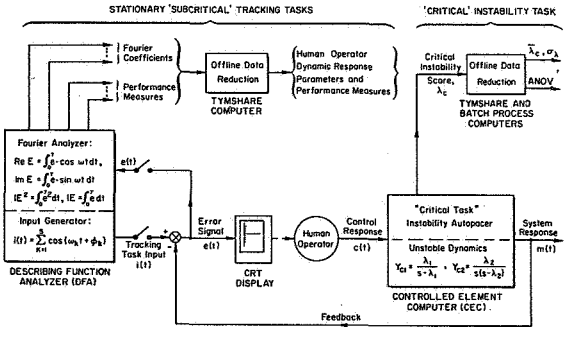

FIGURE 1.—Tracking tasks, *data* measurements, **and** analysis.

point because the line diverges off the CRT more quickly than he can exert compensatory control action. The degree of instability, λ_c, at which the subject loses control is termed his "critical instability" score. It is roughly equal to the inverse of the operator's dynamic time delay as shown in references 3 through 6.

The control of simple first-order divergent dynamics is called the *first-order critical task*, and requires the operator to act as a simple gain (i.e., the operator's stick output looks like a scaled version of the system error signal including a time shift equal to the operator's dynamic time delay). Controlling a first-order divergence in series with a pure integrator is called the *second-order critical task*. In controlling these dynamics the operator must effectively cancel out the effect of the integrator by providing what we term *first-order lead* equalization in order to stabilize the control dynamics. (Lead equalization is equivalent to rate perception or error signal prediction.) Generation of this lead equalization requires additional mental processing time (ref. 7) which increases the operator's effective dynamic time delay. Thus for the second-order critical task the operator can't achieve as high a critical instability score as with the first-order task.

The operator's basic effective time delay, as measured by the first-order critical task, is composed primarily of neural conduction time delays and neuromuscular dynamics of the arm. Thus performance on first-order critical task is a measure of basic neuromuscular dynamics, while the second-order task measure includes a component due to higher center involvement.

The critical task is easily administered since it only requires about one minute per trial and a single number is recorded at the end of each trial. Therefore, the first- and second-order critical instability tasks were selected to be administered routinely during the 90-day confinement test.

Xteady "subcritical" tracking tasks.—For steady tracking tasks the instability level of the unstable dynamics is held constant at a value well below the typical subject's critical instability score. An unpredictable command input is introduced into the tracking loop as shown in Fig. 1, and the subject is asked to maintain minimum tracking error during runs lasting approximately 2 min. Using special apparatus to be described later, the error signal is Fourier analyzed and performance data are computed during the run. These data are further reduced off-line, via a time-sharing computer program, to obtain the subject's open-loop describing function and task performance. The describing functions are fitted with a three-parameter dynamic response model, and the resulting loop closure properties are interpolated. Key parameters presented herein include

Crossover frequency (ω_c).—The unity-amplitude frequency of the open loop describing function; determines the closed-loop bandwidth.

Phase margin (φ_M).—A measure of system stability margin related to the closed-loop damping ratio.

Dynamic time delay (τ_e).—The subject's visual-motor time delay in a continuous tracking task including neural and mental delays and neuromuscular lags.

The performance measures include

Normalized error variance (σ_e^2/σ_i^2).—the ratio of tracking error variance to the variance of the task input.

Error coherence (ρ_{e^2}).—the percentage of total variance predicated by (correlated with) the describing function measurements. The remaining error power ($1-\rho_{e^2}$) is due to the subject's internal noise (remnant).

For this experiment we chose to include both first- and second-order subcritical tracking tasks that are dynamically equivalent to the first- and second-order critical instability tasks. The first-order instability was set at $\lambda = 2$ rad/sec, and the second-order case was set at $\lambda = 1.25$ rad/sec. Although these tasks allow a detailed assessment of the subject's dynamic response and noise properties, they require longer trial durations and a large amount of on-line data collection and reduction. For this reason they were run less frequently than critical tasks during the 90-day test, and were employed to provide realistic tracking task data to correlate with the critical instability scores.

Test Setup and Equipment

The experimental layout and apparatus are shown in figure 2. The test administrators con-

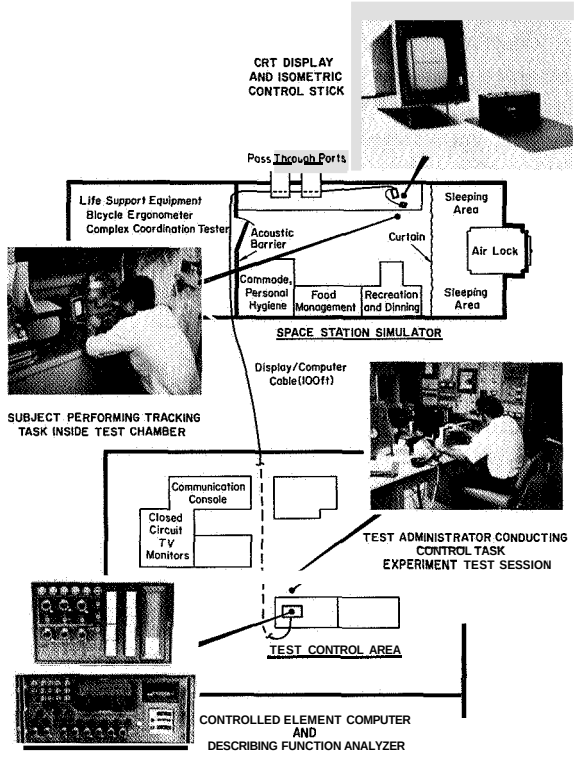

FIGURE 2.—Control task apparatus and experimental setup for the 90-day confinement study.

ducted the experiment from the control room where the task computers were located. The controlled element computer (CEC) provided the unstable dynamics for the tracking tasks, and automatically increased the instability during critical task runs as shown in figure **1.** The describing function analyzer (DFA) provided the subcritical tracking task input, Fourier analyzed the tracking error signal, and measured various performance parameters.

The display and control stick, connected to the computers through a 100 ft cable, were located in the space chamber recreation area. The Douglas Test Administrator communicated with the crewmen through an intercom, and also via interconnected "ready" lights located on the subject's display and the controlled element computer.

TRAINING

Crewmen began training on the first- and second-order critical tasks four months prior to commencing the 90-day confinement period. This training consisted of approximately thirty 1-hr sessions spanning a 5-wk period. At each session the crewmen would track **2** three-trial blocks of the first-order critical task and **2** five-trial blocks of the second-order critical task. These λ_{c1} and λ_{c2} training scores are plotted in figure 3(a). It is evident that all crewmen reached stable levels of critical instability within about **100** trials of distributed practice.

Training of the steady tracking tasks was commenced immediately after critical task training. Because of the dynamic similarity between the critical and subcritical tasks, a favorable transfer of training is assured. The crewmen tracked three first-order and three second-order runs per session for approximately ten sessions spanning a four-week period. Dynamic response data for the first- and second-order tasks is plotted in figure 3(b) and 3(c). From figure 3(b) and 3(c) the crossover gain, ω_c, shows a gradual increase with training, while the stability margin, φ_M, shows a concurrent decrease. Stable training levels were achieved in all cases except for crew-

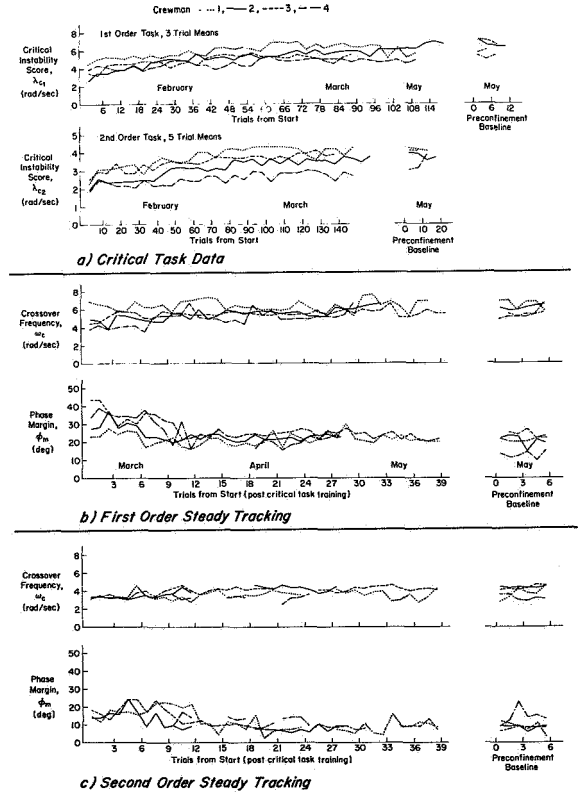

FIGURE 3.—Training data.

man 4 on the second-order task. He had significantly less exposure to this task than the other crew members, and he later exhibited correspondingly larger learning effects during the confinement period.

90-DAY CONFINEMENT TESTS

General

During the confinement period, three trials of first-order and five trials of second-order critical instability task were administered routinely every Monday, Wednesday, and Friday, following the midday meal. These data formed the core of our experimental design, and represent a base from which other tracking data can be compared and extrapolated. Steady tracking sessions were performed twice a week, one session for each order. These sessions began with the critical instability trials of the equivalent dynamics in order to provide a warmup and also to provide concurrent correlations between λ_c and the more comprehensive measures of steady tracking behavior.

The crewmen were split into two shifts, with crewmen 1 and 2 on a nominal day shift (0700 to 2300 hr) and crewmen 3 and 4 on a graveyard shift (2100 to 1300 hr). Illumination was held constant inside the simulation chamber, and all indications are that crewmembers 3 and 4 quickly adjusted to their abnormal work shift. Test sessions were conducted after the midshift meal (nominally 1300 hr for crewmen 1 and 2, and 0200 hr for crewmen 3 and 4). All test sessions began with a warmup critical instability trial.

Critical Instability Results

Weekly mean critical task scores (averaged across the solely λ_c sessions for each week) are plotted in figure 4. Generally, these scores were very reliable (low residual variance) and show a consistent stratification among crewmen. There is a consistent, albeit small, improvement trend apparent over the 90-day period in all cases except for crewman 3 on the second-order task. Experience suggests that this reflects a residual improvement in the neuromuscular system due to continuous practice beyond the initial training asymptote—much as in any athletic skill involving strength. Crewman 1 evidenced the most variable performance, with a definite dip in scores during the initial confinement period compared with his preconfinement baseline. This dip was followed by a return to performance levels significantly above his preconfinement baseline.

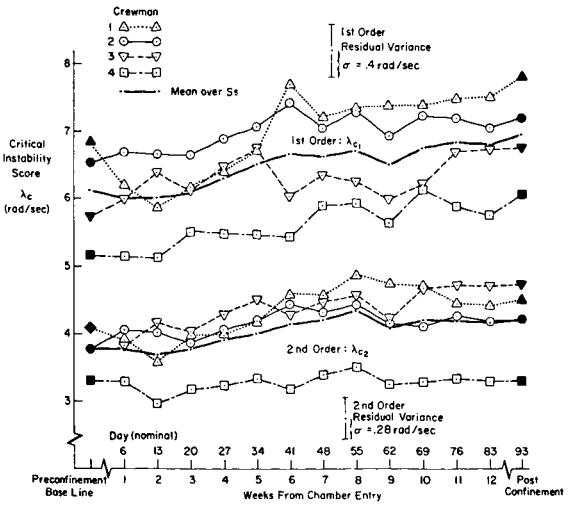

FIGURE 4.—Weekly mean critical instability scores during the 90-day confinement period.

There is one very consistent dip in performance for all crewmembers during week 9, with a preceding performance peak during week 8. These results appear to correlate with assessments of crew psychological status obtained by other investigators (references 8 and 9). Positive "affect" among crew members increased sharply dueing week 8, which was associated with passing the midpoint of the mission. During week 9 the measure of positive affect took a sharp drop and reached a mission low point, accompanied by a corresponding increase in the hostility index among crew members and a drop in reported sleep time. Although the changes in critical task performance which accompanied these behavioral symptoms are not large, operationally, the sensitivity of the subjects' critical task scores to the psychological climate is interesting.

Analysis of variance procedures applied to the data showed subjects and weeks to be significant main effects. The subjects-by-weeks interaction was also statistically significant. The residual variance obtained from the ANOV was quite small, with the standard deviation being on the

order of only 7 percent of the mean score for each task as shown in figure 4. This low variability is one of the virtues of critical task which allows for the efficient measurement of small changes in visual-motor behavior.

Steady Tracking Results

The steady tracking behavior and performance data are plotted in figure 5. (The critical instability data shown here were obtained at the beginning of each subcritical tracking session, and were not included in fig. 4.) The steady tracking data are often missing because these sessions had a somewhat lower priority than the critical task sessions, and were sometimes not performed.

The dynamic response data ω_c and φ_M and critical task scores (λ_c) seem to remain fairly consistent and similar in level over the 90-day period. The normalized error and error coherence performance measures (σ_e^2/σ_i^2 and ρ_e^2) show considerable variations, however. Crewman 4's tracking errors are significantly higher than that of the other crew members. This result seems to be due primarily to an intrinsically higher remnant level (as evidenced by his lower error coherence) and to a poorer loop closure (evidenced by low λ_c and low φ_M).

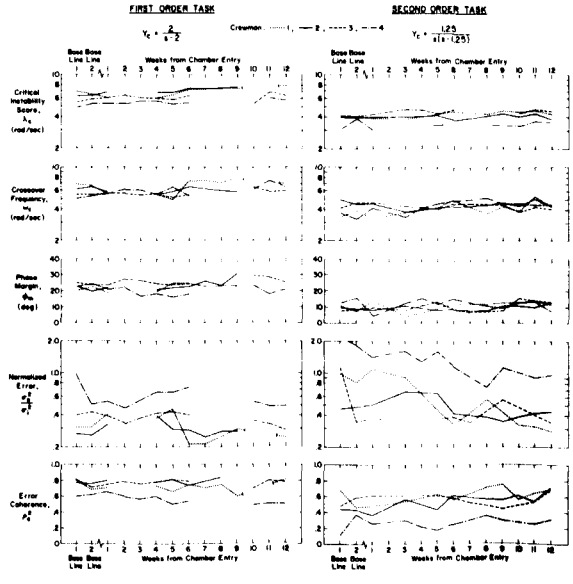

FIGURE 5.—Comparison of tracking-session data for the 90-day test.

Crewman 1 and 4 were still learning the second-order steady tracking task during the first half of the confinement period, as reflected in their normalized error scores. This result seems to be primarily due to dynamic response effects as both subjects show a corresponding increasing trend in crossover gain during the first half of the mission.

Correlation Between Subcritical and Critical Task Results

One of the objectives of this experiment was to tie in the dynamic response measurements with the critical instability scores obtained during the steady tracking sessions. The describing function parameters, performance measures and critical task scores from these sessions were entered in a computer file and subjected to correlation analysis.

The correlation matrix for this data is given in table 1. The inverse dynamic time delay τ_e^{-1} was used for the correlation analysis, because this is the parameter linearly correlated with λ_c, as shown in reference 6. A scatter diagram showed σ_e^2/σ_i^2 to be hyperbolically related to λ_c, so the inverse of this parameter was also employed in the correlation analysis.

As shown in table 1, λ_c is highly correlated with the more detailed steady tracking measures. This indicates that the easily administered critical task can reliably monitor a subject's basic tracking behavior. Furthermore, a network of λ_c runs can be used to supplement a limited number of detailed steady tracking measurements, thereby providing a comprehensive picture of a subject's dynamic response and remnant characteristics over extended time periods. The one describing function measure not correlated with λ_c is the "low-frequency phase droop" parameter, α. This is not surprising since λ_c is primarily dependent on crossover-region phase effects which depend mainly on the time delay τ_e and only secondarily on α (ref. 4).

A scatter plot of the τ_e^{-1} versus λ_c scores obtained during each subcritical tracking session is shown at the top of figure 6 for both first- and second-order tasks. Because it is ultimately bounded by τ_e^{-1} and hence by λ_c, crossover frequency ω_c has also been shown to correlate

TABLE 1.—*Correlation Matrix—90-day Confinement Study Dynamic Response Data*

	Variable	λ_c	$\left(\frac{\sigma_e^2}{\sigma_i^2}\right)^{-1}$	ρ_e^2	ω_c	φ_M	τ_e^{-1}	α	ω_u
	Critical instability score, λ_c	1.000	0.632	0.706	0.801 *	0.813 *	0.859 *	−0.028	0.890 *
Steady tracking data — Performance	Inverse normalized error var., $\left(\frac{\sigma_e^2}{\sigma_i^2}\right)^{-1}$		1.000	0.651	0.406	0.351	0.357	−0.015	0.430
Dynamic response parameters	Error coherence, ρ_e^2			1.000	0.379	0.498	0.499	0.131	0.554 *
	Crossover frequency, ω_c				1.000	0.684	0.799	−0.169	0.838 *
	Phase margin, φ_M					1.000	0.925 *	−0.280	0.923
	Inverse dynamic time delay, τ_e^{-1}						1.000	−0.010	0.940 *
	Low freq. phase droop parameter, α							1.000	−0.122
	Upper phase crossover freq., ω_u								1.000

Note: $N = 65$ degrees-of-freedom
$P = 0.001$ for $R > 0.475$
* Denotes $R \geq 0.80$

with λ_c (ref. 6), and this scatter diagram is shown at the bottom of figure 6. Also, the present regression relationships, with initially naive subjects, are quite similar to those given in ref. 6 among professional pilots, as shown in figure 6.

A high correlation is noted in table 1 between inverse dynamic time delay τ_e^{-1} and phase margin φ_M. Time delay is a basic limiting factor in the human operator's visual-motor dynamic response, whereas phase margin is related to how high a gain (effort) the operator is willing to produce. The theoretical relationship between φ_M and τ_e, obtained from closed-loop analysis using the "crossover-model" for the man/machine system, is (see ref. 3, appendix A):

$$\varphi_M \doteq \tan^{-1}\frac{\omega_c}{\lambda} - \tau_e\omega_c - \frac{\alpha}{\omega_c}$$

where ω_c is related to the subject's gain. The above relationship shows φ_M proportional to τ_e, while the data plotted in figure 7 show a linear correlation with inverse time delay τ_e^{-1}. This behavior was achieved mainly by a covariation of ω_c with τ_e since the α term is small. This effect may represent some form of optimum behavior given the present task and should be further investigated.

Data obtained in a previous experiment with pilot-subjects (ref. 6) has been added to figure 7. The data from the two experiments show good agreement, which implies the universal applicability of results obtainable with the tracking task battery employed in this experiment.

CONCLUDING REMARKS

Crewmen performance in this experiment agrees quite favorably with that of experienced pilots and test subjects tested previously (ref. 6). No serious degradations in performance were noted during the mission, and in fact there appeared to be a slight improvement trend throughout the 90-day period. Some dips in individual performance seem to correlate with crew psychological status as measured by other investigators. While these effects were not operationally serious, they do demonstrate the capability of critical task to efficiently measure small changes in visual-motor response behavior.

The dynamic response psychomotor tests used in this experiment have a well developed theoretical basis and have been thoroughly validated (references 3 through 6). With the present experimental results we have demonstrated that sophisticated human visual-motor properties can be efficiently and reliably measured over an extended period and in spite of adverse living conditions. The control task equipment functioned properly throughout the mission, even though the CRT display and control stick were subjected to the simulator sub-atmospheric pressure. In spite of the apparent complexity of the equipment and test protocols, both the crewmen and test administrators quickly became proficient in the experiment procedures. Test sessions for one subject typically required less than 15 min. Thus the simpler equipment and tests

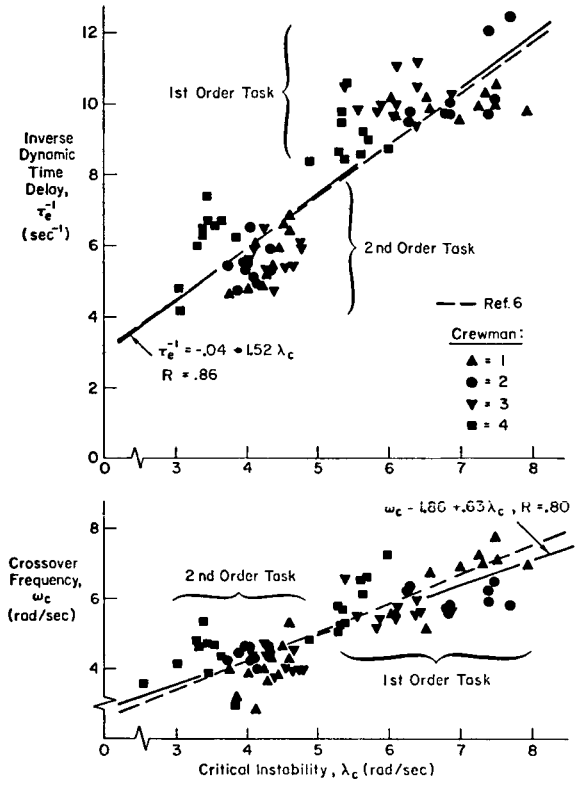

FIGURE 6.—Correlation between critical instability score and steady tracking data.

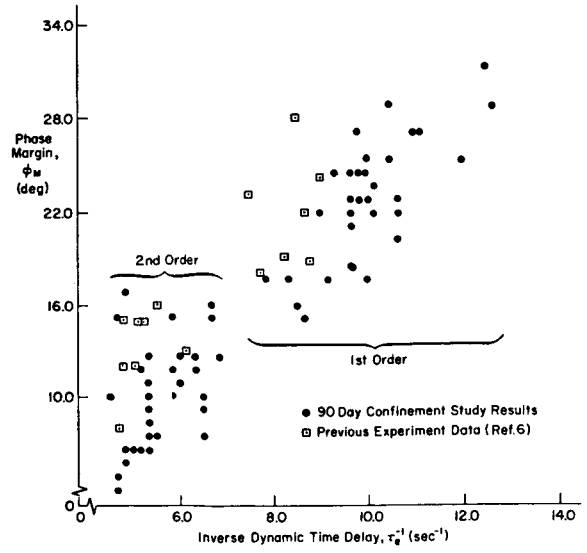

FIGURE 7.—Correlation between 90-day confinement study and reference experiment dynamic response data.

being planned for future orbital use by astronauts should meet with good acceptance and allow us to obtain in-depth information regarding the space environment's effect on human dynamic response properties.

REFERENCES

1. JACKSON, J. K.: Test Objectives and Program Management. NASA SP–261, sec. 2, 1971.
2. PEARSON, A. O.; AND GRANA, D. C.: Preliminary Results From an Operational 90-Day Manned Test of a Regenerative Life Support System. NASA SP–261, 1971.
3. JEX, H. R.; MCDONNELL, J. D.; AND PHATAK, A. V.: A "Critical" Tracking Task for Man-Machine Research Related to the Operator's Effective Delay Time. Part I: Theory and Experiments with a First-Order Divergent Controlled Element. NASA CR–616, Nov. 1966.
4. MCDONNELL, J. D.; AND JEX, H. R.: A "Critical" Tracking Task for Man-Machine Research Related to the Operator's Effective Delay Time. Part II: Experimental Effects of System Input Spectra, Control Stick Stiffness, and Controlled Element Order. NASA CR–674, Jan. 1967.
5. JEX, H. R.; MCDONNELL, J. D.; AND PHATAK, A. V.: A "Critical" Tracking Task for Manual Control Research. IEEE Trans., vol. HFE–7, no. 4, Dec. 1966, pp. 138–145.
6. JEX, H. R.; AND ALLEN, R. W.: Research on a New Human Dynamic Response Test Battery. Part I: Test Development and Validation; Part II: Psychophysiological Correlates. Proceedings of the 6th Annual Conference on Manual Control, Air Force Institute of Technology, Wright-Patterson AFB, Apr. 7–9, 1970, pp. 743–777.
7. MCRUER, D. T.; HOFMANN, L. G.; JEX, H. R.; ET AL.: New Approaches to Human-Pilot/Vehicle Dynamic Analysis. AFFDL–TR–67–150, Feb. 1968.
8. SEEMAN, J. S.; AND MCLEAN, M. V.: Behavioral Program. NASA SP–261, sec. 29, 1971.
9. OKANES, M. M.; FEENEY, W. R.; AND SEEMAN, J. S.: Non-Interference Performance Assessment (NIPA). NASA SP–261, sec. 35, 1971.

N73-10134

30. Prediction and Analysis of Human Performance in a VTOL Hover Task*

SHELDON BARON AND DAVID L. KLEINMAN

Bolt Beranek and Newman Inc.

An optimal control model is used to predict pilot performance in a series of longitudinal hovering tasks. Configurational changes are considered that alter significantly the system response to both control and disturbance inputs. Model predictions of mean-squared performance are compared with measurements obtained in an independent experimental study of the task. In addition, the optimal control model is used to predict describing functions that correspond to the "loop closing" pilot transfer functions frequently employed in classical multiloop manual control analyses.

INTRODUCTION

Modern control theory with its emphasis on state-space techniques and digital computation has provided the basis for systematic analysis and synthesis of multi-input, multi-output systems. In recent years this theory has been blended with results from human response theory to develop a computerized procedure for analyzing manned-vehicle systems (refs. 1 and 2). Central to this approach is an "optimal-control" or "state-variable" model of the human operator. This model has proven to be very successful in predicting human control characteristics and system performance in a variety of single-axis tracking tasks. It has also been used to analyze longitudinal hover control of an XV–5A (ref. 3). In that study, semi-empirical techniques, involving a fairly extensive preliminary experimental program, were used to determine the parameters of the optimal-control model. Using these parameters, human performance in the hover task was predicted and compared with data from simulation experiments. The results showed that the model was capable of reproducing both the correlated and uncorrelated portions of the pilot's control spectra as well as closed-loop system performance. The effects of visual scanning and a change in displayed information were also predicted.

In this paper, we also analyze longitudinal hover control. However, our emphasis is on the ability of the model to predict the effects on performance of a variety of configurational changes (i.e., changes in aircraft stability derivatives). In addition, we shall use the optimal-control model to predict describing functions that correspond to "loop-closing" pilot transfer functions that are frequently employed in classical multiloop manual control analyses.

MODEL FOR THE HUMAN OPERATOR

The optimal-control model of the human operator is predicated on the assumption that he behaves optimally subject to his inherent limitations and his understanding of the requirements of the task. This implies a *normative* approach to developing the model, i.e., we seek to determine what the human should do given his limitations and the task. This leads to a model for the pilot that has as its key elements representations of his limitations and of his compensating "processes." The resulting model has been described in detail in references 1 through 3, so we will only review briefly its basic features.

The structure of the model for the human

* This work was performed for NASA-Electronics Research Center under contract NAS12–104, and is described in greater detail in reference 1.

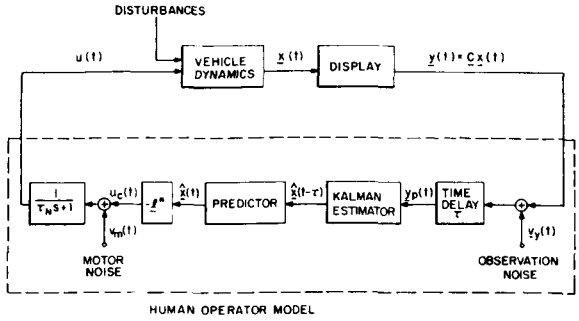

FIGURE 1.—Control theoretic model of optimal human behavior.

operator is shown in figure 1. Also shown is the model of the vehicle-display system. Vehicle dynamics are assumed to be linear and time-invariant.* The state of the vehicle is given by the vector $\underline{x}$ and the displayed variables, $\underline{y}$, are assumed to be linear combinations of the states. Input disturbances are modelled as zero-mean, gaussian, white noises passed through appropriate linear filters.†

Figure 1 illustrates several types of pilot limitations that are represented explicitly in the model. The various internal delays associated with visual, central processing and neuro-motor pathways are modelled, for convenience, by a lumped perceptual delay τ. The "equivalent" observation noise process indicated in figure 1 accounts for the effects of sensory and central processing sources of human randomness. A white, gaussian noise is added to each "observed" variable. The power density level of this noise is assumed to scale with the mean-squared value of the "signal" being observed. The noise-to-signal ratio is a parameter of the model that is expected to depend on the nature (quality, type, form) of the display. The model also includes a "motor-noise" to account for the fact that the human operator cannot generate intended control inputs perfectly. The motor noise is also assumed to be a white gaussian noise and its power density is scaled with the intended or "commanded" control u_c indicated in figure 1. The motor noise and the observation noises together account for human randomness; for situations in which quasilinear, frequency domain representations of the human are appropriate, these noises constitute a model for controller remnant.

Given the above "human" limitations, and our basic assumption, the model of the human operator then includes for "equalization": a Kalman estimator to compensate for the observation noises; a least mean-squared predictor to compensate for the time-delay; and, a set of feedback gains that are optimal in terms of minimizing a quadratic cost functional of the form

$$J=\sum_{i=1}^{n} q_i\overline{x_i^2}+g\overline{\dot{u}^2}. \qquad (1)$$

This quadratic performance index is a natural extension of the mean-squared tracking error criterion of classical compensatory tracking experiments. The cost functional weightings, $q_i \geq 0$ and $g>0$, may be either objective (specified by the experimenter or designer) or subjective (adopted by the human in performing and relating to the task). The inclusion in equation (1) of a term proportional to mean-squared control rate is an important feature of the model. This term may be thought of as constituting a subjective penalty on too rapid control movements or as an indirect method for accounting for physiological limitations on the human's bandwidth. Its inclusion results in the first order controller lag (time constant $=\tau_N$) shown in figure 1.

To apply the model, we must specify the values of its parameters: the time delay τ; the noise-to-signal ratios of the observation noises ρ_i and the motor-noise ρ_m; and the cost-functional weightings q_i, g. Our studies of single-axis control tasks have revealed a consistency of parameter values that is very encouraging. In particular, we have found that for k, k/s, and k/s^2 tracking, excellent agreement between model and measured data is obtained with the following parameter values: $\tau=0.15$ to 0.2 sec; $\rho_i \simeq 0.01$ (-20 dB); $\rho_m \simeq -0.003$ (-25 dB); $\tau_N=0.08$ to 0.1 sec. (ref. 2).

THE HOVERING TASK

The results of an analytic and experimental investigation of precision hover control by Vinje

* The time-invariance assumption is not essential for using the model to predict performance; certain "memoryless" nonlinearities can also be considered (ref. 4).

† Nonrandom inputs can also be considered (ref. 4).

and Miller (refs. 5 and 6) will provide the basic data for our investigation. They conducted a series of simulator experiments in which they measured the effects of variations in aircraft stability parameters on rms hovering performance.

Briefly, the pilot's task was to minimize longitudinal position errors while hovering in turbulent air. Only longitudinal motions were considered and the pilot was not required to control the height of the aircraft. The linearized equations used to simulate this task were

$$\left.\begin{aligned}\dot{q} &= M_u(u+u_g)+M_q q+M_\delta\delta\\ \dot{u} &= X_u(u+u_g)+g\theta\end{aligned}\right\} \qquad (2)$$

where $u=\dot{x}$ is the perturbation velocity along the x-body axis, u_g is the longitudinal component of the gust velocity;* θ and $q=\dot{\theta}$ are pitch and pitch-rate, respectively; δ is the control stick input; g is the gravitational constant; and, X_u, M_u, M_q, M_δ are aircraft stability derivatives. The stability derivatives were assumed to have "nominal" values of $X_u=-0.1$, $M_u=0.0207$, $M_q=-3.0$, and $M_\delta=0.431$. We will examine the effects of the variations in these derivatives indicated in table 1 (the case numbers identifying

TABLE 1.—*Variations in VTOL Stability Derivatives*

Case	X_u	M_u	M_q	M_δ
Nominal (PH8)	−0.1	0.0207	−3.0	0.431
PH1	0	0.0207	−3.0	.287
PH2	−.05	0.0207	−3.0	.420
PH5	−.3	0.0207	−3.0	.516
PH6	−.1	0	−3.0	.300
PH7	−.1	.0104	−3.0	.360
PH9	↓	.0312	−3.0	.481
PH10	↓	.0207	−1.0	.369
PH12	↓	.0207	−5.0	.493

the various conditions are those assigned in reference 6).

The pilot was provided with a Norden contact analog display on which both aircraft attitude θ and position x were indicated explicitly. (The display is described in ref. 5.) We assume, on the basis of much evidence, that the pilot is able to infer $\dot{\theta}=q$ and $\dot{x}=u$ from the display, so that the "displayed output" is $y=\text{col}\,\{u,x,q,\theta\}$.

MULTILOOP-MODEL ANALYSIS

A closed-loop pilot-vehicle analysis of the above hover task, using fixed-form, multiloop pilot models was performed by Vinje and Miller. We present the highlights of their approach in an attempt to provide further context for the results we have obtained with our model.*

In applying the multiloop-model approach, one must *assume* an a priori closed-loop system structure. In other words, an assumption must be made concerning those loops "closed" by the pilot. Vinje and Miller assumed the "series loop" model illustrated in figure 2. (A parallel loop model for this task is also a possibility.) Once the loop topology has been decided upon, it is then necessary to assume specific forms for the individual transfers comprising the pilot model. For the structure of figure 2 this means choosing fixed forms for Y_{p_x} and Y_{p_θ}. The forms chosen by Vinje and Miller were

$$Y_{p_x}=K_{p_x}(T_{L_x}s+1)e^{-\tau_x s} \qquad (3)$$

$$Y_{p_\theta}=K_{p_\theta}(T_{L_\theta}s+1)e^{-\tau_\theta s}/(T_N s+1). \qquad (4)$$

In equations (3 and 4), and the "neuromuscular lag" T_N, the θ-loop transport lag τ_θ, and the x-loop transport lag τ_x were considered to be fixed parameters with values of 0.35 sec, 0.09 sec and 0.08 sec, respectively; the gains K_{p_θ}, K_{p_x} and the lead time constants T_{L_θ}, T_{L_x} were assumed to be "adaptable" parameters, chosen by the pilot to achieve certain desired closed-loop characteristics.

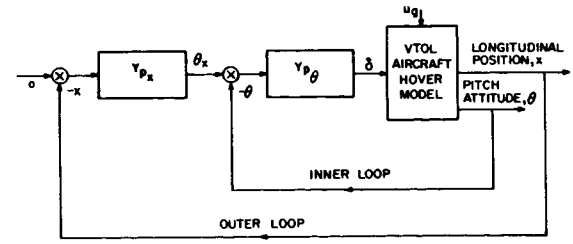

FIGURE 2.—Series loop model for pilot longitudinal control in hover.

* The simulated gust u_g was equivalent to first-order filtered white noise with a bandwidth of 0.314 rad/sec and an rms value of 5.14 ft/sec.

* Details may be found in reference 6.

Inasmuch as Y_{p_x} and Y_{p_θ} cannot be measured directly in this task, Vinje and Miller devised a technique for "identifying" the adaptable parameters. In particular, they iterated on K_{p_θ}, K_{p_x}, T_{L_θ} and T_{L_x} until the rms values σ_u, σ_x, σ_θ, and σ_q computed by using the closed-loop model of figure 2 "matched" the corresponding rms hover performance (as measured in the simulator experiments) to within 0.5 percent. Vinje and Miller did not use rms control activity σ_θ in their matching procedure in an attempt to minimize the effects of ignoring pilot remnant in the computation of the pilot-model adapted parameters. However, they compared measured values of σ_δ with those obtained from calculations based on the computed pilot-model parameters and found that these values of σ_δ differed, on the average, by about 17 percent.

Once values for the parameters of Y_{p_x} and Y_{p_θ} are given, it is possible to compute various loop closure characteristics, e.g., inner- and outer-loop crossover frequencies and phase margins. The inner-loop characteristics are obtained from $Y_{p_\theta}\cdot[\theta/\delta]$. The outer-loop characteristics are calculated by assuming the inner (pitch) loop is closed.

Before leaving this discussion of the multiloop analysis, it is worth repeating and re-emphasizing that the pilot-model adapted parameters and the computed loop closure characteristics are *derived* measures of human performance that are designed to provide additional understanding of the pilot's behavior. The only direct measures made by Vinje and Miller in their experimental study were the measures of closed-loop rms hovering performance σ_x, σ_u, σ_θ, σ_q σ_δ.*

PREDICTIONS WITH THE OPTIMAL CONTROL MODEL

In this section we present the results of applying the optimal control model of the human operator to the analysis of the hover task described earlier. We begin with a brief discussion of the choice of parameters for the optimal control model. Then we present and discuss model predictions for the various configurations listed in table 1.

Model Parameters

Values for τ_N, τ, the ρ_i, and ρ_m as well as cost functional weightings had to be chosen for this task. We felt that, with respect to those parameters related primarily to *intrinsic* human limitations, values representative of those used in the single-axis studies constituted a good a priori choice. Thus, we let $\tau_N = 0.1$ sec, $\tau = 0.15$ sec, $\rho_1 = \rho_2 = \rho_3 = \rho_4 = -20$ dB and $\rho_m = -25$ dB.* It is significant that we were able to keep this (initial) set of model input parameters fixed throughout the entire subsequent study.

The choice of a cost functional is a bit more subtle. Recall that the pilots were instructed to minimize position error σ_x. However, in order to accomplish this the pilot must suppress pitch errors inasmuch as such errors introduce disturbing longitudinal forces. In addition, one may expect that pilots try to avoid excessive attitude changes during the process of minimizing hovering errors. Accordingly, it seems reasonable to include a pitch or pitch-rate term in the cost functional; we chose to add a term proportional to mean-squared pitch rate, σ_q^2. We picked the pitch-rate weighting on the basis of the measured scores for the "nominal" configuration.† In that case, values of σ_x^2 and σ_q^2 of approximately 1.2 ft^2 and 0.0024 rad^2/sec^2 were found. On this basis, we selected a pitch-rate weighting of 400 and we used this value in all subsequent calculations. Thus, the cost functional for this analysis was

$$J = \sigma_x^2 + 400\sigma_q^2 + g\sigma_\delta^2 \tag{5}$$

where g was chosen so that $\tau_N \simeq 0.1$ sec.

Nonimal Case

We now compare model predictions with measured and derived data for the nominal case (PH8 in table 1). Measured and predicted scores are compared below in table 2. The measured

* Another (subjective) measure, namely, pilot opinion rating was also taken but we will not discuss this measure at length here.

* Noise ratios were chosen within ± 0.5 dB and τ_N was within 10 percent of 0.1 sec for all cases.

† Other, a priori, techniques for choosing the weighting are possible.

TABLE 2.—*Comparison of Measured and Predicted Scores for Nominal Configuration* ($X_u = -0.1$, $M_u g = 0.667$, $M_q = -3$, $M_\delta = 0.431$)

	σ_u	σ_x	σ_q	σ_θ	σ_δ
Measured	0.79(0.09)	1.16(0.10)	0.050(0.003)	0.032(0.002)	0.59(0.03)
Predicted	.82	1.08	.055	.036	.63

values are averages of ten runs and the quantities in parenthesis indicate the corresponding standard deviations. It can be seen that the agreement between predicted and measured scores is excellent.*

It would be desirable to obtain comparisons of measured and predicted frequency domain data for this study that might provide a more complete validation of the model. Unfortunately, the data of reference 6 does not include frequency domain measurements. Instead, the fixed-form expressions for Y_{p_x} and Y_{p_θ} were assumed and the parameter values (K_{p_θ}, K_{p_x}, T_{L_θ}, T_{L_x}) were adjusted to match scores.

In an attempt to correlate the multi-loop structure of our optimal-control-model with that of Vinje and Miller's model, we simply computed the equivalent transfers, Y_{p_θ} and Y_{p_x} in the following manner. From figure 2, we see that the control input

$$\delta = -Y_{p_x} Y_{p_\theta} x - Y_{p_\theta} \theta. \tag{6}$$

On the other hand, for this situation, we may write the output of the optimal control model of the human operator as (see ref. 1 and Fig. 1)

$$\begin{aligned}\delta(s) = \underline{h}'\underline{y} &= h_1(s)u(s) + h_2(s)x(s) + h_3(s)q(s) \\ &\quad + h_4(s)\theta(s) \\ &= (sh_1 + h_2)x(s) + (sh_3) + h_4)\theta(s)\end{aligned} \tag{7}$$

Comparison of equations (6) and (7) yields

$$sh_3 + h_4 = -Y_{p_\theta} \tag{8}$$

$$\frac{sh_1 + h_2}{sh_3 + h_4} = Y_{p_x}. \tag{9}$$

Consequently, with these expressions for Y_{p_θ} and Y_{p_x}, it is possible to use the optimal control model to compute equivalent "inner" and "outer" loop characteristics, just as is done in the fixed-form multiloop analysis.

Figures 3 through 5 show the results of performing some of the frequency domain calculations for the "nominal" configuration. Bode plots

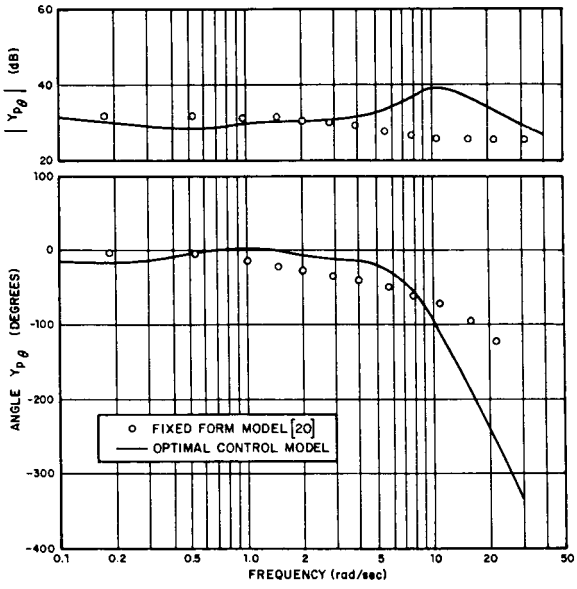

FIGURE 3.—Pitch-loop pilot describing functions Y_{p_θ} for nominal configuration.

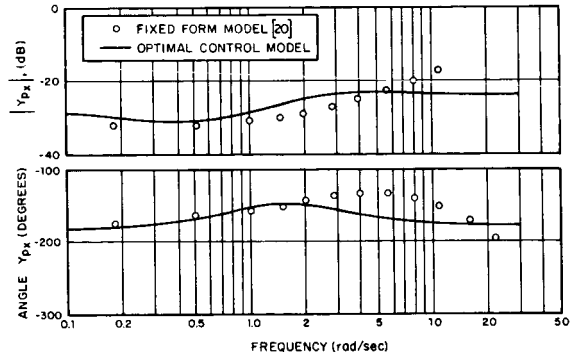

FIGURE 4.—Position-loop pilot describing functions for nominal configuration.

* It should be emphasized the only "parameter" used to "match" this data was the pitch-rate weighting.

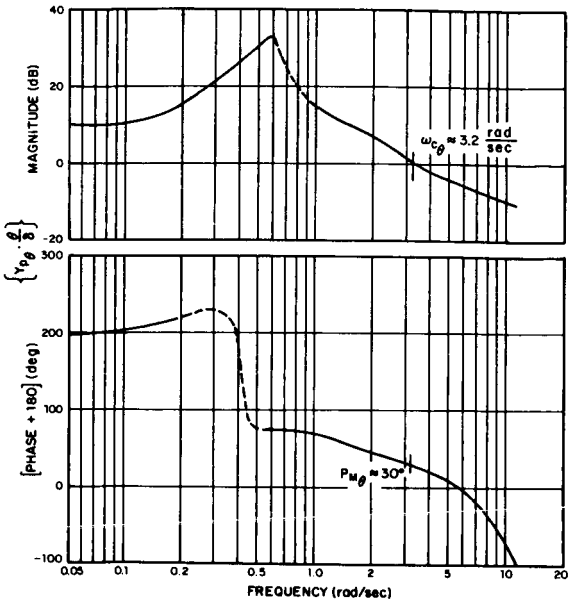

FIGURE 5.—Open loop describing function for pitch loop, $\{Y_{p_\theta} \cdot \theta/\delta\}$.

of Y_{p_θ} and Y_{p_z}, as computed from equations (8) and (9), are presented in figures 3 and 4. Also shown in these figures are the fixed-form Y_{p_θ} and Y_{p_z} corresponding to the parameter values (K_{p_θ}, T_{L_θ}, K_{p_z}, etc.) determined by Vinje and Miller. As can be seen, the corresponding Y_{p_θ}-transfers are in excellent agreement up to about 4 rad/sec; correspondingly good agreement between the Y_{p_z}-transfers is evident up to about 1.5 rad/sec.

In figure 5, the Bode plots for the transfer $\{Y_{p_\theta} \cdot \theta/\delta\}$, necessary to determine "inner"-loop closure characteristics, is presented.* We find that the optimal control model yields, for the pitch loop, "crossover" frequency and phase margin of approximately 3.2 rad/sec and 30°, respectively. Vinje and Miller obtain a pitch loop crossover frequency and phase margin of 3.1 rad/sec and 8°. Similar computations for the "outer" or position loop result in model crossover and phase margin of 1.1 rad/sec and 21° as compared to values of 1.0 rad/sec and 15° derived by Vinje and Miller. Thus, the agreement in these characteristics is good, with the optimal control model providing slightly greater stability margins.

The loop closure characteristics reveal that the Y_{p_θ} and Y_{p_z} predicted by the optimal control model agree closely with the derived values of Vinje and Miller up to frequencies slightly greater than the respective loop crossovers. The disagreements at higher frequencies cannot be resolved on the bais of the available data and they do not appear to be significant from the standpoint of system performance. However, from our studies of single-axis tasks, we can be reasonably certain that the high frequency deviations of the Y_p result from the longer time delay and the inclusion of the predictor in the optimal-control model.

Effects of Pitch Rate Damping, M_q

Predicted and measured rms-scores as a function of changes in pitch rate damping (with other derivatives held at "nominal" values) are plotted in figure 6. It should be re-emphasized that no changes in the parameters of the pilot model are made in computing the effects of changing aircraft parameters. Again, agreement is quite good, especially for the cases with higher damping. For $M_q = -5.0$, all the predicted scores are within the standard deviations of the data and we have already seen similar agreement for the $M_q = -3.0$ case. Model predictions are poorest for the configuration with the least damping ($M_q = -1.0$), although the maximum deviation between predicted and measured scores does not exceed 25 percent. Unfortunately, it is difficult to assess the true mismatch between model scores and data for this case because standard deviations of the measured averages were not available. (Standard deviations were published for the results of a second, different, subject; as might be expected, standard deviations increased as damping decreased.)

What is perhaps most surprising about the score data for the low damping case is that all the scores predicted by the optimal-control model of the human operator *exceed* those achieved by the pilot. This suggests that the observation noise-ratios in the model may have been too high. We

* The dashed portions of these curves correspond to what we believe are reasonable trends in the data. Unfortunately, our programs were designed to compute quantities at discrete frequencies (corresponding to values at which we normally measure). Time did not permit the recomputations necessary to define these frequency plots in more detail.

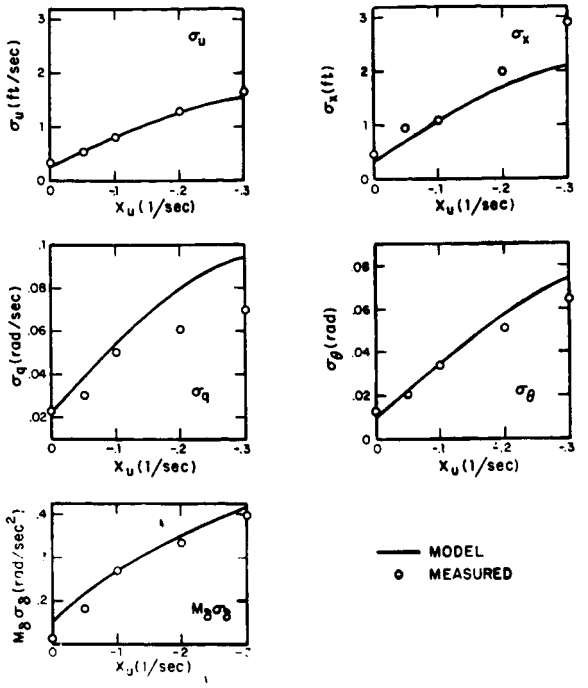

FIGURE 6.—Effect of pitch-rate damping on hovering performance ($M_u g = 0.667$, $X_u = -0.1$).

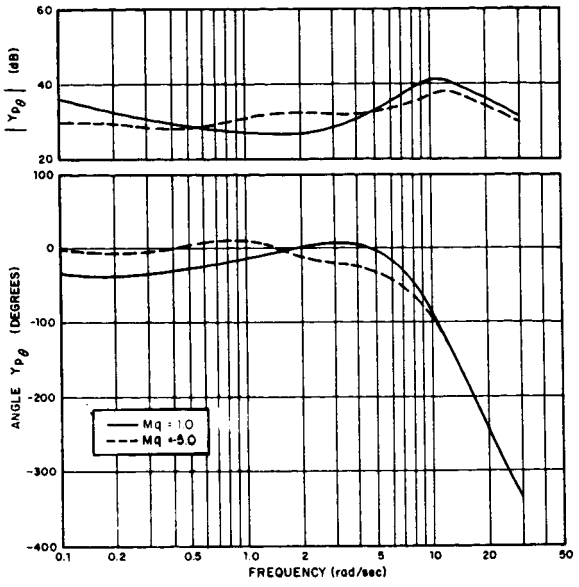

FIGURE 7.—Effect of pitch rate damping on predicted pilot describing function for pitch loop ($M_u g = 0.667$, $X_u = -0.1$).

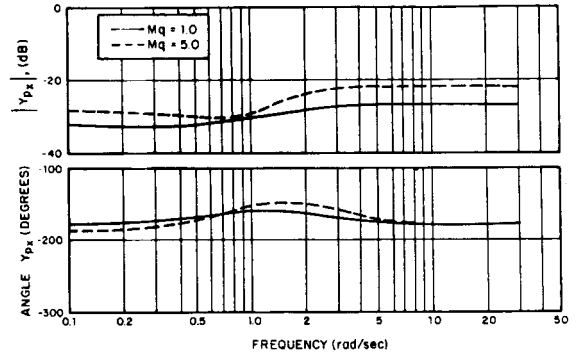

FIGURE 8.—Effect of pitch rate damping on predicted pilot describing function for position loop ($M_u g = 0.667$, $X_u = -0.1$).

decreased these noise-ratios to approximately −23 dB and found that *all* predicted scores were then within 10 percent of measured values. This is an interesting result because it implies that the pilots became less "random," in an attempt to maintain the lower scores. Or, in Levison's (ref. 7) terms, the pilots worked harder to achieve a criterion level. This correlates with the fact that the $M_q = -1.0$ case was rated unsatisfactory by the pilots (ref. 6) whereas the cases with higher damping were rated satisfactory.

The equivalent Y_{p_θ} and Y_{p_x} obtained from the optimal control model are plotted in figures 7 and 8. Naturally, the simplified fixed-form expressions of reference 6 will not duplicate the low-frequency variations seen in the Y_{p_θ} transfer with $M_q = -1.0$. Nor will the high frequency behavior of corresponding transfers be duplicated for the reason mentioned earlier. However, it can be verified that in the neighborhood of crossover, both models yield pitch and position loop gains that agree quite well. Thus, we found inner and outer loop crossover frequencies that agreed with those of reference 21 to within plotting accuracies.

Effects of Speed Stability Parameter, M_u

The effects on predicted and measured scores of changing the speed stability parameter M_u are shown in figure 9. The agreement is again very good except for the smallest value of $M_u = 0$. The less precise agreement for the $M_u = 0$ case is probably attributable to a value of motor noise that is too small. In this case there is no gust component entering in parallel with the stick so the Kalman filter can obtain very good estimates

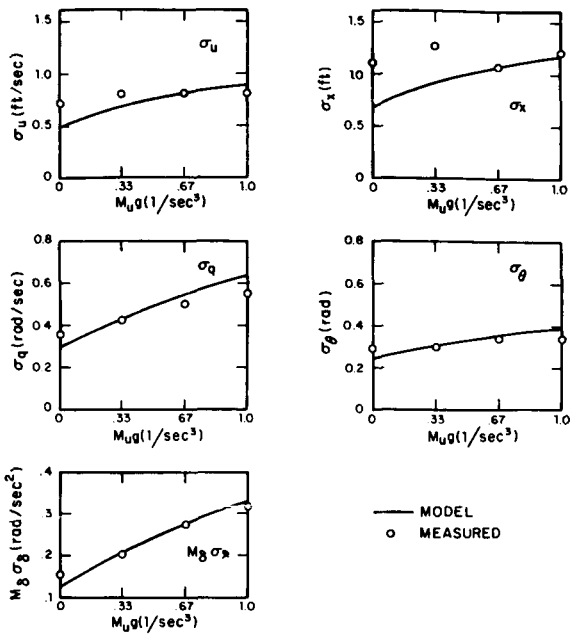

FIGURE 9.—Effect of speed stability parameter on hovering performance ($Mq = -3.0$, $X_u = -0.1$).

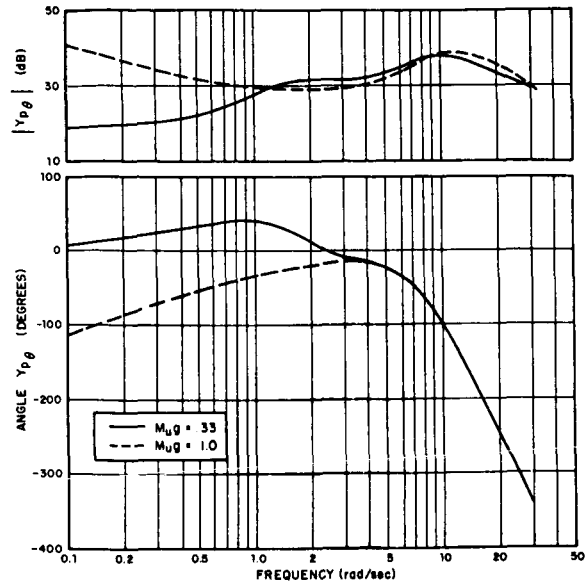

FIGURE 10.—Effect of speed stability parameter on predicted pilot describing function for pitch loop ($Mq = -3.0$, $X_u = -0.1$).

of q and θ. We have found in a previous study (ref. 3), that such a situation may require values of motor noise somewhat greater than -25 dB to model the human operator accurately.*

Equivalent Y_{p_θ} and Y_{p_x} transfers for the cases $M_u g = 0.33$ and $M_u g = 1.0$ are shown in figures 10 and 11. Variations in Y_{p_θ} with $M_u g$ take place almost entirely below 1 rad/sec. (The nominal Y_{p_θ} for $M_u g = 0.667$ falls within those shown.) In the neighborhood of pitch loop crossover ($\sim$3 rad/sec), pitch loop gain decreases very slightly with increasing $M_u g$. This was also true for the fixed-form model of reference 6. The variations in Y_{p_x} (fig. 11) with $M_u g$ are not very dramatic, with relatively small changes in gain appearing to be the principal effect. It should be noted that the position gain of the optimal control model decreases with increasing $M_u g$, whereas the K_{p_x} of the fixed-form model shows the opposite trend. However, the total variation in position loop gain for the fixed-form model is less than 2 dB and the observed trend may not be significant.

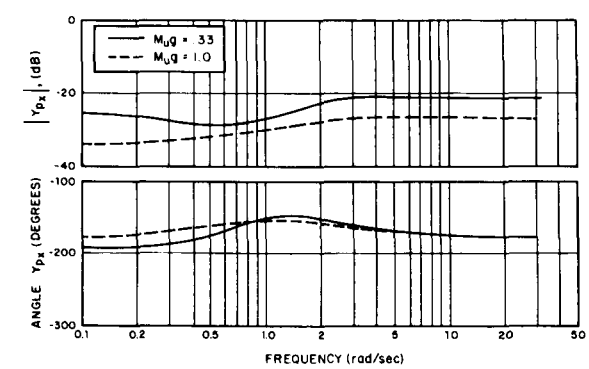

FIGURE 11.—Effect of speed stability parameter on predicted pilot describing function for position loop ($Mq = -3.0$, $X_u = -0.1$).

Effects of Variations in Longitudinal Drag Parameter, X_u

Predicted scores were computed for various values of X_u (with M_q and $M_u g$ kept at their nominal values) and are presented along with measured data in figure 12.* Again, the data

* Note that moderately higher values of motor noise would not increase the scores significantly in the remaining cases examined in this paper because of the relatively large nominal value for $M_u g$.

* Frequency domain data were also computed but they evidenced similar phenomena as in the other cases and are therefore not presented.

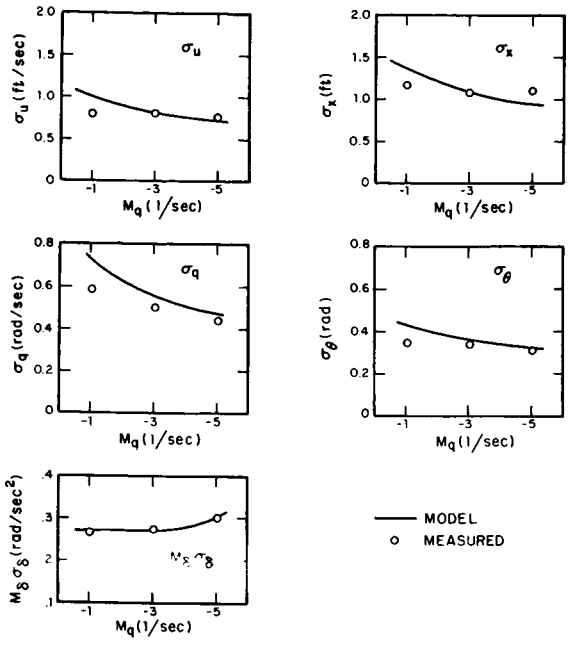

FIGURE 12.—Effect of longitudinal drag parameter on hovering performance ($M_u g = 0.667$, $Mq = -3.0$).

agree almost everywhere; major trends are reproduced and actual values are in close agreement. The only exception is the $X_u = -0.3$ case where the model predicts lower position, and higher pitch scores than were actually measured.

Predicted and measured scores could be brought in closer agreement for $X_u = -0.3$ by increasing the pitch rate weighting. We therefore obtained model predictions for a weighting of $q_4 = 1000$, a two and one-half-fold increase. The results, along with the measured values and those obtained with the lower weighting, are presented in table 3. (Numbers in parentheses are standard deviations.) Thus, it would appear from these results that the pilot was unwilling to accept the higher pitch-rate scores associated with the larger turbulence (X_u multiplies the input) * and increased his pitch-rate weighting accordingly. It is interesting to note that this configuration had the poorest pilot rating of all the cases that we investigated.

SUMMARY AND CONCLUDING REMARKS

We have applied the optimal control model of the human operator to predict performance in a series of longitudinal hovering tasks. The configurational changes that were considered significantly altered the system response to both control and disturbance inputs, yet the model was able to predict performance with exceptional accuracy in almost all cases. Moreover, this was accomplished with a fixed set of model input parameters, whose values were virtually identical to those used in single-axis studies. Also needed in the analysis was a subjective" weighting on rms pitch-rate error (i.e., a measure of performance in the "additional loop"). Results for all but one case were quite good keeping this parameter invariant and reasonable methods for selecting its value appear to be generally available.

Inasmuch as no frequency domain measurements were available for comparison, the optimal control model was used to predict describing functions that corresponded to the "loop closing" pilot transfer functions that are frequently employed in "classical" multiloop manual control analyses. These "equivalent-optimal" describing functions were compared with fixed-form transfer functions that had been derived in the original analyses of the data. The fixed-form transfer

* Vinje and Miller also draw the same inference from their data.

TABLE 3.—*Score Comparison for Different Pitch-Rate Weightings in High Drag Configuration*

	σ_u	σ_x	σ_q	σ_θ	σ_δ
Measured	1.67(0.20)	2.88(0.45)	0.069(0.005)	0.064(0.005)	0.76(0.07)
$q_4 = 400$	1.58	2.10	.095	.074	.82
$q_4 = 1000$	1.66	2.52	.079	.070	.68

functions were of the "crossover-model" genre, and had some preselected parameters (time delays and neuromotor time constant) and some parameters (gain and lead time constants) that were adjusted to match measured score data.

Invariably, the optimal control and fixed-form describing functions agreed quite well in the neighborhood of loop "crossovers." This is not surprising because the optimal control model predicts the measured scores and the fixed-form model, which is designed primarily for the crossover region, is adjusted to match the "same" measured scores. For frequencies outside the crossover range, agreement between the differently obtained describing functions is generally not good. This is particularly evident for pitch-loop pilot describing functions. Those describing functions obtained from the optimal control model exhibit much more complex behavior than do the simpler fixed-form transfers. Many of these complex response characteristics are quite similar to those predicted by the model, and also observed experimentally, in single-axis tasks. On this basis we believe that measured describing functions would bear a closer resemblance to those predicted by the optimal control model than to those obtained from the fixed-form model with "measured" parameters.

There were three cases for which the optimal control model did not yield very accurate score predictions. For one of these cases ($M_u g = 0$) the discrepancies could be largely attributed to our treatment of motor noise. In the other two cases, more accurate predictions were achieved by changing model input parameters. In one case (lowest pitch rate damping), the observation noise ratio was decreased, and in the other case (highest drag) the pitch-rate weighting was increased. It is interesting and important to note that both of these cases were ones in which significantly poorer pilot ratings were obtained. It would appear to be more than coincidental that a change in the basic model parameters correlated with a substantial degradation in pilot rating. Although, much work remains to be done, we are reasonably convinced that the optimal control model will ultimately provide a versatile and fairly general approach to predicting aircraft flying qualities.

REFERENCES

1. KLEINMAN, D. L.; AND BARON, S.: Manned Vehicle Systems Analysis by Means of Modern Control Theory. Rept. No. 1967, Bolt Beranek and Newman Inc., June 1970.
2. KLEINMAN, D. L.; BARON, S.; AND LEVISON, W. H.: An Optimal Control Model of Human Response. Part I: Theory and Validation. Automatica, vol. 6, no. 3, May 1970.
3. BARON, S.; KLEINMAN, D. L.; ET AL.: Application of Optimal Control Theory to the Prediction of Human Performance in a Complex Task. AFFDL–TR–69–81, Wright-Patterson Air Force Base, Mar. 1970.
4. KLEINMAN, D. L.; AND BARON, S.: Analytic Evaluation of Display Requirements for Approach to Landing. Rept. No. 2075, Bolt Beranek and Newman Inc., Mar. 1971.
5. VINJE, E. W.: AND MILLER, D. P.: Interpretation of Pilot Opinion by Application of Multiloop Models to a VTOL Flight Simulator Task. NASA SP–144, Mar. 1967.
6. MILLER, D. P.; AND VINJE, E. W.: Fixed-Base Flight Simulator Studies of VTOL Aircraft Handling Qualities in Hovering and Low-Speed Flight. AFFDL–TR–67–152, Wright-Patterson Air Force Base, Jan. 1968.
7. LEVISON, W. H.; ELKIND, J. I.; AND WARD, J. L.: Studies of Multivariable Manual Control Systems: A Model for Task Interference. Rept. No. 1892, Bolt Beranek and Newman Inc., Dec. 1969. Also NASA CR–1746.

N73-10135

31. A Performance Measure for Manual Control Systems*

THEODOR A. DUKES AND PERSHING B. SUN

Princeton University

A new performance measure is introduced for multivariable closed loop experiments with a human operator. The essential feature of the phase margin performance measure (PMPM) is that the performance of each control loop can be determined independently, with prescribed disturbance and error levels. A variable filter parameter is used as the PMPM within the loop and it assures a high workload at the same time. There is a straightforward relationship between the PMPM and the inner loop feedback augmentation that can be utilized in trade-off studies. An adjustment scheme that seeks the PMPM automatically is described as employed in a single loop control task. This task applies directly to the experimental study of displays for helicopters and VTOL aircraft.

INTRODUCTION

A closed loop dynamic system that includes the human operator in the loop poses many special problems to its designer. The man-machine interfaces and the processing of information inside man are both areas of particular concern in the efforts to represent the human controller with a quantitative model that can be used in system design. Any research in this area must be based on, or supported by, experimental evidence. Ultimately, the goal is always to provide means by which the values of alternative choices of system elements or characteristics (display, controller, system dynamics) can be compared. Besides the comparison of different versions of the same element, there is a considerable interest in trade-off studies, i.e., in establishing the relative merits when improvements are made in different elements; for example, in the controller's display vs. in the dynamics of the controlled system. In all cases a crucial choice must be made: a performance measure must be chosen as the basis for comparison in the experiments.

Performance measures can be separated into two broad classes: subjective and objective measures. Subjective measures are scales constructed to reflect a continuum of opinions, whereas objective measures are performance indices that can be measured by instruments or reduced from the test data. Subjective and objective measures do not necessarily yield the same results, although efforts have been made to match subjective measures with objective ones (ref. 1).

In quantitative manual control studies the independent and dependent variables must be chosen from the input, the output and the system parameters. Therefore, at least one of these is fixed in any experimental design in the sense that its characteristics are not varied. The independent variable is usually a syatem characteristic because most studies are aimed at finding the best choice of a parameter or structure. "Best" is usually defined in terms of a minimum or a maximum of a performance measure. On this basis three distinct types of manual control studies can be identified in terms of test variables, as indicated in the table shown on the next page.

There are advantages and disadvantages connected with any particular choice and some of these are discussed here briefly.

(1) The approach using fixed input characteristics is perhaps the most straightforward. It is

* The work reported in this paper was supported in part by the U.S. Army Electronics Command under contract DA 28-043 AMC-02412(E).

Fixed	Varied (Independent var.)	Max. or min. (Dependent var.)
(1) Input	System	output
(2) output	System	Input
(3) Input & output	System	Auxiliary system

based on the assumption that the smaller the error output, usually in the rms sense, the better the performance. The required performance in an actual system is usually connected with the specification of an error tolerance rather than with minimizing the error. Even if such a tolerance is not given to the human operator, he develops a certain performance level that he considers satisfactory. This can be reflected in an insensitivity of the output performance in the case of a relatively low workload (ref. **2).**

(2) A high workload is provided and the system performance is related to a prescribed error tolerance in the second type of manual control studies (ref. **3).** The level of disturbance inputs is increased automatically if the error output is below the prescribed level and it is decreased if the output level is larger. The resulting input level is a function of the system characteristics and may not reflect realistic requirements for the tested system.

(3) The problem common to approaches **(1)** and **(2)** is that the range of the dependent test variable associated with the operation of the system may exceed the range of realistic magnitudes. The approach taken in reference **4** overcomes this problemby using fixed input and output characteristics. An auxiliary system is used to produce a variable extra workload. This workload is increased when the operator's performance with the tested system is better than specified and it is decreased when the performance is poorer. The auxiliary workload is measured in terms of the location of a variable unstable pole. A good correlation with opinion ratings has been achieved with this system despite the fact that the secondary task does not correspond to any realistic additional workload encountered in practice. Since the adjustment process is in the secondary task, this approach does not lend itself readily to trade-off studies in the primary system if the tested system involves more than one control loop.

A new approach is taken by the authors, aimed at trade-off studies of multivariable control systems with high workloads. The principle and the single loop mechanization of this approach are described in this paper.

THE PHASE MARGIN PERFORMANCE MEASURE (PMPM)

In connection with research on an integrated display for helicopters (ref. 5), it was found desirable to establish a method to determine how various aspects of the display could be evaluated in the multivariable control task of accurate flight path control. An experimental system suitable for this purpose was required to have the following characteristics:

(1) A separate measure of performance for each control loop

(2) Disturbance and error levels to be controlled by the experimenter

(3) Assurance of high workload.

No existing test procedure could meet all three of these requirements. In order to provide individual performance measures for each control loop in the basic task, a system parameter in each loop must be chosen as dependent variable if input and output levels are to be fixed.

A controlled parameter in each loop can be used as dependent variable to increase the workload by making the system more difficult to control. This can be accomplished by inserting a variable filter in series with each controller of the system, as indicated in figure **1.** Variable system dynamics have been used before (ref. *6)* to determine the degree of instability an operator can control. In order to be close to realistic control tasks, the number of integrations between the controller and the controlled variable was chosen as the dependent variable system parameter. There is a very close relationship between this choice and feedback control augmentation, particularly in helicopters and VTOL aircraft. For example, a tight rate control loop can be considered as eliminating one integration; a tight attitude feedback loop closely corresponds to the elimination of two integrations.

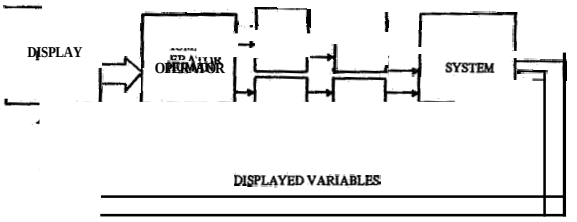

matches the specified error. If K reaches an equilibrium at this state, it represents an additional phase lag or phase margin that can be handled by the operator with prescribed disturbance and error levels. K as a performance mea-

$$G_{01}=\frac{\sqrt{1+K^2}}{S+K}$$

as K varies from infinity to zero. The phase shift of this filter varies gradually from 0" to 90" as shown in the figure. With G_{01} in series, the loop phase shift changes with varying K.

Assume that at the beginning of an experiment, with a prescribed disturbance level and $K=\infty$, the operator is able to control a variable

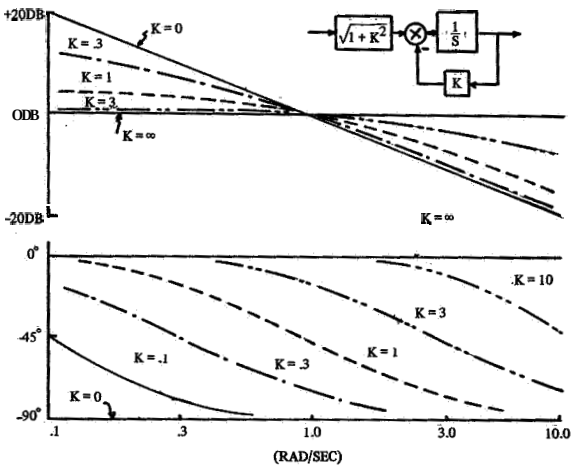

FIGURE 2.—Bode diagrams of variable filter.

DESCRIPTION OF THE ADAPTIVE SYSTEM

The entire manual control system under consideration is shown in figure **3.** This system includes the adaptively controlled element, a model of the pilot equalization, the display feedback, and the input disturbance to the controlled element.

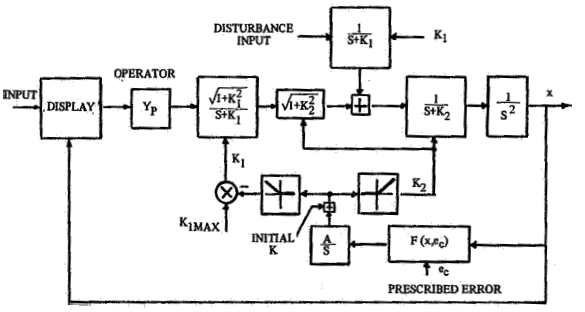

FIGURE 3.—Block diagram of the control loop and the adjustment loop.

Adaptive Filter Adjustment

The adaptively controlled element consists of two variable first order filters which are in series with two fixed integrators. The variation of the filter parameters K_1 and K_2 is produced by the integrated output of the performance calculation network, denoted by $F(x,e_c)$ where e_c is the prescribed error level. The performance calculation is obtained by comparing an even function of the error output with e_c. Continuous variation over a range of two integrations, corresponding to approximately 0° to 180° phase shift, is provided by the filters. As the adjustment loop integrator output varies from a positive maximum value to zero, K_2 varies from $K_{2\max}$ to zero while K_1 remains at $K_{1\max}$. As the integrator output decreases further from zero to a negative maximum range, K_2 remains zero and K_1 varies from $K_{1\max}$ to zero. The maximum values of K_1 and K_2 are chosen so that the phase shift produced by the filter approximates zero within the bandwidth of interest.

If the operator's performance is poorer than the prescribed level, K increases; if the system error is less than the prescribed level, K will decrease. In the case of a VTOL aircraft at hover, e.g., the equilibrium value of K may be viewed as an indicator of the amount of stability augmentation necessary to achieve a prescribed accuracy with a given disturbance level.

Disturbance Input

The disturbance input is entered into the system of figure 3 so as to resemble accelerations resulting from the aerodynamic moments produced by gust inputs. The disturbance is passed through the variable filters with unity filter gains, corresponding to the decreased effect of the disturbance as inner loop feedback gains are increased.

The input gust spectrum employed in handling quality studies of VTOL aircraft at hover is often produced by passing the output of a random noise generator through a first order filter with a break frequency of 0.314 rad/sec (refs. 7 and 2). In order to facilitate a relatively simple measurement of the human pilot transfer function, a random appearing function consisting of discrete frequencies is preferred (ref. 8). Consequently, the desirable input noise spectrum is made up of discrete frequencies with an amplitude envelope approximating a first order filter.

Control Loop Dynamics

For the analysis of the control loop dynamics, a simple linear pilot model is assumed. If the position error is the only element presented on the display, the pilot must generate a low frequency lead equilization, $Y_p = K_p(T_{Lx}s+1)$, in order to achieve stability for the closed loop system (ref. 8). It is assumed that the time delay portion of the pilot transfer function has a negligible effect on the positioning loop dynamics (ref. 2). The root locus plot in figure 4 indicates the variation of the closed loop roots as functions of the pilot equalization and the filter pole locations. For a given pilot equalization, with fixed T_{Lx} and K_p, the closed loop system damping decreases as K_2 decreases. When K_2 becomes less than $1/T_{Lx}$ the closed loop system becomes unstable. In the illustrated case K_1 remains $K_{1\max}$ since K_2 is determined by the characteristics of the disturbance input, the prescribed output error level and the pilot transfer function.

If both position and velocity errors are presented on the display, the pilot model can be represented by $Y_p = K_p(T_{Lx}s^2+T_{Lx}s+1)$. In this case, K_2 can be zero and K_1 becornea the variable parameter. This is shown by the root locus plot in figure 5; again the system damping decreases as K_1 decreases.

The display parameters such as display variables and display gains have been incorporated into the pilot equalization in order to show the

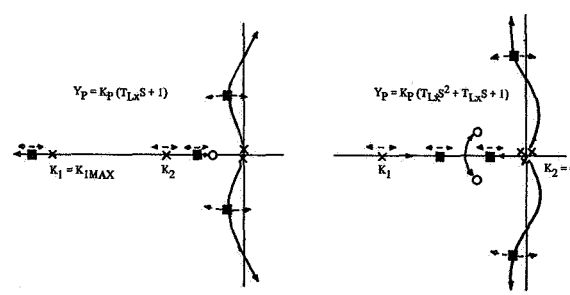

FIGURE 4.—Effects of the operator's gain and lead time constants.

general trend of the closed loop system dynamics. In practice, with a human pilot in the loop, the pilot's equalization parameters can be measured experimentally and the display gains are calculated from the particular display used in the experiment.

PERFORMANCE MEASURE AND THE PARAMETER ADJUSTMENT LOOP

Equilibrium Value of the Performance Measure K

Assuming a random input and a given form of the display-pilot feedback equalization, the mean square error can be calculated from the Phillips integral (ref. 9) as a function of the input and the final system parameters. Since in equilibrium the output of the system is at a prescribed level, the equilibrium value of K can be expressed as a function of the feedback and input characteristics and the prescribed output level.

Assuming again that only the position error is displayed and that the pilot transfer function is

$$Y_p = K_p(T_{Lx}s+1) \tag{2}$$

the closed closed loop error can be expressed as

$$E(s) = \frac{N(s)}{s^3+Ks^2+K_pT_{Lx}(1+K^2)^{1/2}s+K_p(1+K^2)^{1/2}} \tag{3}$$

where $K=K_2$, since $K_1=K_{1\,max}$, and the effect of the first filter on the closed loop dynamics is negligible.

$$N(s) = \frac{\sqrt{4\alpha\overline{n^2}}}{(\alpha s+1)} \tag{4}$$

describes a filtered noise input with a cut-off frequency at $1/\alpha$ and a mean square value of $\overline{n^2}$.

From the Phillips integral table, the resulting mean square error is obtained

$$\overline{e^2} = \frac{2\alpha\overline{n^2}}{K_p^2(1+K^2)(KT_{Lx}-1)} \left[\frac{\alpha^2K_p(1+K^2)^{1/2}(KT_{Lx}-1)+K(\alpha K+1)}{\alpha^2K_p(1+K^2)^{1/2}(T_{Lx}+\alpha)+(\alpha K+1)}\right] \tag{5}$$

The ratio of the rms error to the rms noise level is plotted in figure 5 as a function of the equilibrium K. The increase in rms error as K decreases can be attributed primarily to the decrease in system damping.

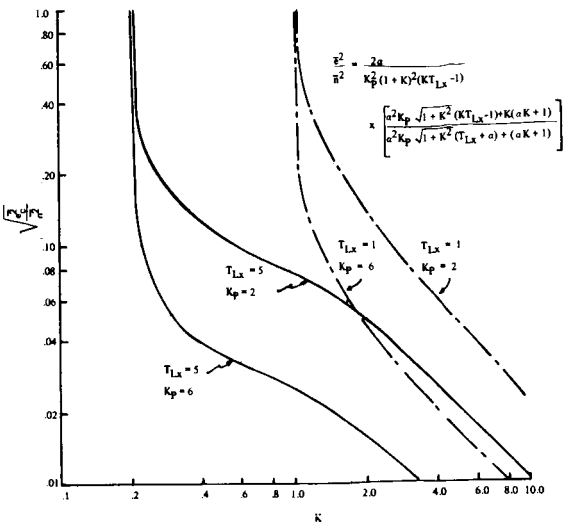

FIGURE 5.—Equilibrium values of the performance measure K.

The Parameter Adjustment Loop

In establishing the described adaptive system as a useful research tool, the importance of the choice of the parameter adjustment scheme cannot be over-emphasized. Crucial criteria in the selection of the adjustment scheme include the following:

(1) The scheme should adjust the performance measure automatically

(2) It should have no influence on the equilibrium value of the adjusted parameter

(3) The parameter should converge to its equilibrium value within the duration of the test run

(4) There should be little variation of the parameter about the equilibrium

(5) The mechanization of the scheme should be simple.

In the past, much effort has been spent on the study of various parameter adjustment schemes in different types of adaptive systems (refs. 10 and 11). The results of these studies depend heavily on the specific nature of the adaptive systems investigated. Furthermore, since the nature of the operator-display portion of the manual control system is generally not specified, it is difficult

to draw analogies between the system discussed in this paper and other existing adaptive systems.

The following adjustment schemes were considered:

Scheme a.—

$$\dot{K} = A(x^2 - e_c^2) \tag{6a}$$

Scheme b.—

$$K = A \log (x^2/e_c^2) \tag{6b}$$

Scheme c.—

$$K = A \operatorname{sgn} (|x| - e_c) \tag{6c}$$

where

$\dot{K}$ = parameter adjustment rate
A = adjustment loop gain
e_c = prescribed error level
x = system error output.

A graphical representation of these functions is shown in figure 6.

Scheme a is the simplest to mechanize. The parameter adjustment rate is proportional to the differencebetween the mean square values of the system error and the prescribed error. The principal difficulty with this scheme can be observed readily in figure 6. The adjustment rate is highly unsymmetrical about the equilibrium point $x^2 = e_c^2$. In the region of $x^2 < e_c^2$, the maximum K, at $x = 0$, is e_c^2, usually a small value. In the region of $x^2 > e_c^2$, K increases rapidly with x and becomes very large at high values of x^2/e_c^2.

The result is demonstrated in Figure 7(a). The unsymmetrical nature of the adjustment and the large variation in K is evident.

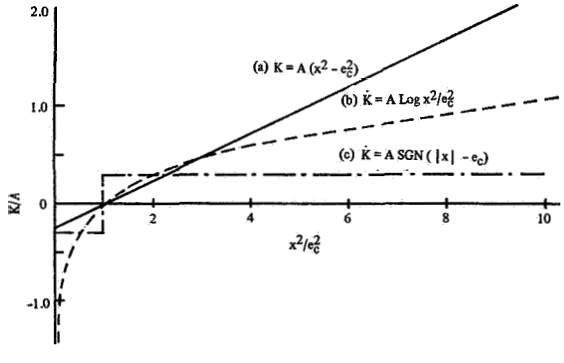

FIGURE 6.—Adjustment laws for the performance measure.

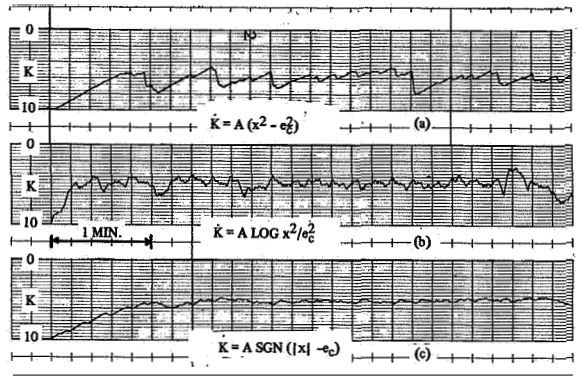

FIGURE 7.—Adjustment loop dynamics with random disturbances and $\overline{Y}_p = \overline{K}_p(T_{Lx}s + 1)$.

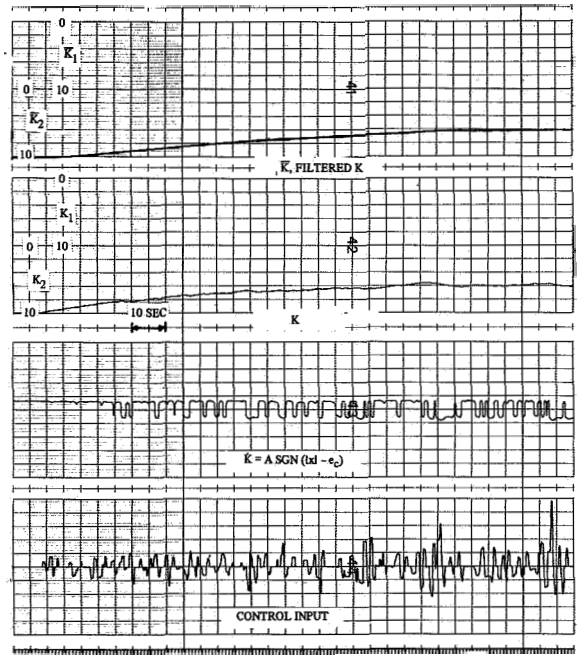

FIGURE 8.—Typical traces of the adjustment loop dynamics with a human operator.

Experimental results indicate that the adjustment loop dynamics become less oscillatory in nature when the loop gain is reduced. This benefit, however, is coupled with an undesirable increase in the time required to reach the equilibrium K value.

Scheme b does not exhibit the difficulties pre-

sented by scheme a. The adjustment rates are reduced at high x^2/e_c^2 and increased at low x^2/e_c^2, providing a more symmetrical parameter adjustment about the equilibrium point of $x^2=e_c^2$. The negative infinite $\dot{K}$ at $x=0$ indicated in figure 6 is naturally limited by the mechanization. This scheme works quite well in practice; however, the adjustment rates at the two ends of the x^2/e_c^2 scale still appear too high. As a result, the variation of K around its equilibrium value, for lightly damped control systems, is still larger than desired, as illustrated in Figure 7(b).

Scheme c is a bang-bang adjustment rule which is symmetrical about the equilibrium point at $x^2=e_c^2$. It is simple to mechanize, and the result obtained with this scheme is comparable to that of scheme b.

With a reduced setting of the bang-bang level at approximately one-third, which is equivalent to reducing the loop gain by a factor of 3, a typical result is shown in Figure 7(c). A relatively smooth convergence in K to its equilibrium value with small variations is obtained.

A sample of experimental runs with the bang-bang adjustment scheme c and a human operator in the loop is shown in figure 8.

CONCLUSIONS

The phase margin performance measure established inside control loops is applicable to multivariable control systems when both the disturbance level and the error tolerance are specified. It features the following properties:

(1) A performance measure can be obtained for each control loop.

(2) A high workload condition is created automatically.

(3) The performance measure can be related directly to inner loop closure requirements.

(4) Trade-off studies between inner loop feedback augmentation and other parameters of system elements (displays, controllers, etc.) can be easily implemented.

A relatively simple mechanization with bang-bang control in the automatic adjustment of the performance measure results in quite satisfactory adjustment dynamics.

REFERENCES

1. Anderson, R. O.; and Dillow, J. D.: Paper Pilot—An Application of Pilot Models to Predict VTOL Flying Qualities in Precision Hover. Proceedings of the Sixth Annual Conference on Manual Control, Apr. 7–9, 1970, pp. 349–364.
2. Miller, D. P.; and Vinje, E. W.: Fixed-Base Flight Simulator Studies of VTOL Aircraft Handling Qualities in Hovering and Low-Speed Flight. AFFDL–TR–67–152, Wright-Patterson AFB, Jan. 1968.
3. Kelley, C. R.: Design Applications of Adaptive (Self-Adjusting) Simulators. Second Annual NASA-University Conference on Manual Control, NASA SP–128, Feb. 28–Mar. 2, 1966.
4. McDonnell, J. D.: Pilot Rating Techniques for the Estimation and Evaluation of Handling Qualities. AFFDL–TR–68–76, Wright-Patterson AFB, Dec. 1968.
5. Dukes, T. A.: An Integrated Display for Trajectory Control of Helicopters and VTOL Aircraft. Proceedings of the Sixth Annual Conference on Manual Control, Apr. 7–9, 1970, pp. 133–146.
6. Jex, H. R.; McDonnell, J. D.; and Phatak, A. V.: A 'Cricital' Tracking Task for Man-Machine Research Related to the Operator's Effective Delay Time. NASA CR–616, pt. I. Nov. 1966.
7. Seckel, E.; Traybar, J. J.; and Miller, G. E.: Longitudinal Handling Qualities for Hovering. Rept. No. 594, Princeton Univ., Dec. 1961.
8. McRuer, D. T.; Graham, D.; Krendel, E.; and Reisner, W.: Human Pilot Dynamics in Compensatory Systems. AFFDL–TR–65–15, Wright-Patterson AFB, July 1965.
9. James, H.; Nichols, N.; and Phillips, R.: Theory of Servo-Mechanisms. McGraw-Hill, 1947.
10. Aseltine, J. A.; Mancini, A. R.; and Sarture, C. W.: Survey of Adaptive Control Systems. IRE Trans. on Automatic Control, Dec. 1958.
11. Rutman, R. S.: Adaptive Systems With Dynamic Characteristic Adjustment. Auto. and Remote Control, vol. 5, no. 23, May 1962, pp. 602–624.

N73-10136

32. Serial Segment Method for Measuring Remnant

R. E. MAGDALENO

Systems Technology, Inc.

For tracking tasks where a sum of sine waves forcing function is used it is often difficult and/or expensive to obtain the pilot's remnant in the vicinity of the sine waves. For the case where each sine wave has at least four times an integer number of cycle per run length, this paper illustrates the Serial Segments method for measuring remnant power spectral density in a frequency band centered on each sine wave. This method can be implemented on digital, hybrid, or analog Fourier coefficient analyzers, and is particularly advantageous on the latter since properties of Fourier coefficients are exploited to yield both a remnant measure and an improved estimate of the correlated component.

INTRODUCTION

There are many techniques available (see especially ref. 1) for measuring the pilot's describing function Y_p and remnant n_c in the compensatory task of figure 1. Generally the remnant is more predictable when referred to the input to the pilot, n_e (refs. 2 and 3). However, if a digital or hybrid computer is not available then remnant measurements with analog equipment (i.e., analog power spectral analyzers) may be expensive and/or lack the accuracy needed to separate signal from noise. For the case where the input is a sum of sine waves, reference 4 describes input-referenced-Fourier coefficient measurements as mechanized on "standard" analog computer equipment as well as on a describing function analyzer (DFA) where the latter uses synchronous motors to drive sine-cosine pots and multiplying pots. The inherent timing precision in the describing function analyzer approach is such that suitable processing of the Fourier coefficients (as they evolve in time) can yield an estimate of both the remnant and the describing function at the same frequency, thus enabling the remnant n_c to be reinterpreted as occurring at n_e by $\Phi_{nn_e}=\Phi_{nn_c}/|Y_p|^2$.

To illustrate the methods to be used, assume that we have a signal which is sine wave plus noise

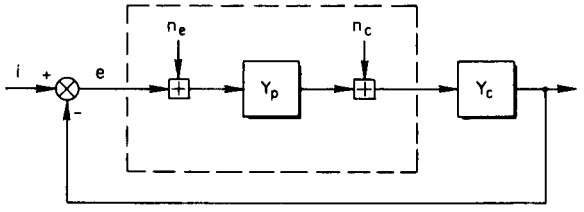

FIGURE 1.—Compensatory situation.

$$x(t)=A\sin(\omega_1 t+\varphi)+n(t) \tag{1}$$

where

A = peak amplitude
φ = phase (arbitrary)
ω_1 = frequency in rad/sec
$n(t)$ = noise component.

The relationship between variance and power spectral density (PSD) used in this paper is

$$\sigma_x^2=\int_0^\infty \Phi_{xx}(f)\,df \tag{2}$$

where $\Phi_{xx}(f)$ = PSD of x; units of power/Hz. The PSD for $x(t)$ is

$$\Phi_{xx}(f)=\frac{A^2}{2}\delta(f-f_1)+\Phi_{nn}(f) \tag{3}$$

For a finite run length T_R the signal xt can be represented by a Fourier series form

$$x(t)=\bar{x}+\sum_{n=1}^{\infty}a_n\cos\omega_n t+\sum_{n=1}^{\infty}b_n\sin\omega_n t \quad (4)$$

where the coefficients are evaluated from

$\bar{x}$ = mean value of x

$$a_n=\frac{2}{T_R}\int_0^{T_R}x(t)\cos\omega_n t\,dt$$

$$b_n=\frac{2}{T_R}\int_0^{T_R}x(t)\sin\omega_n t\,dt$$

$$\omega_n=n\omega_0$$

$$\omega_0=\frac{2\pi}{T_R}$$

Where the fundamental frequency is one cycle per run length, the power in the frequency estimate at ω_n is

$$P_n=\frac{a_n^2+b_n^2}{2}. \quad (5)$$

For cases of interest in this paper the sine wave in equation (1) is assumed to be a harmonic of the fundamental frequency, $1/T_R$. When dealing with data taken over a finite run length T_R, a more useful definition of PSD is to assume that the power in the spike is distributed over the smallest resolvable bandwidth, $1/T_R$(Hz). This bandwidth follows from expanding $x(t)$ in Fourier coefficients which are orthogonal at that frequency spacing. Thus the PSD of $x(t)$ is

$$\Phi_{xx}(f)=\frac{A^2}{2}T_R+\Phi_{nn}(f);\ \frac{(\text{units of } x)^2}{\text{Hz}}. \quad (6)$$

This is sketched in figure 2 in terms of each fundamental frequency band with the sine wave power centered on $f=f_1$ and assumed distributed over $1/T_R$ (Hz). The shaded area is the total power in the sine wave. The remnant sketched in indicates that it fluctuates about on either side of the sine wave portion as well as having a component centered there. The problem is to estimate both the sine wave component and a measure of the average remnant height.

METHOD

The DFA signal processing method can be modified so as to obtain remnant as well as describing function estimates for a 100 sec run length. The key point is to select forcing function frequencies that are orthogonal over 25 sec so that independent estimates of Fourier coefficients can be obtained at this run length as well as for 100 sec. Noting that each Fourier coefficient can be thought of as containing the power in a bandwidth of $(1/T_R)$ Hz where T_R is run length in seconds, then Fourier coefficients obtained over 25 sec have an effective bandwidth four times that of Fourier coefficients obtained over a 100 sec run length. Since the power correlated with the forcing function is common to coefficients obtained over 25 sec as well as those from 100 sec run lengths, then the difference in these powers is that due to remnant.

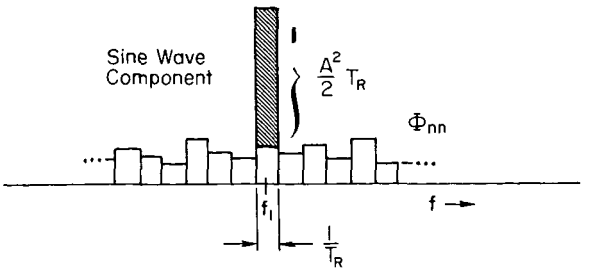

FIGURE 2.—Signal and noise power spectral densities.

It will be convenient to deal with twice the power in a frequency band rather than the PSD,

$$2P_n=2[\Phi_{xx}(f)]\,\Delta f \quad (7)$$

where $\Delta f=1/T_R$.

Inserting equations (5) and (6) into equation (7) yields (for a measurement frequency that falls on a sine wave)

$$a_n^2+b_n^2=A^2+2[\Phi_{nn}(f_n)]\left(\frac{1}{T_R}\right). \quad (8)$$

Equation (8) relates the measured Fourier coefficients a_n, b_n to the sine wave and remnant descriptors A, Φ_{nn}. Two independent evaluations of equation (8) will allow a solution to be found.

Equation (8) evaluated over a 100 sec run length at a frequency corresponding to a forcing function frequency yields

$$M=A^2+\frac{2\Phi_{nn}}{100} \quad (9)$$

where $M=a_n^2+b_n^2$.

Evaluating equation **(8)** over each **25** sec segment and then averaging the power in these four segments together yields

$$M_s = A^2 + \frac{2\Phi_{nn}}{25} \tag{10}$$

where

$$M_s = \frac{1}{4}\sum_{i=1}^{4}[a_{n_i}^2 + b_{n_i}^2]$$

a, is the cosine component of the i^{th} segment

b_{n_i} is the sine component of the i^{th} segment

This method of calculating spectra from successive segments was suggested by Bartlett (ref. 5). The short segment coefficients are related to the full run length coefficients by

$$a_n = \frac{2}{100}\int_0^{100} x(t)\cos\omega t\,dt$$

$$= \frac{1}{4}\Big[\underbrace{\frac{2}{25}\int_0^{25} x(t)\cos\omega_n t\,dt}_{a_{n_1}} + \underbrace{\frac{2}{25}\int_{25}^{50}}_{a_{n_2}} + \frac{2}{25}\int_{50}^{75} + \frac{2}{25}\int_{75}^{100}\Big] \tag{11}$$

$$a_n = \frac{1}{4}\sum_{i=1}^{4} a_{n_i}$$

and similarly for b_n.

The right hand side of equation **(10)** shows that the average power in the four segments contains A^2 since the sine wave is identical in each of the four segments. The amount of measured remnant power is larger than in equation **(9)** since the effective bandwidth for the short run length segments is four times larger. However, the amount of remnant power in the 100 sec estimate is not exactly one-fourth of the remnant power in the averaged **25** sec segments. As shown in figure **2** the remnant component at $f = f_1$ (or any other component) may be higher or lower than the average height. Thus in equation (9) an additional factor ϵ should be added on to reflect the difference from the average remnant, Φ_{nn}.

Equations **(9)** and **(10)** can now be solved for A^2 and Φ_{nn}. However, for generality we are interested in the case where there are Q short segments in the run length T_R. Thus the generalized versions **of** equations **(9)** and (10) are respectively

$$M = A^2 + \frac{2\Phi_{nn}}{T_R} + \epsilon \tag{12}$$

$$M_s = A^2 + \frac{2\Phi_{nn}}{T_R/Q} \tag{13}$$

where ϵ is the deviation of the remnant power from the average level. Since ϵ is a random variable and likely to either be positive **or** negative for any one run it is neglected in the solution of equations **(12)** and **(13)** for average values of A^2 and Φ_{nn}. Thus carrying ϵ through the solution so as to see its effects yields,

$$A^2 = \frac{QM - M_s}{Q-1} - \frac{Q\epsilon}{Q-1}$$

$$\Phi_{nn}(f_n) = (M_s - M)\frac{T_R}{2(Q-1)} + \frac{\epsilon}{Q-1}\frac{T_R}{2} \tag{14}$$

where

Q = number of short run lengths in the basic run length, T_R

$$M_s = \frac{1}{Q}\sum_{i=1}^{Q}(a_{n_i}^2 + b_{n_i}^2)$$

$$M = \left(\frac{1}{Q}\sum_{i=1}^{Q} a_{n_i}\right)^2 + \left(\frac{1}{Q}\sum_{i=1}^{Q} b_{n_i}\right)^2.$$

In addition the sine wave input frequency f_n must have an integer number of cycles in the short run length, T_R/Q. Note that the remnant estimate contains ϵ divided by Q−1, thus the remnant estimate is not sensitive to the scatter. The estimate for A^2 is contaminated by the ϵ term, yet A^2 is usually much larger than the remnant (or its scatter as given by ϵ) so that it is not sensitive either.

RESULTS AND INTERPRETATION

The serial segments method yields a remnant estimate (as well as describing function estimate) at each of the forcing function frequencies. This method of computing remnant was evaluated by simulating the calculations in equation (14), using BOMM (ref. *6*). Using actual human operator data we computed the Fourier coefficients

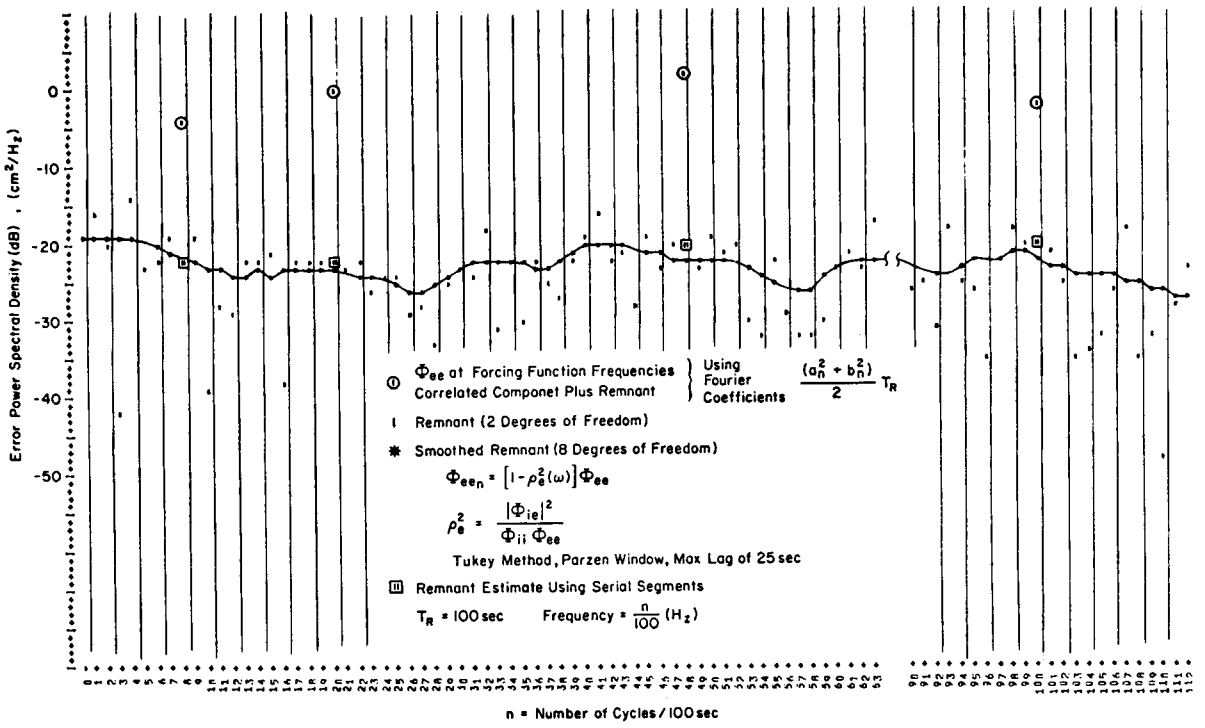

FIGURE 3.—Remnant computed from serial segments, $Y_c = 1/(s-1)$.

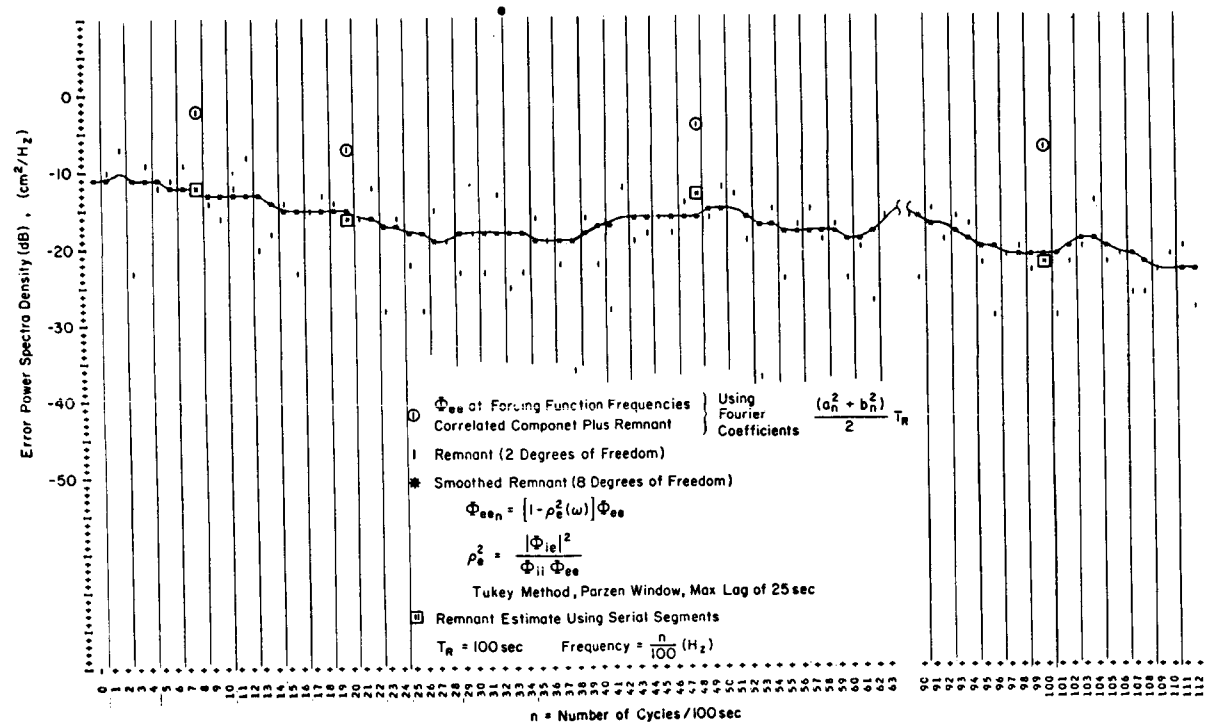

FIGURE 4.—Remnant computed from serial segments, $Y_c = 2/s(s-2)$.

of the error for $T_R = 100$ sec and for each **25** sec segment. These were processed according to equation **(14)** and compared with the remnant found by the Classical Tukey Method (ref. **7).** For the latter a Parzen data window was used with the number of lag values selected so that the effective bandwidth was close to that which results for the Serial Segments method when done four times per run length.

Example calculations are shown in figures **3** and **4,** where the error power spectral density estimates are plotted versus frequency in units of cycles per 100 sec run length. The Fourier components at forcing function frequencies are circled. The pertinent computations using the Serial Segments method are enclosed with a box. Generally these are in good agreement with the remnant power spectral density computed via the Tukey Method, which is included in figures **3** and **4** to give an indication of remnant both at and between the forcing function sine waves. For the Tukey Method (ref. **7),** the maximum number of lags was selected to mimic the 8 degrees of freedom for the Serial Segments (the scatter for 8 degrees of freedom is such that 60 percent of the values should fall within a **4** dB range approximately centered on the true remnant PSD). Note that both the Tukey and Serial Segments methods give smoothed estimates of the remnant, and they are in good agreement with each other. The small differences are partly due to the scatter term ϵ in equation (14).

The Serial Segments method was mechanized using the **DFA** by sampling the Fourier coefficient integrators at the **25, 50,** 75, and **100** sec times and computing the serial segment values per equation **(11).** Typical error spectra results for a pilot (taken from ref. 8) are shown in figure **5.** The measured remnant values are generally well above the worst case system noise (measured with an analog pilot). Even at the highest frequency, the measured remnant is above the actual value of the system noise (about **3** dB lower than the worst case system noise). The normalized injected remnant is consistent with the reference **2** and **3** findings.

Thus the Serial Segments method for measuring remnant is shown to yield excellent remnant estimates over a large dynamic range.

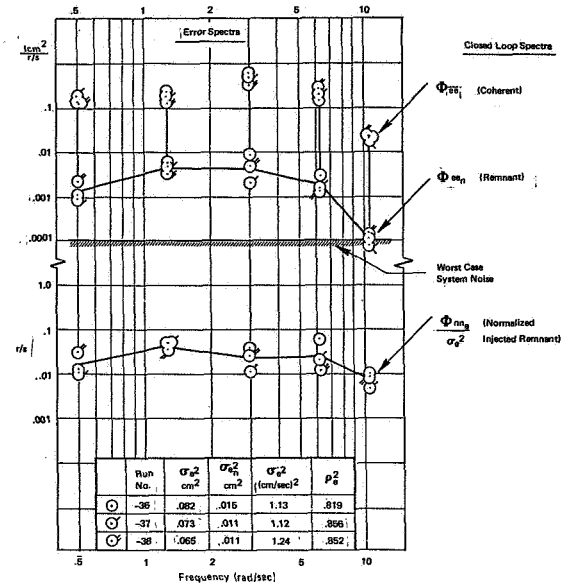

FIGURE 5.—Typical serial segments remnant data.

REFERENCES

1. SHIRLEY, RICHARD S.: A Comparison of Techniques for Measuring Human Operator Frequency Response. Proc. of the Sixth Annual Conference on Manual Control, Apr. 7–9, 1970, p. 803.
2. LEVISON, W. H.; BARON, S.; AND KLEINMAN, D. L.: A Model for Human Controller Remnant. IEEE Trans. on Man-Machine Systems, vol. MMS–IO, no. **4,** pt. **I,** Dec. 1969, p. 101.
3. JEX, H. R.; AND MAGDALENO, R. E.: Corroborative Data on Normalization of Human Operator Remnant. IEEE Trans. on Man-Machine Systems, vol. MMS–10, no. **4,** pt. **I,** Dec. 1969, **p.** 137.
4. ALLEN, R. WADE; AND JEX, HENRY, R.: A Simple Fourier Analysis Technique for Measuring the Dynamic Response of Manual Control Systems. Proc. of the Sixth Annual Conference on Manual Control, Apr. 7–9, 1970, p. 785.
5. BARTLETT, M. S.: Smoothing Periodograms from Time-series with Continuous Spectra. Nature, vol. 161, 1948, p. ***686.***
6. BULLARD, E. C.; ET AL.: A User's Guide to BOMM, **A** System of Programs for the Analysis of Time Series. Published by the Institute **of** Geophysics and Planetary Physics, Univ. of Calif. (San Diego), Jan. 1966.
7. BLACKMAN, R. **B.;** AND TUKEY, **J.** W.: The Measurement **of** Power Spectra. Dover Publications, Inc., 1958.
8. JEX, HENRY **R.;** ALLEN, R. WADE; AND MAGDALENO, RAYMOND E.: Display Format Effects **on** Precision Tracking Performance, Describing Functions, and Remnant. TR–191–1, Systems Technology, **Inc.,** Mar. 1971.

33. A Design Procedure and Handling Quality Criteria for Lateral-Directional Flight Control Systems*

G. STEIN AND A. H. HENKE
Honeywell Systems and Research Center

This paper describes a practical design procedure for aircraft augmentation systems based on quadratic optimal control technology and handling-quality-oriented cost functionals. The procedure is applied to the design of a lateral-directional control system for the F4C aircraft. The design criteria, design procedure, and final control system are validated with a program of formal pilot evaluation experiments.

INTRODUCTION

The work reported here is concerned with two problems in the area of optimal control and its application to the design of augmentation systems for fighter aircraft :

- Specification of performance criteria in terms of handling-quality requirements of the controlled vehicle
- Formulation (and solution) of the optimization problem such that practical control systems are obtained.

These problems have long frustrated efforts of flight control designers to exploit performance improvements and time savings offeredby mathematical optimization. Even for simple performance criteria and system representations (notably quadratic cost functions and linear systema), optimization methods produce controllers too complex for flight control mechanization. When the varied requirements of handling qualities (MIL–F8785B) are imposed as criteria, the methods seem inapplicable altogether.

The objectives of this work were to alleviate these difficulties. Specifically, the objectives were: **(1)** to develop a practical controller design procedure based on quadratic optimal control technology and handling-quality-oriented cost functionals; **(2)** to apply the procedure to the design of a lateral-directional control system for the F4C aircraft; and **(3)** to validate the design criteria, design procedure, and final control system with a program of formal pilot evaluation experiments.

Briefly stated, the design procedure developed involves the computational solution of a reformulated optimal model-following control problem. The optimization problem enforces practicality by including constraints on the structure and scheduling requirements of the final controller, and it enforces handling quality requirements by minimizing quadratic functions of model-following errors. The models themselves are systems of differential equations which satisfy available handling-quality data.

More detailed descriptions of the models, the optimization problem and its computational solution, and their application to the F4 lateral directional axes are presented. Results of the pilot evaluation program which were used to validate the procedure are also presented here.

DESIGN CRITERIA

The first step of the design procedure is to specify handling-quality-oriented design criteria which are usable within the framework of quadratic optimal control technology. Such criteria are described in this section.

There are basically two approaches available for the specification of handling quality criteria.

* This work was performed under AFFDL contract F33615–70–C–1190 (ref. 1).

The first is empirical. Loosely speaking, it consists of measuring the suitability of many different kinds of aircraft configurations to the needs of the pilot and his mission. The configurations are parameterized and catalogued, and the most desirable parameter ranges identified. These desirable ranges define "ideal" configurations. Criteria are then expressed in terms of deviations of an actual airframe's parameters from the ideal. The second approach is analytical. It consists of treating the pilot not as the external judge and evaluator but rather as an integral part of the overall control loop. The loop is analyzed by representing the pilot in terms of mathematical models which are compatible with our descriptions of the vehicle. Optimality is then imposed with respect to some external performance criterion for the overall system, and the system is optimized, pilot model and all. The overall criterion thus provides implicit criteria for the controller/vehicle subsystem.

Needless to say, the second approach requires a very general pilot model which remains valid even under severe manipulations of the control loop. The judgment made here is that, at present levels of sophistication, pilot models fall short of this requirement. In consequence, we have used the first approach to the criteria question and have constructed "ideal" configurations, or handling-quality models, for the F4C lateral-directional axes. These were used as design criteria in an optimal-following control formulation. Our decision is an interim one, subject to change as the sophistication of pilot models grows.

Handling-Quality Models

Assuming that the dominant lateral-directional modes of response of our controlled vehicle configuration correspond to conventional aircraft dynamics, the configuration can be parameterized in the following way:

$$\frac{d}{dt}\begin{bmatrix} p_m \\ r_m \\ \beta_m \\ \phi_m \end{bmatrix} = \begin{bmatrix} L_p & L_r & L_\beta & 0 \\ N_p & N_r & N_\beta & 0 \\ Y_p & Y_r & Y_\beta & Y_\phi \\ 1 & 0 & 0 & 0 \end{bmatrix} \begin{bmatrix} p_m \\ r_m \\ \beta_m \\ \phi_m \end{bmatrix} + \begin{bmatrix} L_{\delta R} & L_{\delta AS} \\ N_{\delta R} & N_{\delta AS} \\ Y_{\delta R} & Y_{\delta AS} \\ 0 & 0 \end{bmatrix} \begin{bmatrix} \delta_R \\ \delta_{AS} \end{bmatrix} \quad (1)$$

where p_m, r_m, β_m and ϕ_m are model roll rate, yaw rate, sideslip and bank angle, respectively, and where δ_R and δ_{AS} are rudder and lateral (coupled aileron and spoiler) commands.

The coefficients L_p, L_r, . . . , $L\delta_{AS}$, N_p, N_r, . . . , $N_{\delta AS}$, and Y_p, Y_r, . . . , $Y_{\delta AS}$ are the parameters of the configuration. Their values are such that the modes of response consist of two exponential modes (spiral and roll subsidence) and one oscillatory mode (dutch roll). Moreover, to correspond to the actual aircraft, certain of the coefficients have nearly constant known values:

$$Y_p \doteq 0, \quad Y_{\delta R} \doteq 0, \quad Y_{\delta AS} \doteq 0.$$
$$Y_r \doteq -1, \quad Y_\phi = g/U_0$$

This leaves 11 free coefficients which characterize the configuration.

Note that the coefficients of equation (1) are not given in conventional notation (ref. 2). Instead, they lump together both aerodynamic and inertia terms. This is consistent with our F4 data source (ref. 4).

Specification of Free Coefficient

The recently-updated Military Specification, MIGF-8785 (ref. 2) and the handling quality data which support it (ref. 3) provide data summaries for specifying ranges of desirable and undesirable values of the model coefficients. It is reasonable to assume that this summary is based upon enough careful analysis of the numerous sources of raw handling-quality data and enough Consideration for various expert opinions to have isolated the results of the most reliable experiments and studies pertinent to any particular specification. Accordingly, 11 handling-quality parameters were taken from references 2 and 3 which implicitly define the remaining coefficients of equation (1).* These are summarized in table 1, together with their approximate literal expressions as functions of the coefficients. The table also indicates the pertinent MIL

*The parameters of table 1 are the end results of several iterations through the available data, each iteration guided by the objective of uniquely specifying the free coefficients. It is quite possible to find additional conditions. However, these will either be redundant or they will overspecify the free coefficients.

TABLE 1.—*Parameters Which Specify Free Model Coefficients*

Handling-quality parameters	Parameter	Literal expression	Ref. 2, paragraph
Dutch roll frequency	$s_1=\omega_d^2$	$=N_\beta+N_r Y_\beta$	3.3.1.1
Dutch roll damping	$s_2=2\zeta_d\omega_d$	$=-\left[Y_\beta+N_r+\frac{L_\beta}{N_\beta}\left(N_p-\frac{g}{U_0}\right)\right]$	3.3.1.1
Roll time constant	$s_3=1/T_R$	$=-L_p+\frac{L_\beta}{N_\beta}\left(N_p-\frac{g}{U_0}\right)$	3.3.1.2
Spiral time constant	$s_4=1/T_s$	$=T_R\frac{g}{U_0}\left(-L_r+\frac{L_\beta}{N_\beta}N_r\right)$	3.3.1.3
Dihedral effect	$s_5=L_\beta$		ref. 3 data, pp. 215, 353
Zero location of p/δ_{AS}	$s_6=(\omega_\phi/\omega_d)^2$	$=1-\frac{L_\beta}{N_\beta}\frac{N_{\delta AS}}{L_{\delta AS}}$	3.3.2.2 and ref. 3 data
Transfer function	$s_7=2(\zeta_\phi\omega_\phi-\zeta_d\omega_d)$	$=\frac{L_\beta}{N_\beta}\left(N_p-\frac{g}{U_0}\right)+\frac{N_{\delta AS}}{L_{\delta AS}}L_r$	3.3.2.2 and ref. 3 data
Sideslip increment	$s_8=\Delta\beta_{\max}$	$L_{\delta AS}\delta_{AS_{\max}}\frac{T_R}{\omega_d^2}\left[2\frac{g}{U_0}\left(\frac{N_{\delta AS}}{L_{\delta AS}}L_r-N_r\right)+\frac{N_{\delta AS}}{L_{\delta AS}}L_p-N_p+\frac{g}{U_0}\right]$	3.3.2.4
Steady-state roll rate	$s_9=\left.\frac{p}{\delta_{AS}}\right\|_{ss}$	$=L_{\delta AS}T_R s_6$	airframe characteristics
Steady-state sideslip	$s_{10}=\left.\frac{\beta}{\delta_R}\right\|_{ss}$	$=N_{\delta R}/\omega_d^2$	airframe characteristics
Roll rate due to rudder	$s_{11}=\left.\frac{p}{\delta_R}\right\|_{ss}$	$=T_R\left(L_{\delta R}-N_{\delta R}\frac{L_\beta}{N_\beta}\right)$	3.3.4.5

F8785 paragraphs or other data sources which define numerical values of each parameter.

Using the 11 parameters of table 1, four handling-quality models were developed for the F4C aircraft. The models are ordered monotonically in terms of predicted handling qualities "goodness"—ranging from poor, model 1, to excellent, model 4. This predicted ranking was later used in the validation experiments to verify the design criteria.

The process of developing models consists simply of choosing numerical values for the 11 parameters and solving the resulting nonlinear algebraic equations (table 1) for the model coefficients. Details of these steps can be found in reference 1. It suffices here to say that we chose parameter values for model 4 which achieve best pilot ratings and chose parameters for the remaining four models such that each successive model was about one-half to one rating unit worse than the previous one. The latter degradations were taken individually along each parameter axis (or, at most, along two axes simultaneously), so the total effective degradation cannot be predicted. It is reasonable, however, to expect that the total degradation will exhibit the intended monotonic ordering of models.

Transient responses of the resulting four models for both lateral and rudder commands are shown in figures 1 through 4.

THE OPTIMIZATION PROBLEM

The second step of the design procedure is to develop a mathematical model for the aircraft which includes all of the dynamic elements judged important for control (e.g., rigid body,

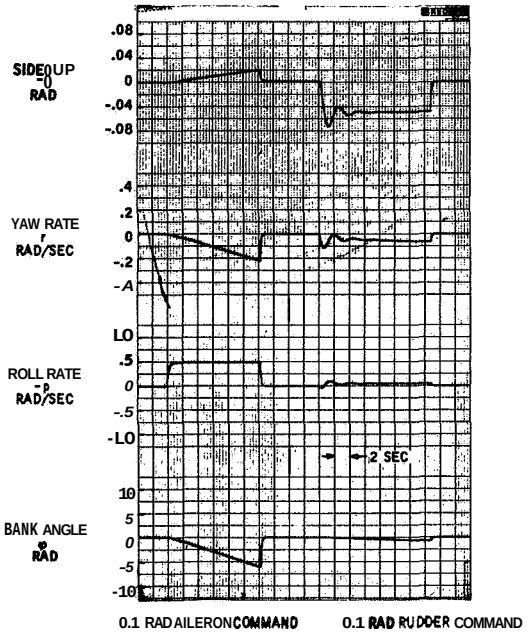

FIGURE 1.—step responses—model 1.

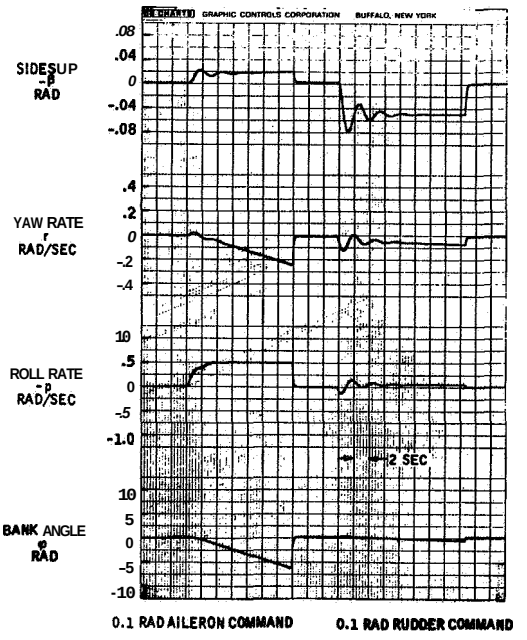

FIGURE 2.—Step responses—model 2.

actuators and servos, flexure modes, sensors, gusts). This vehicle model is then combined with the handling-quality model discussed above, and a controller is computed which satisfies a reformulated version of the usual quadratic optimal model-following control problem (see, for example, refs. **5, 6,** and **7).** The reformulated optimization problem and its computational solution are discussed in this section.

Reformulated Optimal Model-Following Control

Let the aircraft be represented at various points of the flight envelope and for various configurations and mass distributions by a collection of frozen-point linear plants:

$$\dot{x}_p(i) = F_p(i)x_p(i) + G_p(i)u_p + \Gamma_p(i)\eta_p \qquad (2)$$
$$i = 1, 2, \ldots, p$$

where $x_p(i)$ is the plant state vector, u_p is the vector of actuator or servo inputs, and η_p is white noise. The state x, and the system matrixes F_p, G_p, Γ_p, are indexed by the integer i, denoting a particular frozen-point plant. The index ranges from $i = 1$ to $i = p$, meaning that p distinct plants will be handled simultaneously. Further, let

$$\dot{x}_m = F_m x_m + G_m u_m \qquad (3)$$

represent the handling quality model [Equation (1)] with $x_m = (p_m, r_m, \beta_m, \phi_m)^T$ and $u_m = (\delta_R, \delta_{AS})^T$ and let

$$\dot{u}_m = F_u u_m + \Gamma_u \eta_u \qquad (4)$$

represent a stochastic model for pilot commands; i.e., the commands δ_R and δ_{AS} are assumed to be sample functions of a linear system driven by white noise η_u, with magnitudes and spectral content determined by matrixes F, and Γ_u.

We now look for a time invariant controller of the form

$$u_p(i) = K(i)\begin{bmatrix} x_p(i) \\ x_m \\ u_m \end{bmatrix}, i = 1, 2, \ldots, P \qquad (5)$$

such that the following composite performance index is minimized:

$$J = \sum_{i=1}^{p} \alpha_i J(i) \qquad (6)$$

where

$$J(i) = E\{\|H_p(i)x_p(i) - H_m x_m\|^2_{Q(i)} + \|u_p(i)\|^2_{R(i)}\} \qquad (7)$$

This cost functional is a generalization of the

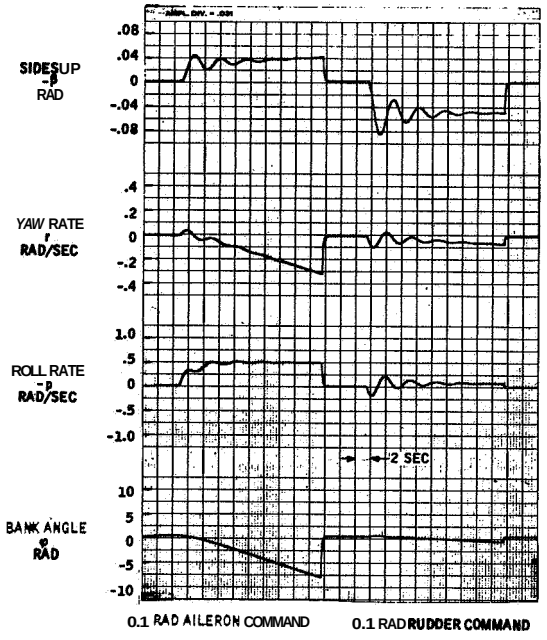

FIGURE 3.—Step responses—model 3.

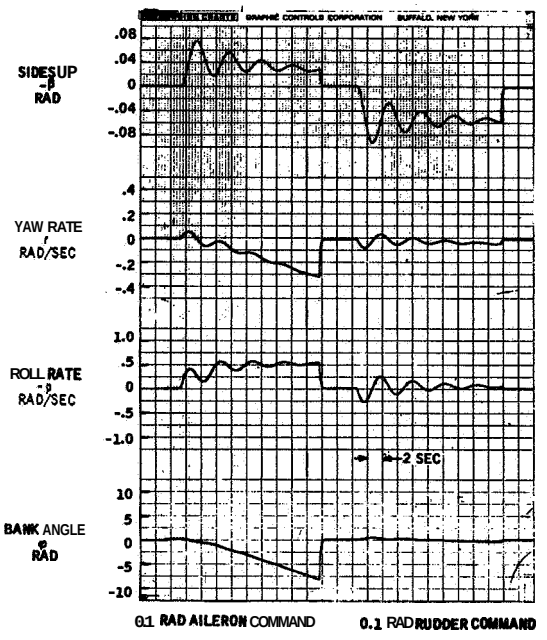

FIGURE 4.—Step responses—model 4.

usual quadratic index, representing weighted average performance over the flight envelope. The symbol $E\{-\}$ denotes mathematical expectation and $\|x\|_Q^2$ denotes the usual quadratic form x^TQx. The quantities $\alpha_i Q(i)$ and $\alpha_i R(i)$ are symmetric weighting matrixes, with $\alpha_i Q(i) \geq 0$ and $\alpha_i R(i) > 0$ for all i. $H_p(i)$ and H_m are matrixes which select certain combinations of plant and model states whose differences are to be minimized.

To achieve practicality, the form of the gain matrixes $[K(1), K(2), \ldots, K(i), \ldots, K(p)]$ cannot remain entirely arbitrary. Measurement realizability implies that certain elements of all gain matrixes must vanish, and elimination of gain scheduling requires that other elements of all matrixes be identical.* These conditions are imposed on the form of $K(i)$ at the outset, thus incorporating the controller simplification requirement directly into the optimization problem. In particular, let y denote a vector of readily observable signals, i.e.,

$$y = M(i)\begin{bmatrix} x_p(i) \\ x_m \\ u_m \end{bmatrix}, i = 1, 2, \ldots, p \qquad (8)$$

where the matrixes $M(i)$ select sensed signals and account for such things as sensor position, orientation, and sensitivity as they vary with flight condition. Then the gains, $K(i)$, most satisfy

$$[K(1), \ldots, K(i), \ldots, K(p)] = [KM(1), \ldots, KM(i), \ldots, KM(p)] \qquad (9)$$

for some constant matrix K.

Unfortunately, this new optimization problem does not yield a unique closed-form solution. Instead, several local minima are possible, each satisfying the necessary conditions of optimality. To solve for even one requires considerable computational effort. This is the price of practicality.

Computational Solutions

As is shown in reference **1,** necessary conditions of optimality for the gains, $K(i)$, can be expressed directly in terms of the performance index J, i.e.,

* **The latter constraint may well mean that adequate performance is impossible. While this is not the case in the F4 designs considered here, the possibility is certainly real and warrants research to remove the no-gain-schedule constraint.**

$$\frac{\partial}{\partial K} J[KM(1), KM(2), \ldots, KM(p)] = 0 \quad \textbf{(10)}$$

or they can be obtained from the maximum principle. The latter approach leads to several iterative algorithms for the solution of our reformulated optimization problem. These include Axsater's algorithms (ref. 8), a modified gradient algorithm (ref. 9), and others (ref. 10). All require large computer budgets (for high-order system), and all suffer from initialization problems, i.e., choosing initial values for K. (Initial values determine which local minimum will finally be found.)

The design procedure described here uses a newly-developed algorithm which is based directly on equation (10). This algorithm exhibits comparable computational speeds but avoids the initialization problem. It proceeds by dividing the gain matrices, $K(i)$ (for the moment these are assumed to be arbitrary), into two components:

$$K(i) = (K^1 + K^3)M(i) + \lambda K^2(i), \quad i = 1, 2) \ldots, p \quad (11)$$

The first component, $(K^1 + K^3)M(i)$, satisfies the constraint conditions [eq. (9)] and will be called "gains to be retained." The second component, $\lambda K^2(i)$, with scalar multiplier λ does not satisfy equation **(9)** and will be called "gains to be discarded." For generality, the first component is further subdivided into parts K^1 and K^3, where K^1 represents free gains to be optimized and K^3 is fixed.

In terms of these subdivisions, the necessary conditions (eq. (10)) become

$$\frac{\partial}{\partial K^1} J[(K^1 + K^3)M(1) + \lambda K^2(1), \ldots, (K^1 + K^3)M(p) + \lambda K^2(p)] = 0$$

or more simply

$$\frac{\partial}{\partial K^1} J(K^1, \lambda) = 0 \quad (12)$$

for fixed $K^2(i)$, $M(i)$, and K^3. This last equation implies that the optimal gains are functions of λ; i.e.,

$$K^1 = K^1(\lambda)$$

where, according to the Implicit Function Theorem (ref. 11), $K^1(\cdot)$ is defined by the following differential equation:

$$\frac{dK^1(\lambda)}{d\lambda} = -\left[\frac{\partial^2 J(K^1, \lambda)}{\partial K^1 \, \partial K^{1T}}\right]^{-1} \frac{\partial^2 J(K^1, \lambda)}{\partial K^1 \, \partial \lambda}. \quad (13)^*$$

From equation (11), however, it follows that the desired constrained gains correspond to $\lambda = 0$. That is,

$$K(i) = [K^1(0) + K^3]M(i), \quad i = 1, 2, \ldots, p. \quad (14)$$

So it is possible to obtain solutions of equation (10) by solving equation (13), starting with any known terminal condition (satisfying eq. (12)) at $\lambda = 1$, and integrating backwards toward $\lambda = 0$. The choice of terminal condition and method of numerical integration is discussed below. The idea of parameterizing solutions of optimization problems and solving the resulting ordinary differential equations was developed by D. K. Scharmack (ref. 12).

Terminal conditions.—The most appealing terminal condition is the global optimum of the performance index, **J**. This corresponds to the gains $[K^*(1), K^*(2), \ldots, K^*(p)]$ which are obtained by optimizing the ith plant with respect to the ith criterion $J(i)$ without gain constraints, for all i. (These gains are readily computed by solving the standard quadratic optimization problem at each flight condition.)

The resulting K^1, K^2, K^3 values for $\lambda = 1$ are:

$$K^3 = \text{given}$$
$$K^1 \text{ arbitrary} \quad (15)^\dagger$$
$$K^2(i) = K^*(i) - (K^1 + K^3)M(i), \quad i = 1, 2, \ldots, p \quad \textbf{(16)}$$

Starting with these terminal conditions amounts to starting in the "deepest valley of J" and forcing K^2 to zero along the trajectory $[K^1(\lambda), \lambda K^2; 1 \geq \lambda \geq 0]$. As long as the matrix of second partials in equation (13) remains nonsingular, the resulting solution, $K^1(0)$, is unique and represents a stable linear controller. Moreover we have the reassurance that it is a point "on the walls of the deepest valley." Together with the knowledge of $J(K^*)$ and $J[K^1(0)]$, this

***Equations (12) and (13) make sense in vector-matrix notation only if the matrix K^1 is written out as a column vector. This is assumed.**

† Reference 1 suggests one possible way to choose K^1 such that $\|K^2(1) \ldots K^2(p)\|^2$ is minimized.

information could well suffice to terminate the search.

Numerical Integration.—The full gamut of integration techniques is available for this problem. In reference 12, a predictor-corrector scheme was found to be particularly useful. It consists of the following equations:

- Adams-Moulton Predictor

$$K^p = K^1(\lambda_k) + \frac{\Delta\lambda}{24}\left[55\frac{dK^1}{d\lambda}(\lambda_k) - 59\frac{dK^1}{d\lambda}(\lambda_{k-1}) + 37\frac{dK^1}{d\lambda}(\lambda_{k-2}) - 9\frac{dK^1}{d\lambda}(\lambda_{k-3})\right] \quad (17)$$

- Newton-Raphson Corrector

$$K^c = K^p - \left[\frac{\partial^2 J(K^p,\lambda_{k+1})}{\partial K^1\,\partial K^{1T}}\right]^{-1}\frac{\partial J(K^p,\lambda_{k+1})}{\partial K^1} \quad (18)$$

The corrector is cycled repeatedly, each time replacing the old value K^p with the new value K^c, until a convergence criterion of the form $|\partial J/\partial K^1| < \epsilon$ is satisfied. The final value of K^c becomes $K^1(\lambda_{k+1})$, where

$$\lambda_{k+1} = \lambda_k + \Delta\lambda,\ \Delta\lambda < 0$$

$$k = 0,\ 1, 2,\ \ldots\ , \frac{1}{|\Delta\lambda|}$$

The integration is initiated at $\lambda_0 = 1$, with $K^1(1)$ given by equation (15).

The utility of these equations depends, of course, on the computer time and memory required to evaluate first- and second-partial derivatives. Equations for this purpose are developed in reference 1. It turns out that all necessary derivatives for a single predictor or corrector step can be obtained by solving $(\ell+3)$ n-dimensional Liapunov-type equations where ℓ is the number of gain components in K^1. These equations can be solved very quickly even for large systems (ref. 13). So it becomes possible, with the algorithm discussed above, to solve some fairly complex control problems. This is shown in the next section with the F4C design applications.

THE F4C TEST CASE

The design procedure discussed in the last two sections was used to design several control systems for the lateral-directional axes of the F4C aircraft. While space does not permit a detailed account of these designs, some of their basic features are discussed briefly below. Greater detail can be found in reference 1.

Mathematical Model

A 20th order dynamic model was used to represent the optimization problem. This model included 14 states for thg plant proper (the aircraft), plus three states for the handling quality model (eq. (1) with the spiral mode extracted), and one state each for the rudder and lateral command models and for a lateral wind gust model. The aircraft model itself included four rigid body states, one actuator state and two servo states in each of the control channels, two states for the lateral accelerometer, and two states for an approximated first asymmetric flexure mode. While flexure is not a primary control consideration on the F4, the first mode was included in order to constrain any tendency of model-following controllers to excite and/or destabilize flexure degrees of freedom.

A total of 11 flight conditions was considered in the design process, providing broad coverage of the flight envelope. Not all conditions were included in the computational procedure, however. Instead, the algorithm was run for a few selected flight conditions treated simultaneously, and the resulting controllers were checked at the remaining conditions.

Sensed signals available for feedback included body axis roll rate, yaw rate, and bank angle, all with unity sensor dynamics, and lateral acceleration near the pilot station, passed through second-order instrument dynamics. Of course, the handling-quality model states and command states were also available for control.

Summary of Designs

Using the problem representation above, the computational algorithm was first used to carry out several single-flight condition designs ($p = 1$). These served to debug the algorithm, to explore sensor complements, and to identify critical flight conditions. Typical run times for these single-flight-condition cases were 20 min on an H–1800

computer. (On present machines this means about 2 min.)

Two designs were then carried out for five flight conditions treated simultaneously (p = 5). The first of these proved disappointing in that too little dutch roll damping was achieved. This was later traced to an improper choice of command magnitudes in the optimization formulization. The second design, however, proved successful and was "flown" in the validation program. Run times for these multi-flight-condition cases came close to 160 min on the H–1800, or about 16 min on current machines.

THE VALIDATION PROGRAM

The design criteria and the controllers developed as discussed earlier were validated with a formal program of piloted experiments. These were conducted on a fixed-base simulator at Honeywell Inc., Minneapolis, Minnesota, and later completely replicated on a limited moving-base simulator at the Air Force Flight Dynamics Laboratory. Our rationale for the validations, the experimental design, procedures, and equipment setup are discussed in this section. Results of the experiments are summarized later.

The objectives of the experimental program were threefold: (1) to validate handling-quality design criteria used in the design phase of the program; (2) to evaluate the resulting practical lateral-directional control system using pilot performance measurement and rating scale values; and (3) to cross-validate pilot opinion measures with performance measures. A basic premise underlying the program is that neither rating data nor performance data alone can provide adequate evaluations of the "quality" of a controller/vehicle configuration. Simply stated, pilot ratings tell us how a pilot feels about flying a system, while performance data tell us how well he can satisfy mission requirements with the system. Both pieces of information are important for evaluation. It is reasonable to expect, of course, that the two measures are interrelated. It was the intent of the third objective to explore this relationship and to add to its data base. Accordingly, the validation program was designed to collect both kinds of data in a form which can be analyzed and interpreted.

The Experimental Design

A 2×5×3 mixed-design analysis of variance (ref. 14) was used to combine factorially five systems and two flight conditions. Three pilot subjects performed under each of the resulting 10 experimental conditions, giving a total of 30 experimental cells.

In the case of performance data, 10 trials were flown in each cell, where a trial was defined as a single flight profile three minutes long. The order of presentation of conditions was randomized to minimize order effects across subjects. In the case of pilot rating data, only two trials were flown in each cell.

Independent variables.—The following fixed variables were of interest: (1) system type, and (2) flight condition.

Five different systems were evaluated, each consisting of an F4C aircraft with a particular lateral-directional controller. The controller for systems 1, 2, 3, and 4 was a quadratic-optimal, model-following controller (no practicality constraints) designed to follow handling-quality models 1, 2, 3, and 4, respectively. As developed in Design Criteria, these models are predicted to exhibit an ascending order of handling-quality "goodness." It was anticipated that systems 1, 2, 3, and 4 would exhibit a consonant ranking, and, in fact, if they did, the design criteria would be validated (the first validation objective).

The controller of system 5 was a practical model-following controller which was designed to follow handling-quality model 4 but involved only practical feedback signals and fixed gains. We did not predict a performance or rating measurement for this system. However, since the four optimal systems were selected along a continuum of "goodness," the data of this experiment would locate the practical system along the same continuum and thus serve to evaluate the practical controller (the second validation objective).

For the second independent variable, two flight conditions—low-speed (Mach 0.5; 328 kt) and high-speed (Mach 1.2; 787 kt)—were selected as representative points of the speed range of the F4 vehicle. The three subjects were treated as random variables.

Dependent variables.—For each performance

data trial, the following variables were recorded on magnetic tape, at the rate of three sample points per second: (1) altitude error, (2) velocity error, (3) lateral error, **(4)** bank angle, (5) sideslip, **(6)** pilot aileron stick command, and (7) pilot rudder command. Several summary scores were also computed on-line and displayed to the experimenter at the end of each trial. For pilot rating trials, the Cooper Harper scale (ref. 15) and the Global scale (ref. 16) were administered after each trial. Voice recordings of pilot commands were collected for all rating and performance trials.

Both performance data and rating data were formally analyzed to evaluate the independent variables. Conclusions reached and numbers obtained were compared to cross-validate the two types of data (the third validationobjective).

The Task

The task consisted of a series of flight profiles of the type illustrated in figure 5. Each profile was composed of twelve 15-sec intervals during which constant bank angle turns or wings-level flight were commanded. Bank angles were randomly selected from the values ± 15, ± 12.5, ± 10, ± 7.5, ± 5, and 0, with approximatelyhalf of the angles taking the zero value. All profiles were initiated at 2000 ft mean sea level and required a 2000-fpm climb to approximately 8000 ft.

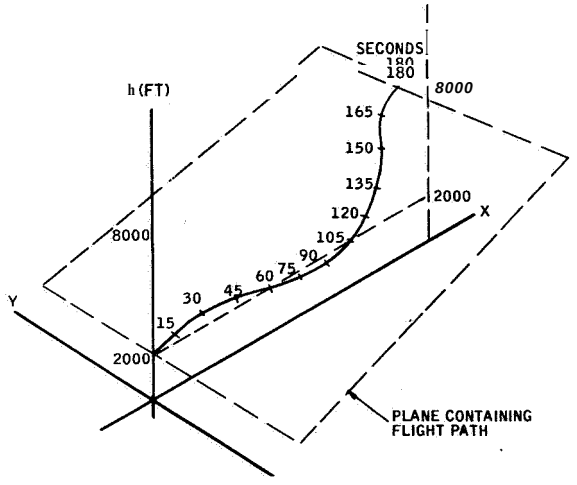

FIGURE 5.—Typical flight profile.

The primary display of the flight path course to the pilot was the flight director. The glide slope portion of the display (pitch command bar) was used to display deviations from the commanded 2000-fpm climb, while the localizer portion of the display (lateral command bar) was used to display deviations from the commanded course centerline. The perceptual motor task for the pilot was simply to detect any deviations from pitch and lateral command bar center and to make appropriate corrections to keep the needles centered.

Subjects

A total of nine pilots were involved in various phases of the validation program. At Minneapolis, two (former) Navy and one (former) Air Force pilot participated. The Air Force subject repeated the experiment at WPAFB along with two current Air Force test pilots. In addition, a second group of four Air Force pilots participated in the Rating Data Phase at WPAFB. The qualifications and experience of the subjects are documented in reference 1.

Simulation Equipment

The experiments were conducted on a fixed-base simulator in Minneapolis and replicated on the limited-moving-base simulator at the Air Force Flight Dynamics Laboratory. In Minneapolis the simulation was mechanized on a **40K** memory, SDS Sigma–5 digital computer with associated A/D and D/A links, and a PACE 231–R–5 analog computer. The simulation was basically all-digital, with analog portions used only to drive instruments of the cockpit mockup. The AFFDL simulation was hybrid, with navigation and control equations mechanized on an EAI 8400 digital computer with associated A/D, D/A links, and aircraft dynamics and cockpit motion mechanized on four PACE 231–R analog computers.

Both simulations used nonlinear 6-degree-of-freedom equations of motion and had comparable complements of cockpit controls and displays. Controls included stick, rudder pedals, and throttles, and flight instruments included airspeed/Mach meter, altimeter, angle-of-attack meter,

flight director, horizontal situation indicator, and a sideslip **or** lateral acceleration indicator.

At each facility, the experiment was divided into two complete phases plus a familiarization phase. Phase I consisted of measuring pilot performance under the restrictions of the $2\times5\times3$ experimental design, and Phase II consisted of pilot rating measurements under the same experimental design. Phase II followed the completion of phase **I.**

RESULTS OF THE VALIDATION PROGRAM

Parametric statistical analyses were performed on the pilot rating scores and on several summary error scores computed from time histories **of** each performance data trial. Results of these analyses lead to the following general findings:

(1) Systems **1** through 4 exhibit the predicted monotonic ordering of "goodness" both when evaluated on the basis of pilot opinion data and when evaluated on the basis of pilot performance data. This verifies that our original design criteria—the handling quality models—do in fact differentiate on a scale of handling-quality goodness, and further, it verifies that the F4 can be made to exhibit the properties of the models, at least with optimal control.

(2) The ranking of system 5 shows an ordering of 5 better than 4 for rating data and 4 better than 5 for performance data. However, neither of these differences is statistically significant. This says that a practical controller designed with the procedure dc,eloped here is sufficient to achieve the required level of model-following.

(3) The effect of flight condition is not significant on all dependent measures analyzed save one—lateral stick activity. This means that the model-following controllers achieved a high degree of performance invariance for the two flight conditions investigated.

Reference **1** contains numerous histograms, graphs and analysis of variance tables to substantiate these findings. Here we will present results for two of the primary dependent measures—RMS lateral error from course centerline and Cooper-Harper ratings, both obtained from the Wright-Patterson AFB (WPAFB) simulation.

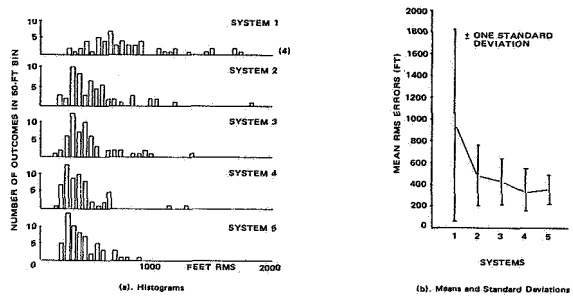

FIGURE 6.—Rms lateral errors at **WPAFB.**

Lateral Error at WPAFB ($\bar{E}_y$)

Figure 6(a) shows some histogram plots of the **300** lateral rms error scores obtained at WPAFB. These plots give the number of experimental outcomes which fell into 50-ft "bins," for bin locations between zero and 2000 ft.* The plots thus constitute crude experimental probability density functions of the random variable $\bar{E}_y$ at WPAFB. The samples are grouped into five plots according to the system with which they are obtained.

The plots of figure 6(a) show qualitatively how the probability density function of $\bar{E}_y$ changes as a function of the independent systems variable, i.e., the main effect of systems. We see first of all that all of the five distributions seem to have the same characteristic shape, something approaching chi-square if we indulge our imagination a little. The average value and spread of the distributions decrease steadily from the predicted worst system **(1)** to the predicted best system (4), and little difference exists between systems 4 and 5. Qualitatively, then, the main effect of systems looks something like this

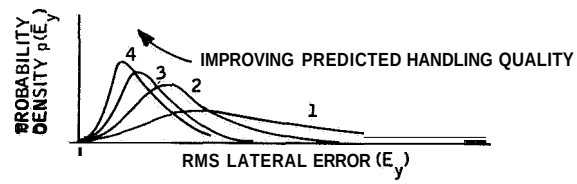

Mean values and standard deviations of the lateral error histograms are presented in Figure

* **As** indicated on the plots by a parenthetical number at the right extreme of the abscissa, four trials fell outside of the 2000-ft range. These are 2068, 2998, 4065, and 5632 ft in magnitude.

6(b). These statistics are again broken down to show the main effects of systems. A monotonic ordering is apparent for systems **1** through **4,** with a slight deterioration for system 5. Note that this is precisely the predicted ordering. The range of error from system **1** to system **4** is approximately 589 ft rms. Likewise, there appears to be a consistent decrease in variability from **1** to **5.** System **1** differs most noticeably from the others both in terms of mean error value and standard deviations.

The statistical significance of these apparent differences was assessed with an analysis of variance (ref. **14)** of the lateral error data and with individual comparisons of systems performed via Scheffe's test (ref. **17).** The analysis of variance showed a highly significant main effect of systems $(F=113)$, with subjects and systems-by-flight condition interactions also significant. All other effects were not significant beyond the **0.05** level. Individual comparisons showed that all differences of system means were significant except for adjacent pairs. In particular, the difference between systems **4** and **5** was not statistically significant.

Cooper-Harper Data at WPAFB

A similar analysis procedure was carried out for the Cooper-Harper rating data. This begins with figure 7 which shows histograms and mean values and standard deviations for this dependent measure. The histograms again show a qualitative main effect of systems which this time appears to match the sketch below:

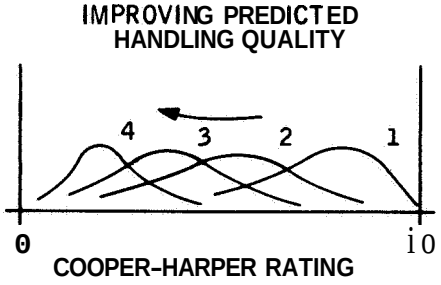

The mean values show a monotonic ordering of systems, with system **1** being the least acceptable and system 5 the most acceptable The average Cooper-Harper value for system **1** is 7.8 with a decreasing trend across systems to an

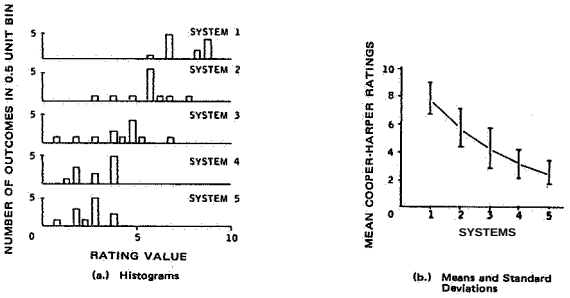

FIGURE 7.—Cooper-Harper ratings at WPAFB (3-subject group).

average of 2.7 for system 5. Note that system *5* obtained a better average rating than system **4.** This is contrary to the performance data which showed that system 5 errors were greater than system **4** and contrary to our original predictions. However, the difference between systems **4** and 5 turns out to be statistically insignificant. For all systems, the standard deviations appear comparable.

The analysis of variance for the Cooper-Harper data showed a significant systems effect $(F=23)$ and also significant flight condition-by-subjects, systems-by-subject, and systems-by-subject-by-flight condition effects. Individual comparisons showed all differences of system means to be significant, except of course, the **4** versus **5** comparison.

Other Dependent Measures

Several other dependent measures were also analyzed. These include altitude errors, velocity errors, global rating scores, and secondary measures such as rms lateral commands and rms rudder commands. All measures were separately analyzed for the Minneapolis and WPAFB versions of the experiment. The results show pretty much the same thing. Systems **1** through **4** are rank ordered as predicted with system *5* a bit better than system **4** for rating scores and a bit poorer for performance scores. In all cases, the latter difference was not statistically significant.

Tables **2** and **3** present the significance levels for the main effects and interactions and the individual comparisons, respectively, for all dependent measures. Entries in these tables are

TABLE 2.—*Summary of Levels of Significance for Main Effects and Interactions of the Dependent Variable Analysis of Variance*

Data source	(A) Systems	(B) Flight condition	(C) Subjects	AXB	AXC	BXC	AXBXC
Lateral error, WPAFB	$p<0.01$	.....	$p<0.05$	$p<0.05$	.....	.....	.....
Lateral error, Minneapolis	$p<0.05$	.....	$p<0.05$	$p<0.05$	$p<0.01$	.....	.....
Altitude error, WPAFB	$p<0.05$	.....	$p<0.01$	$p<0.05$	$p<0.05$	.....	...
Altitude error, Minneapolis	$p<0.05$	.....	.....	.....	.....	.....	.....
Velocity error, WPAFB	$p<0.05$	.....	$p<0.05$	.....	.....	$p<0.01$	.....
Velocity error, Minneapolis	.....	.....	$p<0.05$	.....	.....	$p<0.01$	.....
Cooper-Harper, WPAFB	$p<0.01$	.....	.....	.....	$p<0.01$	$p<0.01$	$p<0.01$
Cooper-Harper, Minneapolis	$p<0.01$	.....	.....	.....	.....	.....	.....
Cooper-Harper, 4-subject group, WPAFB	$p<0.01$	.....	$p<0.01$	.....	$p<0.01$	.....	.....
Global, handling qualities, WPAFB	$p<0.01$	.....	.....	.....	.....	$p<0.05$	$p<0.01$
Global, handling qualities, Minneapolis	$p<0.01$	.....	$p<0.01$	.....	.....	.....	.....
Global, demands on pilot, WPAFB	$p<0.01$	.....	.....	.....	.....	$p<0.05$	$p<0.01$
Global, demands on pilot, Minneapolis	$p<0.01$	.....	$p<0.01$	.....	.....	.....	.....
Global, handling qualities, 4-subject group, WPAFB	$p<0.01$	.....	$p<0.01$	.....	.....	.....	.....
Global demands on pilot, 4-subject group, WPAFB	$p<0.01$	.....	$p<0.01$	.....	.....	.....	.....
Lateral commands, WPAFB	$p<0.01$	$p<0.05$	$p<0.01$	$p<0.05$	$p<0.05$	.....	.....
Rudder commands, WPAFB	$p<0.05$	.....	$p<0.01$	.....	$p<0.05$	.....	.....

probability values indicating significant effects of the independent variables. In those cases where no entries are made there are no significant differences.

In terms of results, the two simulations—fixed base at Minneapolis and moving base at WPAFB—showed only small differences (fig. 8). Moreover, the two types of data—performance and rating—turned out to be complementary not contradictory. The rank orderings of systems are the same whether based on pilot opinion or pilot performance. This suggests a strong relationship between the two types of measures.

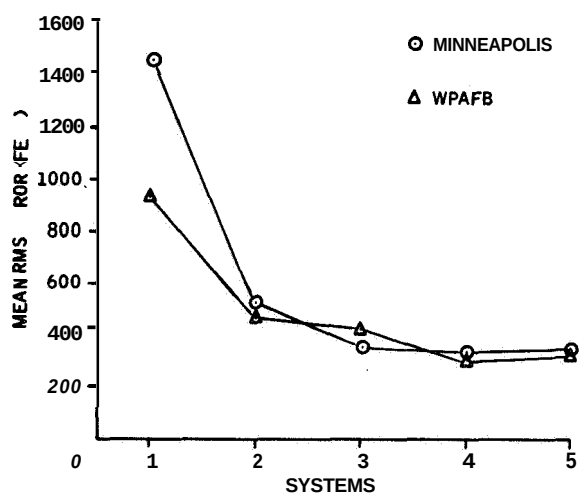

FIGURE 8.—Mean lateral error for both simulations as a function of systems.

CONCLUSION

The validation program has demonstrated that the design procedure developed here represents a powerful approach to the design of augmentation systems. The program has shown that handling-quality models for the controller/vehicle combination are a meaningful way to express design criteria, and that the **F4C** aircraft can be made to follow such models with a practical control system designed by the procedure. This is true at least to the resolution of pilot opinion and performance data gathered in the validation experiments.

TABLE 3.—*Summary of Levels of Significance for Individual Orthogonal Comparisons of All Pairs of Systems*

Data source	1 vs 2	1 vs 3	1 vs 4	1 vs 5	2 vs 3	2 vs 4	2 vs 5	3 vs 4	3 vs 5	4 vs 5
Lateral error, WPAFB	<0.01	<0.01	<0.01	<0.01	.....	<0.01	<0.01	<0.05	.....	...
Lateral error, Minneapolis	<0.01	<0.01	<0.01	<0.01	.....	.....	.....	.....	.....	...
Altitude error, WPAFB	<0.01	<0.01	<0.01	<0.01	.....	.....	.....	.....	.....	...
Altitude error, Minneapolis	<0.05	<0.01	<0.01	<0.01	.....	.....	.....	.....	.....	...
Velocity error, WPAFB	<0.01	.....	<0.01	.....	.....	.....	.....	<0.05	.....	...
Velocity error, Minneapolis		.....	.....	.....	.....	.....	.....	.....	.....	...
Cooper-Harper, WPAFB	<0.05	<0.01	<0.01	<0.01	<0.01	<0.01	<0.01	.....	<0.05	...
Cooper-Harper, Minneapolis	<0.01	<0.01	<0.01	<0.01	<0.01	<0.01	<0.01	.....	.....	...
Cooper-Harper, 4-subject group, WPAFB	<0.01	<0.01	<0.01	<0.01	.....	<0.05	.....	.....	.....	...
Global, handling qualities, WPAFB	<0.01	<0.01	<0.01	<0.01	<0.01	<0.01	<0.01	<0.01	<0.01	...
Global, handling qualities, Minneapolis	<0.01	<0.01	<0.01	<0.01	<0.05	<0.01	<0.01	.....	<0.05	...
Global, demands on pilot, WPAFB	<0.01	<0.01	<0.01	<0.01	<0.01	<0.01	<0.01	<0.01	<0.01	...
Global, demands on pilot, Minneapolis	<0.05	<0.01	<0.01	<0.01	<0.05	<0.05	<0.01	.....	.....	...
Global, handling qualities, 4-subject group, WPAFB	<0.01	<0.01	<0.01	<0.01		<0.05	<0.05			
Global, demands on pilot, 4-subject group, WPAFB	<0.01	<0.01	<0.01	<0.01	<0.01	<0.01	<0.01	.....	.....	...
Lateral commands, WPAFB	<0.01	<0.01	<0.01	<0.01	<0.01	<0.01	<0.01	<0.05	.....	...
Rudder commands, WPAFB	<0.05	<0.05	<0.01	<0.05	.....	.....	.....	.....	.....	...

REFERENCES

1. STEIN, G.; AND Henke, A. H.: A Design Procedure and Handling Quality Criteria for Lateral-Directional Flight Control Systems. AFFDLTR–70–152, Wright-Patterson AFB, Feb. 1971.
2. ANON.: Military Specification—Flying Qualities of Piloted Airplanes. MIL–F–8785B(ASG), Aug. 7, 1969.
3. CHALK, C. R.; NEAL, T. P.; HARRIS, T. M.; PRITCHARD, F. E.; AND WOODCOCK, R. J.: Background Information and User Guide for MIL–F–8785B (ASG). Military Specifications—Flying Qualities of Piloted Airplanes. AFFDL–TR–69–72, Wright-Patterson AFB, Aug. 1969.
4. BRIDGES, B. C.: Calculated Lateral-Directional Stability and Performance Characteristics of the F-4B/C/D/J and RF-4B/C Aircraft Plus the AN/ASA-32H Automatic Flight Control System. Rept. F395, McDonnell Aircraft Corp., May 1968 (revised Sept. 1968).
5. TYLER, J. S., JR.; AND TUTEUR, F. B.: The Use of a Quadratic Performance Index to Design Multivariable Control Systems. IEEE Trans. on Automatic Control, vol. AC–11, no. 1, Jan. 1966.
6. WINSOR, C. A.; AND ROY, R. J.: The Application of Specific Optimal Control to the Design of Desensitized Model-Following Control Systems. IEEE Trans. Auto. Control, vol. AC–15, no. 3, June 1970.
7. YORE, E. E.: Application of Mark III-SOC to Multivariable Control Problems. Part IV: Optimal Decoupling Control Applied to the Lateral-Directional Axes of a Sweep-Wing Aircraft. AFFDL–TR–68–10, Wright-Patterson AFB, Feb. 1968.
8. ÅXSÄTER, S.: Suboptimal Time-Variable Feedback Control of Linear Dynamical Systems with Random Inputs. Int. J. Control, vol. 4, no. 6, 1966, pp. 549–566.
9. WARD, M. D.; AND STEIN, G.: A Gradient Iteration Method for Fixed-Form Control. Research Memo No. MR 10829, Honeywell Systems and Research Center, Oct. 1969.
10. LEVINE, W. S.; AND ATHANS, M.: On the Determination of the Optimal Constant Output Feedback Gains for Linear Multivariable Systems. IEEE Trans. Auto. Control, vol. AC–15, no. 1, Feb. 1970.
11. COURANT: Differential and Integral Calculus. Interscience, 1947.
12. SCHARMACK, D. K.: An Initial Value Method for Trajectory Optimization. Advances in Control Systems. Vol. 5. C. T. Leondes, Ed. Academic Press, 1967.
13. KONAR, A. F.: Improved Iterative Algorithm for Solving the Lyapunov Equation. Honeywell Research Memo No. MR 10702, Honeywell Systems and Research Center, June 1962.
14. WINER, B. J.: Statistical Principles in Experimental Design. McGraw-Hill, 1962.
15. COOPER, G. E.; AND HARPER, R. P., JR.: The Use of Pilot Rating in the Evaluation of Aircraft Handling Qualities. NASA TND–5153, Apr. 1969.
16. MCDONNELL, J. D.: Pilot Rating Techniques for the Estimation and Evaluation of Handling Qualities. AFFDLTR–68–76, Wright-Patterson Air Force Base, Dec. 1968.
17. SCHEFFE, H. A.: The Analysis of Variance. John Wiley and Sons, 1960.

N73-10138

34. Application of Manual Control Theory to the Study of Biological Stress

CLYDE R. REPLOGLE, FRANK M. HOLDEN, AND CARROLL N. DAY

Wright-Patterson Air Force Base

Current techniques used to evaluate the effects of stress on the human operator may be generally divided into two classes: man-machine systems effectiveness models and factor-analytic techniques using test batteries. Each of these methods have inherent difficulties which may be solved by manual control techniques. The use of mission effectiveness metrics provide the essential estimate of system performance but due to the broad range of human operator adaptation, the effects of stress are not observed until catastrophic failure. On the other hand, task batteries can be constructed which are sensitive to changes induced by stress but from which little extrapolation to system effectiveness can be made. It is desirable, therefore, to have a task sensitive to stress induced changes in the human operator while measuring quantities which can be used in an analysis of mission effectiveness and reliability.

A study was run using both a stable, third-order task and an adaptive first-order unstable task singly and in combination to test the effects of 2 min hypoxia (22 000 ft). The results indicate that the RMS error in the stable task does not change as a function of hypoxic stress whereas the error in an unstable task changes significantly. Models involving human operator parameter changes and noise injection are discussed.

INTRODUCTION

This report discusses an experiment the purpose of which is to deminstrate that measurement of human operator parameters is a sensitive technique for evaluation of human operator performance under stress. The task consisted of an adaptive unstable compensatory tracking task and a stable third-order plant compensatory tracking task. The stresses used consisted of three simulated altitudes utilizing oxygen-nitrogen mixtures equivalent to sea level, 12 000 ft, and 22 000 ft.

Research into the effect of stress on the human operator may, in general, be broken into three classes: systems effectiveness evaluation for mission oriented tasks, behavior testing for changes in the operator, and physiological examination. Substantial difficulties have risen in the ability to predict a decrement in operational capability from all three approaches. The general pattern found in heat, hypoxic, acceleration, vibration, vestibular, toxic, and workload stresses is physiological and operator compensation to some limit and then rapid decreases in systems effectiveness. The man in a control situation will utilize his maximum capability to reduce or minimize closed loop error until the environment, task, mission goal or psychological factors, overwhelm him or terminate the control task. For this reason, measurement of system effectiveness alone, while providing necessary mission capability information, is not predictive of the decrement. Behavioral and physiological measures are more sensitive to changes in the human operator but only with great difficulty (if at all) can be related back to changes in operational errors. The task of identification of compensation and limits of human operator control parameters then falls to the control engineer. Not all of the techniques used to study manual control may be adapted to this area. The duration of many stresses may be as short as 30 sec to 1 min. Further the degree of compensation or adaptation may be large in this time frame. Techniques which need a 30 sec

analysis period or which must be done off-line have at best limited uses.

To evaluate the performance of a man in a control situation, the investigator is obligated to evaluate how the man is achieving effective control. If the stresses upon the man are affecting his ability to control the weapons system and the man can switch to alternative modes of control while maintaining closed loop error at a minimum, then evaluation of the man as an input-output processor will show the changes in his operating behavior while analysis of closed loop error will be uninformative. If changes in the man's mode of control are correlated with the stresses upon the man then they ought to be correlated with the psychological and physiological changes induced by the stresses.

TASK DESCRIPTION

The unstable tracking task is a first-order system with a single pole to the right of the imaginary axis. The first-order unstable tracking task as described by Jex et al. (ref. 1) was modified in the following manner (fig. 1). The absolute value of the displayed error was filtered with a first-order linear filter and then divided into a constant K. This provides a real time function called *b*. The function *b* is always positive and is used as the pole in the unstable element. By appropriate choices of the values for the constant *K* and the time constant in the first-order filter, one can prevent skilled trackers from losing control of the task while at the same time forcing him to maintain a low mean squared error.

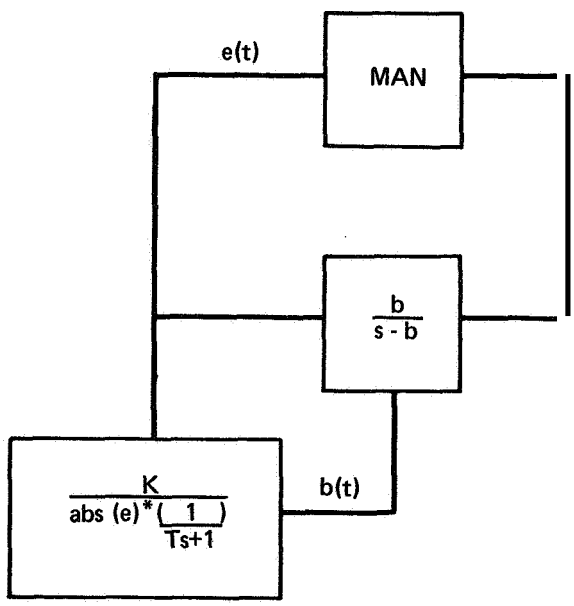

FIGURE 1.—Modified unstable tracking task.

The above modification of the unstable tracking task provides the following advantages. The operator while controlling such a system can optimize one of two variables. He can either optimize the displayed error which he is instructed to do or he can optimize the difficulty of the controlled element by operating at a point which provides a manageable unstable element. In either case in order for the operator to effectively control the system, he must either adjust his internal gain or he must maintain an effective time delay which is smaller than the value of the unstable pole at all times. Jex et al. have observed that the unstable tracking task forces a mode of controlling by the operator which is consistent with pure gain controlling. This is true as long as the operator maintains an effective time delay shorter than the value of the unstable pole. The distribution of the moving pole *b* or the distribution of the displayed error therefore provides a measure of either the operator's gain or his effective time delay. Jex has shown that in his formulation of an unstable element the critical value of the unstable pole is proportional to the effective time delay of the operator and Leviston has demonstrated an increased sensitivity in the unstable task to injected noise.

The stable tracking task was chosen to be representative of the pitch axis dynamics of a high performance aircraft. The dynamics of this stable tracking task are typical of a third-order system with a pole at the origin. The forcing function used in the stable tracking task consisted of the sum of five sine waves whose frequencies were chosen to simulate Gaussian white noise buffeting (fig. 2).

If the operator's performance at 22 000 ft is different than his performance at sea level, then the modification of the unstable tracking task as described above should indicate either a change in the mean value of the signal *b* or a

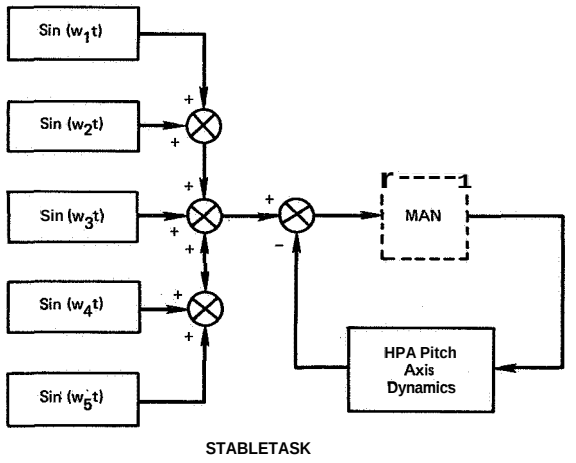

FIGURE 2.—Stable tracking task representative of the pitch axis control system of a high performance aircraft.

change in his rms error. Either of these changes or both in combination indicate that there is an internal change in the structure of the human operator. The operator has no control over the dynamics represented in the stable tracking task. It is, therefore, anticipated that at altitude no effect on rms error will be observed. If the operator is forced by the affects of altitude to change his internal structure as an operator, he can do so while operating the stable task and maintaining identical or similar mean squared error distribution.

EXPERIMENTAL DESIGN

The experiment is designed to evaluate the performance of an operator in a compensatory tracking task at sea level followed by the same task at a simulated altitude of either *12000* or *22 000* ft. Each run of the experiment consisted of two periods of tracking. Each period was preceded by one minute of prebreathing at the indicated altitude followed by one minute of tracking. Randomization of the order of presentation of the simulated altitudes and tasks to the subjects was done in order to minimize the effects of learning and anticipation of experimental factors.

Six subjects were evaluated. Each subject performed the same task on two different occasions. Three Compensatory tracking tasks were employed. The first was a single axis stable tracking task. The dynamics of the stable tracking tasks were representative of a high performance aircraft pitch axis control system. The second task was an unstable single axis tracking task modified as described below. The third task consisted of a dual axis tracking task combining the stable tracking task on the vertical axis and the unstable tracking task on the horizontal axis. The data were sampled at a rate of 50 samples per sec. The data were reduced by calculating the mean error and the variance of the error for the displayed error signals, and the mean unstable pole and the variance of the unstable pole in the unstable tasks. In addition, empirical probability entity functions were generated for the displayed error and the unstable pole-signals. The mean squared error scores and the variance of the mean squared error scores were subjected to analysis of variance utilizing a random variable design.

RESULTS

The results are straightforward and require little interpretation. Referring to table *1,* it is

TABLE *1.*—*Results of Analysis of Variance Comparing the Differences in the Various Scores at Ground Level and 22 000 ft Altitude Across Subjects*

Task	Score	Main effect $df = 1$	Interactions $df = 5$	F ratio
Stable	Rms error	1.69	11.99	.8457
Unstable	Rms error	0.01	64.97	.00092 *
Combined	Mean $b(t)$	6.98	5.54	7.56†

* $p > 0.99$
† $p > 0.95$

apparent that the RMS error in the stable axis was not affected by the 22000 ft altitude. The RMS error in the unstable tracking task is significantly affected by altitude, and the mean operating point b in the combined task unstable axis is significantly affected by the altitude **of 22 000** ft.

Further analysis of the data will include identification of the linear portion of the human operator as a function of altitude. The analysis of variance will be repeated on the parameters of the operators. It is anticipated that examination of the internal parameters of the operator while performing the stable tracking task will demonstrate an effect due to the simulated altitude. Support **for** this statement arises as a result of examining the data for the unstable tracking task at **22** 000 ft. It is apparent that the majority of the operators in the unstable axis attempted to maintain the average operating points b at an identical point irrespective of altitude while allowing mean squared error to change.

Examination of the empirical probability density curves (figs. **3** through 8) verifies that the

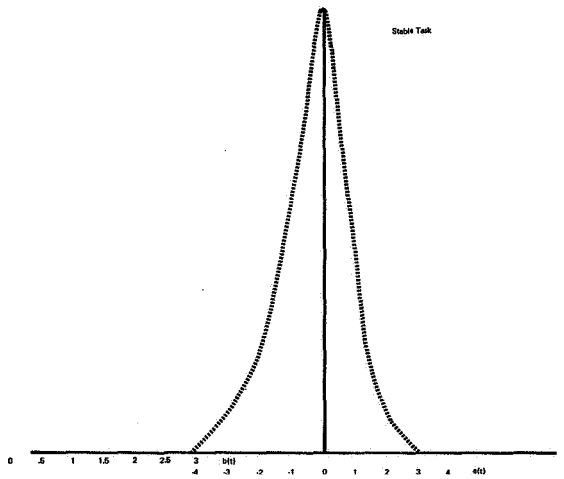

FIGURE 3.—Representative empirical probability density function of closed loop error in the stable task at sea level.

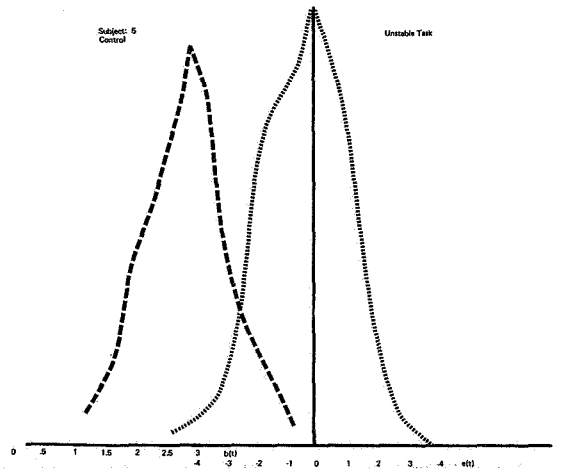

FIGURE 5.—Representative probability density functions for $b(t)$ and closed loop error $e(t)$ in the unstable task at sea level.

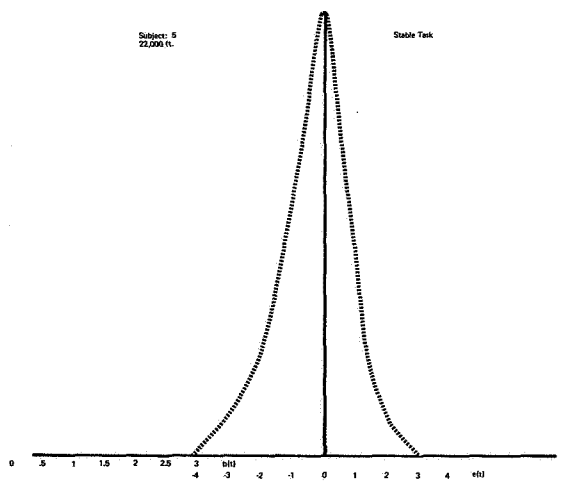

FIGURE 4.—Representative empirical probability density function of closed loop error in the stable task at 22 000 feet.

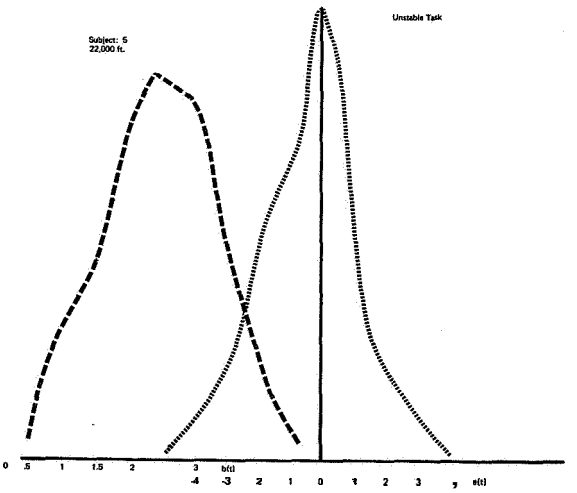

FIGURE 6.—Representative probability density functions for $b(t)$ and closed loop error $e(t)$ in the unstable task at 22 000 feet.

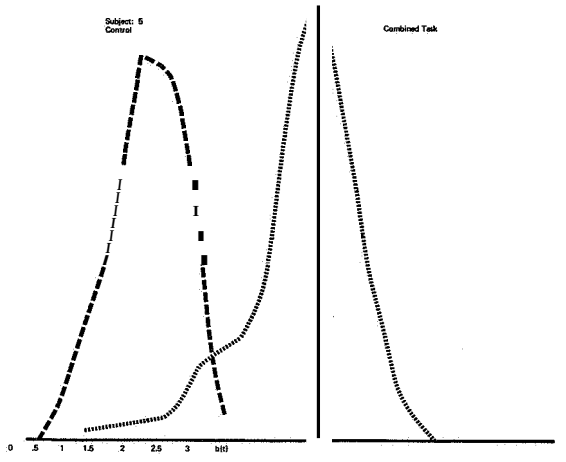

FIGURE 7.—Representative empirical probability density functions of vertical axis closed loop error $e(t)$ and horizontal axis $b(t)$ function at ground level.

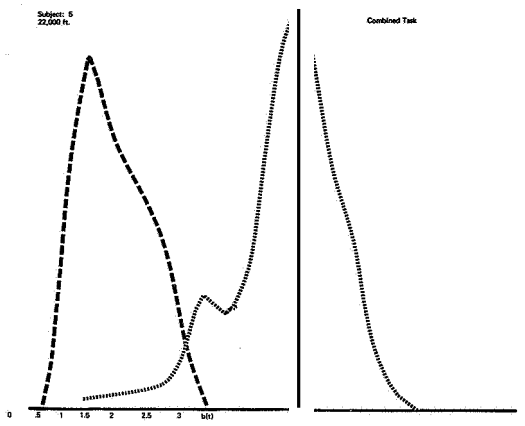

FIGURE 8.—Representative empirical probability density functions of vertical axis closed loop error $e(t)$ and horizontal axis $b(t)$ function at 22 000 feet.

error curve for the unstable task has a broader variance at altitudes. The b curves however shift their mean to a lower value at higher altitudes. The variance due to interaction was too large to demonstrate significance in the change of the mean b at altitude. If the mean b scores are normalized however a student's T test shows significance at the **0.01** level.

Figures **3** and **4** are the empirical probability density functions for the displayed error in the stable tracking task. There is relatively little difference between the curves at the control altitude, sea level, and at the **22** 000 ft altitude. Figures 5 and **6** are the probability density functions for both b and e in the unstable tracking task. Not only does the shape of the error curve e change but also the mean of the b curve is lower at **22** 000 ft and has a broader variance at **22** 000 ft. Figures **7** and 8 are the probability density functions for the combined task at control and at sea level and at **22** 000 ft. Again, there is relatively little change in the error curves for the vertical axis whereas the mean value for the b curve shifts to a lower point at **22** 000 ft.

The purpose of these experiments is not to evaluate a unique way of identifying a performance measure. Rather, the purpose of these experiments is to demonstrate that control theory principles can be used to identify changes in human operator performance as a result of environmental factors. The data clearly demonstrates that standard measurements of error are insensitive to changes in human operator performance at **22000** ft. That changes in the human operator occur at **22** 000 ft is evidenced by the changes in the unstable tracking task parameters. One of the exciting aspects of the experiments was that the same changes and effects were suggested at **12000** ft. The effects at **12** 000 ft, however, were severely masked by the large amount of subject variance and interaction variance.

SUMMARY

Although the performance of a man-machine control system is best represented as a function of the closed loop system error, the compensatory actions of the human operator will obscure the effects of stress on the man until the point is reached where his compensation is not effective. In order to predict this point instead of merely observing it, the parameters of the human operator, the effect of stress on these parameters, and the range of control of these parameters must be described.

REFERENCE

1. JEX, H. R.; MCDONNELL, J. D.; AND PHATAK, A. V.: A Critical Tracking Task for Man-Machine Research Related to the Operator's Effective Delay Time. Part I: Theory and Experiments with a First-Order Divergent Controlled Element. NASA CR-616, Nov. 1966.

SESSION VIII

INTERACTION OF SENSORY MODALITIES

Chairman: ARNOLD SMALL

35. Human Transinformation Rates During One-to-Four Axis Tracking With a Concurrent Audio Task

DANIEL L. BATY

NASA — Ames Research Center

An experiment was conducted to determine the information processing rates of six subjects performing one-, two-, three-, and four-axis compensatory tracking tasks, with and without a concurrent four-choice auditory task. The purpose **was** to obtain further evidence concerning the nature of an hypothesized ceiling on human transinformation rates. Interference was found **among** tasks, but the evidence concerning **a** ceiling on information processing rates was inconclusive.

INTRODUCTION

This study was a continuation of research (refs. **1, 2,** and **3)** investigating the utility of measures of transinformation (infgrmation processing rate in bits/sec) in describing and predicting human performance in tasks related to aerospace missions.

Specifically, this experiment was designed to increase the number of simultaneously performed tasks beyond that used in prior experiments in order to obtain evidence that would either support or refute the evidence found in a prior study (ref. **2)** that a ceiling on total transinformation may exist. That study used a one- and two-axis integrated compensatory display controlled with a single two-axis controller. The subjects responded to a two-choice audio input task with the free hand. **A** portion of the results of that study suggested that a ceiling of some sort existed with the ***K*** and K/S dynamics with no evidence for a ceiling with K/S^2, even though the total transinformation was less than for the other two dynamics.

For the present experiment, provision was made for one, two, three, or four axes of tracking using ***K***, K/S or K/S^2 dynamics. In addition, a four-choice audio task was added for half the trials. When the experiment was designed the choice of which one-axis task, or which two-axis task, etc., should be presented was rather arbitrary. **To** have used all possible combinations of one-, two-, and three-axis tasks would have required too many experimental conditions.

The following, fairly general, hypotheses were made prior to the experiment.

(1) With the successive addition of tasks a limit (ceiling) on total transinformation would be found as evidenced by an approach to some asymptotic value.

(2) The ceiling would be related to the order of the dynamics, i.e., K/S^2 would have a lower ceiling than K/S, which would in turn have a lower ceiling than K.

(3) Each additional task would cause a decrement in transinformation on a "per channel" basis regardless of whether a ceiling was shown. This decrement would be related to the order of the dynamic, i.e., K more than K/S, and K/S more than K/S^2.

(4) When (if) a ceiling was demonstrated with two, three, or four tracking channels, the addition of the auditory task would decrease the total transinformation of the two, three or four channels by at least the amount of transinformation computed for the audio task.

Before the selection of subjects for this experiment began, a few ((interestedvolunteers" spent considerable time learning the task. It was generally agreed that the limits of the subjects would

indeed be found. A fairly extensive coverage of subject selection procedures will be given since it probably had a large influence on the results of the experiment, and it is assumed this will be of general interest to other experimenters because of the ever present problem of subject selection. For this experiment the selection was deemed especially important because the object was to find subjects who could perform well enough that data could be obtained on all conditions.

Following a description of the experiment, the results will be discussed in terms of task interference and the hypothesized transinformation ceiling. Performance comparisons will then be made, both between separate parts of this experiment and between this experiment and prior experiments. The final part of the discussion will be on the more tentative subjects of motivation and transinformation model assumptions.

TASKS AND PROCEDURES

Tasks

Continuous Compensatory Tracking *Task.*— The elements for this task were displayed on a 30 cm (12 in.) oscilloscope. Two 0.635 cm (1/4 in.) reference circles, 6.35 cm (2-1/2 in.) apart remained centered on the scope as shown in figure 1. The two 0.95 cm (3/8 in.) cross hair followers could be electronically driven anywhere on the face of the scope. The two cross hairs were oriented differently as shown to prevent confusion about which was the right and left follower when doing four-axis tracking. The subject's eye was held at 66 cm (26 in.), so that the visual angle between the two references was approximately 5.5° or ±2-3/4° from an imaginary center point.

The task forcing functions were provided by a multichannel FM magnetic tape system. The filtered output of a low-frequency gaussian noise generator had been prerecorded on magnetic tape. The recorded signal had been shaped by a second-order filter, providing a -40 dB/decade power spectrum beyond the break frequency ω_n for a forcing function. All runs were made with ω_n set at 1 rad/sec which corresponds to an effective bandwidth of 0.24 Hz, calculated as in prior studies (refs. 1 through 3). The inputs for multi-

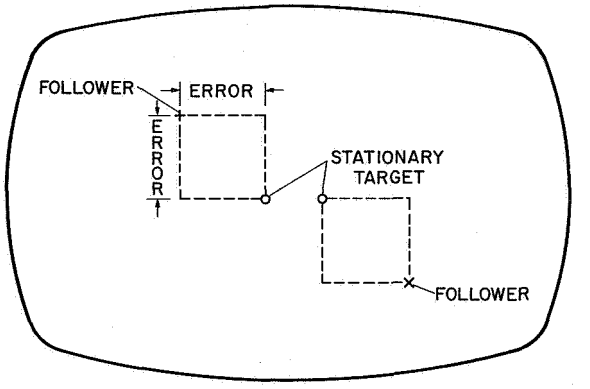

FIGURE 1.—Four-axis compensatory display.

axis tracking were all statistically independent. The 1 rad/sec forcing function was chosen as a compromise between two limitations. As shown in an earlier study (ref. 1), transinformation plotted against signal bandwidth generates a unimodel curve with the peak appearing between 2 and 4 rad/sec. The desire was to choose a frequency as high as possible (without passing this peak) and still have a task that could be controlled in four axes for all dynamics. Preliminary tests showed that 1 rad/sec was the best compromise.

Error control was provided through compatible movements of two, two-axis MSI Model 438 sidearm controllers with special flexible control sticks. The sticks were mounted upright and would deflect 1 cm at the tip with a 6×10^5 dyne side force.

Three controlled element dynamics were used: displacement (5×10^{-5} cm error displacement per dyne stick force), velocity (25×10^{-5} cm/sec error displacement per dyne), and acceleration (25×10^{-5} cm/sec² error displacement per dyne).

Discrete Auditory Task.—A four-choice audio input task was generated by random selection of a 1000 or 350 Hz tone; either was randomly presented as a clear tone or with white noise added. The tones were presented at a rate of 40 per min (i.e., a maximum information rate of 1-1/3 bits/sec). Responses were made with the feet which rested on metal plates pivoted under the arch of the foot. The 350 Hz tone was associated with the left foot and the 1000 Hz tone with the right foot. Clear tones were associated with toes while tones with noise went with the

heels. For example, for a clear **1000** Hz signal the response was made by pushing down with the right toes. This activated a switch under the foot plate and turned off the signal. If an incorrect response was made the tone signal remained on.

Test Subjects

Since the experiment was to be long and difficult, a special effort was made to select *six* subjects who were highly motivated and potentially skillful trackers. First **19** male college students were selected who expressed interest by phone and said they would be available through the entire school year. Subsequently, each of these **19** students made **160** runs on the critical task device (ref. **4),** which is a tracking task that gives a measure inversely related to effective reaction time (i.e., high scores were related to quick corrections to changes in target position). At the end of the day each man was given a simple questionnaire that was designed to point out any differences in goal setting behavior or intentions (ref. *5).* The questionnaire, as designed did not prove to be of any use in establishing a selection criteria.

Seventeen of the students were willing to spend a second day making another **160** runs on the critical task device. The six students with the highest score averaged over the last **120** runs were chosen for the experiment. The mean scores for **17** students ranged from **7.07** to **4.19.** All knew beforehand that their performance on this task would determine whether they would have a chance to participate in a long experiment with pay.

Table **1** shows the criteria task average score for the six selected subjects, along with relative total scores based on cumulative transinformation totals from the entire experiment. Although the pretest scores did not predict the final ranking for the experiment, the selection procedure was considered a success. Not one subject "dropped-out" of the experiment which ran almost seven calendar months, and every one **was** able to learn each task to a "scorable" criterion. One would not expect to be able to predict final ranking within a group whose members were originally so near each other in performance.

Of the six subjects, two were left-handed, all had normal corrected vision, and none had participated in any prior tracking experiments. It may be of interest to note that this selection procedure selected *six* very active young men, which caused some scheduling difficulties. Activities ranged from student government to other jobs. One man had three other jobs plus a full academic load. In retrospect, it would have been of interest to have correlated critical task score with I.Q. or some general measure of vitality.

Procedure

Instructions.—For the compensatory tracking task, the subjects were told, "Keep the crosses as close to the center of the circles as possible at all times; the score is related to the average value of the error for the entire run." For the audio task, they were instructed to respond to each tone within **1-1/2** sec or less after the onset of the tone. They were told that their score was the number of correct responses minus the number of incorrect responses divided by the total number of tones presented during the test

TABLE **1.**—Relative Performance: Critical Task and Main Experiment

Subject	Average critical task score, $\bar{\lambda}$	Relative rating main experiment			Average relative rating	Rank **on** experiment
		K	K/S	K/S^2		
D	**7.07**	**98.1**	**86.6**	**77.1**	**87.3**	**3**
A	**6.92**	**91.0**	**83.8**	**74.0**	**82.9**	**6**
C	**6.83**	**90.6**	**87.2**	**78.0**	**85.3**	**4**
B	**6.80**	**100.0**	**85.2**	**100.0**	**95.1**	**2**
E	**6.44**	**91.3**	**81.0**	**83.4**	**85.2**	**5**
F	**6.29**	**99.5**	**100.0**	**87.4**	**95.6**	**1**

period. They were told that they were not scored on how quickly they responded, so long as they responded within the 1-1/2 sec interval. If an incorrect response was followed by a correct response within the 1-1/2 sec time period, both a correct and an incorrect response were scored.

When the tracking task(s) and the auditory task were presented together, the subjects were not told how to weigh the two tasks. They were only told to do their best on both. At the beginning of each day the subjects were informed of their performances on the previous day and urged to lower their (error) scores. On multiaxis tasks the separate scores for each axis were available but generally the subjects concentrated on bringing down the average score across axes. It was repeatedly emphasized throughout the experiment that each condition was of equal importance and that maximum effort was to be extended on each run, whether it seemed like an easier task or not. It is believed that one other point had considerable bearing on the outcome of the experiment. At no time was it ever conveyed to the subjects that there was any doubt that they would learn the assigned tasks.

Performance Measures.—Two scoring procedures were used for the compensatory tracking task. An on-line relative rms error score was computed for each axis for each run to give a day-to-day indication of subject progress and to inform the subjects of this progress. The other procedure was to digitize and store directly on magnetic tape the system input and output signals for each axis being tracked. These data were used in the off-line computation of transinformation measures.

For the auditory task, the number of input signals, the number of correct responses, and the number of incorrect responses were recorded during each run. To obtain the auditory task transinformation rate for each run, the maximum transinformation rate of 1-1/3 bits/sec ($2/3 \log_2 4$) was multiplied by the ratio formed by subtracting the number of incorrect responses from the correct responses and dividing by the total number of stimuli presented during the run.

Training and Experimental Design.—Table 2 summarizes the sequence of the experiment for the six subjects. Each subject trained with a given controlled-element dynamics, then all data were recorded with those dynamics before presenting him with a new set of dynamics to learn. Using six subjects made it possible to present the dynamics in all possible sequences. The subjects were randomly assigned to each sequence. For phase I there were 75 training runs—15 per day for 5 days. For phases II and III there were 60 training runs (4 days) except for K/S^2 dynamics where 75 training runs were given. This meant that subjects A and D had one day less of training than the other four subjects during the experiment. After the initial introduction to the audio and tracking tasks, training was carried out in the same manner as the main part of the experiment; that is, the ten experimental conditions were presented in random order. For the main experiment, each subject ran six replications of the ten conditions for each set of dynamics in random sequence, making 60 runs per set.

Table 3 shows the combinations of tasks used to make the ten experimental conditions, along with the code designations.

Generally, two subjects were run per day, one resting in another room while the other was tracking so that there was always at least 1/2 hr between each of the three daily sessions for a given subject. The runs were 3-1/2 min long. During a session of five runs, the rest periods were 1-1/2 min between runs.

TABLE 2.—*Sequence of* Experimental Conditions

	Subject					
Phase	**A**	**B**	**C**	D	**E**	**F**
I	K/S^2	K/S	K	K/S^2	K/S	K
II	K	K/S^2	K/S	K/S	K	K/S^2
III	K/S	K	K/S^2	K	K/S^2	K/S

TABLE 3.—*Experimental* Condition Codes

Number of axes tracked	1	2	2	3	4
Axes tracked	LV*	LV and LH	LV and RV	LV, LH, and RV	LV, LH, RV, and RH
Without audio task	*S*	D	*P*	*T*	*F*
With audio task	*S*+	*D*+	*P*+	*T*+	*F*+

* LV—left vertical axis
LH—left horizontal axis
RV—right vertical axis
RH—right horizontal axis.

Data Reduction.—The input and output signals for each of the tracking tasks were digitized on-line (sampled from track-and-store units at the rate of 10/sec). For each pair of input and output signals, **1800** samples per channel were obtained for each run and stored onmagnetic tape for off-line computation. Cross correlation and auto-correlation values with **90** lags and subsequent power spectral densities were computed. The transinformation values were obtained by the following formula:

$$\text{Transinformation} = \int_0^\infty \log_2\left[1+\frac{S(f)}{N(f)}\right] df \cong \Delta f \sum_f \log_2\left[1+\frac{S(f)}{N(f)}\right]$$

where

$$1+\frac{S(f)}{N(f)} = \frac{\Phi_{00}(f)}{\Phi_{00}(f) - \dfrac{|\Phi_{i0}(f)|^2}{\Phi_{ii}(f)}}$$

also

$$\text{Relative error} = \frac{\sqrt{\dfrac{1}{\pi}\displaystyle\int_0^\infty \Phi_{ee}(f)\, df}}{\sqrt{\dfrac{1}{\pi}\displaystyle\int_0^\infty \Phi_{ii}(f)\, df}}$$

RESULTS AND DISCUSSION

Primary Performance *Measures.*—Figures 2, 3, and **4** show the combined performance for the *six* subjects for K, K/S, and K/S^2, respectively. These figures show the total transinformation for each condition, the solid lines indicating continuous tracking transinformation and the dotted lines the audio task transinformation. Also shown part way up on each column are bars indicating the average transinformation per channel for the continuous tracking tasks. From figures **2,** 3, and **4** it is difficult to detect the variation of the audio task transinformation so the actual values are listed in table **4.** It can be seen that the differences in rate were small but consistent, dropping in value as the number **of** axes tracked increased, and dropping from K to K/S to K/S^2.

The average transinformation per channel for the continuous tracking tasks is shown in figure **5.** This figure provides a gross comparison of all conditions for this experiment. Taking the average of all conditions for each dynamic, the average transinformation per channel was **3.71** bits/sec for the K dynamics, **3.12** bits/sec for K/S, and **1.64** bits/sec for K/S^2. The total difference between K and K/S^2 of **2.07** bits/sec was essentially the same as that found in an earlier study (ref. 2). However, where the earlier study showed the K/S results to be more or less equally spaced between K and K/S^2 (i.e., **1** bit/sec difference either way), these results showed the difference to be considerably less between K and K/S (0.59 bit/sec) than between K/S and K/S^2 **(1.48** bits/sec). These results are not directly comparable since the earlier data were obtained using three different forcing function frequencies ($\omega_n = 0.5$, 2.0, and **8.0** rad/sec), but the range did span that used for this experiment (i.e., **1** rad/sec).

Also shown in figure *5* are the averages for each set of dynamics both with and without the concurrent audio task. The difference in transinformation between the tiacking tasks with and without the audio task was **0.27** bit/sec for K dynamics, 0.13 bit/sec for K/S, and 0.09 bit/sec for K/S^2. Although the differences

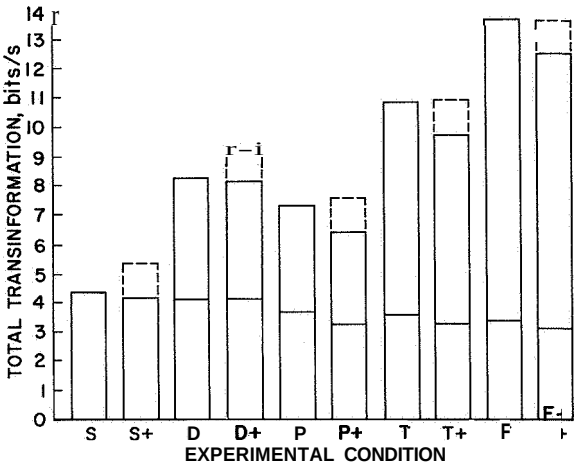

FIGURE 2.—Transinformation rates, K dynamic, all conditions, average 6 subjects.

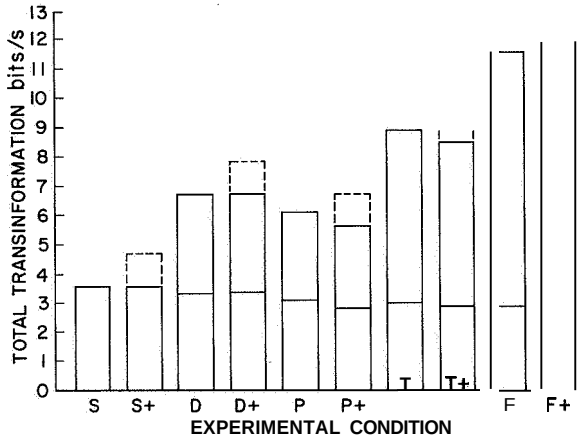

FIGURE 3.—Transinformation rates, K/S dynamic, all conditions, average 6 subjects.

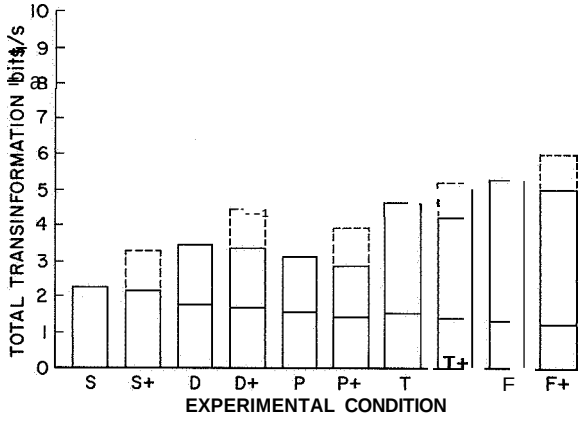

FIGURE 4.—Transinformation rates, K/S^2 dynamic, all conditions, average 6 subjects.

TABLE 4.—*Audio Task Transinformation (bits/sec)*

Condition	K	K/S	K/S^2	Avg
$S+$	1.18	1.18	1.11	1.16
$D+$	1.16	1.16	1.08	1.13
$P+$	1.18	1.14	1.08	1.13
$T+$	1.16	1.12	1.02	1.10
$F+$	1.12	1.12	1.00	1.08
Avg.	1.16	1.14	1.06	1.12

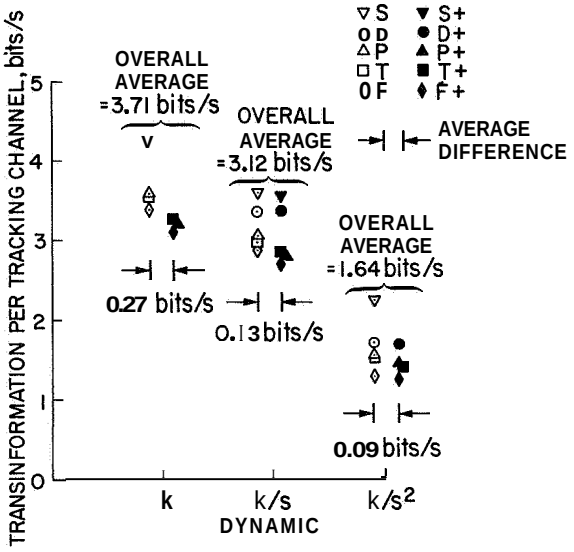

FIGURE 5.—Summary-average transinformation per tracking channel.

are small it can be seen by referring to table 4 that the tendency was to trade performance on the audio task for performance on the tracking tasks as the order of the dynamics is increased.

Table 5 provides a comparison of three different measures of tracking performance for this experiment, transinformation, relative error and open-loop crossover frequency ω_c, shown as overall averages on a per-channel basis. Generally the three measures follow the same trend, best performance (on a per axis basis) for the single task with progressively lower performance as tasks were added. This similarity in trend between performance measures was also found in an earlier study (ref. 3). Figure 6 shows that for this experiment given a value of relative error, one could fairly accurately predict the value of transinformation, particularly for K and K/S. This

TABLE 5.—*Comparison* of Performance *Measures* (average per tracking channel)

Dynamic		Experimental condition									
		S	*S*+	*D*	*D*+	*P*	*P*+	*T*	*T*+	*F*	*F*+
K	I, bits/sec	4.36	4.16	4.14	4.07	3.67	3.21	3.61	3.26	3.44	3.13
	Relative error	.208	.209	.214	.219	.248	.268	.243	.263	.263	.278
	X_{ovr}, Hz	.943	.915	.932	.886	.812	.760	.834	.768	.782	.758
K/S	I, bits/sec	3.60	3.56	3.38	3.39	3.07	2.81	2.99	2.84	2.90	2.71
	Relative error	.259	.267	.277	.280	.320	.344	.320	.339	.332	.348
	X_{ovr}, Hz	.771	.734	.749	.736	.646	.615	.657	.618	.634	.606
K/S^2	I, bits/sec	2.25	2.16	1.72	1.69	1.58	1.43	1.55	1.43	1.34	1.27
	Relative error	.520	.540	.614	.632	.672	.728	.682	.738	.742	.777
	X_{ovr}, Hz	.570	.540	.522	.500	.463	.461	.466	.450	.436	.438

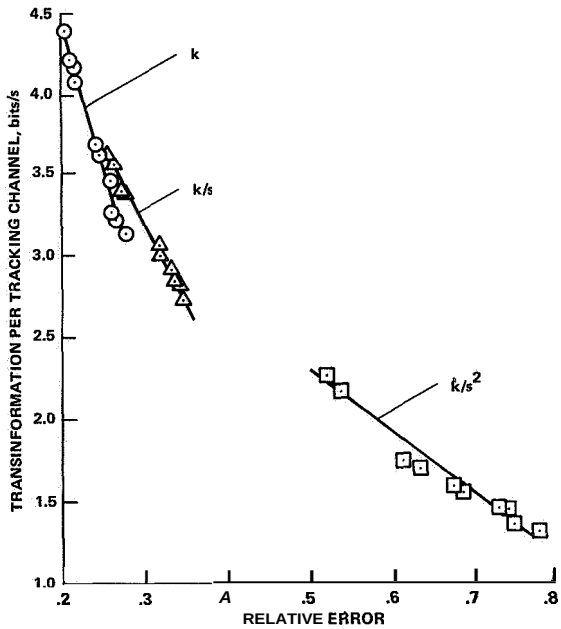

FIGURE 6.—Relationship between transinformation and relative error.

relationship is good only for the averages as calculated, however, and in a random sample of individual runs some showed marked deviations from these curves. Also it is to be stressed that this particular set of curves is good only for the conditions for this experiment. Any change in forcing function, gain, etc., would produce another set of curves.

Task Interference.—It can be seen in figures 2 through 4 that there was additional interference each time a task was added to any task set. For example, when tracking only one axis with *K* dynamics, the average transinformation was 4.36 bits/sec. When tracking the *D* condition the total transinformation was 8.28 bits/sec. If there had been no interference (i.e., if the second task had not affected performance on the first task and was of equal difficulty as the first task), the *D* total transinformation would have been twice 4.36 or 8.72 bits/sec. In like manner, the interference due to the addition of a third tracking channel to a two-axes task would be the difference between three-halves of the two-axes score and the total three-axes score, etc. This is shown graphically in figures 2 through 4 by the lines indicating average transinformation per tracking channel. The downward slope of these values indicate successive task interference.

The above discussion has answered the first part of the third hypothesis (Introduction) concerning per channel decrements in transinformation (interference) with additional tasks. Table 6 and figure 5 together answer the second part of the hypothesis relating to whether the amount of the decrement is related to the order of the dynamics. Listed in table 6 are the average values of transinformation per tracking channel for both single axis tracks (*K* and *S*+), all two-axes tasks (*D*, *D*+, *P* and *P*+), etc. for the three dynamics. Adjacent to these values are the incremental decrements with an additional tracking channel. From this table no clear statement can be made about the relationship between the amount of decrement and the order of the dynamics. It is seen that the largest decrement was for K/S^2, adding a second tracking channel to a single channel. In turn the *K* and K/S data show larger decrements in going from 2 to 3

TABLE 6.—*Transinformation Decrement With Increaed Number of Tracking Tasks* *

Tracking channels	K		K/S		K/S^2	
	Transinformation per tracking channel	Decrease due to added channel	Transinformation per tracking channel	Decrease due to added channel	Transinformation per tracking channel	Decrease due to added channel
1	4.26		3.58		2.21	
2	3.77	0.49	3.16	0.42	1.61	0.60
3	3.44	.33	2.92	.24	1.49	.12
4	3.28	.16	2.80	.12	1.30	.19

* All values in bits/sec.

tracking channels. However, it has already been noted (fig. 5) that the average decrement with the addition of the audio task was 0.27 bits/sec for K dynamics, 0.13 bits/sec for K/S, and 0.09 bits/sec for K/S^2. At least with the addition of the audio task the decrement was related to the order of the dynamics and in the direction indicated.

In a similar experiment using K/S^2 dynamics Levison and Elkind (ref. 6) found that adding a second axis of control resulted in little or no interference. Their experimental conditions corresponded to conditions S and D of this experiment. This does not agree with the present results where the decrement was 1.06 bits/sec (twice the single axis value, 2.25 bits/sec, minus the two axes value, 3.44 bits/sec). Their estimate of 3.6 bits/sec for two axis transinformation was, however, very close to the 3.44 bits/sec found for this experiment.

In an experiment with four separated displays, two hand controllers and no visual scanning allowed, Levison et al. (ref. 7) found that interference was less when two side-by-side axes were tracked with two hands than when two axes (one above the other) were tracked with one hand on a two-axis controller. In the present experiment (figs. 2 through 4) performance was degraded more when the second axis was added as a separate right vertical task to be tracked with two hands than when added as the left horizontal task to be tracked with one hand. These two results are not in disagreement but rather point to the disadvantages of an integrated control when the display is not integrated. Conversely, the results of the present experiment show the advantages of an integrated control and display over a separated control and display.

Transinformation Ceiling

Three of the four hypotheses stated in the Introduction dealt with finding and describing a ceiling on transinformation. The evidence for that ceiling was to be an approach to an asymptotic value of transinformation with additional tasks. The finding of task interference in these results does not necessarily indicate the existence of a transinformation ceiling. Figure 7 was obtained by plotting only the data from conditions S, D, T, and F for each set of dynamics to isolate the effects of successively adding tracking tasks only. If the assumption is made that each additional axis is an equal additional increment of total task load, then the points can be connected as shown by the solid lines. Strictly on the basis of the tracking task results alone it is obvious that there is no evidence for a ceiling on total transinformation, at least for K and K/S. (If condition P had been used instead of condition D a straight line would have been a good approximation for all four points.)

While the combination of tracking tasks alone did not show evidence of an information processing ceiling (figs. 2 through 4), the addition of the audio task did yield results that suggest some kind of limit. The effect is most evident for K, less for K/S and least for K/S^2. For all dynamics the decrease of transinformation with the addition of the audio task was small when all tracking was being done by the left hand, either one- or two-axis. When tracking was done with two hands, however (2, 3, or 4 axes), the interference due to the audio task was evident. For K dynamics this interference was such that the total transinformation for five tasks $F+$ was less than for four tasks F.

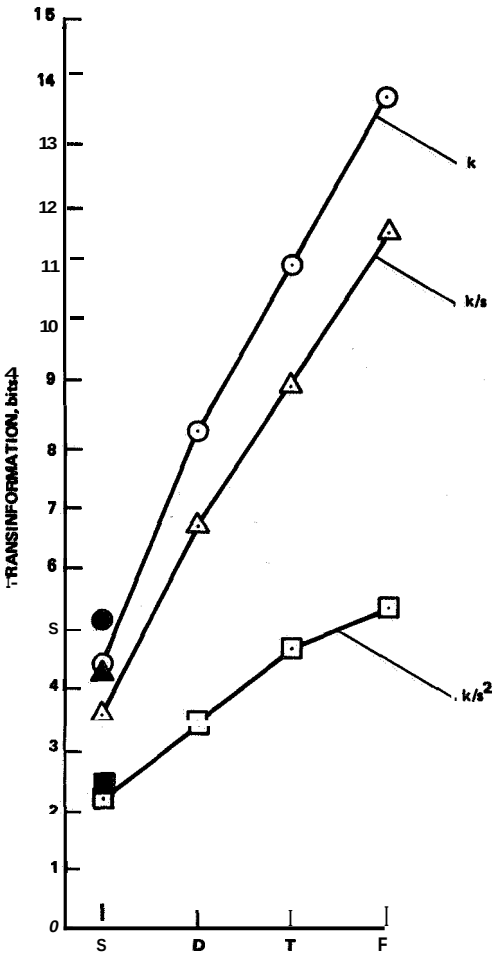

FIGURE 7.—Continuous tracking tasks, showing absence of transinformation ceiling.

Comparison Model for Three Dynamics

Transinformation performance has been presented separately for K, K/S, and K/S^2 data (figs. 2 through 4). From these figures it is difficult to compare the relative effects of additional tasks. It was decided to "adjust" the K/S and K/S^2 data to the magnitude of the K data by some simple mathematical model. The average differences between dynamics shown in figure 5 suggested one approach, That is, the average difference between K and K/S was 0.50 bits/sec per tracking channel. To each data point for K/S was added 0.59 times the number of axes being tracked for that data point. In a similar manner, to each K/S^2 data point was added 2.07 times the number of axes tracked. The results of the application of this procedure are shown in figure 8. Considering that the adjustment values used were gross averages and were also multiplied by as much as a factor of four, the clusters of data points are surprisingly close. If performance with K dynamic is taken as the reference, this means that performance on K/S and K/S^2 can be closely approximated by simply adding a common factor to each tracking channel.

With the data all in the same relative proportion (fig. 8) some of the differences between dynamics can be pointed out. The one-axis performance was very nearly the same. Performance on the two-axis integrated tasks was nearly the same with or without the audio task. There was about 0.9 bit/sec difference between K performance and K/S^2 performance in both cases. Finally, note the small but consistent relationship between K and K/S^2 performance for all two-handed tasks. For tracking without the audio task, performance is nearly the same but with K higher in each case. For the tracking with the audio task, K is lower in each case by an average difference of nearly 0.5 bit/sec. This reinforces the position stated earlier that the addition of the audio task affected performance more for the K dynamics than for the K/S^2 dynamics, both on a relative and an absolute basis.

Comparison of Integrated and Split Axis Tracking

It was pointed out in the Introduction that it would have been prohibitive to have used all possible task combinations as experimental conditions. However, two different 'two-axis tasks were used and the performance on the two tasks was different. The performance was poorer for the P and $P+$ conditions than for the D and $D+$ conditions for all three dynamics but the following discussion is for the K dynamic only.

It was first thought that the subjects' perceptually sampling between the displays might account for this loss. To explore this hypothesis, estimates were made of changes in the subjects' reaction times. The phase angles of the open-loop transfer functions for conditions D, $D+$, P, and $P+$ were measured at 0.67 Hz (where changes in

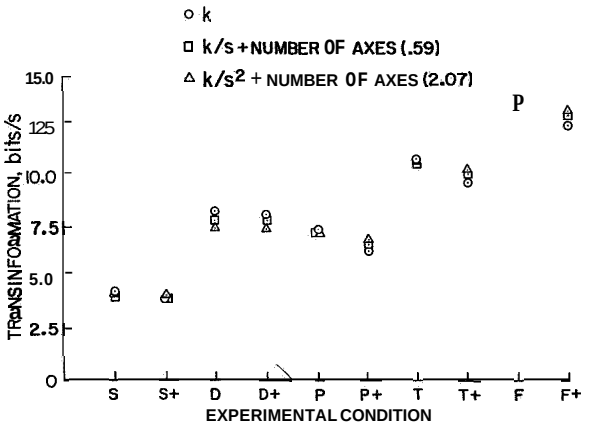

FIGURE 8.—Adjusted data for three dynamics.

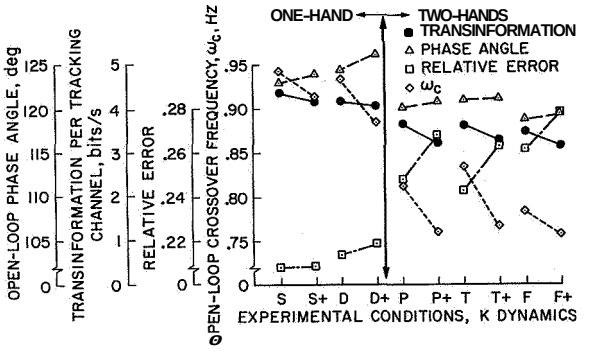

FIGURE 9.—Differences between single and two-handed performance.

reaction time would produce a relatively large change in phase angle, and changes in a lag time constant would produce a relatively small change in phase angle) and averaged across axes for the six subjects. The average phase angle difference between the integrated tasks and the separated tasks was approximately 5° which would occur with a change in reaction time of **0.014** sec, but was in the opposite direction to that needed to support the sampling hypothesis. The integated tasks ***D*** and $D+$ had larger phase angles than the separated tasks, P and $P+$.

The next step was to look at this result in context with the same calculations for all conditions. Figure 9 shows the phase angle for all conditions (K dynamics) along with the per channel values of transinformation, relative error and crossover frequency shown for comparative purposes. In this figure it is apparent that the task results can be partitioned into two groups, those that are one-hand tasks and those that are two-hand tasks. The first pertinent point is that the phase angles for all two-hand tasks are less than for the one-hand tasks. If the subjects perceived all two-hand tasks as more difficult than one-hand tasks, the result could have been a tightening of their control thereby reducing their reaction time. This explanation leaves the problem of explaining why average transinformation was reduced and average relative error increased, opposite from the direction that would be indicated by a reduction in reaction time. In the "crossover model" of the human operator (ref. 9) crossover frequency ω_c is directly proportional to the operator open-loop gain. Referring to figure 9 it can be seen that at the same time the subjects decreased their reaction time they also decreased their gain ω_c. It is tenable that the decrease in gain was large enough to offset the effects of the reduction in reaction time.

Comparison With Prior Study

Data from the earlier study (ref. **2)** that led to this experiment and comparable data from this experiment will be compared to show that there was a performance level difference between the two groups of subjects. The closest points of comparison are those where the two-axis tracking was performed with one two-axis controller, the present ***D*** and $D+$ conditions. The forcing function frequency for the points of comparison was **2** rad/sec for the earlier study, compared with **1** rad/sec for this study. (The effect of this difference will be discussed later.) The secondary task for the earlier experiment was a two-choice auditory task.

With a K/S^2 controlled element, the prior subjects were able to add the auditory task to the two-axis tracking task with only a small decrease in tracking performance, with a total transinformation of **2.7** bits/sec while tracking alone and a total of **3.6** bit/sec with the audio task. **A** similar small effect on tracking due to an added task was also found for the current subjects.

Next, with K/S, the prior subjects showed a decrease in total transinformation of 0.55 bits/sec with the addition of the auditory task. The current subjects added the transinformation of the

4

audio task to the tracking task with no decrease in tracking performance.

With K, the prior subjects were different in their response, one showing a total decrease of 1.5 bits/sec and the other showing a total increase of 1.5 bit/sec with the addition of the auditory task. The current subjects were able to add nearly all of the transinformation of the auditory task to the total, with little decrease in tracking performance.

The above references to the decrease in total transinformation with the addition of the auditory task was the primary evidence in the earlier study from which a transinformation ceiling was inferred. That evidence has not been refuted by this study but the suggestion is made that subjects selected for this experiment performed at a higher proficiency level than the earlier subjects and therefore did not show the evidence for a ceiling at this task level. Compare directly the differences in total transinformation between the two studies for the two-axis tracking without an auditory task. These differences were: 1.0 bit/sec for K, 1.2 bits/sec for K/S, and 0.7 bit/sec for K/S^2, higher for the present study in each case. As already mentioned, another study (ref. 1) of single axis tracking showed that transinformation increases with forcing function frequency and peaks at a value slightly above a 2 rad/sec input. Although further experimentation would be necessary to determine whether this peak would be at the same frequency for two-axis tracking, it does appear that the subjects had a greater transinformation potential at the 2 rad/sec task than those at the 1 rad/sec task. If this were so the performance disparity between these two groups of subjects was even larger than that shown by the above comparison and stands in favor of the hypothesis that the selection procedures for this experiment picked subjects that did not exhibit transinformation limiting at the task levels expected.

ADDITIONAL OBSERVATIONS

Motivation

Levison et al. (ref. 7) found that subjects originally trained with unstable controlled element dynamics were then able to track stable dynamics (K/S^2) such that the operator remnant (observation noise) was 6 dB below that which they had found in several previous experiments.

> The most likely explanation for the relatively low noise ratio is that training on the unstable dynamics provided strong motivation for the subjects to reduce their observation noise. . . . Once trained to achieve a low noise level, the subjects apparently retained this ability when presented with the stable-vehicle tasks.

Motivation *can* cause large variations in performance, even in well controlled experiments. Following this line of reasoning for the present experiment, it is possible that as the number of tasks increased, the subjective difficulty increased with a resulting increase in subject effort. If this happened the total transinformation would have been proportionately inflated for the more complex tasks, masking any actual trend toward a transinformation ceiling. The only protection against this effect during the course of the experiment was by instruction to the subjects. At the beginning of the experiment and at the beginning of each day, after going over the previous day's scores, it was emphasized that maximum effort should be expended on every condition on every run. After the experiment was over each subject was asked to write a review of the experiment covering certain specified areas. Every subject made some mention of this continual emphasis toward overall maximum effort. They generally agreed that: (1) it was impossible to put out absolutely maximum effort on that many runs per day (15); (2) they did attend to all tasks, simpler ones included, with as much effort as possible; and (3) the audio task, although it did interfere with the tracking somewhat, did prevent inadvertent lapses of attention. Two of the subjects affectionately referred to the audio task as being "very irritating to my ears and mind" and as "that infernal beeping."

In order to get some rough idea of what "maximum effort" might be for the simplest task (i.e., one axis without audio) a special session was run at the end of the experiment. Each subject ran five successive runs of the S task with the third dynamic of his sequence (see table 2), therefore, there were data for two subjects for each dynamic. The subjects were informed that this was the last of the experiment, that it was realized that the effort being asked for would have been

impossible for the entire experiment, but now they were being asked to "give everything." They were given their score at the end of each run and then urged to break that score. The average of the resulting ten scores per dynamics is shown as the "filled in" symbols on figure **7.** These scores are in fact greater than those obtained from the main experiment, by about **16** percent for K and K/S, and **10** percent for K/S^2. When looking at these differences there are two things to consider: **(1)** these scores were made by subjects with a high degree of skill since it was the end of a lengthy experiment and *(2)* the subjects did indeed put out extra effort in order to get the higher scores as evidenced by their comments and interest in scores after the runs and reports of hand and forearm cramps from the strain of "really bearing down." (There had been only passing mention of such tensions at the beginning of the experiment.) These reports of the effort needed to get the relatively modest increases in performance are taken as evidence that the level of effort on the simplest task was on the average commensurate with that of the more complex tasks throughout the main experiment.

This conclusion does not agree entirely with the prior discussion concerning the results of the dual integrated tasks and the split axes tasks. Clearly there was an interaction between subject set, motivation and task interference that cannot be fully separated on the basis of these data.

Parallel Channel Hypothesis

Moray (ref. 8) cites the results of an experiment that may provide some further insight into the lack of evidence for a transinformation ceiling for the continuous tasks. His purpose was to test the efficacy of the "many-to-one convergence model" of information processing. The central idea of this model is that there is one limited "narrow throat" or single channel through which information must be processed. In his simple but germane experiment Moray simultaneously presented his subjects with discrete audio stimuli in pairs. When provision was made for making two responses simultaneously, one with each hand, it was found that the subjects could respond at a rate of more than twice that found for other methods of response. He concluded that the "many-to-one convergence model" did not apply **(1)** for practiced subjects and **(2)** for compatible input-output systems. These two conditions are both applicable to the present experiment. Moray's results provide evidence that two parallel channels can function with essentially no interference between them. The present data show that up to four parallel channels can function with fairly small increases in interference as each channel is added.

Task Organization Hypothesis

Lying behind this and prior experiments are two basic, although at this time unproven, assumptions. The first of these is that there is some finite limit to the amount of information the human can process, no matter how cleverly the tasks are designed. Viewing the human subject as a set of input/output devices with an intervening complex central information processer it is intuitive that there is some task or set of tasks which can overload any part of this system.

The other assumption is that there is a lawful combination of tasks and functions. By this it is meant that each function performed ties up some portion of the total capacity so that it is not available for other functions or tasks. This allocation of capacity to function is lawful in the sense that if all these functional allocations could be measured, they would be the same each time under the same conditions and the sum of their proportions would equal unity. These functions include not only those directly associated with external task performance, but also such other ones as set, motivation, attention fluctuation, emotion, and conflicts. This discussion will be confined to task oriented functions.

On the basis of the data from the present experiment the hypothesis of an existing '(task organizing function" will lend a useful structure. This hypothetical function will tie-up" a certain amount of the total capacity as discussed above. Even though the experimenter thinks of a multitask situation as the sum of individual tasks, the operator, when faced with the actual task of doing his best on all tasks at the same time, approaches the situation with an overall task strategy **or** "task organization." That is, with some learning the operator decides the best

approach to take to a particular combination of tasks and then proceeds as if it were one composite task. The performance of each task (in the experimenter's sense) ties up capacity and the ''task organizing functions" tie up capacity. The amount used by the organizing function depends on the nature of the tasks combined.

Refer again to figure 2. (The trends for the following discussion are the same for K/S and K/S^2 (figs. 3 and 4) though less pronounced.) Adding the fourth tracking task F to the three-axes tracking task T reduced the average transinformation less than the amount of reduction caused by the addition of the audio task $T+$ to the three-axis task T. Adding the third tracking task T and the fourth tracking task F to the two split-axes tracking task P both reduced the average transinformation less than the amount of reduction caused by the addition of the audio task $P+$. Addition of the second tracking task D to the single task S caused the same reduction in average transinformation as caused by the addition of the audio task $S+$.

Three levels of "task organization" can be inferred from this. First, as tracking channels are added there is some reduction in transinformation per tracking channel. Second, there was a discontinuity in going from a one-handed task to a two-handed task. Some additional amount of organizational capacity was called into play in this case. And third, tracking was affected the most when the auditory task was added. The organization capacity needed was the highest here with less capacity left to each tracking channel.

There is still another way to state the above hypothesis. Similar tasks can be added together with less interference between them (tracking only) than when dissimilar tasks are added together (tracking and audio). Taking another step away from the data one might further conjecture that there would be less interference between the two tasks of aircraft control and throttle control than say between aircraft control and communication with air traffic control.

CONCLUSIONS

On the basis of the results of this experiment the following conclusions are indicated:

(1) There was task interference for each additional step in task complexity, that is, for each additional task, performance was poorer on the original task(s) than it had been without the added task.

(2) There was no clear evidence for a ceiling on human information processing capacity. The asymptotic approach to a maximum value of transinformation with additional tasks was not found. The addition of the four-choice audio task interfered most with the four-axes tracking score when the controlled element was K, less when it was K/S, and least when it was K/S^2. This is the correct trend assuming the existence of some sort of absolute ceiling on total transinformation, but this was not sufficient evidence that such a ceiling exists.

(3) Comparison of results with a prior experiment provided evidence that the careful selection of subjects had a large impact on the results of this experiment. The requirement that all tasks be controlled within defined boundaries for the entire period of each run placed a constraint on performance that disallowed performance degradation below certain limits.

(4) There was a consistent but small variation in performance on the four choice audio task. The transinformation rate decreased as tracking axes were added, and decreased when the order of the controlled element was increased. The small change and consistency of these values attest to the attention demanding nature of this task.

(5) The order of the controlled element imposed a limit on the amount of transinformation for each channel. A loss of 0.59 bits/sec was found as the order increased from K to K/S, and a loss of **2.07** bit/sec as the order increased from K to K/S^2.

SYMBOLS

K	gain of controlled element
S	Laplace operator used in defining controlled element
$S(f)$	signal power at frequency f
$N(f)$	noise power at frequency f
Φ_{00}	output power spectral density
Φ_{ii}	input power spectral density
Φ_{i0}	input to output cross power spectral density

Φ_{ee} error power spectral density

ω_n natural frequency of the filter used to generate the forcing function

ω_c system crossover frequency

REFERENCES

1. WEMPE, T. E.; AND BATY, D. L.: Usefulness of Trans-information as a Measure of Human Tracking Performance. NASA SP–128, pp. 111–129, 1966.
2. WEMPE, T. E.; AND BATY, D. L.: Human Information Processing Rates During Certain Multiaxis Tracking Tasks With a Concurrent Auditory Task. IEEE Trans. on Man-Machine Systems, vol. MMS–9, no. 4, Dec. 1968, pp. 129–138.
3. BATY, D. L.: Effects of Display Gain on Human Operator Information Processing Rate in a Rate Control Tracking Task. IEEE Trans. on Man-Machine Systems, vol. MMS–IO, no. 4, Dec. 1969, pp. 123–131.
4. JEX, H. R.; MCDONNELL, J. D.; AND PHATAK, A. V.: A Critical Tracking Task for Man-Machine Research Related to the Operator's Effective Delay Time. Part I: Theory and Experiments With a First-Order Divergent Controlled Element. NASA CR–616, 1966.
5. LOCKE, E. A.; AND BRYAN, J. F.: Goals and Intentions as Determinants of Performance Level, Task Choice, and Attitudes. American Institute for Research, (AD 646 393), Feb. 1967.
6. LEVISON, W. H.; AND ELKIND, J. I.: Studies of Multi-Variable Manual Control Systems: Two Axis Compensatory Systems With Compatible Integrated Display and Control. NASA CR–554, 1966.
7. LEVISON, W. H.; ELKIND, J. I.; AND WARD, J. L.: Studies of Multivariable Control Systems: a Model for Task Interference. Rept. No. 1892, Bolt Beranek and Newman (NASA CR–1746, in press).
8. MORAY, N.: Where Is Capacity Limited? A Survey and a Model. Acta psychologica, vol. 27, 1967, pp. 84–92.

36. The Effects of Attention Sharing in a Dynamic Dual-Task Environment*

R. C. **CLIFF**

University of California

There are numerous examples **of** cases where the human operator is confronted with several tasks occurring simultaneously and continuously in time. The current study is an investigation into the nature of attention sharing between two continuous tasks with independent input-output modes. Eleven subjects were tested using a zero order compensatory control task with three levels of difficulty (input bandwidth) for each subject. **As** a secondary task on half of the trials, the subjects were also required to verbally shadow a random auditory input. Results from an extensive time and frequency domain analysis of the data are presented and discussed. The evidence supports a single channel model for continuous dual-task control.

INTRODUCTION

Man is frequently confronted with two or more tasks demanding his attention simultaneously. Such an everyday activity as driving a car while conversing or listening to the radio provides a common example. In the more highly evolved technological occupations such as air traffic control, piloting aircraft, or process control, the examples are even more numerous, and the consequences of inattention can be potentially more disastrous.

There has been much work on the topic of simultaneous task performance for the case of discrete tasks (Broadbent (ref. 1), Berteleson (ref. **2),** and Welford (ref. **3)).** Most of this work has centered around dual task studies in which an auditory and a visual stimulus are presented within several hundred milliseconds of each other and the response latency for each of the two stimuli is measured. In general, it is found that the response to the second stimulus must be deferred until the response to the first has been completed. Although this result seems to be dependent on the amount of event and temporal uncertainty to be resolved in the response (Adams (ref. 4)), the general finding is well verified. By far the most widely held explanation of this phenomenon is embodied in what has become known as the '(single-channel theory." This theory views the human as a single-channel processor capable of processing only one stimulus-response pair at a time.

While there has been much work on dual discrete task performance, the work on simultaneous continuous task performance has been minimal. Furthermore, the research that has been done has not generally attempted to look deeply into the possible underlying causality as was the case with the work on discrete tasks.

The major concern of dual-continuous task studies in the past has been to assess the workload of one of the tasks, the primary task, by measuring the effect on performance caused by the addition of a secondary task. Welford (ref. **3)** has provided a fairly comprehensive review of this literature. Most studies have shown a decrement in performance when a secondary task is added; however, this seems to have been the extent of the analysis in most cases. There has been no major attempt at a detailed analysis of the operator's response records in search of the underlying processes which might account for the decrement. While the single-channel model

*This paper is based on work from the author's Ph.D. thesis in Human Factors Engineering in the Department **of** Industrial Engineering and Operations Research, Univ. **of** Calif.

is often assumed, support for this theory has only come from the discrete task studies.

There have been a number of studies of multiple visual input tasks (Senders (ref. 5), Carbonell et al. (ref. 6), and Merritt (ref. 7)). While these studies have made valuable contributions to our understanding of the allocation of visual attention, they cannot answer the more fundamental questions as to man's ability to control multiple tasks when the task inputs and outputs are independent. This same drawback applies to the numerous studies involving dual auditory inputs (Cherry (ref. 8), and Neisser (ref. 9)).

Wempe and Baty (ref. 10) did look at the effect of the addition of a secondary auditory task on a tracking task. The auditory task involved a binary decision once per second and caused a small (0.18 bit/sec) tracking decrement. Adopting a single-channel model, they attempted to account for the tracking decrement as a sampling loss when the secondary task was added. They found mixed support for this view and felt that sampling alone could not account for the tracking decrement.

A study was undertaken in order to directly investigate the effects of attention sharing for two stimulus-response independent tasks. It was desired that such a study should uncover the underlying mechanisms which account for the decrement in performance so often noted in the workload studies cited above. By using tasks which were uncorrelated and independent with respect to the input receptors and the output effectors, any interaction was limited to the operator's central information processing mechanisms. A visual-manual compensatory tracking task and an auditory-verbal shadowing task were selected as the most appropriate task pair.

DESCRIPTION OF THE TASKS AND PROCEDURES

The subject was seated in a soundproofed room approximately 60 centimeters in front of an oscilloscope displaying a point of light which could move along the 11.5 cm horizontal diameter. In the center was a vertical arrow which represented the zero error condition for the compensatory tracking task. Control was accomplished through a 6:1 cm diameter control knob which had left-right compatability with the display. Figure 1 is a photograph of the tracking station.

The subject was also equipped with headphones through which the shadowing input was received. Volume on the headphones was adjusted for comfortable listening for each subject. The shadowing task required the subject to repeat aloud random number pairs which were received through the headphones. Figure 2 is a sketch of a subject performing both tasks simultaneously. Figure 3 provides a block diagram representation of both tasks, where Y_E and Y_{Ha} represent the human operator's transfer characteristics for the tracking and shadowing tasks, respectively.

The compensatory tracking task—S.T.I. type forcing functions were used as input to the tracking task. Four forcing functions were used and

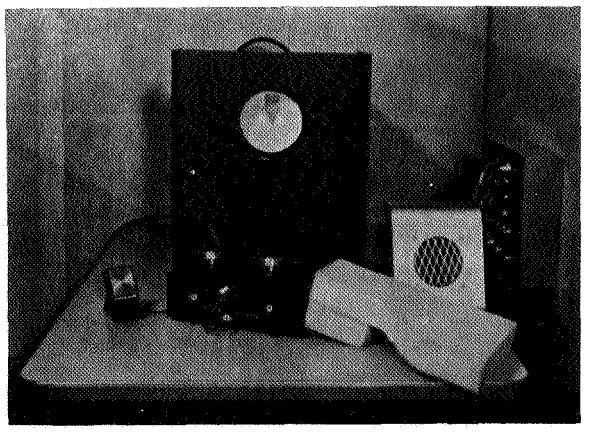

FIGURE 1.—Subjects tracking station.

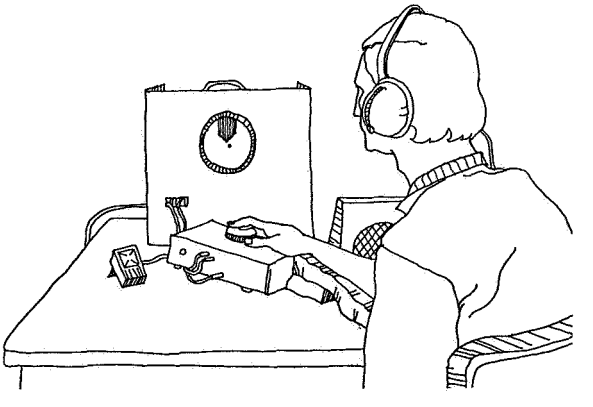

FIGURE 2.—Sketch of subject and equipment.

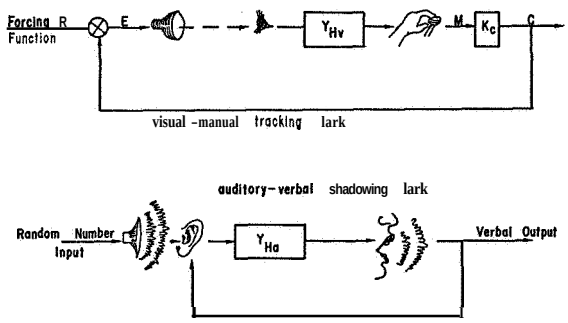

FIGURE 3.—Block diagram of the tasks.

are shown in table *1*. One group of subjects was given forcing functions ***A***, *B*, and ***C***, while the other subjects were given ***3***, ***C***, and ***D***.

Control was accomplished with a zero order controller ($K_c = 5.0$ cm/30° rotation). The control knob was situated with the rotation axis vertical, and an arm rest was provided so that the knob could be comfortably rotated with just the finger tips. The control potentiometer was a precision *360"* slide wire type with absolute linearity of ± 0.5 percent. The tracking task was implemented on an analog computer which was also programmed to produce an on-line computation of the mean squared error.

The *shadowing* task.—The shadowing forcing function consisted of random number pairs (e.g., *71, 49, 90, 44, 69, 25,* . . .) ranging from *10* to *99*. The subject's task was to repeat them aloud as he heard them; no retention was required. Based on the vocabulary size there were *6.49* bits of uncertainty per number pair.

Two levels of shadowing difficulty were used. The first level consisted of approximately one random number pair per second (an average of 5.88 bits/sec as actually measured), the second of approximately **1.5** number pairs per sec (an average of *9.13* bits/sec as actually measured). Subjects using forcing function set ***A***, *B*, ***C*** were given the slower shadowing while subjects using forcing functions *B*, C, ***D*** were given the faster shadowing.

Subjects

All subjects were undergraduates at the University of California, Berkeley, and were paid a standard hourly wage for the time they spent. None of the subjects had previous laboratory tracking experience. The experimental results for eleven subjects will be discussed in this report.* These subjects form two groups: Group I, those who received tracking inputs ***A***, *B*, ***C*** and the slow shadowing (subjects 1 through *6)*; group II, those who received tracking inputs ***B***,

*** In all, 13 subjects were tested, but results for subjects 7 and 8 have been omitted here. These two subjects were given forcing functions *A*, *B*, *C* and the fast shadowing. Their results were similar to those of the group II subjects discussed in this paper.**

TABLE 1.—*Specifications of S.T.I. Type* **Forcing Functions Used**

S.T.I. frequencies		Forcing functions			
		A	*B*	*C*	*D*
Hz	rps	Normalized amplitudes	Normalized amplitudes	Normalized amplitudes	Normalized amplitudes
2.200	13.800	0.1	0.1	0.1	0.1
1.210	7.570	0.1	0.1	0.1	1.0
0.642	4.030	0.1	0.1	1.0	1.0
0.404	2.540	0.1	1.0	1.0	1.0
0.237	1.490	1.0	1.0	1.0	1.0
0.154	0.969	1.0	1.0	1.0	1.0
0.096	0.602	1.0	1.0	1.0	1.0
0.063	0.393	1.0	1.0	1.0	1.0
0.042	0.262	1.0	1.0	1.0	1.0
0.025	0.157	1.0	1.0	1.0	1.0
Rms scope face amplitudes		3.62 cm 1.43 in.	3.42 cm 1.35 in.	3.30 cm 1.30 in.	2.26 cm 1.03 in.

C, D and the fast shadowing (subjects 9 through 13). There were five male subjects (subjects 1, 2, 10, 12, 13) and *six* female subjects (3, 4, *5*, 6, 9, 11).

Procedure and experimental design.—Each subject was first required to practice the shadowing until mistakes were seldom made (almost 100 percent transmission in a *5* min session). Following this, a standard set of instructions were read explaining the experimental procedure. Next, *5* min tracking practice was given followed by *5* min practice of simultaneous tracking and shadowing. After this the actual experiment was started and all stimulus and response functions were recorded on magnetic tape for later processing.

Altogether, each subject performed six runs of *5* min duration each. The subjects tracked each of the three forcing functions twice, once without shadowing and once while simultaneously shadowing. The order in which the forcing functions were presented was selected randomly for each subject. The shadowing or no shadowing condition was also selected randomly for the first trial, and the conditions were alternated thereafter. Rest periods were provided between each run.

Motivation.—In order to keep the subjects' motivational level relatively high, it was desired to supply knowledge of results after each run. However, since it was not possible to compute a shadowing score on-line, it was decided to give the subjects pseudo-knowledge of results. The subjects were given a score after each run which they were told could range from 0 to 100 and indicated how well they had done in relation to other subjects who had performed the same task. In actuality, after each run, the subjects were given a score ranging from 85 to 95, selected randomly. In this way it was hoped to provide scores which were high enough to give incentive, along with a feeling that more improvement was still possible. At the end of the experiment subjects were given an opportunity to receive the actual scores in a few days. None of the subjects claimed to have realized that the scores were not real, and all subjects felt the scores had a facilitating value.

GENERAL RESULTS

Tracking results.—The normalized rms error tracking scores for both groups I and II are shown in table 2. As the table shows, there was no consistent difference in Tracking performance between the no shadowing and shadowing conditions for group I. However, for group II there was a consistent decrement in tracking performance when the shadowing was added. A three way analysis of the variance was conducted and the above observations were supported. The complete ANOVA table is presented in table 3.

TABLE 2.—*Normalized RMS Error* Scores

		Forcing functions							
		A		*B*		*C*		*D*	
Subject		N*	S†	N	S	N	S	N	S
Slow shadowing	1	44.5	46.6	54.2	56.2	76.6	69.0		
	2	32.9	33.2	27.9	42.6	47.8	47.9		
	3	40.0	33.6	45.8	44.0	58.7	52.1		
	4	30.1	42.7	42.6	43.6	67.6	70.7		
	5	35.7	33.8	44.3	43.8	58.5	54.4		
	6	37.3	35.9	51.6	46.6	57.7	63.7		
	Mean	36.8	37.6	46.1	46.1	61.2	59.6		
Fast shadowing	9			37.3	42.5	49.3	74.2	64.6	69.9
	10			34.1	67.8	43.0	67.6	54.5	68.2
	11			49.9	56.8	67.8	84.7	67.7	76.2
	12			44.0	52.6	49.5	58.9	61.5	64.4
	13			43.5	58.4	50.5	61.8	70.9	73.3
	Mean			41.8	56.4	52.0	69.4	63.8	70.4

* No Shadowing. † Shadowing.

TABLE 3.—*Analysis of the Variance of Normalized Rms Error Scores*

Subjects 1 through 6					
	Source	*df*	*MS*	*F*	*p*
A:	Subjects	5	206.17	18.88	<0.005
B:	Forcing function	2	1643.70	150.53	<0.005
C:	Shadowing	1	0.32	0.03	Not significant
AB:	Subjects×forcing function	10	29.58	2.71	<0.10
BC:	Forcing function×shadowing	2	4.47	0.41	Not significant
AC:	Subjects×shadowing	5	19.92	1.76	Not significant
ABC:	Error	10	10.92		

Subjects 9 through 13					
	Source	*df*	*MS*	*F*	*p*
A:	Subjects	4	148.98	7.52	<0.01
B:	Forcing function	2	875.76	44.19	<0.005
C:	Shadowing	1	1193.22	60.21	<0.005
AB:	Subjects×forcing function	8	61.31	3.09	<0.10
BC:	Forcing function×shadowing	2	76.63	3.87	<0.10
AC:	Subjects×shadowing	4	65.66	3.13	<0.10
ABC:	Error	8	19.82		

Also, the mean tracking scores for group II have been plotted in figure 4 for both the shadowing and no shadowing case. The greatest percent decrement in tracking occurred with forcing function C.

Shadowing results.—The shadowing response records were scored for missed number pairs, and from this result percent transmission rates were computed. Table 4 presents the results for groups I and II. As with the tracking task, group I, who had the slow shadowing input, suffered no shadowing decrement when the shadowing was performed in conjunction with the tracking. However, group II subjects did show a significant shadowing decrement in addition to the tracking decrement previously described.

TRANSINFORMATION ANALYSIS

In an attempt to account for the performance decrement for group II subjects, the results were investigated for evidence of an information channel capacity. Tracking transinformation was computed using the linear correlation coefficient measured between the input and response distributions, that is,

$$\text{Transinformation} = w_c \log_2\left(\frac{1}{1-r^2}\right) \text{bits/sec}$$

where

w_c = forcing function bandwidth

r = tracking cross-correlation coefficient.

Results for subjects 9 and 10 are presented

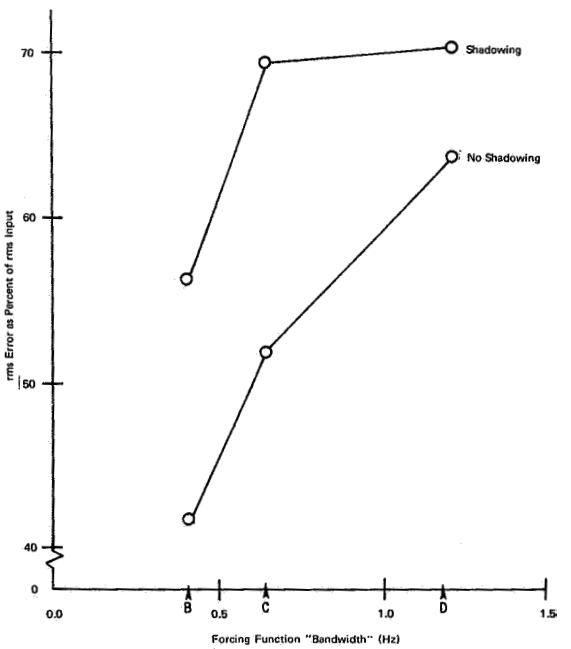

FIGURE 4.—Mean normalized rms tracking error for subjects 9 through 13 vs forcing function bandwidth with and without shadowing.

TABLE 4.—*Shadowing Scores*
[All scores are for 5 min runs and 6.49 bits/message]

	Subject	Trial	Number sent	Number transmitted	Percent transmission	Input, bits/sec	Output, bits/sec	Forcing function
Slow shadowing	1	2	267	265	99.3	5.78	5.73	*A*
		4	284	282	99.3	6.14	6.10	*B*
		6	283	283	100.0	6.12	6.12	*C*
	2	1	263	261	99.2	5.69	5.65	*B*
		3	281	281	100.0	6.08	6.08	*C*
		5	268	268	100.0	5.80	5.80	*A*
	3	2	272	271	99.6	5.88	5.86	*C*
		4	275	272	98.9	5.95	5.88	*A*
		6	269	267	99.3	5.82	5.78	*B*
	4	2	263	257	97.7	5.69	5.56	*C*
		4	278	275	98.9	6.01	5.95	*A*
		6	267	267	100.0	5.78	5.78	*B*
	5	1	269	267	99.3	5.82	5.78	*C*
		3	277	277	100.0	5.99	5.99	*B*
			out	of	Tape			*A*
	6	2	265	264	99.6	5.73	5.71	*B*
		4	277	276	99.6	5.99	5.97	*A*
		6	265	265	100.0	5.73	5.73	*C*
Fast shadowing	7	2	414	338	81.6	8.96	7.31	*B*
		4	417	370	88.7	9.02	8.00	*C*
		6	413	307	74.3	8.93	6.64	*A*
	8	1	426	322	75.6	9.22	6.97	*A*
		3	423	338	79.9	9.15	7.31	*C*
		5	427	338	79.2	9.24	7.31	*B*
	9	2	433	334	77.1	9.37	7.23	*B*
		4	425	340	80.0	9.19	7.36	*D*
		6	429	338	78.8	9.28	7.31	*C*
	10	1	427	337	78.9	9.24	7.29	*C*
		3	411	360	87.6	8.89	7.79	*B*
		5	417	383	91.8	9.02	8.29	*D*
	11	1	433	288	66.5	9.37	6.23	*C*
		3	413	311	75.3	8.93	6.73	*D*
		5	417	340	81.5	9.02	7.36	*B*
	12	2	436	198	45.4	9.43	4.28	*C*
		4	412	148	35.9	8.91	3.20	*D*
		6	425	191	44.9	9.19	4.13	*B*
	13	2	413	373	90.3	8.93	8.07	*D*
		4	422	384	91.0	9.13	8.31	*B*
		6	430	391	90.9	9.30	8.46	*C*

graphically in figure 5. Tracking information lost by the addition of the shadowing was greatly offset by the additional information added due to the shadowing. There was no evidence for a simple information rate channel capacity. Even using normalized information scores, the decrement produced by the addition of the shadowing was not sufficient to fit a channel capacity model. While other measures of tracking transinformation are possible (Wempe and Baty (ref. 11)) further effort in this direction was abandoned.

ANALYSIS OF TRACKING AND SHADOWING HOLDS

Tracking Holds

In the process of examining the tracking records, a striking difference was noted between the subjects' tracking response functions with and without shadowing. During tracking runs which included the shadowing task, the tracking response records were interspersed with periods of

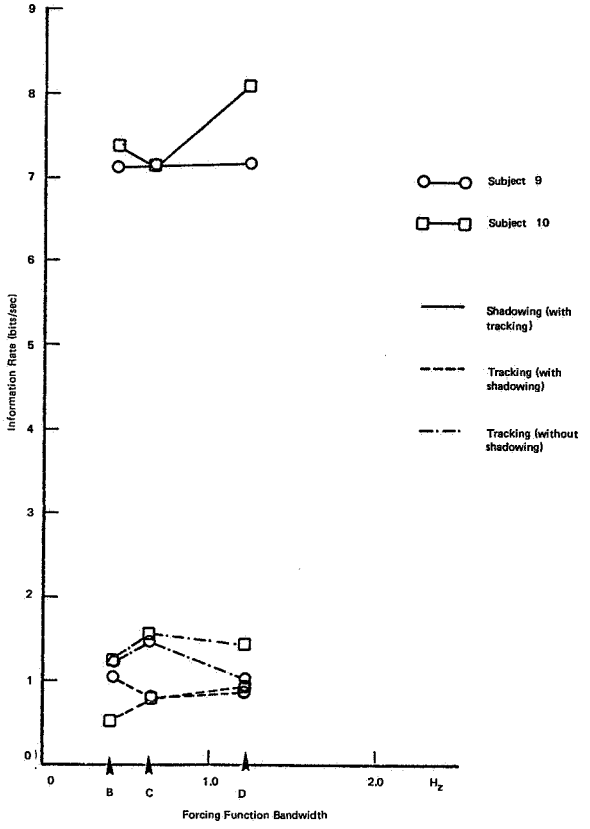

FIGURE 5.—Transinformation.

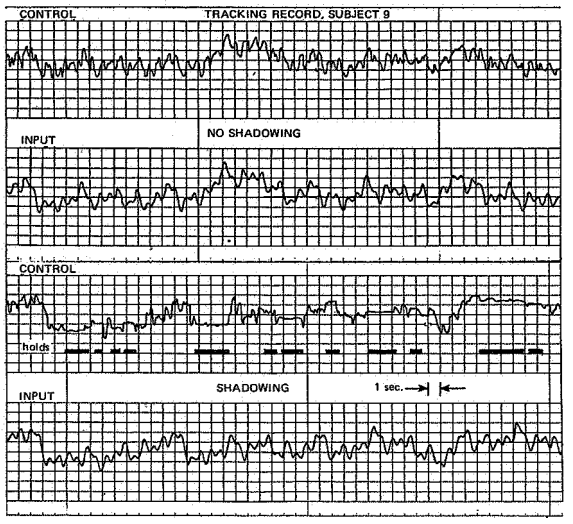

FIGURE 6.—Tracking records for subject 9 with tracking forcing function *D*, illustrating typical input and response (control) functions for tracking both with and without the simultaneous shadowing task. Tracking response holds generated while shadowing have been marked.

complete inactivity or holds on the subjects' tracking output function. In contrast, tracking without shadowing was relatively smooth and uninterrupted. Figure **6** shows a typical portion of tracking record for both the shadowing and no shadowing conditions, and clearly illustrates the difference.

Since forcing function *C* produced the greatest decrement in tracking performance, the input and the operator's control output data for these runs were analyzed for the tracking response holds. Each of the five subjects had two runs with forcing function C, one without shadowing (referred to as condition N) and one with shadowing (condition S). Each of these runs lasted 5 min, and was divided into two consecutive parts of **141** seconds each. The first and last halves of each run are referred to as parts I and II, respectively. The input and response data for these parts were sampled and digitized every **0.1** sec **(1410** samples per part of a run). This data was then digitally analyzed for holds by taking finite differences between successive samples. An interval between samples was counted as **a** hold if the difference was within the specified noise tolerance. Since the forcing function was composed of sinusoids, the input signal also contained some flat splots or apparent "holds" that were within the tolerance limits. For this reason the input was also analyzed in the same manner. The important result is the comparison of the distribution of "holds" for the input forcing function and the holds in the subject's tracking control output. Table 5 presents the results of this analysis.

Referring to table 5, it can be seen that holds in the subjects control output roughly matched the input distribution for the no shadowing condition; however, during runs with shadowing there was a marked increase in the total number of holds and also in the length of the tail of the hold distribution. In every case the addition of the shadowing task produced an increase in the number and mean duration of holds.

One possible explanation for the holds was that they were the result of a fatigue phenomenon. The data were analyzed in several ways to test

TABLE 5.—*Results of the Hold Analysis*

Subject	9								10							
Condition	N				S				N				S			
Part of run	I	II	I	II	I	II	I	II	I	II	I	II	I	II	I	II
Input, I or control, C	I	C	I	C	I	C	I	C	I	C	I	C	I	C	I	C
Hold length, number of points in tolerance																
2	125	106	133	155	108	104	102	112	144	157	134	131	103	108	114	102
3	50	60	47	62	44	30	42	47	36	61	39	51	38	35	46	38
4	18	28	10	22	17	16	20	24	14	21	15	20	29	16	20	12
5	1	19	1	12	4	12	10	15	2	1 1	6	6	6	4	4	1 0
6	2	3	2	2	2	6	2	5	4	2	3	3	3	5	3	9
7		7			1	6	1	4		2	1	3		6		6
8		1				10		2				1		5		6
9		1				10		4		1		1		1		3
10						3								3		3
11		1				2						1		1		2
12						1						1		1		
13						2		2						1		1
14						1								1		1
15														1		
16								1								2
17														1		1
18						1		1								
19														2		3
20																
21														1		1
Over 21 points, length/#						24/1 26/1 31/1								23/1 48/1		
Mean length [points] (total of 1410 pts/part)	2 49	3 07	2 40	2.59	2.59	4 23	2.71	3.25	2.43	2 63	2 53	2.77	2.70	3.96	2.59	3.97
SD [points]	0.77	1.45	0.71	0.89	0.91	3.98	1 0 1	2.23	0 83	1.04	0.93	1.43	0.97	4.75	0.88	3 55
Total number of holds	198	226	193	253	176	207	177	217	200	255	198	218	179	194	187	200
Total number of points	489	694	464	656	455	873	479	706	486	671	500	604	484	768	484	793

this hypothesis. The mean duration of the hold lengths for parts I and parts II was compared across all five subjects. A t-test failed to indicate any significant difference in mean duration between the two halves of the runs. Similarly, a test for increased number of holds gave no significant differencebetween parts I and **11.**

Since it was possible that a five minute run was not sufficiently long enough to produce a differential fatigue effect between the two halves of each run, one other test was applied. If the holds were recuperative in effect, it might be assumed that the longer the period since the last hold, the longer the next rest period, or hold, would be. This hypothesis was tested by generating the distribution of elapsed times since the last hold and classifying according to hold lengths. Based on this analysis, there was no significant

11								12								13							
N				S				N				S				N				S			
I		II		I		II		I		II		I		II		I		II		I		II	
I	C	I	C	I	C	I	C	I	C	I	C	I	C	I	C	I	C	I	C	I	C	I	C
105	52	96	72	114	18	97	16	124	146	138	129	132	118	155	132	95	102	119	102	114	97	135	117 2
40	49	29	52	48	26	45	12	57	36	35	49	56	**44**	51	27	33	69	36	52	58	53	47	47 3
17	34	24	**44**	16	15	**20**	18	16	19	20	24	13	**20**	12	12	18	36	26	39	20	32	13	29 4
7	22	**11**	11	2	14	4	8	1	8	1	8	3	9	1	8	16	28	7	18	**1**	15	**7**	17 5
2	1 8	2	2 6	4	3	4	5	2	4	1	5		2		4	3	12	**1**	12	2	10		10 6
1	9		**11**		2		4		4		2		3		7	2	6	1	1 2		6		5 7
	7		9		3		6				2		3		2		2		5				4 8
	6		6		4		2				**1**		4		1				3		2		1 9
	2		**1**		5		3		**1**		**1**		**1**		**1**						3		**1** 10
	3		**1**		**1**										**1**								**1** **11**
	2		**1**				3						**1**		**1**		**1**				2		12
	1				**1**		2														**1**		**1** 13
	2				**1**		2								**1**				**1**		2		**1** 14
	2		2				2														**1**		1 15
	1				4		5						**1**		2				**1**				16
					4		2																1 17
	1				4																**1**		**18**
					5		2						**1**										**19**
					2																		20
	2				2		2														**1**		21
	40/1				22/2		22/1						24/1		26/1								
					25/1		23/1																
					27/3		24/1																
					28/3		28/2																
					30/1		30/1																
					32/1		31/2																
					52/1		34/1																
					77/1		35/2																
							37/1																
							44/1																
							52/1																
							54/1																
							80/1																
2.63	4.87	2.73	4.04	2.55	9.69	2.66	11.24	2.50	2.65	2.42	2.81	2.45	3.21	2.36	3.18	2.89	3.27	2.62	3.51	2.56	3.65	2.47	3.36
0.97	4.11	1.02	2.29	0.86	10.63	0.94	12.78	0.75	1.21	0.74	1.33	0.68	2.64	0.61	2.82	1 1 9	1.49	0.95	1.99	0.78	2.74	0.77	2.22
172	214	162	236	184	127	170	110	200	218	195	221	204	208	219	200	157	256	190	245	195	226	202	236
452	1042	442	953	470	1230	453	1236	500	578	472	620	499	667	516	636	453	837	498	859	499	825	498	792

difference between elapsed time since last hold for short and long holds, and once again there was no support for the fatigue hypothesis.

Shadowing Holds

Next, the shadowing function was examined. Most of the shadowing decrement was a result of not responding to the input and thereby missing one or more input numbers. Seldom did a subject respond to the input with an incorrect number. Thus, the shadowing decrement was associated with a no response or "hold" condition rather than an incorrect response. In order to analyze the shadowing holds, the recorded shadowing response was passed through a voice key. The output of the key consisted of two exclusive states, either talking or no talking. Figure 7 is a

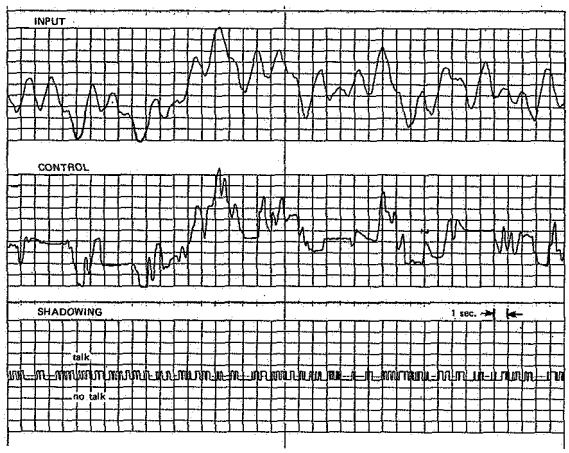

FIGURE 7.—Typical tracking and shadowing records for subject 9 with tracking forcing function C and fast shadowing input, illustrating both tracking and shadowing response holds.

typical portion of tracking record and provides a sample of the keyed shadowing response function. Once again each 5 min run was divided into two parts and the hold distributions compiled. Each part of a run consisted of 1435 samples taken at 0.1 sec intervals. The results are provided in table 6.

As was the case with the tracking, the shadowing holds have a long tailed, skewed distribution. Again, the short holds are primarily due to the properties of the input function. Holds up to three tenths of a second are attributable to normal interverbal spacings and not missed numbers. A t-test indicated no significant difference between the mean hold lengths in parts I and II, once more indicating no support for the fatigue hypothesis.

Test for Tracking and Shadowing Hold Interaction

The next step was to examine both the tracking and shadowing holds to test for possible correlation between the two. This was accomplished by computing the 2X2 contingency table of the percent time spent on the four possible hold and no hold combinations for the two tasks. To test the hypothesis of independence of holds on each task, a chi-squared contingency test was conducted. Under an independence hypothesis the percent expected simultaneous hold time EC during a run was calculated by taking the product of the percent of total time held on each task. The expected contingency table under independence and the measured table were compared using the chi-squared statistic. If the independence hypothesis were rejected, significant association between the shadowing and tracking holds could be assumed.

In analyzing the records and compiling the contingency tables, the holds were partitioned into two groups. Since short holds were attributable mainly to the properties of the respective forcing functions, these holds (those less than 0.3 sec) were analyzed separately. The results of this analysis are given in table 7. The analysis included subjects 9 through 13 using runs with forcing function C. Again, each run was divided into two parts. The table gives the measured percent time spent in tracking holds, in shadowing, and in simultaneous holds on both tasks. Also the expected percent time in simultaneous holds calculated under the independence hypothesis has been tabulated along with the chi-squared values for goodness of fit (values significant at 0.05 level or greater have been marked with an asterisk).

None of the interactions for the short holds were significant as would be expected, since the short holds are due mainly to the two uncorrelated input functions. However, for the long holds subjects 10, 13 and 9 in part II had significantly more simultaneous holds than would have been expected under independence. Subjects 12 and 11 showed no significant deviation from the independence hypothesis. Although these results are mixed, it is important to note that even though the difference from independence was significant for subjects 9, 10 and 13, the percentage difference was only 2 to 4 percent of the total time. This difference would mean about 6 to 15 sec more simultaneous holds out of a five min run than expected. Thus, the interaction effect which was found was small, albeit significant.

A Detailed Analysis of the Tracking Holds

Based on a single-channel model, it might have been hypothesized that when there was a

TABLE 6.—*Distribution of Shadowing Holds for Runs with Forcing Function C*
[1435 points/part of run]

Subj.	9		10		11		12		13	
Part of run	I	II	I	II	I	II	I	II	I	II
hold length, number of points in tolerance										
2	131	133	80	59	54	57	66	56	96	91
3	88	60	32	48	56	35	35	32	64	81
4	26	21	28	20	26	31	14	10	43	28
5	16	13	29	19	17	15	10	9	14	21
6	13	12	13	12	15	14	9	9	14	19
7	11	11	15	15	10	17	11	10	14	9
8	6	8	5	14	11	6	10	7	12	12
9	6	5	11	17	4	6	13	9	9	5
10	3	6	7	4	8	1	9	7	5	10
11	4	3	2	4	5	5	5	2	1	6
12	1	3	1	2	1	5	11	5	3	1
13	1	3	5	2	7	3	6	5	3	1
14	1	1	3	3	3	3	5	2	2	1
15	1				3	1	2	3	1	2
16		1	3	1		1	1	2	1	1
17				2	1	4	3	5	1	
18					3	1		1	1	
19				2			1	1		
20				1	2			3		1
21					2	3	2			
Over 21 points, (length/#)			23/1	24/2	22/1	22/2		24/1	23/1	
			27/1	25/1	26/1	23/2		25/1		
			29/1	26/1		28/1		28/1		
						37/1		39/2		
								32/1		
								35/1		
Mean	2.56	2.75	3.95	4.51	4.54	4.87	4.89	5.82	3.34	3.26
SD	2.30	2.69	3.99	4.41	4.50	5.34	4.40	6.46	3.18	2.92

response hold on one of the tasks the probability of a simultaneous hold on the other would be lower, since the attentional mechanisms were now freer to deal with the other task. This hypothesis was not borne out by the above findings; in fact, there was a tendency in the opposite direction. However, one might view a hold not as a period of freed attention, but rather as a period demanding attention in order to regain control. Furthermore, correlations between holds may be misleading due to the reaction time lags inherent in each task. A more direct approach to investigating the interaction between the two types of holds would involve some indication of the subject's attention as a function of time.

Although it was not possible to obtain a direct record of the attention function, it was possible to isolate times when the focus of attention was fairly well specified. It seemed reasonable to assume that at the termination of a tracking hold, the attention was focused on the tracking task. Based on this assumption, an analysis of the onsets and offsets of tracking holds was made.

At both the start and end of a tracking hold the error state was classified as high H, medium M, or low L, so that for the total error distribution the probabilities of each of these three error classifications were equal (i.e., $P_H = P_M = P_L = 1/3$). The slope of the error magnitude function was also classified as to whether it was increasing (condition I), decreasing (condition D), or approximately zero (condition Z). By classifying the displayed tracking error state

TABLE 7.—*Hold Interaction Results*
[Subjects 9 through 13, forcing function C]

	Subj. 9, part I		Subj. 9, part II		Subj. 10, part I		Subj. 10, part II	
	Long	Short	Long	Short	Long	Short	Long	Short
% SH	23.9	31.4	28.2	25.7	41.4	24.1	52.0	20.3
% CH	28.8	17.6	10.8	25.5	24.7	15.7	24.3	18.4
% Corn	7.3	5.0	4.7	6.5	13.8	3.5	16.9	4.4
% EC	6.9	5.5	3.1	6.6	10.2	3.8	12.6	3.7
χ_1^2	0.5	0.9	14.0 *	0.0	28.3 *	0.3	39.6 *	1.8
	Subj. 11, part I		Subj. 11, part II		Subj. 12, part I		Subj. 12, part II	
% SH	52.0	21.8	53.7	19.7	57.6	15.2	62.1	13.0
% CH	66.9	11.5	71.9	7.9	11.0	21.7	12.4	17.1
% Corn	34.1	2.7	39.3	1.8	7.0	3.5	7.7	2.3
% EC	34.8	2.5	38.6	1.6	6.3	3.3	7.7	2.2
χ_1^2	0.9	0.2	0.9	0.5	1.8	0.2	0.0	0.0
	Subj. 13, part I		Subj. 13, part II					
% SH	38.0	28.6	37.2	29.4				
% CH	14.6	25.0	11.4	26.2				
% Corn	7.9	7.3	6.5	8.3				
% EC	5.5	7.2	4.2	7.7				
χ_1^2	18.8 *	0.0	21.6 *	0.9				

Symbols:
%SH = Percent of time not shadowing (shadowing holds).
% CH = Percent of time not controlling (control holds).
% Corn = Percent of time SH and CH simultaneously.
% EC = (% SH) × (% CH).
χ_1^2 = Chi squared value (1 degree of freedom).
* = Significant chi squared value at <0.05 level.

in these two ways, it was hoped to uncover any rationale underlying the choice for the time of onset and offset of the tracking holds.

Along with the tracking error state, the state of the shadowing task was also examined. At both the onset and offset of each tracking hold the shadowing function was examined for ± 1.0 sec. The shadowing function was then classified into one of four categories: no shadowing hold within ± 1 sec (condition *N*); a shadowing hold which terminated within 1 second before the onset or offset point of interest (condition *B*); a shadowing hold ongoing during the onset or offset point of interest (condition *D*); and a shadowing hold which started after the onset or offset point of the tracking hold (condition *A*). In the *B* condition, the time between the end of the shadowing hold and the onset or offset point was tabulated. In both the *A* and *D* conditions, the time between the start of the shadowing hold and the onset or offset of the tracking hold was tabulated. Thus, for the *B*, *D*, and *A* conditions, both a frequency of occurrence and a time distribution were tabulated.

The frequency distributions for both the tracking error and the shadowing hold classifications described above were converted to percentages in order not to differentially weight subjects. These normalized results have been presented in table 8 for subjects 9 through 13. Again the runs using forcing function *C* were analyzed. The composite results in the form of the means and standard deviations for the results pooled over subjects have been presented at the bottom of the table. Also, the mean times between shadowing holds and tracking holds have been given for the *B*, *D*, and *A* cases described above. While much can be said about the results in table 8, only the main findings will be summarized here.

TABLE 8.—*Analysis* of Onsets *and Offsets* of *Trucking Hold*
[See text for complete explanation]

Onset **of** tracking hold

Subject 9:

Tracking error state, % occur				Shadowing holds			
					Time, 0.1 sec		
	I	D	Z		%	Mean	SD
L	51.2		4.7	N	39.5		
M	20.9			B	11.6	3.6	1.7
H	11.6	2.3	9.3	D	23.3	3.8	1.2
				A	25.6	3.8	2.5

Subject 10:

	I	D	Z		Time, 0.1 sec		
					%	Mean	SD
L	65.9			N	43.2		
M	10.6	4.3	4.3	B	4.5	2.5	0.5
H	6.4	6.4	2.1	D	25.0	4.4	3.8
				A	27.3	3.3	2.1

Subject 11:

	I	D	Z		Time, 0.1 sec		
					%	Mean	SD
L	60.9			N	**61.5**		
M	2.4	12.2		B	10.3	5.0	0.7
H	4.9	14.6	4.9	D	12.8	3.4	5.3
				A	15.4	3.2	2.5

Subject 12:

	I	D	Z		Time, 0.1 sec		
					%	Mean	SD
L	84.0			N	12.0		
M	4.0		12.0	B	24.0	3.5	2.7
H				D	26.0	3.0	2.3
				A	28.0	4.7	3.8

Subject 13:

	I	D	Z		Time, 0.1 sec		
					%	Mean	SD
L	56.4		2.6	N	66.7		
M	15.4	7.7		B			
H	12.8	2.6	2.6	D	7.7	3.3	1.2
				A	25.6	4.1	2.8

Means:

	I	D	Z				Mean time,
L	63.7		1.5	M	Mean	SD	0.1 sec
	11.3		1.9	SD			
M	10.7	4.8	3.3	M	N 44.6	19.3	
	6.9	4.7	4.7	SD	B 10.1	8.1	2.9
H	7.1	5.2	3.8	M	D 21.0	9.0	3.6
	4.7	5.1	**3.2**	SD	A 24.4	4.6	3.8

Offset **of** tracking hold

Tracking error state, % occur				Shadowing holds			
					Time, 0.1 sec		
	I	D	Z		%	Mean	SD
L		4.7		N	26.2		
M	2.3	9.3	**4.7**	B	20.3	3.6	1.7
H	27.9	34.9	16.3	D	14.3	5.7	3.4
				A	28.6	3.8	1.8

	I	D	Z		Time, 0.1 sec		
					%	Mean	SD
L	4.3	10.6		N	43.2		
M		6.4		B	22.7	4.9	2.7
H	14.9	46.8	17.0	D	25.0	5.7	4.6
				A	9.1	3.0	1.2

	I	D	Z		Time, 0.1 sec		
					%	Mean	SD
	2.4	2.4	2.4	N	**61.0**		
L M	2.4	7.3		B	14.6	4.3	1.9
H	24.4	51.2	7.3	D	12.2	2.0	1.8
				A	12.2	6.6	1.3

	I	D	Z		Time, 0.1 sec		
					%	Mean	SD
L		11.5		N	24.0		
M		3.8		**B**	20.0	3.2	2.1
H	34.6	38.5	11.5	D	24.0	7.0	7.0
				A	32.0	3.5	1.8

	I	D	Z		Time, 0.1 sec		
					%	Mean	SD
L	2.6			N	61.5		
M	10.3	12.8	5.1	B	20.5	2.5	2.2
H	17.9	41.0	10.3	D	10.3	3.5	2.7
				A	7.7	5.7	1.2

	I	D	Z				Mean time,
L	1.9	5.8	0.5	M	Mean	SD	0.1 sec
	1.7	4.5	1.0	SD			
M	3.0	7.9	2.0	M	N 43.2	16.2	
	3.8	3.0	2.4	SD	B 21.6	5.1	3.7
H	23.9	42.5	12.5	M	D 17.2	6.1	4.7
	7.0	5.8	3.7	SD	A 17.9	10.3	**4.5**

There was an extremely high probability (65.2 percent) that the tracking error was in the low state at the onset of a tracking hold ($p > 0.005$). This result was still high (by about 25 percent), even if the error distribution excluded errors due to tracking holds. Thus, it seemed that the subjects did not start a hold at random, but that the subjects either chose to start a hold when the error state was low or that they took steps just prior to the hold in order to secure low tracking error. The former explanation seemed to be the case, as there was no evidence of sharp control discontinuities just prior to the onset of the holds. As would be expected at the start of a hold, the most probable (81.5 percent) state for the error rate was an increasing error magnitude.

At the ends of the tracking holds, there was a large proportion (78.9 percent) of high error states; this condition was to be expected at the end of a hold. There was a surprising result however. The rate of change of the error magnitude was most often (71.2 percent) decreasing or zero at the point tracking control was resumed. It appeared as if the subjects had waited for an ideal time to resume tracking control, that is, when the forcing function was headed back toward the subject's current controller position or was at an inflection point and about to head back. If this were the case, it seems that some active monitoring of the tracking task must have gone on during the hold in order to determine when to re-establish control.

The only significant difference between the distribution of shadowing holds at the start of a tracking hold and at the end was an increase in the percent occurrence of shadowing holds which had ended just prior to the end of the tracking hold (condition *B*). This result was mainly due to the fact that there was a fairly high probability of a shadowing hold beginning near (± 1 sec) the onset of a tracking hold, and that these shadowing holds often ended within the 1 see interval prior to the end of the tracking hold.

A PRELIMINARY MODEL

Assuming that the operator is a single-channel processor, a structure was hypothesized which might account for the above findings. Under the single-channel assumption, the operator must rapidly switch his attention from one task to the other in order to maintain simultaneous control. This simultaneous control was accomplished with no signs of decrement when the slow shadowing task was added. With the addition of the fast shadowing task, there was a consistent performance decrement on both tasks, and response holds were generated. It was hypothesized that with the fast shadowing input, the switching rate was not rapid enough to keep pace with both tasks continuously. The evidence may suggest that the subjects took advantage of times when the tracking task was well under control (i.e., low error) in order to allocate extra attention to the shadowing. This would account for the increased probability of holds starting in the low error state condition. If too much time were spent on the shadowing task, then upon the return of attention to the tracking task, the error could have grown too large, thus forcing the operator to hold. In this light, a hold would not be viewed as a release of attention from one task for the benefit of the other, but as an inadvertant

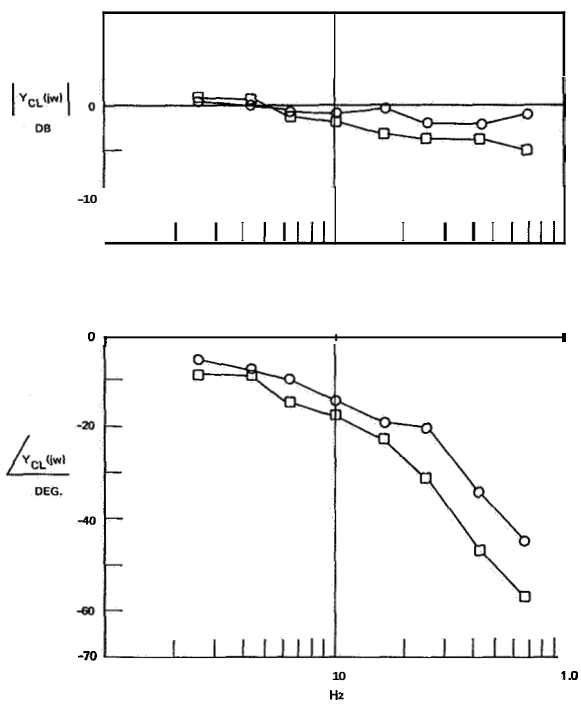

FIGURE 8.—Subject 9 closed loop Bode plot—forcing function *C*.

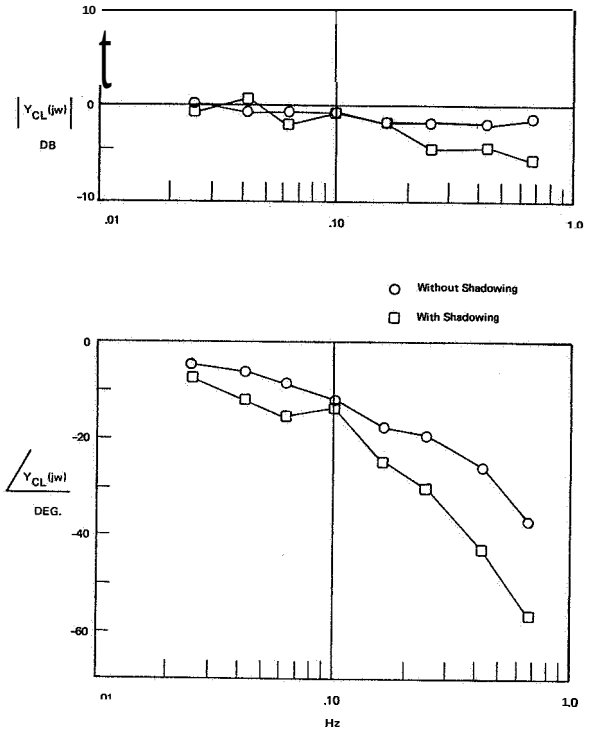

FIGURE 9.—Subject 10 closed loop Bode plot—forcing function *C*.

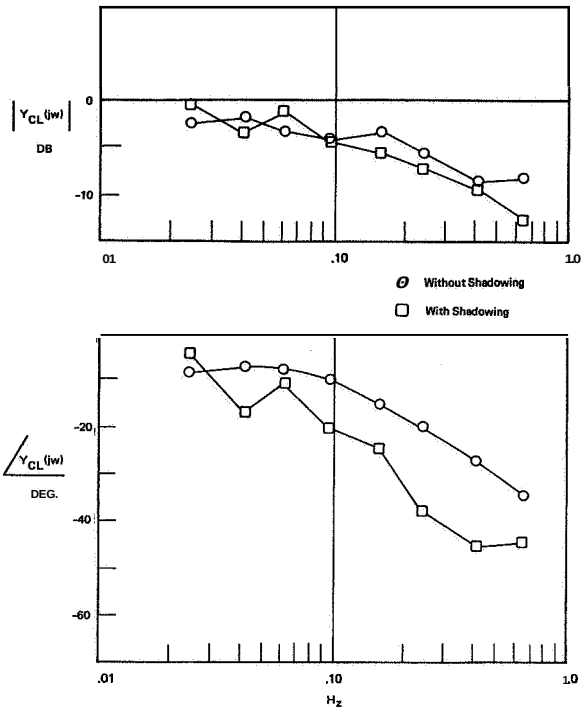

FIGURE 10.—Subject 11 closed loop Bode plot—forcing function C.

loss of control due to the combined effects of a relatively long absence of attention and the local properties of the forcing function at that point. The actual process of regaining control in order to terminate a hold may have even demanded a greater share of attention than ongoing tracking. Consequently, holds on the shadowing task would result from too infrequent sampling of the shadowing input. If the tracking holds do demand more attention than the ongoing tracking, this would account for the increased probability of simultaneous holds.

Although the above discussion is highly speculative and cannot be entirely verified with the data available from the present study, there are some further implications. If there is a single-channel attention mechanism, then the tracking lag should be greater when the shadowing task is added. In addition, if both types of holds actually require more attention than ongoing control, then there should be a differential increase in tracking lag during a shadowing hold. Both of the above hypotheses were tested.

THE TRACKING TRANSFER FUNCTION

The closed loop tracking transfer functions were computed using the Gabor transform technique. The resultant phase and gain plots are presented in figures 8 through **12** for subjects **9** through **13** respectively. As can be seen from the graphs, there is greater closed loop phase lag for the case of tracking with shadowing. This result does support the single-channel assumption. The open loop tracking lag was directly assessed by examining the cross-correlation functions between tracking error and the operator's output. These correlation functions have been plotted in figures **13** through **17,** with the time shifts for maximum correlation interpolated to the nearest 0.05 sec and indicated on the graphs. The resulting differential lag increase with the addition of the shadowing ranged from 0.05 to **0.3** sec.

An attempt was also made to test for the hypothesized differential increase in tracking lag when there was a shadowing hold. To accomplish

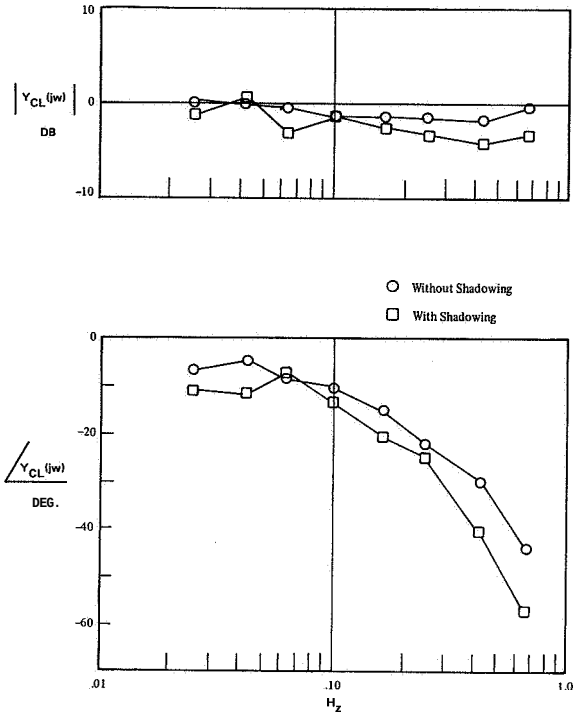

FIGURE 11.—Subject 12 closed loop Bode plot—forcing function C.

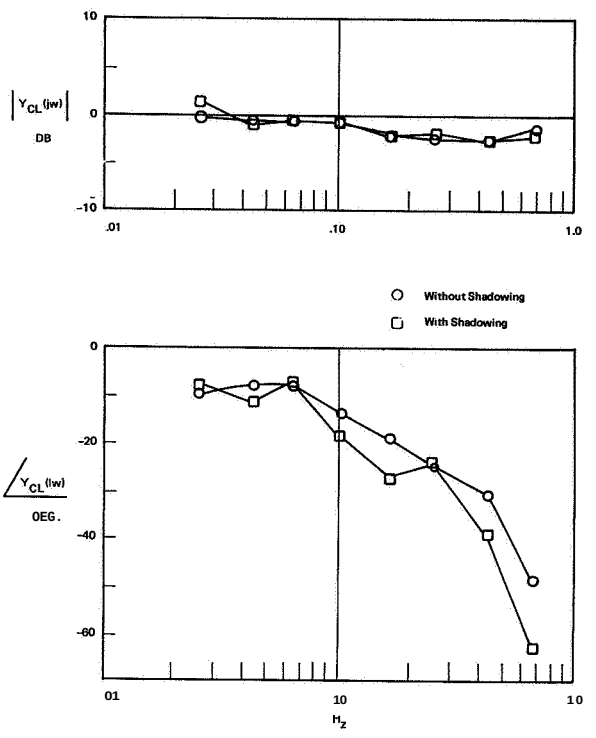

FIGURE 12.—Subject 13 closed loop Bode plot—forcing function C.

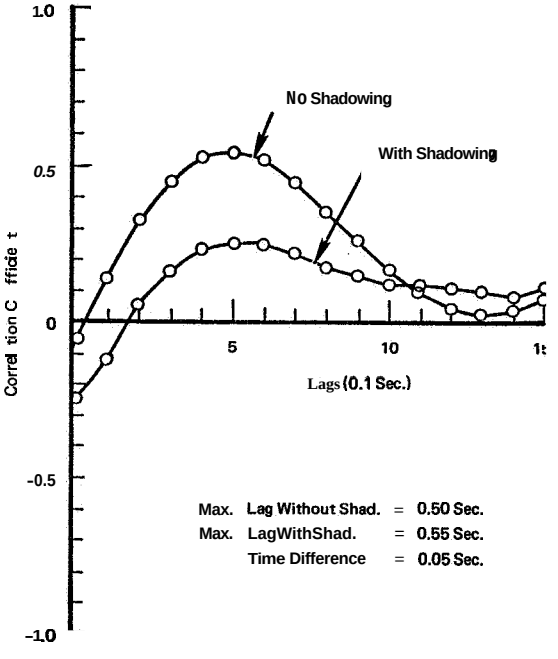

FIGURE 13.—Subject 9 open loop crosscorrelation functions with input C.

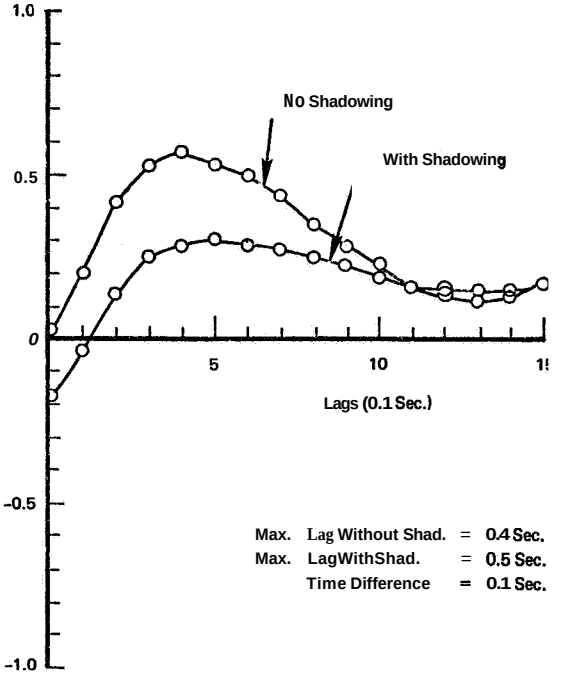

FIGURE 14.—Subject 10 open loop crosscorrelation functions with input C.

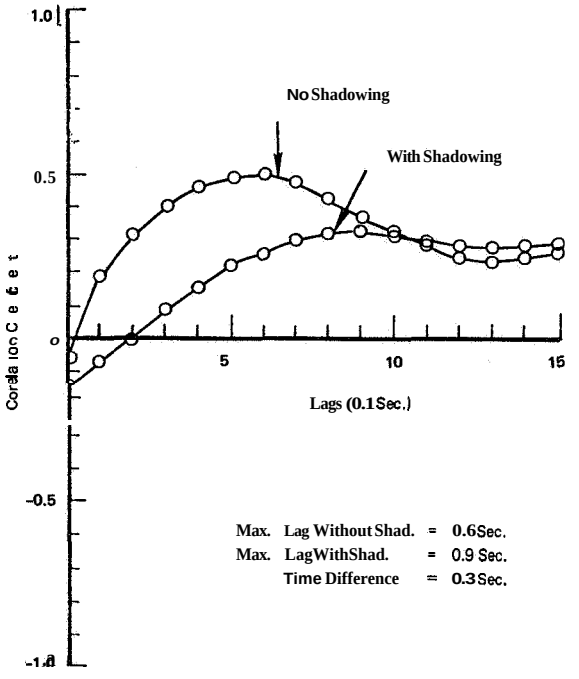

FIGURE 15.—Subject 11 open loop crosscorrelation functions with input C.

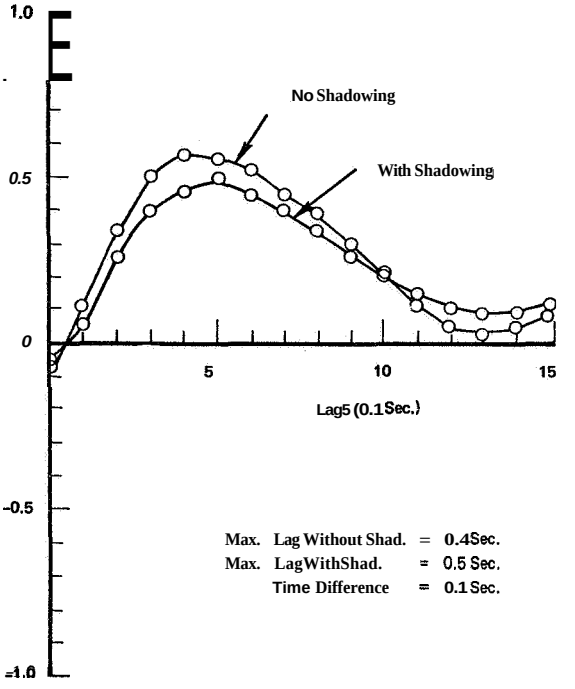

FIGURE 16.—Subject 12 open loop crosscorrelation function with input C.

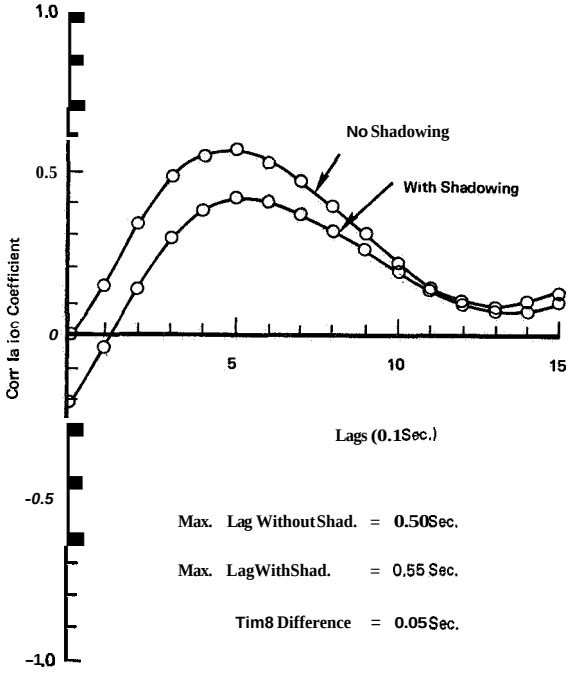

FIGURE 17.—Subject 13 open loop crosscorrelation function with input C.

this, the correlation functions were computed for sections of tracking where there were a number of closely grouped shadowing holds, and also for sections where there were relatively few shadowing holds. For two of the subjects, **11** and **13,** the shadowing holds were so evenly distributed throughout the run that the two types of tracking could not be partitioned. Although records for subjects 9, **10,** and **12** were analyzed, it was very hard to find relatively long sections of record which fit the above two descriptions; therefore, the results from this analysis must be viewed as tentative at best. For subjects 9 and **10** there was a measured increase in tracking lag during times when there were numerous holds on the shadowing function. The average increase for subject 9 was 0.18 sec and for subject **10** was **0.01** sec. For subject **12** there was a decrease of **0.01** sec. At this time the most reasonable conclusion is that the results are mixed and questionable, and that further experimentation is needed to test this specific point. Also further assessment must be made of the attentional demands of the tracking holds.

SUMMARY AND CONCLUSIONS

The experimental findings are summarized below.

(1) When slow shadowing (about one random number pair per second) was performed simultaneously with a zero order compensatory tracking task (forcing functions ***A, B,*** and ***C),*** there was no evidence of a performance decrement on either the tracking or shadowing task attributable to their concurrent performance.

(2) When fast shadowing (about one and a half random number pairs per sec) was performed simultaneously with a zero order compensatory tracking task (forcing functions *B, C,* and D), there was a consistent performance decrement on both the tracking and shadowing tasks attributable to their concurrent performance.

(3) The tracking decrement, as measured by normalized rms error, increased with forcing function bandwidth. The differential increase due to the addition of shadowing was greatest for forcing function ***C.***

(4) There was no evidence to support the view that the dual task decrement could be accounted for by a simple information channel capacity model.

(5) A major source of the dual task decrement on both tasks seemed to stem from holds or cessation of response output for brief periods of time.

(6) It was not possible to account for the holds on either task in terms of a fatigue phenomenon.

(7) A contingency analysis of the shadowing and tracking holds revealed that for three of the five subjects analyzed there were slightly more simultaneous shadowing and tracking holds than would be expected if the two types of holds had been generated independently.

(8) A close analysis of the onsets and offsets of the tracking holds indicated that there was a high probability that the tracking error state was quite low at the onset of a hold, and that the subjects seemed to wait for the error magnitude to begin decreasing before resuming control.

(9) Closed loop frequency plots of the tracking response indicated less loop gain and greater phase lag when the shadowing task was added to the task environment.

(10) Cross-correlation analysis of the tracking records revealed that the open loop tracking lags increased from 0.05 to **0.10** sec with the addition of the shadowing task.

Although there is admittedly still much to be uncovered, these results have helped to illuminate some of the underlying factors which account for the dual task performance decrement. One of the major values of the present study was to offer substantiation for the single-channel hypothesis in the case of independent stimulus-response tasks. It now seems valid to undertake a detailed examination of the determinants of visual attention in an independent, dual, visual task environment. In this way the attention function can be made explicit through the eye position records. With this type of data, fundamental inquiries can be made to clearly define not only the exact function of a hold, but but also the factors which determine when a hold will begin or terminate.

Some very promising progress has been made toward the development of a deterministic model of simultaneous tracking and shadowing control under the single-channel assumption. The model assumes an inherent internal human operator "cycle time" of about 50 msec which governs input, output and switching of attention in relation to the two tasks (Kristofferson (refs. **12** and **13).** Based on the findings in this report, attention is normally allocated to the shadowing task only when the tracking error is in a low state. If, upon return of the attention to the tracking task, the error is in a high state, a tracking hold is initiated. Once a hold is ongoing, the error function is sampled twice in order to determine the slope of the error magnitude. An increasing magnitude results in an attention shift to the shadowing task, while a decreasing magnitude initiates the termination of a hold. The above algorithm implies that more attention is required by the tracking task during a hold, and gives rise to a slightly greater probability of a shadowing hold occurring.

Although the above assumptions need further verification, the model results are promising and show a remarkable similarity to those of the actual subjects. Details of this modelling effort will **be** made available in the near future.

REFERENCES

1. BROADBENT, D.: Perception and Communication. Pergamon Press (London), 1958.
2. BERTELESON, P.: Central Intermittency Twenty Years Later. Quart. J. Exper. Psych., vol. 18, 1966.
3. WELFORD, A. T.: Fundamentals of Skill. Methuen (London), 1968.
4. ADAMS, JACK A.: Some Mechanisms of Motor Responding: An Examination of Attention. E. A. Bilodeau, Ed. Acquisition of Skill, Ch. 4, Academic Press, 1966.
5. SENDERS, JOHN W.: The Human Operator as a Monitor and Controller of Multidegree of Freedom Systems. IEEE Trans. Human Factors in Electronics, vol. HFE–5, Sept. 1964, pp. 2–5.
6. CARBONELL, S. R.; WARD, J. L.; SENDERS, J. W.: A Queueing Model of Visual Sampling Experimental Validation. IEEE Trans. Man-Machine Systems, vol. MMS–9, no. 3, Sept. 1968, pp. 82–87.
7. MERRITT, M. J.: The Application of Discrete Modeling Elements to the Synthesis and Identification of a Deterministic Model for the Visual Scanning Behavior of Human Operators. NASA SP–192, 1968, pp. 289–311.
8. CHERRY, COLIN: On Human Communication. M.I.T. Press (Cambridge, Mass.), 1966.
9. NEISSER, ULRIC: Cognitive Psychology. Appleton-Century-Crofts (New York), 1967.
10. WEMPE, T.; AND BATY, D.: Human Information Processing Rates During Certain Multiaxis Tracking Tasks with a Concurrent Auditory Task. IEEE Trans. on Man-Machine Systems, vol. MMS–9, Dec. 4, 1968, pp. 129–138.
11. WEMPE, T.; AND BATY, D.: The Usefulness of Transinformation as a Measure of Human Tracking Performance. NASA SP–128, 1966, pp. 111–129.
12. KRISTOFFERSON, A. B.: Successiveness Discrimination as a Two-State Quantal Process. Science, vol. 158, Dec. 8, 1967, pp. 1337–1339.
13. KRISTOFFERSON, A. B.: Attention and Psychophysical Time. Acta Psychologica, vol. 27, 1967, pp. 93–100.

37. Motion Cue Effects on Pilot Tracking*

ROBERT F. RINGLAND AND ROBERT L. STAPLEFORD

Systems Technology, Inc.

The results of two successive experimental investigations of the effects of motion cues on manual control tracking tasks are reported. The first of these was an IFR single-axis VTOL roll attitude control task. Describing function data show the dominant motion feedback quantity to be angular velocity. The second experimental task was multiaxis, that of precision hovering of a VTOL using separated instrument displays with reduced motion amplitude scaling. Performance data and pilot opinion show angular position (i.e., g-vector tilt) to be the dominant cue when simulator linear motion is absent.

INTRODUCTION

Motion cues can have an important effect on several aspects of vehicular design and simulation. In this paper, attention is confined to situations involving continuous control or pilot tracking. In particular, the research reported herein was directed toward developing and validating a multimodality (both visual and motion cues) model of the human operator. The experimental portion of the research was conducted on the six-degrees-of-freedom simulator at the Ames Research Center of the National Aeronautics and Space Administration.

Two experimental programs were involved. The first of these was directed toward validating a hypothesized multimodality pilot model (to be described below) in a simple, single-axis task. The major results are in the form of pilot describing function measurements for the visual and motion modalities separately as well as together. The second program was intended to test the multimodality pilot model in a more complex, multiaxis task. The key results are in the form of performance measures and pilot opinion as a function of motion condition. In the following paragraphs we will first outline the features of the pilot model, then discuss the two experiments and the key results therefrom.

MULTIMODALITY PILOT MODEL

The basic structure of the model consists of three parallel, noninteracting feedback paths via the visual, system, the semicircular canals, and the utricles." It is recognized that the three noninteracting feedback paths are a gross simplification. However, for present purposes the simplified model is adequate.

Characteristics of the visual path are well known. A quasi-linear model for control tasks involving only visual cues is described in detail in reference 1. This description includes a describing function model form and adjustment rules for selecting the variable parameters. In the following paragraphs we will confine our attention to the characteristics of the two motion sensing paths of the model. The means by which these paths are integrated with the visual path (i.e., the adjustment rules) for a particular piloting task is inferred later in the discussions of the experimental results.

* This research was sponsored by the Man/Machine Integration Branch, Biotechnology Division, NASA-Ames Research Center, under contracts NAS2–3650 and NAS2–5261.

* Although we directly refer only to the motion sensors of the inner ear, the potential contributions of other sensors is recognized. Since the data on human motion sensing is from tests with live subjects, the contributions of all mechanisms are included.

Characteristics of the Semicircular Canal Path

While the semicircular canals are basically responsive to angular accelerations, their dynamic characteristics are such that over the range of frequencies normally used in manual control they can be considered as rate gyros which provide the pilot with a subjective impression of angular velocity. The model for the semicircular canal path can be represented by the elements shown in figure **1.** The sensor is comprised of the semicircular canals which provide the subjective angular velocity. The time constants, T_1 and T_2, are taken from a survey of the literature (ref. 2), while the threshold values shown are based upon experiments to determine the minimum detectable constant angular acceleration or step velocity change (ref. **3).** In most cases of manual control, the motions are considerably above the thresholds noted above, and the primary concern is in the frequency range of **1** to **5** rad/sec. Then the sensor dynamics for the semicircular canal path are adequately approximated by a single lag or a pure time delay as indicated in figure **1.**

The third block in figure **1** models the effects of pilot equalization and the net effects of any central processing, transmission, and neuromuscular lags. The equalization is assumed to be lead. While lag equalization is theoretically possible, the primary function of the semicircular canal path appears to be one of supplying lead equalization. Unfortunately, there are no direct data on equalization, although some of the data of reference **4** indicate that relatively large lead equalization (roughly **1** sec) is possible. Whether or not the pilot can generate lead equalization as large as that measured for visual tracking is unknown. It is hypothesized herein that the lead in the semicircular path can be as large as that used in the visual path.

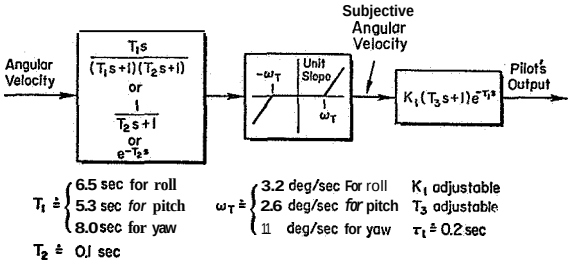

FIGURE 1.—Model for semicircular canal path.

Characteristics of the Utricular Path

The model for the utricular path consists of elements similar to those of the semicircular canal path (fig. *2).* While less data are available on the sensor dynamics of the utricles, it is widely accepted that they act like accelerometers, being sensitive to linear accelerations in the plane of the utricular maculae. This plane is inclined front end upward approximately **30** deg from the horizontal in the upright head.

The most recent data on utricular sensory dynamics is that given in reference *5.* That report suggests a model for the sensory dynamics of the form

$$\frac{\text{Subjective acceleration}}{\text{Actual acceleration}} = \frac{(T_5/T_4)(T_4 s+1)}{(T_5 s+1)(T_6 s+1)} \quad (1)$$

where

$T_4 \doteq 13$ sec
$T_5 \doteq 5.2$ sec
$T_6 \doteq 0.67$ sec.

Over the frequency range of interest in most vehicular-control situations, equation **(1)** can be adequately approximated by a single lag, as shown in figure *2.* The utricular threshold is so small, on the order of **0.01** g or less, that it will have a negligible effect in most vehicular control situations. Therefore, figure *2* shows no threshold element.

The data on possible pilot equalization forms, net lags, etc., shown in the second block of figure *2* are extremely sparse, being limited to the reference *6* analysis of some of the data from reference **3** wherein the results from one case showed the presence of a first-order lead at **3** rad/sec and a time delay of **0.3** sec. Lag equal-

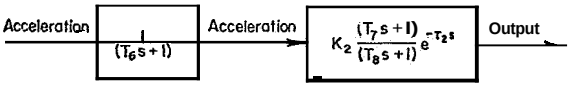

ization for certain circumstances cannot be ruled out because of the extremely wide range of acceleration numerator zeros which can occur in vehicle transfer functions. These zeros are strong functions of the vehicle stability and control properties and the pilot's location. Consequently, the model (fig. **2)** allows for both lead and lag equalization on the sensed accelerations, depending upon the piloting situation.

DESCRIPTION OF THE FIRST EXPERIMENT

The selection of the experimental task was based upon the need for sensitivity to motion cues and simplicity (i.e., single-axis task) to facilitate describing function measurement and analysis with two separate (uncorrelated) inputs. This latter feature permitted separate but simultaneous measurement of the characteristics of both the visual and motion channels.

The general task presented to the subjects was to roll stabilize a high performance VTOL which was hovering in gusty air. They were instructed to keep the roll deviations as small as possible and were given no information on their lateral position (simulator was hooded and the only display was roll angle). In response to visual (display) and motion cues, the pilot manipulated a sidestick controller. Stick position was fed to an analog computer which was used to simulate a variety of controlled element dynamics, derive the input signals to the display and the simulator, and provide a performance measure (see fig. **3).**

The controlled element dynamics were always of the form

$$Y_c = \frac{K_c}{s(s+a)} \qquad (2)$$

The data presented in this paper are for the two extreme values of a tested, 0, and **10** sec^{-1} (see ref. **7** for the complete results). Each subject was allowed to select the value of gain K_c preferred for each value of a.

For all test conditions, a disturbance input d was added to the controlled element output. This input is equivalent to the hand-off gust response of the simulated vehicle. The input was composed **of** ten sine waves and had a rms value

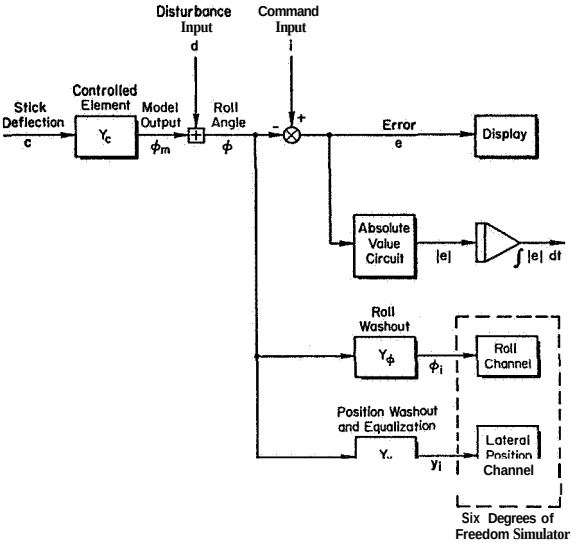

FIGURE 3.—Simulation schematic, first experiment.

of 4.3°. The amplitudes of the four highest frequency components were **1/10** those of the low frequency components.

For those runs where a separate measurement of visual and motion channels was desired, a command input i was also used, see figure **3.** The basic difference between the command and disturbance inputs is that the disturbance input feeds directly into both the display and the moving-base simulator, whereas the command feeds only into the display. Thus d tends to disturb the vehicle and the pilot attempts to cancel its effects and keep the vehicle level, while i is a roll command which the pilot attempts to follow. This input was also composed of ten sine waves of frequencies different (and thus uncorrelated with) from the frequencies of *d.* The highest five frequency components were **1/10** the amplitude of the lowest frequency components. The rms value was either **1/2** or **1/4** that of the disturbance input.

The roll angle error *e* was displayed to the pilot on a *5* in. attitude indicator (8-ball). Without the command input, the ball approximated the true horizon, i.e., the ball was nearly inertially stabilized and the cab rotated around it. The integral of the absolute value of the error was also computed to provide an on-line check on pilot performance.

A washout

$$Y_\varphi = \frac{s}{s+p_\varphi} \tag{3}$$

was used between the roll angle φ and the input to the roll channel of the six-degrees-of-freedom simulator (see fig. 3). The inverse time constant p_φ was an experimental parameter and values of 0.5, 1, and 2 sec^{-1} were tested. The data given subsequently are for the smallest value, 0.5 sec^{-1}.

The equalization between φ and the lateral position channel was used to vary the linear acceleration cues sensed by the pilot. The net transfer function between the roll angle and the input to the lateral position channel of the simulator was

$$\frac{y_i}{\varphi} = Y_y = \frac{(\ell_z - \ell_s)s^2 + bs + g}{(s+p_y)^2}. \tag{4}$$

The variables ℓ_z, b, and p, were all experimental variables, however most of the data presented herein are for the pilot's lead at the c.g. ($\ell_z = 0$), no $\dot{\varphi}$ component of acceleration ($b = 0$), and minimal washout ($p, = 0.5\ sec^{-1}$).

The data presented below are for two of the four subjects used in these experiments. The backgrounds of these two subjects are given below. They were each allowed several practice runs on the various configurations and data runs were made only after their performance, as measured by $\int |e|\, dt$, had stabilized. The data runs were approximately 4.5 min long, of which 4 min was used in the data analysis.

Subject backgrounds, first experiment.—

GB: Retired Air Force pilot; approximately 7000 hr in multi-engine aircraft.

RG: NASA research pilot; approximately 4200 hr total, mostly in single-engine fighters, 500 hr in helicopters and VTOL aircraft.

The data were originally recorded in analog form on a 14-chennel FM magnetic tape recorder. The data were subsequently sampled at 20 samples/sec and converted to a digital format. The data were then analyzed on a large-scale digital computer using the BOMM program (ref. 8) to compute describing functions.

RESULTS OF THE FIRST EXPERIMENT

When only the one input d is used, the effective loop structure is that shown in figure 4, where

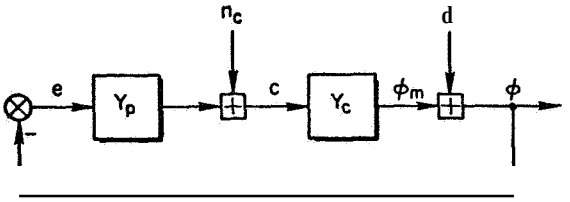

FIGURE 4.—Effective loop structure for one-input runs.

Y_p contains the combined effects of visual and motion feedbacks. The fixed-base results for some of these runs are compared with the moving-base data in figure 5 and 6 for two controlled elements. Examination of these data shows:

- The simple crossover model form of reference 1 with all its ramifications on pilot dynamic performance, adjustment rules, etc., holds for these data.
- A reduction in pilot phase lag when motion cues are added, especially for the three highest frequencies. The phase change is roughly equivalent to a time delay reduction of 0.1 to 0.2 sec.
- With less phase lag, the pilot can and does increase his mid-frequency gain and crossover frequency.
- The motion effects are somewhat different for the two subjects. In particular, the changes are somewhat less for subject GB. This may be due to his background, which is primarily in multi-engine aircraft with their slower responses and smaller motion cues.

With motion cues the crossover frequency is increased 0.5 to 1.5 rad/sec. The changes are less for $Y_c = K_c/s^2$ and less for subject GB for all controlled elements. The phase margin data show large reduction (20 to 40") with motion for $K_c/s(s+10)$, and no change for K_c/s^2. Significant phase margin reductions were not possible for K_c/s^2 as the fixed-base values were already low (5 to 15").

When both inputs are used, the loop structure is that shown in figure 7. Here Y_v is the pilot describing function for visual feedback and Ym is the describing function for motion feedback. It must be noted that Y_m actually represents the sum of two separate motion feedback channels—one angular and one linear. Furthermore, all simulator dynamics, washouts, and equalizations are included in Y_m.

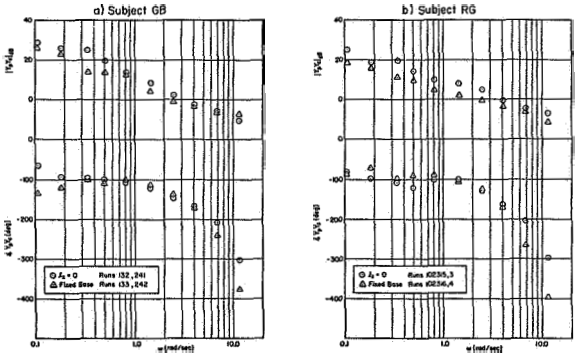

FIGURE 5.—Motion effects for $Y_c = K_c s(s+10)$.

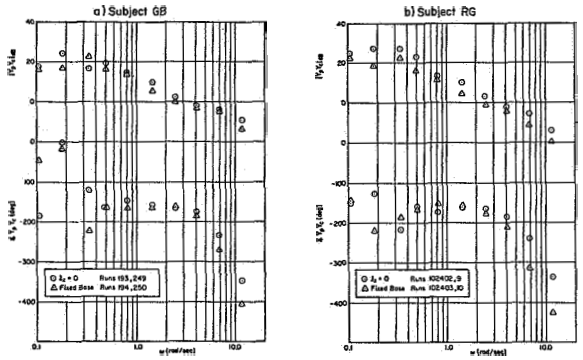

FIGURE 6.—Motion effects for $Y_c = K_c/s^2$.

The faired curves resulting from the data reduction procedure (detailed in ref. 7) are shown in figures 8 and 9. Also shown in these figures are the Y_v data for the fixed-base runs. Since the fixed-base Y_p is a visual feedback, comparison of those data and the Y_v data shows how the pilot adjusts his visual feedback when motion cues are added.

From figures 8 and 9 we see that when motion cues are present the visual feedback gain at low frequency is increased and less lead is used in the visual path, i.e., the low frequency phase lags are greater. To the extent that the semicircular canals act as rate gyros, this result might be expected. With the lead information supplied by the motion cues, the pilot does not need to supply as much visual lead as he does fixed base. He can also increase his gain and achieve a higher crossover frequency because his effective time delay is reduced.

The motion feedback describing function Y_m

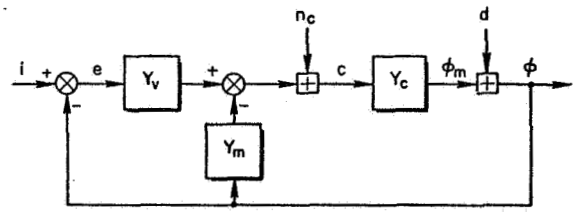

FIGURE 7.—Effective loop structure for two-input runs

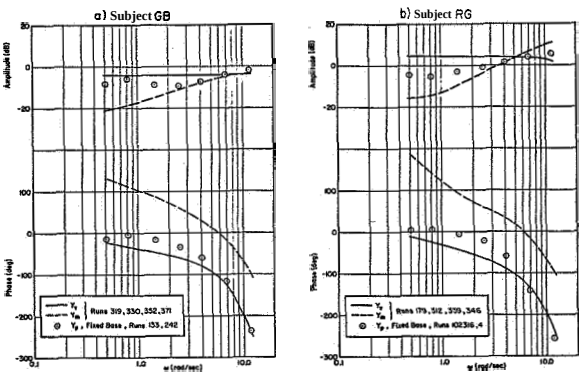

FIGURE 8.—Visual and motion feedbacks for $Y_c = K_c/s(s+10)$, $\ell_z = 0$.

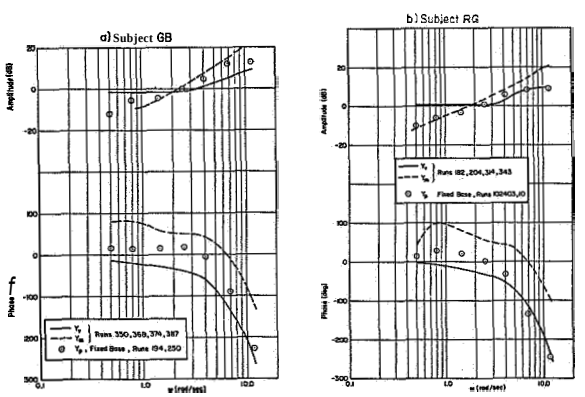

FIGURE 9.—Visual and motion feedbacks for $Y_c = K_c/s^2$, $\ell_z = 0$.

generally appears to be a very low frequency first-order lead and a time delay of roughly **0.26** sec. Comparison of the visual and motion feedbacks shows a definite difference between the two controlled elements. For $Y_c = K_c/s(s+10)$ the magnitudes of Y_v and Y_m are equal for a frequency of 5 to 9 rad/sec. For the more difficult task, $Y_c = K_c/s^2$, the magnitudes are equal at a

frequency of roughly 2 rad/sec. Thus for the task requiring more pilot lead, the relative contribution of the motion feedback is significantly higher.

It was also concluded that the motion feedback was dominantly or exclusively the angular motion. As noted above, Y_m includes simulator dynamics, washouts, and equalization. These represent known elements for both the angular and linear motion paths. If the linear motion was a significant part of the motion feedback, Y_m would not have the simple shape shown in figures 8 and 9.

In addition to the data presented above, many runs were made in which the parameters of equation (4), ℓ_z, p_y, and b, were varied, thus varying the lateral acceleration cues over a wide range. The results were negative in that the pilot describing functions show no significant change. However, the subjective impressions did change—higher lateral accelerations produced pilot complaints of a tendency toward disorientation.

Variations in the roll washout inverse time constant p_w were also tried in some of the runs. Overall describing functions for subject RG showed a slight reduction in pilot gain and therefore crossover frequency for $p_\varphi = 2$ sec^{-1}. The performance measures (integrated absolute error) showed small variations with p_w; RG's performance being degraded for $p_\varphi = 2$ sec^{-1} (which correlated with the describing function measures) and GB's performance being unaffected. This intersubject difference in part may be explained by differences in background: GB's experience is in multi-engine aircraft, while RG's is primarily in fighters. In summary, the data suggest that motion feedback via the semicircular canals is dominant and that utricular cues are relatively unimportant in the experimental tasks.

The overall results of the first experiment suggest certain additions to the multimodality pilot model as follows: For attitude tracking tasks, the overall effects of motion on the equivalent visual describing function are adjustments in the crossover frequency and effective time delay. One can use the existing quasi-linear pilot model to estimate the fixed-base pilot describing function. To allow for motion cues, one increases the crossover frequency by approximately 1 rad/sec and reduces the effective time delay by approximately 0.15 sec. This gives the overall effects of high fidelity angular cues.

The relative magnitudes of the visual and semicircular canal feedbacks depend on the controlled element dynamics; however, the visual path dominates at low frequencies and the semicircular canal path at high frequencies. For controlled elements which do not require low frequency pilot lead ($Y_c \doteq K_c/s$ in the region of crossover), the two feedbacks are of comparable magnitude in the frequency region just above crossover, 5 to 10 rad/sec. For controlled elements which do require low frequency pilot lead ($Y_c \doteq K_c/s^2$ in the region of crossover), the two feedbacks are of comparable magnitude in the frequency region just below crossover, 1.5 to 2 rad/sec. In all cases the lead provided by the angular path allows the low frequency gain of the visual path to be higher than it would be fixed-base, and the lead somewhat lower.

DESCRIPTION OF THE SECOND EXPERIMENT

The selection of the control task for the second experiment was guided, as in the first, by the need for sensitivity to the presence or absence of motion cues. Since the presence of motion cues was expected to alter the pilot's needs for visual information, his display scanning behavior was to be measured on some of the runs. With these factors in mind, a VTOL hovering task using separated instrument displays was selected.

The task presented to the subjects was to hover over a spot in mildly gusty air. They were instructed to keep their position (fore-and-aft and side-to-side) and altitude excursions to a minimum. In response to displayed visual and motion cues, the pilot manipulated a two-axis centerstick and a collective control. The controller positions were fed to an analog computer which was used to simulate the VTOL dynamics and compensate for motion simulator lags. (The displayed longitudinal position was lagged ($\tau = 0.1$ sec) to match the longitudinal response of the simulator because the latter couldn't be compensated sufficiently without introducing undesirable peaking in the simulator response.) Signals from the computer drove both the motion simulator and the displays in the simulator cap

(fig. 10). The displays consisted of an attitude ball, a CRT for display of position in the horizontal plane, and a dial gauge for display of altitude; these are similar to the conventional instrument display of reference 5. The gain on the attitude ball was five times that of the "real world" motion of the cab, and the stick gain was correspondingly reduced from typical values. This was done to keep the motion of the simulator cab within its linear excursion limits of ± 9 ft (no washouts were used in the experiment). The motions felt by the pilot were considerably attenuated from those which would otherwise be felt. Or, to put it another way, the precision of position control was considerably greater than would otherwise (attitude ball gain of 1:1) be possible in these IFR conditions."

The equations of motion for the five-degrees-of-freedom simulated VTOL are given below:

- Longitudinal

$$\begin{aligned} s(s-X_u)x+g\theta &= -X_u u_g \\ -M_u sx+s(s-M_q)\theta &= M_{\delta_e}\delta_e - M_u u_g \end{aligned} \tag{5}$$

- Lateral

$$\begin{aligned} s(s-Y_v)y-g\varphi &= -Y_v v_g \\ -L_v sy+s(s-\mathrm{L}_p)\,\varphi &= L_{\delta_a}\delta_a - L_v v_g \end{aligned} \tag{6}$$

- Vertical

$$s(s-Z_w-Z_{w'})z = Z_{\delta_c}\delta_c - Z_w w_g \tag{7}$$

- Pilot location

$$\begin{aligned} x_i &= x \\ y_i &= y \\ z_i &= z-\ell_x\theta. \end{aligned} \tag{8}$$

The intersection of the motion simulator's pitch and roll axes was the simulated center-of-gravity location of the vehicle except when ℓ_x was nonzero. Several configurations of the vehicle dynamics were tried in the course of the experiment. In this paper we shall confine our attention to the four configurations listed (in increasing order of difficulty) in Table 1—the remaining configurations involved changes in the vertical task dynamics and the pilot location as well as intermediate values of attitude damping. The dynamics are similar to those used in earlier studies (refs. 10 and 11).

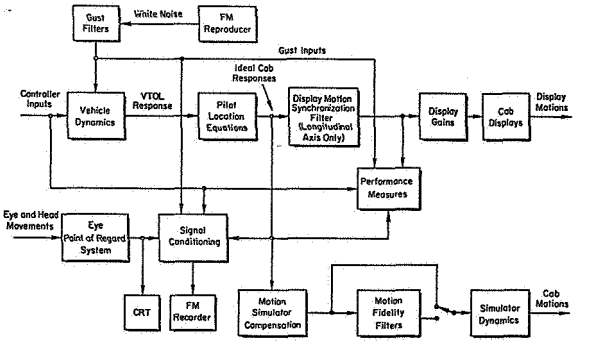

FIGURE 10.—Simulation schematic, second experiment.

TABLE 1.—VTOL *Dynamic Parameters*

Fixed parameters		
Longitudinal task	$gM_u = -0.2\ \mathrm{sec}^{-3}$,	$X_u = -0.1\ \mathrm{sec}^{-1}$
Lateral task	$gL_v = -0.2\ \mathrm{sec}^{-3}$,	$Y_v = -0.1\ \mathrm{sec}^{-1}$
Vertical task	$Z_w = -1.0\ \mathrm{sec}^{-1}$,	$Z_{w'} = -3.0\ \mathrm{sec}^{-1}$
Pilot location	$\ell_x = 0$ ft	
Variable parameters *		

Configuration	$M_q(\mathrm{sec}^{-1})$	$L_p(\mathrm{sec}^{-1})$
1	-4.0	-4.0
3	0	-4.0
4	-4.0	-0.5
6	0	-0.5

*Pilots were asked to select values of M_{δ_c}, La, and Z_{δ_c} which felt best to them for each configuration.

The three gust inputs were simulated by feeding prerecorded noise through "gust filters" having a first-order lag characteristic with $\tau = 1.0$ sec. In order to get repeatable rms level measurements (measured over a 100 sec time interval) the prerecorded noise consisted of a 100 sec white noise sample repeated over and over—a different sample for each of the three inputs. The simulated rms gust levels used were as follows (mean values are zero in all cases):

$$\sigma_{u_g} = 1.0\ \mathrm{ft/sec}$$

$$\sigma_{v_g} = 1.4\ \mathrm{ft/sec}$$

$$\sigma_{w_g} = 1.6\ \mathrm{ft/sec}.$$

Pilot ratings (based on past data, see ref. 12) are relatively insensitive to the precise level of gust excitation with the values of M_u and L_v used in this experiment.

* However, a brief test showed the position excursions could easily be kept within the limits in a VFR situation.

Three subjects were used in the second experiment, one of whom, RG, participated in the first. The backgrounds of the other two are listed below. Because of his extensive research experience and limited availability, subject RG was used as a point of reference for the other two pilots who were inexperienced in giving pilot opinion ratings and commentary.

Subject backgrounds, second experiment.—

GB: Airline flight engineer and pilot, approximately **800** hr; former USAF pilot with **650** hr as instrument instructor, approximately **4300** hr in helicopters in U.S.

EF: Airline flight engineer, approximately 200 hr; former USMC pilot with **1550** hr as primary flight instructor, **1500** hr in helicopters in Vietnam.

Subjects GB and EF were relied upon for most of the data taken. They each received **5** days of training totaling approximately **85** to 90 runs of **2** min or more duration. Nevertheless, there were still evidences of continued learning on these extremely difficult to fly configurations at the conclusion of the program.

RESULTS OF THE SECOND EXPERIMENT

The pilot performance (measured in terms of time-averaged rms motions) and opinion rating for each of the four configurations are shown in figure **11.** The pilot opinion ratings (PR) listed are to be interpreted only relative to this experiment—in the training runs it was discovered that these configurations were so difficult as to merit ratings between **8** and **10** on the Cooper-Harper scale in any motion condition. Consequently, the pilots were instructed to rate the simulation as flyable (pilot opinion rating (Cooper-Harper scale) better than **10.0)** if they were able to keep the position excursions within the motion simu-

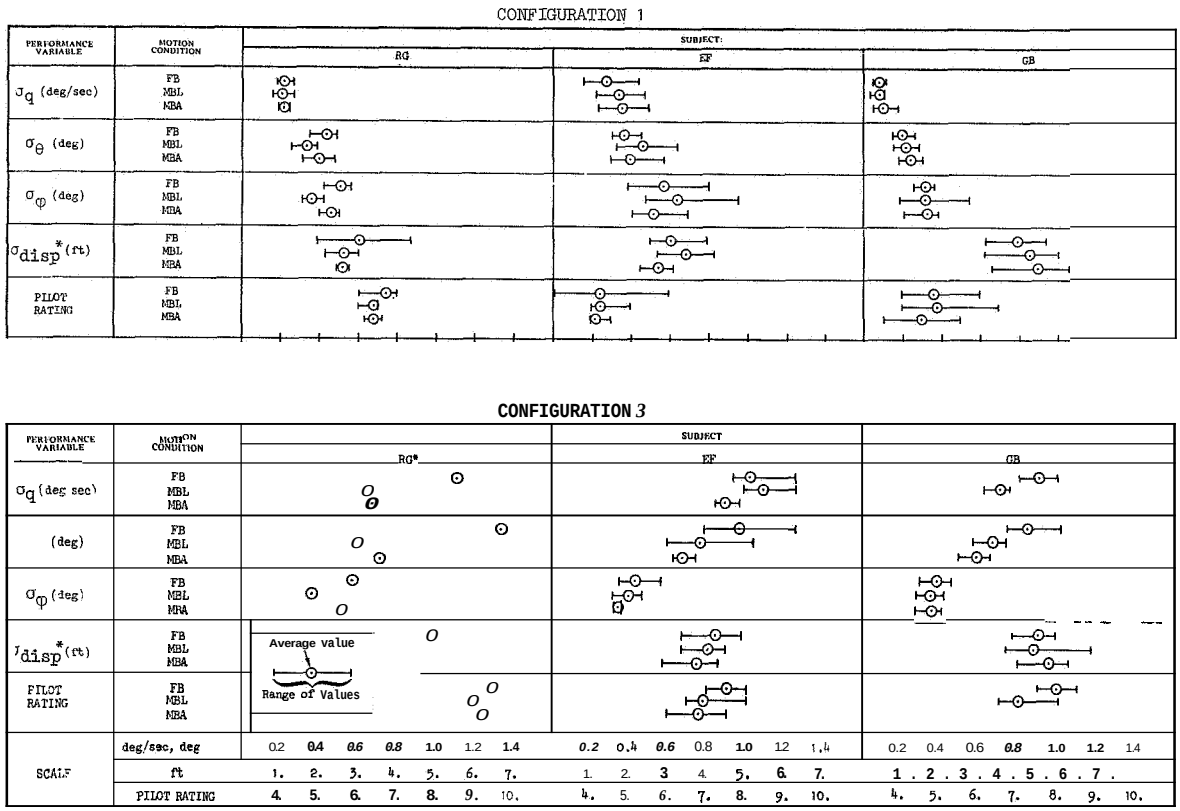

FIGURE 11.—Performance and pilot rating data.

lator limits for the duration of the run, barring momentary exceedances. This made up (at least in part) for the large rating decrement caused by the IFR conditions of the experiment. The more significant results to be drawn from these figures and the pilot commentary are as follows:

- The **MBA** motion condition (moving base, angular motion only) is rated best by all pilots for all configurations with performance

$$(\sigma_{\text{disp}} = (\sigma_x^2 + \sigma_y^2 + \sigma_z^2)^{1/2})$$

confirming this for all subjects but **GB** who is postulated to "relax"—his performance is worst and his rating best in this motion condition for all configurations.

- The **MBL** motion condition (moving base, linear and angular motion) is rated at an intermediate level between the **FB** (fixed base) and **MBA** conditions by all pilots for all configurations with the exception of the easiest (configuration 1) where EF and **GB** rate the **MBL** condition worse than **FB.** Pilot performance confirms this trend.

- Pilot commentary indicated the **MBL** condition to be subjectively "strange," "confusing," "distracting," etc., suggesting a tendency to vertigo in this motion condition. The **MBA** condition was subjectively better because of the "unmistakable" g-vector tilt cue and the absence of the "distractions," etc., of the **MBL** motion condition.

A comparison of these data with those given in reference **11,** plus comparing the data with semicircular canal thresholds (fig. 1) indicate the presence of threshold effects similar to those measured in the simpler task of reference **13.** The angular motions are so small (as a result of the display scaling used to permit position control within the simulator limits) that the ebneficial effects of motion are considerably re-

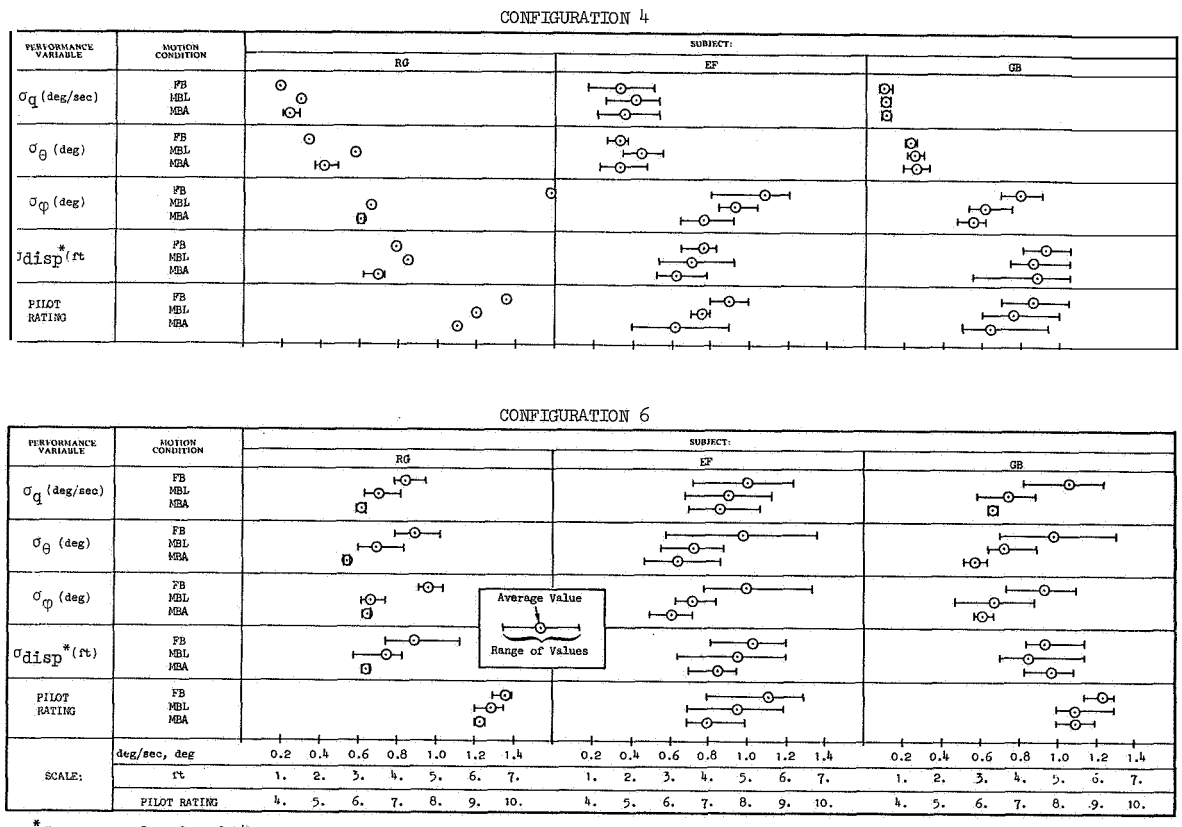

FIGURE 11.—Concluded.

duced. Thus the variation of performance (and opinion with motion condition is less than one might otherwise expect.

On several of the runs (approximately ***50)*** we measured the pilots' display scanning behavior using the eye point-of-regard system developed at Systems Technology, Inc. These raw data were reduced using the techniques on reference **14** for **35** of these runs. The reduced data are available in reference **15.**

Based upon the pilots' Commentary, one would expect them to spend more time on the attitude display, FB, and less time, MBA. Figure **12,** a small sample of the reduced EPR data, graphically shows this to be the case for RG. In this figure the shaded area inside the circles represents the fraction of the time spent looking at that instrument. The width of the arrows connecting two instruments is proportional to the fraction of all changes in the eye point-of-regard attributable to looks between the two instruments indicated. Thus, figure **12** shows that RG spends most of his time shifting his gaze back and forth between the attitude and position displays with little attention to the altitude display. The largest fraction of his time is on the attitude display in all motion conditions, although his need to look at this display is (apparently) least in the MBA condition.

By way of summarizing some of these results, table **2** shows the various cues available to the pilot in the three motion conditions investigated in the second experiment. The data presented indicate a strong preference for the angular motion only (MBA) condition over full motion (MBL). This preference is attributed to the absence of auditory cues and simulator vibration in the MBA condition relative to MBL, and/or the presence and pilot's use of the g-vector tilt cue, in the MBA condition. The latter point of view was confirmed by pilot commentary taken at face value, while the former is certainly a factor in the easiest, No. **1,** configuration, which would ordinarily be expected to show little advantage accruing to the presence of motion. The g-vector tilt cue as an indicator of attitude, present only in the MBA condition, is apparently used by the pilot in addition to his attitude display. It can give him an attitude indication when he is looking elsewhere which can be used at least to alert him to a changing situation, and perhaps even to provide some measure of closed-loop control. The apparent g-vector tilt experienced in the MBL condition is related weakly to attitude and strongly to the simulated gust excitation. It can't help him in control at attitude and, because of the restricted visual world inside the simulator cab (in particular, the absence of an approximation to a real-world display which would aid his perception of orientation), can presumably lead to vertigo. Consequently, a moving-base simulator with angular motion only gives the pilot an additional cue not present in the real world. If this cue can be used advantageously, as it apparently can in the simulated task where attitude control is of paramount importance and separated instrument displays are employed, then the results obtained will be optimistic relative to IFR flight. The multimodality pilot model in this instance includes utriclar as well as semicircular canal feedbacks, the former acting to supplement his relatively poor (in IFR conditions) perception of vehicle attitude.

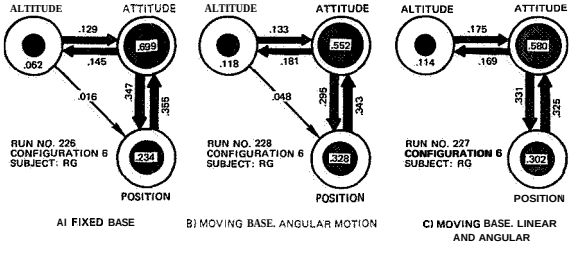

FIGURE 12.—Transition link vectors and dwell fractions.

CONCLUSIONS

In the course of the second experimental program we attempted to predict the performance to be achieved using the multimodality pilot model with adjustments for scanning workload. The predictions (detailed in ref. **15)** correctly predicted the performance trends with configuration changes and motion conditions, but were considerably wide of the mark in predicting actual performance due to a number of factors. Foremost among these were the VFR IFR difference, causing a large decrement in both performance and opinion (the existing pilot models are based upon results measured in simpler

TABLE 2.—*Simulator Motion Conditions and Pilot Sensory Modalities*

Simulator condition \ Pilot modality	Vision	Audition	Vestibular: Canals	Vestibular: Utricle	Other proprioceptive
Fixed-base	Displays				
Moving-base, angular motions only	Displays		Angular velocities near effective threshold level.	G-vector tilt. Pilot's head not at center of cab rotation (simulated c.g.)*	G-vector tilt
Moving base, angular and linear motions	Displays	Simulator rumble. Amplidyne whine (only in training and early experimental runs where motions are large).	Angular velocities near effective threshold level.	G-vector tilt *only* when linear motion limits exceeded. Pilot's head not at center of cab rotation (simulated c.g.)*	G-vector tilt only when linear motion limits exceeded. Simulator vibration in linear degrees of freedom.

* Therefore angular accelerations produce linear accelerations at pilot's head.

tasks). In addition, the predictions did not include any allowance for motion threshold effects, or for the possible benefits of utricular cues.

The lessons are clear: Certain improvements (based upon experimentation) in pilot models are required in the area of multiple display scanning behavior; the data base upon which such behavior is predicted is quite limited, see references 14, **16,** and **17.** Application of the model requires careful examination of simplifying assumptions (e.g., are motion amplitudes large enough to permit ignoring vestibular threshold effects?). Finally, additional experimentation is needed to define the extent to which threshold effects are due to simulator artifacts ("masking" effects due to noise and vibration), actual vestibular thresholds, or pilot workload (stress).

REFERENCES

1. McRuer, Duane T.; Graham, Dunstan; and Krendel, Ezra S.: Manual Control of Single-Loop Systems: Parts I and 11. J. Franklin Institute, vol. 283, no. 1, Jan. 1967, and no. 2, Feb. 1967.
2. Peters, Richard A.: Dynamics of the Vestibular System and Their Relation to Motion Perception, Spatial Disorientation, and Illusions. NASA CR-1309, Apr. 1969.
3. Meiry, Jacob L.: The Vestibular System and Human Dynamic Space Orientation. MIT, Man-Vehicle Control Lab., Thesis No. T–65–1, June 1965.
4. Shirley, Richard S.: Motion Cues in Man-Vehicle Control. MIT, Man-Vehicle Lab., Thesis No. MVT–68–1, Jan. 1968.
5. Young, L. R.; and Meiry, J. L.: A Revised Dynamic Otolith Model. 3rd Symposium on Role of the Vestibular Organs in Space Exploration (Pensacola, Fla.) Jan. 23–27, 1967.
6. Alex, F. R.: Analysis of Two Manually Controlled Compensatory Systems with Inclusion of Motion Cues. Working Paper 162–2, Systems Technology, Inc., Feb. 1967.
7. Stapleford, R. L.; Peters, R. A.; and Alex, F. R.: Experiments and a Model for Pilot Dynamics with Visual and Motion Inputs. NASA–CR–1325, May 1969.
8. Bullard, E. C.; Oglebay, F. E.; Munk, W. H.; and Miller, G. R.: A User's Guide to BOMM. Univ. of Calif. Institute of Geophysics and Planetary Physics, Jan. 1966.
9. Williams, P. R.; and Kronholm, M. B.: Technical Report on Simulation Studies of an Integrated Electronic Vertical Display, Rept. No. 1161 R 0021. United Aircraft Corp., Dec. 31, 1965.
10. Miller, D. P.; and Vinje, E. W.: Fixed-Base Flight Simulator Studies of VTOL Aircraft Handling Qualities in Hovering and Low-Speed Flight. AFFDL–TR–67–152, Jan. 1968.
11. Vinje, E. W.; and Miller, D. P.: Analytical and Flight Simulator Studies to Develop Design Criteria

for VTOL Aircraft Control Systems. AFFDL-TR-68-165, Wright-Patterson AFB, Apr. 1969.

12. CRAIG, S. J.; AND CAMPBELL, A.: Analysis of VTOL Handling Qualities Requirements. Part I: Longitudinal Hover and Transition. AFFDLTR-67-179, Wright-Patterson AFB, Oct. 1968.
13. BERGERON, H. P.; ADAMS, J. P.; AND HUNT, G. J.: The Effects of Motion Cues and Motion Scaling on One- and Two-Axis Compensatory Control Tasks. NASA TN D-6110, Jan. 1971.
14. WEIR, DAVID H.; AND KLEIN, RICHARD H.: The Measurement and Analysis of Pilot Scanning and Control Behavior During Simulated Instrument Approaches. NASA CR-1535, June 1970.
15. RINGLAND, R. F.; STAPLEFORD, R. L.; AND MAGDALENO, R. E.: Motion Effects on an IFR Hovering Task—Analytical Predictions and Experimental Results. Tech. Rept. No. 188-1, Systems Technology, Inc., Oct. 1970.
16. ALLEN, R. W.; CLEMENT, W. F.; AND JEX, H. R.: Research on Display Scanning, Sampling, and Reconstruction Using Separate Main and Secondary Tracking Tasks. NASA CR-1569, July 1970.
17. CLEMENT, W. F.; AND HOFMANN, L. G.: A Systems Analysis of Manual Control Techniques and Display Arrangements for Instrument Landing Approaches in Helicopters. Vol. I: Speed and Height Regulation. Tech. Rept. 183-1, Systems Technology, Inc., July 1969.

N73-10142

38. Human Operator Dynamics for Aural Compensatory Tracking*

EDWARD W. VINJE

United Aircraft Research Laboratories

AND

EDWARD T. PITKIN

University of Connecticut

The human operator's ability to control using aural information only and using combined aural and visual displays was investigated for a simple tracking task. Tracking error was presented to the test subjects using one- and two-ear displays. For both displays the pitch of the tone represented the magnitude of the tracking error. **Error** polarity was indicated in the two-ear display by switching the tone between ears as a function of error sign. **For** the one-ear display, error polarity was indicated by using modulated and unmodulated tones.

The operator's aural control characteristics were modeled as a describing function plus a remnant. The effects on the measured describing function and remnant of different system dynamics, changes in the frequency content of the input and different displays were determined during the study.

The describing function and remnant data indicate that humans can control as well with aural cues as with visual cues for the task considered. However, the reduction in operator time delays, expected because of the generally faster human response to aural stimuli, was not evident in the results. It was also determined that the operators could control equally well with either the one- or two-ear display. Differences which might exist between monaural and binaural signal processing in the human operator were not significant for the displays and task considered. Finally, the operator model results indicate that the combined aural and visual presentation of tracking error neither improves the operator's control capability nor reduces operator time delays. Reduced time delays might have been expected because studies of simple human response have shown faster response to combined aural-visual stimuli, then to either stimulus alone.

INTRODUCTION

There are a number of aircraft control tasks in in which excessive demands are placed on the pilot's capability to control visually. Examples of such tasks are terrain following and V/STOL aircraft IFR approach and hover. Integrated and heads-up displays have been developed in an attempt to reduce the visual workload for such tasks. However, supplying the pilot with control information through one or more of his other sensory channels could also alleviate visual workload. In addition, using these other senses might enable the pilot to be more flexible with his vision than he could be with visual displays alone.

The human's aural sense is an information collecting apparatus which might be used as an alternate to vision in complex control tasks. In some respects, the aural channel may actually be superior to vision as an information gathering and processing device for human control. For example, the human aural receptor delays are considered to be smaller than the visual receptor

*This research was performed at the University of Connecticut to fulfill part of the requirements for E. W. Vinje's Ph.D degree.

latencies (ref. **1).** Also, studies of simple human response indicate that an aural stimulus elicits a response which may be **10** to **30** msec faster than the response to a visual stimulus (refs. **1** and **2).** Thus, it may be that the pure time delays incurred in aural control would be smaller than those for visual control.

Little attention has been given to the human operator's ability to control using aural information in previous man-machine system studies. This study was undertaken, therefore, to quantitatively evaluate the human operator's aural control characteristics. The limits of the human's aural control capability and also his flexibility as an aural controller were considered in the investigation. The effects of combined aural and visual presentation of control information were also examined. Particular emphasis was placed on obtaining results which would permit a quantitative comparison of human aural and aural-plus-visual control characteristics with results for control with visual information only.

MODEL FOR THE HUMAN OPERATOR

The test subject's dynamic characteristics for aural control were modeled as a describing function $Y_p(j\omega)$ plus a remnant $\phi_{nn}(\omega)$ which was assumed to be injected at the subject's output. This model is shown in figure 1. The describing function defines the linear relation between tracking error and operator output at the frequencies contained in the task input $i(t)$. As such, it can be used to define that part of the pilot's output which is linearly correlated with the input. The remnant, in turn, is composed of that part of the operator's output which is not linearly correlated with the input. The describing function and remnant measured in this study were developed from the functions $e(t)$ and $c(t)$ which were recorded during 180-sec tracking periods. These functions were digitized off-line and Fourier coefficients were computed from these data at appropriate frequencies using a fast Fourier transform algorithm. The Fourier coefficients were then used to form the describing function and remnant.

The mean-square value of the operator's output $c^2(t)$ was also measured during the tracking runs. These data were used in conjunction with

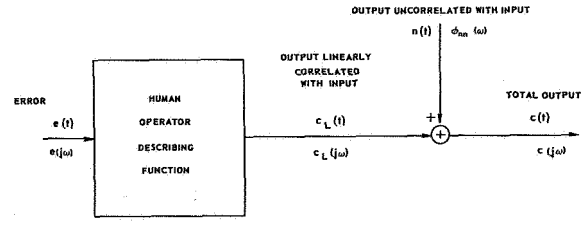

FIGURE 1.—Model for human operator dynamics.

the task input $i(t)$ and the operator's describing function to form operator relative remnant ρ_a^2. Relative remnant is defined as the ratio of the mean-square value of that part of the operator's output linearly correlated with the input $c_L^2(t)$ to the mean-square value of the total operator output $\overline{c^2(t)}$. That is,

$$\rho_a^2 = \frac{\overline{c_L^2(t)}}{\overline{c^2(t)}} = \frac{\overline{c^2(t)} - \overline{n^2(t)}}{\overline{c^2(t)}} \tag{1}$$

where $\overline{n^2(t)}$ is the mean-square value of operator remnant. Relative remnant is, therefore, an indication of relative operator linearity.

Describing functions measured in this study were also fit visually with two linear models. The first representation, McRuer's crossover model, was fit to forward-loop describing functions developed by forming the product $Y_p(j\omega) \cdot Y_c(j\omega)$, where $Y_c(j\omega)$ is the transfer function for the controlled element. The crossover model is defined as

$$Y_p(j\omega) \cdot Y_c(j\omega) \approx \frac{\omega_c e^{-j\omega\tau_e}}{j\omega} \tag{2}$$

where ω_c is the crossover frequency and τ_e is an approximation for the effects of operator lags and delays and high-frequency lead generation. In order for the crossover model to be a valid representation for $Y_p(j\omega) \cdot (Y_c(j\omega)$, the operator must compensate the controlled element dynamics so as to achieve a $K/j\omega$ forward-loop describing function at frequencies near crossover. Such a forward-loop describing function is indicative of "good" closed-loop response (ref. **3).**

The second model used to represent selected operator describing functions, $Y_p(j\omega)$, measured in this study was a more complex transfer function. This representation is McRuer's precision model which is defined as

$$Y_p(j\omega) \approx G\left(\frac{T_K j\omega+1}{T_{KI} j\omega+1}\right)\left(\frac{T_L j\omega+1}{T_I j\omega+1}\right)\frac{e^{-j\omega\tau}}{(T_{N1} j\omega+1)[(T_{N2} j\omega)^2+T_{N3} j\omega+1]} \quad (3)$$

where

G = adaptable operator gain

$\frac{T_K j\omega+1}{T_{KI} j\omega+1}$ = low frequency lag-lead form presumed to describe low-frequency effects of the neuromuscular system dynamics

$(T_L j\omega+1)$ = adaptable lead compensation

$(T_I j\omega+1)$ = adaptable lag compensation

$e^{-j\omega\tau}$ = pure time delay due to latencies in the aural data gathering, coding and transmission process

$\frac{1}{(T_{N1} j\omega+1)[(T_{N2} j\omega)^2+T_{N3} j\omega+1]}$ = representation for the high-frequency characteristics of the neuromuscular system dynamics.

The precision model was found to be a reasonably accurate representation over all measurement frequencies for the visual describing functions measured in reference **3.** Note also that the precision model identifies separate operator dynamic characteristics whose effects had been combined in the crossover model for $Y_p(j\omega)\cdot Y_c(j\omega)$, e.g., the pure time delay and the high-frequency effects of the neuromuscular dynamics.

DESCRIPTION OF THE AURAL CONTROL EXPERIMENT

Control Task, Aural Displays and Manipulator

The control task considered in this study was one-degree-of-freedom compensatory tracking. A schematic of the task is shown in figure **2.** Important features of the task are discussed briefly in the following paragraphs. A more detailed description can be found in reference **4.** The input $i(t)$ which the test subjects tracked was McRuer's "sum-of-sine waves" function (ref. **3).** The bandwidth of this function was varied during the investigation to change the difficulty **of** the task. For aural control the tracking error voltage $e(t)$ was converted to an audio signal and presented using two-ear and one-ear displays. Both two- and one-ear displays were considered in order to provide information on display requirements for the human aural controller.

For both aural displays $e(t)$ was linearly converted to frequency and the magnitude of the tracking error was represented by the pitch of a single tone. The sensitivity used in converting tracking error voltage to frequency was **64** Hz/volt. This was the sensitivity which resulted in the best aggregate tracking performance from the test subjects used in this study. Zero tracking error corresponded to a low-frequency **(330** Hz) bias tone. For the two-ear display, the sign of the tracking error was indicated by switching the tone between the left and right earphones. The convention on the switching was such that the control stick was moved away from the ear in which the tone was heard. This in turn reduced the magnitude of the tracking error and the perceived pitch of the tone. For example, if the tone was heard in the left ear and the stick was moved right, the pitch of the tone decreased until it reached the bias frequency of **330** Hz. At this point the tone would switch to the right ear and begin to increase in pitch,

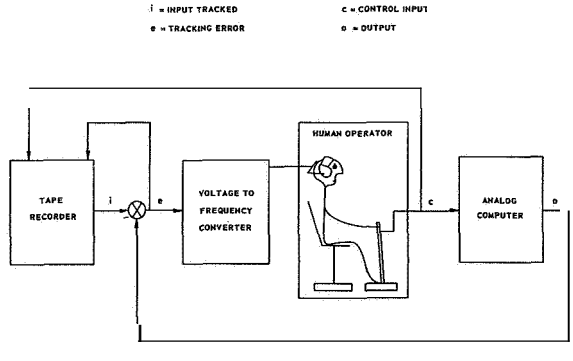

FIGURE 2.—Schematic diagram of the aural compensatory tracking experiment.

indicating that the sign of $e(t)$ had changed and that its magnitude was becoming larger.

The frequency to voltage sensitivity and the bias frequency used for the one-ear display were the same as those for the two-ear display. The only difference between displays was in the manner in which the polarity of $e(t)$ was presented. For the one-ear display, a change in the sign of the error was indicated by changing the character of the presented tone. A negative tracking error resulted in a tone identical to that used in the two-ear display. For positive tracking error the tone was modulated, i.e., for positive error the tone seemed to "whir" as it changed pitch.

The control stick used was a cantilevered rectangular steel rod which provided a stick force gradient of 1.0 lb/in. The top of the stick could be moved ± 3 in. about null before it contacted stops. Motion of the stick was converted to the voltage $c(t)$ using a linear induction transducer. The sensitivity of the control stick was held constant and the forward-loop gain of the system was adjusted to acceptable values by changing the gain of the controlled elements. The controlled element dynamics were simulated using an analog computer as shown in figure 2.

Test Cases and Subjects

The test cases for which describing functions, remnants and relative remnants were measured are shown in table 1. The major part of this study consisted of a relatively complete evaluation of aural human operator dynamics using both the one-ear and two-ear displays. The remainder of the study consisted of a short investigation of the effects on operator dynamics of combined aural and visual presentation of tracking error. Data were obtained from three test subjects for each of the test cases indicated in table 1. All subjects had normal hearing, but none had any special talent for identifying the characteristics of audio tones, e.g., perfect pitch. Also, one of the subjects was an experienced visual tracker, but none had any previous aural tracking experience.

DESCRIBING FUNCTION RESULTS

Results for the Two-Ear Display

Describing functions.—Representative forward-loop describing functions $Y_p(j\omega) \cdot Y_c(j\omega)$ for the two-ear display are shown in figures 3, 4, and 5 for $\omega_b = 2.6$ rad/sec and controlled elements of 10, $10/j\omega$ and $10/(j\omega)^2$, respectively. The standard deviations in these measurements are presented as well. Visual describing functions from reference 3 for corresponding controlled elements and a similar input ($\omega_b = 2.5$ rad/sec) are also plotted for comparison in figures 3, 4, and 5. In addition, the crossover model has been fit to the aural data and is plotted in these figures. The discussion of these describing function results which follows for $\omega_b = 2.6$ rad/sec applies also to similar data obtained with $\omega_b = 1.7$ and 3.5 rad/sec (ref. 4). The aural results presented in figures 3, 4, and 5 indicate that the test subjects adapted to the controlled elements so as to yield describing function magnitudes similar to those of a $K/j\omega$ transfer function. This is especially evident for the $10/j\omega$ and $10/(j\omega)^2$ controlled elements where the crossover model fits the describing function magnitude quite well. Note also, that the magnitudes (and crossover frequencies) of the aural describ-

TABLE 1.—Test Cases Evaluated

Investigation	Display	Controlled element	Input break frequency, ω_b-rad/sec
Aural presentation of tracking error	Two ear	K, $K/j\omega$, $K/(j\omega)^2$	1.7, 2.6, 3.5
	One-ear display on left ear	$K/(j\omega)^2$	1.7, 2.6
	One-ear display on right ear	$K/(j\omega)^2$	1.7
Combined aural and visual presentation of tracking error	Visual only	$K/(j\omega)^2$	2.6
	Two-ear aural	$K/(j\omega)^2$	2.6
	Visual plus two-ear aural	$K/(j\omega)^2$	2.6

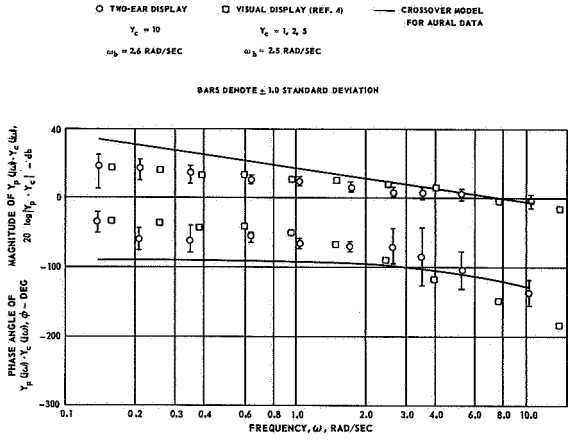

FIGURE 3.—Comparison of aural and visual forward-loop describing functions for gain dynamics.

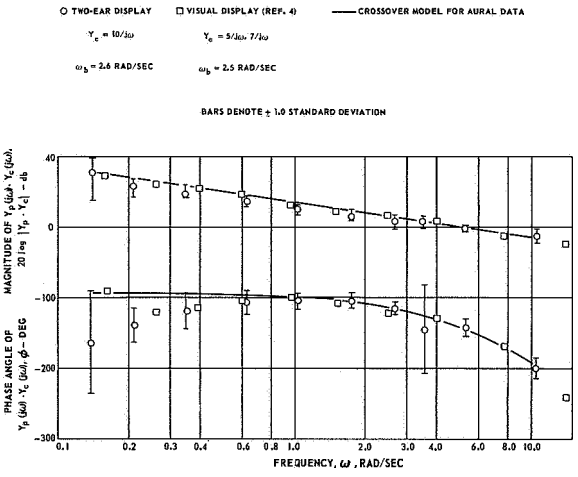

FIGURE 4.—Comparison of aural and visual forward-loop describing functions for rate dynamics.

ing functions generally decreased with increasing order of the controlled element. The effect of ω_b on the aural describing function characteristics will be discussed later in conjunction with the crossover model parameters.

The visual describing function data from reference **3** generally agree well with the corresponding aural results. The magnitudes correspond closely for all controlled elements and the phase angles are also very similar for the $10/j\omega$ and $10/(j\omega)^2$ controlled elements. However, for the gain controlled element the phase lag of the aural data is generally smaller at the higher

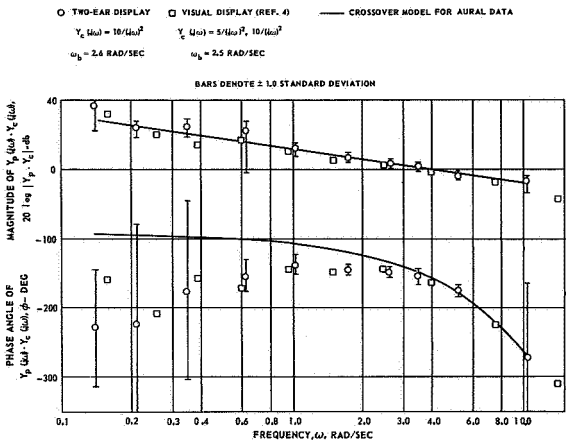

FIGURE 5.—Comparison of aural and visual forward-loop describing functions for acceleration dynamics.

frequencies than the phase lag for the visual results.

Crossover model parameters.—*As* indicated previously, the crossover model accurately represents the magnitude of the aural forward-loop describing functions for the $10/j\omega$ and $10/(j\omega)^2$ controlled elements. However, only for frequencies near crossover is this model a good representation of the magnitude of the describing function for the gain controlled element (see figs. **3, 4,** and 5). For all controlled elements, the model does not represent the describing function phase angles accurately for frequencies much below crossover. These conclusions apply to aural describing functions obtained for all three values of ω_b (ref. **4).**

The crossover model parameters used to fit the aural describing functions for all values of ω_b are listed in table **2.** Phase margins associated with these fits are also presented along with visual describing function parameters computed from empirical formulas developed in reference **3.** It should also be pointed out that the gains of the controlled elements were increased for aural tracking when ω_b was increased. The test subjects desired increased forward-loop gain when ω_b was made larger and the input became more difficult to track. The controlled element gains were not adjusted in this fashion for the visual study of reference **3.**

The relative magnitudes of corresponding aural and visual crossover model parameters are

TABLE 2.—*Comparison* of Aural and Visual *Crossover* Model Parameters

ω_b, rad/sec	Dynamics	Aural, two-ear display			Visual, ref. 3		
		ω_c, rad/sec	PM, deg	τ_e, sec	ω_c, rad/sec	PM, deg	τ_e, sec
1.7	7	5.2	73	0.06	5.1	35	0.19
	$7/j\omega$	4.6	48	0.16	4.7	31	0.22
	$7(j\omega)^2$	3.7	20	0.32	3.3	18	0.38
2.6	10	6.8	63	0.06	5.2	54	0.12
	$10/j\omega$	4.8	41	0.18	4.8	48	0.15
	$10/(j\omega)^2$	3.9	23	0.30	3.5	28	0.31
3.5	15	4.8	78	0.05	5.4	75	0.05
	$15/j\omega$	4.2	54	0.14	5.0	67	0.08
	$15/(j\omega)^2$	3.8	27	0.30	3.7	40	0.24

similar and the trends in the aural and visual parameters with controlled element order are the same. That is, ω_c and PM decrease and τ_e increases with increasing controlled element order for both sets of data. However, there are trends in the visual data with ω_b which are not evident in the aural results. Crossover frequency and phase margin increase and τ_e decreases with ω_b for the visual data and these trends are not evident in the aural results. The aural ω_c does increase slightly as ω_b changes from *1.7* to *2.6* rad/sec, however. Note also that operator regression * is not apparent at $\omega_b = 3.5$ rad/sec in the aural results for the $K/(j\omega)^2$ controlled element. Regression is not evident in the visual data of reference *3* either since the formulas used to fit the data do not account for its effects. However, other visual results in reference *3* show that the operators regressed significantly at $\omega_b = 4.0$ rad/sec with the $K/(j\omega)^2$ controlled element ($\omega_c = 1.8$ rad/sec and PM = 42° at $\omega_b = 4.0$ rad/sec versus $\omega_c = 3.25$ rad/sec and PM = 26° at $\omega_b = 2.5$ rad/sec).

Both the crossover model parameters and the describing functions themselves tend to indicate little difference between human operator dynamics for aural and visual control. In particular, a smaller time delay, which might have been expected for the aural results because of the smaller aural receptor latency, were not evident in the crossover model results. That is, the aural values of τ_e were not significantly smaller than the visual τ_e results.

Precision model parameters.—The precision model (eq. *(3)*) was fit to all the two-ear display describing function data and these results are presented in reference *4*. Two interesting features of these data will be discussed here. First, the values of operator adapted lead used to fit the aural describing function data for the $K/(j\omega)^2$ controlled elements were equivalent to the lead adapted by the subjects in the visual tracking study of reference **3.** The aural lead parameters are presented in the following list:

ω_b	$Y_c(j\omega)$	T_L
1.7	$7/(j\omega)^2$	*3.7*
2.6	$10/(j\omega)^2$	*3.7*
3.5	$15/(j\omega)^2$	*3.0*

Secondly, visual data are available (ref. **3)** which permit a reasonably direct comparison between aural and visual precision model parameters. The aural data are for the $10/j\omega$ controlled element with $\omega_b = 2.6$ rad/sec. The visual parameters are for $Y_c(j\omega) = K/(j\omega - 2)$ and $\omega_b = 2.5$ rad/sec. How well the precision model fits the aural data can be seen in figure **6.** The visual and aural precision model parameters are tabulated in the following list:

	T_L	T_I	T_K	T_{KI}
Visual	*0.11*	0.0	*3.33*	*20.0*
Aural	*0.05*	0.0	*5.50*	*25.0*

* **Regression is a term used to describe the relaxation in operator control characteristics (decreased ω_c and increased PM) which occurs when the tracking task is made too difficult.** In **doing so the operator tolerates a larger tracking error in the interest of maintaining stability.**

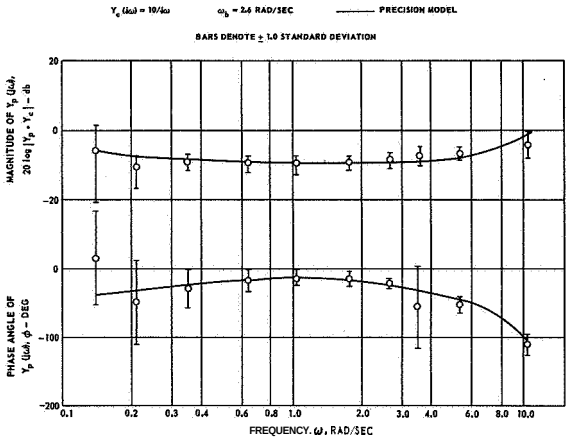

FIGURE 6.—Precision model fit to operator describing function for rate dynamics with two-ear display.

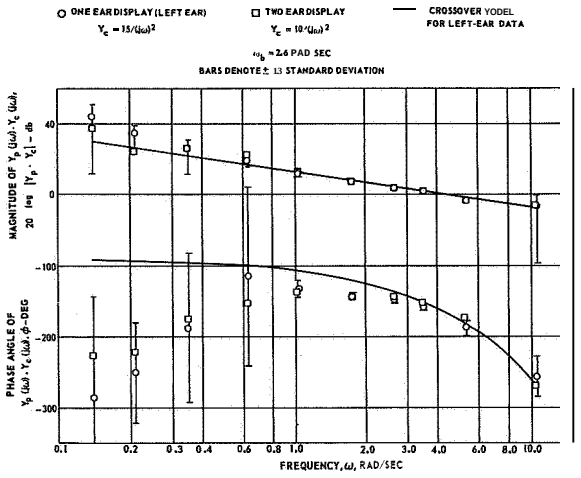

FIGURE 7.—Forward-loop describing functions for acceleration dynamics with one- and two-ear displays.

	τ	T_{N1}	T_{N2}	T_{N3}
Visual	**0.09**	**0.10**	**0.06**	**0.014**
Aural	**0.10**	**0.08**	0.08	**0.016**

The visual and aural parameters are very similar. Note that the pure time delay parameter τ is not smaller for the aural data.

Results for the One-Ear Display

A representative forward-loop describing function for the one-ear display is shown in figure 7. It was measured for $\omega_b = 2.6$ rad/sec and $Y_c(j\omega) = 15/(j\omega)^2$ with the display on the left ear. The crossover model fit to this data is also shown in figure 7. For comparison, a describing function for the two-ear display measured with the same input break frequency and $Y_c(j\omega) = 10/(j\omega)^2$ is presented as well. The controlled element gains used with the one-ear display were larger than those considered for the two-ear display. The test subjects felt the larger gains compensated somewhat for the less precise indication of tracking error sign change in the one-ear display. As indicated in figure 7, the one-ear display and two-ear display describing functions are quite similar. This correspondence between one-ear and two-ear display describing functions holds for the other one-ear display test cases considered as well, i.e., $\omega_b = 1.7$ rad/sec, and $Y_c = 10/(j\omega)^2$ with the display on either the right or left ear. Crossover model parameters obtained for these comparative one-ear and two-ear display test cases are discussed in reference 4. There appears to be no significant difference between the one-ear (used on either the right or left ear) and two-ear display crossover model parameters.

Results for Combined Aural and Visual Displays

Description of visual display.—As indicated in table 1, describing functions were measured in this part of the study using an aural display only, a visual display only and the aural and visual displays in combination. The aural display used was the two-ear display described previously. Initially, a scaled oscilloscope face with a grid and a zero-error reference was considered for use as the visual display. However, experiments indicated that this display provided more precise information than the aural display. The subjects ignored the aural display when it was used in combination with the scaled visual display. This could have compromised the objectives of this part of the study.

The visual display that was finally used was an oscilloscope display designed to be a visual analog of the two-ear aural display. It is shown schematically in figure 8. On this display a dot moved along one of two separate vertical paths. One of the paths was located on the left side of

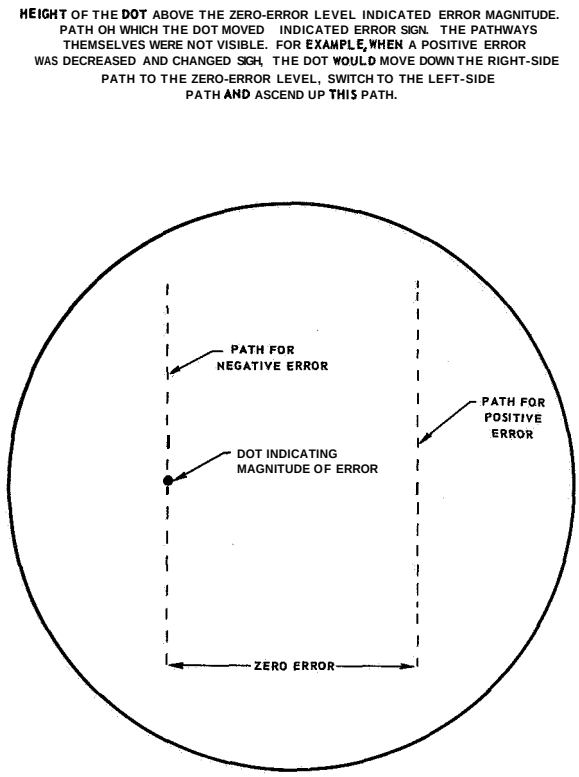

FIGURE 8.—Oscilloscope display used in the evaluation of combined aural and visual displays for tracking error.

the oscilloscope face and the other was located on the right. The magnitude of the tracking error was indicated by the vertical position of the dot and the sign of the error determined which path the dot moved on. The oscilloscope face did not have a scaled grid and there was no reference line for zero error. Measured rms tracking errors for this display were only slightly larger than corresponding tracking error scores measured for the aural two-ear display. It was felt, therefore, that the visual display provided about as much information on tracking error as did the two-ear display.

Describing functions.—Describing functions measured for aural only, visual only and combined (or parallel) aural and visual displays are presented in figure 9. These describing functions were measured for $10/(j\omega)^2$ dynamics and $\omega_b = 2.6$ rad/sec. The one standard-deviation error bars are shown for the combined display data and the crossover model fit to the combined display data is also shown. The describing functions for all

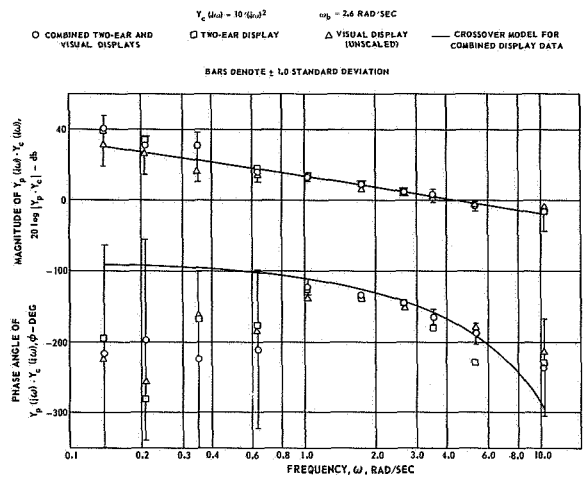

FIGURE 9.—Forward-loop describing functions for acceleration dynamics with aural, visual, and combined displays.

three types of tracking error presentations are generally quite similar.

Crossover model parameters.—Parameters used to fit the crossover model to the three describing functions shown in figure 9 are listed in table 3. The crossover frequency is slightly larger and the phase margin smaller for the combined displays than for either display alone. Although the ω_c and PM differences are small, they do indicate that the operators were slightly more responsive to tracking error when the displays were combined. This correlates with the slightly smaller rms tracking error scores measured for the combined displays (ref. 4). The value of τ_e, however, was no smaller for the combined displays. As was pointed out previously, studies of simple human response (ref. 1) have shown that humans respond more rapidly to combined aural and visual stimuli than to an aural stimulus alone. Studies also indicate, however, that the latency in human response is related to the complexity of the required response (ref. 1). The compensatory tracking task may be sufficiently difficult to obscure differences which are significant for more simple human response tasks.

REMNANT RESULTS

Remnant power spectral densities $\phi_{nn}(\omega)$ measured for the unscaled visual display and the

TABLE 3.—*Crossover Model Parameters for Aural, Visual and Combined Displays*
[$\omega_b = 2.6$ rad/sec, $Y_c/(j\omega) = 10/(j\omega)^2$]

Display	Crossover model parameters		
	ω_c, rad/sec	PM, deg	τ_e, sec
Aural (two-ear)	3.9	18	0.34
Visual	3.8	23	0.30
Combined aural and visual	4.2	8	0.34

two-ear aural display are compared in figure 10. The remnant power spectral density for the scaled visual display mentioned previously is also presented in figure 10. These data were measured for $\omega_b = 2.6$ rad/sec and $Y_c(j\omega) = 10/(j\omega)^2$ and the results are presented in terms of power decibels (pdb) where $\text{pdb}(\omega) = 10\log_{10}\phi_{nn}(\omega)$. It should be noted, also, that the effects of measurement and computational errors become significant in the remnant data for frequencies below 0.6 rad/sec (ref. **4**). Therefore, the remnant data are not reliable at these low frequencies. However, for frequencies equal to or greater than 0.6 rad/sec, the visual and aural remnant data agree quite well. The averaged relative remnant results, ρ_a^2, for these test cases are quite small, however, they also are quite similar. These values of ρ_a^2 are 0.06, 0.06, and 0.07 for the aural, unscaled visual, and scaled visual displays, respectively.

Remnant data from this study are discussed in more detail in reference **4.** Some of the more significant results from the analyses of these data will be briefly outlined here. The remnant power spectral data in reference **4** show that the magnitude of the remnant spectra increased with increasing order of the controlled element. The values of relative remnant, ρ_a^2, varied inversely with controlled element order, ranging in magnitude from about 0.90 for $Y_c = K$ to 0.10 for $Y_c = K/(j\omega)^2$ at $\omega_b = 2.6$ rad/sec. The remnant power spectral magnitudes for a given controlled element decreased with increasing ω_b. This was due chiefly to the increased controlled element gain used as ω_b was made larger. The increased gain resulted in smaller control motions which resulted in lower remnant power spectral densities and also smaller total operator control

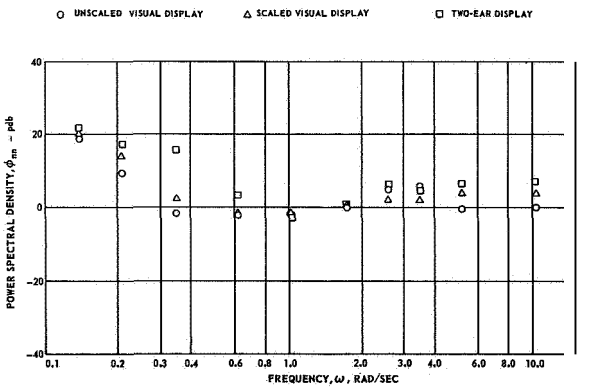

FIGURE 10.—Remnant power spectra for acceleration dynamics with unscaled visual, scaled visual, and aural displays.

output. The averaged values of ρ_a^2 generally decreased when ω_b was increased. Also, the remnant power spectral densities and relative remnant results for the two-ear and one-ear aural displays were not significantly different.

SYMBOLS

c	total operator output, volts
$\overline{c^2}$	mean-square total operator output, (volts)^2
$\overline{c_L^2}$	mean-square value of that part of the total operator output linearly correlated with the input, (volts)^2
db	decibels, $20\log_{10}(\ )$ where $(\ )$ is a magnitude quantity, e.g., Y_p
e	tracking error, volts
G	gain of the precision model, volts/volt
i	input forcing function, volts
j	$\sqrt{-1}$
K	open-loop gain, volts/volt
n	operator open-loop remnant injected at the operator's output, volts
$\overline{n^2}$	mean-square operator open-loop remnant, (volts)^2
0	output from the controlled element, volts
pdb	power decibels, $10\log_{10}(\ )$ where $(\ )$ is the quare of a magnitude quantity, e.g., ϕ_{nn}
PM	phase margin, an indicator of closed-loop stability expressed as the phase lag of the forward-loop describing function, ϕ, plus 180°, deg
s	Laplace operator, 1/sec

T_I time constant for operator adapted lag, sec

T_K lead time constant for the lead-lag representation of operator low-frequency neuromuscular characteristics, sec

T_{KI} lag time constant for the lead-lag representation of operator low-frequency neuromuscular characteristics, sec

T_L time constant **for** operator adapted lead, 0ec

T_{N1} time constant for first-order lag portion of the third-order precision model representation for operator high-frequency neuromuscular characteristics, sec

T_{N2} coefficient in the second-order part of the precision model representation for operator high-frequency neuromuscular characteristics, sec^2

T_{N3} coefficient in the second-order part of the precision model representation for operator high-frequency neuromuscular characteristics, sec

Y_c controlled element transfer function

Y_p measured operator describing function

ρ_a^2 operator relative remnant (see eq. **(1))**

τ time constant representing inherent operator time delays, sec

τ_e time constant approximating the effects of operator time delays, neuromuscular lags and high-frequency operator adapted lead, sec

ϕ phase angle of the forward-loop describing function, $Y_p \cdot Y_c$, deg

ϕ_{nn} power spectrum **of** the open-loop remnant injected at the operator output, $(volts)^2/rad/sec$

ω frequency, rad/sec

ω_b bandwidth of the input to the tracking task, rad/sec

ω_c crossover frequency, that frequency at which the gain of the forward-loop describing function, $Y_p \cdot Y_c$, is equal to one; a measure of closed-loop frequency response, rad/sec

REFERENCES

1. WARGO, M. J.; ET AL.: Human Operator Response Speed, Frequency, and Flexibility: **A** Review, Analysis and Device Demonstration. NASA CR–874, Sept. 1967.
2. SINAIKO, H. W., ED.: Selected Papers on Human Factors in the Design and Use of Control Systems. Dover Publications (New York), 1961.
3. MCRUER, D. T.; GRAHAM, D.; KRENDELL, E. S.; **AND** REISENER, W. : Human Pilot Dynamics in Compensatory Systems. AFFDL–TR–65–15, July 1965.
4. VINJE, E. W.: Human Operator Dynamics for Audio Compensatory Tracking. Ph.D Thesis, Department of Aerospace Engineering, Univ. of Connecticut (in preparation).

N 73-10143

39. A Computer Assisted Teleoperator Control Station With Tactile Feedback*

J. W. HILL AND J. C. BLISS

Stanford Research Institute

This report describes a computer-assisted teleoperator control system for making comparative performance evaluations. A local and remote control station, each with decision-making capability, communicate with each other through a simulated time delay. Supervisory control at three increasingly automatic levels is possible. The highest level of programmed control is facilitated through the ARM language which was developed to permit easily readable program manuscripts to be written and assembled into programs of motions by novice programmers. Experimental results show the advantage of this form of supervisory control with both direct and delayed (3 sec) manipulation tasks. In addition, two systems to measure and reproduce force distributions have been designed. One system reproduces contact on the external surfaces of the remote hand using 21 airjet simulators. Another system reproduces the shape of the contact between object and jaws using 288 piezoelectric (bimorph) stimulators. In the course of this work the Rancho Arm was upgraded through mechanical strengthening and the addition of a proportional control system.

INTRODUCTION

Evaluation of touch-sensing and feedback systems for a mechanical hand require their use in a wide variety of tasks and control situations. Since tactile feedback does not interfere with manipulation as force feedback does in the time-delay situation, one of the variables in these evaluations should be the amount of time delay. Operations with a time delay, however, are so slow and tedious that manipulations without some form of supervisory control are not representative of the state of the art. To fulfillthese requirements for a flexible control system, a computer program was written that simulates different control conditions, time delays, and levels of supervisory control. The advantage of this simulation is the way parameters and control options can be included or modified through program (software) rather than equipment (hardware) changes.

The arm-control program on our LINC–8 computer simulates both a local and a remote control station, each with decision-making capability. The two stations communicate with each other through a communications time delay that may range from milliseconds, seconds, even to minutes. Supervisory control at three increasingly automatic levels is possible using this simulation. The first level is purely manual: the operator moves the arm using the control brace. The second level is automatic: the operator requests that remote sensors be tested or remote actions be carried out by typing a two-character instruction. The third level is programmed control: the operator types in the name of a previously written program containing the list of instructions he wishes to be carried out. This simulation is described under the heading Arm-Control System, and an example of a program to unscrew a nut from a bolt follows. An evaluation experiment comparing manual operation with program-assisted manual operation is also given.

Touch feedback systems for both a manual and automatic operation are described in this report. One system consists of 21 force sensors

* For a more complete presentation refer to Bliss, Hill, and Wilbur (ref. 1) and Hill and Bliss (ref. 2). This investigation was conducted under NASA contract NAS2–5409.

distributed on the outside surfaces of the mechanical hand. These sensors are connected one-to-one with airjet tactile stimulators mounted over corresponding areas of the operator's hand. The second system consists of two 6×24 arrays of sensors distributed on the faces of the tongs. These sensors are connected one-to-one with piezoelectric (bimorph) stimulator arrays positioned on the fleshy pads of the operator's index finger and thumb. These sensors and stimulators provide force distribution feedback instead of force feedback in the conventional sense; thus it is possible to use these touch-reproducing systems in the time-delay situation without interfering with manipulations as force feedback does.

ARM-CONTROL SYSTEM

A control system for carrying out tasks at a distant location with a mechanical arm consists of the following three basic elements:

(1) A control station where the operator controls the motion of the arm by transmitting commands and by supervising the resulting action using various displays and feedback.

(2) A remote-station that accepts the commands and uses them along with information from environment sensors to control the arm.

(3) A communications link that limits information flow. The limitations may take the form of a time delay, a bandwidth limitation, a signal-to-noise ratio, maximum video frame rate, and so forth.

There are obviously many combinations of design options for each of these three basic elements, depending on the task to be carried out. Hot-cell manipulations are usually carried out with simple control and remote stations. Frequently the remote arm is servoed directly to a joystick. This requires that the human operator interpret a TV display, access the situation, and provide manual inputs to carry out the appropriate action. The human operator supplies all the intelligence in this case.

In communication systems with a time delay, such as those involved in exploration of the moon or the planets, direct control by a human operator becomes a very slow and laborious process. To overcome this problem, both control stations and remote stations of varying complexity have been proposed. For example, the control station may include predictor displays, or the remote station may have computing power enabling it to utilize joint positions, force sensors, range finders, or TV cameras to aid the operator by carrying out semi-automatic or "supervisory" operation. Carrying this idea to its logical conclusion, artificial intelligence laboratories are studying computer stations capable of completely automatic control. In this case the operator communicates to the remote station only with sentence-like commands.

Our goal is to design a control scheme that optimizes performance in carrying out remote tasks by combining the best attributes of man and computer. Therefore, man's ability to interpret scenes, estimate distances, and project motion with a multicoordinate control brace, is combined with the computer's ability to save and accurately duplicate arm positions, remember sequences of motions, carry out tests based on arm position, and interpret touch sensors. Background material on such supervision control is given by Johnson and Corliss (ref. 3, pp. 69–74), and Corliss and Johnson (ref. 4, pp. 117–124).

In general, man interprets and directs overall or organizational aspects of a task and the computer-directed arm attends to detailed aspects. The following hypothetical example of picking up a block illustrates this point. First, the operator recognizes the block in the picture transmitted by a TV monitor. He directs the arm to its position using a control brace. Control is then transferred to a computer subroutine which, utilizing feedback from the touch sensors, directs the hand to grasp the block and center it in the jaws. Next, as the operator directs the arm to go to a previously stored position, another subroutine adjusts the jaw pressure so that the block will not be dropped.

In order to study manual control supplemented by such semi-automatic operations in a time-delay environment, we programmed a small computer (LINC–8 with 4K memory) to simulate the entire control system shown in figure 1. The program actually has separate subroutines for the control station and the remote station that interact with each other only through a subroutine that simulates the time delay. Real-time interactions between the two control sta-

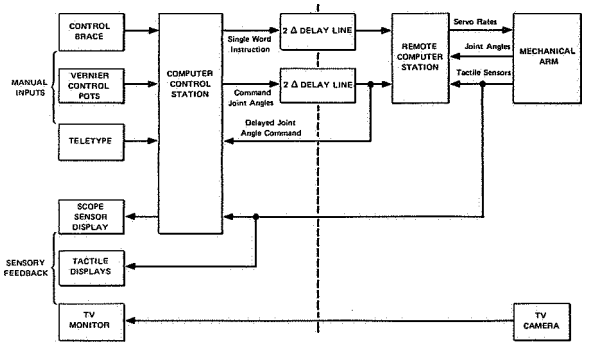

FIGURE 1.—Block diagram of the simulated man-machine control system.

tions are maintained by dividing time into 1/60-sec intervals. During each interval the inputs (if any) to the control station are serviced and a new command is formed for insertion into the delay line. Next, the command is inserted into the front of the delay line and the delayed command removed from the end. Finally, the delayed command is used by the remote-station subroutine to calculate new servo-rate outputs and to sample sensors or joint angles. Thus, the LINC–8 is programmed to share time between the two stations. Sampling and storing manual input signals at 60 Hz is adequate to preserve human accuracy and smoothness of motion.

Control Station

The arm-control station as it currently stands is shown schematically in the left half of figure 1. It consists of several manual inputs, several visual and tactile displays, and a computer program to permit the operator to select and transfer among inputs, displays, and programs of motion to accomplish a given task.

Manual inputs.—The manual inputs are illustrated in figure 2. The Rancho anthropomorphic control brace measures the joint angles of the operator's arm with a set of seven potentiometers. These joint angles can also be controlled with the individual potentiometers mounted on a panel. Manipulations in tasks requiring either a long time to complete or precise positioningare generally best carried out with knob control. Control can also be entered directly from a teletype using the format

#6←45

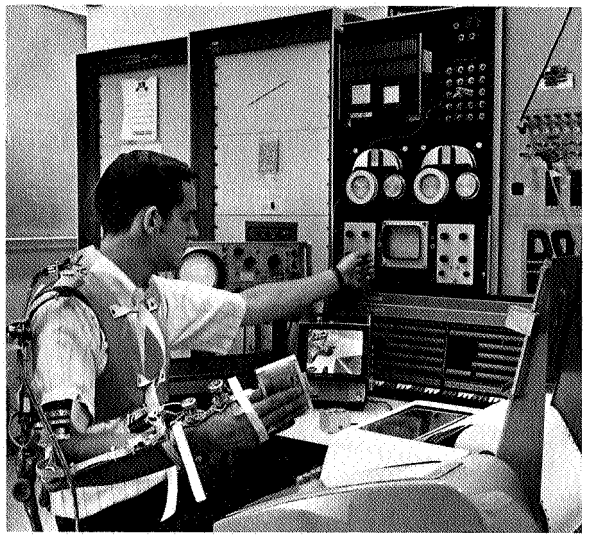

FIGURE 2.—Arm control station. (From left to right are (1) the master brace with single 4 X12 tactile display on index finger, (2) computer-driven display with sensing pad information, (3) TV view of hand grasping block, (4) operator adjusting vernier potentiometer on computer panel, and (5) teletype terminal.

where # and ← are prompts from the teletype, 6 is the joint number, and 45 is the joint angle in degrees. Teletype control has been used largely for testing and debugging manipulation programs. A desirable control input would be a miniature (scaled down) control brace light enough to maintain the position it is put in and small enough to be manipulated with the operator's fingers.

Sensory *feedback*.—Primary visual feedback is supplied by a broadcast-quality, closed-circuit television system. In addition, a computer-driven scope display presents the state of some of the touch-sensor information. One version of this display is shown in figure 3. Here information from three preliminary touch sensors and two simulated jaw sensors are presented in perspective.

Tactile feedback from the arm to the operator is provided by a set of touch sensors on the hand. The touch sensors fall into two groups: a pair of touch-sensing pads on the gripping surface of the manipulator tongs, and a number of individual force sensors covering the outer surface of the tongs and wrist. Since these sensors and the anthropomorphic tactile stimulators represent a

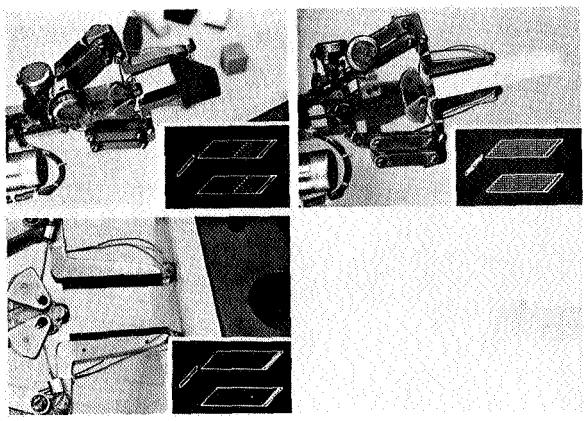

FIGURE 3.—Gripping and touching situations and corresponding displays on the computer scope. (The display program uses simulated data since the sensor multiplexer has not yet been constructed.)

major part of this project they are separately described later.

Control-station operation.—The control-station program is organized to provide three increasingly automatic levels of control. This control structure is described in the command tree shown in figure **4.** By moving from branch to branch, typing single letters or numbers, the operator selects manual or program control to carry out the desired task.

Direct manual control is achieved by typing either *K* (for knobs), *B* (for brace), or *T* (for teletype), followed by either ***A*** (for absolute), or *R* (for relative). Absolute control causes joint positions to be read directly from these devices and to be transmitted to the remote station. Relative control specifies that joint commands from the control source take up where the previous joint commands left off. Thus, after a transfer from brace to knobs (or vice versa), the new control source picks up where the old one left off, and there is no transient motion artifact.

Decision-response control achieved by typing ***D*** permits two character instructions to be transmitted to the remote-control station. The fist character of the pair selects a remote test to be carried out and the second selects a remote action to be carried out if the test is passed. For example, test *T* is "thumb sensor closed," and action **O** is "open jaws." Therefore, the instruction that appears as the sequence "*(T,O)*" means "if thumb sensor closed then open jaws." The instruction "(,*O*)" requires no tests and causes the jaws to open. All of the *six* tests and all of the seventeen actions possible with the subroutines built into the remote computer are thus executable by typing in pairs of characters under decision-response control. Since any test can be used with any action, there are a total of $6 \times 17 = 102$ possible instruction that may be transmitted using this mode. **A** detailed listing of the different tests and actions is given later in figure 8(a).

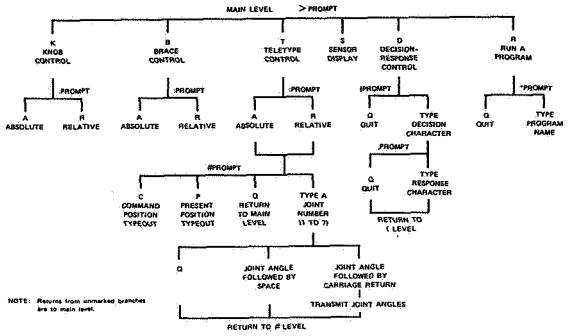

FIGURE 4.—Command tree of the control station.

Program control achieved by typing *R* and then the name of the desired program causes a program of tests and actions to be loaded into the remote computer's 256-word memory. Such programs are then run under decision-response control. Positions of objects are input to the program using the save of $ command in the form "(,20$)." This command causes the seven joint angles to the arm to be stored beginning at location 20 in the program. When the operator is ready to enter the program, he types a go or ***G*** command as "(,100G)." This command causes further instructions to be taken from the list in the program starting at location 100. A usage example involving a program to unscrew a nut from a bolt is given later.

Remote Station

The remote station as it currently stands in the communication system is shown schematically in the right half of figure **1.** It consists of a modified Rancho Arm * with a number of specially

* Model 8A, a 7-degree-of-freedom anthropomorphic manipulator manufactured by R. & D. Electronics, Downey, California.

built touch sensors, a TV camera, and a computer program with several subroutines for automatic operations. The physical layout is shown in figure 5. While the arm and its control system are described in the rest of this section, the touch sensors are separately described.

Mechanical arm.—During this study, the Rancho Arm was upgraded to reduce the amount of play in the joints and to increase the range of motion. In total, all joints but one have been refurnished to some degree, two members have been completely replaced, and two joints completely rebuilt. These changes were deemed necessary, based on our previous experience with the arm, in order to carry out meaningful manipulation experiments with it.

An initial study of the sources of play or looseness in the Rancho Arm revealed that poor design in the three worm-gear-driven joints was the major trouble. Replacing the bearings with commercial roller bearings and incorporating simple backlash adjusters greatly improved smoothness of performance. To lighten the arm, cable drivers for jaw closure and wrist prehension/extension were lengthened in order to mount the motors on the main pedestal. To increase the range of hand motion, thus increasing the number of meaningful tasks that could be carried out, wrist flexion/extension range was increased from 90" to 180°, and wrist rotation (supination/pronation) was increased from 90° to 360". To reduce the play between the tongs, the prehension linkages were rebuilt, replacing the machine-screw bearings with tightly fitting pin bearings.

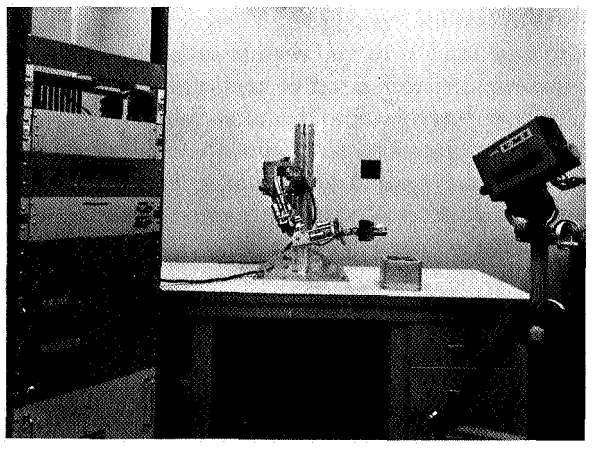

FIGURE 5.—Remote station. (From left to right are (1) the computer interface containing proportional control amplifiers, sensor amplifiers, and power supplies; (2) the modified Rancho Arm; and (3) the TV camera.

Proportional arm controller.—Because of the many difficulties experienced with the original relay-operated bang-bang control system, a new proportional-control system was designed and built. This system has shown the following advantages over the original system:

(1) The time for a given movement can be halved by driving the motors harder than the original system but still retaining stability.

(2) Smaller movements are permissible.

(3) The smooth acceleration and deceleration reduces the mechanical coupling between joints and the vibrations at the beginning and termination of movements.

(4) Proportional control allows computer programs to govern rates of motion as well as position.

The proportional power amplifiers use a pulse-width-modulation drive to keep the power dissipated in the drive transistors low and also limit the drive current to prevent the motors from burning out. Since torque is proportional to motor current, this current limiting also provides a linear and easily adjustable analog to a mechanical clutch. Stiction effects are reduced by incorporating a "negative" dead band or high-grain region into the amplifier's otherwise linear characteristic. Stiction was additionally reduced by lowering the modulation frequency to the point where a slight vibration or mechanical dither is produced by the motors when the error signals are small.

Structure of the remote station.—The block diagram of the remote station is given in figure 6. The delayed instruction (two computer words) and the delayed joint commands (seven computer words) from the control station are the only inputs. The auto-manual switch is under program control and can be either closed to accept manual inputs from the control station or opened to allow commands generated by programs to move the arm. Arm control is quite conventional, with actual joint positions subtracted from the command joint positions, and the difference multiplied by the joint gains and output to the servo-motors as angular rates.

For program control, the following simulated

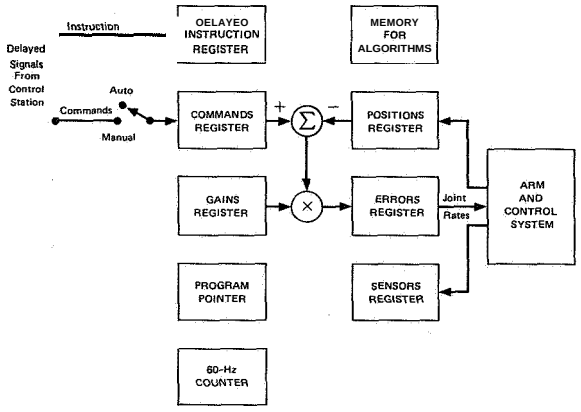

FIGURE 6.—Components of the remote station.

features have been added to the remote station:

(1) The counter, which is decreased by one count every **1/60** sec. There is an instruction that sets the counter to any desired value and a test instruction that detects when it has reached zero. Time delays (or waits) in programs can be achieved by setting the counter to the desired value and waiting for it to become zero.

(2) The 256-word memory, which can be loaded with a list of instructions by a single command from the remote-control station.

(3) The program pointer, containing the address of (or pointing to) the next instruction to be executed. The address may be that of the delayed instruction register or may be any of the instructions in the 256-word memory. There are instructions that back up, skip, or specifically set the program pointer.

With the use of these registers and the memory in combination with the registers in the control system and the sensor information, meaningful tasks can be carried out.

Automatic Subroutines

To experiment with semi-automatic operation of the arm, subroutines that execute simple, remote tests and actions have been built into the remote-control station's computer program. These subroutines are the building blocks used by both single-instruction commands from the control teletype and multi-instruction algorithms executed by the remote computer. The test subroutines are based on both the arm-joint positions and the status of the touch sensors. The action subroutines change the contents of one of the arm-control registers to produce a desired movement or rate of movement, or to tell the program where to obtain the next instruction under program control.

A single instruction transmitted from the control station requests that a specific test be executed and that a specific command be carried out if the test was passed. The first half of the instruction word is used to select one of **64** possible tests by means of a look-up table. If the test is passed, the second half of the instruction is similarly used to select one of **64** possible actions. Even though only *6* tests and 17 actions have been implemented, a rich variety of operations is already possible. An example of a single instruction is as follows:

If "fingertip Sensor closed" then "open jaws."

For the computer, this instruction is the octal number 5157, where the "fingertip sensor closed" test is specified by 51 and the "open jaws" command is specified by 57. A list of the tests and actions is given later in figure 8.

One advantage of this system is the ability to converse with the arm in a language more natural than the machine language normally used to program small computers. Another main advantage in the time-delay situation is that the entire subroutines of machine-language instructions for the given test or action need not be transmitted to the remote computer. These subroutines are already built into the remote computer. Only a single instruction need be transmitted.

These instructions also allow short sequences of operations to be sent from the control station at one time instead of having to be sent one by one, waiting for a return message after each one. Thus the sequence of commands

(1) If "fingertip sensor closed"
(2) Then "stop arm"
(3) And "open jaws"

allows a particular job to be done with one cycle of transmissions through the time delay that would ordinarily take three cycles. Additionally, with long time delays, this sequence of commands specifies a task that would require great caution if performed completely under manual control.

Just touching an object in such a time-delay situation is difficult without producing some overshoot that may knock the object away or without having to use a stop-and-wait strategy with successive motions of decreasing amplitude that may take a great deal of time.

The set of tests and commands is also intended to be used in longer lists (actual programs of movement), each with perhaps 10 to 100 instructions. These programs can provide such simple features as position memory or path memory, or can perform such complicated automatic tasks as unscrewing a nut from a bolt. A single command specifying that successive commands be taken from a list of commands can be a very powerful and flexible method for producing computer-assisted manipulations.

The structure of the remote-computer program executing these special instructions is given in figure 7. Combined with the short test and action subroutines and the control registers this subroutine is all that is required to implement the ARM language. The subroutine is entered every 1/60 sec after a new instruction and command position become available from the delay line, but before the servo subroutine (computing errors from arm positions) is carried out.

ALGORITHMIC LANGUAGE FOR REMOTE MANIPULATION (ARM)

If requests for the automatic operations described in the preceeding section are taken from a list, the list can be considered a program of motions (an algorithm) to carry out a manipulation task. The effective utilization of such programs, however, requires a means of writing them in an easy-to-use language and a means for assembling (or generating) a list of arm operations from the statements in the language. Using a sufficiently powerful computer program, a list of such operations or instructions could be generated from any reasonable language. With a small computer system, care must be exercised when designing a programming language so that the assembly of programs is possible. Under this constraint, we simultaneously developed the separate concepts of the ARM language, the assembler, the instruction set, and the procedure for carrying out instructions.

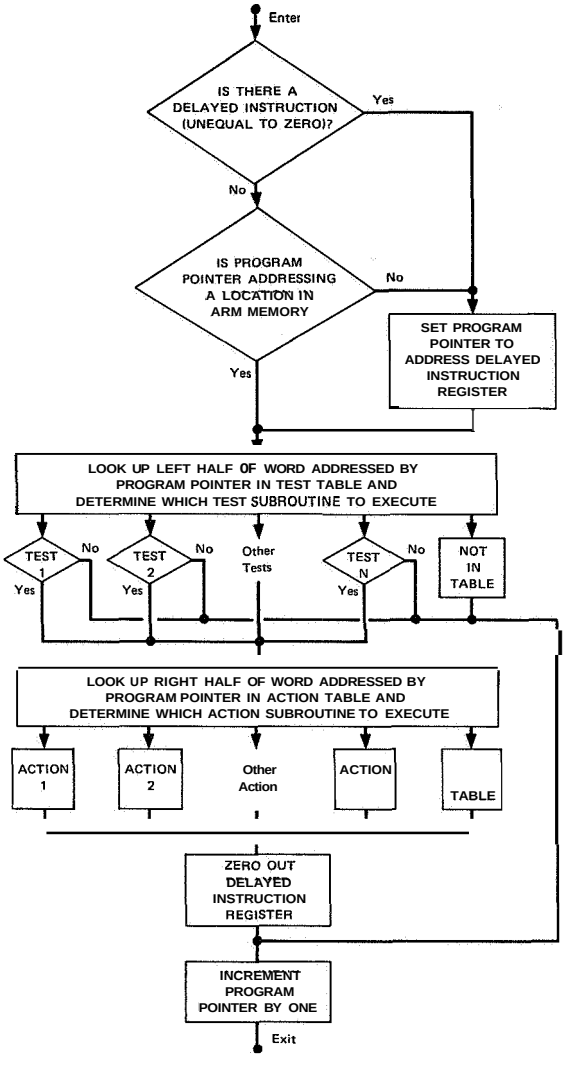

FIGURE 7.—Flow chart of the remote station subroutine. (This subroutine carries out single instructions and programs of instructions. It can be seen that if instructions are being taken from a program in arm memory, an instruction sent from the control station will cause the program to be stopped and the instruction to be carried out.)

ARM differs from the MHI or THI language developed by Ernst (ref. 5) and from MANTRAN reported by Sheridan (ref. 6), in that manual inputs from the operator can be used in addition to teletype inputs. Thus, the operator can move his control brace and request that the arm move to "this" position or move "this" joint "this" much. Each "this" in the preceding sentence is a manually specified quantity that is

difficult to verbalize, much less to quantify as a joint vector for typewriter input. ARM should not be considered an entity itself, but a means of carrying out automatically programmed motions within the scope of the teleoperator control system previously described.

An example of a program (written in ARM), an algorithm to unscrew a nut from a bolt, is given in figure 8. The program honsists of the following three parts:

(1) Definitions of the symbols for the assembler (fig. 8(a)) to use in converting names to instructions.

(2) An algorithm for the task (fig. 8(b)), giving the order of individual motions and tests.

(3) Labeled storage space for arm positions and gains used in various parts of the algorithm (fig. 8(c)).

This entire manuscript is given to an assembler for conversion to a list of numbers (instructions) for execution by the remote computer program.* In this case the compiling is quite straightforward : Values for the various symbols on each line are simply added together to form the instruction. This simple assembler, however, is quite powerful, as indicated by the easy-to-understand phrases of the algorithm shown in the program.

The unscrewing program is designed to receive both typed commands entered from the control-station teletype and manual commands entered from the control brace or knobs. Thus, the pro-

* Note the meaning of some special symbols:
/ A comment.
→ Assign a value to a name.
; The line terminator.
: A label.

```
\BASIC DEFINITIONS FØR THE ASSEMBLER

\DEFINITIØNS ØF THE TESTS

        THUMB←6400      \THUMB TIP SENSØR CØNTACT
        FINGER←5100     \FINGERTIP SENSBR CBNTACT
        BØTH←4200       \BØTH THUMB 6 FINGER CØNTACT
        WEBB←6100       \WEBB ØF JAW SENSØR CØNTACT
        DØNE←4400       \ALL JØINT ERRØRS < 17
        WAIT←6500       \CLØCK NØT YET = 0

\DEFINITIØNS ØF SIYGLE WØRD ACTIBNS

        STØP←63         \LØAD PRESENT PBSITIBN IN CØMMAND VECTBR
        ØPEN←57         \ØPEN JAUS
        CLØSE←43        \CLØSE JAUS
        AUTØ←50         \TAKE PØSITIØN CØMMANDS FRØM PRBGRAM
        MANUAL←62       \TAKE PØSITIØN CØMMANDS FRBM CØNTRØL STATIØN
        REPEAT←42       \SUBTRACT 1 FRØM PRBGRAM CØUNTER
        SKIP←53         \ADD 1 TØ PRBGRAM CØUNTER
        SKIP2←22        \ADD 2 TØ PRBGRAH CBMTER
        BELL←13         \RING TELETYPE B R L
        DDT←44          \STØP PRØGRAM & LØAD DEBUGGING PACKAGE

\DEFINITIØNS ØF TWØ WØRD ACTIBNS WITH PARAMETER IN SECØND WØRD

        GØ←47           \SET PRØGRAM CØUNTER WITH PARAMETER
        CLØCK←67        \SET 60 HZ CLØCK CØUNTER WITH PARAM,

\DEFINITIØNS ØF TWØ WØRD ACTIØNS WITH VECTØR ADDRESS IN SECØND WØRD

        INCREMENT←13    \ADD PØSITIØN UECTBR TØ CØMMAND VECTØR
        DECREMENT←15    \SUBTRACT PØS. VECTBR FRBM CMD. VECTBR
        MBVE←55         \LØAD CMD. VECTØR FRØM PØS. VECTØR
        SAVE←4          \STØRE CMD. VECTBR IN PØS. VECTBR
        GAINS←17        \LØAD GAIY VECTØR FRØM GIVEN VECTØR

\SØME FILL-WØRDS, ØNLY TØ MAKE PRØGRAMS READ EASIER

        BY←0
        IF←0
        THEN←0
        SET←0
        IN←0
        TØ←0
```

(a) BASIC DEFINITIONS OF THE TESTS AND ACTIONS

FIGURE 8.—Program to unscrew a nut from a bolt. (All of the numbers in this program are octal.)

```
\PRØGRAM TØ UNSCREW A NUT FRØM A BØLT
\LABELS---INSTRUCTIØNS----------CØMMENTS

BEGIN
        AUTO                    \SWITCH TO PRØGRAM CONTROL
        CLOSE                   \MAKE SHURE JAWS CLOSE HARD

LØØP:   DECREMENT BY: HALFTURN  \LEFT 180 DEGREE WRIST ROTATION
        SET CLOCK: 140
        IF WAIT THEN REPEAT

        SAVE IN: NUT            \SAVE POSITION ØF NUT

        SET GAINS; TESTGAIN     \MØVE TØ TEST PØSITIØN
        MØVE TO; TEST
        CLBSE
        SET CLØCK: 200
        IF WAIT THEN REPEAT

        SET GAINS; DØNEGAIN     \IS NUT FREE9
        IF DONE THM SKIP2
        GØ TØ; FINISH

        SET GAINS; RETGAIN      \RETURN TØ NUT
        MOUE TØ: NUT
        SET CLØCK: 200
        IF WAIT THEN REPEAT

        SET GAINS; FUGAIN       \ØPEN JAUS
        ØPEN
        SET CLØCK: 200
        IF WAIT THEN REPEAT

        INCRMMT BY: HALFTURN    \RIGHT 180 DEGREE WRIST ROTATION
        SET CLØCK: 140
        IF YAIT THM REPEIIT

        CLBSE                   \CLØSE JAUS
        SET CLOCK; 200
        IF UAIT THM REPEAT
        GØ TO; LØØP
FINISH: SET GAINS, FULLGAIN     \MØVE TØ FINAL PØSITIØN
        CLBSE
        MØVE TØ FINAL
        SET CLOCK) 300
        IF UAIT THEN REPEAT

        ØPEN                    \DRØP NUT
        SET CLØCK: 200
        IF WAIT THEN REPEAT

        B R L                   \RING BELL=ALL DONE
        GØ TØ: 1000             \END PRØGRAM
```

(b) THE ALGORITHM

TA-7948-27b

FIGURE 8.—Continued.

```
\PØSITIØN AND GAIN VECTBRS
\ THE 1 NUMBERS CØRRESPØND TØ THE SEVEN JBINTS
\ BEGINNING AT SHØLDER AND ENDING AT TØNGS

HALFTURN: 0; 0; 01 0; +760; 0; 0        \RIGHT HALF TURN

FINAL:    01 0; 01 01 0; 0; 0           \FINAL PØSITIØN

NUT:      0; 0; 0; 0; 0; 01 0           \TEMPØRARY PØSITIØN

TEST:     0; 01 0; 0; 01 0; 0           \TEST PBSITIBN

TESTGAIN: 2000; 2000; 2000; 2000        \LØWER FBRCE
          0; 0; 2000

RETGAIN:  31771 31711 31111 3171        \RETURN GAIN
          0; 0; 3111

DØNEGAIN: 0; 31111 01 37711 0; 0; 0     \TEST TWØ JBINTS

FULLGAIN: 37711 31711 37111 3711        \FULL GAIWS
          31771 31111 3777

END
```

(c) THE STORAGE LOCATIONS

TA-7948-27c

FIGURE 8.—Concluded.

gram of figure 8 is not completely self-explanatory. For the unscrewing task the operator carries out the following operations:

(1) Load the unscrewing program (a total of **116** instructions) into the remote computer using the run command "*R*UNSCREW."

(2) Sets up Absolute control by the Brace by typing "*B*:*A*."

(3) Moves the arm to the final position where the nut is to be placed and stores the position vector in the "FINAL" storage area of the program under decision control using the command "(,104$)." (The octal number **104** is the location of FINAL; hopefully a more refined version of the control-station program will allow name input).

(4) Moves the arm to the test position located **1** to **2** in. directly behind the nut and similarly saves the position vector in the "TEST" storage area using the command "(,122$)."

(5) Moves the arm to the nut and grasps it using the brace and then starts the program using the command "(,*G*)."

Instructions taken from a list then direct the arm to unscrew the nut by half-turns, attempting to pull the nut to the test position after each half-turn is completed. If the test position is not reached, the arm knows that the nut is still attached and goes back for another half-turn. When the test position is reached, the arm moves to the final position, opens its jaws, and drops the nut into the container.

AN EVALUATION OF A COMPUTER-ASSISTED MANIPULATION TASK

To determine what advantage a program of motions would have in reducing the time required for a task, a task was designed around the unscrewing program previously described. The task was to unscrew a hex nut from a **16** mm (5/8-in.) machine bolt and drop it into a small 5-by-8 cm receptacle located approximately **40** cm away. The two different experimental conditions were as follows:

(1) The communications time delay was either zero or **2.6** sec (the round-trip moon-time delay).

(2) Control was either pure manual or computer-assisted manual. Using knob control for all manual inputs and direct viewing, all four combinations of these two conditions were performed twice by one subject (JH). Knob instead of brace control was used because of the inability to hold the control brace sufficiently stationary for several minutes in the longer tasks and the inability of the human wrist to rotate through 360° for efficient unscrewing.

The computer-assisted manual-control conditions followed the modus operandi for running the unscrewing algorithm detailed in the preceding section: The "final" and "test" positions were found manually and entered into the program and then control was handed over to the computer algorithm, which finished the task. The program was changed only to allow the nut to be removed with full turns by doubling the wrist increment "Halfturn."

The manual removal of the nut followed a slightly different course. No test position was required in this case, so the task began by unscrewing the nut turn-by-turn for the first three of four revolutions. Since the nut would come off in five or six turns, the strategy changed at this point and an attempt was made to pull the nut off before releasing it. If it did not come off, the jaws were opened, the grasping position found again, and another revolution undertaken. When the nut came off, it was manually positioned over the receptacle and dropped.

The results of these tests are given in figure 9. In both time-delay situations, manual-computer control was faster than manual control. The difference is greatest in the time-delay condition where a time reduction of greater than **5** to **1** was achieved by employing the computer-assisted operation.

TOUCH-FEEDBACK SYSTEMS

Two touch-feedback systems for the teleoperator control system have been constructed. Each system consists of a set of sensors mounted on the mechanical arm and a corresponding set of tactile stimulators mounted on the control brace. All of the sensors utilize conducting rubber that is deformed to complete an electrical circuit upon physical contact. Individual sensors activate corresponding stimulators in a binary fashion: a stimulator is either full on or full off. The follow-

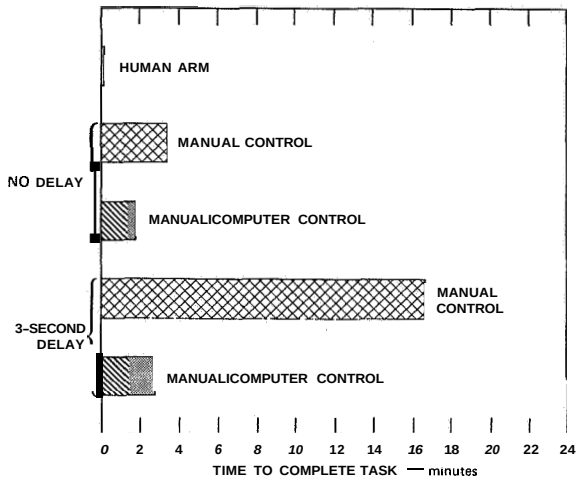

FIGURE 9.—Comparison between manual and computer-assisted manual control. (The time taken to perform the task directly with a human hand is shown only for comparison. Computer-assisted times are broken into two parts: the time required by the program which is the same in both delay conditions, and the time required by the manual portion.)

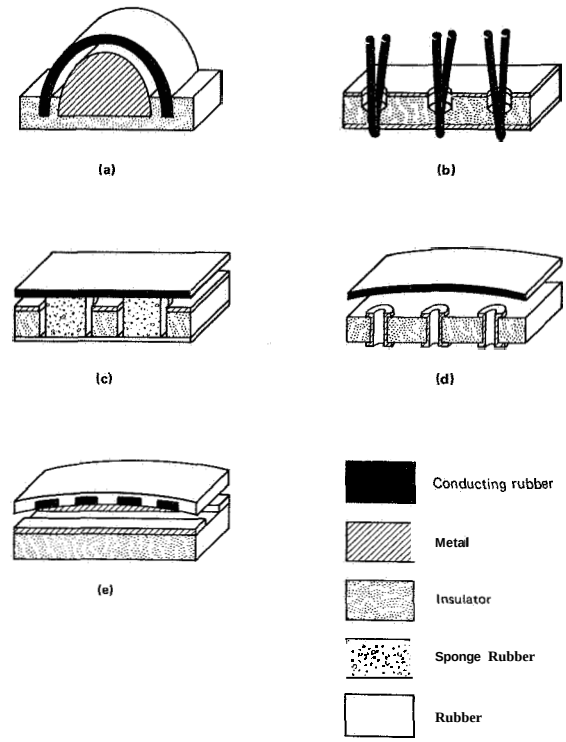

FIGURE 10.—Five types of sensor construction using conducting rubber.

ing sections describe the construction of the sensors and the two touch feedback systems.

Sensor Design

Individual sensors for the hand and wrist areas of the manipulator must have the following properties, which are seldom found together in commercial microswitches:

- Respond to forces over a specified (often large) area.
- Respond to small forces over a range of directions.
- Be small in size.

Prototype sensors having some of these characteristics have been developed to transduce mechanical forces to electrical signals. The sensors, shown in figure 10, all use conducting rubber in some form and have the ability to provide both discrete (binary) and continuous force information. Descriptions of these sensors follow:

(1) The omnidirectional force sensor shown in figure 10(a) consists of a bridge of conducting rubber cast into an insulating mounting block. Sensitivity depends on both the thickness of the conducting rubber and the spacing between the rubber and metal rod.

(2) The whisker sensor shown in figure 10(b) consists of thin conducting rubber strips pulled through holes in two-sided printed circuit boards. This sensor has high sensitivity because of the mechanical advantage of the whiskers and has a wide dynamic range (over 1000 to 1) if several parallel whiskers (10) are employed in the same sensor.

(3) The surface sensor shown in figure 10(c) consists of a conductive rubber sheet held by sponge rubber columns above a sheet of single-sided printed circuit board. If islands of copper foil are made by etching the circuit board, then the contact force can be localized to one or more islands.

(4) The force-distribution sensor shown in figure 10(d) consists of a sheet of conducting rubber arched over an insulating board studded with microeyelets. The shape of the force pattern is measured by measuring the pattern of contact

resistance between the eyelets and the conducting rubber sheet.

(5) The force distribution sensor shown in figure 10(e) consists of rows of conducting rubber imbedded in insulating rubber above perpendicular rows of foil on an insulating board.

Hand Contact-Sensing System

The purpose of this system is to reproduce to the operator the contact between the mechanical hand and the object being touched or manipulated. This system consists of a number of conducting rubber sensors mounted on the outside surfaces of the mechanical hand, as shown in figure 11. The outside of the tongs is completely covered with these sensors, as are other extreme or protruding parts of the upper hand. The sensors are arranged so that any contact with the hand and a flat surface is sensed and that any contact with the tongs is sensed. The locations of these sensors on the remote hand are given in table 1. Each of the sensors is connected via amplifying and gating circuits to an air-jet tactile stimulator. The air jets are positioned on the control brace to produce a touch sensation on a portion of the operator's hand corresponding to the location of the sensor. Each jet produces an area of pulsating pressure on the skin approximately 3/16 in. in diameter. The arrangement of air-jet stimulators on the control brace is shown in figures 12 and 13. The construction of the air-jet stimulators is described by Bliss and Crane (ref. 7, appendix B).

TABLE 1.—*Contact Sensors on Mechanical Hand*

Location	Number	Type, fig. 10
Tips of tongs	2	b
Top of tongs, distal	2	c
Top of tongs, proximal	2	c
Bottom of tongs, distal	2	c
Bottom of tongs, proximal	2	c
Back of tongs, distal	2	c
Back of tongs, proximal	2	c
Web of jaw	1	b
Knuckles	2	c
Top of wrist	2	d
Bottom of wrist	2	d

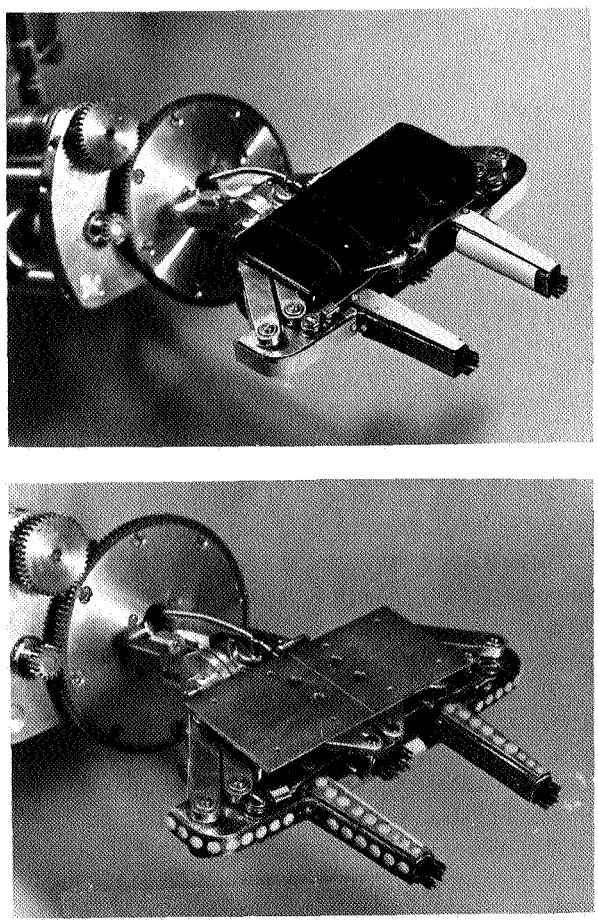

FIGURE 11.—Construction of touch sensors. (Upper photo shows printed circuit board bonded to the tongs and wrist. Lower photo shows finished assembly with conducting rubber covers in place.)

Jaw Shape-Sensing System

The purpose of this system is to reproduce to the operator the shape and location of the object held in the remote jaws. Two sensing pads using the design shown in figure 10(d) are built into the tongs of the mechanical hand as shown in figure 11. Each of these two opposing pads consists of 144 individual contacts in a 6X24 rectangular pattern. Two corresponding 6X24 rectangular arrays of bimorphs contacting the index finger and thumb are built into the control brace as shown in figure 12.

The connections between the sensor and stimulator are one-to-one: If one contact is closed, the

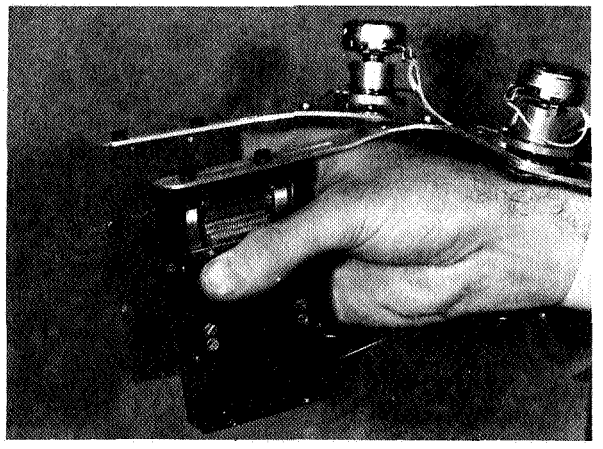

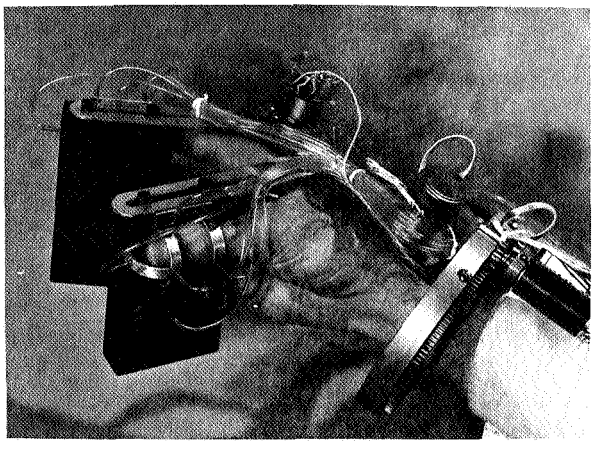

FIGURE 12.—Tactile simulators on the hand controller. (The upper photograph shows the array **of** 6 X24 piezoelectric vibrators positioned under the thumb. The lower photo shows the same hand controller with seven air jets in place on each finger.)

bimorph in the corresponding location vibrates. Bimorphis produce a vibration of the skin restricted to an area about **1** mm in diameter. Thus the pattern of contact closures is reproduced as a pattern of vibration enabling the operator to feel on his own thumb and index finger the shape and location of the object held in the remote jaws. A complete description of nearly identical bimorph arrays used in shape recognition and reading experiments is given by Bliss (ref. **8)** and Bliss, Katcher, Rogers, and Shepard (ref. 9).

This shape-sensing system represents a considerable improvement over our previous jaw shape-sensing system (Bliss, Hill, and Wilber, ref. **1).** The new sensors are exactly the size of

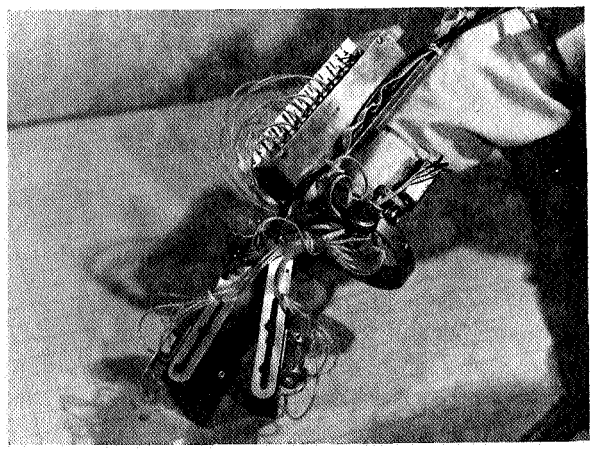

FIGURE 13.—Overall view **of** the tactile stimulators on the control brace. (Air valves in the box on forearm individually activate air jets on the finger and thumb.)

the jaws **(10** by 50 mm) and are only about **3** mm thick, whereas the previous sensors were twice as wide and twice as thick. In spite of their clumsiness, the previous sensors were necessary to carry out obscured manipulations and they greatly reduced the occurrence of drops and fumbles in pickup and extraction tests.

ACKNOWLEDGMENTS

The authors are grateful to those who have substantially contributed to this project. Professor James L. Adams of Stanford University assisted in diagnosing problems with the Rancho Arm and suggesting improvements for it, as well as a philosophy for designing a teleoperator control system, and evaluation experiments to be carried out with the system. Mr. Anthony J. Sword of Stanford University helped set up the initial control-system hardware, suggested several of the features in the control-station simulation, wrote the first two versions of the control-system computer program, and designed and constructed the first touch sensors. His work was supported under grant NASA–NgR–05–020–345 with Stanford University. Mr. John P. Gill of Stanford Research Institute contributed to the design and construction of the piezoelectric bimorph tactile stimulators and built the majority of both touch-sensing systems.

REFERENCES

1. BLISS, J. C.: HILL, J. W.; AND WILBER, B. M.: Tactile Perception Studies Related to Teleoperator Systems. NASA–CR–1775, 1971.
2. HILL, J. W.; AND BLISS, J. C.: Tactile Perception Studies Related to Teleoperator Systems. Final Rept. 2 on Contract NAS2–5409, SRI Project 7948, Stanford Research Institute, 1971.
3. JOHNSON, E. G.; AND CORLISS, W. R.: Teleoperators and Human Augmentation. NASA–SP–5047, 1967.
4. CORLESS, W. R.; AND JOHNSON, E. G.: Teleoperator Controls. NASA–SP–5070, 1969.
5. ERNST, H. A.: A Computer Operated Mechanical Hand. Ph.D. Thesis, Massachusetts Institute of Technology, 1961.
6. SHERIDAN, T. B.: Advancements in Teleoperator Systems. NASA–SP–5081, 1970.
7. BLISS, J. C.; AND CRANE, H. D.: Experiments in Tactual Perception. Final Rept. on Contract NAS2–1679, SRI Project 4656, Stanford Research Institute, 1965.
8. BLISS, J. C.: A Relatively High-Resolution Reading Aid for the Blind. IEEE Trans. on Man-Machine Systems, vol. MMS–10, 1969, pp. 1–9.
9. BLISS, J. C.; KATCHER, M. H.; ROGERS, C. H.; AND SHEPARD, R. P.: Optical-to-Tactile Image Conversion for the Blind. IEEE Trans. on Man-Machine Systems, vol. MMS–11, 1970, pp. 58–64.

☆ U.S. GOVERNMENT PRINTING OFFICE: 1972 O—459-173